Pflügers Archiv

European Journal of Physiology

Vol. 409 No. 1–2 June 1987

A Heart, circulation, respiration and blood; environmental and exercise physiology

Y. Tamaki, T. Nakayama: Effects of air constituents on thermosensitivities of preoptic neurons: hypoxia versus hypercapnia 1

F. P. Gerstheimer, M. Mühleisen, D. Nehring, V. A. W. Kreye: A chloride-bicarbonate exchanging anion carrier in vascular smooth muscle of the rabbit 60

R. S. Staron, D. Pette: Nonuniform myosin expression along single fibers of chronically stimulated and contralateral rabbit tibialis anterior muscles 67

B. Mohr, A. H. Bom, A. J. Kaumann, V. Thämer: Reflex inhibition of efferent renal sympathetic nerve activity by 5-hydroxytryptamine and nicotine is elicited by different epicardial receptors 145

U. Heinrich, J. Hoffmann, D. W. Lübbers: Quantitative evaluation of optical reflection spectra of blood-free perfused guinea pig brain using a nonlinear multicomponent analysis 152

T. P. Geisbuhler, S. Sergeant, F. L. Miramonti, H. D. Kim, M. J. Rovetto: Forskolin inhibition of hexose transport in cardiomyocytes 158

J. E. Ponce-Hornos, P. Bonazzola, A. C. Taquini: The role of extracellular sodium on heart muscle energetics 163

O. I. Pisarenko, E. S. Solomatina, I. M. Studneva, V. I. Kapelko: The relationship between the cardiac contractile function, adenine nucleotides and amino acids of cardiac tissue and mitochondria at acute respiratory hypoxia 169

Z. Szelényi, P. Hinckel: Changes in cold- and heat-defence following electrolytic lesions of raphe nuclei in the guinea-pig 175

B Transport processes, metabolism and endocrinology; kidney, gastrointestinal tract, and exocrine glands

P. Silva, B. Koenig, S. Lear, J. Eveloff, R. Kinne: Dibutyryl cyclic AMP inhibits transport dependent QO_2 in cells isolated from the rabbit medullary ascending limb 74

E. Schlatter, J. A. Schafer: Electrophysiological studies in principal cells of rat cortical collecting tubules. ADH increases the apical membrane Na^+-conductance 81

O. Skøtt: Effects of amines, monensin and nigericin on the renin release from isolated superfused rat glomeruli 93

R. Greger, H. Gögelein, E. Schlatter: Potassium channels in the basolateral membrane of the rectal gland of the dogfish (*Squalus acanthias*) 100

H. Gögelein, R. Greger, E. Schlatter: Potassium channels in the basolateral membrane of the rectal gland of *Squalus acanthias*. Regulation and inhibitors 107

R. Greger, E. Schlatter, H. Gögelein: Chloride channels in the luminal membrane of the rectal gland of the dogfish (*Squalus acanthias*). Properties of the "larger" conductance channel 114

H. Gögelein, E. Schlatter, R. Greger: The "small" conductance chloride channel in the luminal membrane of the rectal gland of the dogfish (*Squalus acanthias*) 122

L. C. Garg, N. Narang: Effects of potassium bicarbonate on distal nephron Na-K-ATPase in adrenalectomized rabbits 126

B. C. Burckhardt, E. Frömter: Evidence for OH^-/H^+ permeation across the peritubular cell membrane of rat renal proximal tubule in HCO_3^--free solutions 132

Continuation see back cover page

Springer International

424 Pflügers Arch

ISSN 0031-6768 PFLABK 409(1–2) 1–222 (1987)

Pflügers Archiv
European Journal of Physiology

The Journal publishes the results of original research considered likely to further the physiological sciences in their broadest sense. Papers on pathophysiological topics will also be considered insofar as the information they contain can be used as a tool for further investigation of physiological mechanisms. In other words, their subject matter must clearly convey a physiological message. Purely clinical papers will be excluded.

The Journal is sub-divided in three sections (A, B, C) according to subject matter. Within these sections and in addition to the regular scientific papers, subject-related papers on purely methodological topics will be published in a subsection, entitled "Instruments and techniques". A further subsection entitled "Short communications", is also reserved for the publication of forefront material not yet in full paper form but of immediate interest to our readers. Once a Short communication has been accepted and resubmitted by the authors in camera-ready form, it can be published in the next available issue.

The Editors of Pflügers Archiv endorse the "Recommendations from the Declaration of Helsinki" and the "Guiding Principles in the Care and Use of Animals". All investigations involving man and all animal experiments reported in this Journal must conform with these principles. Editors are instructed to reject papers in which there is no clear evidence that these principles have been adhered to. Any differences of opinion will be adjudicated by the Editorial Board of the Journal.

Manuscripts in triplicate should be sent to the appropriate Subject Editor

(see inside title page for addresses)

Copyright

Submission of a manuscript implies: that the work described has not been published before (except in the form of an abstract or as part of a published lecture, review, or thesis); that it is not under consideration for publication elsewhere; that its publication has been approved by all coauthors, if any, as well as by the responsible authorities at the institute where the work has been carried out; that, if and when the manuscript is accepted for publication, the authors agree to automatic transfer of the copyright to the publisher and that the manuscript will not be published elsewhere in any language without the consent of the copyright holders.

All articles published in this journal are protected by copyright, which covers the exclusive rights to reproduce and distribute the article (e.g., as offprints), as well as all translation rights. No material published in this journal may be reproduced photographically or stored on microfilm, in electronic data bases, video disks, etc., without first obtaining written permission from the publisher.

The use of general descriptive names, trade names, trademarks, etc., in this publication, even if not specifically identified, does not imply that these names are not protected by the relevant laws and regulations.

While the advice and information in this journal is believed to be true and accurate at the date of its going to press, neither the authors, the editors, nor the publisher can accept any legal responsibility for any errors or omissions that may be made. The publisher makes no warranty, express or implied, with respect to the material contained herein.

Special regulations for photocopies in the USA

Photocopies may be made for personal or in-house use beyond the limitations stipulated under Section 107 or 108 of U.S. Copyright Law, provided a fee is paid. This fee is US$ 0.20 per page, or a minimum of US$ 1.00 if an article contains fewer than five pages. All fees should be paid to the Copyright Clearance Center, Inc., 21 Congress Street, Salem, MA 01970, USA, stating the ISSN 0031-6768, the volume, and the first and last page numbers of each article copied. The copyright owner's consent does not include copying for general distribution, promotion, new works, or resale. In these cases, specific written permission must first be obtained from the publisher.

Subscription information

Volumes 408 and 409 (6 issues each) will appear in 1987.

North America: Annual subscription rate: approx. US$ 857.00 (single issue price: approx. US$ 85.00) including carriage charges. Subscriptions are entered with prepayment only. Orders should be addressed to:
Springer-Verlag New York Inc.
Service Center Secaucus
44 Hartz Way,
Secaucus, NJ 07094, USA,
Telephone (201) 348-4033,
Telex 023125994.

All other countries: Annual subscription rate: DM 1,696.00 plus carriage charges. Volume price: DM 848.00 (single issue price: DM 169.60) plus carriage charges. SAL delivery (surface airmail lifted) is mandatory for Japan, India, Australia and New Zealand. Customers should ask for the appropriate price list. Airmail delivery to all other countries is available upon request. Subscriptions can either be placed via a bookdealer or sent directly to:
Springer-Verlag
Heidelberger Platz 3
D-1000 Berlin 33,
Telephone (0) 30/8207-1,
Telex (0) 1-83319.

Changes of address: Allow six weeks for all changes to become effective. All communications should include both old and new addresses (with Postal Codes) and should be accompanied by a mailing label from a recent issue.

Back volumes: Prices are available on request.

Microform: Microform editions are available from:
University Microfilms International
300 N. Zeeb Road
Ann Arbor, MI 48106, USA.

Production

Springer-Verlag
Journal Production Department II
Postfach 105280
D-6900 Heidelberg 1
Federal Republic of Germany,
Telephone (0) 6221/487-331,
Telex (0) 461723.

Responsible for advertisements

Springer-Verlag
E. Lückermann
Heidelberger Platz 3
D-1000 Berlin 33
Telephone (0) 30/8207-1
Telex (0) 1-85411.

Printers

Wiesbadener Graphische Betriebe GmbH,
D-6200 Wiesbaden

© Springer-Verlag Berlin Heidelberg 1987
Springer-Verlag GmbH & Co. KG
D-1000 Berlin 33
Printed in Germany

Springer International

Pflügers Archiv

European Journal of Physiology

	Subject groups	Subject editors
A	**Heart, circulation, respiration and blood; environmental and exercise physiology**	E. Gerlach Physiologisches Institut Universität München Pettenkoferstrasse 12 D-8000 München 2
B	**Transport processes, metabolism and endocrinology; kidney, gastrointestinal tract, and exocrine glands**	P. Deetjen Physiologisches Institut Universität Innsbruck Fritz-Pregl-Strasse 3 A-6010 Innsbruck
C	**Excitable tissues and central nervous physiology**	O. Pompeiano Istituto di Fisiologia Università di Pisa Via S. Zeno 31 I-56100 Pisa

Springer International

Pflügers Archiv

European Journal of Physiology

Field Editors

J. A. Bernards, Nijmegen
J. P. Bonjour, Geneva
A. J. Brady, Los Angeles, CA
G. ten Bruggencate, München
E. E. Carmeliet, Leuven
R. Casteels, Leuven
P. Cerretelli, Geneva
C. de Rouffignac, Gif-sur-Yvette
J.-M. Dubois, Orsay
B. R. Duling, Charlottesville, VA
J. Durand, Paris
E. Frömter, Frankfurt (Main)
W. Hasselbach, Heidelberg
K. Hierholzer, Berlin
M. Imai, Osaka
C. Jessen, Giessen
F. Kreuzer, Nijmegen
H. Kuriyama, Fukuoka
H. Murer, Zürich
O. H. Petersen, Liverpool
J. Piiper, Göttingen
R. S. Reneman, Maastricht
H. Seller, Heidelberg
H. Shimazu, Tokyo
E. Simon, Bad Nauheim
S. Thesleff, Lund
W. Trautwein, Homburg (Saar)
W. Ulbricht, Kiel
K. J, Ullrich, Frankfurt (Main)
J. A. Young, Sydney
E. M. Wright, Los Angeles, CA
W. G. Zijlstra, Groningen

Subject Editors

E. Gerlach, München
P. Deetjen, Innsbruck
O. Pompeiano, Pisa

Coordinating Editor

K. Thurau, München

Springer International

Pflügers Arch (1987) 409:1–6

Pflügers Archiv
European Journal of Physiology
© Springer-Verlag 1987

Effects of air constituents on thermosensitivities of preoptic neurons: hypoxia versus hypercapnia

Yoko Tamaki and Teruo Nakayama

Department of Physiology, Osaka University Medical School, Nakanoshima 4-3-57, Kita-ku, Osaka 530, Japan

Abstract. The effects of hypoxia (10% O_2) on the thermosensitivities of preoptic neurons were studied in urethanized rats and compared to the effects of hypercapnia (10% CO_2). This was examined by regression of neuronal activity on preoptic temperature. During hypoxia, the slope of the regression line increased significantly in 8 (23%) of 35 warm-sensitive neurons and decreased in eight other neurons ($P<0.05$). During hypercapnia, the slope of the regression line decreased significantly in 7 (30%) of the 23 warm-sensitive neurons ($P<0.05$). No neuron was found that significantly increased the slope of the regression line. The effects of hypoxia on thermosensitivities (i.e. the slope of the regression line) of PO neurons differed from those of hypercapnia in chi-square analysis ($P<0.05$). Responses of the cold-sensitive neurons to hypoxia or hypercapnia did not generally differ from those of the warm-sensitive neurons. During hypoxia and hypercapnia, arterial blood pressure, respiratory frequency, heart rate, and EEG were recorded to examine their relations to neuronal activity. The present results indicate that the thermosensitivities of preoptic neurons are modified by both hypoxia and hypercapnia, but that hypoxic differ from hypercapnic effects.

Key words: Hypoxia – Preoptic area – Thermosensitive neuron – Thermoregulation – Hypercapnia

Introduction

Hypoxia has been known to lower body temperature in many species (Hemingway and Nahas 1952; Bhatia et al. 1969). In kittens, guinea pigs, mice, and pigeons, inducing hypoxia at an environmental temperature below neutral causes oxygen consumption to fall, especially when the initial level of oxygen consumption is high (Hill 1959; Cassin 1963; Gleeson et al. 1986). Hypoxia has been also reported to inhibit shivering in mice, dogs, man, cats, and pigeons (Kottke et al. 1948; Hemingway and Birzis 1956; Gleeson et al. 1986). Blatteis and Lutherer (1973) have suggested that moderate hypoxia eliminates nonshivering thermogenesis in dogs, but that shivering is susceptible only to more severe hypoxia. In golden hamsters, acute exposure to 10% O_2 has been reported to decrease the threshold temperature for cold-induced nonshivering thermogenesis, but this result is not due to an inhibition of nonshivering thermogenesis itself (Kuhnen et al. 1985). Hypoxia in man enhances dissipation of heat from the skin in a cold environment (Kottke et al. 1948). In rabbits 8% O_2 induces a rise of ear skin temperature, indicating increased blood flow, that corresponds to a decrease in cutaneous sympathetic activity (Iriki et al. 1971). Jänig and Kümmel (1977) demonstrated in postganglionic neurons innervating the cat hindpaw that sudomotor neurons were activated and vasoconstrictor neurons were inhibited by systemic hypoxia. As a possible mechanism for its hypothermic effect, hypoxia may alter the neuronal activity involved in thermoregulation. We recently reported that preoptic (PO) thermosensitive neurons generally increase their activities and modify their thermosensitivities during hypercapnia, which also produces hypothermia (Tamaki et al. 1986). The purpose of the present study was to examine the effects of hypoxia on the thermosensitivities of PO neurons and to compare hypoxic to hypercapnic effects. The effects of hypercapnia were analyzed on new data in addition to our previously published results.

Offprint requests to: T. Nakayama

Methods

Male Wistar rats weighing 270–340 g were anesthetized with urethane (1 g/kg, i.p.) and fixed on a stereotaxic instrument after tracheal cannulation. A water-perfused thermode and a needle type thermocouple were implanted into the PO area according to a method already described in detail (Tamaki et al. 1986). Neuronal activity was recorded extracellularly from the PO area with a glass microelectrode filled with pontamine sky blue dissolved in 0.5 M sodium acetate. Rectal temperature (T_{re}) was maintained at about 37°C throughout the experiment.

The rat breathed air and 10% O_2 (with 0.03% CO_2 and the remainder N_2) via a tracheal cannula connected to a small open chamber. CO_2 and O_2 concentrations near the entry of the tracheal cannula in the chamber were monitored using Expired Gas Monitor 1H26 (San-ei, Tokyo, Japan) and maintained at given levels by means of flow-rate controllers. The gas mixture and air passed through the small open chamber at a flow rate sufficiently high to prevent the CO_2 and O_2 concentrations from being altered by respiration of rats. Discharges of single neurons were followed while both T_{po} and T_{re} were maintained at about 37°C. By use of a water-perfused thermode, T_{po} was then changed twice between 33°C and 41°C at a rate of 2–4°C/min to determine the thermal response of the neuron. After T_{po} was returned to 37°C, the rat breathed 10% O_2 gas. After at

least 1 min, T_{po} was changed once more in the same way to compare thermosensitivity during hypoxia with that during air inhalation. When thermally insensitive neurons were being recorded, the rat breathed the 10% O_2 gas mixture for 2 min while both T_{po} and T_{re} were maintained at about 37° C. During some recordings of thermosensitive neurons, the rat breathed air for more than 10 min, followed by a 10% CO_2 gas mixture (with 20% O_2 and the remainder N_2). During the recovery period of air inhalation, T_{po} was sometimes changed once again to confirm the thermal response of the neuron. Some thermosensitive neurons were examined only during hypercapnia. Neuronal discharges were counted by a rate meter and displayed simultaneously on a chart recorder with T_{po}, T_{re}, and inspired O_2 and CO_2 concentrations. At the end of the recording, the dye was deposited by iontophoresis to mark the position of the microelectrode. Following each experiment the rat was perfused with saline followed by 10% formalin. Frozen sections of the brain were prepared in 50 μm slices to confirm the position of the electrode tip.

Using six other rats, arterial blood pressure (BP), EEG, respiratory frequency (RF), and heart rate (HR) were recorded during hypoxia and hypercapnia. For monopolar EEG recording, a stainless steel screw was placed in the skull over the occipital cortex. Another screw was placed in the skull over the frontal sinus as the indifferent electrode. RF was calculated by using a pneumograph, placed across the lower thoracic margin. BP was measured via the femoral artery with a calibrated transducer.

Using six other rats, arterial blood samples (0.4 ml) were drawn anaerobically into heparinized syringes during the first 8–9 min of 10% O_2 or 10% CO_2 inhalation as well as during air inhalation. These blood samples were stored at 0° C until analysis. Po_2, Pco_2, and pH were measured at 37° C using a radiometer blood micro system (BMS3-MK2). During hypoxia, Po_2 decreased from 83.7 mm Hg (mean) to 40.7 mm Hg, Pco_2 decreased from 25.9 mm Hg to 21.3 mm Hg, and pH increased from 7.45 to 7.61. Po_2, Pco_2, and pH for hypercapnia were 85.5 mm Hg, 52.1 mm Hg, and 7.18, respectively. The changes in blood gas composition reached more than 90% of the values mentioned above within 1 min after the beginning of hypoxic or hypercapnic inhalation. After 5–7 min air inhalation in the recovery periods, Po_2, Pco_2, and pH returned close to their respective control levels.

Changes in T_{re} and T_{tail} in conscious rats exposed to a hypercapnic or hypoxic gas mixture had been noted in preliminary observations. The rat was placed in a wire mesh cage (6.5 cm in diameter and 18 cm long), in which it could roll over but not turn around, and was exposed for 30 min to 10% CO_2 or 10% O_2 at 19.2° C average ambient temperature. T_{re} in the air was 37.97 ± 0.36° C (mean ± SD, $n = 7$) for the hypoxic group and 38.07 ± 0.40° C for the hypercapnic group. The pre-exposure T_{re} for the hypoxic group did not differ significantly from that for the hypercapnic group. T_{re} significantly decreased by 0.80 ± 0.48° C (mean ± SD) after the hypoxic exposure and by 0.90 ± 0.45° C after the hypercapnic exposure ($P < 0.01$). Rate of decrease in T_{re} did not differ significantly between the two groups. In 5 of 7 rats, T_{tail} rose 3.7–6.8° C by about 10 min after the beginning of 10% CO_2 exposure, implying vasodilation. In 10% O_2 exposure, T_{tail} rose 2.3–7.2° C after about 10 min in 3 of 7 rats.

Results

From 29 rats, 44 warm-sensitive, 7 cold-sensitive, and 28 thermally insensitive neurons were recorded. Mean firing rate at 37° C T_{po} ranged from 1.5 to 44.9 imp/s. The thermosensitivity of the neuron was determined over the 4–5° C range in which each individual neuron appeared most thermosensitive. A neuron was considered sensitive to T_{po} if, in response to changes in T_{po}, it displayed a positive thermosensitivity of at least 0.8 imp/s° C or a negative thermosensitivity of at least 0.6 imp/s° C (Boulant and Hardy 1974). Changes in thermosensitivity were examined in 39 warm-sensitive and 5 cold-sensitive neurons. Of the 39 warm-sensitive neurons, 27 were examined during hypoxia, 4 neurons during hypercapnia, and the remaining 8 during both hypoxia and hypercapnia. During hypoxia 4 cold-sensitive neurons were examined and 1 during hypercapnia. Average mean firing rate at 37° C T_{po} was 14.4 ± 11.6 imp/s (mean ± SD, $n = 40$) for the warm-sensitive neurons, 7.8 ± 3.4 imp/s ($n = 6$) for the cold-sensitive neurons, and 6.2 ± 4.1 imp/s ($n = 28$) for the insensitive neurons.

Differences in mean firing rate at 37° C T_{po} between inhalation of 10% O_2 and of air, calculated for all neurons recorded during hypoxia, ranged from −5.6 to +7.3 imp/s, but mean firing rate did not change significantly in very many neurons. All neurons were thus classified into three groups. Neurons of the first group increased mean firing rate significantly and those of the second group decreased during hypoxia ($P < 0.01$). Mean firing rate in those of the third group remained relatively constant. Proportions of these three groups in the warm-sensitive, the cold-sensitive, and the insensitive neurons are indicated by percentage at the foot of each column in Fig. 1 (from left to right: the first group, the second group, the third group). Differences in mean firing rate between hypoxia and air inhalation are averaged in the first and second groups and graphed in Fig. 1. During hypoxia, the warm-sensitive and cold-sensitive neurons in the first group increased their firing rates by 3.79 ± 1.65 and 4.16 ± 1.75 imp/s (mean ± SD), whereas the insensitive neurons did so by 1.83 ± 1.55 imp/s. Degree of increase in mean firing rate during hypoxia thus was significantly greater in the thermosensitive neurons of the first group than in the insensitive neurons ($P < 0.025$). Thermosensitive neurons of the second group, on the other hand, had a mean firing rate during hypoxia that resembled the corresponding value for insensitive neurons. Chi-sqare analysis revealed that cold-sensitive and insensitive neurons were distributed differently among the three response groups to hypoxia ($P < 0.025$). Such a difference was not seen between warm-sensitive and insensitive neurons.

Figure 2 shows an example of thermal response of a warm-sensitive neuron during 10% O_2 and 10% CO_2 inhalations. Thermal response curves of this neuron during air and 10% O_2 inhalation are illustrated in Fig. 3. Linear regression was calculated for the data in the entire temperature range (33–41° C T_{po}). The regression line is expressed by the formula Y (firing rate) $= a + b \cdot X$ (T_{po}), in which a is the Y intercept and b is the slope. The slope reflects the thermosensitivity of this PO neuron. As shown in Fig. 3, hypoxia altered the slope of the regression line significantly ($P < 0.01$). The responses to hypoxia thus depend on T_{po}, that is, Fig. 1 may be valid at only 37° C T_{po}. All neurons were tested in the same way and the results are summarized

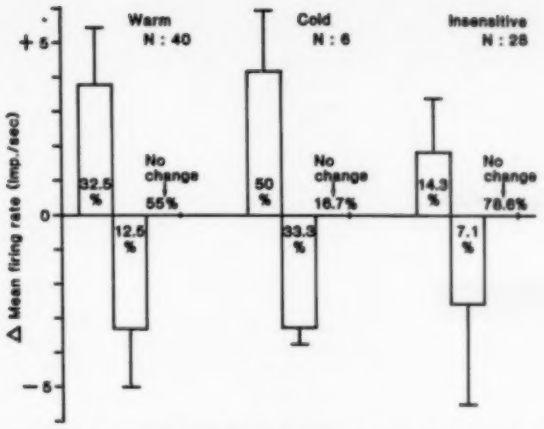

Fig. 1. Relative incidences of three responses groups to hypoxia and differences in mean firing rate between hypoxia and air inhalation in the warm-sensitive, the cold-sensitive, and the insensitive neurons. In the warm-sensitive neurons, the first group (*left*) and the second group (*middle*) indicate the neurons whose mean firing rate significantly increased and decreased, respectively ($P<0.01$). The third group (*right*) is "No change". The incidences of each group are indicated by % at the foot of each column. In the first and the second groups, average differences in mean firing rate between hypoxia and air inhalation are graphed with *bars* indicating ± SD. See the cold-sensitive and insensitive neurons in the same way as warm-sensitive neurons

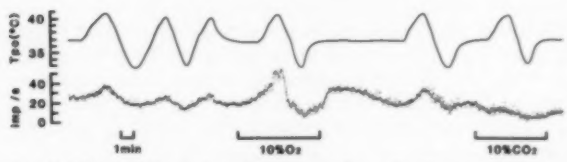

Fig. 2. Effects of hypoxia and hypercapnia on the thermosensitivity of a PO warm-sensitive neuron

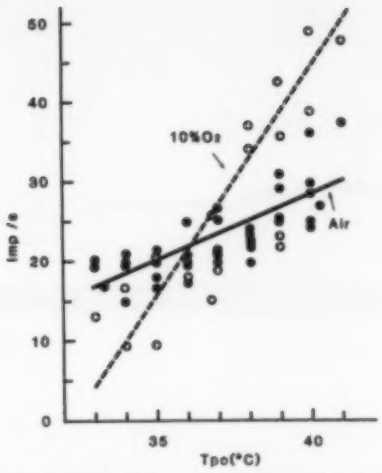

Fig. 3. Relation between T_{po} and firing rate (FR) of the warm-sensitive neuron of Fig. 2 during air and 10% O_2 inhalations. The slopes of the two regression lines differed significantly ($P<0.01$). FR = $-38.08+1.66\ T_{po}$ (air) FR = $-188.37+5.83\ T_{po}$ (10% O_2)

Table 1. Effects of hypoxia and hypercapnia on regression line for T_{po} versus neuronal firing frequency of warm-sensitive neurons

	Hypoxia	Hypercapnia
Change in slope		
Increase	8 (23%)	0 (0%)
Decrease	8 (23%)	7 (30%)
No change in slope, but tested for parallel shift	19 (54%)	16 (70%)
Upward shift	6 (17%)	8 (35%)
Downward shift	6 (17%)	4 (17%)
No parallel shift	7 (20%)	4 (17%)
Total	35 (100%)	23 (100%)

Values indicate number of neurons and percent of sample. All changes judged by significance at $P<0.05$

in Table 1. Of the 23 warm-sensitive neurons summarized in Table 1 under hypercapnia 11 are from our previously published data (Tamaki et al. 1986). Thermosensitivities in only part of the experimentally used range of T_{po} were exhibited by 6 neurons. In such a case, the linear regression was calculated only for that range of temperature in which the firing rate showed changes. Throughout the full temperature range 4 other neurons could not be followed because recorded activity suddenly ceased in the midst of the experiment. As shown in Table 1, the slope of the regression line significantly increased during hypoxia in 8 (23%) of the 35 warm-sensitive neurons and decreased in 8 other neurons ($P<0.05$). Of the 19 neurons that did not undergo singificant changes in the slope of the regression line 6 (17%) did show significant parallel upward shifts in firing rate, while 6 other neurons showed downward shifting. Responses of the PO warm-sensitive neurons to hypoxia were not uniform. As shown in Table 1, the slope of the regression line significantly decreased during hypercapnia in 7 (30%) of the 23 warm-sensitive neurons ($P<0.05$). No neuron was found that had a significantly increased slope of the regression line. Of the 16 neurons that did not have significantly altered slopes, 8 (35%) did show significant parallel upward shifts in firing rate. The effects of hypoxia on thermosensitivities (i.e. the slope of the regression line) of PO neurons differed from these effects of hypercapnia, according to chi-square analysis ($P<0.05$).

Among the cold-sensitive neurons, the slope of the regression line significantly decreased in 1 of 4 neurons during hypoxia and in 1 of 3 neurons during hypercapnia ($P<0.01$). No cold-sensitive neuron had a significantly increased slope of the regression line during either hypoxia or hypercapnia. During hypoxia, 3 neurons did not have significantly altered slopes. One showed a significant upward parallel shift, another a downward shift, and the third no change in firing rate. No cold-sensitive neuron showed a significant downward parallel shift during hypercapnia. Responses of the cold-sensitive neurons to hypoxia or hypercapnia did not appear to be generally different from the responses of the warm-sensitive neurons.

The effects of both hypoxia and hypercapnia were examined in 8 warm-sensitive neurons. One example is shown

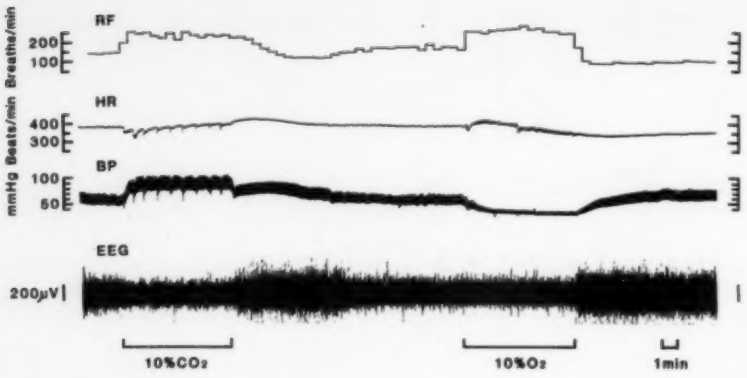

Fig. 4
Responses of respiratory frequency (RF), heart rate (HR), arterial blood pressure (BP), and EEG during hypoxia and hypercapnia

in Fig. 2. The responses to hypoxia or hypercapnia in these 8 neurons were similar to the results shown in Table 1. That is, hypercapnia did not alter the slope of the regression line, but did shift the firing rate upward in 4 neurons. During hypoxia the slope of the regression line increased in 2 neurons and decreased in 2 others. Hypoxic effects differed from hypercapnic effects in 6 of 8 neurons.

Figure 4 shows typical responses of RF, HR, BP, and EEG during hypoxia and hypercapnia. RF increased from 140.3 to 232.6 breaths/min during hypercapnia and from 153.0 to 246.4 breaths/min during hypoxia. Average RF during air inhalation was 115.7 ± 31.1 breaths/min (mean $\pm$ SD, $n = 6$) for the hypoxic group and 116.0 ± 24.6 ($n = 6$) for the hypercapnic group, indicating no significant difference between the two groups. RF increased significantly to 167.5 ± 49.8 breaths/min during hypoxia and to 179.4 ± 39.4 breaths/min during hypercapnia. During hypercapnia BP increased rapidly as soon as the rat breathed the 10% CO_2 gas mixture, and reached a steady level 30 mm Hg higher within about 1 min. After the end of the CO_2 inhalation, BP decreased and remained at an intermediate level for 5–6 min and then returned gradually to the control level. HR decreased to a minimum 1–2 min after the beginning of the CO_2 inhalation and then returned to the control level or a little higher. During hypoxia, BP decreased and reached a steady level 25 mm Hg lower after 1–2 min. HR increased to a maximum at 1 min and then gradually decreased. The responses of HR and BP during hypoxia were opposite to those during hypercapnia. Desynchronization of the EEG was observed during hypoxia as well as during hypercapnia. Change in the EEG during hypoxia was less than during hypercapnia. Sometimes the EEG did not change at all during hypoxia.

Discussion

The effects of hypoxia (10% O_2) on PO thermosensitive neurons were studied in anesthetized rats and compared to the effects of hypercapnia (10% CO_2). The hypoxic and hypercapnic gas mixtures used in this experiment were shown in preliminary work to produce equivalent falls in rectal temperature. As shown in Fig. 1, thermosensitive neurons tended to increase their activities during hypoxia more than thermally insensitive neurons did. A similar tendency was also observed hypercapnia (Tamaki et al. 1986).

During hypoxia as well as hypercapnia, increased activity of warm-sensitive neurons might influence body temperature regulation more than corresponding increased activity of cold sensitive neurons, because warm-sensitive neurons are more numerous than cold-sensitive neurons in the PO area. As a result, hypoxia and hypercapnia would tend to lower body temperature. The tendency for activity of warm-sensitive neurons to increase apperared to be greater during hypercapnia than during hypoxia. This might explain why rise in T_{tail}, implying vasodilation, was seen more frequently during hypercapnia than during hypoxia.

As shown in Table 1, the PO thermosensitive neurons modified their thermosensitivities during both hypoxia and hypercapnia. Responses of the thermosensitive neurons to hypoxia, however, were more varied than responses to hypercapnia. Furthermore, the effects of hypoxia qualitatively differed from those of hypercapnia in 6 of the 8 neurons that were examined during both hypoxia and hypercapnia. We have yet to clearly determine whether the activities of PO thermosensitive neurons are modified directly by hypoxia or whether the effects are transmitted to the PO neurons via thermal and non-thermal afferent pathways.

In this experiment, RF, BP, and HR displayed characteristic and predictable changes during exposure to hypoxia and to hypercapnia. PO thermosensitive neurons might receive afferent inputs from neuronal structures concerned with respiratory, circulatory, and other systems. PO thermosensitive neurons were recently reported to be affected by arterial blood pressure in urethanized rats (Koga et al. 1986). Warm-sensitive neurons mainly (77%) increase their firing rates when blood pressure falls, whereas cold-sensitive neurons mainly (78%) decrease their firing rates to the same stimulus. Hypotension may be responsible for changing neuronal activity of thermosensitive neurons during hypoxia, because BP decreased during hypoxia in this experiment. Other factors might affect thermosensitive neurons as well, because half of the cold-sensitive neurons showed higher firing rates in hypoxia than in air at 37°C T_{po}. The increase in RF prompts consideration of central and peripheral chemoreceptors and of brainstem respiratory neurons as other possible afferent inputs to the preoptic area.

Hypoxia and hypercapnia exert their effects on anesthetized rats in a number of ways. Almost all the ventilatory drive of hypoxia is mediated by carotid chemoreceptors (Hayashi et al. 1983). Cardiovascular responses in hypoxia (as low as 10% O_2) are predominantly derived from peripheral carotid body chemoreceptors,

whereas in hypercapnia (as high as 9% CO_2) other chemoreceptors are mainly responsible, most likely neurons in the central chemosensitive areas (Fukuda et al. 1986). PO thermosensitive neurons might thus receive afferent inputs from peripheral chemoreceptors as well as from baroreceptors during hypoxia, and from central chemosensitive areas during hypercapnia. Stimulation of arterial chemoreceptors has been reported to inhibit shivering in rabbits (Mott 1963). In addition to the medulla and pons, the hypothalamus has also been considered to receive baroreceptor and chemoreceptor inputs. In the posterior and lateral areas of the hypothalamus, 16 units were inhibited and 7 excited by electrical stimulation of the carotid sinus nerve (Thomas and Calaresu 1972).

The thermoregulatory functions of the posterior hypothalamus have been considered generally to be related to the convergence of thermal signals in heat production or shivering from many body locations or to be a part of a thermal efferent pathway. Neurons in the posterior hypothalamus are affected by temperature changes in the PO, skin, and spinal cord (Nutik 1971, 1973; Wünnenberg and Hardy 1972). On the other hand, a high proportion of neurons in the posterior and lateral areas of the hypothalamus that were not identified to be thermal were excited by hypoxia and hypercapnia (Cross and Silver 1963). This indicates a possibility that the posterior hypothalamus and other regions besides the preoptic area may be involved in hypothermia induced by hypoxia and hypercapnia.

Desynchronization of EEG was observed during hypoxia and hypercapnia in this experiment. Thermosensitivities of neurons in the preoptic area/anterior hypothalamus have been shown to vary according to the sleep-awake cycle in kangaroo rats (Glotzbach and Heller 1984). Thus, thermosensitivity of a PO neuron can be modified by not only thermal inputs but also non-thermal inputs from various parts of the brain or body. PO thermosensitive neurons might receive a greater variety of afferent inputs during hypoxia than hypercapnia, because the responses during hypoxia are more varied.

Hypoxia may be able to induce hypothermia in animals with hypothalamic lesions. Regional differentiation of sympathetic efferents has been known to be evoked by hypoxia. For example, 8% O_2 induces a rise of ear skin temperature that corresponds to a decrease of cutaneous sympathetic activity in intact rabbits. In decerebrated rabbits, however, cutaneous sympathetic activity increases during hypoxia (Iriki and Kozawa 1976). If a rise in ear skin temperature, i.e., a dissipation of heat from the skin, is responsible for hypothermia during hypoxia, then suprapontine structures might be involved in producing hypothermia during hypoxia.

Although the effects of hypoxia on thermosensitivity of PO neurons differed from the effects of hypercapnia in this experiment, we do not know what this difference means in thermoregulation. The hypoxic and hypercapnic gas mixtures used in this experiment produced equivalent falls in rectal temperature. Differential response patterns to hypoxic and hypercapnic stimuli of the autonomic nervous system are largely similar in artificially ventilated rabbits (Iriki et al. 1972). Spinal influences on chemosensitivity during systemic hypoxia and hypercapnia have recently been demonstrated by various experiments, which were carried out on sympathetic neurons in the chronic spinal cat (Jänig and Spilok 1978) and acute spinal cat (Rohlicek and Polosa 1981; Zhang et al. 1982) and on vascular resistance in the acute spinal cat (Rohlicek and Polosa 1986). Modification of PO neuron thermosensitivity thus does not appear to be by itself enough to produce hypothermia during hypoxia or hypercapnia.

Factors not of a neurogenic nature should, of course, also be considered in any comprehensive appraisal of hypothermia induced by hypoxia and hypercapnia.

In conclusion, PO thermosensitive neurons changed their activities and modified their thermosensitivities during both hypoxia and hypercapnia, but hypoxic differed from hypercapnic effects. These results suggest that PO thermosensitive neurons play a role in the mechanism for hypothermia during both hypoxia and hypercapnia, and that the role is not identical in these two situations.

Acknowledgement. This work was supported in part by Grant-in-Aid for Scientific Research 59440026 from the Ministry of Education, Science and Culture of Japan.

References

Bhatia B, George S, Rao TL (1969) Hypoxic poikilothermia in rats. J Appl Physiol 27:583–586

Blatteis CM, Lutherer LO (1973) Cold-induced thermogenesis in dogs: its reduction by moderate hypoxia. J Appl Physiol 35:608–612

Boulant JA, Hardy JD (1974) The effect of spinal and skin temperature on the firing rate and thermosensitivity of preoptic neurons. J Physiol 240:639–660

Cassin S (1963) Critical oxygen tensions in newborn, young, and adult mice. Am J Physiol 205:325–330

Cross BA, Silver IA (1963) Unit activity in the hypothalamus and the sympathetic response to hypoxia and hypercapnia. Exp Neurol 7:375–393

Fukuda Y, Sato A, Suzuki A, Trzebski A (1986) Neural mechanisms of the effects of hypoxia and hypercapnia of cardiovascular responses in anesthetized rats. Neurosci Res (Suppl) 3:S14

Gleeson M, Barnas GM, Rautenberg W (1986) The effects of hypoxia on the metabolic and cardiorespiratory responses to shivering produced by external and central cooling in the pigeon. Pflügers Arch 407:312–319

Glotzbach SF, Heller HC (1984) Changes in the thermal characteristics of hypothalamic neurons during sleep and wakefulness. Brain Res 309:17–26

Hayashi F, Yoshida A, Fukuda Y, Honda Y (1983) The ventilatory response to hypoxia in the anesthetized rat. Pflügers Arch 396:121–127

Hemingway A, Birzis L (1956) Effect of hypoxia on shivering. J Appl Physiol 8:577–579

Hemingway A, Nahas GG (1952) Effect of varying degrees of hypoxia on temperature regulation. Am J Physiol 170:426–433

Hill JR (1959) The oxygen consumption of new-born and adult mammals: its dependence on the oxygen tension in the inspired air and on the environmental temperature. J Physiol 149:346–373

Iriki M, Kozawa E (1976) Patterns of differentiation in various sympathetic efferents induced by hypoxic and by central thermal stimulation in decerebrated rabbits. Pflügers Arch 362:101–108

Iriki M, Pleschka K, Walther OE, Simon E (1971) Hypoxia and hypercapnia in asphyctic differentiation of regional sympathetic activity in the anesthetized rabbit. Pflügers Arch 328:91–102

Iriki M, Riedel W, Simon E (1972) Patterns of differentiation in various sympathetic efferents induced by changes of blood gas composition and by central thermal stimulation in anesthetized rabbits. Jpn J Physiol 22:585–602

Jänig W, Kümmel H (1977) Functional discrimination of postganglionic neurons to the cat's hindpaw with respect to the

skin potentials recorded from the hairless skin. Pflügers Arch 371:217–225

Jänig W, Spilok N (1978) Functional organization of the sympathetic innervation supplying the hairless skin of the hindpaws in chronic spinal cats. Pflügers Arch 377:25–31

Koga H, Hori T, Kiyohara T, Nakashima T, Shibata M (1986) Preoptic and anterior hypothalamic neurons responding to changes in local temperature and blood pressure. Thermal Physiol Abstr Satellite Symposium of XXX International Congress of Physiological Sciences, p 35

Kottke FJ, Phalen JS, Taylor CB, Visscher MB, Evans GT (1948) Effect of hypoxia upon temperature regulation of mice, dogs, and man. Am J Physiol 153:10–15

Kuhnen G, Wloch B, Wünnenberg W (1985) Effects of hypoxia and hypercapnia on thermoregulation and hibernation. Abstract for an international symposium, "Living in the Cold", p 203

Mott JC (1963) The effects of baroreceptor and chemoreceptor stimulation on shivering. J Physiol 166:563–586

Nutik SL (1971) Effect of temperature change of the preoptic region and skin on posterior hypothalamic neurons. J Physiol (Paris) 63:368–370

Nutik SL (1973) Posterior hypothalamic neurons responsive to preoptic region thermal stimulation. J Neurophysiol 36:238–249

Rohlicek CV, Polosa C (1981) Hypoxic response of sympathetic preganglionic neurons in the acute spinal cat. Am J Physiol 241:H679–H683

Rohlicek CV, Polosa C (1986) Neural effects of systemic hypoxia and hypercapnia on hindlimb vascular resistance in acute spinal cats. Pflügers Arch 406:392–396

Tamaki Y, Nakayama T, Matsumura K (1986) Effects of carbon dioxide inhalation on preoptic thermosensitive neurons. Pflügers Arch 407:8–13

Thomas MR, Calaresu FR (1972) Responses of single units in the medial hypothalamus to electrical stimulation of the carotid sinus nerve in the cat. Brain Res 44:49–62

Wünnenberg W, Hardy JD (1972) Response of single units of the posterior hypothalamus to thermal stimulation. J Appl Physiol 33:547–552

Zhang TX, Rohlicek CV, Polosa C (1982) Responses of sympathetic preganglionic neurons to systemic hypercapnia in the acute spinal cat. J Auton Nerv Syst 6:381–389

Received November 4, 1986/Accepted February 11, 1987

Pflügers Arch (1987) 409:7–12

Pflügers Archiv
European Journal of Physiology
© Springer-Verlag 1987

Effect of adrenergic agonists on Ca^{2+}-channel currents in single vascular smooth muscle cells

G. Droogmans, I. Declerck, and R. Casteels

Laboratorium voor Fysiologie, Campus Gasthuisberg, K. Universiteit Leuven, B-3000 Leuven, Belgium

Abstract. Ca^{2+}-channel currents have been measured in enzymatically dispersed single smooth muscle cells of the rabbit ear artery using the whole-cell patch clamp technique. Inward currents were elicited by depolarizing test pulses from a holding potential of −50 mV. These currents were activated from −30 mV onward and reached full activation around 0 mV. α-Adrenergic agonists did not affect the background current measured at the holding potential, but markedly reduced the peak amplitude of the voltage-activated Ca^{2+}-channel currents. This α-adrenergic inhibition also occurred in cells which were internally perfused with solutions containing either 10 μM cAMP, 10 μM cGMP or 0.1 mM GTP, but became irreversible when the pipette solution contained a non-hydrolyzable GTP-analog. The action of β-agonists on the voltage-activated Ca^{2+}-channel currents was variable, and ranged from no effect at all to a 50% reduction of the current. It is concluded that α-agonists do not open receptor-operated Ca^{2+}-channels in these smooth muscle cells. The inhibition of the voltage-activated Ca^{2+}-currents does not seem to be mediated through changes in cyclic nucleotide levels, but might be mediated through G-proteins. Its physiological relevance remains however unclear. The action of β-agonists is consistent with their relaxing effect, but the reason for the non-uniform response has not been elucidated.

Key words: Vascular smooth muscle – Patch clamp – Ca^{2+}-channels – Noradrenaline – Isoprenaline – G-proteins

Introduction

It is generally assumed that excitatory agonists induce contraction in vascular smooth muscle cells by mobilizing sequestered Ca^{2+} from an intracellular pool and by opening Ca^{2+}-channels in the plasma membrane allowing thereby a sustained influx of extracellular Ca^{2+}-ions.

This agonist evoked contraction in the rabbit ear artery is not accompanied by a significant change of the resting potential and is more resistant to organic Ca^{2+}-antagonists than that induced by membrane depolarization in most vascular smooth muscle cells. These observations have led to the assumption that these smooth muscle cells present besides the voltage-dependent Ca^{2+}-channels also so-called receptor-operated Ca^{2+}-channels (ROCs). These ROCs would be activated by agonist-receptor interaction and not by a depolarization of the membrane (Bolton 1979; Droogmans et al. 1985).

Up till now the existence of these receptor-operated Ca^{2+}-channels has not been demonstrated by direct electrophysiological techniques, nor have any of their characteristics been described. In the present report we analyze by means of the whole-cell patch-clamp technique the action of α- and β-adrenergic agonists on Ca^{2+}-currents in isolated single smooth muscle cells of rabbit ear artery. The obtained results are not in support of the opening of ROCs by α-adrenergic agonists in the smooth muscle cells of the rabbit ear artery.

Offprint requests to: G. Droogmans

Methods

Isolation procedure. All experiments were performed on single smooth muscle cells isolated from the rabbit ear artery. Rabbits (1–2 kg) were killed by cervical dislocation. The ear arteries were dissected free of connective tissue in oxygenated physiological solution at 37° C. The enzymatic digestion procedure consisted in an exposure for 45 min to a Krebs solution containing 0.2 mM Ca^{2+}, 1.5 mg/ml collagenase, 0.5 mg/ml trypsin inhibitor and 2 mg/ml bovine serum albumin. Thereafter the tissue was exposed for 10 min to a nominal Ca^{2+} free Krebs solution containing 0.5 mg/ml protease and 1 mg/ml trypsin inhibitor. Finally the cells were mechanically dispersed with a wide-bore pipette in a nominal Ca^{2+}-free solution.

A suspension of isolated cells was transferred to a small experimental chamber mounted on the stage of an inverted microscope (Zeiss, IM-35). After adhesion of the cells to the glass bottom of the chamber, they were continuously superfused with a Hepes buffered Krebs' solution containing (mM): 119.6 NaCl, 5.9 KCl, 1.2 $MgCl_2$, 10 $CaCl_2$ or $BaCl_2$, 11.5 HEPES NaOH (pH 7.2), 11.5 glucose. All experiments were done at room temperature (20–22° C).

Electrophysiological recording. Patch pipettes were pulled from Pyrex glass (Jencons H15/10) and heat polished. The resistance of the filled pipettes ranged between 2 and 5 MΩ. The standard filling solution for the pipettes contained (mM): 140 CsCl, 4 $MgCl_2$, 1 $CaCl_2$, 11 EGTA-KOH, 10 HEPES-KOH (pH 7.2), 2 Na_2-ATP. The free Ca^{2+}-concentration in this solution was estimated at $3 \cdot 10^{-8}$ M. CsCl was used in the pipette solution in order to minimize the interference of outward currents with the currents through Ca^{2+}-channels (Droogmans and Callewaert 1986).

Ionic currents were measured using the patch clamp technique in the whole-cell configuration (Hamill et al. 1981). After sealing of the patch pipette against the cell surface, the underlying membrane was broken by a pulse of suction, and the pipette solution was allowed to equilibrate with the cytoplasmic solution.

The currents were measured with a List EPC-7 patch-clamp amplifier, filtered at 0.5–2 kHz with an 8-pole Bessel filter and digitized on line (sampling frequency 2–10 kHz). Membrane potential and data acquisition were software controlled using an IBM personal computer equipped with a Tecmar Labmaster analog interface board (Kegel et al. 1985).

Agonists were applied by changing from an agonist-free perfusion medium to one containing the agonist. Because of the small volume of the experimental chamber (1.5 ml) and the relative high perfusion rate (about 2 ml · min^{-1}) the inflow of the agonist was fast and its maximum response could be recorded after 30–45 s after the start of perfusion.

Drugs used. 5′-guanylyl imidodiphosphate [Gpp(NH)p, Boehringer, Mannheim, FRG], guanosine 5′-O-(3-thio-triphosphate) (GTP-γ-S, Boehringer, Mannheim, FRG), collagenase (Cooper Biomed, Freehold, NJ, USA), trypsin inhibitor (Boehringer, Mannheim, FRG), bovine serum albumin (Sigma, St. Louis, MO, USA, Fraction V powder) portease (Sigma, St. Louis, MO, USA, type VII).

Results

Voltage-activated Ca^{2+}-channel currents

Depolarizing voltage steps from a holding potential of −50 mV elicit time-dependent inward currents, that reached a maximum value and then declined to a steady-state level at a much slower rate (Fig. 1A). Substituting Ba^{2+}-ions in the bathing solution for Ca^{2+}-ions increased the peak amplitude of the currents through the Ca^{2+}-channels about two-fold at all test potentials (Fig. 1B). Because of these larger current values we have mainly used solutions containing Ba^{2+}-ions.

Figure 2A shows current records measured in a solution containing 10 mM Ba^{2+} at different test potentials in the absence and in the presence of 0.1 mM Cd^{2+}. It is obvious that Cd^{2+}-ions effectively block the transient inward current elicited at each test potential. At test potentials positive to +30 mV an outward current is activated that is not blocked by Cd^{2+}. A more detailed description of the characteristics of this current is beyond the scope of this paper. The steady-state current-voltage relationship of the Cd^{2+}-insensitive current is linear in the range from −60 to +20 mV with a slope of 0.5 pA/mV corresponding to an input resistance of 2GΩ (Fig. 2B).

The current-voltage relationship of the peak inward current corrected for the Cd^{2+}-insensitive current (Fig. 2C) shows a threshold for activation around −40 mV, whereas full activation is reached around 0 mV. The maximum value of this peak Ba^{2+}-current varies from cell to cell and ranges between 100 and 400 pA (mean value of 274 pA for 41 cells). The i-v relationship is approximately linear in the voltage range between +10 and +40 mV, but deviates systematically from this linear relation at more positive potentials. No significant Cd^{2+}-sensitive outward currents could be observed at potentials up to +90 mV.

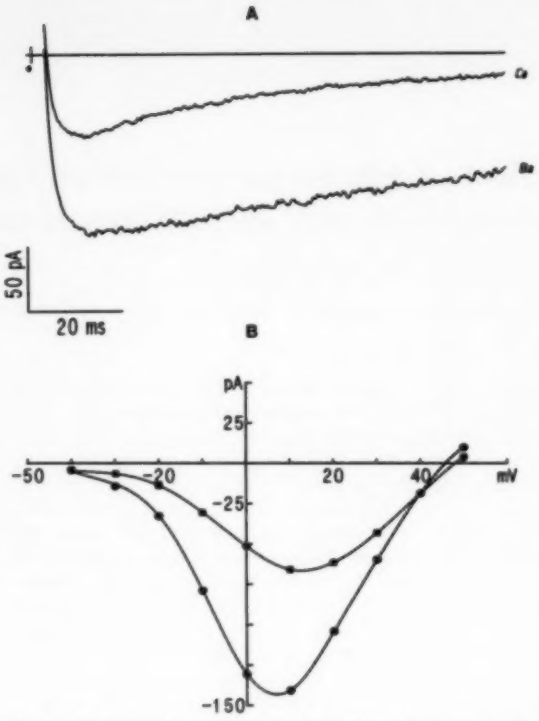

Fig. 1. A Transient inward current induced by a test pulse to 0 mV from a holding potential of −50 mV. The bathing solution contained either 10 mM Ca^{2+} (*upper trace*) or 10 mM Ba^{2+} (*lower trace*). **B** Current-voltage relationship of the peak inward current measured in a solution with 10 mM Ca^{2+} (◆) or 10 mM Ba^{2+} (●)

Effect of noradrenaline on the holding current

Stimulation of rabbit ear artery with noradrenaline evokes a contraction that is not associated with a significant change in resting potential (Droogmans et al. 1977). If it is assumed that the tonic component of the force development is mediated through an increased influx of extracellular Ca^{2+}-ions through receptor-operated Ca^{2+}-channels (ROCs), excitatory agonists should induce an inward Ca^{2+}-current. 10 μM Noradrenaline induced a contraction in unpatched cells, i. e. a cell shortening was observed under the microscope, but the agonist did not affect the background current measured at a holding potential of −50 mV.

Activation of α_1-receptors is believed to be mediated through GTP-binding proteins. The internal dialysis of the cell with the pipette solution might have decreased the cellular GTP-level and might thereby inhibit the activation of ROCs by the agonist. However when pipette solutions containing 0.1 mM GTP or either of its non hydrolyzable analogs Gpp(NH)p or GTP-γ-S were used, there was still no effect of noradrenaline on the holding current.

Effect of α-adrenergic agonists on voltage-activated Ca^{2+}-channels

The preceding observations do not substantiate the hypothesis that noradrenaline opens ROCs. We have therefore investigated whether this agonist modulates the voltage-

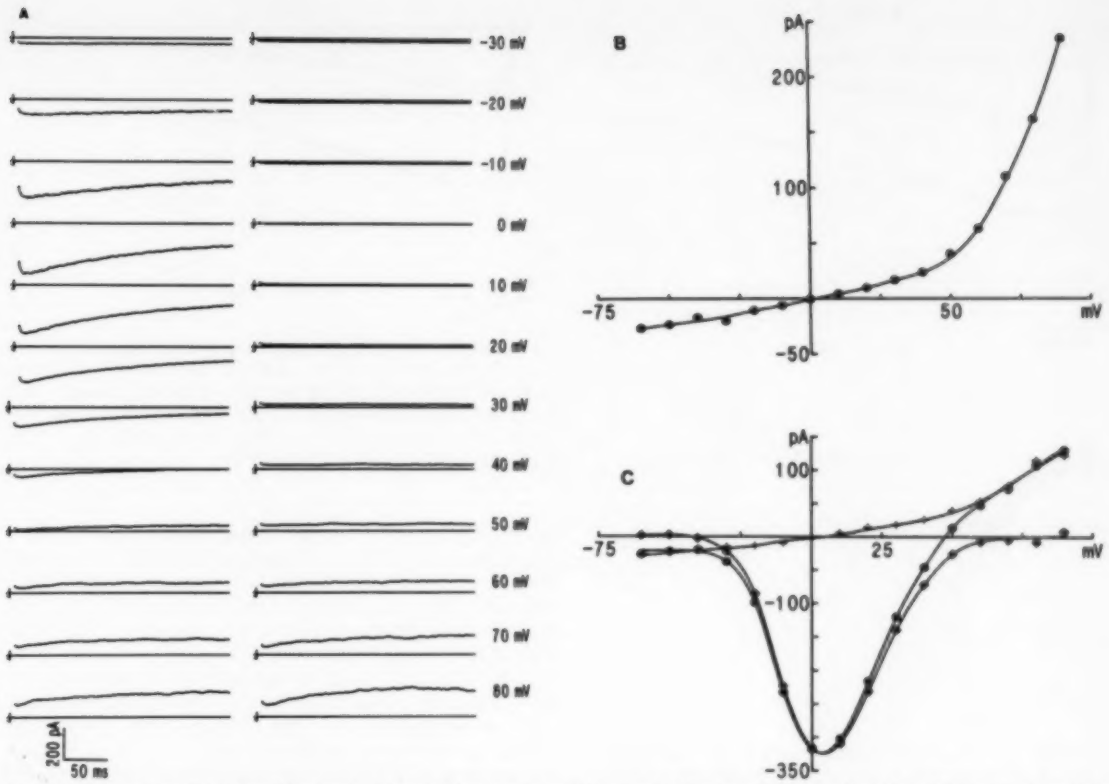

Fig. 2. Current traces (**A**) induced by depolarizing rabbit ear artery cells from a holding potential of − 50 mV to different levels, as indicated at the right. The *left traces* were recorded in a 10 mM Ba^{2+} Krebs' solution, and the *right traces* in the same solution with 0.1 mM $CdCl_2$. I-v relationship of the Cd^{2+}-insensitive current measured at the end of the test pulse (**B**). Peak amplitude (**C**) of the Cd^{2+}-sensitive transient inward current before (●) and after (◆) correction for the Cd^{2+}-insensitive component as a function of the applied test pulse. The Cd^{2+}-sensitive current was obtained by subtracting the current in the presence of Cd^{2+} (+) from the corresponding current in control solution

activated Ca^{2+}-channels by comparing the currents through these channels in the presence and absence of noradrenaline. The records in Fig. 3A show that the agonist appreciably inhibits the voltage-activated Ca^{2+}-channel currents. This effect cannot be due to a time-dependent run-down of the Ca^{2+}-channels because washing out the agonist restores the currents. The record showing this recovery [Fig. 3A(c)] was obtained about 10 min after removal of the agonist, and shows a complete reversibility of the agonist induced inhibition. However in most cells this recovery was only partial, probably because washing out the agonist requires a relatively long time which overlaps with the concomitant run-down of the Ca^{2+}-channels. A second application of noradrenaline induced similar inhibitory effects on the voltage-activated Ca^{2+}-channels. Figure 3B shows the current-voltage relationship before and during application of the agonist and after its washing out. It has to be noted that in this and in subsequent i-v curves the plotted current amplitudes have not been corrected for the Cd^{2+}-insensitive component. The peak inward current was reduced at all potentials, but this inhibition was not accompanied by a significant shift of the i-v curve along the voltage axis. The inhibition of the current in the voltage range from − 10 to + 20 mV amounted to 44.1 ± 3.1% (mean ± SEM of 19 cells).

The effects of noradrenaline could be mimicked by the α_1-agonist phenylephrine, while the voltage-activated Ca^{2+}-channel currents were not affected by the α_2-agonist clonidine. These findings indicate that the current inhibition was caused by activation of α_1-receptors. A concomitant activation of β-receptors was prevented in these experiments by the presence of 1 μM propranolol.

In order to find out whether the down modulation of Ca^{2+} channels induced by α-adrenergic agonists is mediated by changes of the intracellular levels of cyclic nucleotides we have used patch pipettes filled with either 10 μM cAMP or 10 μM cGMP. Dialysis of the cells with these pippette solutions will increase the intracellular levels of either nucleotides, and thereby buffer the putative receptor-mediated changes. However, the inhibitory effects of noradrenaline on the voltage-activated Ca^{2+}-channels also occurred under these conditions, indicating that the effect of noradrenaline is not mediated by changes in cyclic nucleotide levels.

It has recently been suggested by several authors that the α_1-adrenergic receptor is coupled to its signal transduction

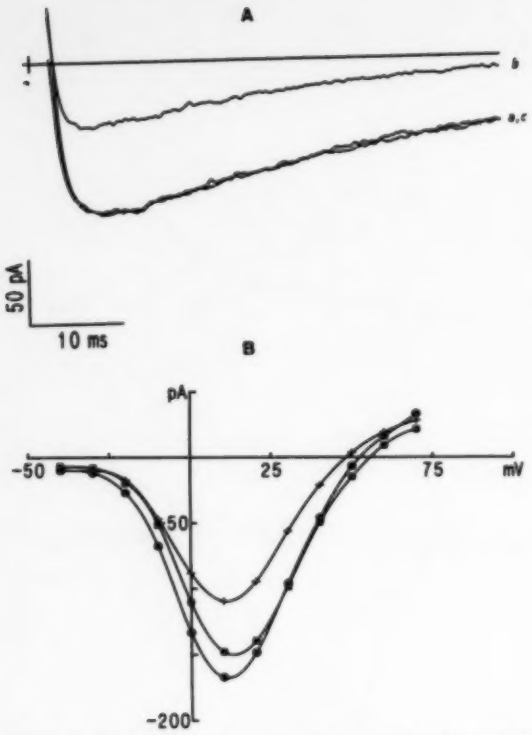

Fig. 3. **A** Effect of 10 μM noradrenaline on the Ba^{2+}-current induced by a depolarizing step from a holding potential of − 50 mV to + 10 mV. Traces *a* and *c* correspond to control currents measured before and after application of the agonist, whereas trace *b* shows the current measured in the presence of the agonist. **B** Current-voltage relationship of the peak inward Ba^{2+}-current before (●), during (+) and after (◆) application of 10 μM noradrenaline

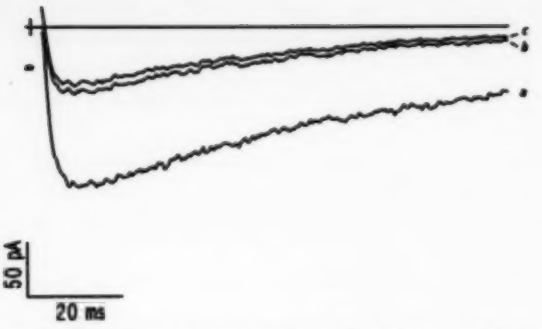

Fig. 4. Effect of 10 μM noradrenaline on the Ba^{2+}-current induced by a depolarizing step from a holding potential of − 50 mV to + 10 mV. The pipette solution contained 10 μM Gpp(NH)p. Traces *a* and *c* correspond to control currents measured before and after application of noradrenaline, whereas trace *b* shows the current measured in the presence of the agonist

mechanism by guanine-nucleotide binding proteins (G-proteins). At least two major mechanisms might be operative, i. e. a mobilization of sequestered Ca^{2+} by IP_3 and activation of protein kinase C by diacylglycerol (see review articles by Berridge and Irvine 1984 and by Nishizuka 1984). In order to establish the role of G-proteins in this down modulation of Ca^{2+}-channels mediated by α-adrenoceptor activation, we have perfused the cells with pipette solutions containing either 0.1 mM GTP, or one of its non hydrolyzable analogs Gpp(NH)p or GTP-γ-S. The amplitude of the peak inward currents recorded with these solutions were of the same order of magnitude as those observed with electrodes filled with the standard pipette solution, suggesting that these substances do not exert a direct effect on these currents. The inhibition of the Ca^{2+}-channel currents induced by noradrenaline occurred with all pipette solutions. The currents returned to the control value after washing out the agonist when the cells were dialyzed with GTP. However this inhibition became irreversible when the pipette solutions contained a non-hydrolyzable GTP analog (Fig. 4).

Effect of β-adrenergic agonists on Ca^{2+}-channels currents

Stimulation of β-receptors and the concomitant changes in cyclic AMP levels have been found to modulate the voltage-activated Ca^{2+}-channels in cardiac muscle (Reuter 1983; Cachelin et al. 1983; Kameyama et al. 1985). From their studies of whole smooth muscle tissues of rabbit aorta, Meisheri and van Breemen (1982) proposed that isoprenaline and dibutyryl cyclic AMP inhibit the ^{45}Ca influx elicited by K-depolarization.

The effects of 10 μM isoprenaline on voltage-activated Ca^{2+}-channels in our single smooth muscle cells were not uniform. In 14 out of 18 cells obtained from 18 different rabbits, the agonist either did not affect the current, or only reduced its peak amplitude by a maximum of 20%. However in the remaining 4 cells the β-agonist caused a pronounced inhibition of the currents elicited by various depolarizing voltage pulses (Fig. 5A). The effect of isoprenaline disappeared within a few minutes after washing out the agonist, whereas the washout of the noradrenaline effect is much slower. Moreover, its effect was almost completely reversible in all cells. The current-voltage relationship of the peak inward current obtained from one of these latter cells before, during and after application of 10 μM isoprenaline is represented in Fig. 5B. Blocking the α-receptor with 10 μM phentolamine did not affect the current inhibition induced by isoprenaline in these cells.

It has to be pointed out that noradrenaline always inhibited the voltage-activated Ca^{2+}-currents irrespective of their response to β-agonists. Also in those cells in which isoprenaline did not affect the Ca^{2+}-currents, noradrenaline still induced a significant inhibition (Fig. 6).

Discussion

The voltage-dependent currents through Ca^{2+}-channels, which have been described in this paper have properties similar to those described in other smooth muscle preparations. Activation occurs at potentials between − 40 and − 30 mV, and full activation is reached around 0 to + 10 mV. The i-v curve shows marked rectification around the reversal potential (Klöckner and Isenberg 1985; Mitra and Morad 1985; Droogmans and Callewaert 1986). These characteristics are also similar to those of the L-type Ca^{2+}-channel in cardiac cells (Nilius et al. 1985; Bean 1985) and in neuronal cells (Nowycky et al. 1985).

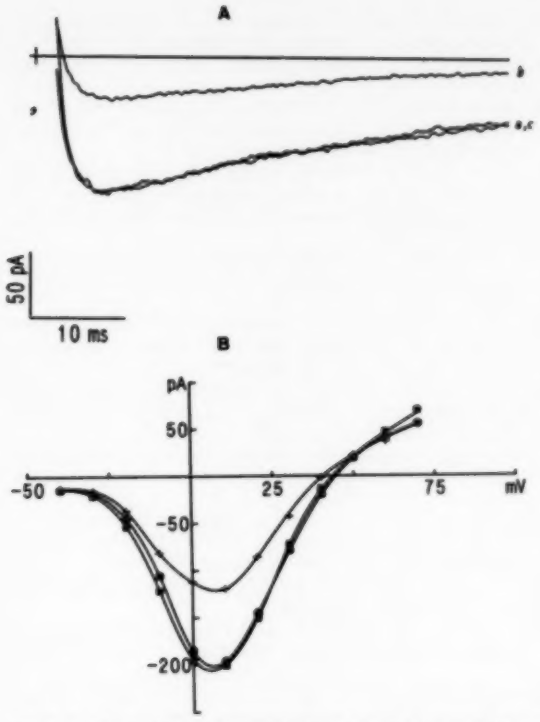

Fig. 5. A Effect of 10 μM isoprenaline on the Ba^{2+}-current induced by a depolarizing step from a holding potential of − 50 mV to + 10 mV. Traces *a* and *c* correspond to control currents measured before and after application of the agonist, whereas trace *b* represents the current observed in the presence of the agonist. **B** Current-voltage relationship of the peak inward Ba^{2+}-current before (●), during (+) and after (◆) application of 10 μM isoprenaline

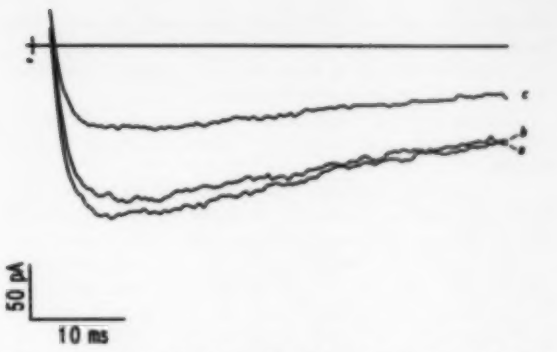

Fig. 6. Effect of 10 μM noradrenaline (trace *b*) and 10 μM isoprenaline (trace *c*) on the inward current induced by a depolarizing voltage step from − 50 mV to + 10 mV. Trace *a* represents the control current in the absence of an agonist

In order to explain the observation that an excitatory agonist such as noradrenaline does not activate receptor-operated Ca^{2+}-channels in our isolated vascular smooth muscle cells, two alternative hypotheses can be proposed. The isolation procedure and/or the intracellular perfusion with the pipette solution might have affected these channels. An effect of the isolation procedure is unlikely because the agonist still induces a contraction of unpatched cells. Our data indicate that a decreased cellular GTP-level cannot explain the lack of agonist effect. However it cannot be excluded that the dialysis procedure dilutes some soluble endogenous second messenger, thereby modifiying the activation of the receptor-operated Ca^{2+}-channels. An alternative explanation is that receptor-operated Ca^{2+}-channels do not exist and that the activation of the contractile proteins induced by α_1-agonists depends solely on the mobilization of intracellular Ca^{2+}-pools. Our experimental data cannot discriminate between these hypotheses, but the second alternative is consistent with the observations of Morgan and Morgan (1984) that the agonist-induced contractile responses are only associated with an initial but transient change of the cytosolic calcium concentration. In this regard it is worth mentioning that the noradrenaline-induced stimulation of ^{45}Ca uptake which has been described in a number of vascular smooth muscle preparations, such as rabbit aorta, has not been observed in rabbit ear artery (Droogmans et al. 1977). The receptor activation of aortic smooth muscle is accompanied by a depolarization of the cell membrane (Mekata 1974), and the observed entry of Ca^{2+} could depend on the opening of voltage-activated Ca^{2+}-channels by this depolarization.

In some recent reports (Byrne and Large 1986; Benham and Bolton 1986) it has been shown that noradrenaline activates an inward current in single vascular smooth muscle cells when pipettes with a low Ca-buffering capacity (low EGTA concentration) were used. It can therefore not be excluded that this current is activated by the agonist-induced release of Ca^{2+} ions rather than by the opening of ROCs. The nature and characteristics of this current have not been investigated in more detail.

The inhibition of the current through voltage-activated Ca^{2+}-channels by α-adrenergic agonists is rather unexpected and is in contrast with the observations of Aaronson et al. (1986). These authors recorded in the same preparation that we used voltage-dependent calcium currents of a much smaller amplitude and which were increased by noradrenaline stimulation. At present we have no obvious explanation for these discrepant results. It is unlikely that this phenomenom is due to a run-down of the Ca^{2+}-channels because of the reversibility of the effects. An alternative explanation is that the agonist-induced release of cellular Ca^{2+} increases the cytoplasmic level of Ca^{2+} and thereby either modifies the Ca^{2+}-gradient or causes inactivation of the Ca^{2+}-channels (Eckert and Chad 1984). Also this explanation is unlikely because of the high Ca^{2+}-buffering capacity of the pipette solutions which prevents a significant increase of the free calcium concentration.

Our results further indicate that the inhibition of inward current by α-agonists is probably not induced by changes in cyclic nucleotide levels. However, because the inhibition of the Ca^{2+}-channel current becomes irreversible when the pipette solution contains a non-hydrolyzable GTP analog, it can be proposed that this down modulation of Ca^{2+}-channels is mediated through G-binding proteins. Our data with α_1-agonists are similar to those obtained in neuronal cells with α_2-agonists. Forscher and Oxford (1985) observed that neither changes in cytoplasmic $[Ca^{2+}]$, nor changes in the levels of cyclic AMP or cyclic GMP could explain the down-modulation of Ca^{2+}-channels induced by nor-

adrenaline in internally dialyzed avian sensory neurons. The inhibition of voltage-dependent calcium channels by noradrenaline was found to be mediated through G-proteins in dorsal root ganglion cells (Holz et al. 1986).

The physiological significance of this α_1-adrenergic inhibition of voltage-activated Ca^{2+}-channels is not clear at present.

β-Adrenergic agonists also inhibit voltage-activated Ca^{2+}-channels, but the degree of inhibition varied from cell to cell, and was even absent in some cells. This inhibition is consistent with the vasodilating action of these agonists, and with the observations of Meisheri and van Breemen (1982) on the effects of isoprenaline on the ^{45}Ca uptake induced by K-depolarization. There is no obvious explanation for the non- uniform response to β-agonists in contrast with the rather homogeneous response to α-agonists.

References

Aaronson PI, Benham CD, Bolton TB, Hess P, Lang RJ, Tsien RW (1986) Two types of single-channel and whole-cell calcium or barium currents in single smooth muscle cells of rabbit ear artery and the effects of noradrenaline. J Physiol 377:36P

Bean BP (1985) Two kinds of calcium channels in canine atrial cells. Differences in kinetics, selectivity, and pharmacology. J Gen Physiol 86:1–30

Benham CD, Bolton TB (1986) Spontaneous transient outward currents in single visceral and vascular smooth muscle cells of the rabbit. J Physiol 381:385–406

Berridge MJ, Irvine RF (1984) Inositol triphosphate, a novel second messenger in cellular signal transduction. Nature 312:315–321

Bolton TB (1979) Mechanism of action of transmitters and other substances on smooth muscle. Physiol Rev 59:606–718

Byrne NG, Large WA (1986) Membrane responses to noradrenaline in dispersed single smooth muscle cells of the guinea-pig pulmonary artery studied with path-pipette technique. J Physiol 377:37P

Cachelin AB, De Peyer JE, Kokubun S, Reuter H (1983) Ca^{2+}-channel modulation by 8-bromocyclic AMP in cultured heart cells. Nature 304:62–4644

Droogmans G, Callewaert G (1986) Ca^{2+}-channel current and its modification by the dihydropyridine agonist BAY k 8644 in isolated smooth muscle cells. Pflügers Arch 406:259–265

Droogmans G, Raeymaekers L, Casteels R (1977) Electro- and pharmacomechanical coupling in the smooth muscle cells of the rabbit ear artery. J Gen Physiol 70:129–148

Droogmans G, Himpens B, Casteels R (1985) Ca-exchange, Ca-channels and Ca-antagonists. Experientia 41:895–899

Eckert R, Chad JE (1984) Inactivation of Ca^{2+}-channels. Prog Biophys Mol Biol 44:215–267

Forscher P, Oxford GS (1985) Modulation of calcium channels by norepinephrine in internally dialyzed avian sensory neurons. J Gen Physiol 85:743–763

Hamill OP, Marty A, Neher E, Sakmann B, Sigworth FJ (1981) Improved patch-clamp techniques for high-resolution current recording from cells and cell-free membrane patches. Pflügers Arch 391:85–100

Holz IV GG, Rane SG, Dunlap K (1986) GTP-binding proteins mediate transmitter inhibition of voltage-dependent calcium channels. Nature 319:670–672

Kameyama M, Hofmann F, Trautwein W (1985) On the mechanism of β-adrenergic regulation of the Ca^{2+} channel in the guinea-pig heart. Pflügers Arch 405:285–293

Kegel DR, Wolf BD, Sheridan RE, Lester HA (1985) Software for electrophysiological experiments with a personal computer. J Neurosci Methods 12:317–330

Klöckner U, Isenberg G (1985) Calcium currents of cesium loaded isolated smooth muscle cells (urinary bladder of the guinea pig). Pflügers Arch 405:340–348

Meisheri K, van Breemen C (1982) Effects of β-adrenergic stimulation on calcium movements in rabbit aortic smooth muscle: relationship with cyclic AMP. J Physiol 331:429–441

Mekata F (1974) Current spread in the smooth muscle of the rabbit aorta. J Physiol 242:143–155

Mitra R, Morad M (1985) Ca^{2+} and Ca^{2+}-activated K^+ currents in mammalian gastric smooth muscle cells. Science 229:269–272

Morgan JP, Morgan KG (1984) Stimulus-specific patterns of intracellular calcium levels in smooth muscle of ferret portal vein. J Physiol 351:155–167

Nilius B, Hess P, Lansman JB, Tsien RW (1985) A novel type of cardiac calcium channel in ventricular cells. Nature 316:443–446

Nishizuka Y (1984) The role of protein kinase C in cell surface signal transduction and tumour promotion. Nature 308:693–698

Nowycky MC, Fox AP, Tsien RW (1985) Three types of neuronal calcium channels with different calcium agonist sensitivity. Nature 316:440–443

Reuter H (1983) Calcium channel modulation by neurotransmitters, enzymes and drugs. Nature 301:569–574

Received October 13, 1986/Accepted February 6, 1987

Pflügers Arch (1987) 409:13–23

Pflügers Archiv
European Journal of Physiology
© Springer-Verlag 1987

Effects of stimulation of vestibular and neck receptors on Deiters neurons projecting to the lumbosacral cord

A. R. Marchand, D. Manzoni, O. Pompeiano, and G. Stampacchia

Dipartimento di Fisiologia e Biochimica, Università di Pisa, Via S. Zeno 31, I-56100 Pisa, Italy

Abstract. 1. The activity of lateral vestibular nucleus (LVN) neurons, antidromically identified by stimulation of the spinal cord at T_{12} and L_1, thus projecting to the lumbosacral segments of the spinal cord (lVS neurons), was recorded in precollicular decerebrate cats during rotation about the longitudinal axis either of the whole animal (labyrinth input) or of the body only while the head was kept stationary (neck input). 2. Among the lVS neurons tested for vestibular stimulation, 76 of 129 units (i.e. 58.9%) responded to roll tilt of the animal at the standard parameters of 0.026 Hz, $\pm 10°$. The gain and the sensitivity of the first harmonic responses corresponded on the average to 0.47 ± 0.44, SD, impulses $\cdot s^{-1} \cdot deg^{-1}$ and 3.24 ± 3.15, SD, %/deg, respectively. As to the response patterns, 51 of 76 units (i.e. 67.1%) were excited during side-down and depressed during side-up tilt, whereas 15 (i.e. 19.7%) showed the opposite behavior. In both instances the peak of the responses occurred with an average phase lead of about $+21.0 \pm 27.2$, SD, deg with respect to the extreme side-down or side-up position of the animal. Moreover, the former group of units showed almost a twofold larger gain with respect to the latter group (t-test, $p < 0.05$). 3. Among the lVS neurons tested for neck stimulation, 75 of 109 units (68.8%) responded to neck rotation at the standard parameters. The gain and the sensitivity of the first harmonic responses corresponded on the average to 0.49 ± 0.40, SD, impulses $\cdot s^{-1} \cdot deg^{-1}$ and 3.30 ± 3.42, SD, %/deg, respectively, thus being similar to the values obtained for the labyrinth responses. However, 59 of 75 units (i.e. 78.6%) were excited during side-up neck rotation and depressed during side-down neck rotation, while 8 of 75 units (i.e. 10.7%) showed the opposite pattern. In both instances the peak of the responses occurred with an average phase lead of $+52.0 \pm 18.3$, SD, deg for the extreme side-up or side-down neck displacements. Further, the former group of units showed a larger gain than the latter group. 4. Histological controls indicated that 102 of 129 (i.e. 79.0%) lVS neurons tested for labyrinth stimulation and 86 of 109 (i.e. 78.9%) lVS neurons tested for neck stimulation were located in the dorsocaudal part of LVN, the remaining lVS neurons being located in the rostroventral part of LVN. 5. The observation that the predominant response pattern of the lVS neurons to roll tilt was just opposite to that of lVS neurons to neck rotation indicates that the motoneurons innervating ipsilateral hindlimb extensors were excited by an increased discharge of vestibulospinal neurons during side-down tilt but they were disfacilitated by the reduced discharge of vestibulospinal neurons during side-down neck rotation; the opposite would occur during side-up animal tilt or neck rotation. These findings were compared with those of previously recorded LVN neurons, whose descending axons were not identified as projecting to upper or lower segments of the spinal cord. It was then possible to evaluate the role that the LVN exerts not only in the control of the limb but also of the neck extensor musculature.

Key words: Vestibulospinal neurons – Response characteristics – Macular vestibular input – Neck input

Offprint requests to: O. Pompeiano

Introduction

Labyrinth and neck afferent volleys elicited either by changing the position of the head with respect to space or the position of the head with respect to the body produce postural adjustments involving the neck and the limb musculature [cf. 26, 39]. In particular, the vestibulospinal reflexes elicited by rotation about the longitudinal axis of the entire animal (roll) or by rotation of the head after neck deafferentation are characterized by excitation of the ipsilateral dorsal neck muscles as the splenius muscle during side-up tilt [3, 6, 40] and the ipsilateral forelimb extensors as the triceps brachii during side-down tilt [5, 18, 23, 28, 31, 40]. For low frequencies of head rotation the peak of these muscle responses was related to position and not to velocity of displacement, thus being attributed to stimulation of macular, utricular receptors. These compensatory vestibulo-collic and vestibulo-forelimb reflexes would then operate to maintain the head stationary in the horizontal plane both by righting the head on the neck and by righting the body over the limbs.

As to the cervicospinal reflexes, rotation of the body about the longitudinal axis while maintaining the head stationary or rotation of the head in labyrinthectomized animals causes postural adjustments, characterized by excitation of the splenius muscle during side-down neck rotation, i.e. when chin is rotated maximally contralaterally and by excitation of the triceps brachii during side-up neck rotation, i.e. when chin is rotated maximally ipsilaterally [17, 18, 23, 27, 28, 30, 32]. For low frequencies of neck

rotation the peak of the muscle responses was usually in phase with position. It has been postulated that the cervicocollic and cervico-forelimb reflexes, originally attributed to stimulation of joint receptors [12, 30], are due in part at least to activation of muscle spindle receptors located in the dorsal and the small perivertebral neck muscles [cf. 37, 38].

The postural adjustments produced by vestibular and neck stimulations may involve not only neck and forelimb extensors, but also hindlimb extensors. As to the vestibulospinal reflexes, myographic [11] or electromyographic experiments [4, 29, 36] performed in decerebrate cats have shown that the gastrocnemius-soleus (GS) muscle either did not respond or displayed only small amplitude modulation of its activity to slow roll tilt of the animal or head rotation after neck deafferentation. In these instances the response pattern of the triceps surae to a given labyrinth signal was similar to that of the triceps brachii, although the gain was much smaller; in fact only a limited number of tonically active GS motoneurons [36; cf. also 16], as well as of a primary and secondary endings of GS muscle spindles [11], were excited during side-down head displacement.

As to the cervicospinal reflexes, the triceps surae either did not respond in the same preparations or showed only a small amplitude modulation of its activity suring slow neck rotation. Even in these instances the response pattern of the triceps surae to a given cervical input was similar to that of the triceps brachii, but the gain was smaller [4].

In conclusion, it appears that at least in decerebrate cats the tonic vestibular and neck reflexes acting on hindlimb extensors are negligible or absent, in contrast to those acting on neck and forelimb extensors which are prominent.

The lateral vestibular nucleus (LVN) of Deiters represents one of the main structures which transmits the positional signal from labyrinth and neck receptors to spinal extensor motoneurons. There is in fact evidence that the LVN, which projects ipsilaterally to the whole segments of the spinal cord [35; cf. 33], exerts mono- and polysynaptic excitatory influences on motoneurons innervating hindlimb [20, 21, 24, 42], forelimb [25, 42] and dorsal neck extensors [2, 42]. Moreover, LVN neurons responded to slow rotation about the longitudinal axis of the whole animal [7, 9, 10, 41] or of the neck [8–10] with a periodic modulation of their discharge rate, which was mainly related to the positional signal. Interestingly, a proportion of units were excited during side-down animal tilt and side-up neck rotation, thus having the potential of being involved in the postural adjustments of the limb musculature; however, other units showed the opposite response pattern as expected if they were involved in the vestibular and cervical control of the dorsal neck musculature [7, 8]. In these experiments the recorded units were found to be histologically located within the whole extent of LVN and some of them could also be identified antidromically as vestibulospinal neurons; however, the stimulating electrode was located at high cervical level, so that nothing could be said as to whether the recorded units projected to upper or lower segments of the spinal cord. Moreover, a proportion of LVN neurons were unresponsive to vestibular and/or neck stimulation.

The main aims of the present study were to find out whether in decerebrate preparations the negligible amplitude or absence of modulation of hindlimb extensors to roll tilt of the animal or neck rotation was due to small amplitude or absence of modulation of the corresponding vestibulospinal neurons and, in the former case, whether these neurons responded to the vestibular or neck inputs with a response pattern similar to that predicted for the LVN neurons controlling the limb musculature. For this purpose the activity of vestibulospinal neurons, antidromically identified as projecting to the lumbosacral segments of the spinal cord, was recorded in decerebrate cats and tested during roll tilt of the animal and neck rotation. The results of these experiments were then compared with those obtained in previous experiments [7, 8], in which responses of unidentified units to the same labyrinth and neck inputs were recorded from the whole extent of the LVN which projects not only to the cervical and the lumbosacral enlargements, thus controlling the limb extensor musculature, but also to the upper cervical segments of the spinal cord which control the dorsal neck musculature.

Methods

The experiments were performed in 14 cats (2.5–3.5 kg). Under ether anesthesia the dorsal neck muscles were disconnected bilaterally from the occipital bone and the vertebral axis and partially removed, while the skin of the neck was fully denervated [7, 8, 14, 15]. The axial musculature was also bilaterally disconnected from the dorsal aspect of the vertebral arcs and removed between T_{10} and L_2, to allow exposure of the underlying spinal cord. The animal was then decerebrated at precollicular level, while the cerebellum was left intact.

After interruption of the anesthesia, the head of the animal was placed in a stereotaxic frame and pitched 10° nose-down as in previous studies [7, 8], while the spinous process of the second cervical vertebra was exposed and held by a clamp rigidly secured on a tilting table. In addition, the lower part of the trunk was fixed to a spinal cord frame at T_{11} and L_3 and pins were inserted through the great trochanter of both femurs to prevent body sway. Both fore- and hindlimbs were extended and clamped. Sinusoidal tilting about the longitudinal axis of the whole animal led to selective stimulation of labyrinth receptors; on the other hand, stimulation of neck receptors was performed by tilting the table sinusoidally while the head remained stationary [14, 15]. Rotation at the standard frequency of 0.026 Hz, and at the peak amplitude of displacement of 10° were used.

Three stimulating electrodes made of insulated 200 μm tungsten wire, electrolytically sharpened at the tip and with an interelectrode distance of 1.5 mm, were implanted into the ventrolateral funiculi of both sides as well as along the midline of the spinal cord at T_{12} and L_1.

After these surgical procedures had been performed, the animals were immobilized with pancuronium bromide (Pavulon, Organon, The Netherlands, 0.6 $mg \cdot kg^{-1} \cdot h^{-1}$, i.v.) and artificially ventilated. At least 2–3 h elapsed in each experiment between the end of the surgical procedures and unit recordings, which allowed a complete recovery of the animal from ether anesthesia.

Neuronal activity was recorded extracellularly with glass microelectrodes (5 to 10 MΩ impedance) filled with a solution of 0.5 M sodium chloride saturated with pontamine blue dye for iontophoretic marking of the recording site.

Rectangular pulses (at 1/s, 0.2 ms in duration, 0.5–10 V) were applied in a unipolar manner between one of the three stimulating spinal cord electrodes (1–10 KΩ impedance) and a reference electrode placed on the body

skin for antidromic activation of LVN neurons. Criteria for identification of antidromic responses including the collision test, and evaluation of the conduction velocity of the corresponding vestibulospinal axons have been previously reported [10]. After application of the antidromic test, the unit activity was selected through a window discriminator and converted to standard pulses. The resting discharge of these neurons was then recorded on magnetic tape and the mean firing rate calculated off line [10]. The unit activity recorded during roll tilt of the animal or neck rotation was processed by a digital signal averager (Correlatron 1024, Laben). Sequential pulse density histograms (SPDHs) with a time base adjusted to cover two full cycles of table movement (128 bins, 0.6 s bin width) were averaged and a Fourier analysis of the unit response was performed following the method described in previous studies [14, 15]. Results are based on the quantitative spectral analysis of the averaged unit activity with respect to the first harmonic of response (output) during the rotational stimuli (angular input).

For each unit, the mean discharge rate or base frequency (impulses/s) was evaluated during animal tilt or neck rotation. For spontaneously active units, this value closely corresponded to the mean firing rate of the same unit recorded at rest. The gain of the first harmonic response was defined as the absolute change of firing rate per degree of displacement (impulses $\cdot s^{-1} \cdot deg^{-1}$) while the sensitivity expressed the same value as percentage of the base frequency (%/deg). According to the terminology used in previous studies [7, 8, 14, 15] the direction of stimulus orientation was indicated as side-down when rotation of the animal (downward displacement of the table) or of the neck (upward displacement of the table) occurred towards the side of the recording electrode and side-up for rotation in the opposite direction. The phase angle of response corresponded to the phase difference in arc degrees between the peak of the side-down displacement of the animal or the neck and the peak of the fundamental component of unit response. We considered as responsive only those units displaying a stable resting discharge, a reliable modulation of their firing rate during the rotatory stimulus, and a coherence coefficient of the first harmonic to successive cycles of stimulation greater than 0.8; a value of 1.0 represents a linear, time-invariant, noise-free system. In a few instances, units firing at low rate or even silent at rest displayed a cutoff of response during periods of stimulation. These units were used for evaluation of the response gain which was corrected according to the method applied in a previous study [43], but not of the response sensitivity, since in these cases the base frequency represents an overestimate of the resting discharge.

Systemic arterial blood pressure, end-tidal P_{CO_2} and rectal temperature were monitored throughout the experiment and maintained within physiological limits (100–140 mm/Hg, 3–4.5% P_{CO_2}, 37–38°C, respectively). At the end of penetrations a mark was made by passing a cathodal current through the tip of the microelectrode (10–15 μA for 10 min). The method of identifying the location of the recorded units has been described previously [11, 12]. The LVN was subdivided in two parts following the criteria described previously [11, 12]: i) the rostroventral part, rvLVN (sections 1, 2 and the ventral part of sections 3, 4 in Fig. 4), and ii) the dorsocaudal part, dcLVN (sections 5, 6 and the dorsal part of sections 3, 4 of Fig. 4), which project mainly – although not exclusively – to the cervical and the lumbosacral segments of the spinal cord, respectively [35].

Results

Response characteristics of lateral vestibulospinal neurons to sinusoidal vestibular stimulation at standard parameters

The activity of 145 neurons histologically identified as being located within the LVN was recorded and examined during roll tilt of the animal at the standard parameters (0.026 Hz, ±10°). Among these units, 129 were activated antidromically by electrical stimulation of the spinal cord between T_{12} and L_1; these were therefore considered as lateral vestibulospinal neurons projecting to the lumbosacral segments of the spinal cord (lVS neurons); 110 of these 129 neurons were spontaneously firing at rest. The conduction velocity of the corresponding axons ranged from 33.8 to 124.8 m/s and corresponded on the average to 90.0 ± 21.5, SD, m/s ($n = 129$). The remaining 16 neurons, 14 of which tonically active in the animal at rest, were not antidromically activated by spinal cord stimulation (LVN neurons).

The following data refer to the lVS neurons. In particular, the base frequency evaluated for all the 110 tonically firing lVS neurons (both responsive and unresponsive to tilt), as well as for 8 silent neurons responsive to tilt (see Methods) varied from 0.5 to 70.1 impulses/s corresponding on the average to 24.0 ± 16.9, SD, impulses/s ($n = 118$); its value, however, was lower for the responsive units (20.0 ± 16.2, SD, impulses/s; $n = 76$) than for the units unresponsive to tilt (31.0 ± 15.9, SD, impulses/s; $n = 42$) (t-test, $P < 0.001$). There was a close correspondence between the base frequency of the units tested during animal tilt and the firing rate evaluated for the same units in the animal at rest (resting discharge) (Table 1).

Among the recorded lVS units, 76 (58.9%) responded with a periodic modulation of their discharge frequency in relation to the sinusoidal stimulus. The remaining 53 (41.1%) units did not meet the criteria for responsiveness and were thus considered unaffected by the stimulus.

The gain of the first harmonic response of the lVS neurons to the labyrinth input varied from 0.04 to 2.01 impulses $\cdot s^{-1} \cdot deg^{-1}$, with a mean value of 0.47 ± 0.44, SD, impulses $\cdot s^{-1} \cdot deg^{-1}$ ($n = 76$), while the sensitivity of the first harmonic response varied from 0.31 to 11.66%/deg, with an average of 3.24 ± 3.15, SD, %/deg ($n = 64$); for the remaining 12 neurons, which were silent or fired at low rate at rest, the sensitivity was not evaluated since the corresponding units showed a cutoff of their responses (Table 1). Histograms of both gain (Fig. 1A) and sensitivity display a rather unimodal long-tailed distribution.

The phase angle of the first harmonic response to standard parameters of tilt was also evaluated and plotted in Fig. 2B. In this histogram, 0° corresponds to the responses displaying a maximal firing rate at the extreme side-down position of the animal and a minimal firing rate at the extreme side-up position, while 180° corresponds to the responses characterized by the reverse pattern. Two main groups of lVS neurons were recognized on the basis of their phase angle distribution. The most prominent group of units (51/76, i.e. 67.1%), which were excited during side-down tilt of the animal, showed a phase angle of responses that ranged from a lead of +75° to a lag of −45°, with an average phase lead of +25.0 ± 23.8, SD, deg (α-responses). The second group of units (15/76, i.e. 19.7%), which were excited during side-up tilt of the animal, showed a phase angle of responses that varied from a lead of +135° to a lag of −105°, with an average phase lag of −172.6 ± 33.9, SD,

Table 1. Response characteristics of antidromic (lVS) and non-antidromic (LVN) neurons to sinusoidal tilt around the longitudinal axis of whole animal (macular input) or rotation of neck (neck input) at standard parameters

	Macular input		Neck input	
	Antidromic	Non-antidromic	Antidromic	Non-antidromic
No of units	129	16	109	13
Responsive (R) units	76 (58.9%) (8 of which silent)	14 (87.5%) (2 of which silent)	75 (68.8%) (5 of which silent)	7 (53.8%) (2 of which silent)
Unresponsive ($\bar{R}$) units	53 (41.1%) (11 of which silent)	2 (12.5%) –	34 (31.2%) (9 of which silent)	6 (46.2%) –
Resting discharge rate of R+$\bar{R}$ units	24.5 ± 15.7 $n = 108$	26.3 ± 15.3 $n = 13$	23.5 ± 16.1 $n = 95$	27.3 ± 16.3 $n = 11$
Resting discharge rate of R-units	21.3 ± 15.4 $n = 68$	26.7 ± 15.9 $n = 12$	21.9 ± 16.5 $n = 70$	23.9 ± 20.8 $n = 5$
Resting discharge rate of $\bar{R}$-units	29.9 ± 14.7 $n = 40$	21.3 $n = 1$	27.8 ± 14.0 $n = 25$	30.2 ± 12.7 $n = 6$
Base frequency of R+$\bar{R}$ units	24.0 ± 16.9 $n = 118$*	23.9 ± 15.9 $n = 16$	23.5 ± 16.8 $n = 100$*	22.2 ± 16.3 $n = 13$
Base frequency of R-units	20.0 ± 16.2 $n = 76$	25.2 ± 16.6 $n = 14$	21.6 ± 17.6 $n = 75$	17.6 ± 20.3 $n = 7$
Base frequency of $\bar{R}$-units	31.0 ± 15.9 $n = 42$*	15.0 ± 6.2 $n = 2$	29.0 ± 12.9 $n = 25$*	27.6 ± 8.9 $n = 6$
Gain of R-units	0.47 ± 0.44 $n = 76$	0.40 ± 0.47 $n = 14$	0.49 ± 0.40 $n = 75$	0.48 ± 0.56 $n = 7$
Sensitivity of R-units	3.24 ± 3.15 $n = 64$	2.00 ± 2.06 $n = 12$	3.30 ± 3.42 $n = 63$	3.08 ± 2.97 $n = 5$
Phase angle of R-units	From +75° lead to −45° lag		From +90° lead to −15° lag	
	51 (67.1%)	8 (57.1%)	8 (10.7%)	3 (42.9%)
	From +135° lead to −105° lag		From +165° lead to −90° lag	
	15 (19.7%)	4 (28.6%)	59 (78.6%)	4 (57.1%)
	From +75° to +135° and from −45° to −105°		From +90° to +165° and from −15° to −90°	
	10 (13.2%)	2 (14.3%)	8 (10.7%)	0

Abbreviations: LVN, lateral vestibular nucleus; antidromic and non-antidromic, LVN units activated or nonactivated antidromically by spinal cord stimulation at $T_{12}-L_1$; resting discharge rate, mean firing rate in impulses/s recorded in the absence of movement; base frequency, mean firing rate in impulses/s evaluated during roll tilt of the animal or neck rotation at standard parameters (0.026 Hz, ± 10°); gain of the first harmonic, change of the mean firing rate per degree of peak displacement (impulses · s^{-1} · deg^{-1}); sensitivity of the first harmonic, percentage change of the mean firing rate per degree (%/deg); phase angle of the first harmonic, in degrees of phase lead (positive values) or phase lag (negative values) with respect to the side-down animal or neck displacement.

Values of resting discharge, base frequency, gain and sensitivity are means ± SD. Figures in parentheses are percentages. The numbers of units used for the evaluation of the base frequency indicated by asterisks are lower than those of the corresponding populations of tested units, due to exclusion of the unresponsive silent units. Moreover, the numbers of units used for sensitivity evaluation of the labyrinh and neck responses were slightly lower than the total numbers of responsive units, since some units that showed a cutoff of their response, either silent or firing at rest, were disregarded; in these instances the cutoff of the unit responses prevented us from taking their base frequency as a reliable indicator of the resting discharge

deg, corresponding to a lead of +7.4° with respect to extreme side-up position (β-responses). In addition to these two populations of units, there were 10 units (i.e. 13.2%) whose phase angle response values were not in the range of the two main populations (intermediate responses) (Table 1).

Fig. 3A represents in a polar diagram both the gain and the phase relation of the responses. Most of the unit responses characterized by an increase in firing rate during side-down tilt (right quadrant) showed a larger gain than that of the units displaying the opposite response pattern (left quadrant).

The results described above were concerned with the first harmonic, which represented the predominant component of responses of the lVS neurons to tilting. A second harmonic was noticeable in most units and had a mean amplitude of 33.7 ± 37.4, SD, expressed in percent of the fundamental ($n = 76$). The response characteristics of the non-antidromic LVN neurons to the same parameters of animal tilt are shown in Table 1.

Localization of units responding to vestibular stimulation

If we consider the localization of all the recorded 145 neurons within Deiters' nucleus, it appears that 34 neurons were located in the rvLVN, while 111 neurons were located in the dcLVN. Moreover, 27 rvLVN and 102 dcLVN units were antidromically identified as lVS neurons (Fig. 4A). Table 2 indicates that the proportion of lVS neurons re-

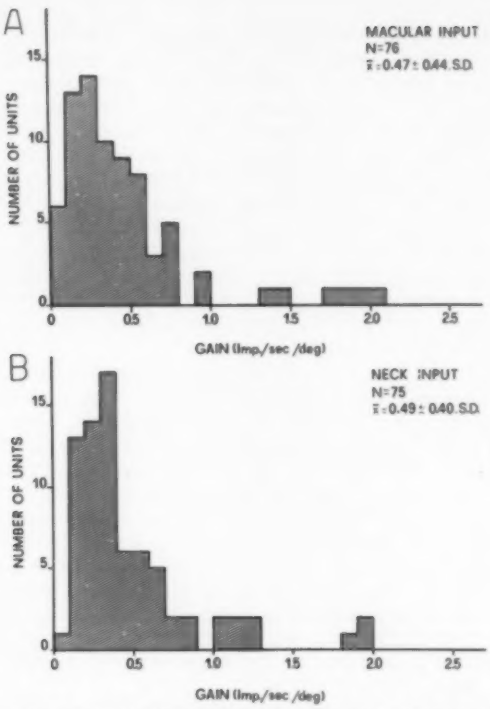

Fig. 1. Gain histograms of the first harmonic of responses of lVS neurons to sinusoidal tilt of the animal (**A**) and neck rotation (**B**) at the standard parameters (0.026 Hz, ± 10°). In particular, 76 LVN units responsive to animal tilt (**A**) and 75 LVN units responsive to neck rotation (**B**) were antidromically activated by stimulation of the spinal cord at $T_{12}-L_1$, thus projecting to the lumbosacral segments of the spinal cord (lVS neurons). Both histograms show a long-tailed unimodal distribution

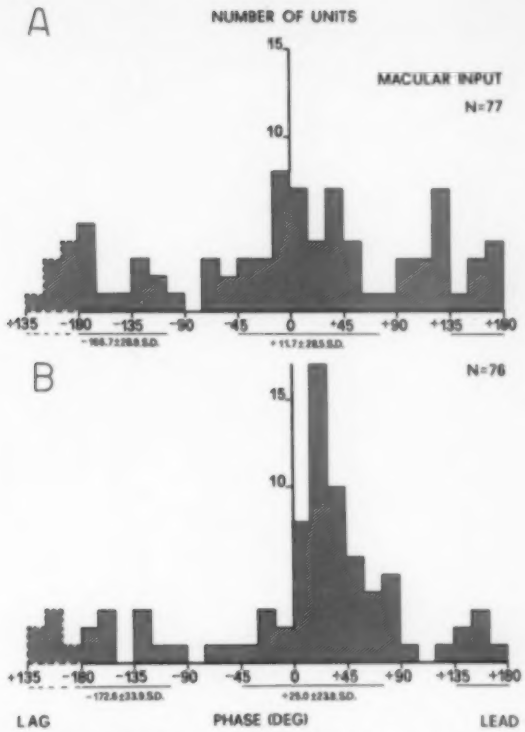

Fig. 2A, B. Distribution of the phase angle of the first harmonic of responses of different populations of LVN neurons tested during roll tilt of the animal at 0.026 Hz, ± 10° − 15°. All the experiments were performed in precollicular decerebrate cats with the cerebellum intact. The upper histogram (**A**) illustrates the distribution of the phase angle of responses to animal tilt of 77 neurons histologically identified as being located within the whole extent of LVN, thus projecting to the whole segments of the spinal cord (slight modified from Fig. 3A, Ref. 7), while the lower histogram (**B**) illustrates the distribution of the phase angle of responses to animal tilt of 76 LVN neurons, antidromically activated by stimulation of the spinal cord at $T_{12}-L_1$, thus projecting to the lumbosacral segments of the spinal cord (lVS neurons). Positive numbers in the abscissas indicate in degrees, the phase lead, whereas negative numbers indicate the phase lag of responses with respect to the extreme side-down position of the animal, as indicated by 0°. Responses of the neurons underlined by horizontal bars have been used to evaluate the average phase angle of units excited during, or near the side-down (0°) or side-up displacement of the animal (180°)

sponding to standard parameters of animal tilt was comparable in the rvLVN (17/27, i.e. 63.0%) and the dcLVN (59/102, i.e. 57.8%), as were the average resting discharge rate and base frequency of the two populations of neurons. The gain as well as the sensitivity of the first harmonic responses of the lVS neurons to vestibular stimulation were on the average higher in the rvLVN than in the dcLVN; however, the differences were not statistically significant. Finally, most of the lVS neurons were excited during side-down tilt of the animal; the proportion of units showing this response pattern was higher in the dcLVN (41/59, i.e. 69.5%) than in the rvLVN (10/17, i.e. 58.8%); the difference, however, was not significant.

Response characteristics of lateral vestibulospinal neurons to sinusoidal neck stimulation at standard parameters

The activity of 122 neurons histologically identified as being located within the LVN was recorded and evaluated during neck rotation at the standard parameters. Among these units, 109 were activated antidromically by electrical stimulation of the spinal cord between T_{12} and L_1 (lVS neurons); 95 of 109 neurons were active at rest. The estimated conduction velocity of their axons ranged from 37.1 to 124.8 m/s and corresponded on the average to 89.8 ± 21.0, SD, m/s ($n = 109$). The remaining 13 neurons, 11 of which tonically active in the animal at rest, were not antidromically identified (LVN neurons).

The following data refer to the lVS neurons. The base frequency evaluated for all the 95 tonically firing neurons (both responsive and unresponsive to neck rotation), as well as for 5 silent neurons responsive to neck rotation varied from 0.4 to 68.9 impulses/s, corresponding on the average to 23.5 ± 16.8, SD, impulses/s ($n = 100$); its value was lower for the responsive (21.6 ± 17.6, SD, impulses/s, $n = 75$) than for the unresponsive units (29.0 ± 12.9, SD, impulses/s, $n = 25$); however, the difference was not statistically significant (see Table 1 for the correspondence between mean values of

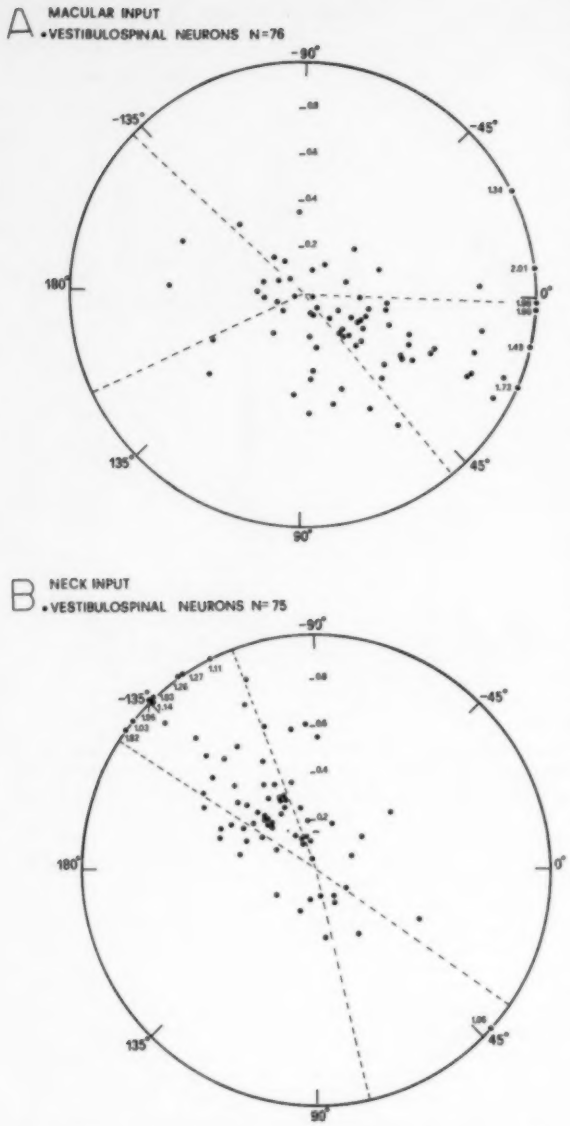

Fig. 3. Polar diagrams showing the gain and the phase angle of the first harmonic of responses of IVS neurons to sinusoidal tilt of the animal (**A**) and neck rotation (**B**) at the standard parameters. The response gain of each unit is indicated by the distance of the corresponding symbol to the center of the diagram (see the scale along the vertical meridian); 6 units in **A** and 9 units in **B** and a gain higher than 1.0. The relative position of the symbol with respect to 0° meridian indicates in degrees the phase lead (positive values) or the phase lag (negative values) of responses with respect to the extreme side-down position of the animal or neck displacement. The dashed lines outline the standard deviation of the phase angle of response of the two main populations of units responsive to animal tilt (**A**) and neck rotation (**B**), as indicated in Figs. 2B and 5B, respectively. In particular, the mean phase angle of the units excited during side-down or side-up animal tilt in **A** corresponded to $+25.0 \pm 23.8$, SD, deg ($n = 51$) and -172.6 ± 33.9, SD, deg ($n = 15$), respectively, while that of the units excited during side-down or side-up neck rotation in **B** corresponded to $+55.9 \pm 21.0$, SD, deg ($n = 8$) and -128.5 ± 18.1, SD, deg ($n = 59$), respectively

base frequency and resting discharge rate of the recorded neurons).

From the total population of recorded IVS units, 75 (68.8%) displayed a periodic modulation of the discharge frequency in relation to the sinusoidal input, while the remaining 34 (31.2%) units did not respond to the stimulus.

The gain of the first harmonic response of the IVS neurons to neck rotation varied from 0.03 to 1.96 impulses $\cdot s^{-1} \cdot deg^{-1}$, with a mean value of 0.49 ± 0.40, SD, impulses $\cdot s^{-1} \cdot deg^{-1}$ ($n = 75$), while the sensitivity of the first harmonic response varied from 0.24 to 13.32%/deg with a mean value of 3.30 ± 3.42, SD, %/deg ($n = 63$); for the remaining 12 neurons the sensitivity was not evaluated, since they were silent or fired at low rate at rest (Table 1). Histograms of both gain (Fig. 1B) and sensitivity display a rather unimodal long-tailed distribution.

The phase angle of the first harmonic response with respect to side-down displacement of the neck was also evaluated. Fig. 5B shows that most of the responsive units (59/75, i.e. 78.6%) were maximally excited by side-up neck displacement (phase angle of responses ranging from a lead of $+165°$ to a lag of $-90°$), with an average phase lag of -128.5 ± 18.1, SD, deg, corresponding to an average lead of $+51.5°$ with respect to the extreme side-up displacement. On the other hand a smaller group of units (8/75, i.e. 10.7%) were maximally excited by side-down neck displacement (phase angle of responses ranging from a lead of $+90°$ to a lag of $-15°$), with an average phase lead of $+55.9 \pm 21.0$, SD, deg. Only 8 units (10.7%) fell outside the two ranges reported above (Table 1).

Both the gain and the phase angle of each unit response at the standard parameters of neck rotation were plotted on a polar diagram (Fig. 3B). Most of the unit responses characterized by an increase in firing rate during side-up neck rotation (left quadrant) showed a larger gain than that of the units displaying the opposite response pattern (right quadrant).

In addition to the first harmonic, a second harmonic component of the responses of the IVS neurons to neck rotation was noticeable in most units and had a mean amplitude of 35.2 ± 29.4, SD expressed in percent of the fundamental ($n = 75$). The response characteristics of the non-antidromic LVN neurons to the same parameters of neck rotation are shown in Table 1.

Localization of units responding to neck stimulation

Among all the recorded 122 neurons, 28 were located in the rvLVN, while 94 were located in the dcLVN. Moreover, 23 rvLVN and 86 dcLVN units were antidromically identified as IVS neurons (Fig. 4B). Table 2 shows that the proportion of IVS neurons responding to standard parameters of neck rotation was comparable in the rvLVN (16/23, i.e. 69.6%) and the dcLVN (59/86, i.e. 68.6%), as were the mean resting discharge rate and base frequency of the two populations of neurons. No significant differences in the average gain and sensitivity of the first harmonic of responses to neck rotation were found between the IVS neurons located in the rvLVN and the dcLVN. Finally, most of the IVS neurons were excited during side-up neck displacement; the proportion of units showing this response pattern was slightly higher in the dcLVN (47/59, i.e. 79.6%) than in the rvLVN (12/16, i.e. 75.0%); the difference, however, was not significant.

Fig. 4. Anatomical localization of IVS neurons tested to sinusoidal tilt of the animal (**A**) and neck rotation (**B**) at the standard parameters (0.026 Hz, $\pm 10°$). For each group of experiments the units were plotted on six representative drawings corresponding to transverse sections of the medulla taken at equal intervals and numbered progressively from rostral to caudal levels. The vestibular and cerebellar nuclei were outlined on each of the illustrated sections. Abbreviations: DVN, descending (inferior) vestibular nucleus; *F*, fastigial nucleus; *I*, interpositus nucleus; *LVN*, lateral vestibular nucleus (Deiters); *MVN*, medial vestibular nucleus. **A** Among the 129 LVN neurons antidromically activated by stimulation of the spinal cord at $T_{12}-L_1$ (IVS neurons), 76 units responded to roll tilt of the animal (●), while the remaining 53 units (×) were unaffected by this stimulus. Moreover, 27 of the 129 units (17 of which responsive) were located in the rvLVN while 102 of the 129 units (59 of which responsive) were located in the dcLVN. **B** Among the 109 IVS neurons, 75 units responded to neck rotation (●), while the remaining 34 units (×) were unaffected by this stimulus. Moreover, 23 of 109 units (16 of which responsive) were located in the rvLVN, while 86 of 109 (59 of which responsive) were located in the dcLVN

Comparison of the response patterns of different populations of lateral vestibular neurons to vestibular and neck stimulations

The response characteristics of the antidromic IVS neurons (which project to the lumbosacral segments of the spinal cord), following sinusoidal stimulation of labyrinth and neck receptors, can hardly be compared with those obtained in the present experiments from the non-antidromic LVN neurons (which may actually project to the cervical segments of the spinal cord), since the latter units were few in number and mainly located in the dcLVN. In order to evaluate the responses of lateral vestibular units projecting to different segments of the spinal cord, we should compare the responses of the IVS neurons with those of unidentified LVN neurons, previously tested to vestibular [7] and neck [8] stimulations. In these experiments, in fact, the units were assumed to project to the whole segments of the spinal cord, since they were quite numerous and homogeneously distributed throughout the whole extent of the LVN; moreover, they

Table 2. Localization of antidromic lVS neurons responsive to sinusoidal animal tilt (macular input) or neck rotation (neck input) at standard parameters

	Macular input		Neck input	
	rvLVN	dcLVN	rvLVN	dcLVN
No of units	27	102	23	86
Conduction velocity	93.8 ± 17.4 $n = 27$	89.0 ± 22.5 $n = 102$	92.6 ± 18.6 $n = 23$	89.1 ± 21.6 $n = 86$
Responsive (R) units	17 (63.0%)	59 (57.8%)	16 (69.6%)	59 (68.6%)
Unresponsive (R) units	10 (37.0%)	43 (42.2%)	7 (30.4%)	27 (31.4%)
Resting discharge rate of R-units	20.6 ± 19.2 $n = 16$	21.5 ± 14.3 $n = 52$	19.8 ± 19.1 $n = 15$	22.5 ± 15.9 $n = 55$
Base frequency of R-units	21.2 ± 19.3 $n = 17$	19.7 ± 15.4 $n = 59$	20.0 ± 19.2 $n = 16$	22.0 ± 17.2 $n = 59$
Gain of R-units	0.59 ± 0.58 $n = 17$	0.44 ± 0.38 $n = 59$	0.58 ± 0.52 $n = 16$	0.46 ± 0.37 $n = 59$
Sensitivity of R-units	4.55 ± 4.17 $n = 14$	2.87 ± 2.74 $n = 50$	4.34 ± 4.56 $n = 12$	3.05 ± 3.10 $n = 51$
Phase angle of R-units	From +75° lead to −45° lag		From +90° lead to −15° lag	
	10 (58.8%)	41 (69.5%)	3 (18.75%)	5 (8.5%)
	From +135° lead to −105° lag		From +165° lead to −90° lag	
	5 (29.4%)	10 (16.9%)	12 (75.0%)	47 (79.65%)
	From +75° to +135° and from −45° to −105°		From +90° to +165° and from −15° to −90°	
	2 (11.8%)	8 (13.6%)	1 (6.25%)	7 (11.85%)

Abbreviations as in Table 1; rvLVN, rostroventral part of LVN; dcLVN, dorsocaudal part of LVN

were not submitted to the antidromic test or else they were antidromically activated by spinal cord stimulation at high cervical level.

Let is consider first the unit responses to vestibular stimulation obtained in the two different groups of experiments. These groups differ first in the proportion of units responsive to sinusoidal tilt of the animal at the standard parameters (0.026 Hz, ± 10°), which was smaller for the antidromically identified lVS neurons (76/129 units, i.e. 58.9%) than for the unidentified LVN neurons (77/102 units, i.e. 75.5%).

As to their response patterns, the neurons recorded in each group of experiments were classified as: 1. units excited during side-down tilt of the animal, with a phase angle of responses ranging from +75° to −45° (α-responses); 2. units excited during side-up tilt of the animal, with a phase angle ranging from +135° to −105° (β-responses), and 3. units showing phase angle of responses outside the range described for the two main populations (intermediate responses). In Fig. 2 the distribution of the response patterns to animal tilt of the identified lVS neurons (B), recorded in the present experiments, is compared with that of the unidentified LVN neurons (A), as recorded in a previous study [7]. Although the majority of the units recorded in both groups of experiments displayed α-responses, their proportion was greater among the lVS neurons (51/76, i.e. 67.1%) than the LVN units (37/77, i.e. 48.0%). Conversely, the proportions of units displaying β- and intermediate responses were smaller among the lVS neurons (15/76, i.e. 19.7% and 10/76, i.e. 13.2%, respectively) than the LVN neurons (20/77, i.e. 26.0% for each group). There are also differences in the average phase angle of responses of the two populations of lVS and LVN units showing α- or β-responses, as shown in Fig. 2. Taken together, the two populations of units showing α- and β-responses displayed an average phase lead with respect to the extreme animal displacements which was larger for the lVS neurons (+21.0 ± 27.2, SD, deg) than for unidentified LVN neurons (+12.3 ± 28.4, SD, deg).

Let us consider now the unit responses to neck stimulation, obtained in the two different groups of experiments. In contrast to the results obtained during animal tilt, the proportion of units responsive to neck rotation at the standard parameters (0.026 Hz, ± 5−10°) was lower for the LVN neurons (70/120, i.e. 58.2%) than for the lVS neurons (75/109, i.e. 68.8%).

As to the response patterns, the neurons were identified as: 1. units excited during side-up neck rotation with a phase angle of responses ranging from +135° or +165° to −90°; 2. units excited during side-down neck rotation with a phase angle ranging from +90° to −15° or −45°, and 3. units showing intermediate responses. Figure 5 compares the distribution of the response patterns to neck rotation of the antidromically activated lVS neurons (B), recorded in the present experiments, with that of the unidentified LVN neurons (A), as recorded in a previous study [8]. The units excited by side-up or side-down neck rotation were almost equally represented among the LVN neurons (38/70, i.e. 54.3% and 31/70, i.e. 44.3%, respectively), while among the lVS neurons there was a predominance of the first population of units with respect to the second one (59/75, i.e. 78.6% and 8/75, i.e. 10.7% respectively). Figure 5 also shows differences in the average phase angle of responses of the

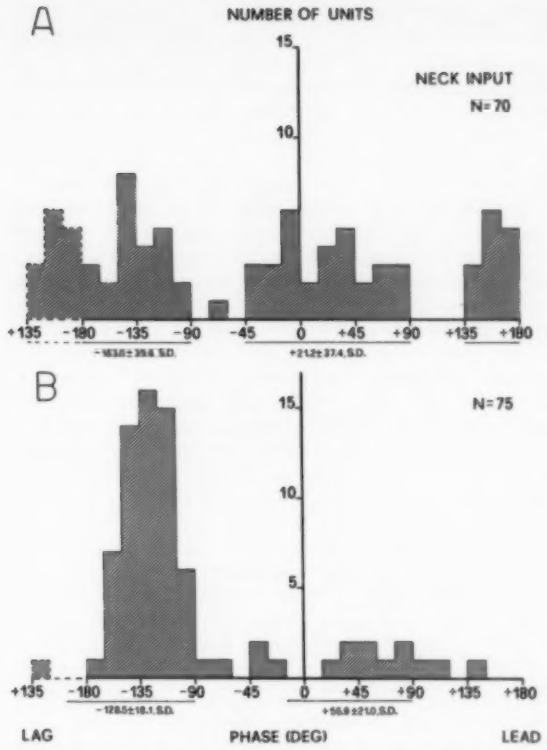

Fig. 5A, B. Distribution of the phase angle of the first harmonic of responses of different populations of LVN neurons tested during neck rotation at 0.026 Hz, $\pm 10°$. All the experiments were performed in precollicular, decerebrate cats, with the cerebellum intact. The upper histogram (**A**) illustrates the distribution of the phase angle of responses to neck rotation of 70 neurons histologically identified as being located within the whole extent of LVN, thus projecting to the whole segments of the spinal cord (slightly modified from Fig. 5A, Ref. 8), while the lower histogram (**B**) illustrates the distribution of the phase angle of responses to neck rotation of 75 LVN neurons antidromically activated by stimulation of the spinal cord at $T_{12}-L_1$, thus projecting to the lumbosacral segments of the spinal cord (lVS neurons). Positive numbers in the abscissas indicate, in degrees, the phase lead, whereas negative numbers indicate the phase lag of responses with respect to the extreme side-down displacement of the neck, as indicated by 0°. Responses of the neurons underlined by horizontal bars have been used to evaluate the average phase angle of units excited during or near side-down (0°) or side-up displacement of the neck (180°)

two populations of lVS and LVN units reported above. Taken together, these two populations of units displayed an average phase lead with respect to the extreme neck displacements, which was larger for the lVS neurons ($+52.0 \pm 18.3$, SD, deg) than for the unidentified LVN neurons ($+18.9 \pm 38.6$, SD, deg).

Discussion

It was previously shown that in decerebrate cats the responses of histologically identified LVN neurons to slow sinusoidal tilt of the animal [7] are mainly related to animal position, thus being attributed to stimulation of macular receptors. Similarly, the responses of LVN neurons to slow neck rotation [8] are related to neck position rather than to velocity of neck displacement, and originate from deep receptors, i.e. joint receptors [12, 30] and/or muscle spindle receptors particularly located in the dorsal and the small perivertebral muscles [cf. 37, 38].

In the experiments reported above [cf. also 34], the proportion of units affected by animal tilt or neck rotation was higher in the rvLVN (91.2% and 73.9%, respectively) than in the dcLVN (67.6% and 48.6%, respectively) which project mainly, although not exclusively, to the cervical and the lumbosacral segments of the spinal cord, respectively [35]. Although the populations of responsive neurons in these two regions of Deiters' nucleus showed a comparable base frequency (43.6 ± 54.4, SD, impulses/s for macular responsive units and 40.7 ± 48.9, SD, impulses/s for neck responsive units), the rvLVN neurons had on the average an higher response sensitivity, but not an higher gain, to both labyrinth and neck inputs with respect to the dcLVN neurons. These differences were attributed to the fact that the primary vestibular afferents from macular receptors as well as the cervical afferents and the related ascending pathways activate more efficiently the rvLVN than the dcLVN.

The rvLVN and dcLVN neurons recorded in the previous studies [7, 8] did not differ with respect to their predominant pattern of response to vestibular stimulation; in fact the proportion of units excited during side-down tilt of the animal (α-responses; 48.0%) was higher than that of the units excited during side-up tilt (β-responses; 26.0%). However, they differ in the distribution of the neck responses; units located in the rvLVN were mainly excited during side-down neck rotation, while most of the units in the dcLVN were excited during side-up neck rotation.

The response patterns characterized by an increase in firing rate during side-down animal tilt and side-up neck rotation have been considered the most appropriate to increase the postural activity in the ipsilateral limb extensors for those directions of animal and neck orientation, while the opposite response patterns have been thought to be quite effective to control the extensor neck musculature (see Introduction). Unfortunately, in the experiments reported above [7, 8] nothing could be said about the precise termination of the vestibulospinal axons originating from the recorded LVN neurons, since the tested units were not identified as projecting to upper or lower segments of the spinal cord.

In the present experiments we recorded the activity of vestibulospinal neurons antidromically activated by stimulation of the spinal cord at $T_{12}-L_1$, thus projecting to the lumbosacral segments (lVS neurons). These neurons were found in both the rvLVN and the dcLVN; however, in our sampled population, the majority of lVS neurons tested to vestibular and neck stimulations were located within the dcLVN (102/129, i.e. 79.0% and 86/109, i.e. 78.9%, respectively).

In spite of the predominant number of antidromic units in the dcLVN, the percentage of lVS neurons responsive to roll tilt of the animal (58.9%) or neck rotation (68.8%) was not significantly different within the two divisions of the nucleus. This finding differs from that previously reported in unidentified LVN neurons, where the proportion of units responsive to standard parameters of animal tilt [7] and neck rotation [8] was higher in the rvLVN than in the dcLVN. Moreover, while the gain and the sensitivity values of all the responsive lVS neurons found in the present study were

on the average similar to those obtained from the whole population of unidentified LVN neurons [cf. also 34], their base frequency evaluated during vestibular stimulation was lower (20.0 ± 16.2, SD against 43.6 ± 54.4, SD, impulses/s); the same was true during neck stimulation (21.6 ± 17.6, SD against 40.7 ± 48.9, SD, impulses/s). Since the unidentified LVN neurons were distributed throughout the whole extent of Deiters' nucleus, thus having the potential of projecting to the whole segments of the spinal cord, our findings indicate that the vestibulospinal neurons projecting to the lower segments of the spinal cord have a mean firing rate lower than that of the units projecting to the upper segments. Moreover, since in the previous experiments [7, 8] no difference in base frequency was found between the two populations of rvLVN and dcLVN neurons, we postulate that at least a proportion of unidentified dcLVN units projected to the cervical rather than to the lumbosacral cord. It appears, therefore, that the whole population of unidentified units histologically located in the dcLVN is less homogeneous than that of the lVS neurons antidromically activated by stimulation of the spinal cord at $T_{12}-L_1$.

In the present experiments the responses of antidromically identified lVS neurons to animal tilt and neck rotation showed on the average phase leads of $+21.0°$ and $+52.0°$, respectively, with respect to the extreme animal and neck displacements, which contrast with the lower values of $+12.3°$ and $+18.9°$, respectively, previously obtained from unidentified LVN neurons [7, 8]. Since these last neurons probably included units projecting not only to the lumbosacral but also to the cervical segments of the spinal cord, it is likely that the latter population of neurons showed by itself a smaller phase lead with respect to that obtained from the whole population of unidentified LVN units. This difference can easily be understood if we consider that the majority of recorded lVS neurons were located in the dcLVN and that this part of Deiters' nucleus receives the direct corticocerebellovestibular projection from the anterior vermis [cf. 13], which is inhibitory in function [1, 19, 22]. Since the Purkinje cells of the anterior vermis giving rise to this direct inhibitory projection on Deiters' nucleus actually collaborate with the excitatory macular or neck input in determining the response of the lVS neurons to animal tilt [14] and neck rotation [14, 15], we may assume that the more prominent phase lead of the lVS neurons with respect to those projecting to the cervical segments of the spinal cord is due to corticocerebellar influences acting on these neurons during dynamic stimulation of labyrinth receptors.

A final comment concerns the predominant patterns of responses of the lVS neurons to animal tilt and neck rotation. The majority of responsive lVS neurons displayed an α-response to animal tilt, being excited during side-down tilt of the animal (67.1%; see Fig. 2B); moreover, a great proportion of lVS neurons were excited during side-up neck rotation (78.6%; see Fig. 5B). These proportions were higher than those reported in previous studies (see Fig. 2A and 5A), where the LVN neurons were tested independently upon their axonal distribution [7, 8]. As pointed out previously [cf. 34], these predominant patterns of response are quite appropriate to produce an increased contraction of ipsilateral hindlimb extensors during side-down animal tilt or side-up neck rotation.

Conversely, units excited during side-up tilt of the animal (β-response) and side-down neck rotation were much less represented in our population of lVS neurons (19.7% and 10.7%, respectively) than in the whole population of unidentified LVN neurons [11, 12] (compare Figs. 2B and 5B with Figs. 2A and 5A). It is likely that these two types of unit responses intervene in the control of the dorsal neck muscles, thus being responsible for the increased contraction of the ipsilateral neck extensors during side-up animal tilt or side-down neck rotation [cf. 34]. As to the lVS neurons, which also showed similar response patterns, the most likely hypothesis is that they project either to ipsilateral hindlimb motoneurons different from those controlling the proximal extensor musculature, or to contralateral hindlimb extensor motoneurons [cf. 41]; their activity, however, was apparently weaker than that of the lVS neurons displaying the opposite response patterns.

The demonstration that in decerebrate cats the lVS neurons showing the predominant patterns of response to animal tilt and neck rotation were quite numerous and highly affected by the labyrinth and neck signals contrasts with the fact that in the same preparations the contraction of limb extensor muscles during side-down tilt of the animal and side-up neck rotation involved particularly the triceps brachii, but not the triceps surae [4, 11, 29, 36]. There must be, therefore, other pathways, such as the reticulospinal pathway, which probably contribute with the excitatory vestibulospinal pathway to the postural adjustments during labyrinth and neck stimulations, whose neuronal activity, however, is greatly impaired by the decerebration [cf. 34].

Acknowledgements. This work was supported by National Institute of Neurological and Communicative Disorders and Stroke Research Grant NS 07685-18 and by a grant from the Ministero della Pubblica Istruzione, Roma, Italy. We thank E. Biagetti, U. Corti and Mrs. M. Vaglini for their valuable technical assistance. Dr. A. Marchand was supported by a fellowship of the "Fondation Simone et Cino del Duca, Paris" on leave of absence from the Département de Psychophysiologie générale, Institute de Neurophysiologie et de Psychophysiologie, C.N.R.S., 31 Chemin Joseph-Aiguier, F-13274 Marseille Cédex 2, France.

References

1. Akaike T (1983) Electrophysiological analysis of cerebellar corticovestibular and fastigiovestibular projections to the lateral vestibular nucleus in the cat. Brain Res 272:223–235
2. Akaike T, Fanardjian VV, Ito M, Ohno T (1973) Electrophysiological analysis of the vestibulospinal reflex pathway of rabbit. II. Synaptic actions upon spinal neurones. Exp Brain Res 17:497–515
3. Anderson JH, Pappas C (1978) Neck motor responses to vertical rotations in the alert cat. Soc Neurosci Abstr 4:609
4. d'Ascanio P, Bettini E, Pompeiano O (1985) Tonic inhibitory influences of locus coeruleus on the response gain of limb extensors to sinusoidal labyrinth and neck stimulations. Arch Ital Biol 123:69–100
5. Berthoz A, Anderson JH (1971) Frequency analysis of vestibular influence on extensor motoneurons. I. Response to tilt in forelimb extensors. Brain Res 34:370–375
6. Berthoz A, Anderson JH (1971) Frequency analysis of vestibular influence on extensor motoneurons. II. Relationship between neck and forelimb extensors. Brain Res 34:376–380
7. Boyle R, Pompeiano O (1980) Reciprocal responses to sinusoidal tilt of neurons in Deiters' nucleus and their dynamic characteristics. Arch Ital Biol 118:1–32
8. Boyle R, Pompeiano O (1980) Responses of vestibulospinal neurons to sinusoidal rotation of neck. J Neurophysiol 44: 633–649

9. Boyle R, Pompeiano O (1981) Convergence and interaction of neck and macular vestibular inputs on vestibulospinal neurons. J Neurophysiol 45:852–868
10. Boyle R, Pompeiano O (1981) Relation between cell size and response characteristics of vestibulospinal neurons to labyrinth and neck inputs. J Neurosci 1:1052–1066
11. Boyle R, Pompeiano O (1984) Discharge activity of spindle afferents from the gastrocnemius-soleus muscle during head rotation in the decerebrate cat. Pflügers Arch 400:140–150
12. Cohen LA (1961) Role of eye and neck proprioceptive mechanisms in body orientation and motor coordination. J Neurophysiol 24:1–11
13. Corvaja N, Pompeiano O (1979) Identification of cerebellar cortico-vestibular neurons retrogradely labeled with horseradish peroxidase. Neuroscience 4:507–515
14. Denoth F, Magherini PC, Pompeiano O, Stanojević M (1979) Responses of Purkinje cells of the cerebellar vermis to neck and macular vestibular inputs. Pflügers Arch 381:87–98
15. Denoth F, Magherini PC, Pompeiano O, Stanojević M (1980) Responses of Purkinje cells of cerebellar vermis to sinusoidal rotation of neck. J Neurophysiol 43:46–59
16. Ehrhardt KJ, Wagner A (1970) Labyrinthine and neck reflexes recorded from spinal single motoneurons in the cat. Brain Res 19:87–104
17. Ezure K, Wilson VJ (1983) Dynamics of neck-to-forelimb reflexes in the decerebrate cat. J Neurophysiol 50:688–695
18. Ezure K, Wilson VJ (1984) Interaction of tonic neck and vestibular reflexes in the forelimb of the decerebrate cat. Exp Brain Res 54:289–292
19. Fanardjian VV, Sarkissian VA (1980) Spatial organization of the cerebellar corticovestibular projection in the cat. Neuroscience 5:551–558
20. Grillner S, Hongo T, Lund S (1970) The vestibulospinal tract. Effects on alpha-motoneurones in the lumbosacral spinal cord in the cat. Exp Brain Res 10:94–120
21. Hongo T, Kudo N, Tanaka R (1975) Effects from the vestibulospinal tract on the contralateral hindlimb motoneurones in the cat. Brain Res 31:220–223
22. Ito M (1972) Cerebellar control of the vestibular neurons: physiology and pharmacology. In: Brodal A, Pompeiano O (eds) Progress in brain research, vol 37; Basic aspects of central vestibular mechanisms. Elsevier, Amsterdam, pp 377–390
23. Lindsay KW, Roberts TDM, Rosenberg JR (1976) Asymmetric tonic labyrinth reflexes and their interaction with neck reflexes in the decerebrate cat. J Physiol (Lond) 261:583–601
24. Lund S, Pompeiano O (1968) Monosynaptic excitation of alpha-motoneurons from supraspinal structures in the cat. Acta Physiol Scand 73:1–21
25. Maeda M, Maunz RA, Wilson VJ (1975) Labyrinthine influence on cat forelimb motoneurons. Exp Brain Res 22:69–86
26. Magnus R (1924) Körperstellung. Springer, Berlin
27. Magnus R, De Kleijn A (1912) Die Abhängigkeit des Tonus der Extremitätenmuskeln von der Kopfstellung. Pflügers Arch 145:455–548
28. Manzoni D, Pompeiano O, Srivastava UC, Stampacchia G (1983) Responses of forelimb extensors to sinusoidal stimulation of macular labyrinth and neck receptors. Arch Ital Biol 121:205–214
29. Manzoni D, Pompeiano O, Srivastava UC, Stampacchia G (1984) Gain regulation of vestibular reflexes in fore- and hindlimb muscles evoked by roll tilt. Boll Soc Ital Biol Sper 60 (Suppl 3):9–10
30. McCouch GP, Deering ID, Ling TH (1951) Location of receptors for tonic neck reflexes. J Neurophysiol 14:191–195
31. Nagaki J (1967) Effects of natural vestibular stimulation on alpha extensor motoneurons of the cat. Kumamoto Med J 20:102–111
32. Peterson BW, Bilotto G, Goldberg J, Wilson VJ (1981) Dynamics of vestibulo-ocular, vestibulocollic and cervicocollic reflexes. Ann NY Acad Sci 374:395–402
33. Pompeiano O (1975) Vestibulo-spinal relationships. In: Naunton RF (ed) The vestibular system. Academic Press, New York, pp 147–180
34. Pompeiano O (1984) A comparison of the response characteristics of vestibulospinal and medullary reticulospinal neurons to labyrinth and neck inputs. In: Barnes CD (ed) Brainstem control of spinal cord function. Research topics in physiology, vol 6. Academic Press, Orlando, pp 87–140
35. Pompeiano O, Brodal A (1957) The origin of vestibulospinal fibers in the cat. An experimental-anatomical study with comments on the descending medial longitudinal fasciculus. Arch Ital Biol 95:166–195
36. Pompeiano O, Wand P, Srivastava UC (1985) Responses of Renshaw cells coupled with hindlimb extensor motoneurons to sinusoidal stimulation of labyrinth receptors in the decerebrate cat. Pflügers Arch 403:245–257
37. Richmond FJ, Abrahams VC (1975) Morphology and distribution of muscle spindles in dorsal muscles of the cat neck. J Neurophysiol 38:1322–1339
38. Richmond FJR, Abrahams VC (1979) What are the proprioceptors of the neck? In: Granit R, Pompeiano O (eds) Progress in brain research, vol 50. Reflex control of posture and movement. Elsevier, Amsterdam, pp 245–254
39. Roberts TDM (1978) Neurophysiology of postural mechanisms. 2nd edn., Butterworths, London
40. Schor RH, Miller AD (1981) Vestibular reflexes in neck and forelimb muscles evoked by roll tilt. J Neurophysiol 46:167–178
41. Schor RH, Miller AD (1982) Relationship of cat vestibular neurons to otolith-spinal reflexes. Exp Brain Res 47:137–144
42. Wilson VJ, Yoshida M (1969) Comparison of effects of stimulation of Deiters' nucleus and medial longitudinal fasciculus on neck, forelimb, and hindlimb motoneurons. J Neurophysiol 32:743–758
43. Xerri C, Gianni S, Manzoni D, Pompeiano O (1983) Central compensation of vestibular deficits. I. Response characteristics of lateral vestibular neurons to roll tilt after ipsilateral labyrinth deafferentation. J Neurophysiol 50:428–448

Received February 18/Accepted December 10, 1986

Pflügers Arch (1987) 409:24–38

Pflügers Archiv
European Journal of Physiology
© Springer-Verlag 1987

Effects of roll tilt of the animal and neck rotation on different size vestibulospinal neurons in decerebrate cats with the cerebellum intact

O. Pompeiano, S. Manzoni, A. R. Marchand, and G. Stampacchia

Dipartimento di Fisiologia e Biochimica, Università di Pisa, Via S. Zeno 31, I-56100 Pisa, Italy

Abstract. 1. In decerebrate cats with the cerebellum intact we recorded the activity of lateral vestibulospinal neurons projecting to lumbosacral segments of the spinal cord (lVS neurons) and related the resting discharge, as well as the response characteristics of these neurons to roll tilt of the animal and neck rotation, with the cell size inferred from the conduction velocity of the corresponding axons. 2. A slight negative correlation was found between resting discharge rate and conduction velocity of the whole population of lVS neurons responsive and unresponsive to animal tilt and neck rotation, so that the faster the conduction velocity, the lower was the unit discharge at rest. This correlation, however, was found only for the dorsocaudal LVN neurons, which contributed to the majority of lVS units, but not for the rostroventral LVN neurons. Moreover, it affected the units unresponsive but not those responsive to vestibular stimulation; the opposite, however, occurred for the units tested to neck stimulation. These findings indicate that the static properties of the lVS neurons can only in part be related to cell size. 3. If we consider the lVS neurons responsive to roll tilt of the animal (76 neurons) and neck rotation (75 neurons) at the standard parameters of 0.026 Hz, $\pm 10°$, no significant correlation was found between gain (impulses $\cdot s^{-1} \cdot deg^{-1}$) of the labyrinth or neck responses and conduction velocity of the axons. Thus, due to the presence of slight negative relation between resting discharge and conduction velocity of the axons, larger neurons exhibited a greater percentage modulation (sensitivity) to the labyrinth and neck inputs than smaller neurons; this correlation involved particularly the dcLVN neurons. These findings suggest that the afferent pathways driven during dynamic stimulation of labyrinth and neck receptors produce an higher number or density of synaptic contacts on lVS neurons of increasing size. 4. No significant differences in the means of resting discharge, conduction velocity, gain and sensitivity were found between all the lVS units responding to labyrinth and neck inputs. These findings indicate that the effectiveness of the two inputs was almost comparable and did not vary in different units as a function of cell size. 5. The lVS neurons were mainly excited during side-down animal tilt and side-up neck rotation. Although these neurons showed the same spectrum of conduction velocity as those displaying the opposite response patterns, the response gains of the predominant populations of units were on the average higher than those obtained from the remaining populations of units. The peak of the unit responses occurred with an average phase lead of $+21.0 \pm 27.2°$, SD with respect to the extreme animal displacements, and an average phase lead of $+52.0 \pm 18.3$, SD with respect to the extreme neck displacements; yet no difference was found in the average phase angle of responses of the two populations of slow and fast units to animal tilt or neck rotation. These findings indicate that the quantitative and qualitative organization of the synaptic inputs represent the critical factor controlling response characteristics of comparable size lVS neurons to vestibular and neck stimulations. 6. A comparison between the present results and those obtained in previous experiments performed after bilateral ablation of the paleocerebellum permitted to evaluate the role that the inhibitory area of the cerebellum exerts on the resting discharge, as well as on the dynamic characteristics of response of different size lVS neurons to animal tilt and neck rotation.

Key words: Vestibulospinal neurons – Cell size – Response characteristics – Vestibular input – Neck input

Offprint requests to: O. Pompeiano

Introduction

The lateral vestibular nucleus (LVN) of Deiters consists of two parts, the rostroventral part (rvLVN) which contains neurons of small to medium size, the axons of which project mainly to the cervical segments of the spinal cord, and the dorsocaudal part (dcLVN) made by small to giant cells, which project particularly to the lumbar spinal cord [40].

The functional role of different size vestibulospinal neurons in the static and dynamic control of posture during the vestibular and neck reflexes has been recently investigated. In particular, Boyle and Pompeiano [6], recorded the activity of individual LVN neurons projecting to the lumbosacral segments of the spinal cord (lVS neurons) and studied the relation between their resting discharge or response characteristics to excitatory labyrinth and neck afferent volleys and the cell size inferred from the conduction velocity of the corresponding vestibulospinal axon; they tried in this way to find out whether the spontaneous discharge as well as the induced responses of these neurons were determined by neuronal properties related to cell size [26] or whether they depended mainly upon synaptic organization, so that a differential control of particular neuronal groups by the relevant input systems could result [11, 12]. Since the lVS neurons are particularly located in the dcLVN, on which the cerebellar cortico-vestibular projection originating from the ipsilateral vermal cortex [cf. 18] exerts a monosynaptic inhibitory influence [1, 2, 22, 30–33], these

experiments were performed in decerebrate cats in which cerebellar reverberation of labyrinth and neck afferent volleys [19, 20, 45, 46] was excluded by a bilateral ablation of the medial corticonuclear zone of the cerebellum.

Obviously, the problem originated as to whether the paleocerebellum exerts an inhibitory influence on different size LVN neurons and if so, whether this influence is either homogeneously distributed within the nucleus or differentially oriented towards particular groups of neurons.

We decided therefore with the present study to extend our unit analysis to lVS neurons recorded in decerebrate cats, but with the cerebellum intact. By comparing the resting discharge as well as the response characteristics of different size lVS neurons the vestibular and neck stimulations, as recorded in the present experiments, with those previously obtained in partially cerebellectomized cats [6] we could obtain informations about the role that the inhibitory area of the cerebellum exerts on the static and dynamic properties of different size LVN neurons projecting to the lumbosacral segments of the spinal cord.

Methods

The present observations were performed in the same precollicular decerebrate cats with the cerebellum intact which were recently used to record the activity of lVS neurons antidromically activated by stimulating the spinal cord at T_{12}-L_1 and study their response characteristics to roll tilt of the animal and neck rotation at the standard parameters of 0.026 Hz, $\pm 10°$ [36]. The animal's head was placed in a stereotaxic frame and pitched 10° nose-down. The methods of securing the animal on the tilting table while rotating the animal or the neck about the longitudinal axis [cf. 19, 20] as well as the methods used to record extracellularly the unit activity, and identify antidromically the lVS neurons have already been described [36].

All the experiments were performed in animals immobilized with pancuronium bromide (Pavulon, Organon, Oss, The Netherlands, 0.6 mg/kg/h, i.v.) and artificially ventilated. In particular, after the antidromic identification of the lVS neurons, raw spike-train data from segments of spontaneous background discharge of lVS neurons were recorded on magnetic tape. The mean resting discharge rate (impulses · s) was evaluated over a period of time sufficiently long to allow the recording of 400–800 spikes. In addition the mean interspike interval, standard deviation interval and coefficient of variation (CV) defined as the standard deviation of interspike intervals divided by the interval mean, were calculated off-line following the criteria described in previous paper [6]. Sequential pulse density histograms (SPDHs) were obtained by superimposing and averaging data of 4–5 successive sweeps, each containing two cycles of unit responses to sinusoidal animal tilt or neck rotation. The analogue output of signal averager (Correlatron 1024, Laben) was then plotted on an X-Y plotter (Hewlett-Packard, HP 7035P) and the digital data transferred to a microprocessor (Pet 2001-8C) and processed online by means of a fast Fourier analysis. Results are based on the quantitative spectral analysis of the averaged unit activity with respect to the first harmonic of response (output) during the rotational stimuli (angular input).

For each unit the mean discharge rate or base frequency (impulses/s) was evaluated during lateral tilt of the animal or neck rotation at the standard parameters. This value corresponded to the mean discharge frequency of the same unit recorded at rest. The response gain was defined as the absolute change of the mean firing rate per degree of displacement (impulses $\cdot s^{-1} \cdot deg^{-1}$) and the sensitivity was expressed as the percentage change of the mean discharge rate per degree (%/deg). When the units displayed a cutoff of their response during periods of stimulation, the gain was corrected according to the method described by Anderson et al. [3]. According to the terminology used in previous studies [5, 19], the direction of stimulus orientation was indicated as side-down when the animal was rotated downward towards the side of the recording electrode (labyrinth input) or the body was rotated upward towards the recording side (neck input); the term side-up was used for rotations in the opposite direction. The phase angle of response was described as the phase difference in arc degrees between the peak of side-down displacement of the animal or the neck and the peak of the fundamental component of unit response. Criteria used to evaluate the responsiveness of the units to the rotatory stimulus have been reported in our previous study [36].

Systemic arterial blood pressure, end-tital P_{CO_2} and rectal temperature were monitored throughout the experiments and maintained within physiological limits (100–140 mm Hg, 3–4.5% P_{CO_2}, 36.5–37.5° C, respectively).

At the end of penetrations a mark was made by passing a cathodal current (15 μA for 10 min) through the tip of the microelectrode [25]. The recording sites were then identified on histological serial sections of the medulla stained with the Nissl method. Only lVS neurons histologically located in LVN, as outlined by Pompeiano and Brodal [40], were investigated.

Results

Unit responses to vestibular stimulation

Resting discharge activity and conduction velocity of lateral vestibulospinal neurons. The results were obtained from a large population of LVN neurons recorded in a previous study [36]. In particular, 129 neurons were antidromically activated by electrical stimulation of the spinal cord between T_{12} and L_1 (lVS neurons), and tested to roll tilt of the animal at the standard parameters. Among these antidromic units; 110 were spontaneously active, while the remaining 19 were silent. Resting discharge rates, evaluated for 108 out of the 110 lVS neurons, ranged from 0.7 to 66.7 impulses/s and averaged 24.5 ± 15.7, SD, impulses/s. Comparable ranges but with different mean values of discharge rate were obtained from the units responsive (21.3 ± 15.4, SD, impulses/s, $n = 68$) and those unresponsive (29.9 ± 14.7, SD, impulses/s, $n = 40$) to animal tilt (Fig. 1 A, inset, shaded and white columns, respectively), the difference being statistically significant (t-test, $P < 0.01$). Similar results were obtained for the base frequency. It is interest that among the 108 neurons reported above the majority, i.e. 85 neurons, were histologically identified as being located in the dcLVN, while the remaining 23 neurons were located in the rvLVN; in particular, 52 out of 68 responsive units and 33 out of 40 unresponsive units were located in the dorsal aspect of LVN.

If we consider the total population of lVS neurons exhibiting a background discharge at rest, a clear-cut positive correlation was found between the mean interval and the

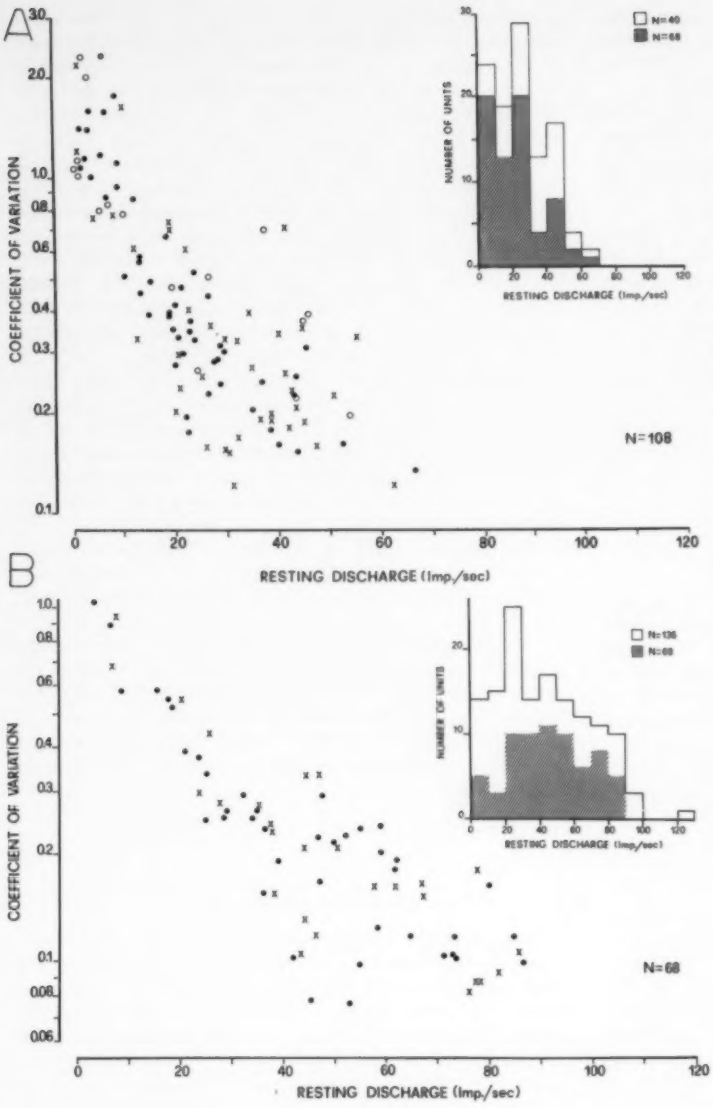

Fig. 1
Resting discharge activity of lVS neurons in decerebrate cats before (**A**) and after partial cerebellectomy (**B**). **A** relation between resting discharge rate (measured in impulses/s) and coefficient of variation (*CV*) of 108 lVS neurons recorded in decerebrate cats with the cerebellum intact. Symbols represent units either responsive (●, ○ $n = 68$) or unresponsive (×, $n = 40$) to roll tilt of the animal at standard parameters. The CV corresponded on the average to 0.64 ± 0.52, SD for the responsive units and to 0.43 ± 0.41, SD for the unresponsive units (mean value of both groups of units was 0.56 ± 0.49, SD). The higher the CV, reflecting a more irregular unit discharge, the lower the mean background discharge (paired rank, $P < 0.001$; $n = 108$). *Inset*: distribution of resting discharge of the general population of lVS neurons showing a spontaneous activity at rest and tested for evaluation of the CV. Both responsive (*shaded columns*, $n = 68$) and unresponsive (*white columns*, $n = 40$) units are indicated. The majority of the units originated from the dcLVN ($n = 85$, 52 of which indicated by *filled circles* in the main graph being responsive), while the remaining units originated from the rvLVN ($n = 23$, 16 of which indicated by *empty circles* in the main graph being responsive). **B** relation between resting discharge rate and CV of 68 lVS neurons recorded in decerebrate cats after ablation of the cerebellar vermal cortex and fastigial nuclei [6]. Symbols represent units either responsive (●, $n = 41$) or unresponsive (×, $n = 27$) to labyrinth stimulation. The CV was on the average comparable for the two populations of responsive and unresponsive units (mean value of both groups of units was 0.26 ± 0.20, SD). The higher the CV, reflecting a more irregular unit discharge, the lower the mean background discharge (paired rank, $P < 0.001$; $n = 68$). *Inset*: distribution of resting discharge of the general population of lVS neurons (*white columns*, $n = 136$) and the population of units illustrated in the main graph (*shaded columns*, $n = 68$). Responsive and unresponsive units were located in the dcLVN or in the rvLVN

standard deviation interval of the examined spike trains. The variability of the resting discharge of these units, as measured by the coefficient of variation (CV), ranged from 0.12 to 2.28 and averaged 0.56 ± 0.49, SD ($n = 108$). These findings should be compared with those obtained from lVS neurons previously recorded in decerebrate cats after ablation of the paleocerebellum [16]. In these experiments, in which 41 units responded to standard parameters of roll tilt, while the remaining 27 units were unresponsive, the CV ranged from 0.078 to 1.09 and averaged 0.26 ± 0.20, SD ($n = 68$). As a result of these findings the proportion of units showing a CV higher than 0.575 was much higher in the present experiments (35/108, i.e. 32.4%) than in partially cerebellectomized animals (6/68, i.e. 8.8%).

A prominent negative correlation was found between the CV of the spike train and the mean resting discharge rate; in fact, the higher the CV, reflecting a more irregular unit discharge, the lower was the mean background discharge (Fig. 1A, paired rank, $P < 0.001$; $n = 108$). Similar results were also obtained for the two populations of units responsive ($n = 68$) and unresponsive ($n = 40$) to vestibular stimulation. The less prominent negative relation between CV and mean resting discharge rate of lVS neurons, previously recorded after partial cerebellectomy, is shown for comparison (Fig. 1B, paired rank, $P < 0.001$; $n = 68$).

Across the whole population of antidromically identified lVS units ($n = 129$) the axonal conduction velocity varied in an unimodal fashion from 33.8 to 124.8 m/s, with an average value of 90.0 ± 21.5, SD, m/s. Moreover, the antidromic units responsive to vestibular stimulation showed on the average a faster conduction velocity than the unresponsive ones (93.4 ± 19.1, SD, m/s, $n = 76$ against 85.2 ± 23.9, SD,

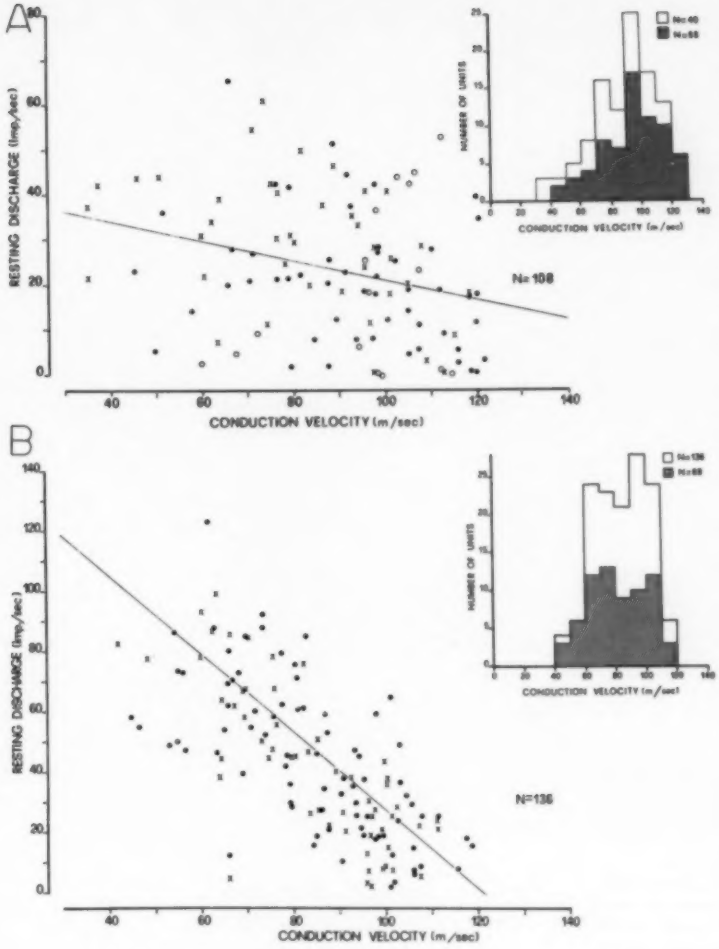

Fig. 2
Relation between resting discharge rate (measured in impulses per second) of lVS neurons and conduction velocity of the corresponding axons in decerebrate cats before (**A**) and after partial cerebellectomy (**B**). **A** the graph shows the data of 108 lVS neurons firing at rest in decerebrate cats with the cerebellum intact. Symbols represent units either responsive (●, ○; $n = 68$) or unresponsive (×, $n = 40$) to roll tilt of the animal of standard parameters; responsive units are indicated by *filled* or *empty circles* if located in the dcLVN or the rvLVN, respectively. A slight negative correlation was found between the unit resting discharge rate and the conduction velocity of the corresponding vestibulospinal axon (paired rank, $P < 0.01$; $n = 108$). Such a negative correlation was also found for the unresponsive units (same test, $P < 0.01$; $n = 40$), but not for the 68 responsive units. *Inset*: distribution of the conduction velocity of the general population of lVS units, including the two groups of 68 responsive (*shaded columns*) and 40 unresponsive units (*white columns*). **B** the graph shows for comparison the data of 136 lVS neurons firing at rest in decerebrate cats after ablation of the cerebellar vermal cortex and fastigial nuclei [6]. Symbols represent units either responsive (●; $n = 80$) or unresponsive (×; $n = 56$) to standard parameters of roll tilt. Responsive and unresponsive units were located in the dcLVN or in the rvLVN. A prominent negative correlation was found between the unit resting discharge rate and the conduction velocity of its axon (paired rank, $P < 0.001$, $n = 136$). Similar correlation was also found for the two populations of responsive (same test, $P < 0.001$; $n = 80$) and unresponsive units (same test, $P < 0.001$; $n = 56$). *Inset*: distribution of the conduction velocity of the general population of lVS units (*white columns*, $n = 136$) and the population of units used to evaluate the CV as illustrated in Fig. 1 B (*shaded columns*, $n = 68$)

m/s, $n = 53$; *t*-test between the means, $P < 0.05$), thus being presumably larger in size. Similar differences were also obtained when considering only the 108 lVS neurons firing at rest, which were either responsive (Fig. 2A, inset, shaded columns) or unresponsive to animal tilt (Fig. 2A, inset, white columns) (93.9 ± 19.3, SD, m/s, $n = 68$ against 80.7 ± 22.8, SD, m/s, $n = 42$; *t*-test, $P < 0.01$).

If we consider now the whole population of responsive and unresponsive neurons which fired at rest, a slight negative correlation was found between the unit resting discharge rate and the conduction velocity of the axons, so that the faster the conduction velocity of its axon, the lower was the unit discharge rate at rest (paired rank, $P < 0.01$; $n = 108$) (Fig. 2A).

Similar results were obtained for the unresponsive units (paired rank, $P < 0.01$; $n = 40$), but not for the responsive units (paired rank, $P > 0.05$; $n = 68$). Interestingly, a negative correlation was found for the total population of dcLVN neurons (paired test, $P < 0.001$; $n = 85$) as well as for the corresponding groups of responsive (same test, $P < 0.05$; $n = 52$) and unresponsive units (same test, $P < 0.01$; $n = 33$); however, no correlation was found with the same test for the total population of rvLVN neurons ($n = 23$) nor for the corresponding groups of responsive ($n = 16$) and unresponsive units ($n = 7$).

The results of these experiments should be compared with those obtained from lVS neurons previously [6] recorded in decerebrate cats after ablation of the paleocerebellum (Fig. 2B).

Gain and sensitivity. Of the 129 lVS neurons, 76 displayed a reliable periodic modulation of their firing rate during sinusoidal tilt of the animal at the standard parameters: among these units, 68 had a spontaneous discharge (see Fig. 2A, ● and ○) and 8 were silent at rest. The remaining 53 units were classified as unresponsive to the stimulus: among these units 42 fired at rest (but for two of them the resting discharge was not recorded) (see Fig. 2A, ×), while 11 were silent.

The gain of the labyrinth response ranged from 0.04 to 2.01 and averaged 0.47 ± 0.44, SD, impulses $\cdot$ s^{-1} $\cdot$ deg^{-1} ($n = 76$). No significant correlation was found across the population of units ($n = 68$) between the gain and either the resting discharge rate (Fig. 3A) or the axonal conduction

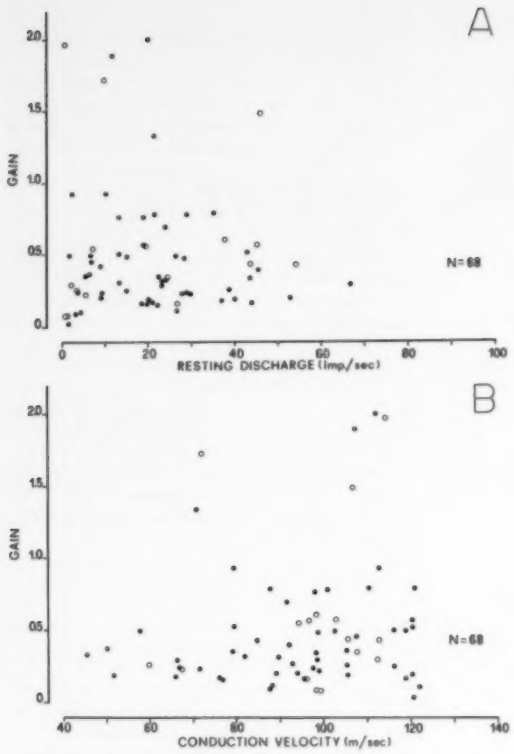

Fig. 3A,B. Relations between resting discharge rate (measured in impulses per second) or conduction velocity of axons and the response gain of lVS neurons to sinusoidal stimulation of labyrinth receptors at standard parameters in decerebrate cats. Among the 68 antidromically identified lVS neurons responsive to roll tilt of the animal at standard parameter, 52 neurons indicated by *filled circles* were located in the dcLVN and 16 neurons indicated by *empty circles* were located in the rvLVN. No significant correlation was found between resting discharge rate and the response gain in **A** (paired rank, $P < 0.05$), nor between conduction velocity of axons and the response gain in **B** (same test, $P > 0.05$). Negative results were also obtained if one considered not only the total population of lVS neurons, but also the two populations of dcLVN and rvLVN neurons separately

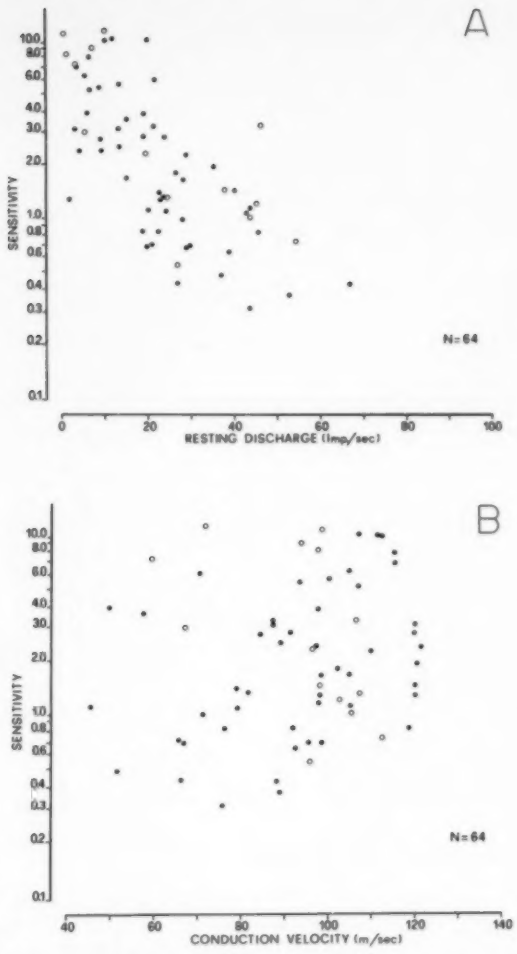

Fig. 4A,B. Relations between resting discharge rate (measured in impulses per second) or conduction velocity of axons and the response sensitivity of lVS neurons to sinusoidal stimulation of labyrinth receptors at standard parameters in decerebrate cats. Among the 64 antidromically identified lVS neurons responsive to roll tilt of the animal at standard parameters, 50 neurons indicated by *filled circles* were located in the dcLVN and 14 neurons indicated by *empty circles* were located in the rvLVN. Four lVS units responding to labyrinth stimulation could not be used for the evaluation of the sensitivity, because they showed a cutoff of their response. **A** a negative correlation was found between resting discharge rate and the response sensitivity (paired rank, $P < 0.001$). A negative correlation was also found for both the dcLVN neurons (same test, $P < 0.001$) and the rvLVN neurons (same test, $P < 0.01$). **B** positive correlation between conduction velocity of axons and the response sensitivity of the dcLVN neurons (same test, $P < 0.01$); however, no correlation was found with the same test for the rvLVN neurons as well as for the whole population of tested neurons

velocity (Fig. 3B). Moreover, units were recorded from the same or different experiments which had a comparable conduction velocity, but showed a different gain.

For the population of units which displayed a background discharge at rest and did not show a cutoff of their response to animal tilt, the sensitivity of responses ranged from 0.31 to 11.66 and averaged 3.24 ± 3.15, SD, %/deg ($n = 64$). Figure 4 illustrates the relation between the response sensitivity and other physiological properties. Units displaying a greater percentage of modulation during roll tilt had in general: i) a lower background discharge (Fig. 4A, paired rank, $P < 0.001$; $n = 64$) and thus a larger variability of instantaneous firing rate as monitored by the coefficient of variation (same test, $P < 0.001$; $n = 64$), and ii) a faster conduction velocity of their axons (Fig. 4B). In this instance, however, the positive relation between conduction velocity of axons and response sensitivity was found only for the dcLVN neurons which represented the predominant population of neurons (same test, $P < 0.01$; $n = 50$), but neither for the 14 rvLVN neurons nor for the two groups of cells taken together. This finding should be related to the fact that a slight but significant negative relation between resting discharge and axonal conduction velocity was found only among the dcLVN neurons.

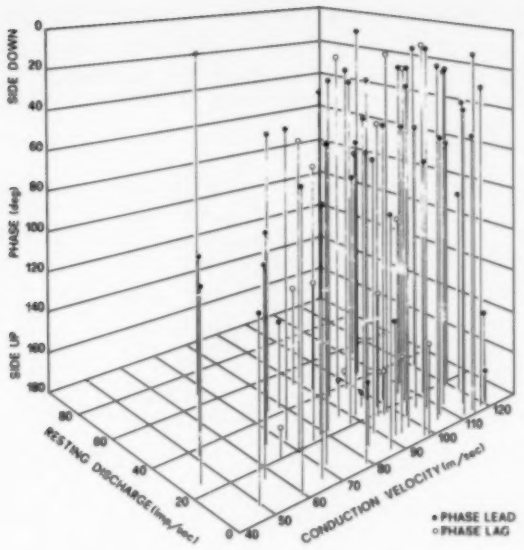

Fig. 5. Three-dimensional diagram relating resting discharge rates (measured in impulses/s), conduction velocities of axons and phase angles of response of 68 lVS neurons to sinusoidal stimulation of labyrinth receptors at standard parameters in decerebrate cats. The relation between resting discharge rate (x axis), conduction velocity of axons (z axis) and phase angle of labyrinth response (y axis) for each unit is shown. Phase angles are relative to peak of side-down displacement of the animal (indicated by 0°) and symbols represent either a phase lead (●, $n = 52$) or a phase lag (○, $n = 16$) from 0°. *Large vertical bars* refer to units excited during side-down tilt, whereas *small bars* refer to units excited during side-up tilt; for these last units *empty circles* actually indicate a phase lead of the response with respect to the extreme side-up animal position

Phase angle. As reported in a previous study [36], a large proportion of lVS units displayed a peak firing rate during side-down tilt ipsilateral to the recording side (α-responses, phase angle ranging from +75° to −45°; $n = 51$), while a smaller proportion of units reached a peak of modulation during side-up tilt (β-responses, phase angle ranging from +135° to −105°; $n = 15$). The remaining 10 unit responses laid outside the two main groups (intermediate responses). The phase angle of the two populations of lVS neurons showing α- and β-responses corresponded on the average to a lead of $+21.0 \pm 27.2$, SD, deg with respect to the extreme animal displacements.

The relationships between resting discharge rate, conduction velocity and phase relation are illustrated in Fig. 5 (see Table 1 for details). The units indicated by long vertical lines (α-responses), although more numerous, were not distinguishable from those displaying the β-response pattern (short vertical lines) in so far as they covered the whole range of resting discharge (and base frequency) as well as the whole spectrum of conduction velocity; moreover, the mean values of these parameters relative to the two populations of units were not significantly different.

The gain as well as the sensitivity of the units showing α-responses were higher than those displaying β-responses, but only the difference in gain was significant (t-test, $P < 0.05$). If we compared, however, the average gain and sensitivity of the units showing α-responses (0.57 ± 0.49, SD, impulses · s^{-1} · deg^{-1} and 3.94 ± 3.32, SD, %/deg) with the corresponding values obtained from the two remaining populations of units showing β- and intermediate responses (0.27 ± 0.17, SD, impulses · s^{-1} · deg^{-1} and 1.98 ± 2.40, SD, %/deg), the differences not only in gains but also in sensitivities became significant (t-test, $P < 0.01$ and $P < 0.02$ for differences in gain and sensitivity, respectively). It is of interest that the response characteristics of the units showing intermediate phase angle of their responses corresponded to those of the units showing a β-pattern of response (see Table 1).

Unit responses to neck rotation

Resting discharge activity and conduction velocity of lateral vestibulospinal neurons. Among the 129 lVS neurons described above, 109 were also examined during neck rotation at the standard parameters. In particular, 95 out of these 109 neurons fired spontaneously and exhibited a discharge rate at rest which averaged 23.5 ± 16.1, SD impulses/s, while the remaining 14 units were silent. The resting discharge rate was on the average lower for the lVS neurons responsive to neck stimulation (21.9 ± 16.5, SD, impulses/s, $n = 70$) than for the unresponsive units (27.8 ± 14.0, SD, impulses/s, $n = 25$); however, the difference was not statistically significant. Similar results were obtained for the base frequency.

The negative correlation found between CV and the resting discharge of the units tested to vestibular stimulation (Fig. 1) also held true for the population of units tested to neck stimulation.

Across the whole population of antidromically identified lVS neurons tested to neck rotation ($n = 109$) the axonal conduction velocity varied in a unimodal fashion from 37.1 to 124.8 m/s with an average value of 89.8 ± 21.0, SD, m/s; similarly to what observed for the units responsive to animal tilt, those responsive to neck rotation showed on the average a faster conduction velocity than the unresponsive ones (91.6 ± 19.7, SD, m/s, $n = 75$, against 85.4 ± 23.2, SD, m/s, $n = 34$). The difference, however, was not statistically significant (t-test between the means, $P > 0.05$), but it became so if we limited the analysis to the lVS neurons firing at rest ($n = 95$), which were either responsive or unresponsive to neck rotation (92.2 ± 19.7, SD, m/s, $n = 70$, against 80.7 ± 20.2, SD, m/s, $n = 25$; t-test between the means, $P < 0.02$).

As for the units tested to vestibular stimulation, a slight negative correlation was found between the resting discharge rate of the whole population of responsive and unresponsive neurons and the conduction velocity of the axons so that the faster the conduction velocity of the axon, the lower was the unit discharge rate at rest (paired rank, $P < 0.01$; $n = 95$). This correlation was significant for the responsive units (paired rank, $P < 0.01$; $n = 70$) but not for the unresponsive units (paired rank, $P > 0.05$; $n = 25$). As shown for the labyrinth responses, a good negative correlation was found for the total population of dcLVN neurons (paired rank, $P < 0.001$; $n = 74$) as well as for the corresponding groups of responsive (same test, $P < 0.001$; $n = 55$) and unresponsive units (same test, $P < 0.05$; $n = 19$); however, no correlation was found with the same test for the total population of rvLVN neurons ($n = 21$) nor for the corresponding groups of responsive ($n = 15$) and unresponsive units ($n = 6$).

Table 1. Response characteristics of antidromic lVS neurons showing different patterns of response to sinusoidal stimulation of labyrinth and neck receptors (at 0.026 Hz, ± 10°)

Phase angle of responses	Number of responsive (R) units	Conduction velocity of R-units	Resting discharge rate of R-units	Base frequency of R-units	Gain of R-units	Sensitivity of R-units	Phase angle of R-units
Labyrinth input							
From +75° to −45°	51 (67.1%)	94.9 ± 17.6	19.5 ± 14.9 $n = 45$	18.1 ± 15.3	0.57 ± 0.49	3.94 ± 3.32 $n = 41$	+ 25.0 ± 23.8°
From +135° to −105°	15 (19.7%)	96.1 ± 15.5	25.3 ± 17.6 $n = 14$	24.1 ± 18.3	0.26 ± 0.19	1.97 ± 2.77 $n = 14$	−172.6 ± 33.9°
From +75° to +135° and from −45° to −105°	10 (13.2%)	81.3 ± 27.6	24.3 ± 14.9 $n = 9$	23.8 ± 17.4	0.29 ± 0.13	2.00 ± 1.82 $n = 9$	
Total population	76	93.4 ± 19.1	21.3 ± 15.4 $n = 68$	20.0 ± 16.2	0.47 ± 0.44	3.24 ± 3.15 $n = 64$	
Neck input							
From +90° to −15°	8 (10.7%)	89.4 ± 11.2	25.6 ± 17.3 $n = 7$	22.9 ± 17.8	0.34 ± 0.32	1.57 ± 1.54 $n = 6$	+ 55.9 ± 21.0°
From +165° to −90°	59 (78.6%)	91.7 ± 20.9	21.1 ± 16.4 $n = 55$	20.8 ± 17.6	0.53 ± 0.43	3.66 ± 3.54 $n = 49$	−128.5 ± 18.1°
From +90° to +165° and from −15° to −90°	8 (10.7%)	93.5 ± 18.7	24.6 ± 18.3 $n = 8$	25.9 ± 18.2	0.26 ± 0.14	2.36 ± 3.43 $n = 8$	
Total population	75	91.6 ± 19.7	21.9 ± 16.5 $n = 70$	21.6 ± 17.6	0.49 ± 0.40	3.30 ± 3.42 $n = 63$	

Abbreviations: Resting discharge rate, mean firing rate in impulses/s recorded in the absence of movement; base frequency, mean firing rate in impulses/s evaluated during sinusoidal tilt of the animal or neck rotation at standard parameters (0.026 Hz, ± 10°); gain of the first harmonic, change of the mean firing rate per degree of displacement (impulses · s^{-1} · deg^{-1}); sensitivity of the first harmonic, percentage change of the mean firing rate per degree (%/deg); phase angle of the first harmonic, in degrees of phase lead (positive values) or phase lag (negative values) with respect to the side-down animal or neck displacement; conduction velocity of axons, in m/s. For each of these parameters, the mean ± SD is given. Figures in parentheses are percentages. The numbers of units used for the evaluation of the resting discharge and the sensitivity are slightly lower than those of the total populations of "responsive units", due to silent or slowly discharging neurons whose resting discharge rate was close to 0 and whose sensitivity could not be evaluated due to a cutoff of their response

Gain and sensitivity. Of the 109 lVS neurons, 75 lVS neurons displayed a reliable periodic modulation of their firing rate to neck rotation at the standard parameters; among these units 70 had a spontaneous discharge and 5 were silent at rest. The remaining 34 units were unresponsive to neck rotation; among these units 25 showed a spontaneous firing at rest, while 9 were silent.

The average gain of neck responses was 0.49 ± 0,40, SD, impulses · s^{-1} · deg^{-1} (range 0.03 − 1.96, impulses · s^{-1} · deg^{-1}, $n = 75$) and the average sensitivity was 3.30 ± 3.42, SD, %/deg (range 0.24 − 13.32 %/deg, $n = 63$). No correlation was observed across the population of units ($n = 70$) between the gain of unit responses and either the resting discharge rate (Fig. 6A) or the conduction velocity of axons (Fig. 6B). Moreover, units were found in the same or in different experiments which had the same conduction velocity but a different gain.

The relation between the response sensitivity and other physiological properties of the units are illustrated in Fig. 7. Units with a greater sensitivity to neck rotation displayed in general: i) a lower background discharge (Fig. 7A, paired rank, $P < 0.001$; $n = 63$) and thus a larger variability of instantaneous firing rate as monitored by the coefficient of variation (same test, $P < 0.001$; $n = 63$), and ii) a faster conduction velocity of their axons (Fig. 7B, same test, $P < 0.01$; $n = 63$).

Phase angle. As shown in a previous study [36], the majority of lVS neurons were excited during side-up neck rotation (phase angle ranging from +165° to −90°; $n = 59$), while fewer units were excited during neck rotation in the opposite direction (phase angle ranging from +90° to −15°; $n = 8$). The remaining 8 unit responses laid outside the two main populations. The phase angle of the lVS units excited during side-up or side-down neck rotation corresponded on the average to a lead of +52.0 ± 18.3, SD, deg with respect to the extreme neck displacements. This lead was higher than that obtained for the labyrinth responses. The two populations of responsive units reported above covered the whole range of resting discharge (and base frequency) as well as the whole spectrum of conduction velocity; moreover, no differences in the mean resting discharge (and base frequency) and conduction velocity were observed. The gain as well as the sensitivity of the units excited during side-up neck rotation were on the average higher than those of the units displaying the opposite response pattern, but the differences were not statistically significant, probably because the sampling of the units excited during side-down neck rotation was too small (see Table 1 for details). However, if we compared the average gain and sensitivity of the units excited during side-up neck rotation (0.53 ± 0.43, SD, impulses · s^{-1} · deg^{-1} and 3.66 ± 3.54, SD, %/deg) with the corresponding values obtained from the two remaining populations of units which where either excited during side-down neck rotation or showed intermediate responses (0.30 ± 0.24, SD, impulses · s^{-1} · deg^{-1} and 2.02 ± 2.72, SD, %/deg), the differences in gains, but not in sensitivities, became statistically significant (*t*-test, $P < 0.05$). It is of in-

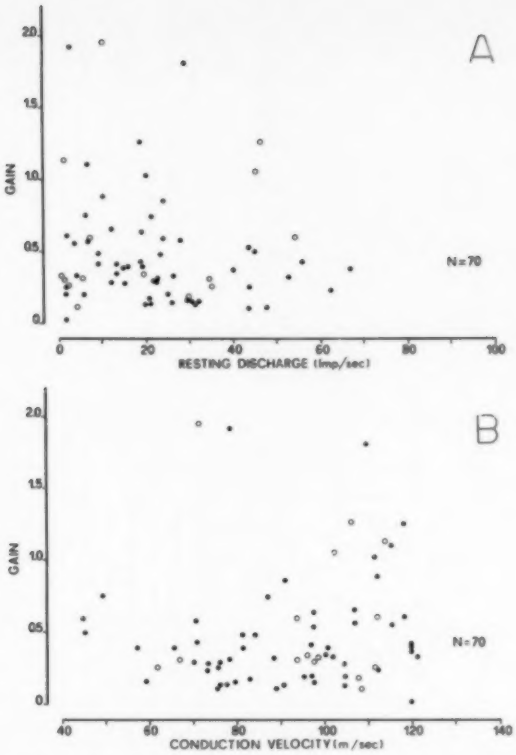

Fig. 6 A, B. Relations between resting discharge rate (measured in impulses/s) or conduction velocity of axons and the response gain of IVS neurons to sinusoidal stimulation of neck receptors at standard parameters in decerebrate cats. Among the 70 antidromically identified IVS neurons responsive to neck rotation at standard parameters, 55 neurons indicated by *filled circles* were located in the dcLVN and 15 neurons indicated by *empty circles* were located in the rvLVN. No significant correlation was found between resting discharge rate and the response gain in **A** (paired rank, $P > 0.05$) nor between conduction velocity of axons and the response gain in **B** (same test, $P > 0.05$). Negative results were also found if one considered not only the total population of IVS neurons but also the two populations of dcLVN and rvLVN neurons, separately

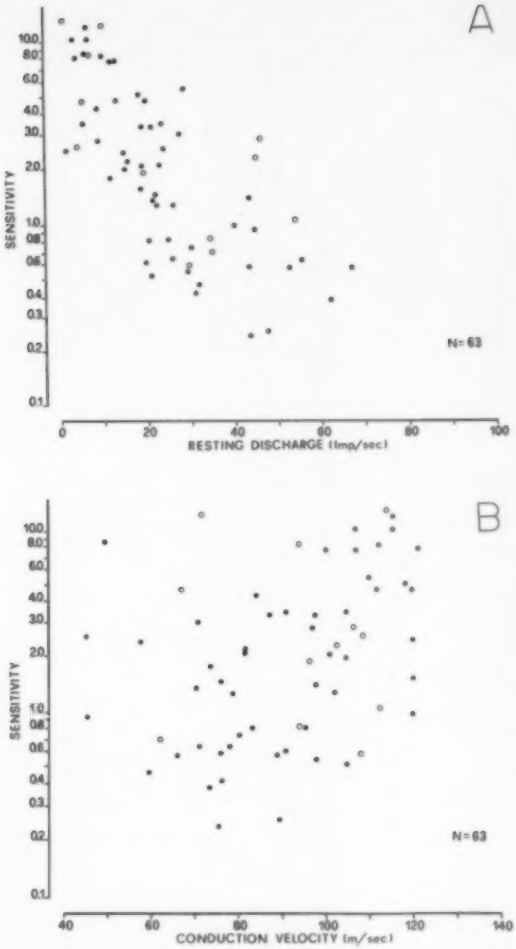

Fig. 7 A, B. Relations between resting discharge rate (measured in impulses/s) or conduction velocity of axons and the response sensitivity of IVS neurons to sinusoidal stimulation of neck receptors at standard parameters in decerebrate cats. Among the 63 antidromically identified IVS neurons responsive to neck rotation at standard parameters, 51 neurons indicated by *filled circles* were located in the dcLVN and 12 neurons indicated by *empty circles* were located in the rvLVN. Seven IVS units responding to neck rotation could not be used for the evaluation of the sensitivity because they showed a cutoff of their response. **A** negative correlation between resting discharge rate and the response sensitivity (paired rank, $P < 0.001$). A negative correlation was also found for both the dcLVN neurons (same test, $P < 0.001$), and the rvLVN neurons (same test, $P < 0.02$). **B** positive correlation between conduction velocity of axons and the response sensitivity (same test, $P < 0.01$). A positive correlation was also found with the same test for the dcLVN neurons (same test, $P < 0.001$) but not for the rvLVN neurons (same test, $P > 0.05$)

terest that the response characteristics of the units showing intermediate phase angle of their responses were similar to those of the units excited during side-down neck rotation (see Table 1).

Comparison of the unit responses to vestibular and neck stimulations. No significant differences in the mean values of resting discharge rate, base frequency, conduction velocity, gain and sensitivity were found between all the units responsive to the labyrinth ($n = 76$) and neck ($n = 75$) inputs as shown in Table 1.

A more detailed comparison of the unit responses to labyrinth and neck stimulations was obtained by subdividing the recorded IVS neurons into two groups according to their axonal conduction velocity (either $\leqslant 90$ m/s, slow units or > 90 m/s, fast units). As expected from the results of the previous sections, the resting discharge rate (and base frequency) was significantly higher for the slow than for the fast vestibulospinal units; this held true for the total populations of IVS units tested to vestibular stimulation and to neck stimulation (including both responsive and unresponsive neurons), as well as for the IVS units which were either unresponsive to labyrinth or responsive to neck stimulation. This difference, however, was not found for

Table 2. Effects of sinusoidal stimulation of labyrinth and neck receptors (at 0.026 Hz, ± 10°) on the act

	Number of responsive (R) units	Conduction velocity of R-units	Resting discharge rate of R-units		Base frequency of R-units		Gain of R-u
Labyrinth input							
Responsive units							
⩽ 90 m/s	26	71.6 ± 12.8	22.9 ± 16.4	n.s.	23.1 ± 17.8	n.s.	0.41 ± 0.39
			$n = 24$				
> 90 m/s	50	104.7 ± 9.6	20.4 ± 15.0		18.5 ± 15.3		0.51 ± 0.46
			$n = 44$				
Unresponsive units							
⩽ 90 m/s	24	65.4 ± 17.4	35.8 ± 13.3	$P < 0.01$	37.8 ± 14.5	$P < 0.01$	
			$n = 23$				
> 90 m/s	18	101.2 ± 8.3	22.0 ± 13.0		22.1 ± 13.1		
			$n = 17$				
Total population							
⩽ 90 m/s	50	68.6 ± 15.4	29.2 ± 16.2	$P < 0.01$	30.1 ± 17.7	$P < 0.001$	
			$n = 47$				
> 90 m/s	68	103.8 ± 9.4	20.9 ± 14.4		19.4 ± 14.7		
			$n = 61$				
Neck input							
Responsive units							
⩽ 90 m/s	31	71.7 ± 11.9	28.6 ± 17.3	$P < 0.01$	28.4 ± 19.2	$P < 0.01$	0.45 ± 0.43
			$n = 29$				
> 90 m/s	44	105.7 ± 9.1	17.2 ± 14.4		16.8 ± 14.7		0.51 ± 0.39
			$n = 41$				
Unresponsive units							
⩽ 90 m/s	15	68.5 ± 16.5	29.0 ± 16.2	n.s.	29.4 ± 14.7	n.s.	
> 90 m/s	10	98.9 ± 7.1	26.0 ± 10.6		28.5 ± 10.5		
Total population							
⩽ 90 m/s	46	70.7 ± 13.5	28.7 ± 16.7	$P < 0.01$	28.7 ± 17.7	$p < 0.01$	
			$n = 44$				
> 90 m/s	54	104.4 ± 9.1	18.9 ± 14.1		19.0 ± 14.7		
			$n = 51$				

Abbreviations as in Tables 1. Resting discharge rate, base discharge frequency, gain, sensitivity and phase ar
velocity of axons ⩽ 90 m/s) and the fast units (conduction velocity of axons > 90 m/s). For each of these pa
of the resting discharge and the sensitivity are slightly lower than those of the total populations of tested
was close to 0 and whose sensitivity could not be evaluated due to a cutoff of their response. Moreover, the re
input was not evaluated, so that they were disregarded. Notice that among the total population of 129 IVS
which were silent at rest were not included in the table. Moreover among the 109 IVS units tested to neck st
disregarded. n.s., no significant difference (*t*-test)

he activity of slow and fast lateral vestibulospinal neurons

of R-units		Sensitivity of R-units		Phase angle of R-units		
				Side-down	Side-up	Intermediate
± 0.39 ↑	n.s.	2.54 ± 2.77 ↑	n.s.	+31.4 ± 25.4	+175.4 ± 37.2	
		$n = 23$		$n = 16$	$n = 5$	$n = 5$
± 0.46 ↓		3.63 ± 3.31 ↓		+22.1 ± 22.9	−166.6 ± 32.4	
		$n = 41$		$n = 35$	$n = 10$	$n = 5$
± 0.43 ↑	n.s.	2.13 ± 2.72 ↑	$P < 0.02$	+56.5 ± 30.7	−130.2 ± 19.4	
		$n = 28$		$n = 4$	$n = 25$	$n = 2$
± 0.39 ↓		4.23 ± 3.67 ↓		+55.4 ± 8.9	−127.2 ± 17.2	
		$n = 35$		$n = 4$	$n = 34$	$n = 6$

ase angle are given for the two populations of responsive units, the slow (conduction ese parameters the mean ± SD is given. The numbers of units used for the evaluation ested units, due to silent or slowly discharging neurons whose resting discharge rate the resting discharge rate of two units (1 slow and 1 fast) "unresponsive" to labyrinth 9 IVS units tested to labyrinth stimulation, 11 unresponsive units (1 slow and 10 fast) eck stimulation, 9 unresponsive units (2 slow and 7 fast) were silent at rest and were

the remaining populations of IVS units which were either responsive to vestibular or unresponsive to neck stimulation (see Table 2, for *t*-test between the means). These findings differ with those obtained after partial cerebellectomy [6], where the resting discharge rate (and base frequency) was much higher for the slow than for the fast IVS neurons, irrespectively of their responsiveness to the labyrinth or neck input. In particular, if we consider only the units responsive to vestibular stimulation no difference in resting discharge rate was found between the slow and fast IVS neurons recorded in the present experiments; in contrast, the resting discharge rate was much higher for the slow than for the fast IVs neurons after partial cerebellectomy (Fig. 8).

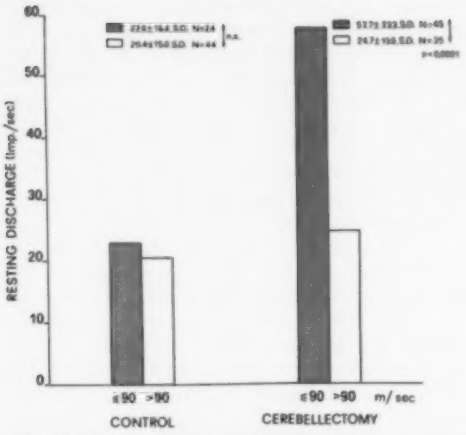

Fig. 8. Effects of partial cerebellectomy on the average resting discharge rate of slow- and fast-conducting IVS neurons responsive to roll tilt of the animal at standard parameters. The conduction velocity of axons of the two populations of LVN neurons ranged between 33.8–90 and 91–124.8 m/s in decerebrate preparations with the cerebellum intact and between 45–90 and 91–118.7 m/s after cerebellectomy [6]. *Striped columns* refer to slow IVS neurons, while *white columns* refer to fast IVS neurons, as recorded either in control experiments or after partial cerebellectomy [6]. The values indicated on the top of the columns refer to the mean resting discharge ± SD of the corresponding populations of neurons. *Arrows* indicate differences of means that are or not statistically significant (*t*-test)

The possibility that in preparations with the cerebellum intact the resting discharge rate of different size IVS neurons is in some way related to their responsiveness to vestibular or neck stimulation was further investigated on a selected population of neurons tested to both vestibular and neck stimulations. Table 3 shows that no differences in resting discharge rate and therefore in base frequency were found between the two populations of small and large size IVS neurons, which received either convergent labyrinth and neck inputs or the labyrinth input only. Conversely, a significant difference in resting discharge rate between slow and fast conducting units was found for the IVS neurons responding only to the neck input. The neurons unresponsive to both inputs also showed the same behaviour; however, the sampling was so small that the result did not reach the significance level. The statement that small size IVS neurons have an higher firing rate than large size neurons can thus apply only to the population of units unresponsive to vestibular stimulation, independently as to whether they receive a neck input. These findings explain why the units which were either unresponsive to animal tilt or responsive to neck rotation showed a significant negative relation between resting discharge rate and conduction velocity of the corresponding axons, whereas the units responsive to animal tilt or unresponsive to neck rotation did not show this correlation.

Observations reported in previous sections indicate that the IVS neurons responsive to animal tilt or neck rotation had on the average a faster conduction velocity than the unresponsive neurons. Table 2 shows that slow and fast units were unequally distributed within the two populations of responsive and unresponsive units. In particular, if we consider the neurons responsive to labyrinth input, it appears that the proportion of fast units (50/76, i.e. 65.8%) pre-

Table 3. Differences in resting discharge rate of slow and fast lateral vestibulospinal neurons classified according to their responsiveness to neck and vestibular stimulations

	Slow units ⩽ 90 m/s		Fast units > 90 m/s		Total population
	Resting discharge rate		Resting discharge rate		
Neurons responsive to both labyrinth and neck inputs	23.4 ± 17.6	$n = 16$	16.8 ± 15.2	$n = 31$	$n = 47$
		n.s.			
Neurons responsive only to the labyrinth input	21.0 ± 15.6	$n = 7$	26.4 ± 7.2	$n = 5$	$n = 12$
		n.s.			
Neurons responsive only to the neck input	36.7 ± 14.5	$n = 12$	18.6 ± 12.2	$n = 10$	$n = 22$
		$P < 0.01$			
Neurons unresponsive to both inputs	35.7 ± 15.0	$n = 7$	25.6 ± 14.2	$n = 12$	$n = 19$
		n.s.			

Resting discharge rate is expressed in impulses/s for the two populations of responsive units, the slow (conduction velocity of axons ⩽ 90 m/s) and the fast units (conduction velocity of axons > 90 m/s). For each population of neurons the mean ± SD is given. n.s., no significant difference (*t*-test)

dominated over the slow units (26/76, i.e. 34.2%), while the opposite occurred among the unresponsive neurons (24/42, i.e. 57.1% slow units and 18/42, i.e. 42.9% fast units) (Yates corrected χ^2, $P < 0.05$). Similarly, if we consider the responses to the neck input, the proportion of fast units (44/75, i.e. 58.7%) predominated over the slow units (31/75, i.e. 41.3%), the opposite being observed among the unresponsive neurons (15/25, i.e. 60.0% slow units and 10/25, i.e. 40% fast units). However, the differences in distribution of the slow and fast units within the two populations of responsive and unresponsive units to neck rotation were not statistically significant.

The gain and the sensitivity of the labyrinth and the neck responses were on the average higher among the fast than among the slow lVS neurons; the differences, however, were statistically significant only between the sensitivity values of the neck responses, probably due to the lower resting discharge of fast conducting units responsive to neck rotation (Table 2).

As to the patterns of unit responses to vestibular and neck stimulations, it appears that the lVS neurons which were excited during side-down or during side-up animal tilt or neck rotation were almost equally distributed between the slow and the fast conducting lVS neurons. In fact, 61.5% slow and 70.0% fast units were excited during side-down animal tilt, while 19.2% slow and 20.0% fast units were excited during side-up animal tilt; moreover 80.6% slow and 77.3% fast units were excited during side-up neck rotation, while 12.9% slow and 9.1% fast units were excited during side-down neck rotation (see Table 2).

As to the phase angle of the units showing α- or β-responses to the labyrinth input, the slow units showed an average phase lead of $+22.8 \pm 31.6$, SD, deg ($n = 21$) with respect to the extreme side-down or side-up animal displacements, which is comparable to the average lead of $+20.2 \pm 25.1$, SD, deg ($n = 45$) found for the fast units (Table 2; see also Fig. 5). As to the phase angle of the unit responses to neck input, the slow units had an average phase lead of $+50.7 \pm 20.7$, SD, deg ($n = 29$) with respect to the extreme side-down or side-up neck rotation; this value is comparable to that displayed by the fast units, which showed an average lead of $+53.1 \pm 16.5$, SD, deg ($n = 38$) with respect to the extreme neck displacements. Slight differences were found among the slow and fast units if we consider separately the units having different patterns of response to animal tilt or neck rotation (Table 2).

Discussion

Relation between cell size and resting discharge of vestibulospinal neurons

In the present study both spontaneous discharge and response properties of lVS neurons to sinusoidal stimulation of macular labyrinth and neck receptors have been related to cell size inferred on the basis of the conduction velocity of their axons. These findings, obtained in decerebrate cats with the cerebellum intact, should then be compared with those obtained in previous experiments in which the medial cortico-nuclear zone of the cerebellum had been bilaterally ablated [6]. This comparison is justified by the facts that in both groups of experiments: 1. only the lVS neurons projecting to the lumbosacral segments of the spinal cord were investigated; 2. the number of identified lVS neurons was comparable ($n = 129$ in the present experiments and $n = 136$ in cerebellectomized animals); 3. the corresponding vestibulospinal axons covered the same range of conduction velocities and had comparable mean values (90.0 ± 21.5, SD, m/s in the present experiments and 84.3 ± 17.1, SD, m/s after cerebellectomy); and finally 4. the majority of these neurons (i.e. 72.7% in both groups of experiments) were histologically located in the dorsocaudal part of Deiters' nucleus (dcLVN), in agreement with the anatomical finding demonstrating the somatotopic organization of the vestibulospinal projection originating from Deiters' nucleus [40].

One of the main results of the present experiments is the demonstration that the resting discharge of the spontaneously firing lVS neurons tested during vestibular stimulation (24.5 ± 15.7, SD, imp/s, $n = 108$) was significantly lower than that obtained in partially cerebellectomized animals (44.1 ± 23.8, SD, imp/s; $n = 136$). In both groups of experiments the recorded lVS neurons formed a continuum between the more regularly discharging units, characterized by an higher firing rate and a low coefficient of variation (CV) and the more irregularly discharging units characterized by a low firing rate and a high CV. However, as expected, the CV obtained in the present study was on the average higher (0.56 ± 0.49, SD) than that obtained in partially cerebellectomized preparations (0.26 ± 0.20, SD), thus reflecting a more irregular unit discharge. In particular, in the preparations with the cerebellum intact the proportion of units showing a CV above 0.575 was higher than that previously obtained in cerebellectomized animals (32.4% instead of 8.8%) (compare Fig. 1 A with Fig. 1 B).

These characteristics of resting discharge and CV of the lVS neurons tested to labyrinth stimulation indicate that the cerebellar vermis of the anterior lobe exerts a tonic inhibitory influence on lVS neurons. This hypothesis is supported by the fact that most of the units recorded in the two groups of experiments were located in the dcLVN, i.e. in the vestibular nuclear region which represents the main area of termination of the direct corticocerebellar vestibular projection [cf. 18] and receives the inhibitory influence of the corresponding Purkinje cells [1, 2, 22, 30–33]. The possibility that this tonic inhibitory influence is more prominent on the lVS units responsive to standard parameters of animal tilt than on the unresponsive units is supported by the fact that in the present preparations with the cerebellum intact the former population of units displayed on the average a lower resting discharge rate (21.3 ± 15.4, SD, imp/s) than the latter one (29.9 ± 14.7, SD, imp/s), a finding which did not occur when the cerebellar influence was removed. Similar results were also found for the population of lVS neurons tested to neck rotation.

An additional finding which emerges from the present experiments is that a slight negative correlation occurred between the resting discharge of all the recorded lVS neurons and the conduction velocity of the corresponding axons, so that the faster the conduction velocity the lower was the unit discharge rate at rest (paired rank, $P < 0.01$; Fig. 2 A). This correlation involved particularly the neurons located in the dcLVN, where the majority of the antidromically identified lVS units were located, and included both groups of units responsive and unresponsive to standard parameters of animal tilt and neck rotation. However, no correlation was found for the total population of rvLVN neurons responsive and unresponsive to labyrinth and neck stimulation. These findings differ from those obtained after

partial cerebellectomy [6], where a prominent negative correlation was found between resting discharge and conduction velocity of all the lVS units responsive to standard parameters of animal tilt and neck rotation (paired rank, $P < 0.001$; Fig. 2B). In these instances the lVS neurons discharging regularly at high rate were characterized by a slower conduction velocity of their axons (smaller neurons), while the units discharging irregularly at low rate by a faster conduction velocity (larger neurons).

If we assume that the excitatory pathways responsible for the background discharge of the LVN neurons are homogeneously distributed among the different size lVS neurons, thus making an equal number of synaptic contacts with different size lVS neurons, then the results described above in cerebellectomized animals could be in agreement with the "size principle" which states that the smaller the size of the neurons, the higher is the input resistance, so that the lower is the threshold and the more effective is the corresponding input in exciting them [26, 47]. In these instances the excess of excitation exerted by the afferent volleys impinging on the lVS neurons in the animal at rest would be smaller in large-sized vestibulospinal neurons, since they fired at lower rate, than in small-sized vestibulospinal neurons, which fired at higher rate.

The reduced slope of the regression line relating the resting discharge of the VS neurons to the conduction velocity of the corresponding axon in the present experiments with the cerebellum intact with respect to the cerebellectomized preparations [6] may depend on the fact that in the former preparations the small size lVS neurons are subjected to a prominent tonic inhibitory influence of the cerebellum, thus firing at a lower rate, in contrast to the large size lVS neurons whose resting discharge was on the average comparable to that obtained after cerebellar ablation (see Fig. 8). In other words the lower resting discharge rate of the small size lVS neurons in the present experiments with respect to the cerebellectomized preparations can be attributed to a greater inhibitibility which affects this population of neurons as a result of the tonic discharge of the related Purkinje cells.

If the distribution of the corticocerebellar inhibition within the LVN were largely uniform and independent of cell size, as postulated for the distribution of the excitatory synapses responsible for the resting discharge in the animal at rest, one would expect that large neurons with their small safety margin would be more sensitive to corticocerebellar inhibition than small neurons; the greater safety margin of the latter would in fact protect them against corticocerebellar inhibition. The situation would then be comparable to that postulated for the distribution of recurrent inhibition within a motor nucleus, which also could be independent of cell size [15, 27–29], an hypothesis supported by the fact that in experiments of ventral root stimulation large motoneurons appeared to be more susceptible to recurrent inhibition of stretch-evoked responses than smaller neurons [15, 27; cf. 38]. Unfortunately electrical stimulation of ventral roots does not represent an appropriate tool to investigate Renshaw cell circuitry, since antidromic stimulation affects Renshaw cells driven by both agonistic and antagonistic motoneurons. Thus, mutual interactions among different populations of Renshaw cells can hardly be avoided [39].

In contrast with the hypothesis reported above, we found that in our experiments small size lVS neurons were apparently more sensitive to corticocerebellar inhibition than large size neurons. This finding is compatible with the results of recent experiments, showing that Renshaw cells anatomically linked with extensor motoneurons and orthodromically activated during vibration of the homonymous muscle, produced a more prominent recurrent inhibition on small motoneurons than on large motoneurons [48]. Moreover, experiments of intracellular recording demonstrated that recurrent inhibitory postsynaptic potentials were generally larger in slow twitch than in fast twitch motoneurons [23].

The great suspectibility of the small size lVS neurons to corticocerebellar inhibition with respect to large size neurons can in part be explained by differences in the input resistance of different size lVS neurons, as shown for the motoneurons [cf. 14]. There is in fact evidence that in small tonic motoneurons, that have higher input resistance than larger motoneurons [34], the same inhibitory input may elicit larger inhibitory post-synaptic potentials [21, 35]. An additional possibility, however, is that the Purkinje cells of the cerebellum make an higher number and density of inhibitory synaptic contacts on small size lVS neurons which counteract the excess of input excitation, in contrast to the large size lVS neurons, where the number and density of inhibitory synaptic contacts are apparently unable, in the animal at rest, to overcome the weak excitatory input impinging upon them. Moreover, the inhibitory synapses could be located closer to the cell body and/or proximal dendrites of small size than of large size neurons.

It is of interest that in the present experiments slow-conducting lVS neurons of comparable size, although firing at low rate, showed different discharge rates. This finding suggested that the corticocerebellar inhibitory influence on neuronal discharge did not equally affect the small-size lVS neurons, in analogy with the observation that the firing rate of small-size motoneurons can also be differentially affected by an inhibitory segmental input [24, 48]. The observation, however, that slow conducting lVS neurons of comparable size did not show the same discharge rates in cerebellectomized cats [6] indicates that even the excitatory input is not apparently homogeneously distributed among the same population of small size lVS neurons. These considerations demonstrate how difficult is to evaluate in the present experiments the relative role that the excitatory and inhibitory pathways exert in determining the resting discharge of a given population of lVS neurons.

A final comment concerns the fact that in decerebrate cats with the cerebellum intact, the difference in firing rate between small- and large-sized lVS neurons involved particularly the units unresponsive to vestibular stimulation, while those receiving a vestibular input fired irrespectively of their cell size. Interestingly, each of these neuronal populations consisted of units which were either affected or not affected by neck rotation (see Table 3). These findings explain why the units unresponsive to vestibular or responsive to neck stimulation showed a slight negative correlation between resting discharge and conduction velocity of the corresponding axons. However, after partial cerebellectomy, a prominent negative correlation was found between resting discharge and conduction velocity of the lVS units, independently on their responsiveness to animal tilt or neck rotation [6]. All these findings taken together indicate that the inhibitory influence exerted by the cerebellum on small sizes lVS neurons is particularly stronger on units responsive to vestibular than to neck stimulation.

Relation between cell size and response characteristics of vestibulospinal neurons to labyrinth and neck inputs

Let us examine now the responses of different size lVS neurons to dynamic stimulation of macular labyrinth receptors [41, 44] and neck (joint and muscle spindle) receptors [16, 17, 37, 42, 43] and compare the results obtained in preparations with the cerebellum intact with those obtained after partial cerebellectomy.

The proportions of lVS neurons responsive to standard parameters of animal tilt (58.9%) and neck rotation (68.8%) in the present experiments were almost comparable with those obtained in our previous study after cerebellectomy for both labyrinth (58.8%) and neck responses (50.6%). Moreover, the gains of these unit responses, which are similar in the present experiments with the cerebellum intact (0.47 ± 0.44, SD, impulses $\cdot s^{-1} \cdot deg^{-1}$ for the labyrinth responses and 0.49 ± 0.40, SD, impulses $\cdot s^{-1} \cdot deg^{-1}$ for the neck responses), closely corresponded to the values obtained after removal of the cerebellum (0.48 ± 0.41, SD, impulses $\cdot s^{-1} \cdot deg^{-1}$ and 0.40 ± 0.36, SD, impulses $\cdot s^{-1} \cdot deg^{-1}$, respectively). These findings seem to indicate that at least in decerebrate animals the cerebellum is not very effective in modifying the average responsiveness nor the amplitude of modulation, i.e. the gain of the lVS neurons to animal tilt and to some extent also to neck rotation.

As to the response patterns of the lVS neurons to labyrinth and neck stimulation, it appeared that both in the present experiments as well as after partial cerebellectomy [6] the majority of the units were either excited during side-down or during side-up animal tilt and neck rotation. However, while in preparations with the cerebellum intact most of the lVS neurons tested to vestibular and neck stimulation were excited during side-down animal tilt (67.1%) and side-up neck rotation (78.6%), after cerebellectomy the proportion of lVS neurons showing these response patterns (26.25% and 46.2%, respectively) decreased in favour of units which displayed the opposite ones [6][1]. These data indicate that the cerebellum intervenes in determining the response patterns of lVS neurons to animal tilt and a lesser extent to neck rotation [cf. also 4, 7].

The demonstration that in preparations with the cerebellum intact as well as after cerebellectomy, a proportion of lVS neurons did not respond to animal tilt and neck rotation excludes that the vestibulospinal neurons projecting to the lumbosacral segments of the spinal cord represent a homogeneous population differing only in cell size. Although in the present study the units responsive to labyrinth and neck inputs displayed on the average a faster conduction velocity (and thus a lower resting discharge) than the unresponsive ones, thus being presumably larger in size, it appears that the two populations of responsive and unresponsive units covered the entire range of conduction velocity and were similarly distributed within the LVN, namely within the dorsocaudal part of the structure. Similar results were also obtained after cerebellectomy [6]. These findings indicate that in both types of preparations there are differences in connectivity of the same afferents which affect the lVS neurons of comparable size.

Obviously, we cannot exclude that the behaviour of the lVS neurons responsive to labyrinth and neck stimulations is in part at least specified by intrinsic neuronal properties related to cell size [8–10, 13, 34, 35].

Strict application of this hypothesis, however, is not supported by the experimental findings. First of all it appears that in the present experiments the response gains of the lVS units displaying the predominant response patterns to vestibular and neck stimulations (i.e. excitation during side-down animal tilt and side-up neck rotation) were on the average significantly higher than those of the units showing the opposite response patterns; however, no differences were found in the average conduction velocity of the corresponding axons and thus in the cell size of these two populations of units. These differences in gains, which were not observed after cerebellectomy [6], suggest that in the intact preparations fibers of the macular vestibular and neck afferent pathways originating from different populations of otolith and neck receptors, having opposite polarization vectors, are not homogeneously distributed among the different size lVS neurons.

Furthermore, if we relate to the cell size the gain of the unit responses to standard parameters of animal tilt and neck rotation independently on their response patterns, it appeared that the corresponding values were slightly although not significantly higher for the large than for the small neurons. This finding suggests that the influence of size on input resistance is cancelled and possibly overwhelmed by the influence of size on the number and density of the synaptic contacts [49], made by the afferent pathways driven during dynamic stimulation of labyrinth and neck receptors. In this way the gain of the responses would be equal for both the small and the large neurons or even higher in the latter ones. An overall increase of synaptic contacts on the cell body and/or proximal dendrites of the large size neurons could also enhance the effectiveness of the vestibular and neck stimulations. The fact that large size lVS neurons did not increase their resting discharge after cerebellectomy does not exclude that the cerebellum might enhance the response gain of these large size neurons; there is in fact evidence that during vestibular or neck stimulation the related Purkinje cells usually discharge 180° out of phase with respect to the vestibulospinal neurons [19, 20], thus contributing to their amplitude of modulation. It is of interest, however, that even after cerebellectomy no acceptable correlation was found between response gain of lVS neurons to animal and neck rotation and conduction velocity of their axons [6].

Whatever are the mechanisms responsible for the response gain, they do not intervene equally in determining the magnitude of response of comparable size vestibulospinal neurons. In particular in the present study, as well as after cerebelloectomy [6], units were recorded from the same or different experiments which had a comparable conduction velocity, i.e. size, but showed a different response gain to labyrinth and neck stimulations.

[1] There were some differences in the phase angle values used in these studies to delimit the main populations of units excited during side-down or side-up animal tilt and neck rotation. These differences, however, were justified by the fact that the responses of the lVS neurons showed, on the average, a more prominent phase lead relative to the extreme animal and neck displacements in the present experiments with the cerebellum intact than in partially cerebellectomized animals [6]. Therefore, a comparison of the results obtained in the two groups of experiments is to some extent acceptable

Acknowledgements. This work was supported by National Institute of Neurological and Communicative Disorders and Stroke Research Grant NS 07685-18 and by a Grant from the Ministero della

Pubblica Istruzione, Roma, Italy. We thank E. Biagetti, U. Corti and Mrs. M. Vaglini for their valuable technical assistance. Dr. A. R. Marchand was supported by a fellowship of the "Fondation Simone et Cino del Duca, Paris" on leave of absence from the Département de Psychophysiologie Générale, Institute de Neurophysiologie et de Psychophysiologie, C.N.R.S., 31 Chemin Joseph-Aiguier, F-13274 Marseille Cédex 2, France.

References

1. Akaike T (1983) Electrophysiological analysis of cerebellar corticovestibular and fastigiovestibular projections to the lateral vestibular nucleus in the cat. Brain Res 272:223–235
2. Akaike T, Fanardjian VV, Ito M, Nakajima H (1973) Cerebellar control of the vestibulospinal tract cells in rabbit. Exp Brain Res 18:446–463
3. Anderson JH, Blancks RHI, Precht W (1978) Response characteristics of semicircular canal and otolith systems in cat. I. Dynamic response of primary vestibular fibers. Exp Brain Res 32:491–507
4. Boyle R, Pompeiano O (1981) Cerebellar influences on the response characteristics of vestibulospinal neurons to sinusoidal tilt. Arch Ital Biol 119:208–225
5. Boyle R, Pompeiano O (1981) Convergence and interaction of neck and macular vestibular inputs on vestibulospinal neurons. J Neurophysiol 45:852–868
6. Boyle R, Pompeiano O (1981) Relation between cell size and response characteristics of vestibulospinal neurons to labyrinth and neck inputs. J Neurosci 1:1052–1066
7. Boyle R, Pompeiano O (1981) Response of vestibulospinal neurons to neck and macular inputs in the presence or absence of the paleocerebellum. Ann NY Acad Sci 374:373–394
8. Burke RE (1967) Motor unit types of cat triceps surae muscle. J Physiol (Lond) 193:141–160
9. Burke RE (1968) Group Ia synaptic input to fast and slow twitch motor units of cat triceps surae. J Physiol (Lond) 196:605–630
10. Burke RE (1968) Firing patterns of gastrocnemius motor units in the decerebrate cat. J Physiol (Lond) 196:631–654
11. Burke RE (1973) On the central nervous system control of fast and slow twitch motor units. In: Desmedt JE (ed) New developments in electromyography and clinical neurophysiology, vol 3. Karger, Basel, pp 69–94
12. Burke RE (1979) The role of synaptic organization in the control of motor unit activity during movement. In: Granit R, Pompeiano O (eds) Progress in brain research, vol 50. Reflex control of posture and movement. Elsevier, Amsterdam, pp 61–67
13. Burke RE, ten Bruggengate G (1971) Electrotonic characteristics of alpha motoneurons of varying size. J Physiol (Lond) 212: 1–20
14. Burke RE, Rudomín P (1977) Spinal neurons and synapses. In: Kandel ER (ed) Handbook of physiology, sect 1: The nervous system, vol I. Cellular biology of neurons, part 1. American Physiological Society, Bethesda, pp 877–944
15. Clamann HP, Gillies ID, Henneman E (1974) Effects of inhibitory inputs on critical firing level and rank order of motoneurons. J Neurophysiol 37:1350–1360
16. Cohen LA (1961) Role of eye and neck proprioceptive mechanisms in body orientation and motor coordination. J Neurophysiol 24:1–11
17. Cooper S, Daniel PM (1963) Muscle spindles in man: their morphology in the lumbrical and the deep muscles of the neck. Brain 80:563–586
18. Corvaja N, Pompeiano O (1979) Identification of cerebellar corticovestibular neurons retrogradely labeled with horseradish peroxidase. Neuroscience 4:507–515
19. Denoth F, Magherini PC, Pompeiano O, Stanojević M (1979) Responses of Purkinje cells of the cerebellar vermis to neck and macular inputs. Pflügers Arch 381:87–98
20. Denoth F, Magherini PC, Pompeiano O, Stanojević M (1980) Responses of Purkinje cells of cerebellar vermis to sinusoidal rotation of neck. J Neurophysiol 43:46–59
21. Eccles JC, Eccles RM, Iggo A, Ito M (1961) Distribution of recurrent inhibition among motoneurones. J Physiol (Lond) 159:479–499
22. Fanardjian VV, Sarkissian VA (1980) Spatial organization of the cerebellar corticovestibular projection in the cat. Neuroscience 5:551–558
23. Friedman WA, Sypert GW, Munson JB, Fleshman JW (1981) Recurrent inhibition in type-identified motoneurons. J Neurophysiol 46:1349–1359
24. Harris DA, Henneman E (1979) Different species of alpha motoneurons in same pool: Further evidence from effects of inhibition on their firing rates. J Neurophysiol 42:927–935
25. Hellon RF (1971) The marking of electrode tip positions in nervous tissue. J Physiol (Lond) 214:12P
26. Henneman E, Mendell LM (1981) Functional organization of motoneuron pool and its inputs. In: Brooks VB (ed) Handbook of physiology, sect 1. The nervous system, vol II: Motor control, part 1. American Physiological Society, Bethesda, Maryland, pp 423–507
27. Henneman E, Somjen G, Carpenter DO (1965) Excitability and inhibitility of motoneurons of different sizes. J Neurophysiol 28:599–620
28. Henneman E, Clamann HP, Gillies ID, Skinner RD (1974) Rank order of motoneurons within a pool: Law of combination. J Neurophysiol 37:1338–1349
29. Hultborn H, Pierrot-Deseilligny E, Wigström H (1978) Distribution of recurrent inhibition within a motor nucleus. Neurosci Lett (Suppl 1):S97
30. Ito M (1972) Cerebellar control of the vestibular neurons: physiology and pharmacology. In: Bródal A, Pompeiano O (eds) Progress in brain research, vol 37. Basic aspects of central vestibular mechanisms. Elsevier, Amsterdam, pp 377–390
31. Itoh M, Yoshida M (1966) The origin the cerebellar-induced inhibition of Deiters neurones. I. Monosynaptic initiation of the inhibitory post-synaptic potentials. Exp Brain Res 2:330–349
32. Ito M, Obata K, Ochi R (1966) The origin of cerebellar-induced inhibition of Deiters neurons. II. Temporal correlation between the trans-synaptic activation of Purkinje cells and the inhibition of Deiters neurons. Exp Brain Res 2:350–364
33. Ito M, Kawai N, Udo M (1968) The origin of cerebellar-induced inhibition of Deiters neurones. III. Localization of the inhibitory zone. Exp Brain Res 4:310–320
34. Kernell D (1966) Input resistance, electrical excitability and size of ventral horn cells in cat spinal cord. Science 152:1637–1640
35. Kuno M (1950) Excitability following antidromic activation in spinal motoneurones supplying red muscles. J Physiol (Lond) 149:374–393
36. Marchand AR, Manzoni D, Pompeiano O, Stampacchia G (1987) Effects of stimulation of vestibular and neck receptors on Deiters neurons projecting to the lumbosacral cord. Pflügers Arch 409:13–23
37. McCouch GP, Deering ID, Ling TH (1951) Location of receptors for tonic neck reflexes. J Neurophysiol 14:191–195
38. Mendell LM, Henneman E (1971) Terminals of single Ia fibers: Location, density and distribution within a pool of 300 homonymous motoneurons. J Neurophysiol 34:171–187
39. Pompeiano O (1984) Recurrent inhibition. In: Davidoff RA (ed) Handbook of the spinal cord, vols 2 and 3. Anatomy and physiology. Marcell Decker, New York Basel, pp 461–557
40. Pompeiano O, Brodal A (1957) The origin of vestibulospinal fibers in the cat. An experimental-anatomical study, with comments on the descending medial longitudinal fasciculus. Arch Ital Biol 95:166–195
41. Precht W (1974) The physiology of the vestibular nuclei. In: Kornhuber HH (ed) Handbook of sensory physiology, vol VI. Vestibular system, part 1: Basic mechanisms. Springer, Berlin Heidelberg New York, pp 353–416

42. Richmond FJR, Abrahams VC (1975) Morphology and distribution of muscle spindles in dorsal muscles of the cat neck. J Neurophysiol 38:1322–1339
43. Richmond FJR, Bakker DA (1982) Anatomical organization and sensory receptor content of soft tissues surrounding upper cervical vertebrae in the cat. J Neurophysiol 48:49–61
44. Shimazu H, Precht W (1965) Tonic and kinetic responses of cat's vestibular neurons to horizontal angular acceleration. J Neurophysiol 28:991–1013
45. Stanojević M (1981) Responses of cerebellar fastigial neurons to neck and macular vestibular inputs. Pflügers Arch 391:267–272
46. Stanojević M, Erway B, Ghelarducci B, Pompeiano O, Willis WD Jr (1980) A comparison of the response characteristics of cerebellar fastigial and vermal cortex neurons to sinusoidal stimulation of macular vestibular receptors. Pflügers Arch 385:95–104
47. Stuart DG, Enoka RM (1983) Motoneurons, motor units, and the size principle. In: Rosenberg RN (ed) The clinical neurosciences, sect 5. Neurobiology (Willis WD, ed). Churchill Livingstone, New York, pp 471–517
48. Wand P, Pompeiano O, Fayein NA (1980) Impulse decoding process in extensor motoneurones of different size during the vibration reflex. Arch Ital Biol 118:205–242
49. Zucker RS (1973) Theoretical implications of the size principle of motoneuron recruitment. J Theor Biol 38:587–596

Received February 26/Accepted December 10, 1986

Pflügers Arch (1987) 409:39–46

Pflügers Archiv
European Journal of Physiology
© Springer-Verlag 1987

Stiffness of frog muscle fibres during rise of tension and relaxation in fixed-end or length-clamped tetani

G. Cecchi, F. Colomo, V. Lombardi, and G. Piazzesi

Dipartimento di Scienze Fisiologiche, Università degli Studi, Viale G.B. Morgagni 63, I-50134 Firenze, Italy

Abstract. 1. Stiffness measurements were performed during the rise, the plateau and the relaxation of tetanic contractions both in whole single muscle fibres and in tendon-free fibre segments under either fixed-end or length-clamp conditions. Fibres were isolated from the tibialis anterior muscle of the frog. Experiments were performed at 2–6°C. Changes in length of tendon-free fibre segments were monitored by means of a "striation follower", an opto-electronic device which, during contraction, measured sarcomere displacement at the level of two selected regions of a fibre. 2. Fast length perturbations imposed at one tendon end of a fibre during the plateau of tetanic contractions distribute uniformly along its length. 3. During the tetanus rise stiffness led isometric tension in whole fibres under fixed conditions as well as in tendon-free fibre segments under length-clamp conditions. 4. It was confirmed that a significant part of the unlinearity of T_1 relations is determined by tendon compliance. 5. During the isometric phase of relaxation in fixed-end tetani, the decline of tension led that of stiffness both in whole fibres and in tendon-free fibre segments. 6. It is concluded that the shift observed between stiffness and tension during tetanus rise and relaxation represents a true specific event in the contractile process.

Key words: Muscle contraction – Force-stiffness relation – Activation

Introduction

The findings by Cecchi et al. (1982, 1984a, 1986; but see also Buchthal and Kaiser 1944; Hill 1949, 1950; Sten-Knudsen 1953; Herbst and Piontek 1974; Bressler and Clinch 1974; Wells 1976; Mason and Hasan 1980; Haugen 1982; Tamura et al. 1982; Ambrogi Lorenzini et al. 1983; Schoemberg and Wells 1984) that in an isolated muscle fibre during an isometric tetanus stiffness, a measure of the number of attachments between actin and myosin filaments (Huxley 1957, 1974; Ford et al. 1977, 1981), leads and lags the force, respectively during the initial rise of tension and the relaxation, require further attention. It was noticed that both these time shifts between stiffness and force could be determined by a specific event in the contractile mechanism. For instance, according to Cecchi et al. (1982, 1986) a long-lived state between force generation and cross-bridge attachment or detachment could be responsible for the stiffness-tension shift observed during tetanus rise and relaxation. On the other hand, however, since the above experiments were performed in whole fibres under fixed end conditions, it was not excluded that both during the rise of tension and the relaxation the elastic characteristics of the tendons could produce an overestimation of instantaneous stiffness or that internal shortening of the fibre could depress the development of tension during the tetanus rise.

The experiments described in the present paper were performed in order to elucidate these points. The influence on stiffness estimation of either the elastic characteristics of tendon or the length changes undergone by tendons and sarcomeres during contraction and relaxation was eliminated by using a "striation follower" (Huxley et al. 1981a, b; see Methods), an opto-electronic device which measures, under fixed end or length-clamp conditions, the actual change in length undergone by a short tendon-free segment of a muscle fibre during contraction and relaxation. The main result is that the lag between rise of stiffness and development of isometric tension is present besides in whole muscle fibres under fixed end conditions also in tendon-free segments of fibres under length clamp conditions. In addition, in tendon free fibre segments under fixed end conditions, during the isometric phase of the tetanus relaxation, before the "shoulder" (Huxley and Simmons 1970), the decline of tension led that of stiffness, in the same way as already described by Cecchi et al. (1984a) for whole muscle fibres. It is clear thus that during the contraction and relaxation phases of a tetanus the time shift between stiffness and tension represents a specific event in the force-producing mechanism. In terms of cross-bridge theories of contraction it could be assumed that an unknown activation factor is responsible for a non-force generating long-lived state of attached cross-bridges. Preliminary reports of the results have been already published (Cecchi et al. 1983, 1984b).

Methods

Preparation and mounting of the fibres. Frogs (*Rana esculenta*) were obtained in the surrounding country during all the year and were kept in running water tanks at about 6°C for not more than 2 weeks before use. Single fibres, dissected from the tibialis anterior, muscle were horizontally mounted in a glass trough between the lever-arms of a capacitance force transducer and a loudspeaker length transducer. Dissection was performed at room temperature under Ringer's solution with the aid of a stereo-microscope, small knives and scissors. Dark field illumination was used during

Offprint requests to: F. Colomo

the dissection. In order to reduce the amount of passive compliance in series with the sarcomeres and to minimize transversal movements of the fibres consequent to contraction or to imposed length changes, special care was taken in dissecting and in mounting the muscle fibres. The passive series compliance was minimized by making the length of the tendon attachments as short as possible; this reduced the transmission time of the preparations and improved the performance of the length-clamp system. In addition, the connections between fibre tendons and force and length transducers were made by means of aluminium foil clips (Ford et al. 1977) to obtain an optimal alignment between the fibres and the transducer lever-arms. This eliminated, when the sarcomeres in the regions selected for measurements were oblique in respect with the longitudinal axis of the fibres, striation-follower signal artefacts due, during contraction, to transversal displacement of fibres. In all the experiments the average sarcomere spacing of the resting muscle fibres was about 2.1–2.2 μm. The experimental chamber, fastened to a metal block which could be cooled by a thermoelectric module (Thermagotrons, TL-0812, M.C.P. Electronics Ltd., Alperton Wembley, UK), was mounted on the moveable stage of an ACM microscope stand (Zeiss, Oberkochen, FRG). Two micromanipulators, carrying the force and the length transducers, were mounted on the same stage so as to adjust the position of the fibre in the trough as well as its resting length. Experiments were made at a low temperature between 2 and 6°C. During each experiment the temperature in the trough was continuously monitored with a thermistor and remained constant to ± 0.1°C.

Tension transducer. Tension (kN/m^2) was measured by means of a capacitance gauge transducer similar to that described by Huxley and Lombardi (1980). The free frequency of resonance of the tension transducers used here ranged from 40 to 60 kHz. The tension produced by the muscle fibre was directly applied to the centre of the moving plate of the transducer by means of a fine glass lever-hook which was attached to it. Capacitance changes produced by forces applied to the transducer were detected with a phase-discriminator circuit (Cecchi 1983) derived from that described by Cambridge and Haines (1959) and working at the frequency of 7.8 MHz. With this circuit the sensitivity of the tension transducer ranged from 80 to 250 mV/mN and the noise from 0.2 to 0.5 mV peak to peak.

Striation follower. The apparatus is a two channel opto-electronic device similar to that described by Huxley et al. (1981 a, b). It is composed by a light source (a 5 mW He-Ne laser, Spectraphysics, Darmstadt, FRG, model 120), a modified microscope mounted on the ACM stand (Zeiss, Oberkochen, FRG), and two photodiode arrays feeding analog-digital electronics. The instrument measures the longitudinal displacement of two distinct regions along a muscle fibre, bounding a 0.5–3 mm tendon-free segment, each about 10 μm broad and containing six consecutive sarcomeres, by counting the number of sarcomeres crossing the optical fields of the two channels. The sarcomere displacement signal was converted into length units on the basis of the actual sarcomere length in each of the fibre regions selected for the measurements. Different regions along a fibre were selected on the basis of the quality of sarcomere image, by translating longitudinally the moveable stage and therefore the muscle fibre across the field of the microscope objective. Single or double channel mode of operation could be selected. The first operation mode was used in experiments concerning the distribution along a tetanized muscle fibre of fast length changes imposed at one tendon end. When the striation follower was operated in single channel mode the length changes undergone by a given tendon-free segment of the fibre were measured by the difference of the sarcomere displacements observed in successive contractions at the level of the two regions selected to bound the segment. The sensitivity was adjusted to 100 mV/sarcomere. In the double channel mode of operation the sarcomere displacements occurring at the level of the two fibre regions bounding the selected tendon-free segment were measured during the same contraction and then subtracted each other so that the output signal gave the actual length change undergone by the selected fibre segment. This signal was converted in nm per half-sarcomere on the basis of the average sarcomere length in the segment. The sensitivity was adjusted to 250 mV/nm per half-sarcomere. The rise time was about 2 μs. The noise, for a segment of about 700 sarcomeres, was less than 0.01 nm per half sarcomere.

Loudspeaker-length transducer servo-system. Step-length changes were imposed on the muscle fibres by means of a loudspeaker length transducer derived from that already described by Cecchi et al. (1976). The length transducer was driven by an electronic pulse generator producing step signals, the amplitude and the rise time of which could be varied independently. Displacements of the loudspeaker lever-arm up to 70 μm were complete within about 100 μs. The electronics of the driving circuit were derived from those described by Cecchi et al. (1976) and by Ford et al. (1977). The length transducer was servo controlled. Fixed end conditions were obtained by using as feed-back signal the output of the photodiode sensor signaling the position of the loudspeaker lever arm. Length clamp conditions were obtained by using as feedback signal the output from the striation follower so as to hold constant the length of the selected fibre segment, independent of the length changes undergone by the tendons and by the parts of the fibre beyond the segment edges. The procedure was as follows. The length transducer was first operated to obtain fixed end conditions and then, at a preset time during the rise of tetanic tension, was switched by a command signal to length-clamp conditions. A second command signal during the relaxation, usually before the tension "shoulder", returned the length transducer to fixed end conditions. A sample-hold circuit, storing the position of the lever-arm of the length transducer just before the start of the length clamp command signal, was used to avoid changes in fibre length, caused at the start of the length clamp period during the tetanus rise by previous shortening of the selected segment and, at the end, by the return of the length transducer to its original position. The system is illustrated by the block diagram in Fig. 1.

Determination of fibre length, cross-sectional area, sarcomere spacing. All the measurements were made under ordinary illumination on the moveable stage of the ACM microscope. A 40× dry objective (Zeiss, Oberkochen, FRG, NA 0.6, working distance 4.9 mm) and 10× or 25× micrometer eyepieces were used. The fibre length was determined by means of a dial gauge mounted on the stand of the ACM microscope by measuring the displacement of the moveable

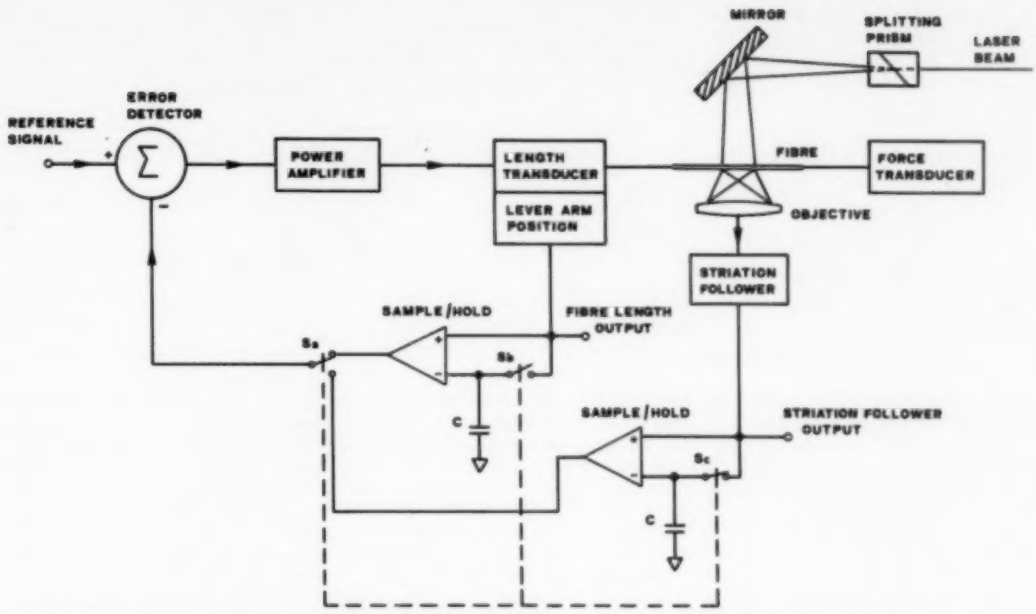

Fig. 1. Schematic diagram of the apparatus. Positions of the switches S_a, S_b and S_c are for fixed-end conditions

stage along the fibre axis required to bring the two tendon ends of the fibre in the centre of microscope optic field. Striation spacings were determined by averaging the measurements of sequences of 20 sarcomeres at different points along the fibre. The cross-sectional area of the fibres was calculated at about 2.20 μm sarcomere length, as if the section were elliptical, from measurements of the major and minor diameters.

Solutions. The Ringer's solution had the following composition: 115 mM NaCl, 2.5 mM KCl, 1.8 mM $CaCl_2$, 3 mM phosphate buffer at pH 7.1.

Stimulation. Stimuli of alternating polarity were applied transversely to the muscle fibre by means of a pair of platinum plate electrodes (10 mm long and 4 mm apart) across which up to 25 V could be applied with a constant voltage pulse generator. Stimuli of 0.5 ms duration and 1.5 times the threshold strength were used. Tetanic stimulation was applied in brief (0.4–0.6 s duration) volleys at 4-min intervals. The optimal stimulation frequency was determined for each fibre and ranged in different fibres from 14/s to 25/s.

Recording and measurement of the responses. The outputs from the tension and length transducers were recorded on a digital oscilloscope (type 2090 or 4094, Nicolet, Madison, WI, USA) and stored in its floppy disk memory. The time base of the Nicolet oscilloscope was triggered externally by different pulse frequency trigger trains so as to obtain an adequate temporal resolution of the records. Measurements of the responses were made directly with the Nicolet oscilloscope by means of its internal reading system.

Determination of stiffness. Stiffness for either whole muscle fibres or tendon free segments was determined at different tensions throughout the rise, the plateau and the relaxation of isometric tetani and was measured by the ratio of the instantaneous tension change in response to a length step imposed at one tendon end over the actual length change undergone by the whole fibres or the selected tendon-free segments. Length steps were produced by the loudspeaker length transducer described above and were complete in 90–120 μs.

Definitions. l_0 is the resting length of fibres or segments. T_0 is the maximum tetanic tension at the plateau. T is the isometric tension at which during the tetanus rise or the relaxation length steps are imposed on the fibre. T_1 is the extreme instantaneous tension attained in response to a length step. Y_0 is the extrapolated intercept on the length axis of the linear portion of the tension-extension or T_1 curves (Huxley and Simmons 1971).

Results

Striation-follower performance

Figure 2 shows the results of control experiments performed to demonstrate the reliability of striation follower measurements. It can be seen that the striation-follower operates so as to minimize the errors due to sarcomere length variation.

Longitudinal distribution of fast length changes in tetanized muscle fibres

The changes in length imposed on an active muscle fibre for stiffness determination are required to be fast enough to make negligible the amount of truncation of the instantaneous tension response by the early recovery (Huxley and Simmons 1971; Ford et al. 1977). This requirement has caused the time resolution of the experimental apparatus to

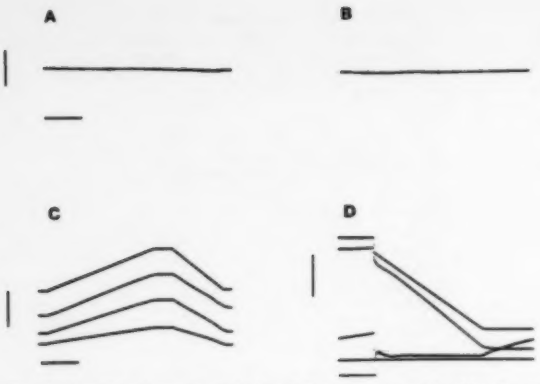

Fig. 2. A and **B** show the striation follower output (double channel operation mode) during 100 sarcomere longitudinal translation of a resting fibre. Because of the saturation of sarcomere counter system, translation was performed in two times. The two fibre regions selected to define a segment were 1,205 μm or 1,156 half-sarcomeres apart. Each region contained 6 sarcomeres with average sarcomere length of 2.095 μm, that closer to the length transducer, and of 2.08 μm, that closer to the force transducer. The *ordinate* measures the length of the segment in nm per half-sarcomere; the *abscissa* measures the amount of displacement in number of translated sarcomeres. Thickness of the traces changed according to the velocity of fibre displacement, which was made by manual translation of the moveable stage of the ACM microscope. The vertical shift of the traces represents the error introduced by variation in sarcomere length throughout the 100 translated sarcomeres: in this case ± 1.5 nm per half-sarcomere or $\pm 0.14\%$ l_0. This represents an absolute error of ± 1.734 μm, and a length variation of ± 0.017 μm or $\pm 0.83\%$ at least for sarcomeres crossing during fibre translation the optical fields of the striation follower. *Vertical calibration*: 40 nm per half-sarcomere. *Horizontal calibration*: 10 sarcomeres. **C** refers to longitudinal distribution of a constant velocity stretch imposed at rest on the same preparation as above. Traces from top to bottom measure fibre length, segment length and sarcomere displacement at the fibre regions selected for measurements. The lengthening undergone by the segment was proportional, within about 1.9%, to that of the whole fibre. The irregularities of the traces during subsequent shortening are due to slackness of the fibre. *Vertical calibration:* 190 μm (fibre length), 40 nm per half-sarcomere (segment length), 50 sarcomeres (sarcomere displacement). *Horizontal calibration:* 20 ms. **D** refers to a controlled velocity release imposed on another fibre at a tension of 0.48 T_0 during the tetanus rise. Traces from top to bottom measure fibre length, segment length, tetanic tension and resting tension. The shortening velocity of the whole fibre was 2.79 l_0/s and that of segment, after the end of the transient, 2.85 l_0/s. *Vertical calibration*: 100 μm (fibre length), 22 nm per half-sarcomere (segment length), 120 kN/m^2 (tension). Temperature: 5°C

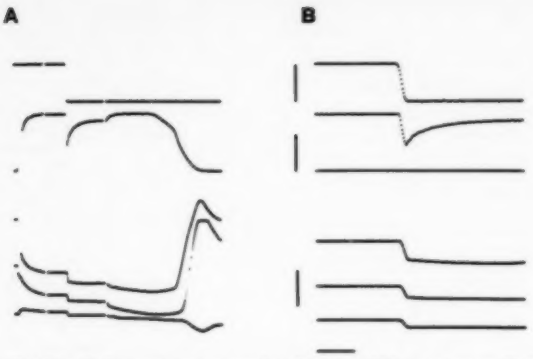

Fig. 3 A, B. Step releases, complete in about 100 μs, were applied at the plateau of a tetanic contraction on one tendon end of a muscle fibre and tension was recorded at the other end. **A** records from top to bottom refer to fibre length, active tension, and sarcomere displacements at three different points along the fibre, i.e. at 1,630, 3,000 and 3,750 μm from the tendon end connected to the length transducer. **B** same records as in **A**, but at a faster time base. In upper frame the third trace from top to bottom is the resting tension of the fibre. Note that sarcomere displacement decreases as the distance from the length transducer is increased. *Vertical calibrations*: from top to bottom, 0.46% l_0 or 20 μm, 180 kN/m^2 and 18 (**A**) or 9 (**B**) sarcomeres. *Horizontal calibrations*: **A** 0.2 s before and after trace interruptions or 2 ms between trace interruptions; **B** 0.5 ms. Fibre length: 4.33 mm. Average sarcomere length: 2.25 μm. Cross-sectional area: 5,200 μm^2. Temperature: 6°C

be progressively improved so that it is possible now to perform stiffness measurements by using length steps which are complete within 50–100 μs. This, however, rises the question whether, because of inertial effects of fibre mass, stiffness measurements performed by using so fast length steps are reliable. This kind of verification can be done by showing that a very fast length step imposed at one end of a tetanized muscle fibre distributes uniformly up to the other end.

Figures 3 and 4 show the results of one experiment, but comparable results were obtained in all the fibres used during the course of the present work. The distribution of a length step along the tetanized muscle fibre was determined by measuring with the striation follower the longitudinal displacement of individual sarcomere sequences selected at different points along the muscle fibre. Length steps of different amplitude were used. The rise time of the steps was less than 100 μs. The striation follower operated in single channel mode. It can be seen that in either releases or stretches, independent of the amplitude of the length steps imposed on the fibres, the amount of displacement of each selected sarcomere sequence decreased proportionally to the distance from the end connected to the length transducer. Apparently, at the tetanus plateau, within the range of fibre lengths and step speeds used in the present experiments, stiffness measurements are not significantly affected by fibre inertia. In addition, assuming that the linear relation between step amplitude and fibre length holds up to the extreme ends of the fibre, it can be calculated that about 20% of the step amplitude is taken by the tendon compliance.

Stiffness measurements at the tetanus plateau

The results described in this section refer to measurements performed under either fixed-end or length-clamp conditions. Figure 5 shows the T_1 relations determined under length-clamp conditions for a whole muscle fibre and for a tendon-free segment bound by sarcomeres at 2,818 and 4,519 μm from the fibre end connected to the length transducer. It was confirmed in accordance with the results of Ford et al. (1977) that the slope of the T_1 relation was significantly smaller in the whole muscle fibre than in the tendon-free segment. The value of Y_0 for 4 muscle fibres at about 5°C was in fact 0.558% $l_0 \pm 0.015$ or 6.32 nm per half-sarcomere ± 0.02 (means and SEs) for the whole fibre

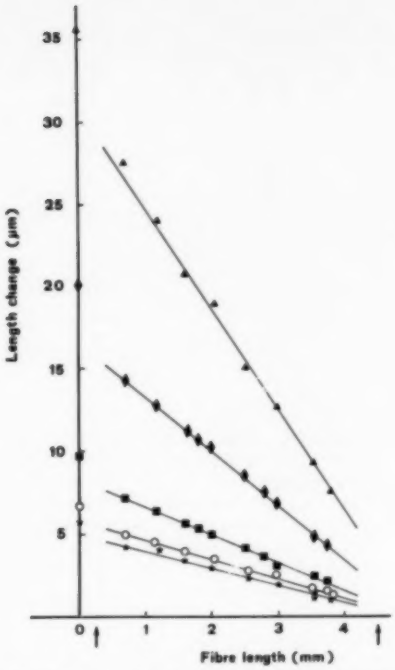

Fig. 4. Longitudinal distribution of length step amplitude along the same muscle fibre as in Fig. 3. The *abscissa* measures the fibre length: the origin and the end of the axis correspond to the edges of the tendon clips connected respectively to length and tension transducers; the arrows at 0.225 mm and at 4.5 mm indicate the points of attachment of the fibre to tendons. The *ordinate* measures the amplitude of the length steps (releases, *filled* symbols, and stretches, *open* symbols) imposed on the fibre. Different symbols refer to steps of different amplitude

and 0.429% $l_0 \pm 0.001$ or 4.85 nm per half-sarcomere ± 0.02 (means and SEs) for the segment.

Stiffness measurements during the tetanus rise

The results described in this section refer to measurements performed under either fixed-end or length-clamp conditions in whole fibres and in tendon-free segments. Figure 6 shows the results of one experiment on a muscle fibre at 5.3°C. The graph illustrates the relation between relative stiffness and relative tension during the tetanus rise of a whole fibre under fixed-end conditions (open squares) and of a tendon-free segment from the same fibre under either fixed-end conditions (open circles) or length-clamp conditions (filled circles). It can be seen (i) that in the range from about 0.5 T_0 to 0.8 T_0 the ratio of stiffness over isometric tension is the same in the whole fibre under fixed-end conditions as in the segment under either fixed-end or length-clamp conditions and (ii) that in all three cases, independent of the conditions at which the measurements were performed, the stiffness value is significantly greater than that expected for a constant ratio of stiffness over tension. In other words, development of stiffness led that of tension during tetanus rise, irrespective of the length changes in the tendon attachments and in the end-parts of the muscle fibre beyond the edges of the length clamped segments. In the fibre of Fig. 6, throughout the tension range from 0.5 T_0 to 0.8 T_0, development of stiffness advanced that of tension by about 10 ms.

Results comparable to those illustrated in Fig. 6 were constantly obtained in all the muscle fibres used during the course of the present work. Table 1 summarizes the results from four experiments. It can be seen that in length-clamped segments during the tetanus rise at isometric tensions of 0.51 T_0 and 0.74 T_0 stiffness had already risen respectively to 0.63 and to 0.81 the maximum value attained at T_0. Apparently, since the measurements were performed in length-clamped fibre segments, this effect is not attributable to either tendon lengthening or sarcomere shortening within the selected fibre segments.

Stiffness measurements during the tetanus relaxation

The results reported in this section refer to measurements performed under fixed-end conditions. Step-length changes were imposed on the fibres at decreasing tensions during the tetanus relaxation before the "shoulder", i.e. as already shown by Huxley and Simmons (1970) under true isometric conditions. The "striation follower" operated in single channel mode and the length changes undergone by a tendon-free segment were measured by recording in successive contractions the movement of two selected sarcomere regions along the muscle fibre and by subtracting the amounts of displacement. Figures 7 and 8 refer to the results from one experiment. It can be seen, in accordance with what shown above for the rise of tension, that at about 0.7 T_0 during the relaxation the relation between stiffness and tension deviates from linearity in either whole fibres or tendon-free segments. The decline of stiffness lagged that of tension by about 50 ms.

Discussion

Stiffness at the tetanus plateau

The results reported in this section agree with those of previous work of Ford et al. (1977) using a spot follower device to control the length of tendon-free segments selected along muscle fibres. Since the value of Y_0 was about 24% greater for whole fibres than for tendon-free segments it is confirmed here that a significant part of series compliance of an active fibre is determined by tendon attachments. Anyway, it is clear that the main source of instantaneous elasticity of an active muscle fibre resides in the contractile element. Moreover, since the stress-strain relation of the tendons has an exponential shape, the contribution of tendon compliance to determine the unlinearity of T_1 relations of whole fibres becomes more and more significant as tension decreases. Finally, the finding that fast mechanical perturbations distribute uniformely along fibres excludes the possibility that the presence of an extra-compliance in the regions beyond the edges of selected segments contributes to increase the plateau value of Y_0. In conclusion, in the range of fibre lengths and step speeds used for experiments at the tetanus plateau, the mechanical behaviour of the contractile component of an active muscle fibre is comparable to that of an undamped spring with negligible inertia and constant stiffness along its length.

The discrepancy between the mean values of Y_0 found for length-clamped segments, 4.85 nm per half-sarcomere

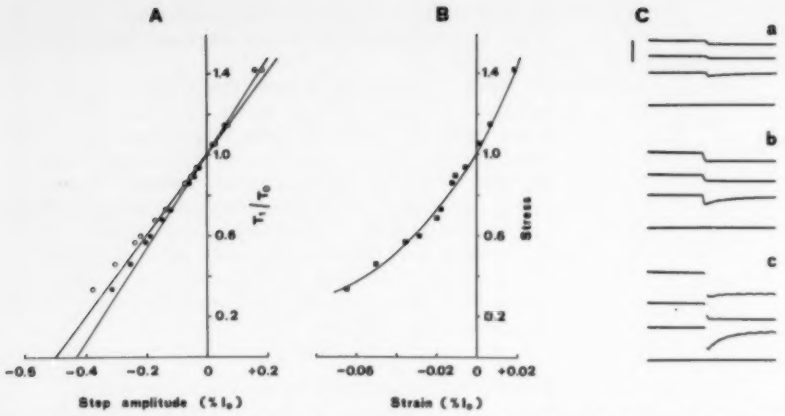

Fig. 5. **A** tension-extension (T_1) relations at the tetanus plateau for a whole muscle fibre (○) and for a tendon-free segment (●) under length clamp conditions. *Abscissa:* amplitude of the length steps as % of l_0 for either the whole fibre or the tendon-free segment. *Ordinate:* relative T_1 values. Straight lines were plotted to T_1 data points obtained in response to length steps ranging from $+0.15\%$ l_0 to -0.15% l_0. **B** stress-strain relation for tendon attachments, obtained by subtracting the compliance of the tendon-free segment from that of the whole muscle fibre. The continuous line was plotted to data points by means of the Eqn.: stress = exp (16.88 strain). **C** sample records of the responses used for determining the T_1 relations shown in **A**. In each frame traces from top to bottom measure fibre length, segment length, active tension, and resting tension. Vertical calibration: 115 kN/m^2 and 21 μm or 5 nm per half-sarcomere, respectively for fibre length and segment length. Sweep duration: 5 ms. Fibre length: 5.98 mm. Segment length: 1.70 mm. Sarcomere length: 2.25 μm. Cross sectional area: 8,405 μm^2. Temperature: 5.3° C

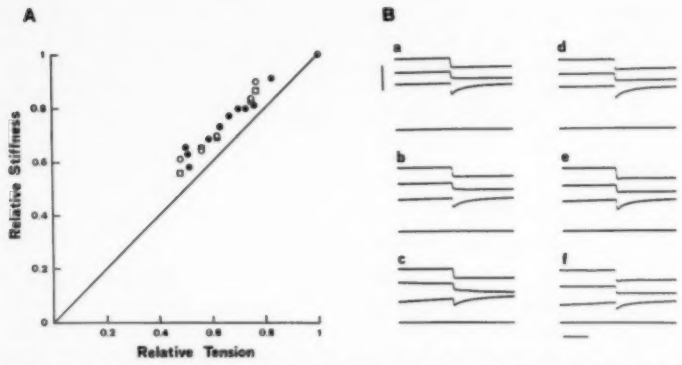

Fig. 6. **A** relations between relative stiffness and relative tension during a tetanic contraction in the same fibre as in Fig. 5. *Open squares* refer to measurements performed in the whole fibre under fixed-end conditions; *circles* refer to measurements performed in a tendon-free segment under either fixed-end conditions (○) or length-clamp conditions (●). The straight line represents the relation for a constant ratio of stiffness to tension. **B** sample records from the experiment illustrated in **A**. The frames refer to records obtained under fixed-end conditions (*left hand column*) and under length-clamp conditions (*right hand column*). Step-releases were applied either during the rise of tension, 55 ms (*c*, *f*) and 75 ms (*b*, *e*) after the beginning of the stimulus volley, respectively at 0.54 T_0 and 0.76 T_0, or later at 300 ms (*a*, *d*) when tension had already attained the plateau. In each frame traces from top to bottom refer to fibre length, segment length, active tension and resting tension. *Vertical calibration:* 115 kN/m^2 for tension and 21 μm or 5 nm per half-sarcomere respectively for fibre length and segment length. *Horizontal calibration*: 2 ms

that reported here, and 5.8 nm per half-sarcomere that reported by Ford et al. (1977), is attributable to the use in the present experiments of about twice faster length steps and consequently to smaller truncation of T_1 responses by the early recovery phase during the tension transient (Huxley and Simmons 1971; Ford et al. 1977).

Stiffness during tetanus rise and relaxation

The observation that during the tetanus rise the ratio of stiffness over isometric tension is the same in whole muscle fibres as in tendon-free fibre segments may be explained by assuming stiffness in the tendons to rise with tension according to a roughly exponential curve, approximately in the same way as stiffness of the contractile component of the fibre is observed to rise with time during the development of a tetanus. Actually, as shown in Fig. 5 the stress-strain relation of the tendons has an exponential shape.

The question which rises here, even using length steps of 100 μs duration, is (i) whether the residual unlinearity of tetanus plateau T_1 relations after exclusion of tendon compliance is entirely attributable to truncation of T_1 re-

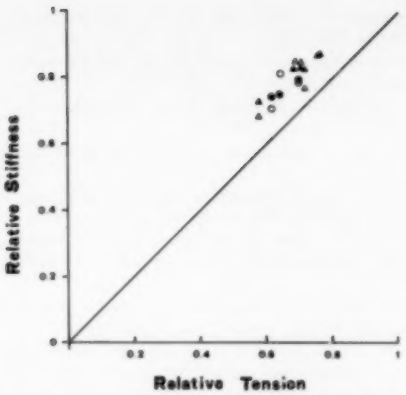

Fig. 7. Relation between relative stiffness and relative tension during tetanus rise (△, ▲) and relaxation (○, ●). As in Fig. 6 the continuous line represents the relation for a constant ratio of stiffness over tension. *Filled symbols* refer to measurements performed in the whole fibre, *open symbols* refer to measurements performed in a tendon-free segment. Note that the relation between stiffness and force deviates from linearity during the tetanus rise and the relaxation in either the whole fibre or in the tendon-free segment. Fibre length: 5.14 mm. Segment length: 1.90 mm. Sarcomere length: 2.22 μm. Cross-sectional area: 8,020 μm². Temperature: 4.4° C

Table 1. Means and SEs of stiffness values in length-clamped segments and fixed-end whole fibres at different levels of isometric tensions throughout the tetanus rise. Data refer to 4 preparations. The average sarcomere length was 2.26 μm ± 0.01 (mean and SE), the average temperature 4.9° C ± 0.25 (mean and SE)

	Isometric tension (T/T_0) at which length steps were imposed on fibres	Relative stiffness	Stiffness/ tension
Length-clamped segments	0.507 ± 0.006	0.626 ± 0.009	1.235
	0.739 ± 0.006	0.812 ± 0.007	1.099
Fixed-end whole fibres	0.485 ± 0.026	0.585 ± 0.022	1.206
	0.734 ± 0.012	0.839 ± 0.013	1.143

sponses (Huxley and Simmons 1971; Ford et al. 1977) and (ii) whether this truncation effect may produce a significant underestimation of the value reported above, 10–15 ms, for the lead of stiffness over tension during the tetanus rise. The situation is complicated. The presence of a very fast recovery phase during the tension transient in response to length steps of 40 μs (Blangé and Stienen 1985), as well as the observation of Bagni et al. (1985) that the value of the rate constant for the early recovery phase of the tension transient described by Huxley and Simmons (1971) increases twice at least during the tetanus rise may represent additional factors for further truncation of T_1 responses, with consequent increase both in the unlinearity of T_1 relations and in the degree of underestimation of the stiffness over tension lead. In this connection, however, it is interesting to note the findings by Bagni et al. (1985) that either at the tetanus plateau or at initial tetanic tensions of 0.3–0.5 T_0, T_1 values are scarcely dependent on step duration between 120 and 85 μs.

Fig. 8A–C. Sample records from the experiment illustrated in Fig. 7. Step releases were imposed at increasing times and various tensions throughout a tetanic contraction: **A** at 35 ms or 0.7 T_0 during the tetanus rise; **B** at 195 ms or T_0; **C** at 515 ms or 0.65 T_0 during the relaxation. In each frame traces from top to bottom refer to fibre length, tension and sarcomere displacements at 1,600 μm and 3,500 μm from the fibre end connected to the length transducer. *Vertical calibrations:* from top to bottom: 0.19% l_0 or 10 μm, 200 kN/m², 18 sarcomeres. *Horizontal calibration*: 0.2 s before and after trace interruption or 2 ms between trace interruption

As to the nature of the shift between stiffness and tension during the tetanus rise or the relaxation, the results reported above indicate that this phenomenon represents a true specific event in the contractile mechanism. As already emphasized by Cecchi et al. (1982, 1984a, 1986) in terms of any cross-bridge model of contraction it could be assumed that an unknown activation factor is responsible for a long-lived state between force generation and cross-bridge attachment or detachment. Actually, while in the model of Huxley and Simmons (1971) force generation is attributed to transition within about 1 ms from a state in which attached cross-bridges contribute to stiffness but do not develop force to a successive force-producing state, in the mechanism suggested above an additional long-lived state is postulated to exist between cross-bridge attachment and force generation during the tetanus rise, and conversely, during relaxation, between force generation and cross-bridge detachment. The time constant for the transfer from one to the next state should be, at 2–6° C, 10–15 ms during the tetanus rise and 50–75 ms during the relaxation. It is possible that during the tetanus rise and the relaxation an unknown factor of activation is responsible for this non force generating state of attached cross-bridges.

Acknowledgements. The volume of the Journal of Physiology (1986, 372:595–609), with an article of L. E. Ford, A. F. Huxley and R. M. Simmons, showing that the lead of stiffness over tension throughout the tetanus rise is present, besides under fixed end conditions, also under length clamp conditions, was still in the press when the authors submitted the manuscript of the present paper to the Pflügers Archiv editor for publication. The authors wish to thank Mrs M. Baldini for typing the manuscript, Mr. A. Vannucchi for preparation of the illustrations and Mr. M. Dolfi for technical assistance. This work was supported by grants from the Ministero della Pubblica Istruzione, Italy.

References

Ambrogi Lorenzini C, Colomo F, Lombardi V (1983) Development of force-velocity relation, stiffness and isometric tension in frog single muscle fibres. J Muscle Res Cell Motility 4:177–189

Bagni MA, Cecchi G, Colomo F (1985) The velocity of "quick tension recovery" during the rise of tension in an isometric tetanus in frog single muscle fibres. J Physiol (Lond) 365:68P

Blangé T, Stienen GJM (1985) Transmission phenomena and early tension recovery in skinned muscle fibres of the frog. Pflügers Arch 405:12–18

Bressler BH, Clinch NF (1974) The compliance of contracting skeletal muscle. J Physiol (Lond) 237:477–493

Buchthal F, Kaiser E (1944) Factors determining tension development in skeletal muscle. Acta Physiol Scand 8:38–74

Cambridge QW, Haines J (1959) A new versatile transducer system. J Physiol (Lond) 149:2–3P

Cecchi G (1983) A circuit specially suited for use with high frequency capacitance gauge force transducers. Archs Ital Biol 121:215–217

Cecchi G, Colomo F, Lombardi V (1976) A loudspeaker servo system for determination of mechanical characteristics of isolated muscle fibres. Boll Soc Ital Biol Sper 52:733–736

Cecchi G, Griffiths PJ, Taylor SR (1982) Muscular contraction: kinetics of cross-bridge attachment studied by high frequency stiffness measurements. Science 217:70–72

Cecchi G, Colomo F, Lombardi V (1983) Longitudinal distribution of step length changes in tetanized fibres from frog skeletal muscle. J Physiol (Lond) 345:146P

Cecchi G, Griffiths PJ, Taylor SR (1984a) The kinetics of cross-bridge attachment studied by high frequency stiffness measurements. In: Pollack GH, Sugi H (eds) Contractile mechanisms in muscle. Plenum, New York, pp 641–655

Cecchi G, Colomo F, Lombardi V, Piazzesi G (1984b) Stiffness and isometric tension during tetanus rise in frog muscle fibre segments under length-clamp conditions. J Physiol (Lond) 357:104P

Cecchi G, Griffiths PJ, Taylor SR (1986) Stiffness and force in activated frog skeletal muscle fibres. Biophys. J 49:437–451

Ford LE, Huxley AF, Simmons RM (1977) Tension responses to sudden length change in stimulated frog muscle fibres near slack length. J Physiol (Lond) 269:441–515

Ford LE, Huxley AF, Simmons RM (1981) The relation between stiffness and filament overlap in stimulated frog muscle fibres. J Physiol (Lond) 311:219–249

Haugen P (1982) Increase of resistance to stretch during the latent period in single muscle fibres of the frog. Acta Physiol Scand 114:187–192

Herbst M, Piontek P (1974) Changes of stiffness of skeletal muscle during latency relaxation. Biochem Biophys Res Commun 57:120–125

Hill AV (1949) The abrupt transition from rest to activity in muscle. Proc Roy Soc B 136:399–420

Hill AV (1950) The development of the active state of muscle during the latent period. Proc Roy Soc B 137:320–329

Huxley AF (1957) Muscle structure and theories of contraction. Prog Biophys Biophys Chem 7:255–318

Huxley AF (1974) Muscular contraction. J Physiol (Lond) 243:1–43

Huxley AF, Lombardi V (1980) A sensitive force transducer with resonant frequency 50 kHz. J Physiol (Lond) 305:15–16P

Huxley AF, Simmons RM (1970) Rapid "give" and the tension "shoulder" in the relaxation of frog muscle fibres. J Physiol (Lond) 210:32–33P

Huxley AF, Simmons RM (1971) Proposed mechanism of force generation in striated muscle. Nature (Lond) 233:533–538

Huxley AF, Lombardi V, Peachey LD (1981a) A system for fast recording of longitudinal displacement of a striated muscle fibre. J Physiol (Lond) 317:12–13P

Huxley AF, Lombardi V, Peachey LD (1981b) A system for recording sarcomere longitudinal displacements in a striated muscle fibre during contraction. Boll Soc Ital Biol Sper 57:57–59

Mason P, Hasan H (1980) Muscle crossbridge action in excitation and relaxation. Experientia 36:949–950

Schoemberg M, Wells JB (1984) Stiffness, force and sarcomere shortening during a twitch in frog semitendinosus muscle bundles. Biophys J 45:389–397

Sten-Knudsen O (1953) Torsional elasticity of the isolated cross striated muscle fibre. Acta Physiol Scand 28:suppl 104

Tamura Y, Hatta I, Matsuda T, Sugi H, Tsuchiya T (1982) Changes in muscle stiffness during contraction using ultrasonic waves. Nature (Lond) 299:631–633

Wells JB (1976) Onset of mechanical change following stimulation in frog striated muscle. Biophys J 16:122a

Received March 13/Accepted December 17, 1986

Pflügers Arch (1987) 409:47–51

Pflügers Archiv
European Journal of Physiology
© Springer-Verlag 1987

An inexpensive dual-excitation apparatus for fluorescence microscopy

John Kassotis, Susan F. Steinberg, Samuel Ross, John P. Bilezikian, and Richard B. Robinson

Departments of Pharmacology and Medicine, Columbia University, College of Physicians and Surgeons, 630 W. 168th Street, New York, NY 10032, USA

Abstract. Ion sensitive indicator molecules can be employed in conjunction with fluorescence microscopy in single cells to measure rapid changes in the intracellular concentration of several ionic species. A number of these probes (e.g. fura-2) require the capability of measuring emission intensity at two excitation wavelengths to quantitate properly intracellular ion concentration. We have developed a simple dual-excitation apparatus for use in such applications. The apparatus switches the excitation filter within 150 ms. This economical apparatus is well suited in situations where the ionic concentration of interest is changing relatively slowly. Moreover, by synchronizing the device's action with an external stimulus, rapid and reproducible ionic changes in excitable tissue also can be measured.

Key words: Fura-2 – Fluorescence microscopy – Dual-excitation – Instrumentation – Excitable tissue – Ion sensitive probe

Introduction

The development of new ion sensitive indicator molecules has led to the emergence of fluorescence microscopy as a powerful technique for the study of intracellular events in living cells. Of particular interest are the dyes fura-2 and 2′,7′-bis-(carboxylethyl)-5,6-carboxy fluorescein (BCECF) that are used for determining intracellular calcium and pH, respectively (Grynkiewicz et al. 1985; Paradiso et al. 1985). These molecules fluoresce in both their free and ion bound forms. However, binding of Ca^{2+} to fura-2 or H^+ to BCECF shifts the excitation peak. This property allows one to monitor the ratio of fluorescence intensity at two appropriate excitation wavelengths, and thereby establish intracellular pH or calcium concentration, independent of the absolute amount of dye in the cell.

Fura-2 and BCECF are ideally suited for single cell microscopic spectroscopy because of their high fluorescence quantum yield. However, such experiments require an elaborate mechano-optical system to permit rapid alteration (ms range) of the excitation wavelength focused on the single cell. In addition to the considerable expense of such complex mechanical devices, these systems must be able to analyze separately the emission intensity associated with each excitation wavelength. This generally requires computer control of both the dual-excitation apparatus and the data acquisition process.

We have designed a simpler dual-excitation apparatus that employs a dual filter mount engaged by a stepper motor and controlled by a digital sequencing circuit. This apparatus switches excitation filters within 150 ms in response to a signal from a timing circuit. It has application in two specific situations: (1) when the ionic concentration of interest is changing with a time constant of seconds; (2) when the changes are occurring with a time constant of ms, but are reproducible and synchronized to an external trigger, such as in electrically driven muscle or nerve cells. In this report, we describe this apparatus and illustrate, using fura-2, its convenience, utility and experimental application.

Materials and methods

Apparatus. The dual-excitation apparatus is a 45° sector, machined from a 1/16 inch thick aluminum disk to minimize mass. Individual 1 inch diameter barrier filters (Oriel Corp., Stratford, CT, USA) are secured in circular cutouts of the sector by means of threaded rings. The sector is secured to a 1/4 inch shaft via a flange which is mounted through an opening in a box-shaped supporting arm. The supporting arm and girder, prepared from an extruded rectangular box section, are designed to support the filter mount, stepper motor and accompanying pulley system (Fig. 1A, B). The stepper motor (no. 4SH12A56S, 12 V, 56 mm; Airpax Corp., Cheshire, CT, USA) is separated from the supporting arm by a rubber spacer to minimize vibration, and is mechanically linked to the sector by means of two timing pulleys (no. TB7EF2-160; Winfred M. Berg, Inc., East Rockaway, NY, USA) and a 1/8 inch timing belt. This indirect mounting configuration allows the entire device to be attached to the fixed front ledge of a vibration-isolation table, thereby further reducing any vibration artifacts associated with the filter motion. The sector is positioned between the lamp and the microscope. In the case of the Leitz Diavert microscope used in this study, adequate clearance for rotation of the sector was obtained by removing a non-structural tube at this locotion which had been designed as a filter housing. The angle of the supporting arm was designed to position the axis of rotation slightly above and to the side of the light path.

Offprint requests to: R. B. Robinson, Department of Pharmacology, at the above address

Supported by grants AM-01186, DK-32333, HL-20859 and HL-28958 from the USPHS; Dr. Robinson is an Established Fellow of the New York Heart Association; Dr. Steinberg held a Squibb Cardiovascular Research Fellowship Award during the time this research was accomplished

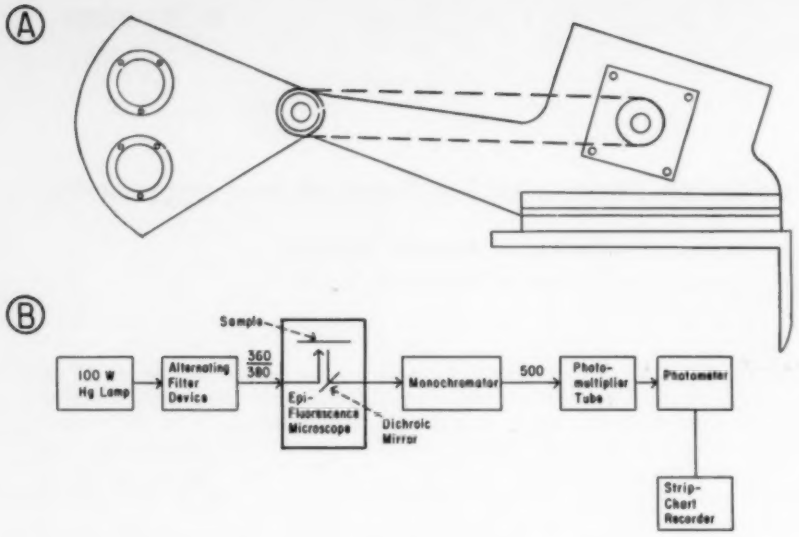

Fig. 1 A, B
Schematic diagram of dual-excitation apparatus and fluorescence microscope. **A** Diagram of filter mounting apparatus and supporting arm. **B** Diagram of fluorescent light path through the optical system. The light passes through the alternating filter device, exiting as either 360 or 380 nm, which then is absorbed by the single cell on the microscope stage. The emitted light from the cell passes through a monochromator tuned to 500 nm, then a photomultiplier. The output from the photomultiplier is transmitted to a photometer and then to a chart recorder

The control circuitry is diagrammed in Fig. 2A. The timing is controlled via a series of digital counters driven by an external clock. Counter 1 acts as a recurrent signal generator with an adjustable basic cycle length (BCL). It delivers trigger pulses to counter 2, which controls the motor pulse duration (MPD), and to a separate divide-by-2 counter. The divide-by-2 circuit element signals the motor control integrated SAA1027 logic circuit, thus effecting a change in the subsequent direction of motor rotation. Upon receiving a trigger pulse MPD delivers, at terminal Q, a rectangular pulse of fixed duration to one input of a two-input AND circuit. The second input is supplied by a divide by 6 counter, designed to divide a 1 kHz clock by 6. Thus, a 150 ms duration output from MPD will result in the generation of 25 discrete pulses generated at the AND output, driving the stepper motor. Each pulse results in a rotation of the motor shaft of 1.8°, resulting in a net rotation per cycle of 45° at a rate of 167 steps/s. Because of the action of the divide by two counter, motor direction is reversed on alternate BCL pulses. In addition, the Q output of MPD supplies a pulse to counter 3 (stimulus delay), which in turn triggers counter 4 (stimulus duration). The result is that with each BCL pulse the excitation filter changes; then after an appropriate delay a stimulus is generated that can be used to excite the cell being studied. It is only at this time, after the filter assembly has reached the correct position, that data sampling occurs. Data are not collected during filter translation (with the exception of Fig. 3). To measure a rapid change in ionic concentration, two sequential records are collected and the ratio computed as a function of time after the stimulus. The timing relation between the various counters is illustrated schematically in Fig. 2B.

Experimental protocol and analysis. Bovine aortic endothelial cells and single adult canine left ventricular cardiac cells are prepared as previously described (Ryan et al. 1978; Hewett et al. 1983). To load the cells with fura-2, the cells are incubated in HEPES buffered saline (pH 7.4) containing (in mM) 20 HEPES, 124 NaCl, 5.0 KCl, 0.5 $MgSO_4$, 1.0 $CaCl_2$, 1.0 Na_2HPO_4, 5.6 dextrose and 2 μM fura-2/AM

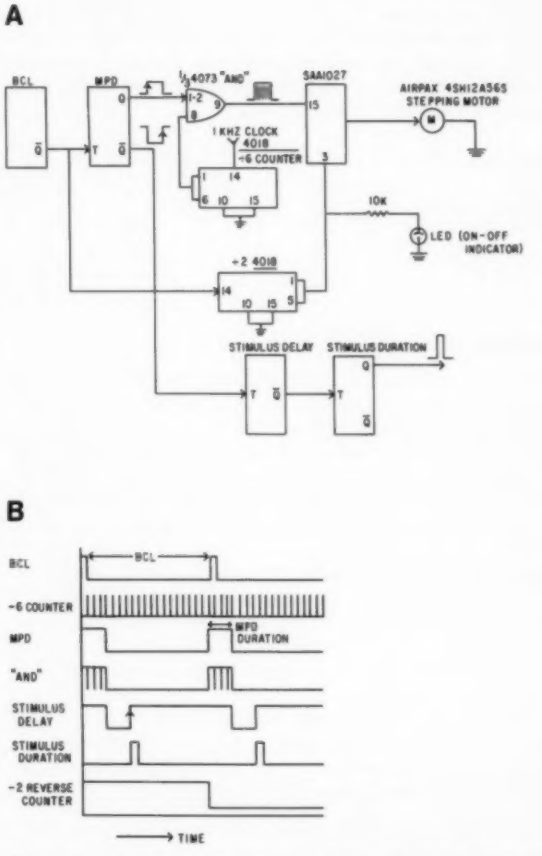

Fig. 2. Circuit and timing diagram for controlling dual-excitation apparatus. **A** Circuit diagram demonstrating configuration of digital counters used to control switching of filters. **B** Schematic representation of output of various digital counters, illustrating relationship between timing pulses

at 37°C for 1 h (endothelial cells) or 15 min (cardiac cells). The cells are rinsed in dye-free buffer to remove extracellular dye. For the fluorescence studies, a modification of a previously described cell superfusion chamber is employed (Hermsmeyer and Robinson 1977). The cells are grown on (endothelial cells) or allowed to adhere to (cardiac cells) a 25 mm diameter round glass coverslip, which serves as the replaceable bottom of the superfusion chamber. Solution entering the chamber is pre-warmed, and the chamber temperature is maintained at 37°C by means of a feedback circuit connected to a thermistor in the chamber. The chamber also contains two strips of silver foil along either side to permit field stimulation of the cells. The chamber is placed on the stage of the Leitz Diavert inverted microscope, which is equipped with an epi-fluorescence system, glass optics, a 40× oil objective and a dichroic mirror that passes wavelengths above 400 nm. The emission path contains a monochromator, set at 500 nm, and a spot photomultiplier (Farrand Optical, Valhalla, NY, USA). The output of the photomultiplier is fed into an amplification circuit and then electronically filtered using either the passive filter of the photometer or an active Bessel filter (Frequency Devices, Haverhill, MA, USA). The final signal is displayed on a Tektronix Oscilloscope or Western Graphtec chart recorder.

For fura-2 studies, the dual-excitation apparatus contains 10 nm wide barrier filters with approximate wavelength maxima of 360 and 380 nm (precise peaks are 361.9 and 381.9 nm, respectively). Fluorescence intensity is recorded during excitation with each of these filters in turn. At 380 nm the emission intensity decreases as the calcium concentration increases; at 360 nm, which is the isosbestic point of fura-2, the emission intensity is insensitive to a change in calcium concentration. We measure the 360/380 ratio, rather than 340/380, because excitation wavelengths below 360 nm are significantly attenuated by the glass optics of our system. Background fluorescence at each wavelength is determined for each cell type by measuring the fluorescence from several cells that are not loaded with dye, and calculating an average value. This average background value (27% of the signal from the loaded endothelial cells, $n = 7$; 3% of the signal from the loaded adult cardiac cells, $n = 20$) is then subtracted from the emission value of the loaded sample at the corresponding excitation wavelength. The calcium concentration in the cell under a given condition was calculated according to the equation of Grynkiewicz et al. (1985). The limiting fluorescence values (at saturating and zero calcium) were determined for each cell type by taking the average values from 8 cells after exposure to the calcium ionophore ionomycin (100 nM) in the presence of 1 mM calcium, and after addition of 5 mM EGTA, respectively.

Results

We first determined whether the photomultiplier response is sufficiently rapid to monitor the sudden change in output associated with alteration of the excitation wavelength, and whether the transient filter vibration associated with this change affects the reading. The chamber is filled with a simple saline solution containing the calcium sensitive form of fura-2. The photomultiplier output is recorded on an oscilloscope as the dual-excitation apparatus switches excitation wavelength (Fig. 3). It can be seen that the filter

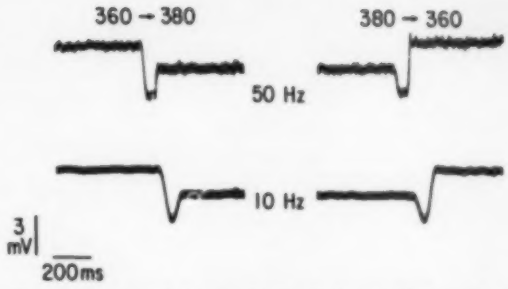

Fig. 3. Response of photomultiplier during rapid change in excitation wavelength. *Top row* Switch from 360 to 380 nm filters, and return, with an active Bessel filter set for a cutoff frequency of 50 Hz. *Bottom row* Switch from 360 to 380 nm filters, and return, with an active Bessel filter set at 10 Hz. During filter transition, when the fluorescent output is not transmitted to the cell, there is a transient downward deflection of the output signal

change occurs, and the photomultiplier output stabilizes, within 150 ms. Reducing the cutoff frequency of the active Bessel filter from 50 to 10 Hz to minimize electronic noice slows the response somewhat, but still permits equilibration within 150 ms.

Using endothelial cell cultures, we next employed the dual excitation apparatus to monitor the fluorescence intensity at two wavelengths during pharmacological perturbation of intracellular calcium levels (Fig. 4). The strip chart depicts the photomultiplier output during continuous alteration of excitation filters every 6 s. In this case a passive filter circuit is used to minimize noise, which slows the response time of the photomultiplier amplifier to 1–2 s. Exposure of cells to the calcium ionophore, ionomycin, results in a reduction of the output signal at 380 nm, with minimal change of the signal at 360. When EGTA is added in the continued presence of ionomycin to chelate free calcium, the signal at 380 nm returns toward its initial value. After background subtraction, the ratio from the two wavelengths is computed, and the corresponding $[Ca^{2+}]_i$ levels are calculated, using the equation described in Methods (Fig. 4B).

We next investigated the suitability of the dual-excitation apparatus to monitor a rapid but reproducible change in intracellular calcium. For this purpose, adult cardiac cells are electrically driven by field stimulation at a frequency of 1 Hz. The timing pulse controlling the dual-excitation apparatus is synchronized with the electrical stimulation such that the excitation wavelength is switched just prior to each contraction of the cardiac cell. The electrical stimulus can then be used as a reference point to superimpose successive emission records at alternative excitation wavelengths (Fig. 5A). The digitized strip chart record of the photomultiplier output contains a transient response at 380 nm excitation, corresponding to the calcium change associated with a contractile response. The 360 nm record lacks such a transient since this filter's maximum is close to the isosbestic point of fura-2. After point by point background subtraction, ratio calculation and corresponding calcium determinations were performed, and the result is shown in Fig. 5B. In this particular experiment, basal calcium was calculated to be 300 nM. This value was at the high end of the range observed in other cells. Also

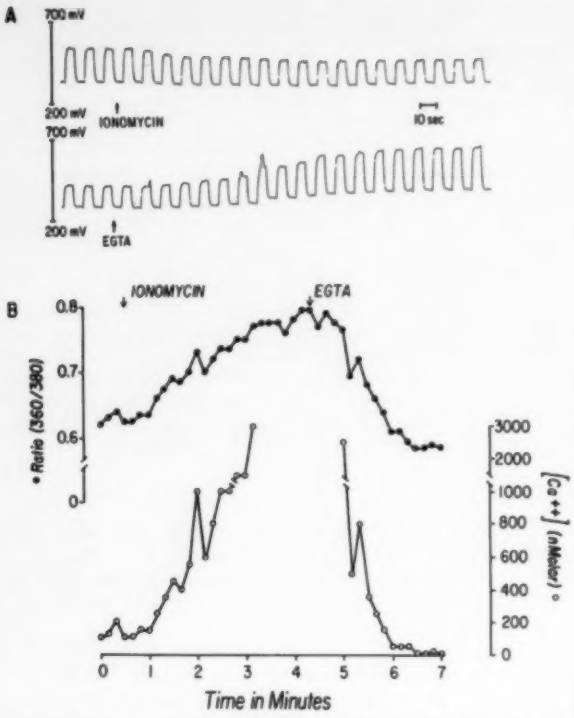

Fig. 4A,B. Measurement of time course of change in intracellular calcium in a cultured endothelial cell in response to ionomycin (100 nM) and EGTA (5 mM). **A** Continuous strip chart of photometer output during operation of dual-excitation apparatus at BCL = 6 sec. The times when ionomycin and EGTA are added are indicated. **B** Calculated ratio of 360 to 380 fluorescence intensities and corresponding intracellular calcium values. A single emission value is obtained after each filter change and ratios calculated for successive readings. Ratios and calcium are calculated as described in Methods. Calculated calcium levels in excess of 3 μM are not shown, since this exceeds the concentration that can be reliably measured with fura-2

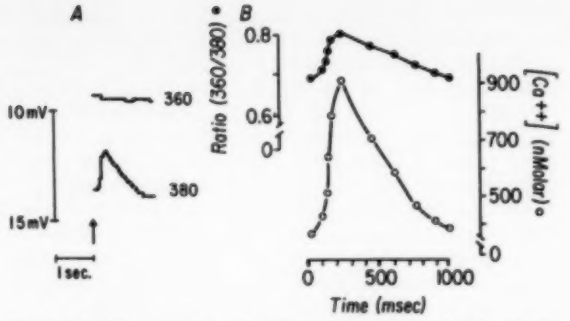

Fig. 5A,B. Measurement of calcium transient associated with the contraction of a field stimulated single adult cardiac myocyte. **A** Digitized strip chart records of fluorescence intensity during two successive contractions, the top at 360 nm excitation and the bottom at 380 nm. *Arrow* represents time of stimulation. A 20 Hz active filter was employed during data collection. **B** Calculated ratio of 360 to 380 fluorescence intensities and corresponding intracellular calcium values. The emission profile at each wavelength is digitized using a digitizing tablet (Summagraphics MM1201, Fairfield, CT, USA) connected to an IBM-PC. Background subtraction and ratio calculation are then performed at selected points, as described in Methods

shown is the calculated calcium transient associated with the contraction.

Discussion

The apparatus described in this paper provides an inexpensive and versatile method for dual-excitation fluorescence microscopy. The results clearly demonstrate the suitability of this method to certain specific experimental situations. The change in excitation wavelength occurs within 150 ms, with no additional delay from photomultiplier response time or vibration artifact. Although we employed a BCL of 6 s in the endothelial cell study, it is clear from the filter response demonstrated in Fig. 3 that the system can be driven at a BCL of 300 ms or less when employing active filtering. This would allow the calculation of a ratio value every 600 ms and permit the measurement of calcium changes occurring over the course of only a few seconds. Further, if a more powerful motor with a larger incremental change is employed, the time required to change filters can be reduced. In addition, the rate at which we can drive the motor is limited by the fact that on alternative cycles the sector is rotating upward against gravity. By constructing a somewhat more complicated linking mechanism that translates motor rotation into horizontal motion, this problem can be eliminated and the stepping rate increased. With such modifications it should be possible to reduce the filter switching time to less than 100 ms.

For more rapid changes, such as those resulting from excitation of cardiac cells, the protocol demonstrated by Fig. 5 can be employed. This approach, which involves digitization of the emission transient at each excitation wavelength, could also be used in association with voltage clamp protocols. The only requirement is that the cell must be at steady state for that particular transient, so that successive excitation cycles are identical. It should be noted that the system described in this paper does not extend to all experimental needs involving fluorescent indicator molecules. When subcellular localization is desired, a video imaging system and a more sophisticated computer interface is required (Williams and Fay 1986). When rapid and non-synchronizable ionic transients occur, excitation wavelengths must be switched far more rapidly than can be accomplished with this apparatus. Nevertheless, the present system has a large number of applications that can be used at considerable advantage in cost and complexity over other approaches. Although we have illustrated the apparatus only in the case of the calcium sensitive dye fura-2, minor modifications (changing to barrier filters with peaks near 438 and 492 nm, and using a dichroic mirror with a 500 nm cutoff) would permit pH studies using BCECF.

The new generation of fluorescent indicator molecules provides the possibility of directly correlating, in a single cell, transient changes in intracellular ionic constituents with pharmacological or electrical perturbations. The realization of that promise has been slowed by the cost and complexity of the requisite hardware. It is likely that the approach

described in this article will make this powerful new technique more accessible to a greater number of investigators.

References

Grynkiewicz G, Poenie M, Tsien RY (1985) A new generation of Ca^{2+} indicators with greatly improved fluorescence properties. J Biol Chem 260:3440–3450

Hermsmeyer K, Robinson KB (1977) High sensitivity of cultured cardiac muscle cells to autonomic agents. Am J Physiol 233:C172–C179

Hewett K, Legato MJ, Danilo P Jr, Robinson RB (1983) Isolated myocytes from adult canine left ventricle: Ca^{2+} tolerance, electrophysiology, and ultrastructure. Am J Physiol 245: H830–H839

Paradiso AM, Tsien RY, Machen TE (1985) Na^+-H^+ exchange in gastric glands as measured with a cytoplasmic-trapped fluorescent pH indicator. Proc Natl Acad Sci USA 81:7436–7440

Ryan US, Clements E, Habliston D, Ryan JW (1978) Isolation and culture of pulmonary artery endothelial cells. Tissue Cell 10:535–554

Williams DA, Fay FS (1986) Calcium transients and resting levels in isolated smooth muscle cells as monitored with quin 2. Am J Physiol 250:C779–C791

Received July 28, 1986/Accepted January 10, 1987

Pflügers Arch (1987) 409:52–59

Pflügers Archiv
European Journal of Physiology
© Springer-Verlag 1987

Effect of menthol on two types of Ca currents in cultured sensory neurons of vertebrates

D. Swandulla, E. Carbone*, K. Schäfer, and H. D. Lux**

Max-Planck-Institut für Psychiatrie, Abteilung Neurophysiologie, D-8033 Planegg-Martinsried, Federal Republic of Germany

Abstract. The effect of menthol on voltage-dependent Ca currents was investigated in cultured dorsal root ganglion cells from chick and rat embryos. Bath application of menthol (0.1–1 mM) had different effects on the various Ca currents present in these neurons. Below −20 mV, the low threshold Ca currents were reduced in amplitude in a dose-dependent manner by menthol with little changes of their activation kinetics. In contrast to this, the time course of inactivation of the high-threshold Ca currents, activated above −20 mV from a holding potential of −80 mV, was drastically accelerated by external menthol. The action of menthol was unchanged with more positive holding potentials (−50 mV). Thus, a proposed third type of Ca current with transient activation and complete deactivation below −50 mV was either not present or not affected by menthol. Menthol exerted its action only when applied from the outside. Its effect was completely reversible within 15–20 min of wash-out. Our findings are consistent with the idea that menthol acts on two types of Ca channels coexisting on the membrane of cultured sensory neurons. Menthol blocks currents through the low voltage-activated Ca channel, and facilitates inactivation gating of the classical high voltage-activated Ca channel.

Key words: Ca channels – Ca-inactivation – Menthol – Sensory neurons – Patch-clamp

Introduction

Different types of Ca channels have been characterized in various excitable cells (Carbone and Lux 1984a, b; Fox and Krasne 1984; Armstrong and Matteson 1985; Bean 1985; Bossu et al. 1985; Fedulova et al. 1985; Nowycky et al. 1985; DeRiemer and Sakmann 1986). One of them, activated at high voltages (HVA), resembles the classical Ca channel of other membrane preparations (for a review see Hagiwara and Byerly 1981) which exerts most of its effects by inducing changes in intracellular Ca concentration. In this way it activates other channels, triggers secretion and contraction and facilitates its own inactivation. Another Ca channel, activated at low voltages (LVA), differs both kinetically and pharmacologically from the classical one. Its time-dependent inactivation is fast and complete and survives large doses of dihydropyridine derivatives (Boll and Lux 1985; Fedulova et al. 1985; Bean 1985). In some cells, LVA channels contribute more than HVA channels to the total Ca current flowing through the cell (Carbone and Lux 1986a). This channel seems to be important for a variety of cell functions such as: (i) cell contraction in ciliates (Deitmer 1984), (ii) patterned firing of central neurons (Llinas and Yarom 1981; Llinas and Jahnsen 1982). (iii) hormone secretion in endocrine cells (DeRiemer and Sakmann 1986) and (iv) pace-making in heart cells (Bean 1985; Hagiwara et al. 1987).

Currents through LVA and HVA channels overlap to form the Ca inward current of the cell and, in some cases, their time course might be further complicated by the contribution of a third type of Ca current (Nowycky et al 1985). Under normal conditions it is therefore difficult to study accurately their kinetics or single channel properties.

Pharmacological tools are required to separate the various Ca currents, and to study them into more detail. All drugs and chemicals tested so far except dopamine (Marchetti et al. 1986), monohydroxyl alcohols (Llinas and Yarom 1986), Ni^{2+} (Hagiwara et al. 1987; Carbone et al. 1987) and phenytoin (Yaari et al. 1987) are found to suppress HVA and leave LVA currents unaltered (Nowycky et al. 1984; Boll and Lux 1985; Bossu et al. 1985; Fedulova et al. 1985; Carbone and Lux 1986a; McCleskey et al. 1986). Recently we described that menthol, a cyclic alcohol, facilitates the inactivation gating of the classical Ca current in *Helix* neurons (Swandulla et al. 1986). Therefore we thought it of interest to investigate the action of menthol on the various types of Ca channels of sensory neurons. Our results indicate that menthol affects LVA and HVA channels differently. Menthol speeds up inactivation of HVA currents similarly to its action on Ca currents in *Helix* neurons. On the other hand, like dopamine and Ni^{2+}, menthol blocks LVA currents. The open-close kinetics of both Ca currents are not affected. The action of menthol appears independent of the presence of a fast inactivating Ca channel which activates at high voltages (> +10 mV) and deactivates below −50 mV as recently described in the same preparation (N-type, Nowycky et al. 1985).

A preliminary account of this work has already appeared (Swandulla et al. 1985).

* *Present address:* Dipartimento di Anatomia e Fisiologia Umana, Sezione di Neuroscienze, Corso Raffaello 30, I-10125 Torino, Italy
** *Present address:* Institut für Zoophysiologie, Universität Hohenheim, Garbenstrasse 30, D-7000 Stuttgart 70, Federal Republic of Germany
Offprint requests to: H. D. Lux

Materials and methods

Preparation and recording. Dorsal root ganglion (DRG) cells from 10 day old chick or 18 day old rat embryos were dissociated and grown according to the method of Barde et al. (1980). Cells were used 6–12 h following plating.

The experimental set up was as recently described (Brown et al. 1984; Carbone and Lux 1984a). Patch electrodes were made of Duran glass (Schott Ruhrglas, Mainz, FRG) with a tip resistance of about 3 MΩ. Whole cell clamp currents were measured according to the method of Hamill et al. (1981). Data were filtered at 5 kHz using a 4-pole Bessel filter and stored on FM magnetic tape. Analog recordings were digitized at a frequency of 7–12 kHz by a 12 bit A/D converter and analyzed by computer (LSI 11/23). Leakage and capacitative currents were minimized by subtraction of a scaled signal which was the average of ten hyperpolarizing pulses of appropriate amplitude. Pipette series resistance was compensated as previously described (Carbone and Lux 1986b). To achieve optimal space clamp control all experiments were performed 6–12 h after cell preparation. During this period of incubation, cells stuck to the substrate. They were of spherical shape without visible processes and could be easily "patched". Cells had a total capacitance of 3–12 pF corresponding to cell diameters of 10–20 μm.

Cells at rest were normally held at −80 mV which was sufficiently negative for the recording of LVA currents (Carbone and Lux 1984a). Depolarizing pulses lasting 100–200 ms were applied every 30 s to minimize possible HVA channel inactivation. Run-down of Ca currents (Kostyuk et al. 1981b; Byerly and Hagiwara 1982; Fenwick et al. 1982) was observed. However, in several cells, currents persisted for more than 30 min and fully recovered after menthol application. A test of current run-down was always done before drug application. Cells which rapidly lost Ca currents were discarded. Temperature was 20–22° C in all experiments.

Solutions. The standard bathing solution (mM) was: 120 NaCl, 20 $CaCl_2$, 2 $MgCl_2$, 10 HEPES (pH 7.3). Tetrodotoxin (TTX, 3μM) was added to the bath to fully block Na currents. The intracellular pipette contained (mM): 120 CsCl or N-methyl-glucamine Cl, 20 tetraethylammonium (TEA) Cl, 10 EGTA, 2 $MgCl_2$, 10 HEPES (pH 7.3). Assuming Ca impurities of the salt solutions in the order of 60–100 μM, the calculated intracellular free Ca^{2+} concentration was about 1×10^{-9} M. (−)Menthol (2-isopropyl-5methyl-cyclohexanol) and cyclohexanol (Sigma, St. Louis, MO, USA) were dissolved in the external fluid at the desired concentration. The chemical structure of these two alcohols is shown in Fig. 1.

In a preliminary series of experiments we found that menthol quickly lost its efficacy in solutions containing choline, probably due to a chemical interaction between the two molecules. Since there was little or no difference between Ca currents recorded in the presence of 120 mM choline or Na, we decided to use Na rather than choline in all the external solutions. The similarity of inward currents in the presence of choline or Na also suggested a negligible contribution of TTX insensitive Na currents (Kostyuk et al. 1981a) in this preparation. To minimize concentration changes due to menthol evaporation, test solutions were always freshly prepared just before starting the experiments.

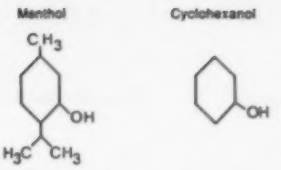

Fig 1. Chemical structure of menthol and cyclohexanol (the cyclic alcohol from which menthol is derived)

Solutions were either pressure ejected via a double barrelled glass pipette (20–50 μm tip diameter) placed 50–100 μm from the cell (Marchetti et al. 1986) or applied by a multibarrelled perfusion pipette (100–200 μm tip diameter) the flow through which was regulated by hydrostatic pressure (Carbone and Lux 1987). Complete perfusion of the cell was assured in control experiments with phenol red stained solutions.

Results

Action of menthol on LVA and HVA currents in chick DRG cells

Figure 2 left shows a series of current recordings obtained at control during whole-cell clamp steps to various membrane potentials starting from a holding potential of −80 mV. Typical LVA currents appeared at a membrane potential of −60 mV, increased from −60 to −40 mV and settled between −40 and −20 mV. HVA currents, which were more prominent and inactivated more slowly, were recorded at potentials more positive than −20 mV. In the presence of external menthol the size of LVA currents was strongly reduced (Fig. 2, center). In 21 cells the reduction was 70 ± 15% in 0.5 mM menthol. Activation and inactivation kinetics were hardly affected by this and even higher concentrations (see below). HVA currents elicited with depolarizing steps positive to −30 mV were less affected in amplitude. Their inactivation time course, however, which was slow and largely incomplete in our experimental conditions with 10 mM EGTA inside the cell, was drastically accelerated and became almost complete. Figure 2 right, shows nearly full reecovery from menthol's action of LVA as well as HVA currents within 5 min of washing. HVA currents were reduced in amplitude after washing, most likely due to their intrinsic rundown during internal perfusion. In some cells treated with menthol full recovery was obtained within 15 min.

The finding of HVA peak reductions with menthol was not consistent. In three neurons a 10–15% increase in HVA peak current was observed at potentials between 0 and +20 mV while LVA currents were strongly reduced. We attributed this to the fact that the I–V relationship of HVA currents assumed maximum negative slope in this range of potential and that menthol had little influence on the amplitude of HVA currents (Fig. 3). A 2–5 mV horizontal shift to the left of the I–V characteristics, due to internal dialysis of the cell (Carbone and Lux 1987), might then account for the small increase of the HVA current amplitude observed at +10 to +20 mV. In other five DRG cells, application of 0.5 mM menthol caused on the average a 5–15% reduction of the HVA current amplitude and a 4–6 mV increase of the current reversal potential, E_{rev},

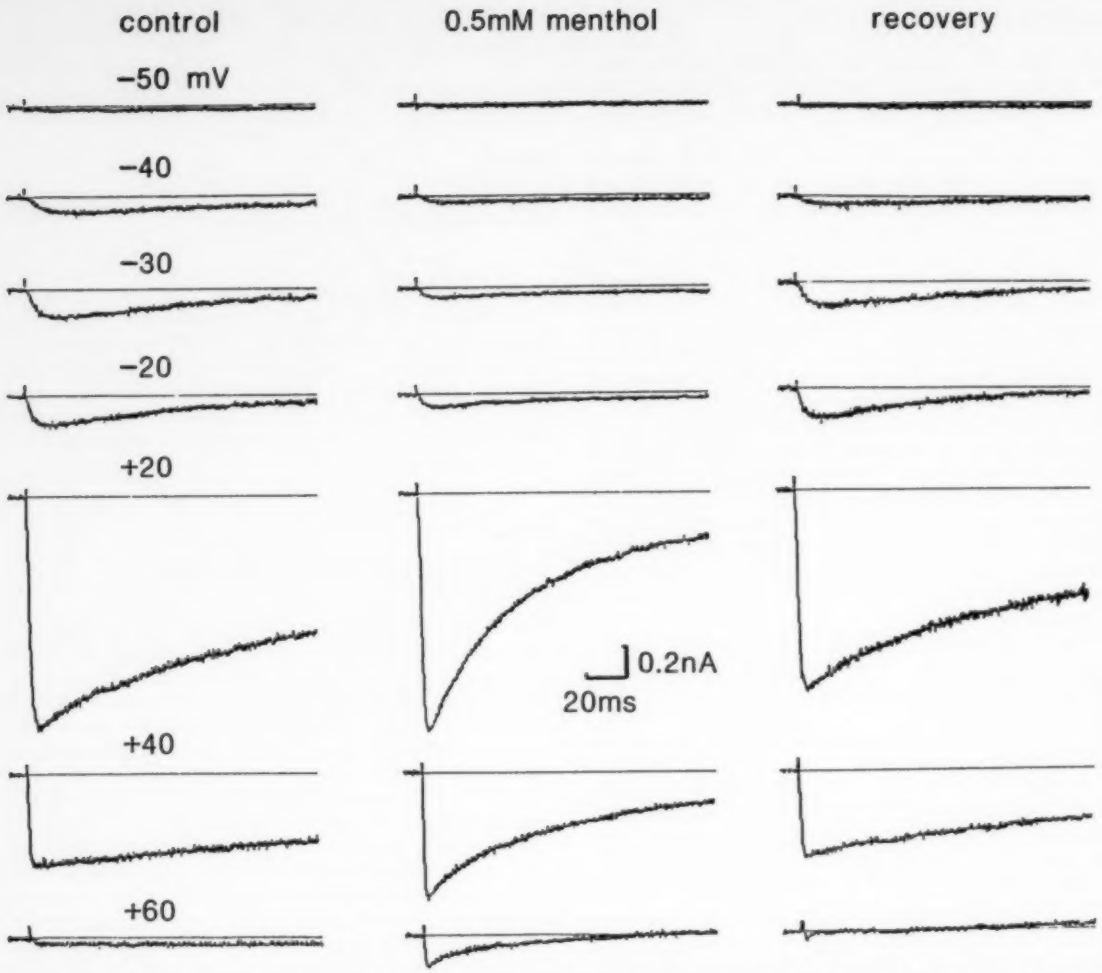

Fig. 2. Effect of menthol on Ca currents in a chick DRG cell. The traces are whole-cell Ca currents recorded at the potentials indicated: before (*left*), during (*middle*) and after (*right*) application of 0.5 mM menthol. Menthol was dissolved in the external medium and ejected from a multi-barrelled glass pipette positioned 50–100 μm from the cell (see Methods). Records in the middle were taken 3 min after the perfusion had started. Currents recovered nearly completely within 5 min of washing. Holding potential was −80 mV. *Out*: 20 mM $CaCl_2$. *In*: 120 mM CsCl

estimated by linear extrapolation near zero current (see Fig. 3). The effect on E_{rev} was reversible when menthol was washed out suggesting a real drug action rather than a consequence of internal cell perfusion.

In two cells, prolonged applications of 10 mM of cyclohexanol to the external bath had no significant effects on the time courses of both types of Ca^{2+} currents.

Menthol speeds up HVA current inactivation

HVA currents elicited by pulses of 150 ms in duration normally decayed with a time course which followed a single exponential function (Fig. 4, left). The time constant of HVA inactivation, τ_h, increased with increasing voltage. At +10 mV the average value of τ_h was 40 ms ($n = 5$), and increased monotonically to 300 ms at larger depolarizations (Fig. 5b, diamonds). This increase of τ_h was well correlated to the peak reduction of HVA currents indicating a dependency of current inactivation on Ca ions entering the cell (see also Carbone and Lux 1987). Menthol accelerated and enhanced HVA current inactivation (Fig. 4, right). As a consequence, τ_h drastically decreased (40 ms at +40 mV) and became rather insensitive to membrane potentials positive to +10 mV (Fig. 5b, circles). In the presence of menthol, τ_h also showed little dependency on Ca current amplitudes.

These effects were striking in DRG cells incubated for 15 min in solutions containing 1 mM menthol (Fig. 6). Positive to +10 mV, inactivation developed with a time constant of approximately 30 ms (Fig. 6a) and was nearly complete for depolarizing pulses of 500 ms duration (Fig. 6b). In addition, Ca current inactivation was found largely independent of the rise and peak amplitude of the current (Fig. 6c). Taken together these findings suggest that HVA current inactivation in the presence of menthol becomes insensitive

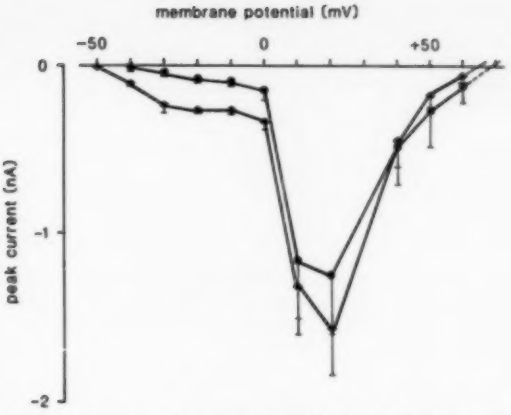

Fig. 3. Average peak current from five chick DRG cells plotted against membrane potential at control (◆) and with 0.5 mM menthol (●). *Bars* represent standard error from the mean. The *dashed lines* drawn between +60 and +70 mV are a linear extrapolation of the I−V characteristics. Their crossing point with the voltage axis was taken to indicate the current reversal potential, E_{rev}

to changes in $[Ca^{2+}]_i$. Similar results have been recently reported in identified snail neurons (Swandulla et al. 1986).

The action of menthol on Ca current inactivation did not depend on the presence of a fast inactivating current which has been reported to activate positive to +10 mV and to strongly deactivate at low resting potentials (−50 mV) (N-current, Nowycky et al. 1985). This was concluded from the following observations. (i) Menthol produced acceleration of Ca current inactivation also in cells with weakly inactivating Ca currents (Fig. 7a). (ii) The action of menthol on Ca inactivation was insensitive to changes of the holding potential from −80 to −50 mV (Fig. 7b). (iii) Cells which were incubated for 15 min in 0.75 mM menthol had fully inactivating Ca currents at +20 mV, independently of whether the membrane was held at −80 or −50 mV, (Fig. 7c). Under these conditions, there was a 10−25% reduction in the size of the currents at −50 mV, which we attributed to an increased slow inactivation of the high-threshold Ca current at more positive holding potentials.

It was unlikely that these effects were due to a menthol action other than on Ca channels. Activation of outward current components such as K currents was excluded by the finding that menthol did not affect the remaining linear current components after blocking Ca channels by Cd^{2+} (0.2 mM) or Ni^{2+} (5 mM) (see also Swandulla et al. 1986).

Menthol does not affect the turning-on and -off of LVA and HVA channels

The time to peak of Ca currents, t_p, was used as a representative parameter for studying the inactivation kinetics of LVA and HVA channels. Figure 5 shows that t_p of LVA and HVA channels changes very little during menthol application (circles). Except for a 3−5 mV shift to the left, the voltage-dependency and absolute values of t_p remained nearly unchanged with menthol. The slight shift of t_p might have been caused by the internal cell perfusion.

Also the deactivation of Ca currents was little affected by menthol. Figures 8 and 9 show tail currents associated with the closings of LVA and HVA channels, before (C) and during (M) menthol application. Both types of tail currents could be well approximated by a single exponential function with time constant, τ_t. In 20 mM Ca^{2+}, τ_t measured at the peak of LVA currents on repolarization to −80 mV was 0.83 ms at control and 0.97 ms with menthol (Fig. 8a, b). In agreement with previous observations on the same preparation (Carbone and Lux 1987) tail currents measured after depolarizations of variable duration were different in amplitude but had similar time constants (Fig. 8a).

To minimize the contribution of LVA currents, HVA tail currents were measured in cells held at −70 mV (Fig. 9). Repolarizations from +20 mV were also to −70 mV. At this potential HVA tail currents are sufficiently slow (with 20 mM Ca^{2+}, τ_t = 0.34 ms) to be accurately resolved with the time resolution of our recording amplifier. Application of menthol reduced the tail current amplitude proportionally to the Ca current depression, with little effect on their time course (Fig. 9b).

Block of LVA currents by menthol

Menthol depressed LVA peak currents in a dose dependent manner following a 1:1 stoichiometry. This is shown in Fig. 10 where the average LVA current amplitudes obtained from 5 different cells at various menthol concentrations, [M], are fitted with the equation:

$$I_M/I_{LVA} = (K_m/(K_m + [M])\,, \qquad (1)$$

where I_{LVA} and I_M indicate the amplitude of LVA currents at control and with menthol (V = −30 mV). K_m is the apparent dissociation constant of the menthol-receptor complex.

Block of LVA currents by menthol was neither voltage nor time dependent. It could also not be explained by a negative shift of the steady state current inactivation characteristics. This was indicated by the finding that changes in the holding potential to more negative values (up to −120 mV) for several minutes did not affect the percent of current block by menthol.

Action of menthol on Ca currents in rat DRG cells

The effects of menthol on LVA and HVA currents in rat sensory neurons are illustrated in Fig. 11a. As in chick DRG, 0.5 mM menthol produced a 60−70% depression of LVA currents (top) and considerable acceleration of HVA current inactivation (bottom). In this case, however, the latter effect could not be clearly resolved because of the prominent contribution of LVA channels to the total current. Ca current inactivation at large voltages had an unusual double exponential time course which results from the simultaneous inactivation of LVA and HVA currents of comparable size. The inactivating action of menthol on HVA currents of normal size and time course observed in most rat DRGs is shown in Fig. 11b. Similar to avian DRGs, menthol increases by about a factor of 7 the rate of inactivation at +20 mV with little effect on the rising phase of the currents.

Discussion

Our results demonstrate that bath application of menthol has different effects on the HVA and LVA Ca currents of

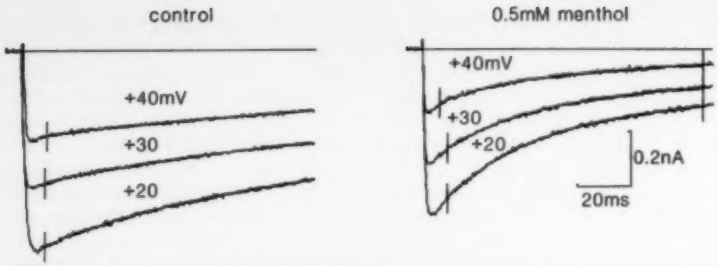

Fig. 4. Effect of menthol (0.5 mM) on HVA current inactivation. The time course of the current decline was fitted (starting from the *vertical bars*) with a single exponential function at the potentials indicated, using a least square criterion for all parameters (Bevington 1974). Time constants (τ_h) of the exponentials were 81.3 ms (+20 mV), 124 ms (+30 mV) and 180 ms (+40 mV) in control (*left*) and 39.8 ms (+20 mV), 40.2 ms (+30 mV) and 40.6 ms (+40 mV) after menthol application (*right*). Holding potential was −80 mV

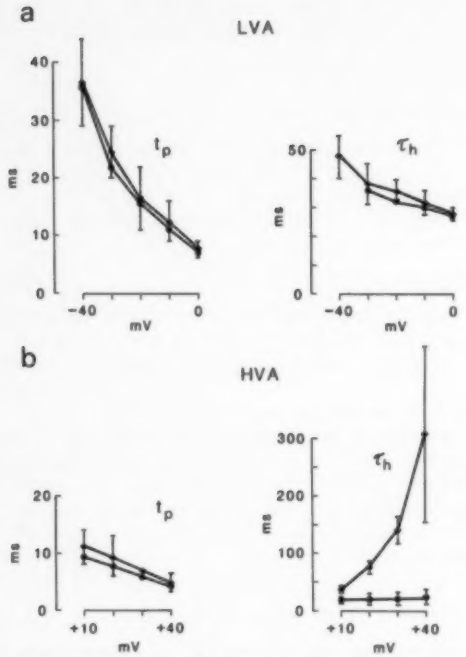

Fig. 5. Comparison of the time to peak (t_p) and inactivation time constant (τ_h) of LVA (**a**) and HVA (**b**) Ca currents in chick DRG cells in control (◆) and with menthol (0.5 mM) (●). τ_h was estimated by fitting a single exponential function to the current decay (see also Fig. 4). Note the drastic decrease of the τ_h of HVA currents with menthol. (●) and (◆) are averaged values of five cells. *Bars* indicate standard deviations. Holding potential was −80 mV. Outside: 20 mM $CaCl_2$. Inside: 120 mM N-methylglucamine-Cl

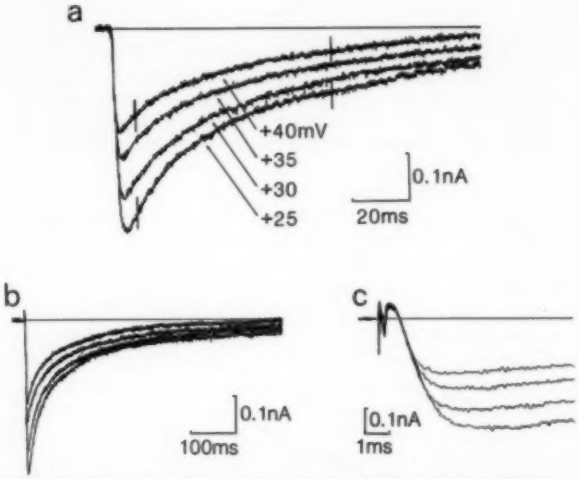

Fig. 6. Time course of inactivation (**a, b**) and activation (**c**) of HVA currents in a DRG cell after incubation in menthol. The cell was incubated in menthol solution (1 mM) for 15 min to achieve steady-state action of menthol. **a**, **b** and **c** show recordings of the same experiment at different time scales. **a** Current decay from the peak was fitted by a single exponential function (between *vertical bars*). τ_h was 31.3 ms at +25 mV and 27.9 ms at +40 mV. Note the slight decrease of τ_h, despite peak Ca current amplitudes were reduced with more positive potentials. **b** Complete inactivation of HVA currents with menthol. **c** Turning-on of Ca currents at the potentials in **a**. Holding potential was −80 mV

vertebrate sensory neurons. It reversibly reduces LVA currents and speeds up inactivation of the HVA current component. Menthol's action differs clearly from those of other substances such as dopamine, which also acts differently on the two types of Ca channels (Marchetti et al. 1986). In contrast to dopamine which produces irreversible effects, menthol is one of the few examples of a drug which reversibly blocks LVA channels by binding to an external receptor site.

Menthol's action is specific. As an alcohol derivative it could possibly act by modifying membrane structure or fluidity (Grisham and Barnett 1973; Haydon et al. 1977). However, several lines of evidence argue against this hypothesis: (i) Cyclohexanol, the highly lipid soluble alcohol from which menthol is derived (Fig. 1), failed to produce any effects on Ca currents even at millimolar concentrations. (ii) Menthol has a diverse action on different populations of Ca channels in the same membrane, it blocks specifically the low-threshold Ca channel while it affects inactivation of the high threshold one. (iii) No significant shift in the I−V characteristics typical of local anesthetics (Hille 1984) was observed with menthol (Fig. 3).

As recently described, the inactivation time course of a Ca current in an identified type of *Helix* neuron is modulated by menthol (Swandulla et al. 1986). Menthol was found to introduce a fast phase in the time course of Ca inactivation

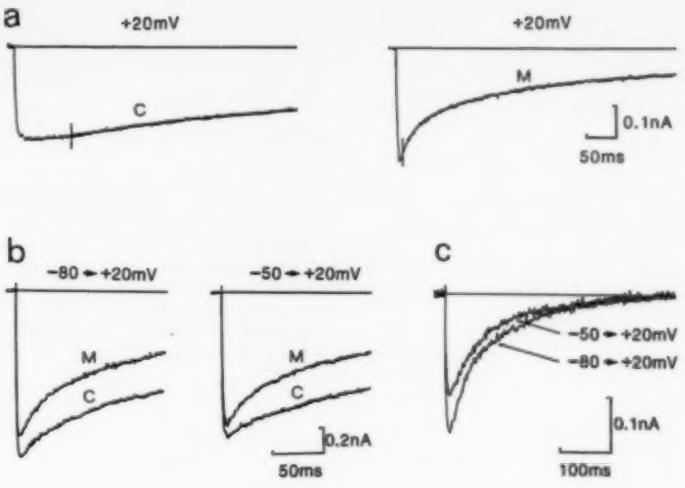

Fig. 7a–c
The inactivating action of menthol is independent of the presence or absence of a fast inactivating high-threshold Ca current. **a** Speeding-up of HVA current inactivation with menthol. *C* control; *M* 0.5 mM menthol. Single exponential functions were fitted to the current decay (after *vertical bars*, curves superimposed). τ_h was 300 ms in control and 117 ms after menthol application. Voltage steps were from −80 to +20 mV. **b** The menthol induced inactivation time course was nearly unchanged when changing the holding potential from −80 mV (*left*) to −50 mV (*right*). This became particularly evident when cells were incubated in menthol (0.75 mM) for several minutes (**c**). Note that inactivation was complete under these conditions

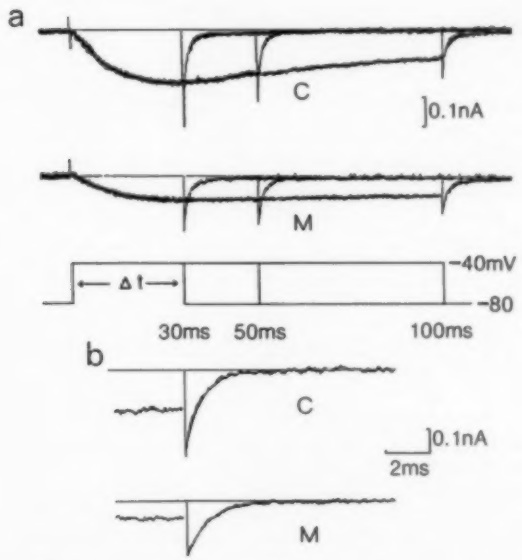

Fig. 8a, b. The effect of menthol on LVA tail currents. *C* control; *M* menthol (0.5 mM). **a** Tail currents measured on repolarization to −80 mV voltage steps to −40 mV at the time indicated. **b** Tail currents measured after 30 ms to −40 mV on a different time scale. The time course of the tails was fitted with a single exponential function, which is shown superimposed on the original trace. τ_t was 0.83 ms at control and 0.97 ms during menthol application. These values of τ_t are about a factor of 3 smaller than those previously reported on the same preparation at room temperature and 5 mM $[Ca^{2+}]_o$ (Carbone and Lux 1987). This may be due to a 10–15 mV shift of τ_t (V) toward positive potentials caused by the increased external $[Ca^{2+}]_o$ (20 mM) used in the present experiments. Out: 20 mM $CaCl_2$

which was independent of the presence of $[Ca^{2+}]_i$ and showed a weak voltage-dependency between −10 and +20 mV in 40 mM Ca^{2+} (see Fig. 3B in Swandulla et al. 1986). The inactivation of HVA currents in DRG cells have close similarities to that of HVA currents in *Helix* neurons (Carbone and Lux 1987). For instance, in *Helix* as well as in chick DRG neurons the HVA channel inactivation shows, to a different degree, a marked sensitivity to the level of free intracellular Ca^{2+}. This is suggested by the following observations: (1) inactivation is largely incomplete in the presence of internal Ca-EGTA buffers as used in our experiments, (2) inactivation is potentiated with increasing Ca entry into the cell and (3) Ba^{2+} and monovalent cations (Na^+, Li^+ and Cs^+) used as charge-carriers make inactivation less complete (Lux et al. 1987). Thus, it is likely that menthol acts on HVA channels similarly as described in *Helix* i.e., facilitating their inactivation gating thereby suppressing the inactivating action of intracellular Ca^{2+}. Our failure to detect a weak voltage-dependency of τ_h (V) between −20 and +10 mV, in menthol treated cells, might be simply due to the difficulty in DRG cells of clearly separating HVA from LVA currents in this potential range.

Our data show that menthol has practically no action on a third type of Ca current (Nowycky et al. 1985) which has been reported to activate transiently at high voltages (> +10 mV) and is fully deactivated below −50 mV (Fig. 7). However, it could be possible that menthol acts on the high-threshold Ca channels by transforming the slowly inactivating HVA channel into a fast inactivating one similar to the N-type described by Nowycky et al. 1985. We think this possibility is rather unlikely for the following reasons. First, Ca current inactivations in cells bathed in menthol solutions should be steeply voltage-dependent in the voltage range +10 to +40 mV (see Fig. 3 in Nowycky et al. 1985), while in our case the inactivation of Ca currents in the presence of menthol appears largely Ca^{2+}- and voltage-independent (Figs. 4–6). Second, lowering the holding potential from −80 to −50 mV should nearly abolish all the Ca currents in menthol-treated cells, while we observed only a 10–25% reduction of their size (Fig. 7).

Menthol speeds up inactivation despite intracellular Ca buffering. Similarly to menthol a variety of substances including local anesthetics and thiazin dyes have been found to accelerate inactivation of Na and K channels in other preparations (for a review see Hille 1984). They simulate inactivation by slowly blocking those channels opened up by depolarization. On repolarization, channels have to be

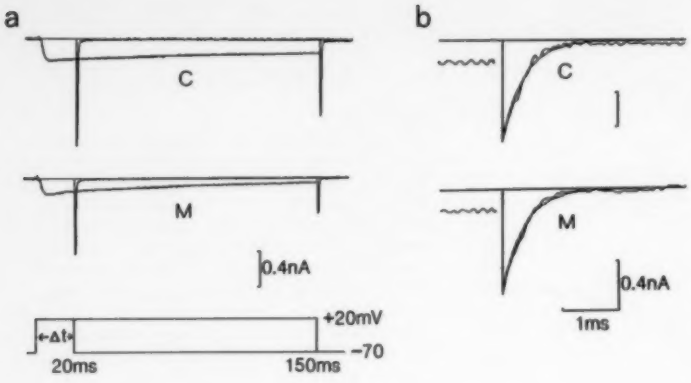

Fig. 9a,b
Effects of menthol on HVA tail currents, *C*, control; *M*, menthol (0.5 mM). **a** HVA tail currents recorded on repolarization to −70 mV from step depolarizations to +20 mV at the time indicated. **b** Tail currents measured 20 ms after the onset of the depolarizing pulse from a different cell, on an expanded time scale. The decay of the tail currents was fitted with a single exponential function, with a τ_i of 0.34 ms at control and 0.36 ms during menthol application. Theoretical and experimental curves are superimposed. Out: 20 mM $CaCl_2$

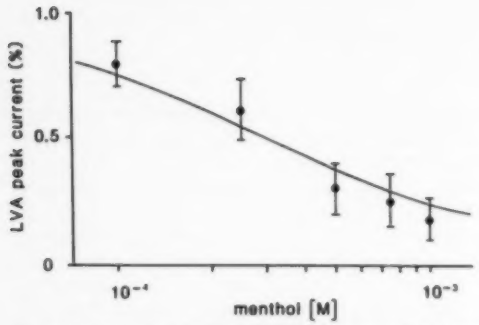

Fig. 10. Concentration dependence of the menthol-induced reduction of LVA currents. The plot shows a dose-response curve of normalized peak current reduction vs. the logarithm of the external menthol concentration. Each point is the mean value of five cells. *Vertical bars* indicate standard deviation from the mean. Equation (1) in the text was derived under the assumptions that: (i) menthol interacts with a receptor site (R) following a first order chemical reaction of the type: menthol $+R \underset{k_{-1}}{\overset{k_1}{\rightleftharpoons}}$ menthol $-R$, where k_1 and k_{-1} are the forward and reverse rate constants with $K_m = k_{-1}/k_1$, (ii) the menthol-bound channels are fully blocked and do not contribute to the total current. The theoretical curve was calculated from Eq. (1) for $K_m = 0.3$ mM. Holding potential was −80 mV

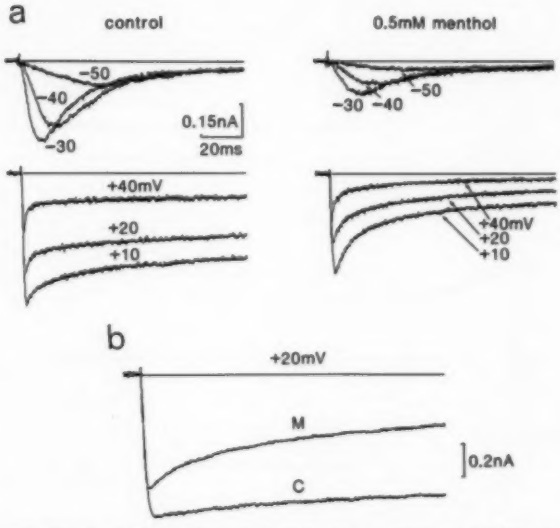

Fig. 11a,b. Action of menthol (0.5 mM) on LVA and HVA Ca currents in rats DRG cells. **a** LVA and HVA currents recorded at the potentials indicated in control (*left*) and after menthol application (*right*). Recovery of the currents was nearly complete after 20 min of washing (not shown). Note the initial fast phase of HVA current inactivation above +10 mV at control. Since HVA current amplitudes were comparatively small in this cell (see also Carbone and Lux 1987), the fast current component at these potentials reflects inactivation of the overlapping LVA currents which normally contribute much less in DRG cells with large HVA currents. **b** Effects of 0.5 mM menthol on HVA currents of normal size from a rat DRG. Voltage steps were to +20 mV. *C* control: *M* 0.5 mM menthol. Holding potential was −80 mV

cleared from these substances before they can close and this process always leads to a considerable slowing of tail currents. The analogy with these other systems fails in this important point: menthol was never observed to affect the kinetics of tail currents (see Figs. 8 and 9).

From the present data little can be inferred about the location of menthol's binding sites. In the case of HVA channels, it may bind to receptors on the external side of the channel. However, since it is uncharged and therefore lipid soluble it may reach deeper structures of the channel protein, such as the inner inactivation gate, by hydrophobic pathways as described for certain uncharged local anesthetics (Hille 1984). In this case, however, one would expect that menthol also acts from the inside of the membrane. This was never observed, even after long internal perfusions (20 min) with menthol concentrations which produced drastic effects from the outside (1 mM).

Like menthol, other high molecular weight alcohols (octanol, nonanol and decanol) have been recently reported to exert a selective action on the low-threshold Ca current in inferior olivary neurons (Llinas and Yarom 1986). The amount of these alcohols required to block neuronal LVA currents is sufficiently low (< 1 μM) to support the existence of a high-affinity binding site for these compounds at the LVA channel. The question remains, whether such receptor is also present in DRG neurons and is common to menthol or other alcohols. Independently of this, however, the high-

affinity and specificity of various alcohols for neuronal LVA channels appear promising for the search of suitable molecules which allow the separation and identification of LVA from other membrane channels.

Acknowledgements. We thank Mrs. H. Tyrlas for excellent technical assistance throughout all stages of this project.

References

Armstrong CM, Matteson DR (1985) Two distinct populations of calcium channels in a clonal line of pituitary cell. Science 227:65–67

Barde Y, Edgar D, Thoenen H (1980) Sensory neurons in culture: changing requirements for survival factors during embryonic development. Proc Natl Acad Sci USA 77:1199–1203

Bean BP (1985) Two kinds of calcium channels in canine atrial cells. J Gen Physiol 86:1–30

Bevington PR (1969) Data reduction and error analysis for the physical sciences. McGraw-Hill, New York, p 336

Boll W, Lux HD (1985) Action of organic antagonist on neuronal calcium currents. Neurosci Lett 56:335–339

Bossu JL, Feltz A, Thomann JM (1985) Depolarization elicits two distinct calcium currents in vertebrate sensory neurons. Pflügers Arch 403:360–368

Brown AM, Lux HD, Wilson DL (1984) Activation and inactivation of single calcium channels in snail neurons. J Gen Physiol 83:751–769

Byerly L, Hagiwara S (1982) Calcium currents in internally perfused nerve cell bodies of *Limnea stagnalis*. J Physiol (Lond) 322:503–528

Carbone E, Lux HD (1984a) A low voltage-activated calcium conductance in embryonic chick sensory neurons. Biophys J 46:413–418

Carbone E, Lux HD (1984b) A low voltage-activated fully inactivating calcium channel in vertebrate sensory neurons. Nature (Lond) 310:501–503

Carbone E, Lux HD (1986a) Low and high voltage-activated Ca channels in vertebrate cultured neurons: properties and function. Exp Brain Res (Suppl) 14:1–8

Carbone E, Lux HD (1986b) Sodium channels in cultured chick dorsal root ganglion neurons. Eur Biophys J 13:259–271

Carbone E, Lux HD (1987) Kinetics and selectivity of a low voltage-activated Ca^{2+} current in chick and rat sensory neurons. J Physiol (Lond) (in press)

Carbone E, Morad M, Lux HD (1987) External Ni^{2+} selectively blocks the low-threshold Ca^{2+} current of chick sensory neurons. Pflügers Arch 408 (Suppl) R 60

Deitmer JW (1984) Evidence for two voltage-dependent calcium currents in the membrane of the ciliata *Stylonychia*. J Physiol 355:137–159

DeRiemer SA, Sakmann B (1986) Two calcium currents in normal rat anterior pituitary identified by a plaque assay. Exp Brain Res (Suppl) 14:139–154

Fedulova SA, Kostyuk PG, Veselovsky NS (1985) Two types of calcium channels in the somatic membrane of new-born rat dorsal root ganglion neurons. J Physiol (Lond) 359:431–446

Fenwick EM, Marty A, Neher E (1982) Sodium and calcium channels in bovine chromaffin cells. J Physiol (Lond) 331:599–635

Fox AP, Krasne S (1984) Two calcium currents in *Neanthes arena ceodentatus* egg cell membranes. J Physiol (Lond) 356:491–505

Grisham CM, Barnett RE (1973) The effect of long chain alcohols on membrane lipids and the (Na^+ + K^+)-ATPase. Biochim Biophys Acta 311:417–422

Hagiwara S, Byerly L (1981) Calcium channel. Annu Rev Neurosci 4:69–125

Hagiwara N, Irisawa H, Kameyama M (1987) Transient-type calcium current contributes to the pace-maker potential. J Physiol (Lond) (in press)

Hamill OP, Marty A, Neher E, Sakmann B, Sigworth FJ (1981) Improved patch-clamp techniques for high-resolution current recording from cells and cell-free membrane patches. Pflügers Arch 391:85–100

Haydon DA, Hendry BM, Levison SR, Requena J (1977) Anesthesia by the n-alkanes. A comparative study of nerve impulse blockage and the properties of black lipid bilayer membrane. Biochim Biophys Acta 470:17–34

Hille BJ (1984) Ionic channels of excitable membranes. Sinauer Associates, Sunderland, MA, USA

Kostyuk PG, Veselovsky NS, Tsyndrenko AY (1981a) Ionic currents in the somatic membrane of rat dorsal root ganglion neurons. I. Sodium currents. Neuroscience 6:2423–2430

Kostyuk PG, Veselovsky NS, Fedulova SA (1981b) Ionic currents in the somatic membrane of rat dorsal root ganglion neurons. II. Calcium currents. Neuroscience 6:2431–2437

Llinas R, Jahnsen H (1982) Electrophysiology of mammalian thalamic neurons in vitro. Nature (Lond) 297:406–408

Llinas R, Yarom Y (1981) Properties and distribution of ionic conductances generating electroresponsiveness of mammalian inferior olivary neurones in vitro. J Physiol (Lond) 315:569–584

Llinas R, Yarom Y (1986) Specific blockage of the low-threshold calcium channel by high molecular weight alcohols. Neurosciences (Abstract) 12:174

Lux HD, Carbone E, Davies N (1987) Monovalent cation currents through low- and high-threshold Ca^{2+} channels in chick sensory neurons. Pflügers Arch 408 (Suppl): R 60

Marchetti C, Carbone E, Lux HD (1986) Effects of dopamine and noradrenaline on Ca channels of cultured sensory and sympathetic neurons of chick. Pflügers Arch 406:104–111

McCleskey EW, Fox AP, Feldman D, Olivera BM, Tsien RW, Yoshikami D (1986) The peptide toxin ωCgTX blocks particular types of neuronal Ca channels (Abstract). Biophys J 49:431a

Nowycky MC, Fox AP, Tsien RW (1984) Multiple types of calcium channel in dorsal root ganglion cell distinguished by sensitivity to cadmium and single channel properties (Abstract). Soc Neurosci 10:526

Nowycky MC, Fox AP, Tsien RW (1985) Three types of neuronal calcium channels with different calcium agonist sensitivity. Nature 316:440–443

Swandulla D, Carbone E, Schäfer K, Lux HD (1985) Menthol modulates Ca inactivation in neurons. Pflügers Arch 405(Suppl): R 39

Swandulla D, Schäfer K, Lux HD (1986) Ca channel current inactivation is selectively modulated by menthol. Neurosci Lett 68:23–28

Yaari Y, Hamon B, Lux HD (1987) Development of two distinct types of calcium channels in cultured mammalian hippocampal neurons. Science (USA) (in press)

Received July 30, 1986/Accepted January 21, 1987

Pflügers Arch (1987) 409:60–66

Pflügers Archiv
European Journal of Physiology
© Springer-Verlag 1987

A chloride-bicarbonate exchanging anion carrier in vascular smooth muscle of the rabbit*

F. P. Gerstheimer, M. Mühleisen, D. Nehring, and V. A. W. Kreye

II. Physiologisches Institut der Universität Heidelberg, Im Neuenheimer Feld 326, D-6900 Heidelberg, Federal Republic of Germany

Abstract. Cl^- efflux into various incubation media (PSS) was studied in pieces of rabbit aortae loaded with ^{36}Cl. Replacement of HCO_3^-/CO_2 by HEPES/O_2 in the PSS increased the rate of Cl^- efflux by a factor of 2.4. This effect was suppressed in Cl^--free PSS containing isethionate, propionate, or benzenesulfonate, but not in NO_3^--PSS, or Br^--PSS. The stimulant effect of HCO_3^- withdrawal on Cl^- efflux was reduced by 140 µM DIDS, but not by 1 mM furosemide. The Cl^- efflux was temperature-dependent ($Q_{10} = 2.3-2.5$), and it was not affected on depolarisation by high $[K^+]_o$. – The $[Cl^-]_i$ of rabbit aorta determined by uptake studies with ^{36}Cl, decreased slightly (by 15%) below controls in PSS containing 140 µM DIDS, but drastically (from 32.6 to 13.5 mM, i.e. by 59%) in PSS containing 1 mM furosemide. – Withdrawal of HCO_3^-/CO_2 depolarized rabbit pulmonary artery in standard PSS and in Br^--PSS or NO_3^--PSS, but not in benzenesulfonate-PSS. – The pH_i of rabbit aorta determined by the distribution of (^{14}C)-DMO, increased in Cl^--free PSS containing isethionate or glucuronate. – It is concluded that transport mechanisms play a major role in the distribution of Cl^- in vascular smooth muscle, and that a membrane anion carrier operates in this tissue which can transport Cl^- and HCO_3^- across the cell membrane. This mechanism seems to be involved in the regulation of pH_i. However, the known high $[Cl^-]_i$ of vascular smooth muscle is rather mediated by the furosemide-sensitive Na-K-Cl cotransport than by this anion carrier.

Key words: Vascular smooth muscle – Ion flux studies – Membrane potential – Intracellular pH – Diuretics – Furosemide – DIDS

Introduction

Vascular smooth muscle (vsm) is characterized by a high intracellular concentration of Cl^- ($[Cl^-]_i$) which cannot be explained by passive ion distribution; values between 25 to 90 mM (i.e. an E_{Cl} between −47 and −10 mV) were measured in various laboratories by indirect techniques (Jones 1980; Kreye and Ziegler 1982), and confirmed by the electron probe in the rabbit portal-anterior vein (Somlyo et al. 1979). In the dog carotid artery (Villamil et al. 1979), and in rabbit vascular tissues (Kreye et al. 1981), the loop diuretic, furosemide, reduces $[Cl^-]_i$. In the latter tissues, furosemide interfered potently with the $^{36}Cl/Cl$-exchange, and hyperpolarized the cell membrane (Kreye et al. 1981). Subsequently, the existence of a Na-K-Cl cotransport operating in vsm, was suggested (Owen 1984).

In the guinea-pig vas deferens (Aickin and Brading 1984), the distribution of Cl^- ions has been attributed to the action of a Cl^-/HCO_3^- countertransport. It was the aim of this study to investigate whether such a mechanism also operates in vsm, and to compare it to the Na-K-Cl cotransport with respect to the high $[Cl^-]_i$ in this tissue. Ion flux studies and microelectrode experiments were performed in rabbit isolated aortae and main pulmonary arteries, respectively.

Methods

Preparations and solutions. For Cl^- flux studies, pieces (10–20 mg) of carefully prepared aortae from White New Zealand rabbits were mounted on stainless steel holders, and equilibrated for 1 h in physiological salt solution (PSS) at 37° C. Standard PSS contained (in mM): NaCl 128, KCl 4.7, $NaHCO_3$ 11.9, $CaCl_2$ 2.5, $MgCl_2$ 1.2, Ca-Na_2-EDTA 0.1, NaH_2PO_4 1.2, glucose 10. It was gassed with 95% O_2/5% CO_2 resulting in a pH of 7.1–7.2 which is standard in this laboratory since in contraction studies, vascular preparations perform better at this pH than at 7.4. In Cl^--free PSS, $NaNO_3$, NaBr, Na-isethionate, Na-benzenesulfonate, Na-propionate, or Na-glucuronate, respectively, was substituted for NaCl, K-isethionate for KCl, Ca-acetate for $CaCl_2$, and Mg-acetate for $MgCl_2$. HCO_3^--free PSS (i.e. HEPES-buffered PSS) contained 11.9 mM HEPES instead of HCO_3^-, and the pH was adjusted with NaOH to 7.2. Pure O_2 was taken for gassing.

Efflux studies. Equilibrated preparations were loaded for 90–120 min in PSS containing ^{36}Cl (1.5–2 MBq/ml). Then, the holders with the tissues were placed on the rotating shafts of small motors fixed to an electropneumatic hoisting device which dipped them sequentially for periods of 2 min into 18 tubes moved by a circular fraction collector. Each tube contained 5 ml of standard or modified PSS to which drugs were added if required. The standard protocol consisted of changing the kind of PSS after the tissues had

* Supported by the Deutsche Forschungsgemeinschaft. Parts of this study have been reported to the German Physiological and Pharmacological Societies (Kreye and Gerstheimer 1982; Kreye et al. 1984a, b), and at the First International Congress on Diuretics, Miami/USA (Kreye et al. 1984c)
Offprint requests to: V. A. W. Kreye

passed the first 10 tubes. 6.8 ml of a hydrophilic scintillation cocktail (6 g PPO, 100 ml Triton X-100, 200 ml Triton X-114, made up to 1 l with xylene) were added to the effluents, and their radioactivity counted. Tissue wet weight was determined after blotting with filter paper for 5 s. The residual radioactivity in the tissue was calculated by regression analysis on the late mono-exponential part of the curve relating the radioactivity of effluents with time. To calculate the rate coefficient of Cl^- efflux, the radioactivities of single effluents were divided by the tissue activities obtained by reverse addition of the effluent activities to the tissue residual. Values are given as $\bar{x} \pm SE$, n = number of observations. Mean rates were calculated from the plateau phases before and after the change of PSS, and compared by Student's t-test for paired data.

Influx studies. The preparations were loaded for 2, 4, 6, and 8 min, respectively, in PSS containing ^{36}Cl. To clear the extracellular space from ^{36}Cl, they were then washed for 20 min at 0° C in non-labelled PSS. After blotting, weighing, and solubilization in Soluene-350 (Packard Instruments, Frankfurt, FRG), their radioactivity was counted. To determine the $[Cl^-]_i$, preparations were treated as above, but loaded with ^{36}Cl for 90 min. According to preceding studies, tissue labelling was complete after this period. The intracellular label was used for the determination of $[Cl^-]_i$ by assuming a cell water space of 24% of the tissue wet weight (Kreye et al. 1981).

Electrophysiological studies. The E_m was measured with glass microelectrodes made from Omega Dot capillary tubing (HR-30-30-1, F. Haer & Co., Brunswick, ME, USA; outer diameter: 1 mm; resistance: 50–100 megohms) in rabbit pulmonary arteries, since aortae were difficult to penetrate. They were mounted in a bath with a volume of 3 ml, and superfused with PSS at a flow rate of 2 ml/min.

Determination of intracellular pH (pH_i) by equilibrium distribution of the weak acid, DMO. Equilibrated aortae (10–20 mg) were incubated for 1 h in standard or modified PSS which for the last 30 min, contained (^{14}C) DMO (12.5 µg/ml; 5.6 kBq/ml) and (^3H)sorbitol (14.8 kBq/ml). Their wet weights were determined as usual, and their dry weights after drying at 80°C (8 h). The dry material was solubilized in 0.1 ml H_2O and 0.5 ml Soluene-350, bleached with 30% H_2O_2, and its (^3H) and (^{14}C) activities counted using Dimilume-30 (Packard) as scintillation cocktail. pH_i was calculated by the algorithm of Waddell and Butler (1959):

$$A = 10^{(pH_e - pK')} + 1$$
$$pH_i = pK' + \log\left(A \times (C_i/C_e \times (1 + V_e/V_i) - V_e/V_i) - 1\right),$$

where pH_e = pH of PSS, pK' = negative logarithm of apparent acid dissociation constant of DMO (i.e. 6.13), V_e = extracellular volume (i.e. sorbitol space), V_i = intracellular volume (i.e. total tissue volume − V_e − volume of dry tissue matter which is tissue wet weight − weight of extracellular tissue water − tissue dry weight), C_i = DMO concentration in total tissue volume, and C_e = concentration of DMO in PSS.

Calculation of apparent Cl^- permeability. The formulas used were: Flux = $[Cl^-]_i \times k_{Cl} \times V/A$ (Keynes and Lewis 1951), and Permeability = Flux/$(\beta \times [Cl^-]_i)$ (Katz 1966; Casteels 1969), where $\beta = (zE_mF/RT)/(1 - e^{-E_mF/RT})$ (Goldman 1943), V/A = volume/area ratio, k_{Cl} = rate coefficient of Cl^- efflux, and $z = -1$.

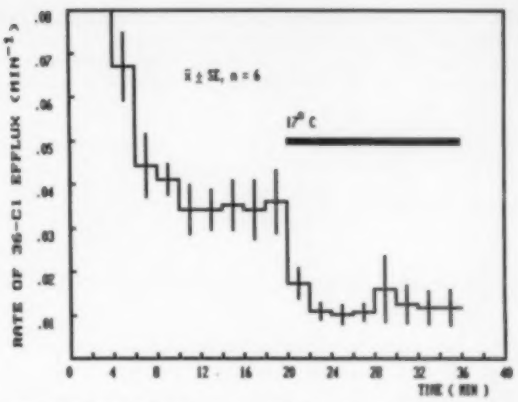

Fig. 1. Effect of temperature reduction on the rate of Cl^- efflux (min^{-1}) from rabbit isolated aorta. After 20 min (*bar*), the standard PSS of 37° C was replaced by standard PSS of 17° C

Chemicals. The salts used (Merck, Darmstadt, FRG) were of analytical grade. HEPES, Ca-Na_2-EDTA, Triton X-100, and Triton X-114 were purchased from Serva (Heidelberg, FRG), DIDS (4,4′-diisothiocyanatostilbene-2,2′-disulfonic acid) and PPO (2,5-diphenyloxazole) from Sigma (Taufkirchen, FRG), and (^{14}C) DMO (5,5-dimethyl-2,4-oxazolidinedione), (^3H)sorbitol, and ^{36}Cl from NEN (Dreieich, FRG). Furosemide (4-chloro-N-furfuryl-5-sulfamoylanthranilic acid) was kindly provided by Hoechst AG (Frankfurt, FRG).

Results

Temperature dependence of Cl^- efflux

The control efflux rate of the tissues at 37° C was reduced by 44%, 66%, and 80%, respectively, when the temperature of the PSS had been reduced to 27° C, 17° C (Fig. 1), and 0° C, respectively. Table 1 gives the rates of Cl^- efflux, the calculated Q_{10} values, and the corrected Q_{10}' values of these experiments.

Effect of HCO_3^- withdrawal on Cl^- efflux

Replacement of HCO_3^-/CO_2 by HEPES/O_2 induced a rise of the Cl^- efflux rate from -0.0476 ± 0.0031 min^{-1} to 0.1164 ± 0.0088 min^{-1} ($n = 13$, $p < 0.0001$, Fig. 2), i.e. an increase by a factor of 2.45. This effect was complete only after 6–8 min. When standard PSS was replaced by PSS containing both 11.9 mM HCO_3^- and 11.9 mM HEPES, no increase of the efflux rate was observed (control in standard PSS: -0.0527 ± 0.0061 min^{-1}, after addition of HEPES: -0.0339 ± 0.0035 min^{-1}, $n = 7$; Fig. 2). Thus, the augmentation of Cl^- efflux was the result of the HCO_3^- withdrawal, and not of a stimulant action of the HEPES buffer.

When in the PSS, Cl^- was replaced by NO_3^- (Fig. 3), or Br^-, the exchange of HCO_3^-/CO_2-PSS by HEPES/O_2-PSS resulted in a similar increase of Cl^- efflux as in standard PSS (Table 2). In contrast, when large anions (isethionate, propionate, or benzenesulfonate (Fig. 3), respectively), were

Table 1. Temperature-dependence of the Cl^- efflux from rabbit isolated aorta. The preparations were initially incubated in standard PSS at temperature t_1, and subsequently at temperature t_2. k_1 and k_2 are mean rates of Cl^- efflux before and after the change of temperature. For the calculation of Q_{10} values, see [a]. Q_{10}' values represent corrected values based on the assumption that the efflux rate at 0° C is the basal loss of Cl^- from the tissues without contribution of carrier-mediated processes, i.e. k_2 (0°C) was subtracted from the other k-values for the calculation of Q_{10}'

t_1 (° C)	t_2 (° C)	n	k_1 (min^{-1}) ($\bar{x} \pm$ SE)	k_2 (min^{-1}) ($\bar{x} \pm$ SE)	Q_{10}[a]	Q_{10}'
37	0	4	-0.0387 ± 0.0061	-0.0076 ± 0.0023	1.59	–
37	27	6	-0.0369 ± 0.0036	-0.0206 ± 0.0023	1.79	2.25
37	17	6	-0.0352 ± 0.0072	-0.0120 ± 0.0039	1.71	2.50

[a] Q_{10} values based on $\log Q_{10} = [10/(t_1-t_2)] \times \log (k_1/k_2)$ (Höfer 1977)

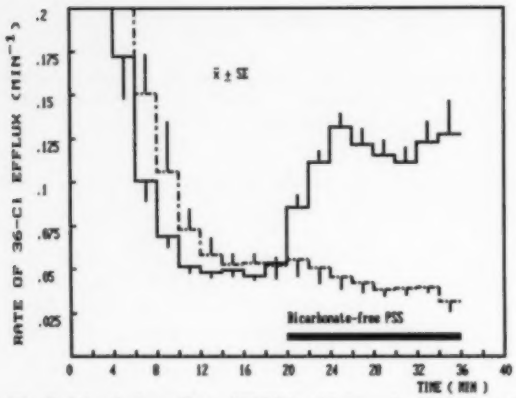

Fig. 2. Stimulating effect of HCO_3^- withdrawal on the rate of Cl^- efflux (min^{-1}) from rabbit isolated aorta ($n = 13$, *whole line*). After 20 min (*bar*), HCO_3^-/CO_2-buffered standard PSS was replaced by HEPES-buffered PSS. In the control experiment ($n = 7$, *broken line*), standard PSS was replaced by standard PSS containing 11.9 mM HEPES at min 20

substituted for Cl^-, HCO_3^- withdrawal was not followed by a rise of Cl^- efflux from the tissues; rather, a reduction in the efflux rate was encountered (Table 2, Fig. 3) in most experiments.

Effect of HCO_3^- withdrawal on Cl^- efflux in the presence of DIDS and furosemide

The potent and immediate effect of the loop diuretic, furosemide, on the basal efflux of Cl^- from rabbit aorta has been described previously (Kreye et al. 1981). DIDS, a known inhibitor of anion transport in various tissues, was less potent in this respect; in one series of such experiments, 140 µM DIDS partially and slowly (within 10–15 min) reduced the basal Cl^- efflux from -0.0522 ± 0.0019 min^{-1} to -0.0355 ± 0.0060 min^{-1}, $n = 5$), whereas in another study, an effect of DIDS on resting Cl^- efflux was barely visible.

In contrast, 10^{-4} M DIDS significantly reduced the rise of Cl^- efflux on withdrawal of HCO_3^-/CO_2; whereas in the absence of DIDS, the rate of Cl^- efflux after HCO_3^- withdrawal was -0.1164 min^{-1} (see above, and Fig. 2), it rose to only -0.0836 ± 0.0074 min^{-1} ($n = 6$, Fig. 4) on HCO_3^- withdrawal in the presence of DIDS ($t = 2.35$, $df = 17$, $2p < 0.05$). 1 mM furosemide was inactive in this respect (rate of Cl^- efflux after withdrawal of HCO_3^-: -0.1102 ± 0.0160 min^{-1}, $n = 6$, Fig. 4). This was not significantly different from the above mentioned control value ($t = 0.37$, $df = 17$, n.s.).

Effect of altered E_m on Cl^- efflux

Withdrawal of HCO_3^- reduces the E_m of vsm (see below). Therefore, by varying $[K^+]_o$, it was studied whether the stimulation of Cl^- efflux on HCO_3^- withdrawal was secondary to the altered electrical driving forces at the cell membrane. In the rabbit main pulmonary artery, a $dE_m/d\log [K^+]_o$ of 42 mV was established for a tenfold increase of $[K^+]_o$, and this data was assumed to be valid for rabbit aorta. Hence, the $[K^+]_o$ of the PSS was either increased from the standard 4.7 mM to 8.7 mM, or to 15 mM, respectively (i.e. by 4, or 11.3 mM, corresponding to an extrapolated depolarization by 11.2, or 21.2 mV, respectively). This procedure had no effect on the rates of Cl^- efflux from rabbit aorta (controls: -0.0360 ± 0.0031, or -0.0339 ± 0.0035 min^{-1}, respectively; in 8.7 mM KCl-PSS: -0.0342 ± 0.0026 min^{-1}, $n = 6$; in 15 mM KCl-PSS: -0.0334 ± 0.0041 min^{-1}, $n = 4$).

Effect of HCO_3^- withdrawal, DIDS, and furosemide on Cl^- uptake

The rate of Cl^- uptake by rabbit aorta calculated from data sampled within the first 8 min of incubation was found to be faster in HCO_3^--free PSS than in standard PSS. The means ($\pm$ SE) of the slopes of the regression curves indicating the time-dependent uptake of Cl^- were 0.150 ± 0.035 µmoles/g wet weight/min ($n = 6$) in HCO_3^--buffered standard PSS, and 0.202 ± 0.081 µmoles/g w.w./min in HEPES-buffered PSS ($n = 6$, difference not significant).

In standard PSS containing 140 µM DIDS, Cl^- uptake was moderately reduced (slopes of regression curves; controls: 0.127 µM/g w.w./min, $n = 13$, $r = 0.863$; with DIDS: 0.077 µM/g w.w./min, $n = 14$, $r = 0.516$). With 1 mM furosemide in the loading PSS, the retardation of Cl^- uptake was more pronounced (controls: 0.134 µmoles/g w.w./min, $n = 16$, $r = 0.558$; with furosemide: 0.053 µmoles/g w.w./min, $n = 16$, $r = 0.769$).

Determination of $[Cl^-]_i$

On incubation for 90 min in HEPES-buffered PSS, an only slightly larger amount of radioactively labelled Cl^- was found in aortic preparations than in controls loaded in standard PSS. In tissues incubated for 90 min in standard PSS

containing 140 μM DIDS, a slightly reduced Cl^- content was found in comparison to controls. In contrast, aortic preparations incubated in the presence of 1 mM furosemide took up substantially less Cl^- than control preparations. The calculated $[Cl^-]_i$ based on the data of this study are shown in Fig. 5.

Effect of HCO_3^- withdrawal on E_m

The E_m of rabbit isolated pulmonary arteries depolarized reversibly on HCO_3^- withdrawal (Fig. 6a); from 21 such prolonged penetrations, a depolarization by 7.3 ± 1.7 mV was obtained. PSS containing 11.9 mM of both HCO_3^- and HEPES, had no effect on E_m (Fig. 6a). On single penetrations ($n = 50$) of 1 min each, the E_m was -60.1 ± 2.9 mV ($\bar{x} \pm SE$) in standard PSS, and -52.8 ± 3.8 mV ($n = 50$) in HEPES-buffered PSS. In bromide-PSS (Fig. 6b) and in nitrate-PSS (Fig. 6c), withdrawal of HCO_3^- also induced depolarization. In contrast, in benzenesulfonate-PSS, the withdrawal of HCO_3^- did not depolarize the pulmonary artery (Fig. 6d).

In another series, the E_m of pulmonary arteries increased from -61.1 ± 0.8 mV ($\bar{x} \pm SE$, 21 single penetrations) in standard PSS to -65.9 ± 1.1 mV ($n = 17$) after superfusion for 1 h with PSS containing 10^{-4} M DIDS. Subsequent withdrawal of HCO_3^- in the presence of DIDS reduced the E_m only to -64.7 ± 0.7 mV ($n = 15$). Furosemide had no immediate effect on the E_m, but induced hyperpolarization after prolonged incubation as shown previously (Kreye et al. 1981). It did not prevent the depolarization induced by withdrawal of HCO_3^-; from 6 prolonged impalements, a decrease of E_m by 7.2 ± 0.62 mV was recorded after exchanging the standard PSS by HEPES-buffered PSS in the presence of 1 mM furosemide.

The superfusion of rabbit pulmonary arteries with isethionate-PSS was followed by a slight and slowly developing hyperpolarization; E_m increased to -64.7 ± 3.6 mV (20 single penetrations), i.e., by 4 mV over controls (see above). In none such experiments did we find an initial depolarization after Cl^- withdrawal.

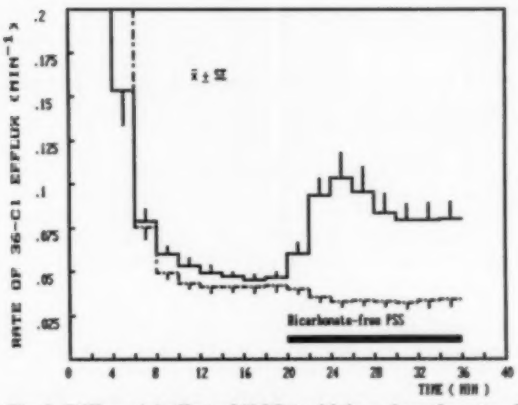

Fig. 3. Differential effect of HCO_3^- withdrawal on the rate of Cl^- efflux (min^{-1}) from rabbit isolated aorta incubated in Cl^--free PSS containing nitrate ($n = 5$, *whole line*) or benzenesulfonate ($n = 6$, *broken line*), respectively. After 20 min (*bar*), nitrate-PSS or benzenesulfonate-PSS buffered with HCO_3^-/CO_2 was exchanged by the same type of PSS buffered with HEPES

Determination of the pH_i by the (^{14}C) DMO distribution method

The pH_i of rabbit aorta incubated in standard PSS (pH 7.1) containing (^{14}C) DMO differed from pH_e by -0.19 units (Table 3). In Cl-free PSS with large anions as substitutes for Cl^-, the pH_i increased above pH_e (Table 3). In contrast, incubation of rabbit aorta in standard PSS containing DIDS or in HEPES-buffered PSS being nominally free of HCO_3^-/CO_2, induced only minor albeit significant changes of the pH_i (Table 3).

Calculation of apparent Cl^- permeability

Assuming a volume/area-ratio (V/A) of 0.8 μm (Jones 1980), and using relevant data from this study (k_{Cl}: $-0.0476\ min^{-1}$, i.e. $7.933 \times 10^{-4}\ s^{-1}$; $[Cl^-]_i$: 27.1 mM; and E_m: -60.1 mV), an apparent Cl^- permeability of 2.5×10^{-8} cm/s is calculated.

Discussion

In HCO_3^--free PSS, the rate of Cl^- efflux from vsm was substantially increased. This most prominent finding of our study can be explained by an anion carrier which transports Cl^- from the cytoplasm to the extracellular space in exchange for $HCO_3^-{}_e$ and $Cl^-{}_e$. If this carrier resembles the anion carrier of human erythrocytes (Dalmark 1976; Wieth 1979; Lowe and Lambert 1983; Jennings 1985), Cl^- and HCO_3^- ions would compete for the same binding sites of the carrier (Dalmark 1976). At a pH_i of 6.9 in rabbit aorta, a $[HCO_3^-]_i$ of approximately 8 mM is calculated which comprises one third to one fourth of the $[Cl^-]_i$ in this tissue. Removing HCO_3^- from the PSS reduces $[HCO_3^-]_i$ considerably as has been shown for guinea-pig vas deferens by Aickin and Brading (1984). Thus, the ratio of $[Cl^-]_i$:$[HCO_3^-]_i$ (i.e.

Table 2. Effect of the withdrawal of HCO_3^-/CO_2 on the rate of Cl^- efflux from rabbit isolated aorta incubated with physiological salt solutions (PSS) containing different types of anions; standard-PSS contained 128 mM NaCl, and the other solutions contained the same amount of NaX instead. k_1 and k_2 are mean rate coefficients of Cl^- efflux in HCO_3^--buffered PSS and HEPES-buffered PSS, respectively

Types of PSS	k_1 (min^{-1}) ($\bar{x} \pm SE$)	k_2 (min^{-1}) ($\bar{x} \pm SE$)	n	t	$2p$
Standard-PSS	-0.0430 ± 0.0040	-0.0980 ± 0.0112	6	5.09	<0.01
Nitrate-PSS	-0.0464 ± 0.0031	-0.0926 ± 0.0122	5	4.14	<0.02
Bromide-PSS	-0.0529 ± 0.0108	-0.0875 ± 0.0179	5	2.84	<0.05
Isethionate-PSS	-0.0335 ± 0.0025	-0.0259 ± 0.0032	5	7.65	<0.01
Propionate-PSS	-0.0484 ± 0.0056	-0.0393 ± 0.0045	5	2.38	n.s.
Benzenesulfonate-PSS	-0.0410 ± 0.0038	-0.0344 ± 0.0075	6	2.11	n.s.

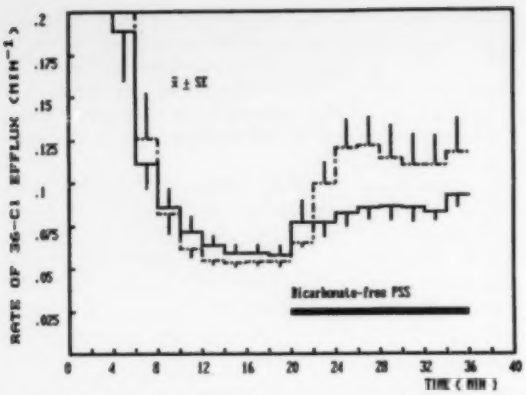

Fig. 4. Effect of 140 μM DIDS ($n = 6$, *whole line*), or of 1 mM furosemide ($n = 6$, *broken line*), respectively, on the stimulant effect of HCO_3^- withdrawal on the rate of Cl^- efflux (min^{-1}) from rabbit isolated aorta. After 20 min (*bar*), standard PSS containing DIDS was replaced by HEPES-PSS containing DIDS, or standard PSS was replaced by HEPES-PSS containing furosemide

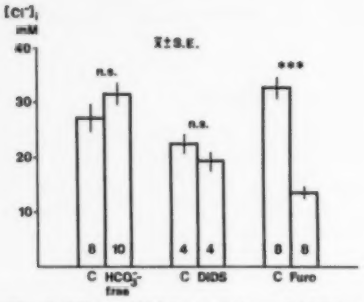

Fig. 5. Effect of HCO_3^- withdrawal (HCO_3^--free), of 140 μM DIDS, and of 1 mM furosemide (*Furo*), respectively, on $[Cl^-]_i$ of rabbit isolated aorta. Number of preparations given within the columns. *Ordinate* $[Cl^-]_i$ in mM. n.s.: not significant, *** $2p < 0.0005$

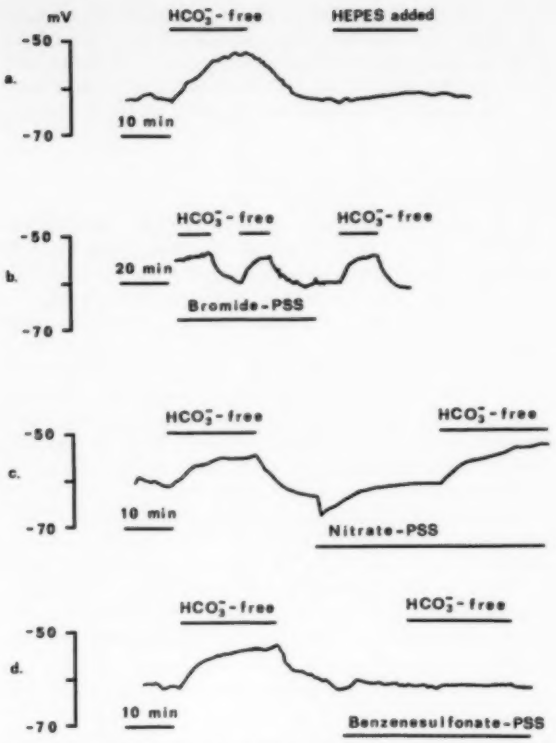

Fig. 6a–d. Effect of HCO_3^- withdrawal on the E_m of rabbit main pulmonary artery (redrawn from original long-term recordings with glass microelectrodes). At the bars titled "HCO_3^--free", the preparations were superfused with HEPES-buffered PSS instead of HCO_3^-/CO_2-buffered PSS. **a–d** Depolarization induced by withdrawal of HCO_3^- in standard PSS, bromide-PSS, and nitrate-PSS, respectively. Addition of 11.9 mM HEPES to standard PSS containing HCO_3^-/CO_2 had no effect on E_m (**a**). **d** In benzenesulfonate-PSS, withdrawal of HCO_3^- was not followed by depolarisation

Table 3. Effect of anion replacement, bicarbonate withdrawal, and DIDS on intracellular pH-values (pH_i) of preparations from rabbit isolated aortae as determined by the (^{14}C)-DMO distribution technique according to Waddell and Butler 1959 (see Methods). The preparations were incubated for 1 h in the appropriate solutions (PSS). Since the pH of the solutions (pH_e) varied within a range of 0.2 units, differences of intracellular and extracellular pH-values (ΔpH, i.e. $pH_i - pH_e$) are given instead of absolute data. ΔpH_i-values represent ΔpH in PSS other than standard PSS minus ΔpH in standard PSS to show deviation from control pH_i. ΔpH in standard PSS was also used as control value for statistical comparisons with the other ΔpH-values using Student's t-test for unpaired data

Type of PSS	ΔpH ($\bar{x} \pm SE$)	ΔpH_i	n	df	t	$2p$
Standard PSS	-0.19 ± 0.02	–	16	–	–	–
Glucuronate-PSS	$+0.34 \pm 0.03$	+0.53	16	30	16.00	<0.0005
Isethionate-PSS	$+0.26 \pm 0.03$	+0.45	24	38	10.26	<0.0005
HEPES-buffered PSS	$+0.02 \pm 0.01$	+0.21	8	22	8.12	<0.0005
140 μM DIDS in standard PSS	-0.10 ± 0.04	+0.09	8	22	2.50	<0.025

3:1 to 4:1) would turn high, and Cl^-/HCO_3^- exchange would be converted into Cl^- self exchange. In addition, the affinity of the anion carrier for HCO_3^- has been found to be 1.5 times the affinity for Cl^- in human erythrocytes (Wieth and Brahm 1980), i.e. under standard conditions, HCO_3^- is transported overproportionally in comparison to Cl^-. Hence, removal of HCO_3^- relieves the carrier from the HCO_3^- load thereby enhancing Cl^- transport. Provided that these observations are applicable to vsm, too, they would explain our finding of a stimulant effect of HCO_3^- withdrawal on Cl^- efflux.

Compared to the substantial effect of HCO_3^- withdrawal on Cl^- efflux, the rate of ^{36}Cl influx increased only slightly in the absence of HCO_3^-. This was expected since the rate of Cl^- influx was calculated from uptake data within the first 8 min of loading with ^{36}Cl, whereas the full effect of

HCO_3^- withdrawal on Cl^- efflux became only stable after this period.

Small anions can substitute for Cl_o^- as transport partners for Cl_i^- in erythrocytes (Dalmark 1976; Obaid 1980; Wieth 1979). In this study, the stimulant effect of HCO_3^- withdrawal on Cl^- efflux was maintained in Br^--PSS or NO_3^--PSS. In contrast, large anions not only suppressed it, but even reduced Cl^- efflux below its basal rate. Obviously, these anions are not countertransported for Cl_i^-; by additional omission of HCO_3^-, the anion carrier would be completely blocked, as no substrates for its outward facing binding sites would be available.

As a further support for an anion carrier in vsm, DIDS, an inhibitor of anion carriers (Aickin and Brading 1983; Brodsky et al. 1979; Candida 1980; Jennings 1985), partially suppressed the Cl^- efflux in resting rabbit aorta, and even more in preparations stimulated by withdrawal of HCO_3^-. In contrast, furosemide, a selective inhibitor of Na-K-Cl cotransport (Schlatter et al. 1983; Owen 1984), reduced Cl^--efflux in the resting tissue, but not in aortae stimulated by withdrawal of HCO_3^-. As in guinea-pig vas deferens (Aickin 1984), withdrawal of HCO_3^- reduced E_m in rabbit pulmonary artery. The mechanism of this effect is not clear, but it required small anions in the PSS. Also, after 1 h of incubation with DIDS, withdrawal of HCO_3^- did not depolarize the tissue. These findings suggest a tight relationship between these E_m changes and the mutual dependence of Cl^- and HCO_3^- ions in vsm, and an at least indirect role of the putative anion carrier for the depolarizing effect of HCO_3^- withdrawal.

Inhibition of Na-K-Cl cotransport by furosemide reduced $[Cl^-]_i$ in aorta drastically, i.e. by more than 50%, whereas only small changes of $[Cl^-]_i$ by incubation with DIDS or in HCO_3^--free PSS were found. Thus, the high $[Cl^-]_i$ of vsm cells is obviously not mediated by the anion carrier, but by the Na-K-Cl cotransport.

Vsm has no measurable activities of carbonic anhydrase (Mühleisen and Kreye 1985). Thus, for rapid adjustments of pH_i, the cell requires fast imports or exports of HCO_3^- by the anion carrier. In Cl^--free PSS, the pH_i increased since only HCO_3^- was available extracellularly for the carrier thereby increasing $[HCO_3^-]_i$. This mechanism seems to be common to smooth muscle cells; in the guinea-pig vas deferens incubated in Cl^--free PSS, the alkaline pH_i was found to recover towards physiological pH_i rapidly on readdition of Cl^- (Aickin and Brading 1984).

The calculated apparent Cl^- permeability of 2.5×10^{-8} cm/s compares with the K^+ permeability of 1.4×10^{-8} cm/s in the same tissue (Jones 1980). However, the exchange of Cl_o^- by isethionate had no acute effect on the E_m of the rabbit pulmonary artery, and the Cl^- efflux from rabbit aorta was found insensitive to E_m changes. In addition, passive ion fluxes across cell membranes are characterized by a low dependence on temperature (Q_{10} = 1.3; Jones 1980), but Cl^- fluxes in rabbit aorta were highly sensitive to temperature changes. These findings argue against a high Cl^- permeability, and suggest that Cl^- is mainly moved by transport processes in vsm. Hence, the permeability calculated from ion flux data is overestimated, and only documents the activity of Cl^- transport mechanisms in this tissue.

Acknowledgements. The skilful technical assistance of Miss Isolde Villhauer is gratefully acknowledged.

References

Aickin CC (1984) Direct measurement of intracellular pH and buffering power in smooth muscle cells of guinea pig vas deferens. J Physiol 349:571–585

Aickin CC, Brading AF (1983) Towards an estimate of chloride permeability in the smooth muscle of guinea-pig vas deferens. J Physiol 336:179–197

Aickin CC, Brading AF (1984) The role of chloride-bicarbonate exchange in the regulation of intracellular chloride in guinea-pig vas deferens. J Physiol 349:587–606

Brodsky WA, Durham J, Ehrenspeck G (1979) The effects of disulfonic stilbene on chloride and bicarbonate transport in the turtle bladder. J Physiol 287:559–573

Candia OA (1980) Use of stimulants and inhibitors for studying the mechanisms of Cl^--transport. Ann NY Acad Sci 241:117–124

Casteels R (1969) Calculation of the membrane potential in smooth muscle cells of the guinea-pigs taenia coli. J Physiol 205:193–208

Dalmark M (1976) Effects of halides and bicarbonate on chloride transport in human red blood cells. J Gen Physiol 67:223–234

Goldman DE (1943) Potential, impedance and rectification in membranes. J Gen Physiol 27:37–60

Höfer M (1977) Transport durch biologische Membranen. Das Konzept der Trägerkatalyse. Verlag Chemie, Weinheim New York, p 68

Jennings ML (1985) Kinetics and mechanism of anion transport in red blood cells. Annu Rev Physiol 47:519–533

Jones AW (1980) Content and fluxes of electrolytes. In: Bohr DF, Somlyo AP, Sparks HV (eds) Vascular smooth muscle. Handbook of physiology, sect II, vol II. Williams and Wilkens, Baltimore, pp 253–299

Katz B (1966) Nerve, muscle, and synapse. McGraw-Hill, New York

Keynes RD, Lewis PR (1951) The resting exchange of radioactive potassium in crab nerve. Pflügers Arch 405:234–236

Kreye VAW, Gerstheimer F (1982) Bicarbonate and carboanhydratase dependence of active chloride transport in vascular smooth muscle (v.s.m.). Pflügers Arch 394 (Suppl): R29

Kreye VAW, Ziegler FW (1982) Anions and vascular smooth muscle function. In: Altura BM, Davis E, Harders H (eds) Adv Microcirc, vol 11. Karger, Basel, pp 114–133

Kreye VAW, Bauer PK, Villhauer I (1981) Evidence for a furosemide-sensitive active chloride transport in vascular smooth muscle. Eur J Pharmacol 73:91–95

Kreye VAW, Gerstheimer F, Mühleisen M, Nehring D, Walter K (1984a) Effects of diuretics, DIDS and anion replacement on 36-Cl/Cl exchange in isolated vascular smooth muscle. Pflügers Arch 400 (Suppl): R12

Kreye VAW, Gerstheimer F, Mühleisen M, Nehring D, Walter K (1984b) Effects of diuretics and bicarbonate withdrawal on chloride transport in isolated vascular smooth muscle. Naunyn-Schmiedebergs Arch Pharmacol 325 (Suppl): R38

Kreye VAW, Gerstheimer F, Mühleisen M, Nehring D, Walter K (1984c) Chloride ions in vascular smooth muscle. In: Puschett JB, Greenberg A (eds) Diuretics, chemistry, pharmacology, and clinical applications. Elsevier, New York Amsterdam Oxford, pp 431–437

Lowe AG, Lambert A (1983) Chloride-bicarbonate exchange and related transport processes. Biochim Biophys Acta 694:353–374

Mühleisen M, Kreye VAW (1985) Lack of soluble carbonic anhydrase in aortic smooth muscle of the rabbit. Pflügers Arch 405:234–236

Obaid AL, Leininger TF, Crandall ED (1980) Exchange of HCO_3 for monovalent anions across the human erythrocyte membrane. J Membr Biol 52:173–179

Owen NE (1984) Regulation of Na/K/Cl cotransport in vascular smooth muscle cells. Biochem Biophys Res Commun 125:500–508

Schlatter E, Greger R, Weidtke C (1983) Effect of "high ceiling" diuretics on active salt transport in the cortical thick ascending

limb of Henle's loop of rabbit kidney. Pflügers Arch 396:210–217

Somlyo AP, Somlyo AV, Shuman H (1979) Electron probe analysis of vascular smooth muscle. J Cell Biol 81:316–335

Villamil MF, Ponce J, Amorena C, Müller A (1979) Effect of furosemide on the ionic composition of the arterial wall. TIT J Life Sci 9:9–14

Waddell WJ, Butler TC (1959) Calculation of intracellular pH from the distribution of 5,5-dimethyl-2,4-oxazolidinedione (DMO). Application to skeletal muscle of the dog. J Clin Invest 38:720–729

Wieth JO (1979) Bicarbonate exchange through the human red cell membrane determined with (^{14}C) bicarbonate. J Physiol 294:521–539

Wieth JO, Brahm J (1980) Kinetics of bicarbonate exchange in human red cells. Physiological implications. In: Lassen UV, Ussing HH, Wieth JO (eds) Membrane transport in erythrocytes. Alfred Benzon Symposium 14. Munksgaard, Copenhagen, pp 467–487

Received September 15, 1986/Accepted January 7, 1987

Pflügers Arch (1987) 409:67–73

Pflügers Archiv
European Journal of Physiology
© Springer-Verlag 1987

Nonuniform myosin expression along single fibers of chronically stimulated and contralateral rabbit tibialis anterior muscles

Robert S. Staron* and Dirk Pette

Fakultät für Biologie, Universität Konstanz, Postfach 5560, D-7750 Konstanz, Federal Republic of Germany

Abstract. Using a combined histochemical and biochemical technique, single fiber analyses were performed on chronically stimulated and contralateral tibialis anterior (TA) muscles of the rabbit. The major fiber population (60%) in 30 days stimulated TA was transforming fibers (type IIC). Some of these fibers displayed a nonuniform distribution of histochemically assessed myofibrillar actomyosin ATPase (mATPase) activity. This heterogeneity of mATPase activity along the fibers was verified in longitudinal sections and by microphotometric evaluation of mATPase staining intensities in serial cross-sections. Biochemical analyses of single fiber segments revealed that these C fibers not only coexpressed fast- and slow-myosin subunits but did so nonuniformly along their length. The distribution of fast- and slow-myosin subunits in these fibers was not random but focal. Variations in myosin expression were also observed in some of the C fibers in the contralateral TA. As opposed to the transforming fibers in the stimulated TA, heterogeneities of mATPase activity and myosin subunits in these contralateral C fibers were less focal and more gradual. These findings suggest that muscle fibers in chronically stimulated TA and the contralateral muscle do not transform synchronously or uniformly along their length.

Key words: Chronic stimulation – Skeletal muscle – Myosin light and heavy chains – Single fiber analysis – Myosin ATPase microphotometry – Fiber transformation – Nonuniform myosin expression

Introduction

Skeletal muscle develops from postmitotic myoblasts which fuse to form multinucleated myotubes, the precursors of adult muscle fibers. Although assumed, it is unknown whether all nuclei of a given fiber are synchronously active and contribute in a concerted manner to the expression of fiber type-specific proteins. Microphotometric measurements of enzyme activities in single fibers of adult rat psoas muscle (Pette et al. 1980) revealed no major metabolic heterogeneity along the fiber length. However, Hintz et al. (1984) have detected some variability in single rat and human muscle fibers for certain metabolites and enzyme activities of energy metabolism. These differences appeared to be gradual over distances of 0.5–2 mm. Recently in this laboratory, using a combined histochemical and biochemical approach, single fibers from normal (Staron and Pette 1986, 1987a, b) and chronically stimulated rabbit muscles (Staron et al. 1987) were analysed for myosin heavy and light chains and other proteins of the myofibrillar apparatus. No variations were found in the distribution of the histochemically assessed myosin ATPase activity or of the myofibrillar proteins along single fibers of normal rabbit tibialis anterior (TA) and soleus muscles. However, certain fibers undergoing transformation during chronic, low frequency stimulation (30 days, 10 Hz, 24 h/day) displayed nonuniform myosin ATPase activity and nonuniform myosin expression along their length (Staron et al. 1987). In addition, this phenomenon was seen in some fibers of the contralateral TA muscles. These observations imply that nuclei of transforming muscle fibers no longer act in a concerted manner. We decided to study these relationships in greater detail in the current work.

* Present address: College of Osteopathic Medicine, Ohio University, Athens, OH 45701-2979, USA
Offprint requests to: D. Pette

Materials and methods

Muscles. Tibialis anterior (TA) muscles from adult White New Zealand rabbits were chronically stimulated (10 Hz, 24 h/day) for either 30 days ($n = 2$) or 60 days ($n = 3$). Electrode implantation and stimulation procedures have been previously described (Pette et al. 1973; Schwarz et al. 1983). The same animals were used in a preceding study (Staron et al. 1987). Stimulated and contralateral TA muscles were removed and divided into three pieces, (1) for myofibrillar actomyosin ATPase (mATPase) staining of (5 or 8 µm thick) longitudinal sections, (2) for mATPase staining of serial thin (12 µm thick) cross-sections over a distance of 4–6 mm, and (3) for combined mATPase histochemistry and single fiber analyses (Staron and Pette 1986, 1987a, b). In addition, sections were stained with hematoxylin and eosin (HE) for periodic histological examination.

Combined histochemical and biochemical single fiber analysis. The method of combining histochemical and biochemical analyses for single fibers has been previously described (Staron and Pette 1986, 1987a, b). Basically, six serial, thin (12 µm) cross-sections were alternated with one thick (200–300 µm) serial cross-section until a total of 14–16 thick sections were obtained. The thin sections were processed for myofibrillar actomyosin ATPase (mATPase) at preincubation values of pH 4.3, 4.5, and 9.6. The thick sections were freeze-dried in series and subsequently, fragments of 50

single fibers per muscle were identified, dissected and separately stored under vacuum at −38°C until used. Therefore, a total of 16 segments from a selected, single fiber was available for biochemical analyses. Segments of single fibers were sorted according to their variable mATPase staining intensities, stored, and analysed separately. Likewise, single fiber segments with no variability in mATPase staining were separated and used as controls. Single fiber segments from contralateral TA were transferred to a glass capillary, lysed and separately analysed for myosin light and heavy chains in the same fiber. Segments of single fibers from stimulated TA were analysed for only myosin heavy chains. Therefore, two light chain and/or two heavy chain analyses were possible for each fiber.

Microphotometry. Cross-sections stained for mATPase after preincubation at pH values of 4.5 (for contralateral TA and 30 days stimulated TA) or 9.6 (for 60 days stimulated TA) were microphotometrically evaluated by spot-measurement. The different preincubations were necessary to give optimal differences between staining intensities of the different fiber types. The measurements were performed on sixteen 12 μm thick sections which were 260−360 μm apart, covering a total distance of 4−5 mm. Using a computer-controlled Leitz MPV 2 microscope photometer (Pette et al. 1979), light absorbance was measured in selected single fibers of serial cross-sections. The selected fibers were automatically positioned by a stepping motor-controlled stage into a circular (20 μm diameter) measuring beam (548 nm). A maximum of 23 fibers plus one blank outside the section was measured at one time. A total of approximately 45 fibers was analysed. These same fibers were then analysed in each subsequent section. The recorded absorbance values were corrected by subtracting the blank value recorded outside the section. For each section, the absorbance of the darkest (or lightest for 60 days stimulated TA) staining fiber was set equal to 100% (reference fiber) and all other values in that particular section were referred to it. This procedure was necessary to standardize absorbance from section to section and to eliminate experimental errors arising from variations in section thickness, whole section staining intensity, etc.

Results

Histochemical analyses of contralateral and stimulated TA

Myosin ATPase histochemistry of contralateral TA displayed fiber types I, IC, IIC, IIA, IIAB and IIB. Type I fibers were dark following preincubation at pH values of 4.3 and 4.5 and light after pH 9.6. The reverse was true for type IIA fibers. Type IIB fibers were light at pH 4.3, intermediate at pH 4.5 and dark at pH 9.6. Type IIAB fibers reacted like IIB fibers after preincubation at pH values 4.3 and 9.6, but stained less intensely than IIB fibers at pH 4.5. Although variable, the C fibers (types IC and IIC) were stable at all three pH values with the IIC fibers staining similar to the IIA and the IC fibers staining similar to the type I fibers (see Staron and Pette 1986, 1987a).

Serial, thin (12 μm) cross-sections covering a distance of 4−6 mm and thin (12 μm) cross-sections, that were alternated with thick sections (for biochemistry) were stained for mATPase activity and analysed for differences in staining intensity along the length of single fibers. In the contralateral, unstimulated TA, a loss of acid stability of mATPase along the length of certain IIC fibers was observed in both the serial cross-sections and those separated by 260−360 μm (Fig. 1). This change appeared to occur in a gradual manner. Upon histological examination, these fibers were normal in shape and appearance, e.g. no macrophages, central nuclei, etc.

Myosin ATPase histochemistry of the 30 days stimulated TA demonstrated a pronounced increase in the C fiber population (Staron et al. 1987). Similar to the contralateral muscle, variations in the acid stability of mATPase were observed along the length of some C fibers (Fig. 2). Approximately 30% of the C fibers were drastically affected. These changes were highly irregular between and within particular fibers. This was best seen in longitudinal sections where the acid stability of mATPase gradually disappeared and reappeared in some fibers (Fig. 3). With the exception of an overall decrease in the cross-sectional area of all fibers, the histological appearance was normal.

Microphotometry of mATPase stained cross-sections

Microphotometric analyses of the staining intensities for mATPase in contralateral TA cross-sections revealed a tight grouping for fiber types I, IIA, IIAB and IIB (Fig. 4). This grouping was retained along the muscle although absorbances varied from section to section due to unavoidable methodical variations, e.g. in preincubation and reaction conditions, temperature, etc. The methodical cause of these changes was supported by the maintenance of similar proportions in the absorbances of types I, IIAB, IIA and IIB in different cross-sections. However, the staining intensity of the C fiber population varied greatly between and within single fibers and gradually decreased along their length. Within the 4−6 mm distance investigated, most of the IIC fibers (plotted in Fig. 4) were indistinguishable from type IIA at one end of the segment. Therefore, these IIC fibers changed their absorbances from section to section independent of the systematic variations mentioned above and displayed disproportionate staining intensities compared with the other fiber types.

Microphotometric analyses revealed an increased heterogeneity in the staining intensities of the C fiber population in 30 days stimulated compared with the contralateral TA (Figs. 4 and 5). This population displayed pronounced fluctuations of relative absorbances along the fiber lengths whereas the type IIA fibers in the same muscle were tightly grouped and showed negligible longitudinal variations. The few type I_t fibers investigated in the 30 days stimulated TA also displayed some variations in mATPase activity along their length (Fig. 5). These atypical slow fibers have been previously identified as the mayor fiber type (97%) in long-term (60 days, 24 h/day), low-frequency stimulated rabbit fast-twitch muscle (Staron et al. 1987). Microphotometrically assessed absorbances for mATPase staining along the length of these fibers in the 60 days stimulated animals also exhibited pronounced heterogeneities (results not shown).

Biochemical analyses of contralateral and stimulated TA

Single fiber analyses for both myosin light and heavy chains were performed on contralateral TA of 30 days stimulated rabbits. Because microphotometry revealed gradual longitudinal changes in mATPase in some C fibers, biochemical

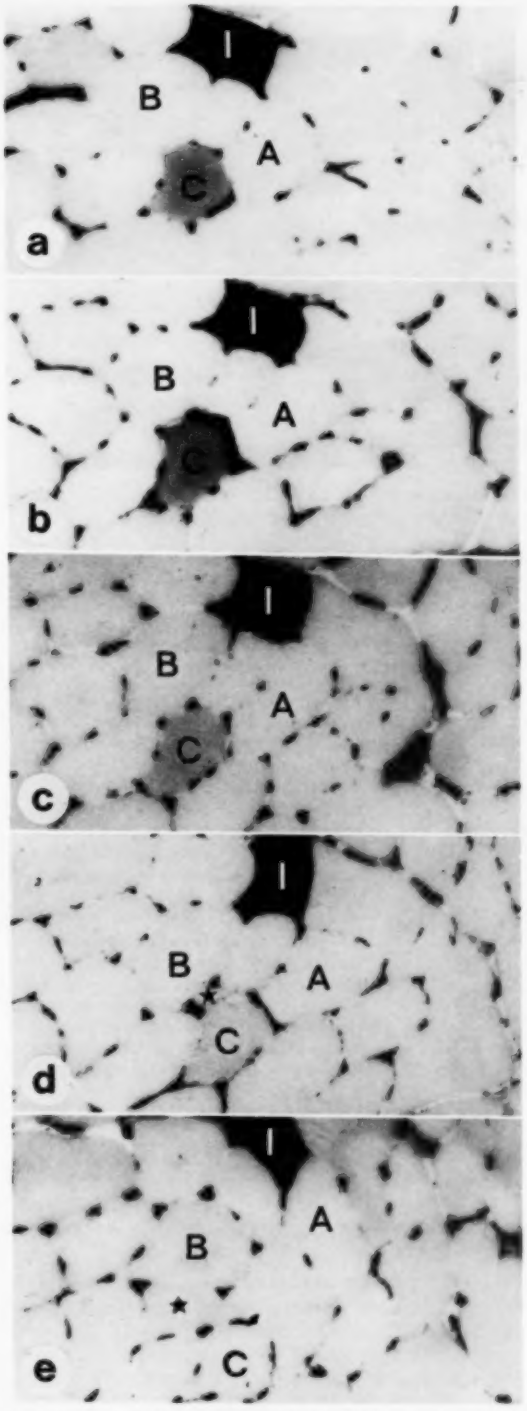

Fig. 1. Cross-sections of contralateral tibialis anterior muscle of a 30 days stimulated rabbit at different levels. Sections were processed for myosin ATPase activity after preincubation at pH 4.3. Sections **a–d** are each approximately 1 mm apart, and sections **d** and **e** are approximately 2 mm apart. Note the gradual disappearance of myosin ATPase activity in the marked C fiber. The *asterisk* marks the appearance of a "new" fiber. The marked fibers were analysed for myosin light and heavy chains shown in Fig. 6a, b. *I* = fiber type I, *A* = fiber type IIA, *B* = fiber type IIB, *C* = fiber type IIC. ×160

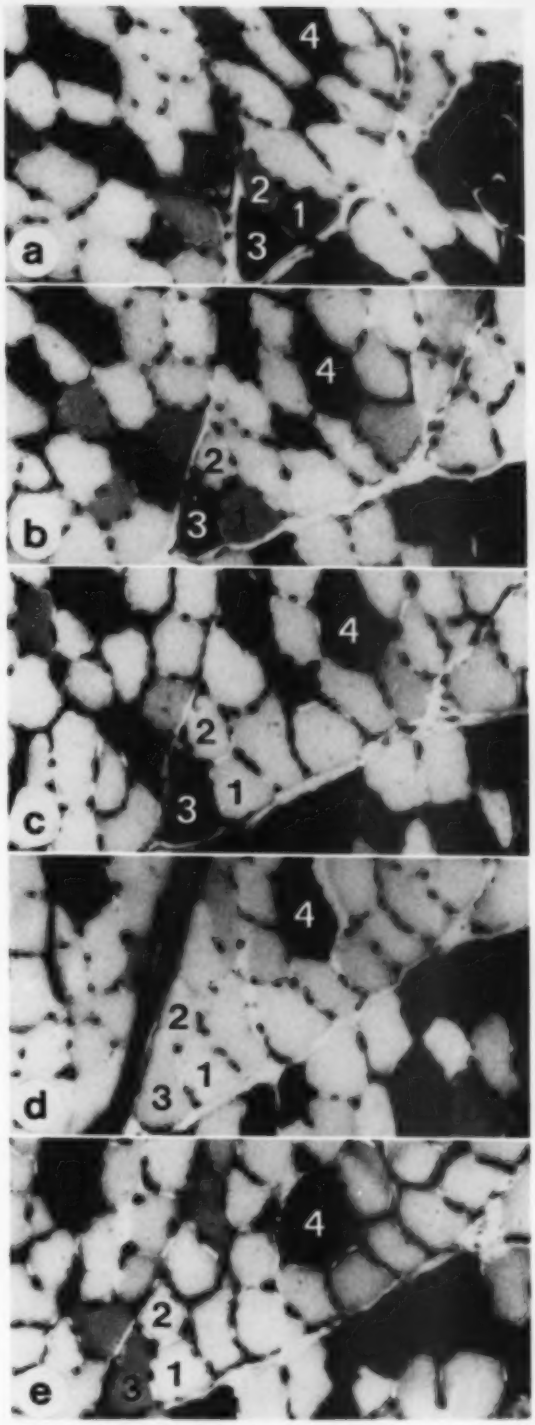

Fig. 2a–e. Cross-sections of 30 days stimulated tibialis anterior muscle processed for myosin ATPase activity after preincubation at pH 4.3. Sections **a–e** are each approximately 1 mm apart. The numbered fibers were analysed for myosin heavy chain composition along their length (see Fig. 6c). Note the variations in myosin ATPase activity in certain C fibers, e.g. fibers 1, 2 and 3. Fiber 4 is a type I, fiber with stable mATPase activity over this distance. ×160

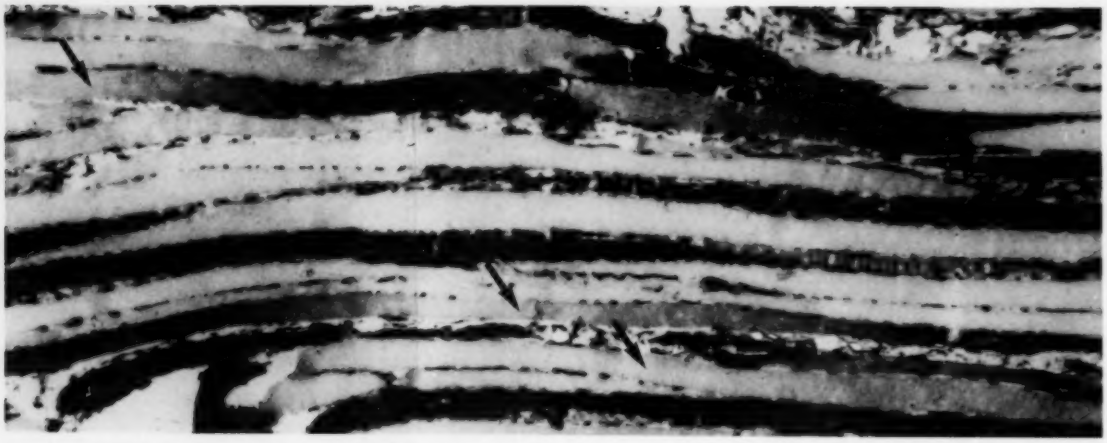

Fig. 3. Longitudinal section of a 30 days stimulated rabbit tibialis anterior muscle processed for myosin ATPase activity after preincubation at pH 4.3. *Arrows* designate three fibers with apparent focal variation of myosin ATPase activity along their length. × 100

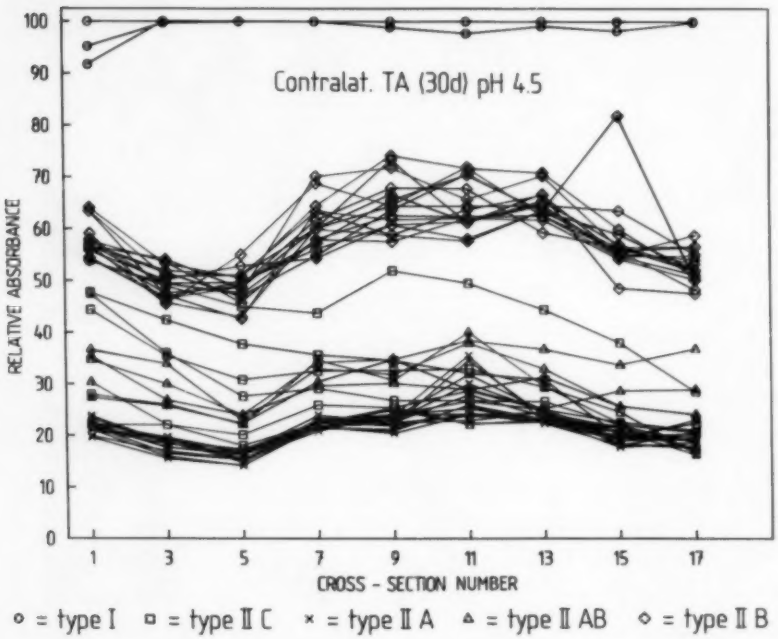

Fig. 4
Microphotometric evaluations of myofibrillar actomyosin ATPase staining intensities in 44 fibers of the contralateral tibialis anterior muscle of a 30 days stimulated rabbit. The cross-sections (12 µm thick) were run together for histochemical analysis (preincubation pH 4.5) and span a distance of 4–6 mm. Normalized absorbances (*ordinate*) are plotted for each fiber along its length according to measurements from only the odd numbered sections (*abscissa*). Each section is approximately 0.5 mm from the next one. Absorbances were referred to the darkest staining fiber (type I) in each section. It is obvious that individual fibers can not be followed in this plot, however, note the tight grouping of fiber types I, IIA, IIB and IIAB and the gradual decrease in absorbance of most type IIC fibers

analyses were performed on different segments of the same fiber. Therefore, single fiber segments from thick sections 1–8 were used for analysis of myosin light and heavy chains, and sections 9–16 of the same fiber were separately analysed in the same way. Thus, it was possible to investigate the myosin light and heavy chain composition along the length of selected C fibers.

The distribution of myosin light and heavy chains within specific C fibers of contralateral TA confirmed the qualitative and quantitative histochemical findings. Segments of a single C fiber which stained intermediate after preincubations at pH 4.3 and 4.5 contained fast- and slow-myosin light and heavy chains (Fig. 6a, b). Segments of that same single fiber which were for the most part unstained under these conditions, displayed negligible amounts of the slow-myosin heavy and light chains (Fig. 6a, b). This correlation between the myosin composition and the histochemical mATPase staining intensity along single fibers was also observed in the fibers of 30 days stimulated TA (Fig. 6c). Biochemical analyses of these fibers revealed that the fluctuations in the mATPase staining along the fiber length reflected altered ratios of the two myosin heavy chains which were identified as HCI and HCIIa according to their electrophoretic mobility. Segments of C fibers which stained light to intermediate after pH 4.3 preincubation contained a predominance of heavy chain HCIIa (type IIC), whereas

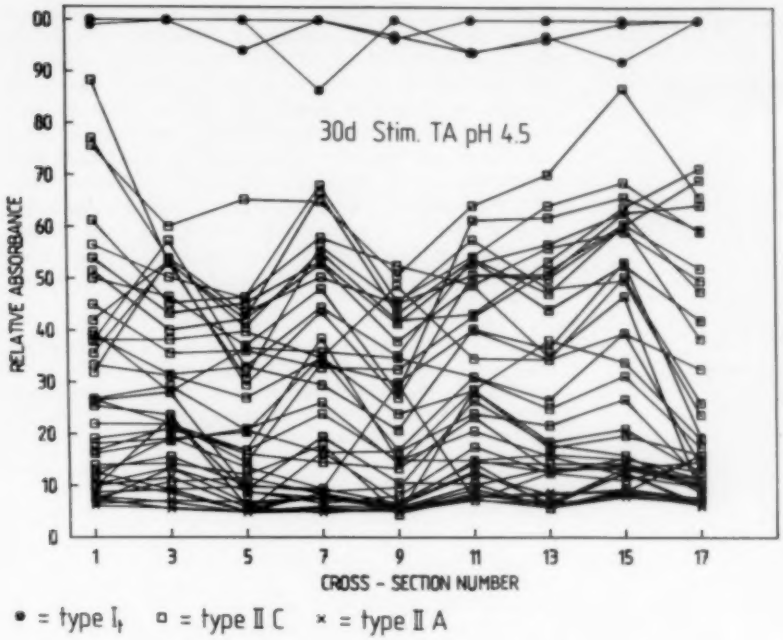

Fig. 5
Microphotometric evaluations of myofibrillar actomyosin ATPase staining intensities (pH 4.5 preincubation) in 12 µm thick cross-sections (approximately 0.5 mm apart) covering a distance of 4–6 mm in 45 fibers of a 30 days stimulated tibialis anterior muscle. Absorbances were referred to the darkest staining fiber (type I_t) in each section. Note the extreme scattering of absorbances. For further explanations, see Fig. 4

segments of the same fibers which stained intermediate to dark under the same conditions displayed a higher content of heavy chain HCI (type IC) (Fig. 6c).

Discussion

The expression of specific proteins is generally assumed to be uniform along the length of normal mammalian muscle fibers. However, nonuniform myosin distribution has been demonstrated in regenerating fibers following local injury. Kelly and Rubinstein (1980) found slow-twitch soleus fibers express fast-myosin in the portion adjacent to the injury. In addition, heterogeneities in the mATPase staining intensities have been observed along the length of specific fibers undergoing transformation (Staron et al. 1987). Because a correlation exists between the mATPase staining intensity and the myosin heavy chain composition (Staron and Pette 1986, 1987a), these phenomena suggest that myosin is nonuniformly expressed along the length of certain fibers undergoing transformation or regeneration. Indeed, the present study confirms this and gives further support to the relationship between the histochemical staining intensity of mATPase and myosin heavy chain composition.

Nonuniform changes in myosin expression may result from repair following focal injuries (Riley 1973) or reflect an asynchronous transformation of the myosin complement along the fiber. Indeed, regenerative processes have been observed in chronically stimulated muscle (Maier et al. 1986; Maier and Pette 1987). However degeneration-regeneration occurs primarily after short-term stimulation (4–8 days), is restricted to a minor population (10–20% of the total fiber population and mainly fast-twitch glycolytic fibers), leads to the replacement of entire fibers by newly formed myotubes, and is believed to be essentially complete after 30 days of stimulation (Maier et al. 1986). On the other hand, recent immunohistochemical data indicates the presence of embryonic myosin in some of these C fibers in long-term stimulated muscles (A. Maier, D. Pette, S. Schiaffino, unpublished observations).

The transforming C fibers contain fast- and slow-myosin light chains and display the coexistence of two heavy chain which are electrophoretically identified as the slow-myosin HCI and the fast-myosin heavy chain IIa. Following 60 days of chronic stimulation, the fast fiber population appears histochemically transformed into a slow population. However, these slow fibers are atypical and have been termed type I_t (Staron et al. 1987). Type I_t fibers display, in addition to a predominant slow-myosin light and heavy chain complement, high concentrations of the fast-myosin alkali light chain LC1f. Microphotometric analyses indicate that the I_t fibers also display nonuniform mATPase staining along their length.

Segmental differences in the maximal speed of shortening have recently been observed along the length of normal frog skeletal muscle fibers (Edman et al. 1984, 1985). These differences correlate with the myofibrillar ATPase activity (te Kronnie et al. 1985, 1986). These variations in the contractile properties appear to be nonrandom and may reflect functional differences along the fibers (Edman et al. 1985). Therefore, a change in function, e.g. during chronic stimulation, may elicit different regional effects. Chronic stimulation during 24 h/day is unphysiologic, especially for fast-twitch fibers unaccustomed to continuous activity, and may elicit transformation processes at multiple sites of the fiber. In addition, any crossover effect is likely to be much smaller in the contralateral muscle and, therefore, the transformation process may occur in a more ordered or gradual manner in these fibers.

Previous cross-reinnervation experiments (Srihari et al. 1981; Reichmann et al. 1983) indicate the occurrence of various contralateral changes which may be due to crossover

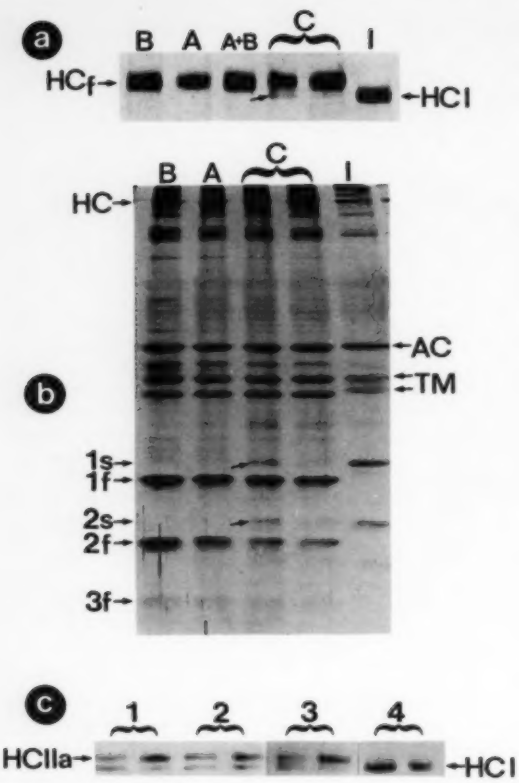

Fig. 6a–c. Electrophoretic analyses of myosin heavy and light chains of single fiber segments collected from cross-sections of contralateral and 30 days stimulated rabbit tibialis anterior muscles. In the contralateral muscle, analyses were performed for myosin heavy chains **a** and light chains **b** on the same fibers. Letters *A*, *B*, *C* and *I* represent the fibers marked in Fig. 1. The first eight and last eight sections of the C fiber were analysed separately (see Methods). Therefore, two heavy and two light chain electrophoreses are shown for this C fiber. The *arrows* denote the presence of slow heavy and slow light chains in the first eight sections of this C fiber. A coelectrophoresis of type IIA and type IIB fiber segments (*A* + *B*) is shown in the upper panel (**a**). Heavy chain analyses of single fiber segments from 30 days stimulated rabbit tibialis anterior are shown in **c**. Numbers 1–4 represent the fibers shown in Fig. 2. For each fiber, two heavy chain analyses were performed at two different levels. Note the variations in HCIIa/HCI ratio for fibers *1–3*. Fiber *4* is a type I_t fiber. Abbreviations: *AC*, actin; *HC*, myosin heavy chain; HC_f, fast-myosin heavy chain (either HCIIa or HCIIb); *HCIIa* fast-myosin heavy chain IIa; *HCI*, slow-myosin heavy chain; *TM*, tropomyosin; *1s*, *2s*, slow-myosin light chains; *1f*, *2f*, *3f*, fast-myosin light chains

effects or reflex activity. In a similar fashion, chronic stimulation may induce slight contralateral changes such as the observed increases in fiber types IIA and IIC with concomitant decreases in type IIB fibers (Staron et al. 1987). Also, some C fibers in the contralateral TA of 30 days and 60 days stimulated animals exhibit nonuniform myosin expression. Compared to the stimulated muscle, these contralateral C fibers appear to transform gradually over greater distances.

In conclusion, stimulation-induced fast-to-slow conversion involves the exchange of fast-myosin with slow-myosin subunits in single fibers. Apparently, this exchange is not complete after continuous (24 h/day) stimulation during 30 days or even 60 days. Transforming fibers are characterized by the coexistence of fast- and slow-myosin subunits which may be unevenly distributed along the fiber length. The reprogramming of myosin expression in these fibers does not appear to be random but is localized with gradations. These fluctuations in myosin expression may reflect various levels of activity of the myonuclei along transforming fibers. It is unknown to what extent local factors, such as metabolic (Maier and Pette 1987) and ionic imbalances or injury, contribute to these regional differences in nuclear activities.

Acknowledgements. This study was supported by the Deutsche Forschungsgemeinschaft, Sonderforschungsbereich 156. R.S.S. is grateful to the Alexander von Humboldt-Stiftung for a postdoctoral stipend. The authors express their thanks to Mrs. B. Gohlsch for excellent technical assistance.

References

Edman KAP, Reggiani C (1984) Redistribution of sarcomere length during isometric contraction of frog muscle fibres and its relation to tension creep. J Physiol (Lond) 351:169–198

Edman KAP, Reggiani C, te Kronnie G (1985) Differences in maximum velocity of shortening along single muscle fibres of the frog. J Physiol (Lond) 365:147–163

Hintz CS, Chi MM-Y, Lowry OH (1984) Heterogeneity in regard to enzymes and metabolites within individual muscle fibers. Am J Physiol 246:C288–C292

Kelly AM, Rubinstein NA (1980) Patterns of myosin synthesis in regenerating normal and denervated muscles of the rat. In: Pette D (ed) Plasticity of muscle. W de Gruyter, Berlin New York, pp 161–175

Maier A, Pette D (1987) The time course of glycogen depletion in single fibers of chronically stimulated rabbit fast-twitch muscle. Pflügers Arch 408:338–342

Maier A, Gambke B, Pette D (1986) Degeneration-regeneration as a mechanism contributing to the fast to slow conversion of chronically stimulated fast-twitch rabbit muscle. Cell Tissue Res 244:635–643

Pette D, Smith ME, Staudte HW, Vrbová G (1973) Effects of long-term electrical stimulation on some contractile and metabolic characteristics of fast rabbit muscles. Pflügers Arch 338:257–272

Pette D, Wasmund H, Wimmer M (1979) Principle and method of kinetic microphotometric enzyme activity determination in situ. Histochemistry 64:1–10

Pette D, Wimmer M, Nemeth P (1980) Do enzyme activities vary along muscle fibres ? Histochemistry 67:225–231

Reichmann H, Srihari T, Pette D (1983) Ipsi- and contralateral fibre transformations by cross-reinnervation. A principle of symmetry. Pflügers Arch 397:202–208

Riley DA (1973) Histochemical changes in ATPase activity during regeneration of adult skeletal muscle fibers. Exp Neurol 41:690–704

Schwarz G, Leisner E, Pette D (1983) Two telestimulation systems for chronic indirect muscle stimulation in caged rabbits and mice. Pflügers Arch 398:130–133

Srihari T, Seedorf U, Pette D (1981) Ipsi- and contralateral changes in rabbit soleus myosins by cross-reinnervation. Pflügers Arch 390:246–249

Staron RS, Pette D (1986) Correlation between myofibrillar ATPase activity and myosin heavy chain composition in rabbit muscle fibers. Histochemistry 86:19–23

Staron RS, Pette D (1987a) The multiplicity of combinations of myosin light chains and heavy chains in histochemically typed single fibres. Rabbit soleus muscle. Biochem J 243:687–693

Staron RS, Pette D (1987b) The multiplicity of combinations of myosin light chains and heavy chains in histochemically typed single fibres. Rabbit tibialis anterior muscle. Biochem J 243:695–699

Staron RS, Gohlsch B, Pette D (1987) Myosin polymorphism in single fibers of chronically stimulated rabbit fast-twitch muscle. Pflügers Arch 408:444–450

te Kronnie G, Reggiani C, Edman KAP (1985) Segmental differences in maximum speed of shortening and myofibrillar ATPase activity in frog skeletal muscle fibres. J Muscle Res Cell Motil 6:108

te Kronnie G, Reggiani C, Schiaffino S, Edman KAP (1986) Shortening velocity correlated with myosin isoform composition and myofibrillar ATPase activity in frog single fibres. J Muscle Res Cell Motil 7:77

Received December 15, 1986/Accepted February 10, 1987

Pflügers Arch (1987) 409:74–80

Pflügers Archiv
European Journal of Physiology
© Springer-Verlag 1987

Dibutyryl cyclic AMP inhibits transport dependent QO_2 in cells isolated from the rabbit medullary ascending limb

Patricio Silva [1], Barbara Koenig [2], Stephanie Lear [1], Jill Eveloff [2], and Rolf Kinne [2]

[1] Charles A. Dana Research Institute, The Harvard-Thorndike Laboratory of Beth Israel Hospital, 330 Brookline Avenue, Boston, MA 02215, USA
[2] Max-Planck Institut für Biophysik, D-6000 Frankfurt 70, Federal Republic of Germany

Abstract. Because the medullary thick ascending limb of the loop of Henle is the target of several polypeptide hormones that stimulate adenyl cyclase in this nephron segment, we examined the effects of cyclic AMP on thick ascending limb of the loop of Henle cells isolated by enzymatic digestion and density gradient centrifugation from the outer medulla of the rabbit kidney. The functional parameter that was measured was transport dependent oxygen consumption. Oxygen consumption was measured using a polarographic oxygen electrode in a constant temperature chamber. We found that dibutyryl cyclic AMP inhibited oxygen consumption in a dose dependent way. Maximal inhibition was observed at a concentration of 10^{-5} M. The effect of dibutyryl cyclic AMP was not present in the absence of either sodium, chloride or both implying that its effect is restricted to the sodium and chloride dependent oxygen consumption. The effect of dibutyryl cyclic AMP was additive to that of furosemide 10^{-4} M while that of furosemide was not additive to that of cyclic AMP suggesting that the site of action of cyclic AMP is distal to that of furosemide. The effect of dibutyryl cyclic AMP was not additive to that of ouabain and was absent in cells where oxygen consumption was stimulated with amphotericin B in the absence of chloride indicating that it has no effect on Na-K-ATPase. On the basis of these results, and by analogy with other epithelia where the effect of cyclic AMP on chloride transport has been demonstrated to be at the chloride conductance, the effect of cyclic AMP on transport dependent oxygen consumption can be most probably localized to the chloride conductance. The hormone responsible for the primary step was not identified in these experiments.

Key words: Cyclic AMP – Oxygen consumption – Epithelial transport – Thick ascending limb – Na,K and Cl cotransport – Ouabain – Furosemide – Amphotericin

Introduction

The medullary thick ascending limb of the loop of Henle is the target of several polypeptide hormones as judged by their capacity to increase in vitro the intracellular concentration of cyclic AMP or to stimulate adenyl cyclase [41]. More difficult is to establish the functional effects of these hormones on the transport of electrolytes by this nephron segment. Experiments with isolated perfused mouse thick ascending limbs show that vasopressin, in physiological concentrations, stimulates sodium and chloride transport and that this effect is inhibited by PGE_2 that by itself has no effect [11, 12, 26, 31, 46]. In the rabbit, however, ADH has no effect [46] and PGE_2 decreases basal chloride reabsorption [54]. Functional effects have been indirectly demonstrated by microperfusion or sampling at the late proximal or tip of the loop of Henle and early distal tubules for calcitonin which stimulates calcium and magnesium reabsorption and may increase sodium and chloride transport under certain conditions [14, 44], parathyroid hormone that increases calcium, magnesium and potassium reabsorption in thyroparathyroidectomized animals [3, 43] and glucagon that increases calcium, magnesium and potassium reabsorption in thyroparathyroidectomized rats [3]. Suki and Rouse have shown that calcitonin increases calcium reabsorption in isolated medullary thick ascending limb of the rabbit [55].

Polypeptide hormones and other hormones exert their effect on the target cells by increasing the activity of adenyl cyclase, and thereby increasing the intracellular concentration of cyclic AMP. In most experimental preparations, exogenous cyclic AMP evokes a functional effect that is similar in nature to that induced by the hormone that triggers its generation. In the intact kidney cyclic AMP increases sodium, calcium, phosphate and water excretion [1, 4, 19, 39, 48]. Micropuncture experiments have localized this effect to the proximal tubule [18, 28, 40]. In the distal convoluted and collecting tubule cyclic AMP enhances sodium and fluid absorption [10, 20]. In the thick ascending limb of the loop of Henle, cyclic AMP increases chloride reabsorption mimicking the effect of AVP [11, 31]. The effect of AVP is found in the mouse, to a much lesser extent in the rat [57] and absent in the rabbit [46]. To date, of the polypeptide hormones that stimulate adenyl cyclase only calcitonin has been demonstrated to have a functional effect in the thick ascending limb of the rabbit [55]. In that series of experiments, 8-bromo cyclic AMP mimicked the effect of calcitonin and reduced, although not significantly so, the transepithelial potential difference, suggesting that transepithelial transport was reduced. In the present experiments we investigated the effect of cyclic AMP on isolated rabbit medullary thick ascending limb of the loop of Henle cells. The functional parameter that was followed was the transport dependent oxygen consumption.

Methods

Isolation of cells from the medullary thick ascending limb of the loop of Henle. Cells were isolated from medullary thick

Offprint requests to: P. Silva

ascending limb of the loop of Henle by the technique of Eveloff et al. [15]. White New Zealand rabbits were used in all experiments. The rabbits were killed by cervical dislocation and carotid exsanguination and both kidneys were removed. The kidneys were then perfused through the artery with 30 ml of cold minimum essential culture medium containing 10% fetal calf serum to remove red blood cells. Perfusion was continued with another 5 ml of minimum essential culture medium containing 0.2% collagenase and 0.25% hyaluronidase under pressure, with the vein occluded until the capsule of the kidney ruptured. The kidney was then cut in half and the outer medulla dissected out and minced with scissors into 1 mm pieces. The minced medulla was then incubated for 1 h at 37° C, in 0.2% collagenase and 0.25% hyaluronidase in continuously oxygenated minimum essential culture medium with 10% fetal calf serum, using a shaking water bath. Two or 3 times during this incubation the tissue was aspirated through a wide mouth pipet to disrupt the mucus conglomerates that tend to form. At the end of the incubation, the bulk (70–80%) of the tissue was composed of long tubular segments. The tubules were harvested by centrifugation at $50 \times g$ for 5 min and washed in minimum essential culture medium containing fetal calf serum. The tubules were then incubated in oxygenated minimum essential culture medium, with fetal calf serum, containing 0.25% trypsin at 20° C for 20 min with gentle mechanical agitation. At the end of the 20 min of incubation with trypsin the tubules were sedimented by rapid ($750 \times g$) centrifugation for 25 s. Isolated cells remained in the supernatant. The cells were harvested by further centrifugation at $500 \times g$ for 5 min, resuspended in minimum essential culture medium and kept on ice. The trypsinization step was repeated 8 times and the cells were then combined, washed once more with minimum essential medium containing calf serum and suspended in 50 ml of the same medium. The cell suspension was then filtered through a nylon mesh and layered over a Ficoll gradient. The Ficoll was dissolved in a buffer of the following composition (mM): NaCl 137; KCl 5; Na_2HPO_4 0.33; KH_2PO_4 0.44; $MgCl_2$ 1; $CaCl_2$ 1; $MgSO_4$ 0.8; Tris-HCl 20, at a pH of 7.4. The gradient was constructed linearly from a concentration of 2.7% (w/v) to 43% (w/v) Ficoll and maintained at 0° C. After layering the cells the gradient was spun at $1900 \times g$, at the heaviest end, for 45 min. The gradient was then removed in 4 ml fractions. Fraction 10 contains thick ascending limb cells. The identity of the thick ascending limb cells was ascertained by both morphological and biochemical means. Phase contrast microscopy was done routinely and occasional electronmicroscopic studies were also performed. The morphological characteristics were those of thick ascending limb cells. Biochemically, the enrichment in Na-K-ATPase and calcitonin stimulated adenyl cyclase was 10.5 ± 2.0 and 9.5 ± 1.7 respectively, the depletion in alkaline phosphatase was 0.58 ± 0.08. These biochemical characteristics identify thick ascending limb cells. The Ficoll fractions were diluted with the same buffer used to prepare the Ficoll and the cells collected by centrifugation at $1400 \times g$ for 15 min. The cells were resuspended in the buffer and kept in an ice bath until used for further experiments.

Oxygen consumption. The consumption of oxygen by the isolated cells was measured using a Clark type polarographic oxygen electrode in a thermostated constant temperature cell (37° C). The buffer used for suspending the cells and for filling the measuring chamber was, unless otherwise specified, of the following composition (mM): NaCl 137; KCl 5; Na_2HPO_4 0.33; KH_2PO_4 0.44; $MgCl_2$ 1; $CaCl_2$ 1; $MgSO_4$ 0.8; Tris-HCl 20, at a pH of 7.4. The volume of measurement ranged between 1.5–2 ml. The rate of oxygen consumption was recorded continuously. Glucose 5 mM, pyruvate 10 mM and acetate 2 mM were dissolved in the same buffer and added to the chamber prior to the addition of cells. The mass of cells usually used was between 8 and 15 mg in 0.1–0.15 ml of buffer. A control period long enough to establish a constant slope was run at the beginning of the experiment followed by one or more experimental periods. Two or more determinations were done with each batch of cells for every experimental condition. The slopes were linear until less than 3% oxygen content was left in the chamber. All subsequent additions to the incubation chamber or inhibitors were made in volumes that did not exceed 1% of the volume of the measuring chamber to eliminate potential dilutional problems. The rate of oxygen consumption was calculated from the slope of the recorded curve by measuring its angle against the 100% oxygen baseline and calculating its tangent.

When the measurement of oxygen consumption was ended, a measured aliquot of the cell suspension, still under constant stirring in the measuring chamber, was removed and centrifuged in a tared centrifuge tube in an Eppendorf microcentrifuge. After centrifugation the supernatant was removed and the inside of the centrifuge tube carefully wiped with filter paper to remove all traces of supernatant. The tube was then reweighed to determine wet weight of the packed cells. Results were expressed as μmoles of O_2 utilized per min per gram wet weight.

All chemicals used were reagent grade. Dibutyryl cyclic AMP, ouabain and amphotericin B were purchased from Sigma Chemical Co., St. Louis, MO, USA. Furosemide was a gift from Hoechst Pharmaceuticals, Frankfurt, FRG.

Statistical analysis was done using Student's *t*-test or paired *t*-test wherever applicable.

Results

Effect of dibutyryl cyclic AMP on oxygen consumption

The average oxygen consumption by medullary thick ascending limb cells in vitro in separate determinations in 70 experiments was 2.01 ± 0.09 μmoles O_2/min/g ww. This value is not different from the value of 31.6 μl O_2/mg of protein/h (which converts to 1.88 μmoles O_2/min/g ww) reported previously by Eveloff et al. [16] for these cells.

Dibutyryl cyclic AMP induced a dose dependent decrease in oxygen consumption by isolated thick ascending limb cells. The dose response curve is shown in Fig. 1. The oxygen consumption during the control periods in these experiments averaged 1.90 ± 0.13, $n = 15$. A significant decline in oxygen consumption to 79 ± 10%, $n = 4$, of control was observed at a dose of dibutyryl cyclic AMP of 10^{-7} M. Maximal inhibition was seen at doses of 10^{-5} M or greater, and averaged 60 ± 3% of control. In all subsequent experiments dibutyryl cyclic AMP was used at a concentration of 10^{-3} M. Because in all the experiments dibutyryl cyclic AMP was added together with theophylline 10^{-3} M, the effect of theophylline alone on oxygen consumption was tested in eight separate experiments. Theophylline by itself did not inhibit oxygen consumption, the average control

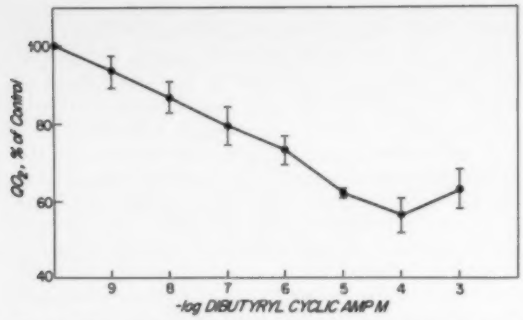

Fig. 1. Effect of dibutyryl cyclic AMP on oxygen consumption in isolated medullary thick ascending limb cells. Oxygen consumption is shown as a percentage of control that averaged 1.90 ± 0.13 μmoles O_2/min/g ww, $n = 15$. A significant decline was observed at a concentration of 10^{-7} M. Maximal inhibition was seen at 10^{-5} M

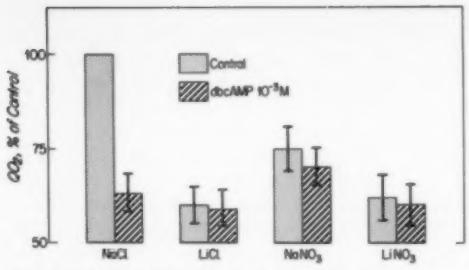

Fig. 2. Effect of dibutyryl cyclic AMP on oxygen consumption in the absence of sodium, chloride or sodium and chloride. In these experiments, sodium was replaced by lithium and chloride by nitrate. Dibutyryl cyclic AMP had no effect on oxygen consumption in the absence of sodium, chloride or both sodium and chloride

values were in these experiments 2.32 ± 0.17 μmoles O_2/min/g ww and after the addition of theophylline 2.25 ± 0.18, $n = 8$. Another potential experimental problem may arise from the hydrolysis of dibutyryl cyclic AMP into butyrate and cyclic AMP while in the reagent bottle or once in solution in the measuring chamber. We therefore tested for the effect of cyclic AMP and butyrate on oxygen consumption. In two experiments, cAMP 10^{-5} M produced an inhibition oxygen consumption of 38% and 36% of the same magnitude as that of dibutyryl cyclic AMP. Butyrate at a final concentration of 2×10^{-3} M, in addition to the substrates present in the incubation solution, did not alter oxygen consumption by the isolated cells.

Effect of dibutyryl cyclic AMP on transport dependent oxygen consumption

This series of experiments was designed to determine whether the effect of dibutyryl cyclic AMP was on transport dependent or transport independent oxygen consumption. In one group of experiments, sodium, chloride or both were removed from the incubation solution to ascertain the effect of dibutyryl cyclic AMP in the absence of these ions. In a second group of experiments furosemide, an inhibitor of the $Na^+:K^+:2Cl^-$ cotransporter present in these cells, and ouabain, a specific inhibitor of Na-K-ATPase, were used in combination with dibutyryl cyclic AMP to locate its effect. In a third series of experiments the effect of dibutyryl cyclic AMP on amphotericin B stimulated oxygen consumption was measured to further locate the effect of dibutyryl cyclic AMP.

Sodium and chloride substitution. In these experiments the cells were suspended, after the final wash, in a solution of lithium nitrate, without any sodium or chloride. As previously reported [16], replacement of sodium by lithium reduced oxygen consumption by 40 ± 5%, $n = 7$, from an average of 1.89 ± 0.19, in simultaneously run controls, to 1.10 ± 0.08 ($p < 0.01$). Dibutyryl cyclic AMP in the absence of sodium did not alter oxygen consumption as shown in Fig. 2, the latter remaining at 1.06 ± 0.07. Replacement of chloride by nitrate reduced oxygen consumption by 25 ± 6%, from 1.84 ± 0.18 to 1.36 ± 0.15, $n = 8$, this reduction was smaller than that noted previously by Eveloff et al. [16]. In the absence of chloride, oxygen consumption after dibutyryl cyclic AMP was 1.27 ± 0.13, not different from that seen after only removing chloride. When both sodium and chloride were removed and replaced with lithium nitrate, the oxygen consumption was decreased by an average of 38 ± 6%, from 1.89 ± 0.19 to 1.12 ± 0.07, $n = 7$, a value not different from that of removing sodium alone. Oxygen consumption remained at 1.08 ± 0.08 after dibutyryl cyclic AMP. From these experiments we conclude that dibutyryl cyclic AMP reduces oxygen consumption only when sodium and chloride are present in the incubation solution. Thus, it inhibits sodium and chloride dependent oxygen consumption.

Inhibition of the $Na^+:K^+:2Cl^-$ cotransporter with furosemide. Furosemide 10^{-4} M reduced oxygen consumption by medullary thick ascending limb cells by 25 ± 3% of total oxygen consumption or 64% of transport dependent (ouabain inhibitable) oxygen consumption. When dibutyryl cyclic AMP 10^{-3} M was given after furosemide it evoked a further decrease of 11 ± 3% of total oxygen consumption or 47 ± 11% of the furosemide inhibitable oxygen consumption, $p < 0.005$. When furosemide was given after dibutyryl cyclic AMP the effect was negligible, 5 ± 4%. The total reduction in oxygen consumption when dibutyryl cyclic AMP was given after furosemide was 35 ± 4% and 40 ± 5% when furosemide was added after dibutyryl cyclic AMP, values that are not significantly different. These experiments show that dibutyryl cyclic AMP has a small additive effect after furosemide but furosemide has no additive effect when given after dibutyryl cyclic AMP (Table 1).

Inhibition of Na-K-ATPase with ouabain. Ouabain inhibits oxygen consumption by medullary thick ascending limb cells by 39 ± 3%. Dibutyryl cyclic AMP after ouabain did not reduce oxygen consumption any further, average reduction 41 ± 8%. When the efflux of sodium via the pump is blocked by ouabain, dibutyryl cyclic AMP has no effect on oxygen consumption (Table 1).

Stimulation of oxygen consumption by increasing the influx sodium. The influx of sodium into the cell can be increased

Table 1. Effect of furosemide, ouabain and dibutyryl cyclic AMP on oxygen consumption

	Oxygen consumption		
	μmoles/min/g		
Control	2.02 ± 0.19	1.93 ± 0.18	1.87 ± 1.12
Furosemide 10^{-4} M	1.50 ± 0.12*		
Ouabain 10^{-4} M			1.12 ± 0.06*
Dibutyryl cAMP 10^{-3} M	1.30 ± 0.14*	1.25 ± 0.15*	1.08 ± 0.04
Furosemide 10^{-4} M		1.16 ± 0.16	
n	9	11	9

Values are mean ± SEM. *n* = number of experiments
* $p < 0.01$

Table 2. Effect of dibutyryl cyclic AMP on amphotericin B stimulated oxygen consumption of isolated medullary thick ascending limb cells

Experimental condition	*n*	Control	Amphotericin B 10 μg/ml	Dibutyryl cAMP 10^{-3} M
Regular Ringer's	14	2.44 ± 0.36	3.97 ± 0.55*	3.34 ± 0.45*
Nitrate Ringer's (no chloride)	8	1.58 ± 0.13	2.92 ± 0.38*	2.70 ± 0.37

Values are μmoles/min/g, mean ± SE. *n* = number of experiments
* $p < 0.01$

by the addition of amphotericin B to the incubation solution. The increase in sodium influx stimulates the activity of the sodium pump and thereby oxygen consumption. The administration of amphotericin B at a final concentration of 10 μg/ml produced a 61 ± 11%, $n = 14$, increase in oxygen consumption (Table 2). The addition of dibutyryl cyclic AMP reduced oxygen consumption by 25 ± 3% of the initial control value. Thus, dibutyryl cyclic AMP produces the same absolute changes in oxygen consumption in cells in which oxygen consumption has been stimulated by increasing the sodium influx using amphotericin B as in the absence of amphotericin B. This suggests that dibutyryl cyclic AMP inhibits transport dependent oxygen consumption by interfering with a discrete component of the transcellular electrolyte transport. To further test this hypothesis, the effect of dibutyryl cyclic AMP on amphotericin B stimulated oxygen consumption was measured in the absence of chloride, the latter replaced by nitrate. Amphotericin B stimulated oxygen consumption by 80% in the absence of chloride (Table 2) but there was no effect of dibutyryl cyclic AMP.

To test for the possibility that the oxygen consumption in the presence of amphotericin B had reached a maximum and also to determine whether dibutyryl cyclic AMP had a non-specific effect on cellular respiration, additional experiments were carried out in which oxygen consumption was uncoupled with 2,4-dinitrophenol 2×10^{-5} M. Oxygen consumption was increased by the uncoupler by 153 ± 24%, $n = 6$, 2.00 ± 0.29 to 5.08 ± 0.81. Dibutyryl cyclic AMP added after 2,4-dinitrophenol did not significantly alter oxygen consumption that averaged 4.67 ± 0.70, $p < 0.05$.

Effect of calcitonin and vasopressin. Because calcitonin and vasopressin are the two polypeptide hormones that evoke the largest response by adenyl cyclase in this segment of the nephron, we tested their effect on oxygen consumption by the isolated cells. Neither calcitonin at concentrations of 10^{-8} to 10^{-6} M nor vasopressin at the same concentrations produced any change in oxygen consumption, even though both hormones were able to stimulate adenyl cyclase in vitro in these cells.

Discussion

The present experiments show that dibutyryl cyclic AMP has an inhibitory effect on sodium and chloride dependent oxygen consumption in cells isolated from the medullary thick ascending limb of the loop of Henle. This effect should be contrasted with that on the mouse medullary thick ascending limb where it stimulates chloride transport [11, 31] and presumably transport related oxygen consumption. The rabbit thick ascending limb is clearly different from that of the mouse. Although its adenyl cyclase can be stimulated by AVP [41] isolated perfused thick ascending limbs do not exhibit a functional response to it [46]. Moreover, in the rabbit ileum, another epithelium that reabsorbs chloride by a sodium coupled mechanism sensitive to furosemide equivalent to that of the loop of Henle, cyclic AMP and theophylline inhibit chloride absorption [17, 42]. We would conclude, on the basis of the experiments reported here, that the rabbit thick ascending limb of the loop of Henle responds like rabbit ileum to cyclic AMP and not like rodent thick ascending limb.

Since sodium and chloride dependent oxygen consumption in this isolated cell preparation can be equated with transcellular electrolyte transport [15], dibutyryl cyclic AMP inhibits transcellular electrolyte transport. Although the present experiments cannot discriminate between sodium or chloride as the electrolyte being transported the available evidence indicates that chloride is transported by secondary active transport in this portion of the nephron [5, 21, 45], it is likely therefore that dibutyryl cyclic AMP inhibits chloride transport in this segment of the nephron.

The dose at which dibutyryl cyclic AMP first showed a significant effect was 10^{-7} M. This concentration is within the range of cyclic AMP concentrations found under basal conditions in isolated medullary thick ascending limbs of the loop of Henle and lower than those observed after stimulation with vasopressin [13]. It should be noted that concentrations of exogenous cyclic AMP that mimic the effect of the hormone are usually much higher than the intracellular levels of cyclic AMP found after hormonal stimulation [13, 26].The fact that in all of our experiments theophylline was added to the incubation medium at a concentration of 10^{-3} M may have helped evoke the response at a lower concentration of dibutyryl cyclic AMP.

The observation that dibutyryl cyclic AMP decreased oxygen consumption only in the presence of sodium and chloride indicates that it interferes with the mechanism of transcellular electrolyte transport. The mechanism of chloride transport in the cortical and medullary thick ascending limb has been worked out using electrical measurements by Greger [21, 24] and Hebert [30], respectively. Chloride enters the cell at the luminal membrane together with sodium and potassium. The energy for this entry step is provided by the

Table 3. Biochemical and functional effects of hormones on medullary thick ascending limb of the loop of Henle

Hormone	Species	Biochemical effect	Functional effect
AVP	Rat	Stimulates adenyl cyclase [13, 34, 37, 46] Increases cAMP levels [13] Activates protein kinase [13]	Increases sodium and chloride reabsorption [57]
	Rabbit	Stimulates adenyl cyclase [33]	
	Mouse	Stimulates adenyl cyclase [7, 46]	Increases PD [26, 29, 31, 46] Increases sodium and chloride reabsorption [26, 31]
Calcitonin	Rat	Stimulates adenyl cyclase [6, 13] Activates protein kinase [13]	
	Rabbit	Stimulates adenyl cyclase [9, 41]	Decreases calcium reabsorption [55]
	Human	Stimulates adenyl cyclase [8]	
PTH	Human	Stimulates adenyl cyclase [18]	
Glucagon	Rat	Stimulates adenyl cyclase [2] Increases cAMP levels [2]	
Aldosterone	Rat	Stimulates Na-K-ATPase [51]	
PGE_2	Rat	Suppresses AVP stimulated increase in cAMP [56]	
	Rabbit		Decreases PD. Decreases chloride reabsorption [54]
	Mouse		Decreases AVP stimulated chloride reabsorption [11, 12]

References in parenthesis

gradient for sodium directed into the cell. This gradient for sodium is maintained by the activity of Na-K-ATPase located in the basolateral membrane. Chloride leaves the cell through a conductance in the basolateral membrane [22, 30]. Potassium recycling across a luminal membrane potassium conductance appears to be critical [23, 32]. We attempted to locate the inhibitory effect of dibutyryl cyclic AMP along the different steps of the chloride transport pathway by using furosemide, ouabain and amphotericin B. The effect of cyclic AMP could be located at any of four different steps of the transport system: in the basolateral membrane Na-K-ATPase and the chloride conductance; in the luminal membrane the sodium, potassium, chloride cotransport system and the potassium conductance. The absence of an effect of dibutyryl cyclic AMP on oxygen consumption after the latter was stimulated with amphotericin in the absence of chloride (Table 2) indicates that Na-K-ATPase can be activated by the admission of sodium into the cell and that this activation is not inhibited by dibutyryl cyclic AMP. Therefore, the effect of dibutyryl cyclic AMP to inhibit sodium and chloride dependent oxygen consumption cannot be on Na-K-ATPase. An effect of dibutyryl cyclic AMP was not expected because whenever an effect of cyclic AMP on Na-K-ATPase in a transporting epithelia has been observed, it has been stimulatory rather than inhibitory [47, 52, 53]. The present experiments show that dibutyryl cyclic AMP has an additional inhibitory effect on oxygen consumption after furosemide. On the other hand, furosemide had no effect when given after dibutyryl cyclic AMP. Previous experiments using this isolated cell preparation indicate that the dose of furosemide used here is at a maximal concentration [16]. The finding that dibutyryl cyclic AMP has an inhibitory effect that is additive to that of furosemide suggests that it inhibits chloride transport at a site different from that of furosemide. Thus, the effect of dibutyryl cyclic AMP on transport dependent oxygen consumption is not on Na-K-ATPase or the sodium, potassium and chloride cotransporter. The only remaining alternatives are the basolateral chloride conductance and the luminal potassium conductance. Without ion flux or electrical measurements, the site of the inhibitory action of dibutyryl cyclic AMP cannot be localized further. However, by analogy with the mouse medullary thick ascending limb of the loop of Henle and the rectal gland of the dogfish where the effect of AVP and cyclic AMP, respectively [25, 49], is on the choride conductance, it would seem likely that the effect of dibutyryl cyclic AMP observed in these experiments may be on the chloride conductance.

Cyclic AMP is the intracellular messenger of polypeptide hormones, it is of great interest to consider which hormone could be the primary stimulus that brings about inhibition of chloride transport in this region of the kidney. Morel and collaborators, and other investigators have mapped the response of adenyl cyclase of the different segments of the kidney to various hormones [13, 35, 36, 41, 46]. The functional effects of some of these hormones have been tested using isolated perfused medullary thick ascending limbs. A summary of the biochemical and functional effects of the different hormones that have an effect on this segment of the nephron is shown in Table 3. It is noteworthy that for all the polypeptide hormones shown in the table a biochemical effect has been demonstrated but only for some of them has a functional effect been shown. Furthermore, some of the hormones have their functional effect restricted to some species, as in the case of AVP where the effect on chloride transport in the medullary thick ascending limb is present

in the mouse [26, 31, 46] and to much lesser extent in the rat [57] where others have seen an effect only when the bath is made hypertonic to the luminal perfusate [46]. The functional effects described for PTH and glucagon have been seen in classical micropuncture or microperfusion experiments where the effect cannot be precisely located to either the medullary or the cortical thick ascending limb [2, 14, 44, 57]. A functional effect of PTH on medullary thick ascending limb may be restricted to humans because adenyl cyclase stimulation by PTH has not been demonstrated in other species in this nephron segment.

The two polypeptide hormones tested in these experiments, salmon calcitonin and synthetic arginine vasopressin, were used because they evoke the largest response by adenyl cyclase in this segment of the nephron. However, neither hormone caused a change in oxygen consumption by the isolated cells at the same experimental conditions where dibutyryl cyclic AMP caused a substantial decrease. These results are in agreement with the absence of a functional effect of AVP on electrolyte transport in the rabbit [46]. Suki and Rouse have demonstrated an effect of calcitonin to increase net calcium absorption by the medullary thick ascending limb of the rabbit an effect mimicked by 10^{-3} M 8-bromo cAMP [55]. In the same series of experiments these authors found that 8-bromo cAMP reduced, although not significantly so, transepithelial potential difference suggesting that transepithelial electrolyte transport was also reduced, in keeping with the reduction in transport dependent oxygen consumption reported here.

Acknowledgements. The excellent technical assistance of Frau Brunhilde Moewes is gratefully acknowledged. This work was done while Dr. P. Silva was an Established Investigator of the American Heart Association on sabbatical leave at Max-Planck-Institut für Biophysik, Frankfurt am Main, Federal Republic of Germany.

References

1. Agus ZS, Puschett JB, Senesky D, Goldberg M (1971) Mode of action of parathyroid hormone and cyclic adenosine 3′,5′-monophosphate on renal tubular phosphate reabsorption in the dog. J Clin Invest 50:617–626
2. Bailly C, Imbert-Teboul M, Chabardes D, Hus-Citharel A, Montegut M, Clique A, Morel F (1980) The distal nephron of rat kidney: a target site for glucagon. Proc Natl Acad Sci USA 77:3422–3424
3. Bailly C, Roinel N, Amiel C (1984) PTH-like glucagon stimulation of Ca and Mg reabsorption in Henle's loop of the rat. Am J Physiol 246:F205–F212
4. Besarab A, Pomerantz P, Swanson JW (1982) Effect of exogenous adenosine 3′:5′-cyclic monophosphate, parathyroid hormone and acetazolamide on electrolyte excretion by the isolated perfused rat kidney. Renal Physiol 5:124–135
5. Burg MB, Green N (1973) Function of the thick ascending limb of Henle's loop. Am J Physiol 224:659–668
6. Chabardes D, Imbert-Teboul M, Montegut M, Clique A, Morel F (1976) Distribution of calcitonin-sensitive adenylate cyclase activity along the rabbit kidney tubule. Proc Natl Acad Sci USA 73:3608–3612
7. Chabardes D, Imbert-Teboul M, Gagnan-Brunette M, Morel F (1978) Different hormonal target sites along the mouse and rabbit nephrons. Curr Probl Clin Biochem 8:447–454
8. Chabardes D, Gagnan-Brunette M, Imbert-Teboul M, Gontcharevskaia O, Montegut M, Clique A, Morel F (1980) Adenylate cyclase responsiveness to hormones in various portions of the human nephron. J Clin Invest 65:439–448
9. Chamberlin ME, LeFurgey A, Mandel LJ (1984) Suspension of medullary thick ascending limb tubules from the rabbit kidney. Am J Physiol 247:F955–F964
10. Costanzo LS, Windhager EE (1980) Effects of PTH, ADH, and cyclic AMP on distal tubular Ca and Na reabsorption. Am J Physiol 239:F478–F485
11. Culpepper RM, Andreoli TE (1983) Interactions among prostaglandin E2, antidiuretic hormone, and cyclic adenosine monophosphate in modulating Cl-absorption in single mouse medullary thick ascending limbs of Henle. J Clin Invest 71:1588–1601
12. Culpepper RM, Andreoli TE (1984) PGE2, forskolin, and cholera toxin interactions in modulating NaCl transport in mouse mTALH. Am J Physiol 247:F784–F792
13. Edwards RM, Jackson BA, Dousa TP (1980) Protein kinase activity in isolated tubules of rat renal medulla. Am J Physiol 238:F269–F278
14. Elalouf JM, Roinel N, de Rouffignac C (1984) ADH-like effects of calcitonin on electrolyte transport by Henle's loop of rat kidney. Am J Physiol 246:F213–F220
15. Eveloff J, Haase W, Kinne R (1980) Separation of renal medullary cells: isolation of cells from the thick ascending limb of Henle's loop. J Cell Biol 87:672–680
16. Eveloff JS, Bayerdorffer E, Silva P, Kinne R (1981) Sodium-chloride transport in the thick ascending limb of Henle's loop. Pflügers Arch 389:263–270
17. Field M (1971) Ion transport in rabbit ileal mucosa. II. Effects of cyclic 3′,5′-AMP. Am J Physiol 221:992–997
18. Fulgraff G, Meiforth A (1974) Effects of cyclic nucleotide monophosphates (cAMP, cGMP, cIMP, dibutyryl-cAMP) on transtubular net fluxes in rat kidneys. Naunyn-Schmiedeberg's Arch Pharmacol 283:425–429
19. Gill JR, Casper AGT (1971) Renal effects of adenosine 3′,5′-cyclic monophosphate and dibutyryl adenosine 3′,5′-cyclic monophosphate. J Clin Invest 50:1231–1240
20. Grantham JN, Burg MB (1966) Effect of vasopressin and cyclic AMP on permeability of isolated collecting tubules. Am J Physiol 211:255–259
21. Greger R (1985) Ion transport mechanisms in thick ascending limb of Henle's loop of mammalian nephron. Physiol Rev 65:760–797
22. Greger R, Schlatter E (1983) Properties of the basolateral membrane of the cortical thick ascending limb of Henle's loop of rabbit kidney. A model for secondary active chloride transport. Pflügers Arch 396:325–334
23. Greger R, Schlatter E (1983) Properties of the lumen membrane of the cortical thick ascending limb of Henle's loop of rabbit kidney. Pflügers Arch 396:315–24
24. Greger R, Schlatter E, Lang F (1983) Evidence for electroneutral sodium chloride cotransport in the cortical thick ascending limb of Henle's loop of rabbit kidney. Pflügers Arch 396:308–314
25. Greger R, Schlatter E, Gogelein H (1985) Cl^--channels in the apical cell membrane of the rectal gland "induced" by cAMP. Pflügers Arch 403:446–448
26. Hall DA, Varney DM (1980) Effect of vasopressin on electrical potential difference and chloride transport in mouse medullary thick ascending limb of Henle's loop. J Clin Invest 66:792–802
27. Hall DA, Barnes LD, Dousa TP (1977) Cyclic AMP in action of antidiuretic hormone: effects of exogenous cyclic AMP and its new analogue. Am J Physiol 232:F368–F376
28. Hamburger RJ, Lawson NL, Dennis VW (1974) Effects of cyclic adenosine nucleotides on fluid absorption by the different segments of proximal tubule. Am J Physiol 227:396–401
29. Hebert SC, Andreoli TE (1984) Control of NaCl transport in the thick ascending limb. Am J Physiol 246:F745–F756
30. Hebert SC, Andreoli TE (1984) Effects of antidiuretic hormone on cellular conductive pathways in mouse medullary thick ascending limbs of Henle. II. Determinants of the ADH-mediated increases in transepithelial voltage and in net Cl-absorption. J Membr Biol 80:221–233

31. Hebert SC, Culpepper RM, Andreoli TE (1981) NaCl transport in mouse medullary thick ascending limbs. I. Functional nephron heterogeneity and ADH-stimulated NaCl cotransport. Am J Physiol 241:F412–F431
32. Hebert SC, Friedman PA, Andreoli TE (1984) Effects of antidiuretic hormone on cellular conductive pathways in mouse medullary thick ascending limbs of Henle. I. ADH increases transcellular conductance pathways. J Membr Biol 80:201–219
33. Imbert M, Chabardes D, Montegut M, Clique A, Morel F (1975) Vasopressin dependent adenylate cyclase in single segments of rabbit kidney tubule. Pflügers Arch 357:173–185
34. Imbert-Teboul M, Chabardes D, Montegut M, Clique A, Morel F (1978) Vasopressin-dependent adenylate cyclase activities in the rat kidney medulla: evidence for two separate sites of action. Endocrinology 102:1254–1261
35. Jackson BA, Edwards RM, Dousa TP (1980) Measurements of cyclic AMP and cyclic GMP phosphodiesterase activity in isolated tubular segments. Kidney Int 18:512–518
36. Jackson BA, Edwards RM, Valtin H, Dousa TP (1980) Cellular action of vasopressin in medullary tubules of mice with hereditary nephrogenic diabetes insipidus. J Clin Invest 66:110–122
37. Kim JK, Jackson BA, Edwards RM, Dousa TP (1982) Effect of potassium depletion on the vasopressin-sensitive cyclic AMP system in rat outer medullary tubules. J Lab Clin Med 99:29–38
38. Kurokawa K, Torikai S (1982) Differential effects of prostaglandin E_2 on cAMP levels in intact single nephron segments of rats. Kidney Int 21:262
39. Martinez-Maldonado M, Eknoyan G, Suki WN (1971) Natriuretic effects of vasopressin and cyclic AMP: possible site of action in the nephron. Am J Physiol 220:2013–2020
40. McKinney TD, Myers P (1980) Bicarbonate transport by proximal tubules: effect of parathyroid hormone and dibutyryl cyclic AMP. Am J Physiol 238:F166–F174
41. Morel F (1981) Sites of hormone action in the mammalian nephron. Am J Physiol 240:F159–F164
42. Nellans HN, Frizzell RA, Schultz SG (1973) Coupled sodium-chloride influx across the brush border of rabbit ileum. Am J Physiol 225:467–475
43. Pastoriza-Munoz E, Colindres RE, Lassiter WE, Lechene C (1978) Effect of parathyroid hormone on phosphate reabsorption in rat distal convolution. Am J Physiol 235:F321–F330
44. Quamme GA (1980) Effect of calcitonin on calcium and magnesium transport in rat nephron. Am J Physiol 238:E573–E578
45. Rocha AS, Kokko JP (1973) Sodium chloride and water transport in the medullary thick ascending limb of Henle. Evidence for active chloride transport. J Clin Invest 52:612–623
46. Sasaki S, Imai M (1980) Effects of vasopressin on water and NaCl transport across the in vitro perfused medullary thick ascending limb of Henle's loop of mouse, rat, and rabbit kidneys. Pflügers Arch 383:215–221
47. Scheid CR, Honeyman TW, Fay FS (1979) Mechanism of beta-adrenergic relaxation of smooth muscle. Nature 277:32–36
48. Scheinman SJ, Stec WJ, Coulson R (1985) Effects of (Sp)- and (RP)-adenosine cyclic 3′,5′-phosphorothioates on electrolyte excretion by the isolated perfused rat kidney. Miner Electrolyte Metab 11:85–90
49. Schlatter E, Greger R (1984) Mechanism of cyclic AMP stimulation of active NaCl reabsorption in the isolated perfused medullary thick ascending limb of Henle's loop (mTAL) of mouse nephron. Pflügers Arch 400:R22
50. Schlondorff D, Carvounis CP, Jacoby M, Satriano JA, Levine SD (1981) Multiple sites for interaction of prostaglandin and vasopressin in toad urinary bladder. Am J Physiol 241:F625–F631
51. Schmidt U, Schmid J, Schmid H, Dubach UC (1975) Sodium- and potassium-activated ATPase. A possible target of aldosterone. J Clin Invest 55:655–660
52. Silva P, Stoff JS, Epstein FH (1979) Indirect evidence for enhancement of Na-K-ATPase activity with stimulation of rectal gland secretion. Am J Physiol 237:F468–F472
53. Silva P, Epstein JA, Stevens A, Spokes K, Epstein FH (1983) Ouabain binding in rectal gland of *Squalus acanthias*. J Membr Biol 75:105–114
54. Stokes JB (1979) Effect of prostaglandin E_2 on chloride transport across the rabbit thick ascending limb of Henle. Selective inhibition of the medullary portion. J Clin Invest 64:495–502
55. Suki WN, Rouse D (1981) Hormonal regulation of calcium transport in thick ascending limb renal tubules. Am J Physiol 241:F171–F174
56. Torikai S, Kurokawa K (1983) Effect of PGE2 on vasopressin-dependent cell cAMP in isolated single nephron segments. Am J Physiol 245:F58–F66
57. Work J, Galla JH, Booker BB, Schafer JA, Luke RG (1985) Effect of ADH on chloride reabsorption in the loop of Henle of the Brattleboro rat. Am J Physiol 249:F698–F703

Received March 6/Accepted December 1, 1986

Pflügers Arch (1987) 409:81–92

Pflügers Archiv
European Journal of Physiology
© Springer-Verlag 1987

Electrophysiological studies in principal cells of rat cortical collecting tubules

ADH increases the apical membrane Na^+-conductance *

Eberhard Schlatter ** **and James A. Schafer**

Nephrology Research and Training Center, Departments of Physiology, Biophysics, and Medicine, University of Alabama at Birmingham, Birmingham, AL 35294, USA

Abstract. The mechanism of ion transport across principal cells of rat cortical collecting tubules (CCT) and its regulation by vasopressin (ADH) has been studied in the isolated perfused tubule. To amplify the response to ADH rats were treated with 5 mg I. M. desoxycorticosterone 4–9 days prior to the experiments. Addition of $2 \cdot 10^{-10}$ mol · l^{-1} ADH increased the transepithelial voltage from -5.1 ± 0.7 mV to -16.1 ± 1.4 mV ($n = 37$) and decreased the transepithelial resistance from $51 \pm 4\,\Omega\,cm^2$ to $39 \pm 2\,\Omega\,cm^2$ ($n = 33$). Optical and functional differentiation of impalements of principal and intercalated cells was made and only data of principal cells are presented. ADH depolarized the apical membrane from 79 ± 1 mV to 66 ± 2 mV ($n = 26$) and decreased the fractional resistance of the apical membrane from 0.76 ± 0.04 to 0.70 ± 0.04 ($n = 13$). These ADH effects were prevented by 10^{-5} or 10^{-4} mol · l^{-1} luminal amiloride which hyperpolarized the apical membrane when added in the presence or absence of ADH. Apical and basolateral membranes were dominated by large K^+ conductances and addition of 3 mmol · l^{-1} barium to bath or lumen perfusates increased transepithelial resistance almost two-fold, whereas luminal amiloride increased the transepithelial resistance only by 26 −35%. Ouabain (0.5 mmol · l^{-1}, bath) depolarized the basolateral membrane and decreased its K^+ conductance. These effects were prevented by the simultaneous presence of apical amiloride suggesting that the only route of Na^+ entry into the principal cells occurred via the amiloride sensitive Na^+ conductance. We conclude that ADH stimulates Na^+ reabsorption and K^+ secretion in the rat CCT primarily by increasing the Na^+ conductance in the apical cell membrane.

Key words: Cortical collecting tubule – Rat – ADH – Principal cells – Intercalated cells – Barium – Amiloride – Ouabain

Introduction

It has long been accepted that aldosterone is the primary regulator of Na^+ transport in the late distal tubule and collecting duct (CCT) [9, 20, 24–26, 33]. It has also been recognized that vasopressin (ADH) can stimulate Na^+ transport in various amphibian epithelia [10, 17], in the medullary thick ascending limb of Henle's loop of the mouse [30], and in the rabbit CCT [4, 32]. However, in the rabbit CCT ADH produced only a transient stimulation of Na^+ absorption and hyperpolarization of the transepithelial voltage. Within 15 min of hormone addition these parameters fell to control levels [4]. These earlier studies were conducted only in the rabbit cortical collecting tubule because of the greater ease of dissection in this species. More recently it has been possible to study the rat cortical collecting tubule by using pathogen-free rats [23, 36]. In the distal tubule [3] and the CCT from this species ADH was shown to have its expected effect in producing a marked increase in water permeability [23], but in addition it also increased net Na^+ absorption and K^+ secretion [24, 29, 36, 37].

In CCT segments from untreated rats there was no net Na^+ reabsorption and only a small net K^+ secretion [24, 29, 36]. Addition of physiologic levels of ADH resulted in an increase in the lumen-negative transepithelial voltage [23], an increased absorptive flux of Na^+ [24], and an increased secretory flux of K^+ [29]. Furthermore, these effects were sustained for at least 3 h in marked contrast to the rabbit.

As expected from studies in the rabbit CCT [14, 20, 25, 33], CCT segments from rats that had been treated for several days with high doses of desoxycorticosterone (DOC) exhibited significantly higher rates of net Na^+ reabsorption and K^+ secretion than observed in the control tubules. In vitro administration of ADH to these DOC-treated tubules resulted in an even further increase in Na^+ and K^+ transport which was greater than in control tubules [24, 28, 36, 37]. The enhancement of Na^+ reabsorption and K^+ secretion by both DOC and ADH was entirely due to increases in their unidirectional reabsorptive and secretory fluxes, respectively, with no change in passive backflux of either cation [24, 28]. It was also found that 10^{-5} mol · l^{-1} luminal amiloride abolished the net Na^+ absorptive flux in the DOC-treated tubules in the presence or absence of ADH [24]. Luminal barium at 2 mmol · l^{-1} reduced the secretory K^+ flux in DOC-treated tubules but not sufficiently to block completely the net flux in the presence of ADH [28]. The results of these inhibitor studies strongly suggest that the Na^+ absorptive flux stimulated by either DOC or ADH occurs via the amiloride-sensitive Na^+ channel in the apical membrane and that the K^+ secretory flux involves barium-inhibitable apical K^+-channels. Both conductances have previously been shown to be increased by the action of mineralocorticoids in the rabbit CCT [14, 21, 25, 26].

* Parts of this study have been presented at the 19th ASN meeting in Washington, DC, USA 1986

** Recipient of a Fogarty International Fellowship from the NIH No 1 F05 TWO 3748-01

Offprint requests to: J. A. Schafer

Na^+ reabsorption and K^+ secretion in the rabbit CCT have been associated with the principal cell, whereas the other cell type in this segment, the intercalated cell, is thought to be involved in H^+ secretion or HCO_3^- transport and possibly K^+ reabsorption [19, 34]. It also appears that ADH receptors are localized exclusively to the principal cells of the rabbit CCT [12] suggesting that this is the ADH-responsive cell type in cation transport.

Until the present study, there have been no reports of the electrophysiologic properties of the rat CCT. Therefore, this study was undertaken to study the mechanism of ion transport and its regulation by ADH in principal cells of DOC-treated rats. Because intracellular data were obtained from principal as well as intercalated cells, optical and functional criteria (see Methods) have been used to subdivide the two populations. We present evidence that ADH increases Na^+ reabsorption and K^+ secretion in the rat CCT by an increase in the apical amiloride-sensitive Na^+-conductance of the principal cells.

Methods

In this study 86 CCT segments of 59 male Sprague-Dawley rats, body weight 75–125 g, have been used. The pathogen-free rats were obtained from Taconic Farms (Germantown, NY, USA) and were kept in filter-top cages as described earlier [23]. The rats were treated with 5 mg I.M. desoxycorticosterone pivalate 4–9 days prior to the experiments. Animals were killed by decapitation and tubules were dissected at 18°C in a bathing solution containing 6% purified bovine serum albumin. The technique of in vitro perfusion of the isolated CCT segments used in this study has been described previously [5, 7, 8]. The in vitro perfusion system used was obtained from Luigs-Neumann, Ratingen, FRG. In this study, the bath perfusate reservoirs and lines were enclosed by water jackets through which heated water was passed to maintain perfusate temperature at 38°C. The bath flow rate varied between 20 and 40 ml/min through a perfusion chamber with a volume of 1.5 ml, which allowed rapid changes of the bath perfusate. The tubule lumen was perfused at flow rates > 10 nl/min to avoid concentration changes of the perfusate along the tubule. The perfusates were identical on both sides of the epithelium and contained in mmol $\cdot l^{-1}$: Na^+ 160, K^+ 5, Ca^{2+} 1.5, Mg^{2+} 1, Cl^- 140, HCO_3^- 25, phosphate buffer 2, HEPES 5, and glucose 5. In the high K^+ solution used in the K^+ concentration step experiments 15 mmol $\cdot l^{-1}$ Na^+ were replaced by K^+. In the low Cl^- solution used in the Cl^- concentration step experiments 90 mmol $\cdot l^{-1}$ Cl^- were replaced either by NO_3^- or gluconate. Osmolality was always 320 mosmol $\cdot l^{-1}$. All solutions were equilibrated with 95% O_2/5% CO_2 and adjusted to pH 7.4 at 38°C. Bath perfusate reservoirs were continuously gassed with 95% O_2/5% CO_2 during the experiment. The ADH-solution contained in addition $2 \cdot 10^{-10}$ mol $\cdot l^{-1}$ arginine vasopressin (Pitressin, Parke-Davis, Morris Plains, NJ, USA).

The electrical circuit and methods to measure or calculate the transepithelial voltage (PD_{te}) and resistance (R_{te}), the basolateral or apical membrane potentials (PD_{bl}, PD_a), and the fractional resistance of the basolateral or apical membrane (FR_{bl}, FR_a) have been described in detail previously [8]. Fractional resistances of apical or basolateral membranes are calculated as the deflections of the basolateral or apical membrane potential, respectively, induced by current pulses divided by the change in the transepithelial voltage. Although voltage deflections were always recorded only across the basolateral membrane and are shown as such on some of the original recordings, average FR_a values are calculated and presented when changes obviously occurred at the apical membrane. Current pulses used to measure transepithelial and fractional cell membrane resistances ranged from 23 to 80 nA and lasted 80 ms at a pulse rate of 10 pulses/min.

Single barreled microelectrodes (Ling-Gerard) were pulled from Pyrex filament glass (O.D. 1.5, I.D., 0.78 mm, Hilgenberg, Malsfeld, FRG) with a horizontal puller (Brown-Flaming, Model P-80, Sutter Instrument, San Francisco, CA, USA). The electrode resistances varied between 80 and 200 MΩ when filled with KCl (1 mol $\cdot l^{-1}$). Stable impalements which lasted several minutes to approximately 3 h were obtained with the aid of a piezodrive (Frankenberger, München, FRG). The criteria for an acceptable intracellular voltage recording were: (1) a sudden change in a potential read by the electrode; (2) an increase in electrode resistance of $\leq 30\%$ (in most instances there was no change in the electrode resistance at all); (3) stability of PD_{bl} (± 2 mV) for at least 5 min; (4) a return to the same original baseline upon withdrawal of the microelectrode. An L-MPR-20 Electrometer (List-Medical, Darmstadt, FRG) was used for the intracellular voltage recordings.

Differentiation of cell types. From a total of 107 impalements in the CCT segments, 72 were identified as principal cells according to the following criteria: First, the impaled cell was examined under high power (400×) Hoffmann contrast microscopy (Nikon Diaphot, Tokyo, Japan). Some cells were observed to be round shaped, to protrude into the lumen, and to show often a clear vesiculation and were considered to be intercalated cells. These observations have also been reported for the rabbit CCT [1, 19]. Second, functional tests were used as objective criteria to separate cell types: (a) In one cell type addition of luminal amiloride hyperpolarized PD_{bl} and increased FR_a. Also in these cells ADH addition to the bath depolarized PD_{bl} and decreased FR_a. These cells were considered to be principal cells. (b) The other cell type showed a depolarization of PD_{bl} upon addition of luminal amiloride and a hyperpolarization of PD_{bl} after addition of ADH with no significant change in FR_a (see Fig. 1). These cells were considered to be intercalated cells. The observed changes of PD_{bl} in intercalated cells with ADH and amiloride addition are probably due to circular current loops across the epithelium generated by the change in PD_{te} induced by ADH or amiloride effects on the principal cells. As both membranes of both cell types are partially short circuited through the paracellular shunt any primary voltage change of one membrane of the principal cell will not only alter the membrane voltage of the opposite membrane of that cell but also both membrane voltages of the intercalated cell. The optical verification together with at least one of the functional tests were used to identify the cell type for each impalement reported. Six impaled cells could not be identified primarily because none of the above mentioned functional parameters were measured to support the optical observation and, therefore, were not considered for this study. As this study focuses on the mechanism and regulation of Na^+ and K^+ transport only data from principal cells are reported in detail.

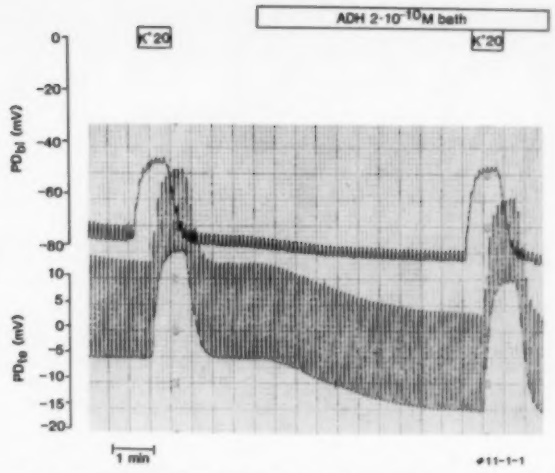

Fig. 1. Effects of ADH and a bath K^+-concentration step (5 to 20 mmol · l^{-1}) on transepithelial voltage (PD_{te}) and resistance of an isolated perfused rat CCT (*lower tracing*) and on basolateral membrane voltage (PD_{bl}) and fractional resistance of an intercalated cell (*upper tracing*). Note the hyperpolarization of PD_{bl} upon ADH with no change in the pulse height (which is proportional to the fractional resistance of the basolateral membrane)

Transference numbers for K^+ (t_K) of the apical and basolateral membrane were calculated from the changes in the membrane potential (ΔPD_x) induced by K^+-concentration steps from 5 (C_1) to 20 (C_2) mmol · l^{-1} in bath or luminal perfusates. The peak depolarization of PD_{bl} was always used with fast bath exchange rates (2–5 s) to minimize secondary effects such as changes in cellular ion activities.

$$t_K = \Delta EMF_x \cdot F / [R \cdot T \cdot \ln (C_2/C_1)] .$$

The electromotive force for K^+ across membrane x (apical or basolateral) is equal to: $\Delta EMF_x = \Delta PD_x$ – liquid junction potential – $\Delta PD_{x,cc}$ where $\Delta PD_{x,cc}$ is the change in membrane voltage induced by circular current across the epithelium. $\Delta PD_{x,cc}$ was calculated using ΔPD_{te} and voltage divider ratio measurements.

$$VDR = (\Delta PD_{te} - \Delta PD_{bl}) / \Delta PD_{bl}$$
$$\Delta PD_{a,cc} = \Delta PD_{te} \cdot VDR / (VDR + 1)$$
$$\Delta PD_{bl,cc} = \Delta PD_{te} / (VDR + 1) .$$

Liquid junction potentials were measured separately with free flowing KCl electrodes.

For this study 5 series of experiments were performed. The first series examined the effects of ADH in the bath perfusate on PD_{te}, R_{te}, PD_{bl}, PD_a, FR_{bl} and FR_a. In addition the effects of luminal amiloride were tested before and after the addition of ADH. The second series described the effects of K^+ and Cl^--concentration steps and barium in both bath and luminal perfusates. In a third series the effects of ouabain in the bath were examined especially with respect to the K^+-conductance. In addition, the effect of ouabain in the presence of amiloride was tested. Series 4 examined the selectivity of the shunt pathway by measuring dilution potentials when 80 mmol · l^{-1} NaCl were replaced by mannitol either in the luminal or bath perfusate. In a fifth series the effects of ADH were monitored when either barium or amiloride was added to the luminal perfusate prior to the ADH addition.

Data are presented as original recordings or as mean values ± standard error with n referring to the number of tubules (transepithelial measurements) or cells (transmembrane measurements). All differences reported here were from paired observations in the same tubule or within the same impalement so that a paired t-test was used to determine statistical significance. A p-value of ≤ 0.05 was accepted to indicate statistical significance.

Results

General data

The CCT segment used in this study had an average length of 345 ± 12 µm ($n = 86$). The optical inside diameter of these tubules was 20.9 ± 0.3 µm. The optically measured and the electrical radius calculated from transepithelial resistance measurements did not differ significantly from each other. The length constant of these tubules was 205 ± 7 µm.

Effects of ADH and amiloride on intercalated cells

For this study of ion transport mechanisms in principal cells of CCT's functional tests as well as morphological criteria were used to identify principal cells (see Methods). Figure 1 shows the effect of ADH on PD_{bl} in an intercalated cell. The original recording clearly demonstrates that opposite to the effects in the principal cells (described below) PD_{bl} hyperpolarized upon addition of ADH, parallel to the increase in the lumen negative PD_{te}. In addition, there was no change in the pulse height on the PD_{bl} tracing, indicating that neither the apical nor the basolateral membrane fractional resistance changed. Upon addition of ADH PD_{bl} of 15 intercalated cells hyperpolarized significantly from −83 ± 1 mV to −87 ± 1 mV. FR_a was 0.82 ± 0.02 and 0.81 ± 0.03 ($n = 13$) before and after ADH, respectively, and, thus not significantly different in the two states. Luminal amiloride (10^{-4} or 10^{-5} mol · l^{-1}) depolarized PD_{bl} of intercallated cells from −85 ± 1 mV to −84 ± 1 mV ($n = 21$) before ADH and from −87 ± 1 mV to −85 ± 1 mV ($n = 12$) after ADH. Both changes were statistically significant on the basis of paired comparison. The changes in FR_a upon addition of amiloride of +0.04 ± 0.02 (−ADH, $n = 12$) and +0.04 ± 0.02 (+ADH, $n = 7$) were not statistically significant.

Effects of ADH and amiloride

Figure 2 shows the rapid increase of the lumen negative PD_{te} upon addition of ADH and its decline after removal of the hormone. On this original recording a close inspection of the voltage deflections induced by transepithelial current pulses, representing R_{te}, shows that ADH reversibly decreased R_{te}. The original recording of Fig. 3 (upper part of the continuous recording) demonstrates the effect of ADH on PD_{te} and PD_{bl}. The basolateral membrane depolarized by 26 mV in contrast to the hyperpolarization seen in the intercalated cells (Fig. 1). On average the effects of ADH began about 1 min after the addition of the hormone to the bath perfusate and were maximal within 5–10 min. Removal of ADH led to the opposite effects with a similar time course. The frequency distributions of PD_{bl} and PD_a

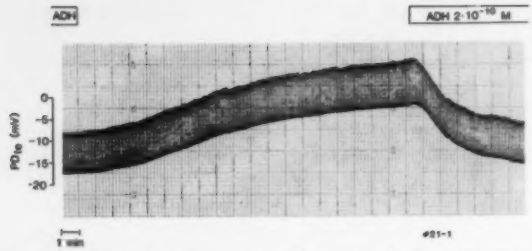

Fig. 2. Effect of ADH ($2 \cdot 10^{-10}$ mol $\cdot$ l^{-1}) on transepithelial potential (PD_{te}) and resistance of an isolated perfused rat CCT segment. The original recording shows initially the effects of ADH removal and then another stimulation of PD_{te} by readdition of ADH. Careful analysis of the transepithelial voltage pulses, corresponding to the input resistance of the tubule segment, reveals that the transepithelial resistance is lower (31 versus 40 Ωcm^2) in the presence of ADH

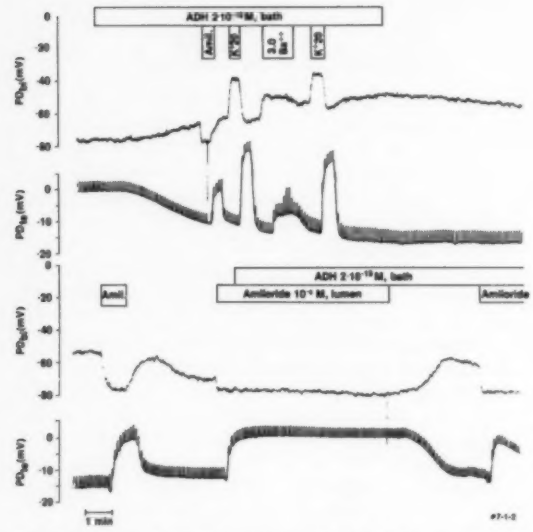

Fig. 3. Effects of ADH on transepithelial (PD_{te}) and basolateral membrane voltage (PD_{bl}) of a principal cell in the absence and presence of luminal amiloride (Amil.) (10^{-5} mol $\cdot$ l^{-1}). This original recording is a continuous tracing of PD_{bl} of a principal cell. This particular cell showed very high transport rates (effects of inhibitors and ADH on PD_{bl} are larger than average values). In addition the effects of a K^+-concentration step from 5 to 20 mmol $\cdot$ l^{-1} in the bath perfusate and of barium (3.0 mmol $\cdot$ l^{-1}) in the bath are shown

without and with ADH in the bath perfusate are shown in Fig. 4. Whereas the frequency distributions of PD_{bl} and PD_a are quite close together in the absence of ADH, both voltages are depolarized with ADH with the PD_a values being significantly more depolarized than PD_{bl} values.

Table 1 summarizes the effects of ADH on PD_{te}, R_{te}, PD_{bl}, PD_a and FR_a. The lumen negative PD_{te} increased by a factor of more than 3 and R_{te} decreased by approximately 24%. Both PD_{bl} and PD_a depolarized significantly with the depolarization of PD_a exceeding that of PD_{bl} ($\Delta PD_a = 13 \pm 2$ mV, $\Delta PD_{bl} = 6 \pm 1$ mV). FR_a decreased slightly but

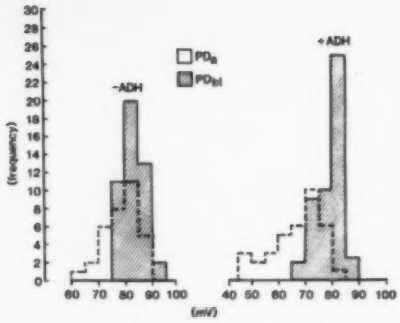

Fig. 4. Frequency distribution of basolateral (PD_{bl}, *shaded area*) and apical (PD_a, *area bounded by dashed lines*) membrane potential of principal cells in the absence and presence of ADH. PD_{bl} values are negative, PD_a values positive with respect to the grounded bath

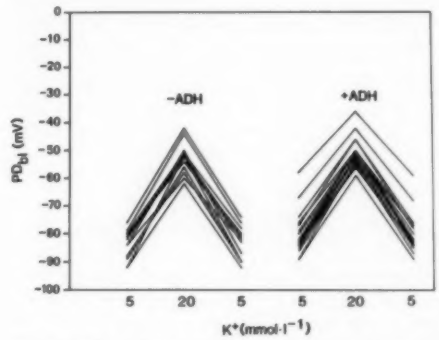

Fig. 5. Effect of K^+-concentration steps (5 to 20 mmol$\cdot l^{-1}$) in the bath perfusate on basolateral membrane voltage (PD_{bl}) in principal cells in the absence and presence of ADH. The mean depolarizations of PD_{bl} are 31 ± 1 mV ($n = 13$) and 30 ± 1 mV ($n = 19$), respectively

significantly by 7.9%. Figure 13 shows the change in the voltage deflections produced by transepithelial current pulses after ADH addition. Because R_{te} decreased, the simultaneous increase in the voltage deflections across the basolateral membrane indicate a decrease in FR_a.

Table 2 summarizes the effects of luminal amiloride before and after ADH addition to the bath. Concentrations of either 10^{-5} or 10^{-4} mol $\cdot$ l^{-1} were used. As there was no significant difference in the effects of these two concentrations the data were pooled. Luminal amiloride reversed the polarity of the lumen negative PD_{te} in both functional states to about +1 mV. The change in PD_{te} with amiloride addition was 3-fold greater after ADH treatment. R_{te} increased with amiloride by 27% without ADH and by 35% with ADH. Amiloride hyperpolarized both membranes in the absence and presence of the hormone. The hyperpolarization especially of PD_a, however, was greatly enhanced after ADH. FR_a increased under both conditions to similar values. The original recording of Fig. 3 shows an example of the amiloride effect on PD_{te} and PD_{bl}.

Effects of K^+ and Cl^--concentration steps and Ba^{2+}

Figure 5 summarizes the effect of a K^+-concentration step in the bath perfusate from 5 to 20 mmol $\cdot$ l^{-1} on PD_{bl}. In

control tubules PD_{te} and PD_{bl} of principal cells depolarized by 19.5 ± 2.0 mV ($n = 10$) and 31 ± 1 mV ($n = 19$), respectively. In ADH treated tubules ΔPD_{te} and ΔPD_{bl} were 21.8 ± 1.8 mV ($n = 14$) and 30 ± 1 mV ($n = 19$), respectively. The differences between the K^+-concentration step induced voltage changes with and without ADH were even bigger in 6 paired observations: $\Delta PD_{te} = 16.8 \pm 1.9$ without ADH versus 23.2 ± 2.6 mV with ADH. The same holds true for the depolarization of PD_{bl}: $\Delta PD_{bl} = 34 \pm 2$ mV versus 30 ± 2 mV without and with ADH respectively. This difference indicates that there is a change in the circular current with ADH that alters the observed ΔPD_{bl} with the K^+ concentration steps. The same K^+-concentration steps performed in the lumen perfusate led to a hyperpolarization of PD_{te} by 10.4 ± 3.2 mV ($n = 4$) without and by 9.4 ± 1.5 mV ($n = 8$) with ADH. Figure 6 summarizes the effect of the K^+-concentration steps in the lumen perfusate on PD_a. PD_a depolarized by 19 ± 3 mV ($n = 7$) and by 12 ± 2 mV ($n = 10$) without and with ADH, respectively.

Table 1. Effects of ADH in rat CCT on PD_{te} and R_{te}, and PD_{bl}, PD_a and FR_a of principal cells

	PD_{te} (mV) $n = 37$	R_{te} (Ωcm^2) $n = 33$	PD_{bl} (mV) $n = 28$	PD_a (mV) $n = 26$	FR_a $n = 13$
−ADH	-5.1 ± 0.7	51 ± 4	-83 ± 1	79 ± 1	0.76 ± 0.04
+ADH	-16.1 ± 1.4	39 ± 2	-78 ± 1	66 ± 2	0.70 ± 0.04

$\bar{x} \pm$SEM, PD_{te} and R_{te} = transepithelial voltage and resistance, PD_{bl} and PD_a = basolateral and apical membrane voltages, FR_a = fractional resistance of the apical membrane. All changes between −ADH and +ADH (paired observations) in this table are significant

The transference numbers for K^+ of the basolateral membrane calculated from the unpaired observations were 1.00 ± 0.03 ($n = 14$) and 1.02 ± 0.03 ($n = 19$) without and with ADH. The transference numbers for K^+ of the luminal membrane were 0.73 ± 0.07 ($n = 7$) and 0.50 ± 0.06 ($n = 10$) without and with ADH, respectively. The Cl^- concentration step experiments in the bath (from 140 to 50 mmol · l^{-1}) in the presence of ADH resulted in no change in PD_{bl} ($\Delta PD_{bl} = 0.5 \pm 0.6$ mV, $n = 10$). Four experiments with the chloride-channel blocker diphenylamine-2-carboxylate [2] at 10^{-5} mol · l^{-1} in the bath did not change PD_{te}, PD_{bl}, R_{te}, or FR_{bl}.

Figure 7 demonstrates the dose response curves for the effect of barium added to the lumen perfusate on PD_{te} and

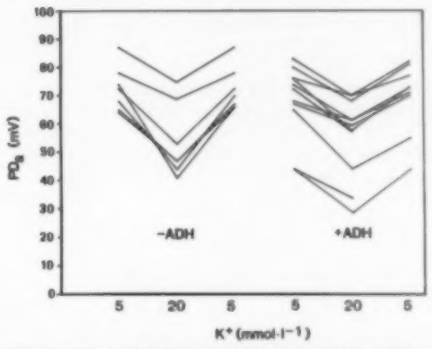

Fig. 6. Effect of K^+-concentration steps (5 to 20 mmol·l^{-1}) in the lumen perfusate on apical membrane voltage (PD_a) in principal cells in the absence and presence of ADH. The mean depolarizations of PD_a are 19 ± 3 mV ($n = 7$) and 12 ± 2 mV ($n = 10$), respectively

Table 2. Effects of amiloride (10^{-5} or 10^{-4} mol · l^{-1}, lumen) and barium (3 mmol · l^{-1}, lumen or bath) on PD_{te} and R_{te}, and PD_{bl}, PD_a, FR_a and FR_{bl} of principal cells of rat CCT

	−ADH		+ADH		−ADH		+ADH		−ADH		+ADH	
	C	Amil. lumen	C	Amil. lumen	C	Ba^{2+} lumen	C	Ba^{2+} lumen	C	Ba^{2+} bath	C	Ba^{2+} bath
PD_{te} (mV)	−4.4 ±0.4 (49)	0.9 ±0.2	−13.5 ±1.3 (34)	1.1 ±0.3	−3.4 ±0.6 (13)	−7.1 ±1.4	−14.7 ±1.5 (17)	−25.9 ±3.1	−5.5 ±0.7 (22)	−1.5 ±0.5	−16.6 ±1.9 (14)	−7.8 ±1.3
R_{te} (Ωcm^2)	49 ±4 (31)	62 ±5	43 ±3 (26)	58 ±5	53 ±9 (15)	90 ±15	48 ±5 (18)	83 ±10	53 ±6 (13)	88 ±13	49 ±6 (11)	83 ±13
PD_{bl} (mV)	−83 ±0.5 (50)	−85 ±0.5	−81 ±1 (35)	−85 ±1	−85 ±1 (9)	−76 ±5	−80 ±1 (18)	−77 ±2	−85 ±1 (11)	−62 ±6	−82 ±1 (18)	
PD_a (mV)	78 ±1 (49)	85 ±0.5	68 ±2 (28)	85 ±1	81 ±2 (8)	75 ±2	69 ±2 (8)	57 ±4	79 ±2 (11)	61 ±6	64 ±3 (14)	45 ±5
FR_a	0.76 ±0.02 (26)	0.87 ±0.02	0.74 ±0.04 (17)	0.89 ±0.02	0.76 ±0.05 (7)	0.96 ±0.01	0.62 ±0.07 (6)	0.93 ±0.02				
FR_{bl}									0.21 ±0.05 (5)	0.83 ±0.10	0.26 ±0.07 (6)	0.60 ±0.06

Mean ± SEM (n), C = control, PD_{te} and R_{te} are the transepithelial voltage and resistance, respectively. PD_{bl} and PD_a are the basolateral and apical membrane voltages, respectively. FR_{bl} and FR_a are the basolateral and apical membrane fractional resistances, respectively. All changes in this table between control (C) and experimental (Amil. or Ba^{2+}) periods are statistically significant

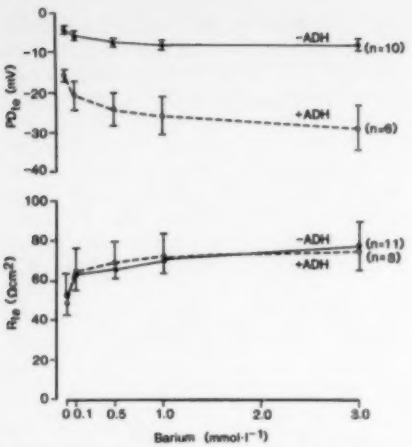

Fig. 7. Dose response curves for the effect of luminal barium on transepithelial voltage (PD_{te}) and resistance (R_{te}) in the absence and presence of ADH. The PD_{te} changes between 1.0 and 3.0 mmol $\cdot l^{-1}$ are not significant, the R_{te} changes, however, are still significant on a paired basis. (●——●) −ADH, (○----○) +ADH

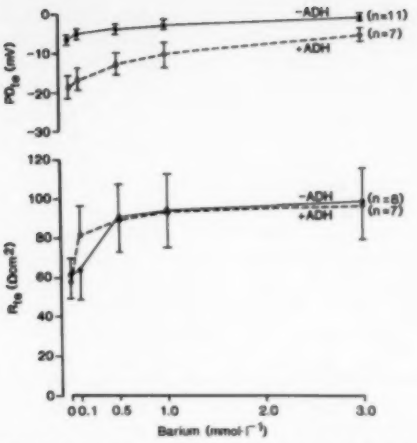

Fig. 8. Dose response curves for the effect of bath barium on transepithelial voltage (PD_{te}) and resistance (R_{te}) in the absence and presence of ADH. The PD_{te} changes, but not the R_{te} changes between 1.0 and 3.0 mmol $\cdot l^{-1}$ are significant on a paired basis. (●——●) −ADH, (○----○) +ADH

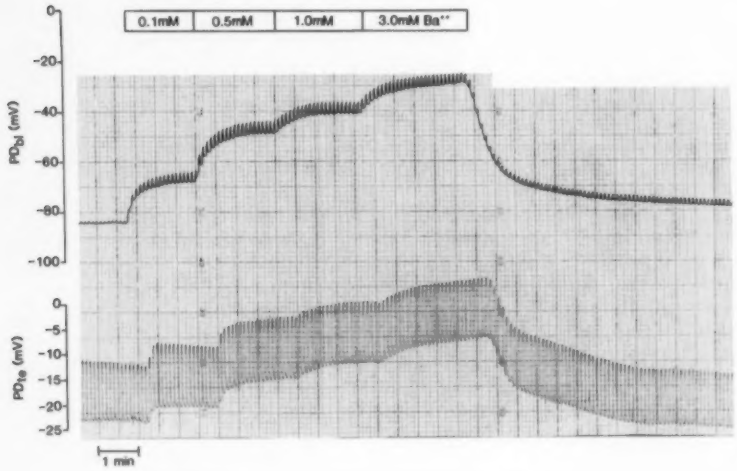

Fig. 9
Effects of increasing bath barium concentrations on transepithelial (PD_{te}) and basolateral membrane voltages (PD_{bl}) and resistances in a principal cell of a rat CCT. Note the marked increase from 0.51 to 1.00 in the fractional resistance of the basolateral membrane (increase in pulse height on the PD_{bl} tracing) upon barium addition

R_{te} in both functional states, i.e., without and with ADH in the bath perfusate. Under both conditions there was only a small further increase in PD_{te} as well as in R_{te} between 1.0 and 3.0 mmol $\cdot l^{-1}$ barium. The dose response curves for the effects of barium added to the bath perfusate on PD_{te} and R_{te} are shown in Fig. 8. Again, for both PD_{te} and R_{te} 1.0 mmol $\cdot l^{-1}$ barium seemed to exert almost maximal effects. Figure 9, an original recording, shows the change of PD_{te}, PD_{bl}, R_{te}, and FR_{bl} upon increasing concentrations of barium added to the bath perfusate. Table 2 summarizes the changes induced by luminal or bath barium in PD_{te}, R_{te}, PD_{bl}, PD_a, FR_a, and FR_{bl}. PD_{te} increased upon luminal addition of barium and decreased upon barium addition to the bath perfusate. The absolute changes were larger in the presence of ADH. Luminal or bath barium increased R_{te} in both functional states to values between 83 and 90 Ωcm^2. Barium added to either side of the epithelium depolarized both membranes with the bath barium effects exceeding those of luminal barium. With 3 mmol $\cdot l^{-1}$ barium in the lumen FR_a approached 1.0, whereas the increase of FR_{bl} by bath barium was smaller.

Effect of ouabain on the basolateral K^+-conductance

Ouabain reduced PD_{te} in both functional states from -2.5 ± 0.2 mV ($n = 3$, −ADH) and -14.7 ± 2.6 mV ($n = 13$, +ADH) to -0.2 ± 0.3 mV and -2.6 ± 1.5 mV, respectively (see Fig. 11). The effects of $5 \cdot 10^{-4}$ mol $\cdot l^{-1}$ ouabain in the bath perfusate on the magnitude of the depolarization of PD_{bl} of 6 principal cells induced by a bath K^+-concentration step (5 to 20 mmol $\cdot l^{-1}$) are summarized in Fig. 10. PD_{bl} depolarizes upon the K^+-concentration steps by 32 ± 2 mV

before and by 30 ± 2 mV after the experimental period with ouabain. In the presence of ouabain ΔPD_{bl} reaches only 14 ± 4 mV. See also the original recording of Fig. 11 for the effect of ouabain on the depolarization of PD_{bl} induced by a K^+-concentration step.

Effect of amiloride on the ouabain induced depolarization of PD_{bl}

Figure 11 shows an experiment similar to that in Fig. 10. However, in this case ouabain was added after luminal amiloride (10^{-5} mol $\cdot$ l^{-1}) had been given. Ouabain did not depolarize PD_{bl} in the presence of amiloride (tested for 5–6 min which is enough to reach a substantial depolarization without amiloride present). As soon as amiloride was removed, with ouabain still present, PD_{bl} depolarized. In addition, this experiment shows that the depolarization of PD_{bl} induced by K^+-concentration steps in the presence of both amiloride and ouabain was similar to the control K^+-concentration step before amiloride addition. Figure 12 summarizes 10 experiments of this type. The control K^+-concentration steps were performed before and/or after the amiloride and ouabain addition. In Fig. 12 these control K^+-concentration steps are summarized at the end of the graph. ΔPD_{bl} for the K^+-concentration steps was 31 ± 2 mV in the presence of amiloride and ouabain, 21 ± 3 mV with ouabain alone, and 32 ± 2 mV under control condition.

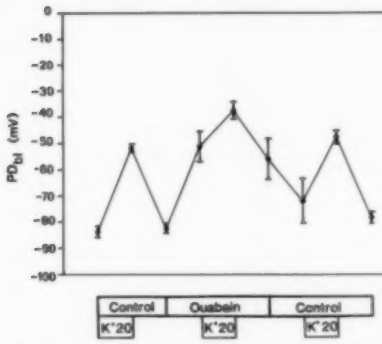

Fig. 10. Effect of ouabain ($5 \cdot 10^{-4}$ mol $\cdot$ l^{-1}) on the change in basolateral membrane potential (PD_{bl}) caused by K^+-concentration steps (5–20 mmol $\cdot$ l^{-1}) in the bath perfusate. The results are from 6 principal cells. The depolarization of PD_{bl} induced by the K^+-concentration steps is significantly lower in the presence of ouabain than in the pre and post control periods

Shunt selectivity

Replacing 80 mmol $\cdot$ l^{-1} NaCl by mannitol in the bath perfusate led to a decrease in the lumen negative PD_{te} by 2.8 ± 0.4 mV ($n = 5$) without ADH and by 2.3 ± 0.5 mV ($n = 7$) with ADH. The same dilutions were performed in the lumen perfusate. To avoid PD_{te} changes due to the luminal Na^+-conductance especially after ADH, the luminal dilutions were performed in the presence of 10^{-4} mol $\cdot$ l^{-1} amiloride. ΔPD_{te} observed under these conditions were -1.0 ± 0.3 mV ($n = 5$) without ADH and -2.2 ± 0.5 mV ($n = 5$) with ADH. All numbers were corrected for the liquid junction potential. There was no significant difference between the PD_{te}'s for bath dilutions $\pm$ ADH and luminal dilutions in the presence of amiloride $\pm$ ADH.

ADH effects on voltages and resistances in the presence of luminal amiloride or barium

Figures 3 (lower half of the continuous recording) and 13 illustrate the effects of ADH on PD_{bl} and FR_{bl} (or FR_a) in the presence of luminal amiloride (10^{-5} mol $\cdot$ l^{-1}). PD_{bl} first hyperpolarized slightly upon addition of amiloride, but did not depolarize with ADH unless amiloride was removed from the lumen perfusate. FR_a did not change in the presence of amiloride but decreased after its removal (indicated in Fig. 13 by the change in the voltage deflections produced by the current pulses).

Table 3 summarizes the effects of ADH both in the presence of luminal amiloride or luminal barium on PD_{te}, R_{te}, PD_{bl}, PD_a and FR_a. All five parameters changed significantly after removal of amiloride. The values in the presence of ADH were also significantly different from the controls without ADH, with the exception of the change in R_{te}, which

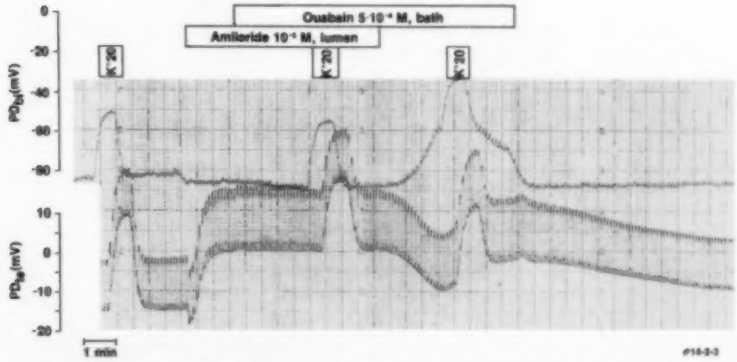

Fig. 11. Effects of amiloride (10^{-5} mol $\cdot$ l^{-1}, lumen) and ouabain ($5 \cdot 10^{-4}$ mol $\cdot$ l^{-1}, bath) on the changes in transepithelial (PD_{te}) and basolateral membrane potential (PD_{bl}) induced by a bath K^+-concentration step (5 to 20 mmol $\cdot$ l^{-1}). The recording is from a principal cell in the presence of ADH. Note that in the presence of amiloride ouabain has no effect on either PD_{bl} or the depolarization of PD_{bl} induced by a K^+-concentration step. The transient increase in PD_{te} after removal of amiloride suggests that ouabain did not bind to all ($Na^+ + K^+$)-pumps after the pump turnover was stopped by amiloride. The hyperpolarization of PD_{bl} after the K^+-concentration step in the presence of ouabain indicates an increase in cellular K^+-activity under these conditions

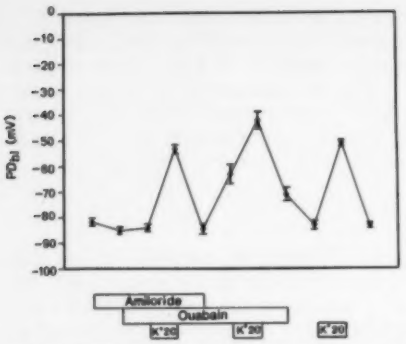

Fig. 12. Effects of amiloride (10^{-5} mol · l^{-1}, lumen) and ouabain ($5 \cdot 10^{-4}$ mol · l^{-1}, bath) on the depolarization of PD_{bl} induced by a K^+-concentration step (5 to 20 mmol · l^{-1}) in 10 principal cells. The depolarization of PD_{bl} is significantly lower in the presence of ouabain than either in the post control period or in the presence of amiloride and ouabain

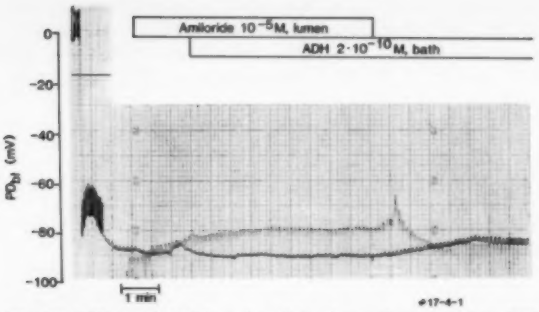

Fig. 13. Effects of ADH on basolateral membrane voltage (PD_{bl}) and fractional resistance of a principal cell in the presence of luminal amiloride (10^{-5} mol · l^{-1}). Note that the depolarization of PD_{bl} after amiloride removal (5 mV) exceeds the initial hyperpolarization (2 mV) of amiloride. Also the pulse height at the end of the tracing (+ADH) is larger than before the addition of amiloride

Table 3. Effects of ADH in the presence of luminal amiloride or barium on PD_{te} and R_{te}, and on PD_{bl}, PD_a and FR_a of principal cells of rat cortical collecting tubule

Bath lumen	*n*	−ADH	−ADH +Amil.	+ADH +Amil.	+ADH	−ADH	−ADH +Ba^{2+}	+ADH +Ba^{2+}	+ADH	*n*
PD_{te} (mV)	7	−6.7 ±1.8	0.9[a] ±0.6	1.5 ±0.3	−11.2[a] ±2.2	−5.3 ±2.0	−4.2 ±1.0	−16.1[a] ±4.0	−13.6[a] ±2.0	10
R_{te} (Ωcm^2)	5	36 ±6	47[a] ±11	53 ±15	33[a] ±5	50 ±8	83[a] ±16	91 ±22	50[a] ±9	10
PD_{bl} (mV)	7	−79 ±2	−82[a] ±2	−82 ±2	−73[a] ±4	−85 ±1	−85 ±1	−80[a] ±2	−81 ±2	9
PD_a (mV)	7	72 ±3	83[a] ±2	84 ±2	62[a] ±5	79 ±3	80 ±2	63[a] ±5	67 ±5	8
FR_a	6	0.82 ±0.05	0.87[a] ±0.05	0.89 ±0.04	0.77[a] ±0.05	0.76 ±0.07	0.96[a] ±0.02	0.91 ±0.03	0.80[a] ±0.04	5

Mean ± SEM, [a] indicates statistically significant difference from previous period. Ba^{2+} added to lumen perfusate at 3.0 mmol · l^{-1}, amiloride at 10^{-5} or 10^{-4} mmol · l^{-1}; PD_{te} and R_{te} are the transepithelial voltage and resistance, respectively; PD_{bl} and PD_a are the basolateral and apical membrane voltages, respectively; FR_a is the fractional resistance of the apical membrane; *n* is the number of tubules or impaled cells

did not reach significance in this series. Barium addition to the lumen increased R_{te} and FR_a significantly. ADH even in the presence of luminal barium led to a significant increase in PD_{te} and a depolarization of PD_{bl} and PD_a. There was, however, no significant change in R_{te} or FR_a until barium was removed from the lumen.

Discussion

This study is directed primarily at an examination of the properties of principal cells of the rat CCT and the regulation of ion transport across these cells by ADH, however, intracellular voltage and resistance recordings were obtained from both principal and intercalated cells. As discussed in Methods and shown in Results, it was possible to differentiate between the two cell types using optical and functional tests. About 1/3 of the cells examined in this study could be identified as intercalated cells, 2/3 as principal cells. The fact that PD_{bl} of principal cells and intercalated cells responded oppositely upon ADH stimulation or amiloride addition to the lumen perfusate allows separate study of the properties and the function of both cell types. There is apparently no or only little cell-to-cell coupling between principal and intercalated cells. Only data from principal cells will be discussed in this report.

This study provides the first electrophysiological data on the luminal Na^+- and K^+conductances, the basolateral K^+-conductance and its dependence on the (Na^+ + K^+)-ATPase in the principal cell of rat CCT. Furthermore, it provides strong evidence for a stable ADH mediated increase in the apical Na^+-conductance of these cells as the primary event for a stimulation of ion transport in this nephron segment. In the following the individual properties of principal cells will be discussed.

Properties of the basolateral membrane

PD_{bl} values reported here for the rat CCT are comparable to those reported earlier for the rabbit CCT [14, 21]. The

high PD_{bl} of −83 mV under control conditions (Table 1) is consistent with the dominance of a K^+-conductance for that membrane. The analysis of the K^+-concentration steps in the bath (Fig. 5) revealed a transference number for K^+ across the basolateral membrane of 1.0. Since the chloride channel blocker diphenylamine-2-carboxylase did not exert any detectable effect on the basolateral membrane and the Cl^- concentration step experiments in the bath did not significantly depolarize PD_{bl}, the presence of a Cl^- conductance parallel to the K^+ conductance in the membrane is unlikely. The transference number for K^+ of 1.0, however, may be an overestimation since cellular ion activity changes cannot be completely excluded even at the fast bath exchange rates used. In addition, because in the Cl^- concentration step experiments large corrections for liquid junction potentials have to be made and changes in intracellular Cl^- activity could occur faster than the bath exchange rate, the presence of a small chloride conductance could be overlooked.

At the higher dose (0.1 − 1 mmol · l^{-1}) required for the rat, ouabain depolarized PD_{bl} reversibly and abolished PD_{te} in both functional states. Therefore, active transport of Na^+ and K^+ through principal cells of the rat CCT is entirely mediated by the (Na^+ + K^+)-ATPase in the basolateral membrane. The K^+-conductance of the basolateral membrane is reduced when the (Na^+ + K^+)-ATPase activity is lowered by ouabain (Figs. 10 − 12). The decrease of the K^+-conductance, however, is not linked to the pump activity itself but rather to the voltage of the basolateral membrane or the K^+-activity in the cell. This is evident from the fact that indirect inhibition of the pump by luminal amiloride does not alter the K^+-conductance (Figs. 11, 12). Under these conditions the pump stops because the Na^+ entry into the cell is blocked but PD_{bl} remains hyperpolarized. Recently a voltage dependence of the apical K^+-channel of rabbit CCT has been reported [11]. A similar interdependence of the K^+-conductance and the ($Na^+ + K^-$)-ATPase has been reported earlier for other epithelia including the thick ascending limb and the proximal tubule [6, 16, 31, 39]. The basolateral membrane is Ba^{2+}-sensitive with a maximal inhibition at approximately 1 − 3 mmol · l^{-1} (Fig. 8). The basolateral membrane is the low resistance membrane in the rat CCT as its fractional resistance is only 0.24 in control conditions. This fractional resistance can be greatly increased by barium in the bath perfusate (Tables 1, 2, Fig. 9). The fact that FR_{bl} does not approach 1 with bath barium could indicate an incomplete inhibition of the K^+ conductance especially after the cell is depolarized in the presence of ADH.

Properties of the apical membrane

It is generally accepted that the dominant conductances of the apical membrane of principal cells of the rabbit CCT are a K^+-conductance and a Na^+-conductance. Luminal K^+-concentration steps confirmed this finding for the rat CCT (Fig. 6). Analysis of these experiments gave a transference number for K^+ of 0.73 across the apical membrane in the absence of ADH. Even assuming the only other conductance is a Na^+-conductance, the K^+-conductance dominates the apical membrane total conductance in the control state. As a result of the dominating K^+-conductance of that membrane PD_a is only slightly depolarized with respect to PD_{bl} in the absence of ADH (Table 1, Fig. 4). This dominance of the apical K^+-conductance also has been reported for the rabbit CCT [15, 18, 21]. The transference number for K^+ decreases moderately to 0.5 upon addition of ADH. Although PD_a significantly depolarizes upon ADH addition, due to an increased Na^+-conductance, the total fractional resistance of the apical membrane changes only by about 8% (Table 1). The ratio of apical over basolateral membrane resistances is 2.3, still well above unity after ADH stimulation. Similar to the basolateral K^+-conductance the apical K^+-conductance is sensitive to Ba^{2+}. Luminal amiloride in the presence or absence of ADH rapidly inhibited the lumen-negative PD_{te} (Table 2). We assume that the remaining small lumen-positive voltage was due to H^+ secretion by the intercalated cells [19]. Amiloride also hyperpolarized both apical and basolateral membranes in the presence of ADH (Fig. 3, Table 2). The apical membrane change is an expected direct effect of amiloride in blocking apical Na^+-channels that is also manifested by the inhibition of the Na^+ lumen-to-bath flux reported previously [24]. We suggest the amiloride induced hyperpolarization of the basolateral membrane occurs as a result of a change in the circular current flow across this membrane due to the primary change in the electromotive force for Na^+ across the apical membrane.

It has recently been proposed that neutral NaCl cotransport serves as a second mode for Na^+ entry across the apical membrane of distal nephron segments. Evidence for this cotransporter has been obtained in the rat distal convoluted tubule where it has been shown to be inhibited by chlorothiazide [38]. The evidence for its presence in the rat CCT is more indirect [37], and appears to be contradicted by some of our present results. In particular, we observed the presence of lumen amiloride prevented the depolarization of PD_{bl} normally observed upon addition of bath ouabain (Figs. 11, 12). This finding would strongly suggest that the only pathway for Na^+ entry in these cells is the amiloride-sensitive apical Na^+-conductance. However, amiloride may also inhibit the NaCl cotransporter, a possibility that has not been examined directly. Incidentally, the stability of PD_{bl} in the presence of ouabain plus lumen amiloride indicates that the microelectrode impalements in these experiments did not induce nonspecific leaks for Na^+ entry.

Properties of the paracellular shunt

From the NaCl dilution potentials, which are symmetrical when NaCl is partially replaced in the bath or lumen perfusate (lumen changes are performed in the presence of amiloride) the paracellular shunt selectivity is close to free solution mobility. The relative permeability for Cl^- over Na^+ ranges from 1.1 − 1.3 for the various dilutions described in Results compared to 1.5 for free solution mobilities. We, therefore, conclude that at least part of the Cl^- reabsorption in the rat CCT occurs across the paracellular shunt. For the rabbit CCT a value for P_{Cl}/P_{Na} of 1.5 has also been reported [40]. In other studies a highly Cl^--selective shunt, different from free solution mobilities, has been reported for the rabbit CCT [22, 27] in addition to Cl^- movement across intercalated cells [35] in this species. An evaluation of the shunt resistance with the present data is difficult as even after inhibition of the basolateral K^+-conductance of principal cells with barium there may still be a sizable contribution of a small basolateral Cl^- conductance of these cells and/or of the intercalated cells to the transepithelial conductance. The latter contribution, however, may be small

especially in the presence of bath barium, as our preliminary data suggest a large basolateral K^+-conductance in intercalated cells (Fig. 1). This conductance is also sensitive to barium. Therefore, it seems likely that bath barium may inhibit most of the transcellular conductance and the R_{te} of 90 Ω cm^2 (Table 2) obtained under these conditions would be close to the shunt resistance. Using a shunt conductance of 90 Ω cm^2, we calculate from the transepithelial resistance of 51 Ωcm^2 (Table 1) that the transcellular resistance would be about 120 Ωcm^2.

Regulation of ion transport by ADH

As has been discussed in the introduction the effect of ADH seems to be limited to the principal cells of the CCT [1, 12, 19]. This study confirms the finding that ADH increases the lumen-negative PD_{te} rapidly and reversibly in the rat CCT (Fig. 2). The transepithelial voltages reported here are lower than some published in other studies. In those studies either asymmetrical solutions were used in bath and lumen perfusates [23, 24, 29] or lower perfusion rates had been applied [13, 36, 37]. Both facts would increase the lumen negative PD_{te} by the diffusion potential across the epithelium, as NaCl was lower in the lumen or decreased along the tubule at low perfusion rates. The transepithelial resistance of 51 and 39 Ωcm^2 without and with ADH, respectively, are the first values reported for the rat (Table 1), and are lower than those reported for the rabbit CCT [18, 21, 22]. This may reflect the fact that the rat CCT exhibits higher transport rates than the rabbit CCT. No decrease of R_{te} upon addition of ADH could be shown for the rabbit so far [see Ref. 18] and may, indeed, not be easily detectable as ADH has only a transient effect in the rabbit CCT [4].

Using the PD_{te} and R_{te} values of this study, net ionic reabsorptive fluxes of approximately 39 and 161 pmoles $\cdot$ min^{-1} $\cdot$ mm^{-1} without and with ADH can be calculated from the equivalent short-circuit current (ISC = PD_{te}/R_{te}). Taking the net Na^+, Rb^+ and total CO_2 transport (HCO_3^- transport) rates from References [13, 24, 28, 37], the total net reabsorptive fluxes are calculated to vary from 5 to 50 pmoles $\cdot$ min^{-1} $\cdot$ mm^{-1} without ADH and from 87 to 142 pmoles $\cdot$ min^{-1} $\cdot$ mm^{-1} with ADH. The slightly higher electrically-determined ionic net fluxes with ADH can possibly be due to different driving forces in the two studies. The higher, more negative PD_{te} of the flux studies probably is due to additional diffusion potentials across the epithelium and not to increased active transport (see above). This would reduce Na^+ reabsorption and enhance K^+ secretion and thus reduce total net reabsorptive fluxes.

The effect of ADH on Na^+ transport in this tissue appears to be due to a direct effect to increase the apical Na^+-conductance. This is directly supported by the rapid depolarization of the apical membrane observed with ADH addition. Presumably a resulting increase in intracellular Na^+ activity serves to increase basolateral (Na^+ + K^+)-ATPase activity. This increased activity would in turn require that the recycling of K^+ out of the cell across either or both the basolateral or apical membrane would increase (see Fig. 14). The small depolarization of PD_{bl} with ADH can again easily be explained by circular current induced by the change in the electromotive force across the apical membrane by ADH. Because the shunt resistance seems to be relatively low, the two membranes are coupled. The same circular current effect leads to the observed small hyperpolarization of PD_{bl} with luminal amiloride (Fig. 2, Table 2). Although ADH changes FR_a only slightly, the influence of this change on the transepithelial resistance is considerably larger, because the apical membrane is the high resistance barrier for the cellular pathway.

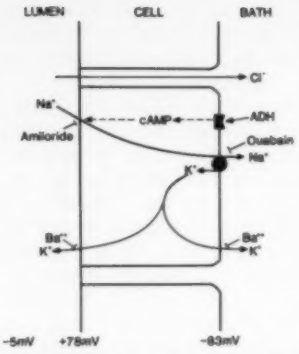

Fig. 14. Cellular model for ion transport across a principal cell of the rat CCT. ●ATP = active transport, → diffusion, —| inhibition, ---→ action of ADH, ■← hormone receptor

Further evidence for an action of ADH primarily on the apical Na^+-conductance stems from the experiments in series 5. In the presence of luminal amiloride ADH does not affect transepithelial or transmembrane voltages or resistances. Thus, amiloride at 10^{-5} or 10^{-4} mol $\cdot$ l^{-1} completely inhibits the ADH effects. This finding has been reported also in Na^+ flux measurements in the rat [24].

Luminal barium on the other hand, does not inhibit the changes in transepithelial and transmembrane voltages by ADH (Table 3). Recently, it has been reported, that luminal barium (2 mmol $\cdot$ l^{-1}) is not only ineffective in inhibiting the ADH induced hyperpolarization of PD_{te}, but also does not completely inhibit the K^+ secretion in the rat CCT [28]. There may be two explanations. It is well known that barium inhibition of K^+-channels is voltage dependent and, thus, the depolarization of PD_a upon ADH addition may diminish the barium blockage, resulting in an increase in K^+ secretion under this condition. This would explain why in the above study [28] barium completely inhibited K^+ secretion in control state but not in the ADH stimulated state. Alternatively, ADH could open up a barium-insensitive K^+ pathway across the apical membrane. It seems unlikely that this could be a conductive pathway because the depolarization of PD_a by barium is twice as large with ADH compared to the control conditions, which would not be expected if ADH opens up a barium-insensitive K^+-conductance parallel to the Na^+-conductance increase.

In conclusion, we arrive at the model shown in Fig. 14 for the ADH regulation of NaCl transport across the CCT epithelium of the rat. Na^+ reabsorption occurs at least predominantly if not exclusively across the principal cells. The same holds true for K^+ secretion. The primary driving force for both transepithelial transport processes is delivered by the action of the basolateral (Na^+ + K^+)-ATPase. Potassium leaves the cell across both barium-sensitive K^+-conductive cell membranes. The relative magnitude of the two K^+-conductances together with the driving force, determines the rate of K^+ secretion into the tubule lumen.

Na^+ enters the cell across the amiloride-sensitive Na^+-conductance of the apical membrane. This seems to be the only pathway for sodium to enter the principal cell. The basolateral K^+-conductance is regulated in accordance with the activity of the ($Na^+ + K^+$)-ATPase. Candidates for the mediator of this coupling are the membrane voltage or the cellular K^+ activity. Cl^- moves at least in part across the slightly anion selective paracellular shunt. A small portion of the Cl^- reabsorption may occur through the principal cell but its exact mechanism is still unclear. A possible electrogenic or electroneutral Cl^- movement across intercalated cells awaits further investigation.

ADH primarily increases the apical Na^+-conductance with the same time course of a few minutes as for the concomitant increase in water permeability [23] which would be compatible with a process involving cAMP-mediated phosphorylation of membrane proteins. This effect of ADH on Na^+-channels has also been reported for the frog skin [10]. The increased apical Na^+-conductance, possibly via the increased cellular Na^+ activity, enhances the activity of the ($Na^+ + K^+$)-pump. The increased pump activity and the depolarization especially of the apical membrane may be sufficient to account for the increased K^+ secretion into the lumen. The apical membrane depolarizes to a far greater extent than the basolateral membrane resulting in an increased lumen negative transepithelial voltage. This increases the driving force for passive movement of Cl^- across the paracellular shunt.

Acknowledgements. The authors acknowledge the expert assistance of S. L. Troutman and S. K. Williams. We thank Dr. D. R. Halm for the helpful comments during the preparation of this paper. This work was supported in part by an NIH Research Grant No. DK25519-08.

References

1. DiBona DR, Kirk KL, Johnson RD (1985) Microscopic investigation of structure and function in living epithelial tissues. Fed Proc 44:2693–2703
2. DiStefano A, Wittner M, Schlatter E, Lang HJ, Englert H, Greger R (1985) Diphenylamine-2-carboxylate, a blocker of the Cl^--conductive pathway in Cl^- transporting epithelia. Pflügers Arch 405:S95–S100
3. Field MJ, Stanton BA, Giebisch GH (1984) Influence of ADH on renal potassium handling: A micropuncture and microperfusion study. Kidney Int 25:502–511
4. Frindt G, Burg MB (1972) Effect of vasopressin on sodium transport in renal cortical collecting tubules. Kidney Int 1:224–231
5. Greger R (1981) Cation selectivity of the isolated perfused cortical thick ascending limb of the loop of Henle. A sodium dependent process. Pflügers Arch 390:30–37
6. Greger R (1984) The $Na^+2Cl^-K^+$ carrier of the lumen membrane of the diluting segment of rabbit kidney. Fed Proc 43: 2473–2487
7. Greger R, Hampel W (1981) A modified system for in vitro perfusion of isolated renal tubules. Pflügers Arch 389:175–176
8. Greger R, Schlatter E (1983) Properties of the lumen membrane of the cortical thick ascending limb of Henle's loop of rabbit kidney. Pflügers Arch 396:315–324
9. Helman SI, O'Neil RG (1977) Model od active transepithelial Na and K transport of renal collecting tubules. Am J Physiol 233:F559–F571
10. Helman SI, Cox TC, van Driessche W (1983) Hormonal control of apical membrane Na transport in epithelia. Studies with fluctuation analysis. J Gen Physiol 82:201–220
11. Hunter M, Lopes AG, Boulpaep E, Giebisch G (1986) Regulation of single potassium ion channels from apical membrane of rabbit collecting tubule. Am J Physiol 251:F725–F733
12. Kirk KL, Buku A, Eggena P (1987) Cell specificity of vasopressin binding in renal collecting duct: Computer-enhanced imaging of a fluorescent hormone analog. Proc Natl Acad Sci USA (in press)
13. Knepper MA, Good DW, Burg MB (1985) Ammonia and bicarbonate transport by rat cortical collecting ducts perfused in vitro. Am J Physiol 249:F870–F877
14. Koeppen BM, Giebisch G (1985) Cellular electrophysiology of potassium transport in the mammalian cortical collecting tubule. Pflügers Arch 405:S143–S146
15. Koeppen BM, Biagi BA, Giebisch G (1983) Intracellular microelectrode characterization of the rabbit cortical collecting duct. Am J Physiol 244:F35–F47
16. Lang F, Messner G, Rehwald W (1986) Electrophysiology of sodium-coupled transport in proximal renal tubules. Am J Physiol 250:F953–F962
17. Macknight ADC, DiBona DR, Leaf A (1980) Sodium transport across toad urinary bladder: A model "tight" epithelium. Physiol Rev 60:615–715
18. O'Neil RG, Boulpaep EL (1982) Ionic conductive properties and electrophysiology of the rabbit cortical collecting tubule. Am J Physiol 243:F81–F95
19. O'Neil RG, Hayhurst RA (1985) Functional differentiation of cell types of cortical collecting duct. Am J Physiol 248:F449–F453
20. O'Neil RG, Helman SI (1977) Transport characteristics of renal collecting tubules: influences of DOCA and diet. Am J Physiol 233:F544–F558
21. O'Neil RG, Sansom SC (1984) Characterization of apical cell membrane Na^+ and K^+ conductances of cortical collecting duct using microelectrode techniques. Am J Physiol 247: F14–F24
22. O'Neil RG, Sansom SC (1984) Electrophysiological properties of cellular and paracellular conductive pathways of the rabbit cortical collecting duct. J Membr Biol 82:281–295
23. Reif MC, Troutman SL, Schafer JA (1984) Sustained response to vasopressin in isolated rat cortical collecting tubule. Kidney Int 26:725–732
24. Reif MC, Troutman SL, Schafer JA (1986) Sodium transport by rat cortical collecting tubule. Effects of vasopressin and desoxycorticosterone. J Clin Invest 77:1291–1298
25. Sansom SC, O'Neil RG (1985) Mineralocorticoid regulation of apical cell membrane Na^+ and K^+ transport of the cortical collecting duct. Am J Physiol 248:F858–F868
26. Sansom SC, O'Neil RG (1986) Effects of mineralocorticoids on transport properties of cortical collecting duct basolateral membrane. Am J Physiol 251:F743–F757
27. Sansom SC, Weinman EJ, O'Neil RG (1984) Microelectrode assessment of chloride-conductive properties of cortical collecting duct. Am J Physiol 247:F291–F302
28. Schafer JA, Troutman SL (1987) Potassium transport in cortical collecting tubules from mineralocorticoid-treated rat. ADH increases Rb^+ secretory flux. Am J Physiol (in press)
29. Schafer JA, Troutman SL (1986) Effect of ADH on rubidium transport in isolated perfused rat cortical collecting tubules. Am J Physiol 250:F1063–F1072
30. Schlatter E, Greger R (1985) cAMP increase the basolateral Cl^--conductance in the isolated perfused medullary thick ascending limb of Henle's loop of the mouse. Pflügers Arch 405:367–376
31. Schultz SG (1981) Homocellular regulatory mechanisms in sodium-transporting epithelia: avoidance of extinction by "flush-through". Am J Physiol 241:F579–F590
32. Schuster VL (1987) Bradykinin and vasopressin actions on rabbit cortical collecting tubule: mechanism of their interaction and effects on Na transport. Am J Physiol (in press)
33. Schwartz GJ, Burg MB (1978) Mineralocorticoid effects on cation transport by cortical collecting tubules in vitro. Am J Physiol 235:F576–F585

34. Stokes JB (1982) Ion transport by the cortical and outer medullary collecting tubule. Kidney Int 22:473–484
35. Tago K, Warden DH, Schuster VL, Stokes JB (1986) Effects of inhibitors of Cl^- conductance and Cl^- self-exchange in the rabbit cortical collecting tubule. Am J Physiol 251:F1009–F1017
36. Tomita K, Pisano JJ, Knepper MA (1985) Control of sodium and potassium transport in the cortical collecting duct of the rat. Effects of bradykinin, vasopressin, and desoxycorticosterone. J Clin Invest 76:132–136
37. Tomita K, Pisano JJ, Burg MB, Knepper MA (1986) Effects of vasopressin and bradykinin on anion transport by the rat cortical collecting duct. Evidence for an electroneutral sodium chloride transport pathway. J Clin Invest 77:136–141
38. Velàzquez H, Wright FS (1986) Effects of diuretic drugs on Na, Cl and K transport by rat renal distal tubule. Am J Physiol 250:F1013–F1023
39. Völkl H, Geibel J, Greger R, Lang F (1986) Effects of ouabain and temperature on cell membrane potentials in isolated perfused straight proximal tubules of the mouse kidney. Pflügers Arch 407:252–257
40. Warden DH, Schuster VL, Stokes JB (1986) The paracellular pathway of rabbit cortical collecting tubule (CCT): A high resistance, non-selective barrier. Fed Proc 45:517

Received October 30, 1986/Accepted January 5, 1987

Pflügers Arch (1987) 409:93–99

Pflügers Archiv
European Journal of Physiology
© Springer-Verlag 1987

Effects of amines, monensin and nigericin on the renin release from isolated superfused rat glomeruli

Ole Skøtt

University Institute for Experimental Medicine, The Panum Institute, Blegdamsvej 3, DK-2200N Copenhagen, Denmark

Abstract. Renin release (RR) in vitro has been shown to depend upon exocytosis, which is brought about by osmotically induced swelling of the acidic secretory granules. Since granule acidity has been suggested to be responsible for the exocytosis of other secretory granules (the chemiosmotic hypothesis), experiments were designed to test its possible significance in the RR from isolated superfused rat glomeruli. Each experiment comprised 5–6 series each of 14 consecutive 12 min periods. Changes in the extracellular pH from 7.4 to 7.8 by an increase in the concentration of bicarbonate inhibited the RR transiently. Alkalinization of the cell interior was achieved with weak permeable bases and ionophores. At low concentrations (5 mM NH_4Cl; 0.2 mM chloroquine) the weak bases caused a delayed inhibition of the RR, while at higher concentrations (15 and 30 mM NH_4Cl; 10 mM methylamine) the inhibitory effect was overlaid with a transient stimulation. 1.5 mM NH_4Cl and 10 and 20 μM chloroquine had no effect. Addition of 10 μM of the Na-H ionophore monensin also caused a transient stimulation followed by a progressive inhibition. 0.1 μM monensin had no effect. The above procedures cause increases in both the granular and the cytosolic pH. The K-H ionophore nigericin will cause an increase in the granular pH but a decrease in the cytosolic pH because of the prevailing ionic gradients. Since the effect of 10 μM nigericin was similar to that of monensin, it is concluded that the above effects are due to the increase in the intragranular pH. Thus, the maintenance of a low intragranular pH is of importance for a continuous RR. The inhibitory effect of the alkalinization can be transiently overridden, most likely due to pH-induced swelling of cell-membrane-associated granules which are sensitive to such stimulation.

Key words: Renin release – Ammoniumchloride – Methylamine – Chloroquine – Monensin – Nigericin – Intracellular pH

Introduction

A morphological (Taugner et al. 1984) and a functional study (Skøtt 1986b) have given evidence, that the renin release process involves the excretion of single secretory granules. It was suggested that the mechanism responsible for the fusion of the granules with the cell membrane involves swelling of the granules which is brought about by an osmotically induced water movement into the granule.

An osmotical swelling has been suggested to be an essential step in exocytosis also in other secretory cells (e.g. parathyroid cells, thrombocytes, chromaffin cells, isolated Langerhans islets) (e.g. Pollard et al. 1981; Hampton and Holz 1983; Serck-Hanssen 1984). The swelling is thought to be induced by an increase in the intragranular amount of osmotically active particles. In some of the hypotheses the increase is suggested to be driven by a proton gradient which is directed out of the granule, and which is maintained by a proton pump located at the granule membrane. Thus, Pollard et al. (1981) suggest that the granular proton excess results in anion (Cl^- or OH^-) entry at the site where the granule is attached to the cell membrane. Others (Geisow and Burgoyne 1982; Grinstein et al. 1982) suggest that cations are exchanged for intragranular buffered protons.

The pH of renin granules is considered to be low (e.g. Harada 1967), isolated renin granules are sensitive to changes in the osmolarity, and they are stabilized in the presence of Mg^{2+} and ATP (Männistö and Poisner 1981). Thus, a proton-pump of importance for the renin secretion might also exist in the JG-granule membrane. Furthermore, measurements of renin release from isolated rat glomeruli after superfusion with different synthetic buffers have previously given indirect evidence suggesting that pH_i or its regulation could be of importance in the regulation of the renin release process (unpublished observations).

The renin release rate in vivo is a balanced result of many different stimulatory and inhibitory factors, and therefore the interpretation of results may be a difficult task. This has lead to the introduction of several in vitro preparations, of which the preparation of isolated glomeruli has the advantage of being free of the changing influences of pressure, neural and tubular factors, as well as circulating or local humoral substances.

Glomeruli prepared by the magnetic iron technique remain metabolically active, consume oxygen, incorporate amino acids into particulate protein and nucleotides into nucleic acid (Brendel and Meezan 1973a, b) and in this laboratory the renin release from such glomeruli have been found to be sensitive to blockers of the respiratory chain, to removal of oxygen and to changes in the temperature (Blendstrup et al. 1975; Baumbach et al. 1976). Furthermore, the release of adenylate kinase, which is considered a marker for cytoplasmic leak, is uncorrelated to the renin release process (Baumbach and Skøtt 1982).

The aim of the present study was to investigate to which extent changes in the pH_o and pH_i were of importance for the renin secretion in a preparation of isolated glomeruli. pH_i was changed either by the addition of permeable weak

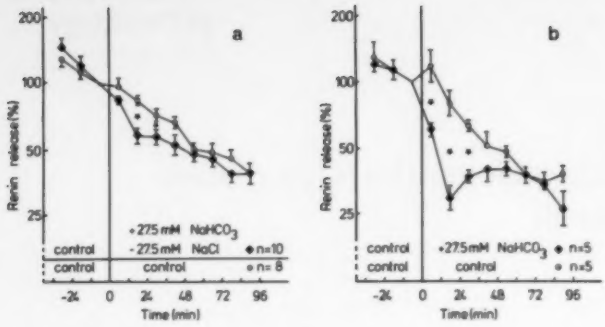

Fig. 1a, b
Effect on renin release of an increase in pH_o from 7.4 to 7.8 achieved by addition of $NaHCO_3$. In (**a**) the $NaHCO_3$ concentration was increased from 17.5 to 45 mM at zero time. An equimolar amount of NaCl was removed simultaneously. (**b**) represents the same procedure except that the $NaHCO_3$ was added with no other correction. In all figures, ○, undisturbed control series; *bars*, SE

bases or by taking advantage of the existing ionic gradients by the addition of ionophores, which dissipate these gradients.

Methods

Male Sprague-Dawley rats (250–350 g) were given a normal diet and had free access to food and water. The rats were anaesthetized with sodium amobarbital (12.5 mg per 100 g bw i.p.). Batches of 300 microscopically selected glomeruli with attached juxtaglomerular cells (5 batches per rat) were then prepared by the magnetic iron technique of Cook and Pickering (1959) and were mounted separately in five parallel polyethylene lines as described previously by Blendstrup et al. (1975). The batches were held by a magnetic field during superfusion at a rate of 10 µl/min from one of 2 pumps (Braun, Melsungen, FRG) each mounted with 5 infusion syringes. All superfusions were started in the control Ringer solution described below. At zero time the superfusion was shifted to the second Braun pump with 5 syringes containing either experimental solution or control Ringer solution. This arrangement permitted abrupt changes of superfusate composition during an experiment without disturbing the glomeruli.

The glomeruli were prepared in a bicarbonate Ringer solution of the following composition (mmoles/l): NaCl 101.0; $NaHCO_3$ 17.5; KCl 7.0; $CaCl_2$ 2.0; $MgSO_4$ 1.2; NaH_2PO_4 1.2; glucose 11.0; and sucrose 30.0; giving a calculated osmolality of 301 mosmoles/kg. The Ringer solution was adjusted to pH 7.4 by bubbling with 4% CO_2 and 96% O_2. This solution is referred to as "control" Ringer solution. The oxygen tension in the superfusate was measured to be 28.3 kPa after 4 h.

Methylamine (hydrochloride), chloroquine (diphosphate salt), monensin (sodium salt) and nigericin were obtained from Sigma (St. Louis, MO, USA). The ionophores were dissolved in ethanol before use. The final concentration of ethanol was 0.1‰.

Superfusate was collected over 12 min periods and frozen for later assay. The renin concentration was measured in 25 µl volumes by radioimmunoassay of generated angiotensin I using the "trapping" technique of Poulsen and Jørgensen (1974). In short 25 µl of superfusate was added to 25 µl of a mixture of angiotensin-I antibody and substrate-enriched rat plasma (4,000–6,000 ng angiotensin-I/ml). The endogenous renin content was about 4 nGU/ml, resulting in a detection limit of 10^{-7} Goldblatt Units in 25 µl. The incubation period was 3 h at 37° C.

All experiments were performed at a temperature of 30° C. When the glomeruli were exposed to changes in the superfusate composition these changes were introduced after approximately 60 min of superfusion with the control medium, and the moment of change is referred to as zero time. After the experiments the remaining renin in the batches was extracted by freezing and thawing three times (Blendstrup et al. 1975).

The absolute value of renin release in the last period preceding the zero time was used for normalizing the renin release rates for the individual experiments and ascribed the value of 100%. The term 'total renin content' means the amount of renin remaining in the glomeruli after the experiment plus the amount of renin released during the experiment.

When comparing the same experiment at two different times, a paired Student's *t*-test was used, and when comparing the release rates of two series which were run in parallel, an unpaired Student's *t*-test was used. The group means of absolute values (100% and total renin content) were compared by one way analysis of variance, and the experimental and control series which are presented in each individual figure were compared by the Bonferroni method for multiple comparisons (Wallenstein et al. 1980). $P < 0.05$ was considered significant.

Since relative renin release rates are used, the logarithm to the renin release rate is presented in the figures. The asterisks means significant difference between the series which are presented in the individual figure. *n* refers to the number of batches of glomeruli.

Results

Increase in pH_o by addition of bicarbonate

Figure 1 shows the effect of an increase in the extracellular concentration of sodium bicarbonate from the 17.5 mM used in the normal Ringer solution to 45 mM at zero time. In this way pH_o was increased from 7.4 to 7.8. The CO_2 concentration was left unchanged at 4%. In Fig. 1a, the osmolality of the Ringer solution was held constant by simultaneous removal of an isosmolal amount of NaCl, while in Fig. 1b, the 27.5 mM $NaHCO_3$ was added to the Ringer solution with no correction for osmolality. In both instances the change resulted in a transient inhibition of renin release with a duration of 36–48 min. The inhibition was most marked when the $NaHCO_3$ was added without correction for osmolality.

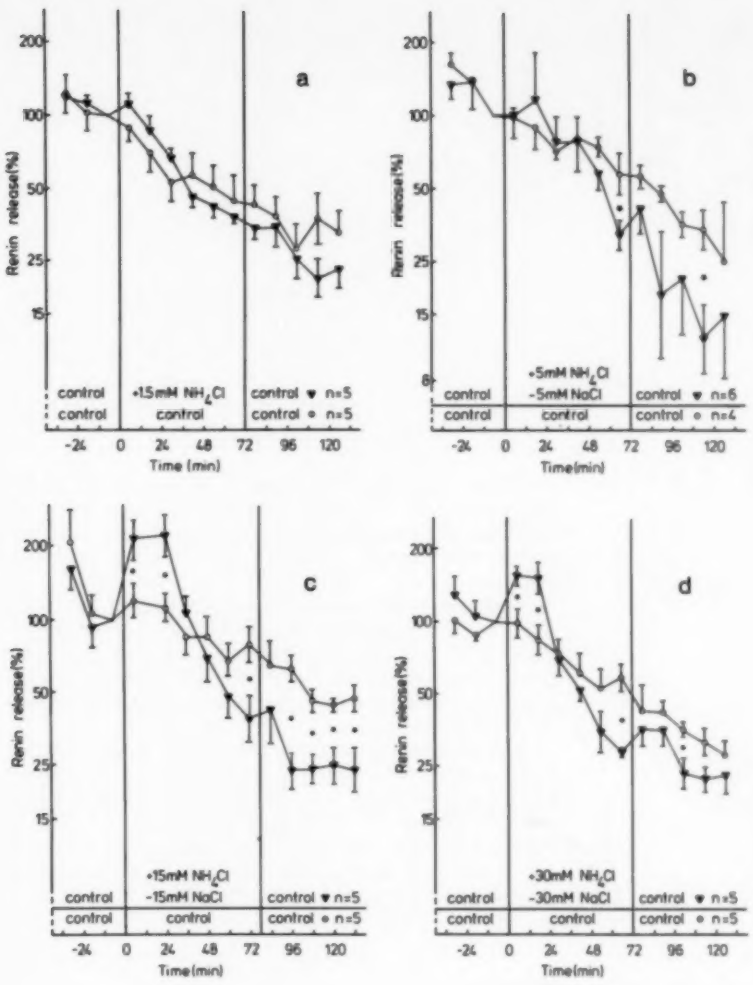

Fig. 2a–d
Effects of the addition of NH_4Cl on renin release. The composition of the superfusion fluid was changed at zero time and at 72 min as indicated in the figures. In (**b–d**) the change in NH_4Cl was accompanied by an equimolar decrease in the NaCl concentration. In (**a**) NH_4Cl was added with no other correction

Weak permeable bases, constant pH_o

The dose- and time-dependent effects of isosmolal addition of different concentrations of ammonium-chloride are shown in Fig. 2. Addition of 1.5 mM ammonium-chloride did not change the renin release rate significantly (Fig. 2a), but the addition of higher concentrations (5, 15 and 30 mM) influenced the renin release rate significantly. 5 mM NH_4Cl (Fig. 2b) did not change the release rate immediately after its introduction, but after 60 min an inhibition of the release became evident. The effects of the addition 15 or 30 mM NH_4Cl (Fig. 2c, d, respectively) were not different from each other: the renin release rate was stimulated during the first 2 periods (~ 24 min) after the introduction of the permeable base. Then a progressive inhibition was observed. After reintroduction of the normal Ringer solution, the renin release maintained a lower release rate than observed in the control series.

Figure 3 shows the effects of chloroquine on the release process. 10 μM chloroquine (Fig. 3a) did not change the renin release rate. 20 μM chloroquine (data not shown) did not change the release either, whereas 194 μM (Fig. 3b) resulted in a delayed inhibition, corresponding to the inhibition seen after treatment with 5 mM NH_4Cl.

In Fig. 4 is shown the effect of the addition of another ammonium salt, methylamine. The effect of isosmolal addition of 10 mM of this salt gave a result similar to that observed after the introduction of ammonium chloride, i.e. initially a stimulatory 24 min period, followed by a progressive inhibition and a low release rate after reintroduction of the normal Ringer solution.

Cation-ionophores

Figure 5 shows the response in renin release rate to addition of cation-ionophores to the normal Ringer solution.

The addition of 0.1 μM monensin (Na-H ionophore, Fig. 5a) did not change the renin release rate significantly at any time.

The introduction of 1 μM monensin (Fig. 5b), however, stimulated the renin release rate significantly as indicated by asterisks in the figure. The stimulation was maximal within

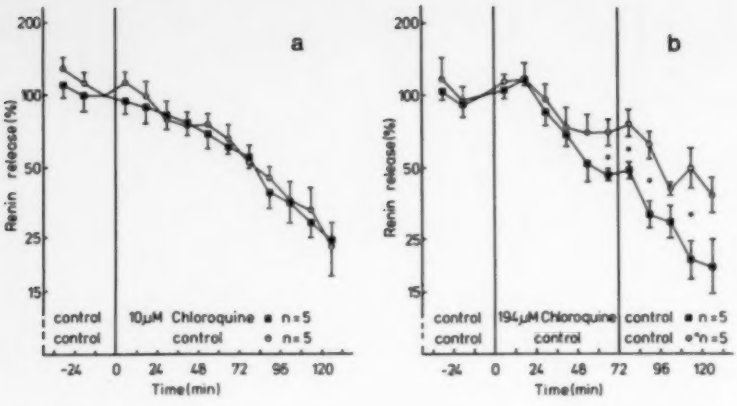

Fig. 3a, b
Effect of the addition of chloroquine on renin release. 10 μM chloroquine was added at zero time in (**a**), 0.2 mM chloroquine was added at zero time, and removed at 72 min in (**b**)

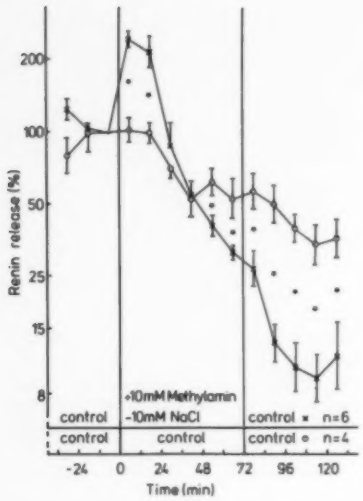

Fig. 4. Effect of the addition of methylamine on renin release. 10 mM methylamine was added at zero time, and removed at 72 min

the second period after the change. After the peak, the release rate decreased progressively until reintroduction of the Ringer solution without ionophore. At this time the renin release rate fell to values significantly below the control series.

10 μM monensin (Fig. 5c) resulted in a initial stimulation of the renin release rate with a maximum in the second period after the change. The stimulatory period was followed by a marked progressive inhibition of the release rate. The decrease continued after removal of the ionophore.

When 10 μM of the K-H ionophore nigericin was added (Fig. 5d), the renin release response was similar to that seen after addition of monensin. The decrease continued after removal of the ionophore.

Absolute values of 100%, and total renin content

The mean renin release rate at the 100% level was 5.62 ± 2.37 (SD) μGU per 12 min per 300 glomeruli for all the series ($n = 149$).

A one-way analysis of variance between the 28 groups was significant ($F = 2.95$). However, there were no differences between the sets of experimental series and their appropriate controls which are shown in the individual figures.

The total renin content amounted to 1.48 ± 1.17 (SD) mGU per 300 glomeruli ($n = 144$). The one way analysis of variance showed significant difference between the groups ($F = 2.33$). There were no differences between the experimental series and the appropriate controls which are shown in the same figure.

The fractional release rate at zero time was about 2%/h, which is similar to that found previously in both isolated superfused glomeruli and isolated superfused afferent arterioles (Skøtt and Baumbach 1985; Itoh et al. 1985). Furthermore the release rate is within one order of magnitude from what can be calculated to be the in vivo secretion rate (Blendstrup et al. 1975; Skøtt 1986b).

Discussion

An increase in the extracellular pH achieved by the addition of sodium bicarbonate resulted in a transient inhibition of the renin release rate (cf. Fig. 1). This inhibition was blunted by a simultaneous correction for the change in osmolality. However, even when the osmolality was held constant by the removal of equiosmolar amounts of NaCl, a slight transient inhibition of the release rate remained. Since the bicarbonate ion is considered less permeable than chloride, the basis for this inhibition might still be the transient inhibitory effect of the less permeable ion due to its osmotic effect. The effects of partially permeable molecules on the renin release rate have been reported previously (Frederiksen et al. 1975; Baumbach et al. 1976).

The results were different when it was attempted to increase the intracellular pH. The addition of weak permeable bases (e.g. amines) is recognized as a means of obtaining intracellular alkalinization (see e.g. review by Dean et al. 1984) as exemplified by NH_4Cl. The ammonia enters the cytosol electroneutrally at a rate depending on the extracellular concentration and the intracellular pH. Within the cytosol, which is more acidic than the exterior, the NH_3 will be trapped by a proton forming NH_4^+, thus raising the intracellular pH.

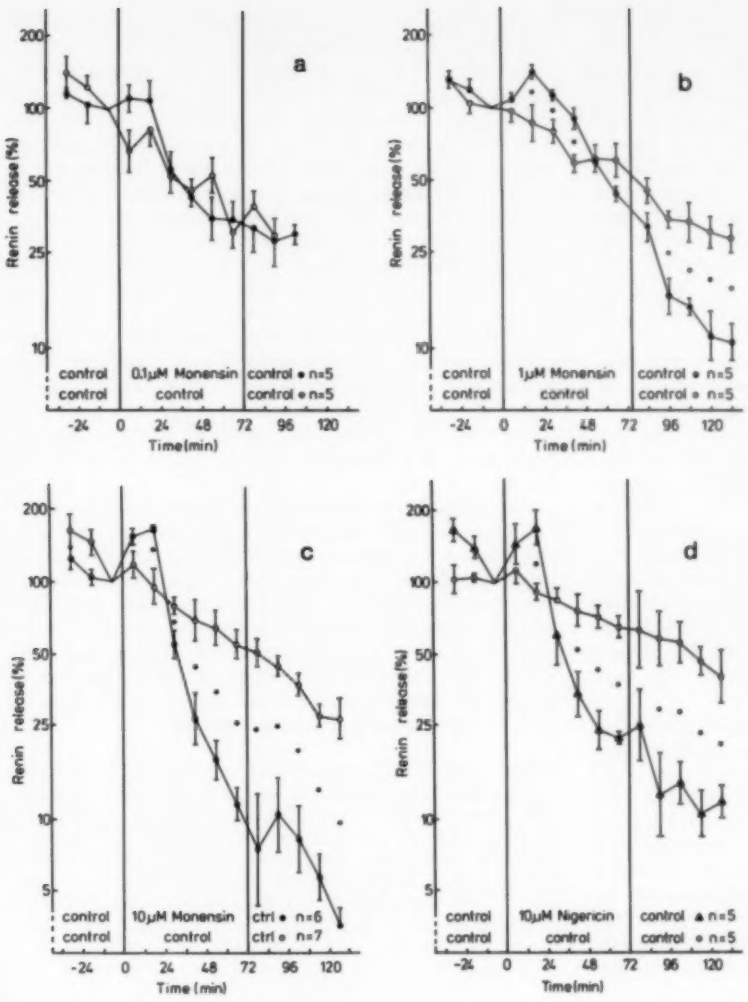

Fig. 5a–d
Effect of ionophores on renin release. 0.1 μM, 1 μM and 10 μM of monensin was added at zero time in (**a**), (**b**) and (**c**), respectively, and removed at 72 min. (**d**) shows the effect of addition of 10 μM nigericin at zero time, and its removal at 72 min

The amines had dose- and timedependent effects on the renin release rate (cf. Figs. 2–4). In low concentrations an inhibition was observed after approximately 60 min of superfusion, whereas higher concentrations initially resulted in a prompt stimulation, followed by a progressive inhibition. The inhibitory effect continued after reintroduction of the control superfusion medium. Similar inhibitory effects of amines at low concentrations overlaid with stimulation of exocytosis at higher concentrations have also been suggested from data on fibroblasts by Dean et al. (1984). The present data (to be discussed below) support the interpretation that these effects of amines on the renin release could be due to phenomena related to the intracellular pH.

Monensin and nigericin are ionophores of the carboxylic carrier group. They move as undissociated acid in one direction, and as a neutral cation-anion complex in the other. Thus, these compounds catalyze electroneutral cation-proton exchange. Their specificity differ: monensin transports Na^+ rather selectively ($K^+:Na^+ = 0.1$), while nigericin is more specific for the transport of potassium ($K^+:Na^+ = 45$) (Pressman 1976).

The results of the addition of the Na-H ionophore monensin (cf. Fig. 5) were similar to the results seen after the addition of the weak permeable bases: initially the renin release rate increased, subsequently this was followed by a progressive inhibition of the release rate. The induction of a Na-H exchange would increase the intracellular pH, and therefore the effect of monensin could be mediated by phenomena related to pH_i.

The changes in the renin release following addition of the ionophore or amines in the experiments mentioned above could be mediated by an increase in the cytosolic pH, or, alternatively, by an increase in the pH inside the secretory granules. It is possible to distinguish between these two possibilities by taking advantage of the different cation-specificities of monensin and nigericin, as previously suggested by Nilsen-Hamilton et al. (1981). The two ionophores should move H^+ in opposite directions across the cell membrane, because of the distribution of Na^+ and K^+ between the extra- and intracellular phases. This prediction has been verified experimentally by Grinstein who demonstrated that nigericin acidified the cytosol of lymphocytes

(Grinstein et al. 1985), while monensin increased the cytosolic pH in the same cell type (Grinstein and Goetz 1985). However, the pH-effect on acidic intracellular organelles (e.g. lysosomes – or JG-cell secretory granules) would be the same for the two ionophores: in the absence of significant gradients for K^+ and Na^+ between the granule and the cytosol, the outward directed proton gradient would drive H^+ out of the organelle and result in alkalinization of the organelle. In fact, Poole and Ohkuma (1981) have demonstrated that the addition of nigericin increases the lysosomal pH in macrophages, and Schwartz and Al-Awqati (1985) observed an increase in the pH of vesicles in cells of collecting ducts and proximal tubules after the addition of this ionophore.

The effect of nigericin on the renin release rate is analogous to that seen after the addition of monensin (cf. Fig. 5). According to the arguments above, this allows the conclusion that the biphasic change in renin release rate seen after the addition of nigericin, monensin, and weak permeable bases, is due to an increase of the pH inside an intracellular acidic organelle, probably the secretory granule. After the removal of the alkalinizing substances the release continued to be low, thus supporting the interpretation that these substances are trapped within the granules. This interpretation is also supported by the study of Ålund and Olson (1979), who demonstrated that JG-cell granules had such a high affinity for quinacrine (another amine) given in vivo, that it was possible to visualize the individual granules by fluorescence light microscopy.

The mechanism by which the intragranular pH affects the renin release process is not clarified by the present experiments. However, Taugner et al. (1985) showed that long-term administration of the weak bases chloroquine and chlorphentermine resulted in vacuolation of the secretory granules of the JG-cells. Swelling of acidic organelles after their alkalinization by treatment with amines, monensin and nigericin is common. Thus, amines and nigericin lead to vacuolation of lysosomes in macrophages (Poole and Ohkuma 1981). Pazoles et al. (1980) found that the addition of ammonium chloride or nigericin lysed isolated chromaffin granules, and the same was found to be true for monensin by Geisow and Burgoyne (1982), who also demonstrated that the basis for the granule lysis was osmotic, since addition of sucrose to the granule suspension inhibited lysis. Since the renin release rate is sensitive to challenges thought to result in granule swelling (Skøtt 1986a), the observed initial stimulatory effect of the increase in granule pH, would most likely be due to the concomitant swelling of the granules.

Such granule swelling has been suggested to be due to an exchange of osmotically active external K^+ or Na^+ for internally buffered protons (Pazoles et al. 1980). Introduction of NH_3 will also result in the formation of one osmotically active NH_4^+ at the expense of one buffered H^+. On this basis and using an estimate of the intragranular buffer capacity Grinstein et al. (1982) have calculated that an increase of one pH unit in the chromaffin granule would lead to an increase in the volume of the granule of more than 50%. The increase in the renin release rate observed after the present addition of alkalinizing substances was of a magnitude to be expected after an increase in the granule volume of only 5–10% (Skøtt 1986a). Although there exists no estimate of the JG-cell buffer capacity, these figures are quite compatible with the interpretation that the swelling could be due to such an exchange of osmotically active particles for intragranular buffered protons.

However, this interpretation does not account for the inhibition, which seems to be mediated by a different mechanism, since its dose-response characteristics was different. The similar inhibitory effects of monensin and nigericin suggest that changes within the secretory granules are responsible for the inhibition. Data on secretion of intracellular products and previously endocytosed materials have suggested that amines can inhibit processes closely related to the vesicle-plasma membrane fusion (Dean et al. 1984). On the other hand, the inhibitory effect could also be due to interference with the intracellular traffic. Thus, monensin has been shown to arrest intracellular transport at the level of the Golgi apparatus in a series of cells (Tartakoff 1983); and furthermore Zhang and Schneider (1983) have suggested that at Golgi secretion in animal cells requires acidification of the cisternal contents. An inhibitory effect at this level could result in a delayed inhibition as seen in the present study.

In summary, the addition of amines has a biphasic effect on the renin release rate: a slow inhibitory effect is evident already at low concentrations, while it is overlaid with an initial stimulation of the exocytosis at higher concentrations. Results obtained with cation-proton ionophores support the findings. The results suggest that the maintenance of a low intragranular pH is of importance for a continuous renin release. The inhibitory effect of the alkalinization can be transiently overridden by pH-induced osmotic effects on granules susceptible to release by swelling.

Acknowledgements. The present work was supported by grants from the Danish Medical Research Council, King Christian X Foundation and the Danish Heart Association. The author is indebted to Dr. P. P. Leyssac for advice throughout the study, to P. Christensen M. Sc. for angiotensin-I antibody and help with the renin assay, and to Dr. N.-H. Holstein-Rathlou for criticism of the manuscript. Mrs. C. Temdrup gave skillful technical assistance, and Mrs. L. Wybrandt drew the figures.

References

Ålund M, Olson L (1979) Quinacrine affinity of endocrine cell systems containing dense core vesicles as visualized by fluorescence microscopy. Cell Tissue Res 204:171–186

Baumbach L, Skøtt O (1982) Isolated glomeruli in vitro: an approach to the macula-densa-mediated renin release. Kidney Int 22:(suppl 12) S73–S77

Baumbach L, Leyssac PP, Skinner SL (1976) Studies on renin release from isolated superfused glomeruli: effects of temperature, urea, ouabain and ethacrynic acid. J. Physiol (Lond) 258:243–256

Blendstrup K, Leyssac PP, Poulsen K, Skinner SL (1975) Characteristics of renin release from isolated superfused glomeruli in vitro. J Physiol (Lond) 246:653–672

Brendel K, Meezan E (1973a) Properties of a pure metabolically active glomerular preparation from rat kidneys. I. Isolation. J Pharmacol Exp Ther 187:332–341

Brendel K, Meezan E (1973b) Properties of a pure metabolically active glomerular preparation from rat kidneys. II. Metabolism. J Pharmacol Exp Ther 187:342–351

Cook WF, Pickering GW (1959) The location of renin in rabbit kidney. J Physiol (Lond) 149:526–536

Dean RT, Jessup W, Roberts CR (1984) Effects of exogenous amines on mammalian cells, with particular reference to membrane flow. Biochem J 217:27–40

Frederiksen O, Leyssac PP, Skinner SL (1975) Sensitive osmometer function of juxtaglomerular cells in vitro. J Physiol (Lond) 252:669–679

Geisow MJ, Burgoyne RD (1982) Cation-dependent lysis of chromaffin granules – an alternative hypothesis for osmotically driven exocytosis. Cell Biol Int Rep 6:353–359

Grinstein S, Goetz JD (1985) Control of free cytoplasmic calcium by intracellular pH in rat lymphocytes. Biochim Biophys Acta 819:267–270

Grinstein S, Vander Meulen J, Furuya W (1982) Possible role of H-alkali cation countertransport in secretory granule swelling during exocytosis. FEBS Lett 148:1–4

Grinstein S, Goetz JD, Cohen S, Rothstein A, Gelfand EW (1985) Regulation of Na^+/H^+ exchange in lymphocytes. Ann NY Acad Sci 456:207–219

Hampton RY, Holz RW (1983) Effects of changes in osmolality on the stability and function of cultured chromaffin cells and the possible role of osmotic forces in exocytosis. J Cell Biol 96: 1082–1088

Harada K (1967) The demonstration of two acid groups in juxtaglomerular granules with basic triphenyl methane dyes, aldehyde-fuchsin and Schiff's reagent. Histochem J 10:74–87

Itoh S, Carretero OA, Murray RD (1985) Renin release from isolated afferent arterioles. Kidney Int 27:762–767

Männistö PT, Poisner AM (1981) Further studies on properties of renin granules isolated from rat kidney cortex. Acta Physiol Scand 112:365–371

Nilsen-Hamilton M, Hamilton RT, Allen WR, Massoglia SL (1981) Stimulation of the release of two glycoproteins from mouse 3T3 cells by growth factors and by agents that increase intralysosomal pH. Biochem Biophys Res Commun 101:411–417

Pazoles CJ, Creutz CE, Ramu A, Pollard HB (1980) Permeant anion activation of MgATPase activity in chromaffin granules. J Biol Chem 255:7863–7869

Pollard HB, Creutz CE, Pazoles CJ (1981) Role of ions and intracellular proteins in exocytosis. Methods Cell Biol 23:313–333

Poole B, Ohkuma S (1981) Effect of weak bases on the intralysosomal pH in mouse peritoneal macrophages. J Cell Biol 90: 665–669

Poulsen K, Jørgensen J (1974) An easy radio-immunological microassay of renin activity, concentration and substrate in human and animal plasma and tissues based on angiotensin-I trapping by antibody. J Clin Endocrinol Metab 39:816–825

Pressman BC (1976) Biological applications of ionophores. Annu Rev Biochem 45:501–530

Schwartz GJ, Al-Awqati Q (1985) Carbon dioxide causes exocytosis of vesicles containing H^+ pumps in isolated perfused proximal and collecting tubules. J Clin Invest 75:1638–1644

Serck-Hanssen G (1984) Different osmotic stability of two storage pools of adrenomedullary catecholamines: Possible relevance to exocytotic release of the hormones. Acta Physiol Scand 120:137–140

Skøtt O (1986a) Calcium and osmotic stimulation in renin release from isolated rat glomeruli. Pflügers Arch 406:485–491

Skøtt O (1986b) Episodic release of renin from single isolated superfused rat afferent arterioles. Pflügers Arch 407:41–45

Skøtt O, Baumbach L (1985) Effects of adenosine on renin release from isolated rat glomeruli and kidney slices. Pflügers Arch 404:232–237

Tartakoff A (1983) Perturbation of vesicular traffic with the carboxylic ionophore monensin. Cell 32:1026–1028

Taugner R, Bührle CP, Nobiling R (1984) Ultrastructural changes associated with renin secretion from the juxtaglomerular apparatus of mice. Cell Tissue Res 237:459–472

Taugner R, Whalley A, Angermüller S, Bührle CP, Hackenthal E (1985) Are the renin-containing granules of juxtaglomerular epithelioid cells modified lysosomes? Cell Tissue Res 239:575–587

Wallenstein S, Zucker CI, Fleiss JL (1980) Some statistical methods useful in circulation research. Circ Res 47:1–9

Zhang F, Schneider DL (1983) The bioenergetics of Golgi apparatus function: evidence for an ATP-dependent proton pump. Biochem Biophys Res Commun 114:620–625

Received April 14, 1986/Accepted January 23, 1987

Pflügers Arch (1987) 409:100–106

Pflügers Archiv
European Journal of Physiology
© Springer-Verlag 1987

Potassium channels in the basolateral membrane of the rectal gland of the dogfish (*Squalus acanthias*)*

Rainer Greger[1,3], **Heinz Gögelein**[2,3], **and Eberhard Schlatter**[1,3]

[1] Lehrstuhl II Physiologie, Hermann-Herder-Strasse 7, D-7800 Freiburg, Federal Republic of Germany
[2] Max-Planck-Institut für Biophysik, Kennedyallee 70, D-6000 Frankfurt, Federal Republic of Germany
[3] Mount Desert Island Laboratory, Salsbury Cove, ME 04672, USA

Abstract. Previous studies in isolated, in vitro perfused rectal gland tubules (RGT) have revealed that the basolateral membrane possesses a K^+ conductive pathway. In the present study, we have utilized the patch clamp technique in RGT segments to characterize this pathway. The basolateral membrane was approached with patch pipettes at the open end of in vitro perfused segments [5]. Recordings were obtained in cell-attached as well as in excised inside-out patches. In cell-attached patches with the pipette filled with a KCl solution (274 mmol/l) and the bath containing NaCl shark Ringer (275 mmol/l), inward K^+ currents (from pipette into cell) with a mean slope conductance of 123 ± 26 pS ($n = 3$) were observed. We were unable to generate outward K^+ currents at high depolarizing (cell more positive) clamp voltages. This indicates inward rectification of this channel. To examine the rectification properties further, excised (inside out) patches were exposed to K^+ concentration gradients, directed out of, as well as into the pipette. With NaCl in the pipette and KCl in the bath, K^+ outward currents were observed. The current-voltage (IV) relation revealed Goldman-type rectification, with a mean single channel conductance of 185 ± 28 pS ($n = 7$) at high positive voltages (linear range of the IV curve). The single-channel permeability coefficient for K^+ was $0.26 \pm 0.04 \cdot 10^{-12}$ cm^3/s ($n = 7$). In the reversed experiment (pipette KCl, bath NaCl), inward currents of similar kinetics and amplitude were obtained. The single channel conductance was 146 ± 21 pS ($n = 7$) at high negative voltages (linear range of the IV curve). The single channel permeability coefficient for K^+ was $0.21 \pm 0.03 \cdot 10^{-12}$ cm^3/s ($n = 7$). We were not able to reverse the currents in any of these experiments, indicating that this channel is highly selective for K^+ over Na^+. In all three series of experiments, the kinetic appearance of the channels was similar. Bursts of activity were followed by interburst pauses. The open state was described by a single time constant of 3.0 ± 0.2 ms, whereas the closed state was described by two time constants of 0.7 ± 0.2 ms and 2.8 ± 0.5 ms ($n = 8$). It can be concluded that these channels permit K^+ inward and outward currents. They are probably the equivalent of the basolateral K^+ conductance as observed in a previous study [12]. Under physiological conditions a single channel conductance of some 20 pS is predicted from the present data. In cell-attached patches, with a high K^+ concentration in the pipette, the channel behaves as an inward rectifier.

Key words: K^+-channel – Patch clamp analysis – Rectal gland – Shark

Introduction

Previously [12–14], we have shown that the mechanism of hormonally (VIP, rectin) [28] stimulated chloride secretion in the rectal gland of the shark (*Squalus acanthias*) involves carrier mediated cell uptake of $Na^+2Cl^-K^+$ across the basolateral membrane. This uptake process is energized by the basolateral ($Na^+ + K^+$)-ATPase. Chloride leaves the cell via an apical chloride conductance. Potassium recycles across the basolateral membrane via a conductive pathway [12]. The movement of chloride into the lumen, and that of potassium to the peritubular side polarizes the epithelium: the lumen becomes electrically negative with respect to the bath solution. This drives paracellular sodium secretion. The above model of Na^+Cl^- secretion is comparable to the mechanisms present in the colon [18, 21] and in the trachea [29]. Study of the rectal gland of the shark, however, offers several major methodological advantages over the other two epithelia: it is a simple single cell layer epithelium, both cell membranes are accessible, and the relative change in Na^+Cl^- secretion induced by VIP and/or rectin [28] or the second messenger cAMP is profound [12, 14], characterized by increases of more than 10-fold.

The present study is part of a larger series of patch clamp experiments [8, 9, 16], undertaken to examine the conductive pathways for chloride and potassium present in the luminal and in the basolateral membranes. Using this technique, the channel properties, possible mechanisms of control of channel activity and putative inhibitors were tested. This report presents our analysis of the potassium conductance in the basolateral membrane, and indicates the presence of a K^+ selective channel of about 20 pS unitary conductance under physiological conditions. This channel permits K^+ influx and efflux, depending on the driving force. The analysis of single channel kinetics reveals burst appearance with only one open time-constant (of the order of 3 ms) and two closed time-constants (0.7 and 3 ms). In this respect, the channel is comparable to the K^+-channel in the basolateral membrane of the proximal tubule [5] and in other epithelia [10]. Under physiological conditions, this channel allows for

* Supported by Deutsche Forschungsgemeinschaft Gr 4808 and by NSF and NIH grants to the MDIBL. Parts of this study have been published in the Mount Desert Island Biol. Bulletin 1984, 1985.
Offprint requests to: R. Greger

Table 1. Composition of solutions. Concentrations in mmol/l

Abbreviation	Na^+	K^+	Ca^{2+}	Mg^{2+}	Cl^-	Hepes	D-Glucose	Urea	EGTA
NaCl	275	4	2.5	3	285	10	5	350	0
KCl	5	274	0.97	3	282	10	5	350	1

K^+ recycling from the cell to the peritubular space, required for the mechanism of Na^+Cl^- secretion described above.

Methods

The present study comprizes some 150 specimens of *Squalus acanthias* (b.w. 7–15 kg, 80% male, 20% female). The animals were killed by decapitation, and the rectal gland was removed and transferred into ice-cold shark Ringers solution. The gland was cut into slices and individual rectal gland tubules were dissected out, as described previously [12]. The individual tubules were transferred into a perfusion chamber mounted on the stage of an inverted microscope. The tubules were cannulated at one end by a perfusion system [11], while the other end was accessible to patch pipettes [5, 15]. No pretreatment of the tubules was necessary. At the non-cannulated side of the tubule, a patch pipette could be inserted into the lumen or brought in contact with the basolateral cell membrane. Gigaseals were obtained on the luminal as well as on the basolateral cell membrane.

The potassium channels, described below, were only found in basolateral membrane patches; conversely chloride channels were only found in luminal membrane patches [15]. Approximately half of the rectal gland segments (ca. $n = 200$) were stimulated to secrete Na^+ and Cl^- by addition of forskolin ($5 \cdot 10^{-6}$ mol/l), adenosine ($5 \cdot 10^{-4}$ mol/l), and dibutyryl cyclic adenosinemonophosphate (db-cAMP, $5 \cdot 10^{-4}$ mol/l) to the peritubular NaCl solution (cf. Table 1). The remainder of the rectal gland tubules were untreated. No difference was apparent with respect to the incidence of K^+-channels found in the basolateral cell membrane [15], nor with respect to the properties of the K^+-channels found in both series. For this reason, the data of the two series are pooled in the present report.

The methods to manufacture patch pipettes for this study, as well as the method used to obtain isolated membrane patches have been described previously [7, 17]. Modified shark Ringer solutions were used in the present study. The compositions are given in Table 1. The NaCl solution contained a high Ca^{2+} concentration (corresponding to an extracellular solution), and the KCl solution had low free-Ca^{2+} concentration (about $4 \cdot 10^{-6}$ mol/l). Details of the equipment used have been given in previous reports [5–7]. All experiments were carried out at about 20° C. When the bath composition was changed the rate of exchange was such that a 95% exchange was achieved within less than 1 min.

Single channel current carried by positively charged ions flowing into the patch pipette (i.e. out of the cell) is presented as upward (positive) deflection. The sign of the potential refers to the bath with respect to the pipette interior. The existence of cell-attached configurations was ascertained by the following criteria: (1) The voltage across the patch was −10 mV to −50 mV (in zero current clamp mode) [6]. This voltage reflects the attenuated membrane potential, and it collapsed upon excision. (2) Disappearance or modification of channel activity when the membrane patch was excised. In some experiments air exposure of the excised patch for a few seconds was required to regenerate channel activity, indicating that a vesicle had formed. The method for excised membrane patches most likely produced the inside-out configuration [17]. Data were recorded on an FM tape at 9.5–152.4 cm/s. The low-pass filter of the patch clamp amplifier was set to 10 kHz. The data were analysed using a LSI 11/23 computer system. The general principles of the analysis have been published previously [6, 7]. The large unitary conductance of the K^+-channel, analyzed in this (and a subsequent) study, permitted us to use ca. 3–5 kHz as the upper frequency limit. For each clamp voltage (Vc), the current amplitude (I) was assessed in frames of 500 ms to 2 s duration; 10–1,000 frames were averaged to arrive at the mean value of I. It was assumed to be indistinguishable from zero if the events were no longer detectable in the baseline noise. The limits of a signal over noise ratio of $\leqslant 2$ are indicated in the individual current-voltage relationships as filled symbols.

The data are presented as individual recordings. For series of experiments mean values ± SEM are given. The current-voltage relations were fitted by the Goldman-Hodgkin-Katz (GHK) current equation

$$I = \frac{F^2}{RT} z P_K V \frac{K_o - K_i e^{(zFV/RT)}}{1 - e^{(zFV/RT)}} \quad (1)$$

where I and V are the single channel current and membrane voltage, R, T, z, and F have their usual meaning. K_o and K_i are the K^+ activities in the pipette and on the cytosolic side. P_K refers to the single channel permeability coefficient for K^+. The value of P_K was obtained by linear regression analysis. This simplified version of the GHK equation could be used since the channel under study is highly selective for K^+, i.e. no Na^+ currents can be driven through this channel (Fig. 2). The single channel conductances were calculated from the differential $g = \delta I / \delta V$. The single channel conductance was analysed for two voltage ranges: at the normal membrane voltage of around −60 to −80 mV [12], $g(V_{bl})$, and at infinite voltage, where the current-voltage curve is linear and where the single channel conductance is maximal, $g(V_\infty)$ (cf. Fig. 2).

Results

Figure 1 shows recording of K^+ channels in cell-attached mode. When both the bath and the pipette contained NaCl-Ringer solution (upper half), and when the rectal gland tubule segment was stimulated to secrete NaCl, the physiological driving force present across the patch ($Vc \approx$ OmV) generated channel currents in the upward direction, i.e. K^+ extrusion from the cell. The channels appeared in bursts

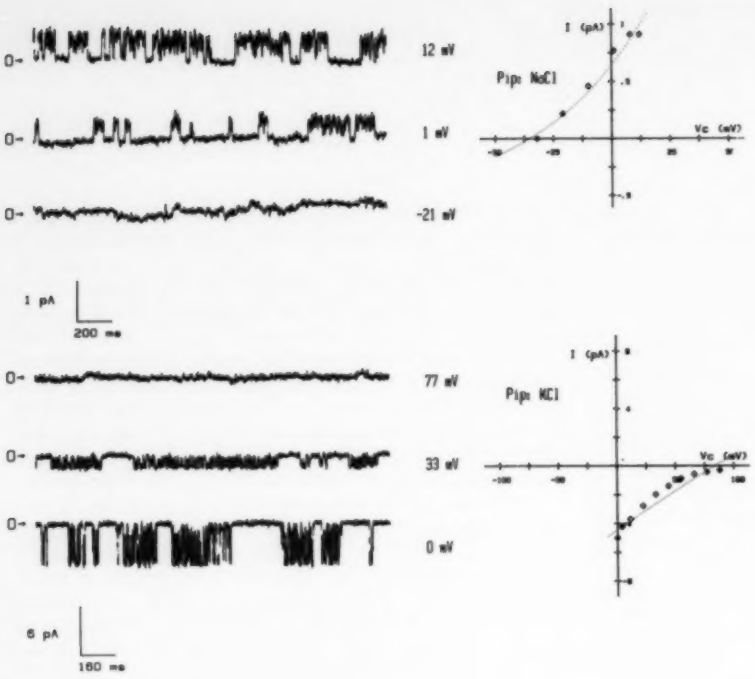

Fig. 1
K^+ channels in cell attached patches of the basolateral membrane of rectal gland cells. The *upper panel* shows a typical recording, when the pipette was filled with NaCl and the bath contained NaCl (Table 1). The voltage at the right side refers to the clamp potential. At clamp voltage → 0 mV (*middle trace*) the normal membrane potential of about −64 mV [12], cytosolic side negative, is present across the membrane patch. At clamp potential −21 mV the voltage across the patch is hyperpolarised by 21 mV. Channel openings in the upward direction indicate outflow of K^+ (from the cell into the pipette). The corresponding current voltage relationship is shown at the right hand side. The single channel current I is plotted as a function of the clamp voltage V_c. The *dotted line* is a least square fit according to the Goldman-Hodgkin-Katz current equation, assuming an intracellular K^+ activity of 130 mmol/l and a basolateral membrane potential of −60 mV. The *filled symbols* mark a signal noise ratio of ⩽ 2. The *lower panel* shows a corresponding experiment with KCl (Table 1) as the pipette solution

with fast transitions to the closed state (flickering). Cell hyperpolarization by −20 mV and more negative values reduced or abolished these current events. This finding confirms that the channel conducts K^+ out of the cell, since intracellular K^+ is above its electrochemical equilibrium [12]. No other major ion has a similar driving force and current direction: chloride efflux as well as Na^+ influx would have been increased by the cell hyperpolarization. The right upper panel of Fig. 1 depicts the current-voltage relation. The data are fitted by the Goldman-Hodgkin-Katz equation, using a K_i of 130 mmol/l and a basolateral membrane potential of −60 mV, as it has been reported previously for the same preparation [13]. The single channel conductance at the membrane potential $g(V_{bl})$ was 35 pS and $g(V_\infty)$ was 194 pS.

Similar experiments in the cell-attached mode were performed with a KCl solution (Table 1) in the pipette and NaCl solution in the bath. Under these conditions a negative current (K^+ flowing into the cell) was observed (lower part of Fig. 1). The channel amplitude decreased with positive (depolarizing) potentials and was indistinguishable from zero at about +70 mV. No channel activity in the reversed direction could be observed at clamp potentials as high as +90 mV. These data indicate that the channel current is due to an inward K^+ movement, driven by the negative cell potential. Apparently the channel behaves as an inward rectifier under these conditions, which means that only inward K^+ flow (from the pipette into the bath) is possible. This is most clearly apparent from the corresponding current-voltage relation (lower right panel of Fig. 1). The data points suggests a curved function and do not fit well to the GHK equation (dotted curve). The single channel conductance was extrapolated for the range (V = 0 − 30 mV) and is 127 pS. The mean value of this series is 123 ± 26 pS ($n = 3$) (Table 2). The kinetic appearance of these channels was similar to that shown in Fig. 1: phases of activity were followed by interburst pauses. Within the bursts, the channel closed and opened rapidly. In the next series, basolateral membrane patches were excised and were examined with NaCl solution in the pipette and KCl solution (Table 1) in the bath. A typical experiment is shown in Fig. 2 (upper part). At ≈ 0 mV clamp potential, a positive current (from the bath into the pipette) of potassium is driven by the respective potassium concentration gradient. With depolarizing clamp voltages (positive on the cytosolic side of the patch) the current amplitude increases. With hyperpolarizing voltages (negative on the cytosolic side of the patch) the amplitude is reduced, and approaches a current level not distinguishable from zero at clamp voltages of −50 mV or more negative values. The corresponding current-voltage relationship for this channel (upper right panel of Fig. 1) indicates that the data points can be fitted reasonably well by the GHK equation. Since we have not observed negative currents at voltages as high as −90 mV, Na^+ ions can be considered to be practically impermeant for this channel. The single channel permeability coefficient, P_K, obtained by the GHK fit, was $0.33 \cdot 10^{-12}$ cm³/s. The conductance values obtained for this channel are: $g(V_{bl})$ = 31 pS and $g(V_\infty)$ = 238 pS. The mean values obtained for the entire series of 7 experiments are summarized in Table 2. P_K was $(0.26 \pm 0.04) \cdot 10^{-12}$ cm³/s, $g(V_{bl}) = 24 \pm 4$ pS and $g(V_\infty) = 185 \pm 28$ pS. These experiments indicate that, with Na^+ ions at the membrane outside, K^+ ions flow from the cytosolic to the extracellular side, as was observed in the cell-attached configuration (Fig. 1).

In the next series of experiments the patch pipette was filled with the KCl and the bath contained the NaCl solution (Table 1). A typical experiment is shown in the lower half of

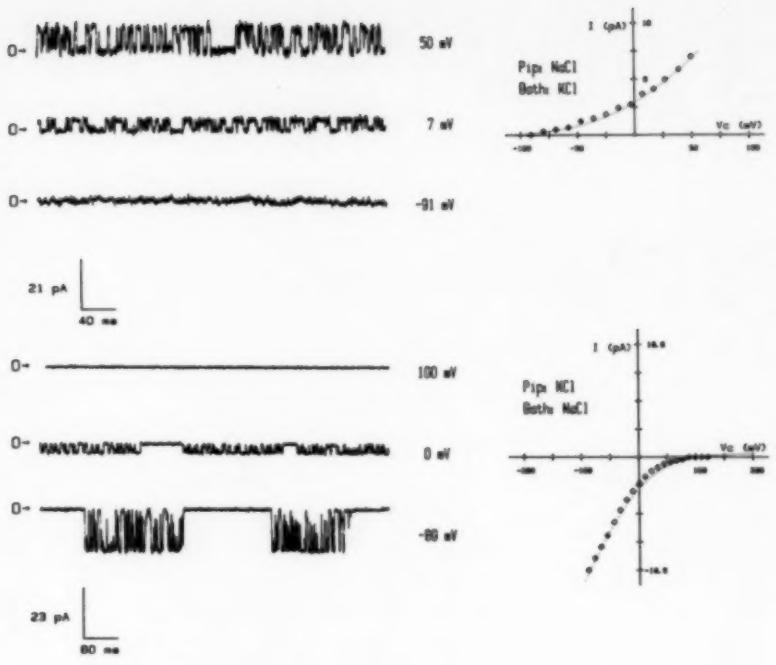

Fig. 2
K^+ channels in cell excised (inside out oriented) basolateral membrane patches of rectal gland cells. The *upper panel* shows a typical recording with NaCl in the pipette and KCl (Table 1) in the patch. The clamp voltage, given at the right side, refers to the bath (cytosolic side) with respect to the pipette interior. 0 → indicates the zero current level. Channel openings in the upward direction indicate K^+ flow from the bath (cytosolic side) into the patch pipette. On the right hand side the current voltage relationship of this channel is shown. The single channel current I is plotted as a function of the clamp voltage Vc. The *dotted line* was obtained by a least square fit to the Goldman-Hodgkin-Katz (GHK) current equation. The *filled symbols* mark a signal noise ratio of $\leqslant 2$. The *lower panel* displays a comparable experiment with KCl in the pipette and NaCl (Table 1) in the bath

Table 2. Permeability coefficient and single channel conductances of K^+ channels in the basolateral membrane of rectal gland cells

Cell	Attached		Excised	
	Pipette NaCl Bath NaCl	Pipette KCl Bath NaCl	Pipette NaCl Bath KCl	Pipette KCl Bath NaCl
P_K (cm^3/s)	$0.39 \cdot 10^{-12}$ (1)	–	$(0.26 \pm 0.04) \cdot 10^{-12}$ (7)	$(0.21 \pm 0.03) \cdot 10^{-12}$ (7)
$g(V_{bl})$ (pS)	35 (1)	–	24 ± 4 (7)	19 ± 3 (7)
$g(V_\infty)$ (pS)	194 (1)	123 ± 26 (3)	185 ± 28 (7)	146 ± 21 (7)

The permeability coefficients P_K were obtained by least square fits of the current-voltage curves to the Goldman-Hodgkin-Katz (GHK) equation. $g(V_{bl})$ are the single channel conductances at the physiological membrane potential and $g(V_\infty)$ are the single channel slope conductances at infinite potential (linear range of the current-voltage curves)

Fig. 2. At zero mV clamp potential, negative current events, corresponding to the movement of K^+ ions from the pipette into the bath, were observed. Again, note the similarity of the kinetic appearance to the other original recordings obtained under differing experimental conditions. With negative clamp voltages, the single channel current amplitude increased, and it was reduced with positive voltage. The current-voltage curve of this recording conforms reasonably well to the GHK equation, indicating that this channel is selective for K^+ ions. The conductance values for this channel were: $g(V_{bl}) = 28$ pS and $g(V_\infty) = 216$ pS; the P_K was $0.3 \cdot 10^{-12}$ cm^3/s. The mean values obtained for this entire series are summarized in Table 2: $g(V_{bl})$ was 19 ± 3 pS, $g(V_\infty)$ was 146 ± 21 pS and P_K was $0.21 \pm 0.03 \cdot 10^{-12}$ cm^3/s ($n = 7$). These values are not significantly different from those obtained for the outward K^+ currents in excised patches (Table 2).

A close inspection of the single-channel recordings (Figs. 1 and 2) reveals that the channel does not always open to the complete current amplitude, nor does it always reach the zero current line. We have examined this in further detail and an example at high time resolution is shown in Fig. 3. Note that substates of approximately 23% and 64% of complete amplitude are clearly apparent. An amplitude histogram of this channel (lower panel) indicates that 3 current levels are clearly discernable. The main peaks are fitted by a Gaussian function (dots). The first peak, scattering around zero mV, corresponds to the zero current level when no channels are open (baseline noise). The second peak has a shallow amplitude at −3.8 pA, corresponding to the small substate. Its incidence was about 5% of that of the fully open state. The larger substate (−9 pA) is occupied even less frequently and therefore is difficult to detect in the amplitude histogram. The third sharp peak reflects the fully open state of this channel (−14 pA). The existence of similar substates was observed under all experimental conditions described in this study. Substates have previously been reported in inward-rectifying K^+ channels of HeLa cells [27] and molluscan neurons [20] and in ventricular cells from guinea-pig [24].

In all series of experiments the kinetic appearance of the channel activity was examined quantitatively by open- and

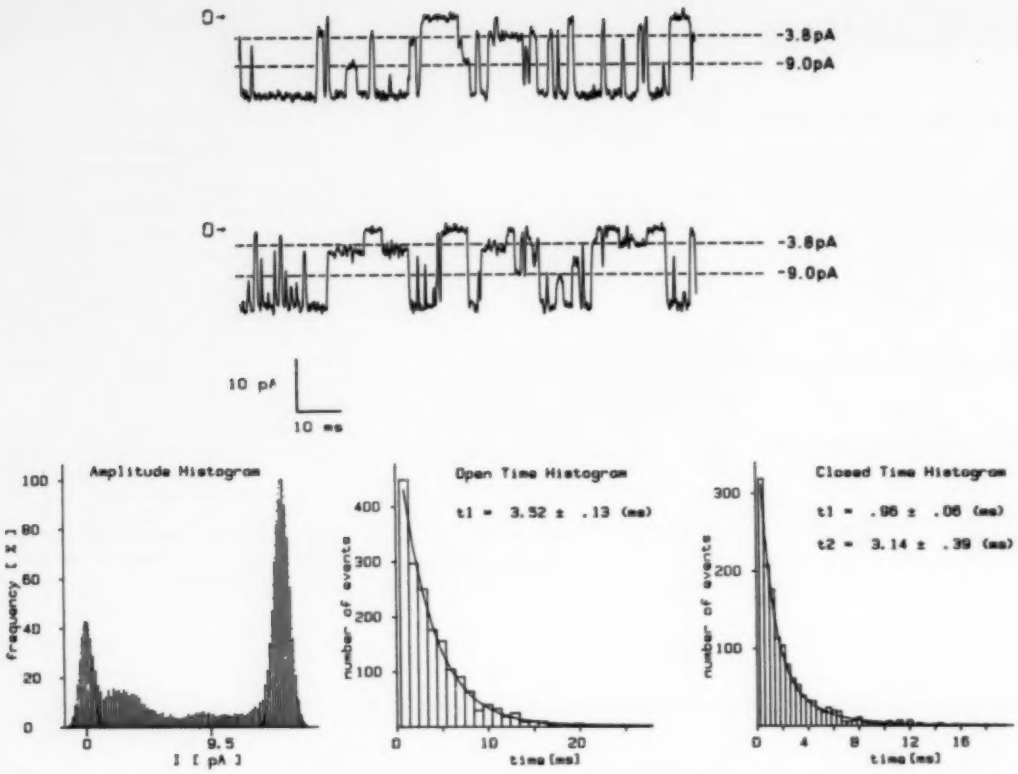

Fig. 3. Substates and time constant analysis of a K^+ channel in a cell excised (inside out) basolateral membrane patch of a rectal gland cell. Pipette KCl, bath (cytosolic side) NaCl (Table 1). *Upper panel* shows original recording at high time resolution. The clamp potential was −60 mV. It refers to the bath with respect to the pipette interior. 0 → indicates the zero current level. Channel openings in the downward direction indicate K^+ flow from the pipette (extracellular side) into the bath. The *dotted lines* correspond to the substates at −3.8 pA and −9.0 pA. *Lower panel* left side: current amplitude histogram of this recording. The *dotted curves* were obtained by Gaussian fits. Note the two main peaks at the zero current level (baseline noise) and at the fully open state. In addition, two shallow peaks at −3.8 pA and −9.0 pA are apparent, corresponding to the sublevels. *Lower panel* right side: open and closed time histograms of this channel. The sample interval was 0.25 ms. The 3 dB point of the Bessel filter was 2 kHz. The *solid curves* were obtained by least square fits to corresponding exponential equations. The open time histogram could be fitted by a single exponential, yielding a time constant *t1* of 3.5 ms. The closed time histogram could be fitted by a double exponential, yielding two time constants *t1* and *t2* of 1 ms and 3.1 ms, respectively. The long interburst pauses (cf. single channel recording in Figs. 1 and 2) were too infrequent to permit a histogram analysis of the time constants of these gaps

closed-time histograms. With this procedure, the small subconductance levels, according to their relative infrequency, were ingnored, and the larger, but very infrequent, substate was considered to be a fully open state [3, 25, 27]. A typical analysis is shown in the lower panel of Fig. 3. For the open state, a single time constant of 3.5 ms was obtained, whereas for the closed state, two time constants of 1 ms and 3.1 ms were obtained. The long gaps between bursts (cf. Figs. 1 and 2) would probably yield yet a third time constant [1, 2, 25]. However, their appearance was too infrequent to allow for a histogram analysis. As the time histograms were similar in all three series of experiments, the data were pooled. Since two operational channels were present in many patches, the mean values refer to 8 experiments in which only one active channel was present. The open time-constant was 3.0 ± 0.2 ms, the first closed time-constant was 0.7 ± 0.2 ms and the second closed time-constant was 2.8 ± 0.5 ms. These results indicate that the K^+ channel observed in this study has at least 4 functional states: 1 open state and 3 closed states (including the interburst state).

Discussion

The present study focusses on the ionic channels in the basolateral membrane of the rectal gland of the dogfish. In this epithelium, microelectrode experiments indicate the presence of only one ionic conductance, namely that for potassium [12–14]. A previous report [15] utilizing the patch clamp technique, has established that only K^+ channels are present in the basolateral membrane of this epithelium, and that these K^+ channels are demonstrable in both secreting (hormonally stimulated) and in resting cells [15]. In the present study we aimed to define this channel more closely in terms of its ionic selectivity, ionic unitary conductance and kinetic appearance and in its rectifying properties.

The first series of experiments, obtained in the cell-attached mode, indicate that this channel permits K^+ efflux from the cell under physiological conditions. In this sense the channel serves as the pathway for K^+ recycling, as we have previously identified using intracellular electrical measurements [12–14]. In excised patches the channel apparently functions symmetrically in as much as it allows K^+ fluxes in both directions depending on the K^+ concentration gradient. In addition, the current pattern (kinetic appearance) is not distinguishable for cell attached patches (NaCl or KCl in the pipette) and for excised patches (inward and outward currents). This apparent symmetry of the channel is probably only true for the experimental situation described thus far. If the pipette solution consisted of KCl in cell-attached patches (Fig. 1, lower half), we were unable to record "normal" K^+ currents from the cytosolic side to the extracellular side. These results indicate that this channel functions as an inward rectifier (permitting only inward K^+ currents) when exposed to symmetrical high K^+ solutions. This rectification can be caused either by the presence of high K^+ on both sides, or by the absence of Na^+ on the *trans* side. The mechanism, however, is thus far unknown. It is important to recall, however, that such behavior was not observed if a K^+-concentration gradient was present across the cell membrane. Specifically, this channel functions perfectly well as an outward conductor if the K^+ concentration is high on the cytosolic side and K^+ is low on the outside (Figs. 1 and 2), as it is the case under physiological conditions. In intact cells, and more specifically in the rectal gland cell, it has been shown [13] that inhibition of the basolateral (Na^+ + K^+)-pump leads to concomitant depolarization and also to a reduction in the basolateral K^+ conductance. The present experiments make it seem unlikely that this effect is mediated by the membrane voltage. (1) As a consequence of a Goldman type of rectification, the single channel conductance increases with depolarization (Fig. 1). (2) We were unable to show any marked voltage dependence of the open state probability in the physiological voltage range (data not shown).

The current-voltage relation reported here allows conclusions with respect to the selectivity of potassium over that for sodium. It is clearly apparent that in cell-free patches this channel is highly selective for potassium. Even at high driving forces favoring sodium currents, such currents were not observed (Fig. 2). In the succeeding report we shall provide evidence that this channel is also poorly conductive to and even blocked by Rb^+ [8].

The kinetic appearance of this channel, with burst phases interrupted by flickering to the closed state and with long interburst pauses, is similar to that observed in K^+ channels of other tissues [5, 19, 22, 25, 26]. Specifically, the K^+ channel observed by us in the basolateral membrane of the proximal tubule of the rabbit has an almost identical kinetic appearance [5]. Bursting behaviour, interrupted by long gaps between bursts, can be explained by binding of agents to the channel protein, leading to activation of the channel. Such agents can be neurotransmitters, as in the case of acetylcholine-activated channels [3], or it can be Ca^{2+} ions in Ca^{2+} dependent K^+ channels [22, 23]. The K^+ channel described in this study is probably not Ca^{2+} activated [8]. Factors which activate and regulate this channel are unknown at present. The existence of several closed time-constants as well as the presence of sublevels indicate that the channel protein may exist in several configurations. At present, this complexity prohibits simple kinetic models.

We can estimate the number of K^+ channels per rectal gland cell and also their density per unit area. Using our previously published K^+ current across the basolateral membrane [12], the cross-sectional area of the cell and the single channel current multiplied by the mean open probability of about 50%, we arrive at a number of some 2,000 K^+ channels per cell. Assuming now that the real area of basolateral membrane is 10–30 times larger than the cross-sectional area, we arrive at a channel density of 0.2–0.6 channels per μm^2. Using the size of our patch pipettes, and the corresponding membrane area of 1.5–3 μm^2, we predict a frequency of 0.3–1 K^+ channel per patch. This accords with what was found in the present and in a previous report [15].

Finally, this K^+ channel should be compared to other K^+ channels. It is obvious that the usual "fingerprinting" using the unitary conductance is of very limited value. Table 2 clearly indicates that, irrespective of the experimental conditions, this channel has a low conductance at physiological voltages, but an eight times higher conductance in the linear range of the current-voltage curve. A similar conclusion has been deduced for the K^+ channel present in the basolateral membrane of submandibular salivary secretory cells [4]. The P_K values are voltage-independent and allow for ready comparison. Under three experimental states tested here (Table 2), very similar P_K values of about $0.25 \cdot 10^{-12}$ cm^3/s have been determined. This value is also very similar to that reported for K^+ channels in other tissues [1, 4, 26].

In conclusion, the present study provides evidence for a potassium-selective channel in the basolateral membrane of the rectal gland cell. This channel has a permeability to K^+ of $0.25 \cdot 10^{-12}$ cm^3/s and it permits K^+ outward and inward currents. It is highly selective for K^+ over Na^+. A subsequent study describes potential regulatory mechanisms of this channel as well as its inhibitors [8].

Acknowledgement. The authors acknowledge gratefully the assistance by Jörg Dreinhöfer and Vinzenz and Walter Greger.

References

1. Benhan CD, Bolton TB, Lang RJ, Takewaki T (1986) Calcium-activated potassium channels in single smooth muscle cells of rabbit jejunum and guinea-pig mesenteric artery. J Physiol 371:45–67
2. Coloquhoun D, Sakmann B (1983) Burst of openings in transmitter-activated ion channels. In: Sakmann B, Neher E (eds) Single-channel recording. Plenum Press, New York London, pp 345–364
3. Coloquhoun D, Sakmann B (1985) Fast events in single-channel currents activated by acetylcholine and its analogues at the frog muscle end-plate. J Physiol 369:501–557
4. Gallacher DV, Morris AP (1986) A patch-clamp study of potassium currents in resting and acetylcholine-stimulated mouse submandibular acinar cells. J Physiol 373:379–395
5. Gögelein H, Greger R (1984) Single channel recordings from basolateral and apical membranes of renal proximal tubules. Pflügers Arch 401:424–426
6. Gögelein H, Greger R (1986) Na^+ selective channels in the apical membrane of rabbit late proximal tubules (pars recta). Pflügers Arch 406:198–203
7. Gögelein H, Greger R (1986) A voltage-dependent channel in the basolateral membrane of late proximal tubules of the rabbit kidney. Pflügers Arch 407 (Suppl 2):S142–S148

8. Gögelein H, Greger R, Schlatter E (1987) Potassium channel in the basolateral membrane of the rectal gland of *Squalus acanthias*. Regulation and inhibitors. Pflügers Arch 409:107–113
9. Gögelein H, Schlatter E, Greger R (1987) The "small" conductance chloride channel in the luminal membrane of the rectal gland of the dogfish (*Squalus acanthias*). Pflügers Arch 409:122–125
10. Greger R, Gögelein H (1986) Role of K^+ conductive pathways in the nephron. Kidney Int (in press)
11. Greger R, Hampel W (1981) A modified system for in vitro perfusion of isolated renal tubules. Pflügers Arch 189:175–176
12. Greger R, Schlatter E (1984) Mechanism of NaCl secretion in the rectal gland of spiny dogfish (*Squalus acanthias*). I. Experiments in isolated in vitro perfused rectal gland tubules. Pflügers Arch 402:63–75
13. Greger R, Schlatter E (1984) Mechanism of NaCl secretion in rectal gland tubules of spiny dogfish (*Squalus acanthias*). II. Effects of inhibitors. Pflügers Arch 402:364–375
14. Greger R, Schlatter E, Wang F, Forrest JN (1984) Mechanism of NaCl secretion in rectal gland tubules of spiny dogfish (*Squalus acanthias*). III. Effects of stimulation of secretion by cyclic AMP. Pflügers Arch 402:376–384
15. Greger R, Schlatter E, Gögelein H (1985) Cl^--channels in the apical cell membrane of the rectal gland "induced" by cAMP. Pflügers Arch 403:446–448
16. Greger R, Schlatter E, Gögelein H (1987) Chloride channels in the luminal membrane of the rectal gland of the dogfish (*Squalus acanthias*). Properties of the "larger" conductance channel. Pflügers Arch 409:114–121
17. Hamill OP, Marty A, Neher E, Sakmann B, Singworth FJ (1981) Improved patch-clamp technique for high resolution current recording from cells and cell-free membrane patches. Pflügers Arch 391:85–100
18. Heintze K, Stewart CP, Frizzell FR (1983) Sodium-dependent chloride secretion across rabbit descending colon. Am J Physiol G357–G365
19. Hunter M, Lopes AG, Boulpaep EL, Giebisch GH (1984) Single channel recordings of calcium-activated potassium channels in the apical membrane of rabbit cortical collecting tubules. Proc Natl Acad Sci USA 81:4237–4239
20. Kazachenko VN, Geletynk VI (1984) The potential-dependent K^+ channel in molluscan neurons is organized in a cluster of elementary channels. Biochim Biophys Acta 773:132–142
21. Mandel KG, Dharmsathaphorn K, McRoberts JA (1986) Characterization of a cyclic AMP-activated Cl^--transport pathway in the apical membrane of a human colonic epithelial cell line. J Biol Chem 261:704–712
22. Methfessel C, Boheim G (1982) The gating of single calcium-dependent potassium channels is described by an activation/blockade mechanism. Biophys Struct Mech 9:35–60
23. Moczydlowski E, Latorre R (1983) Gating kinetics of Ca^{2+}-activated K^+ channels from rat muscle incorporated into planar lipid bilayers. J Gen Physiol 82:511–542
24. Sakmann B, Trube G (1984) Conductance properties of single inwardly rectifying potassium channels in ventricular cells from guinea-pig heart. J Physiol 347:641–657
25. Sakmann B, Trube G (1984) Voltage-dependent inactivation of inward-rectifying single-channel currents in the Guinea-pig heart cell membrane. J Physiol 347:659–683
26. Sakmann B, Norma A, Trautwein W (1983) Acetylcholine activation of single muscarinic K^+ channels in isolated pacemaker cells of the mammalian heart. Nature 303:250–253
27. Sauve R, Roy G, Payet D (1983) Single channel K^+ currents from HeLa cells. J Membr Biol 74:41–49
28. Shuttleworth TJ, Thorndyke MC (1984) An endogenous peptide stimulates secretory activity in the elasmobranch rectal gland. Science 225:319–321
29. Welsh MJ (1983) Intracellular chloride activities in canine tracheal epithelium. J Clin Invest 71:1392–1401

Received July 4, 1986/Accepted January 5, 1987

Pflügers Arch (1987) 409:107–113

Pflügers Archiv
European Journal of Physiology
© Springer-Verlag 1987

Potassium channels in the basolateral membrane of the rectal gland of *Squalus acanthias**

Regulation and inhibitors

Heinz Gögelein[1,2], Rainer Greger[2,3], and Eberhard Schlatter[2,3]

[1] Max-Planck-Institut für Biophysik, Kennedyallee 70, D-6000 Frankfurt, Federal Republic of Germany
[2] Mount Desert Island Biological Laboratory, Salsbury Cove, ME 04622, USA
[3] Lehrstuhl II Physiologie, Hermann-Herder-Strasse 7, D-7800 Freiburg, Federal Republic of Germany

Abstract. The present study examines the influences of pH and Ca^{2+} and several putative inhibitors on the basolateral K^+ channel of the rectal gland of *Squalus acanthias*. Excised membrane patches were examined using the patch clamp technique. It is shown that reduction of the calcium activity on the cytosolic side to less than 10^{-9} mol/l has no detectable inhibitory effect on this channel. Conversely, increase in calcium activity to some 10^{-3} mol/l reduced the activity of this channel. Variations in cytosolic pH had only a moderate effect on the current amplitude: alkalosis by one pH unit increased and acidosis reduced the single current amplitude by some 15%. Several inhibitors were tested in excised patches when added to the cytosolic side. Ba^{2+} ($\approx 5 \cdot 10^{-3}$ mol/l), quinine ($\approx 10^{-3}$ mol/l), quinidine ($\approx 10^{-4}$ mol/l), lidocaine (≈ 1 mmol/l), tetraethylammonium (≈ 10 mmol/l), Cs^+ (≈ 10 mmol/l), and Rb^+ (≈ 20 mmol/l) all blocked this K^+ channel reversibly. We conclude that the basolateral K^+ channel of the rectal gland is distinct from other epithelial K^+ channels inasmuch as it is not stimulated by Ca^{2+} directly, but that it is qualitatively similar to many other known K^+ channels with respect to its sensitivity towards blockers.

Key words: Rectal gland – K^+ channel – Rb^+ – Ca^{2+}-regulation – Patch clamp

Introduction

In the preceding report [13] we have described the properties of a K^+ channel present in the basolateral membrane of rectal gland cells. In the present study we aimed to analyse the influence of known regulatory factors of K^+ conductive pathways, namely cytosolic calcium activity and cytosolic pH. In addition, we examined the question whether this channel, like the K^+ conductance of the basolateral membrane [10], was inhibited by known blockers of K^+ conductive pathways in other epithelia, such as Ba^{2+} [23], tetraethylammonium [32], Cs^+ [44], quinine and quinidine [31], lidocaine [34], and Rb^+ [33]. The rectal gland of the dogfish (*Squalus acanthias*) was chosen since it represents a model for chloride secretory epithelia such as trachea and colon, and has a major experimental advantage in that both cell membrane are accessible for patch clamp measurements in the in vitro perfused gland segment [7] without pretreatment. The present results indicate that this K^+ channel is not inactivated at low cytosolic calcium activities and, moreover, is only slightly affected by cytosolic pH. All tested inhibitors were able to block this channel reversibly.

* This study was supported by Deutsche Forschungsgemeinschaft Gr 480/8 and by NSF and NIH grants to the Mount Desert Island Biological Laboratory
Offprint requests to: R. Greger

Methods

Experiments were performed in isolated in vitro perfused tubules [9] of the rectal gland of *Squalus acanthias*. Data from hormonally stimulated and resting glands have been pooled since no differences in the properties of excised K^+ channels in the two settings were observed previously [12, 13]. The methods of in vitro perfusion have been described in detail elsewhere [8]. Also the method to obtain recordings of individual channels and the methods of data analysis have been provided in the preceding report [13]. Briefly, individual tubules of rectal glands were dissected manually and perfused with a pipette inserted into the lumen [9]. The free and open end of the tubule segment was approached by a patch pipette at the edge, in order to obtain a basolateral membrane patch [6]. After gigaseal formation and appearance of a K^+ channel, the membrane patch was excised, and single channel currents were examined in response to variations in the composition of the bath. Since the way in which these patches were obtained leads to the inside out configuration [13, 16], the cytosolic side of the channel was exposed to the bath solution. The pipette solution was either NaCl shark Ringer or a high K^+ solution. The composition of the solution is given in Table 1. Ca^{2+} activities were calculated from a simple equation [28] taking into account the concentrations of Mg^{2+}, Ca^{2+}, and EGTA. The Ca^{2+} activity was also measured with Ca^{2+} selective electrodes calibrated with standard solutions, and the measured Ca^{2+} activity matched reasonably well with the theoretical values. Blockers were added as chloride salts to the KCl-10^{-6} Ca^{2+} solution. The pH of the solutions was adjusted by titration with NaOH: if not stated otherwise, it was 7.5. Chemicals employed were of highest available grade of purity, and were obtained from Sigma (St. Louis, MO, USA). The data are shown as original recordings. Mean values ± SEM are provided for the experimental series.

Results

Effects of variations of cytosolic free calcium concentration

Figure 1 shows two experiments in which the pipette was filled with NaCl solution (NaCl, Table 1) and the bath

Table 1. Composition of solutions. Concentrations in mmol/l

Abbreviation	Na^+	K^+	Rb^+	Ca^{2+}	Mg^{2+}	Cl^-	Hepes	D-glucose	Urea	EGTA
NaCl	275	4	0	2.5	3.0	285	10	5	350	0
KCl-10^{-3} Ca^{2+}	5	274	0	1.0	3.0	282	10	5	350	0
KCl-10^{-6} Ca^{2+}	7	274	0	0.97	3.01	282	10	5	350	1
KCl-10^{-7} Ca^{2+}	7	274	0	0.74	3.09	282	10	5	350	1
KCl-Ca^{2+} free	15	274	0	0	3.0	280	10	5	350	5
RbCl-10^{-6} Ca^{2+}	7	0	274	0.97	3.01	282	10	5	350	1

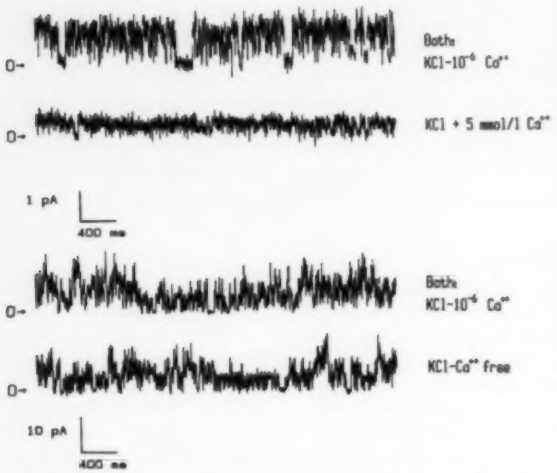

Fig. 1. Effect of Ca^{2+} on K^+ channels in a cell excised (inside out) patches of the basolateral membrane of rectal gland cells. Pipette NaCl, bath KCl-10^{-6} Ca^{2+}. The *upper panel* shows the effect of high Ca^{2+} concentration. Clamp potential 0 mV. 0 → indicates the zero current level. Channel openings in the upward direction indicate K^+ flow from the bath (cytosolic side) into the patch pipette, driven by the chemical gradient of K^+. Note the marked and reversible decrease in single channel amplitude at 5 mmol/l Ca^{2+}. The *lower panel* examplifies the lack of effect of Ca^{2+} free solutions. The clamp potential was 0 mV. 0 → indicates the zero current level. Channel openings in the upward direction indicate K^+ flow from the bath (cytosolic side) into the patch pipette, driven by the chemical gradient of K^+. Up to three channels are open simultaneously in this experiment. Note that the Ca-free solution did not change the channel activity significantly

Fig. 2. Effect of pH on K^+ channels in a cell excised (inside out) patch of the basolateral membrane of a rectal gland cell. Pipette NaCl, bath KCl-10^{-6} Ca^{2+}, clamp potential 0 mV. 0 → indicates the zero current level. Channel openings in the upward direction indicate K^+ flow from the bath (cytosolic side) into the patch pipette, driven by the chemical gradient of K^+. Changing the bath solution (cytosolic side) from pH = 7.5 to pH = 5, reduced the single channel current from 1.5 pA to 0.8 pA. An increase of bath pH to 8.8 slightly increased the single channel current to 1.9 pA. The pH effects were entirely reversible. The open state probability was about 0.7 under all experimental conditions

contained the KCl solution (KCl-10^{-6} Ca^{2+}, Table 1). This figure shows K^+ outward currents (directed from the bath into the pipette), driven by the chemical gradient for potassium. At 10^{-6} mol/l of Ca^{2+} one K^+ channel is fairly active. The channel activity was reduced strongly when calcium activity was increased to 5 mmol/l. This inhibitory effect of calcium was fully reversible. In the five experiments of this series, a marked inhibition was seen at 10^{-3} mol/l, while a variable degree of inhibition was found at 10^{-5} and 10^{-4} mol/l (data not shown). Therefore, these K^+ channels are not activated by moderate increases in calcium activity, but are even inhibited at very high Ca^{2+} activities. A similar inhibition of single K^+ channels by Ca^{2+} was reported in Ca^{2+} activated K^+ channels from rabbit muscle, incorporated into planar bilayers [35]. The effects of a reduction of Ca^{2+} activity is shown in the lower half of this figure.

The control recording (trace 3) shows 3 discrete current levels. When the bath was rinsed for 5 min (bath exchange rate greater than 10 times/min) with a solution with a free Ca^{2+} concentration of less than 10^{-9} mol/l (NaCl-Ca^{2+} free, Table 1), K^+ channel activity remained unaltered. This experiment was repeated 6 times. In all experiments, exposure to the calcium free solution had no significant influence on the open probability or on current amplitude. These data are in sharp contrast to many previously described Ca^{2+} activated K^+ channels, in which channel activity is markedly reduced when cytosolic free Ca^{2+} is decreased [27]. This anomalous reaction to calcium prompted us to test another likely modulator of the K^+-channel, namely cytosolic pH.

pH effects

Figure 2 shows an experiment in which bath pH was reduced from 7.5 to 5.0 and increased to 8.8. The patch was excised, the pipette was filled with NaCl, the bath contained KCl solution and the clamp voltage was 0 mV under all conditions. It is apparent that pH changes alter the current amplitude for a given driving force. Acid pH reduced (27% per unit pH), while alkaline pH increased (27% per unit pH) the single channel current. Changes in pH had no influence on the open state probability. The effects of pH, however, were not very marked if one considers the expected physiological changes in cytosolic pH. In four comparable experi-

Fig. 3. Effect of barium on K^+ channels in a cell excised (inside out) patch of the basolateral membrane of a rectal gland cell. Pipette KCl-10^{-6} Ca^{2+}, bath NaCl (Table 1). Clamp potential: 0 mV. 0 → indicates the zero current level. Channel openings in the downward direction indicate K^+ flow from the pipette (extracellular side) into the bath, driven by the chemical gradient of K^+. Addition of 0.4 mmol/l of $BaCl_2$ increases the gaps between the bursts (*middle traces*) without affecting significantly the single channel current. As a consequence, the open state probability decreased from 0.6 (bath NaCl, no Ba^{2+}) to 0.2 (bath NaCl + 0.4 mmol/l Ba^{2+}). 5 mmol/l Ba^{2+} in the bath completely abolished the channel activity. These effects were completely reversible

ments, a mean change of current amplitude of about 15% per unit pH was obtained.

Effects of blockers

Next we examined the effects of putative K^+ channel blockers. Our intention was not to examine the blocker kinetics, i.e. to describe the mechanism of blocking, but rather to test whether this K^+-channel which is different from other K^+ channels with respect to its sensitivity to Ca^{2+}, was also different with respect to its sensitivity towards known blockers. Therefore, most experiments were performed only at one clamp voltage, chosen to maximize the sensitivity of the experiment. Figure 3 shows an experiment in which the pipette was filled with KCl-10^{-6} Ca^{2+} solution (Table 1), and in which the bath contained NaCl (Table 1). The inward (to the cytosolic side) K^+ concentration gradient resulted in negative (downward) current events through the single channels. The addition of 0.4 mmol/l barium to the bath (cytosolic side) led to a marked reduction in the open state probability of this K^+ channel (from 0.62 to 0.2). When 5 mmol/l barium was added this led to a complete and (not shown) reversible inhibition. In three comparable experiments, identical observations have been made. Complete inhibition required some 2−5 mmol/l Ba^{2+}. Thus, barium is able to block K^+ inward current from the cytosolic side. The effect of barium appeared to result in an increase in the silent periods (gap time) between the bursts. In five other experiments NaCl (Table 1) was present in the pipette, and KCl-10^{-6} Ca^{2+} (Table 1) in the bath, and the effect of cytosolic barium on K^+ outward current was examined. Three mmol/l Ba^{2+} led to a partial and reversible inhibition of the K^+ outward current (at 0 mV clamp potential) (results not shown). Again, the effect of barium affected gap times between the bursts. Similar effects of Ba^{2+} block, namely decrease of channel open probability without an effect on the single channel current, have been observed in K^+ channels in other tissues [1, 18, 20, 35].

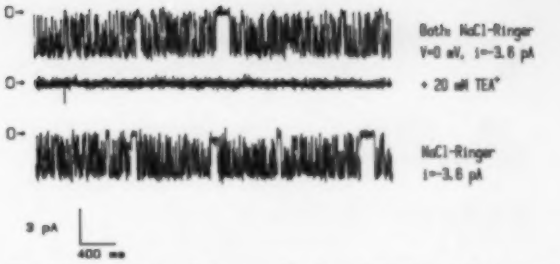

Fig. 4. Effect of tetraethylammonium ions (TEA^+) on K^+ channels in a cell excised (inside out) patch of the basolateral membrane of a rectal gland cell. Pipette KCl, bath NaCl (Table 1), clamp potential 0 mV. 0 → indicates the zero current level. Channel openings in the downward direction indicate K^+ flow from the pipette (extracellular side) into the bath, driven by the chemical potential of K^+. 20 mmol/l TEA^+ abolished the channel activity completely. The effects were completely reversible. The respective single channel currents are given at the right side of the traces

Tetraethylammonium (TEA^+), like other quarternary amines, blocks K^+ channels in other epithelial membranes [4, 32]. A typical experiment, using TEA^+, is shown in Fig. 4. The pipette was filled with KCl-10^{-6} Ca^{2+} (Table 1), and the bath contained NaCl solution. An inward current (from the pipette into the bath), at 0 mV clamp voltage, driven by the K^+ concentration gradient, was observed. Addition of tetraethylammonium to the cytosolic side abolished all channel activity. The effect of tetraethylammonium was entirely reversible. Tetraethylammonium also blocked K^+ outward currents. In five experiments we confirmed the findings shown in Fig. 4. Notably, low concentrations of tetraethylammonium caused an effect exclusively on the current amplitude. This effect of tetraethylammonium on the current amplitude has been reported for other K^+ channels [2, 19, 30, 36, 42].

Next we examined the effect of quinine and quinidine. Whereas the effect of these compounds is difficult to interpret in intact epithelial cells, because the effect on Ca^{2+}-channels [41] may be superimposed on a direct effect on K^+ channels, no such complication was expected for excised membrane patches. Figure 5 shows a typical experiment for quinidine. The pipette was filled with NaCl (Table 1) and the bath contained KCl-10^{-6} Ca^{2+} (Table 1). At 0 mV clamp voltage a K^+ outward current (from the bath into the pipette) was observed. At a concentration of 0.1 mmol/l quinidine inhibited this channel activity due to an increase in the interburst times. It had no effect on the current amplitude. The effect was fully reversible. In a series of 5 experiments quinidine inhibited almost completely at 10^{-3} mol/l ($n = 2$), whereas the effect at 10^{-4} mol/l was only partial ($n = 3$).

The related compound quinine was also tested on K^+ outward and inward currents. In the three experiments performed, 10^{-4} mol/l slightly increased the interburst gaps, but 10^{-3} mol/l inhibited the single channel current completely and reversibly (data not shown). A decrease of single channel open state probability by quinidine or quinine was reported for K^+ channels in other tissues [4, 14, 20].

We also determined whether this K^+ channel was blocked by lidocaine, a substance that has been suggested to act on the basolateral K^+ channel in the tadpole skin [34].

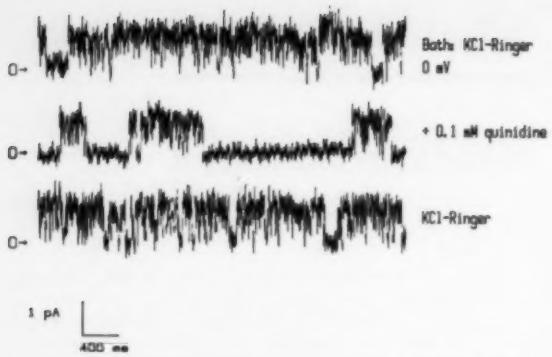

Fig. 5. Effect of quinidine on K^+ channels in a cell excised (inside out) patch of the basolateral membrane of a rectal gland cell. Pipette NaCl, bath KCl-10^{-6} Ca^{2+} (Table 1). Clamp potential 0 mV. 0 → indicates the zero current level. Channel openings in the upward direction indicate K^+ flow from the bath (cytosolic side) into the patch pipette, driven by the chemical gradient of K^+. Addition of 0.1 mmol/l quinidine to the bath increased the intra-burst gaps (*second trace*), leading to a decrease of the open state probability from 0.7 (bath no quinidine) to 0.4 (bath 0.1 mmol/l quinidine). The effect was completely reversible (*lowest trace*)

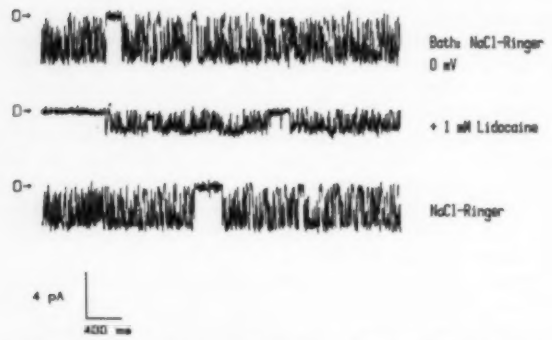

Fig. 6. Effect of lidocaine on K^+ channels in a cell excised (inside out) patch of the basolateral membrane of a rectal gland cell. Pipette KCl-10^{-6} Ca^{2+}, bath NaCl (Table 1). Clamp potential 0 mV. 0 → indicates the zero current level. Channel openings in the downward direction indicate K^+ flow from the pipette (extracellular side) into the bath, driven by the chemical gradient of K^+. Addition of 1 mmol/l lidocaine to the bath (*middle trace*) decreased the single channel current from −3.6 pA (bath no lidocaine) to −1.2 pA (bath 1 mmol/l lidocaine). The effect was completely reversible (*lowest trace*)

Figure 6 shows an experiment in which lidocaine was tested on single channel K^+ inward current. A strong reduction of current amplitude was reached by 1 mmol/l lidocaine and the effect was fully reversible. In this series of 3 experiments, we tested $10^{-4}-10^{-2}$ mol/l of lidocaine. The concentration of 10^{-3} mol/l led to a partial inhibition, 10^{-4} mol/l was devoid of effect, and 10^{-2} mol/l led to a complete inhibition. The effect of lidocaine is, therefore, comparable to that of tetraethylammonium (see above).

Selectivity. The selectivity of this channel to Na^+ [13] suggested that, even with a fairly high conductance, it could discriminate well between the monovalent alkali metal cations. Therefore, we examined the permeability of this channel to Cs^+ and to Rb^+. Cs^+ was added to the cytosolic side at 5–10 mmol/l. Partial and reversible inhibition of K^+ channel activity was observed at this concentration in 3 out of 4 experiments (data not shown).

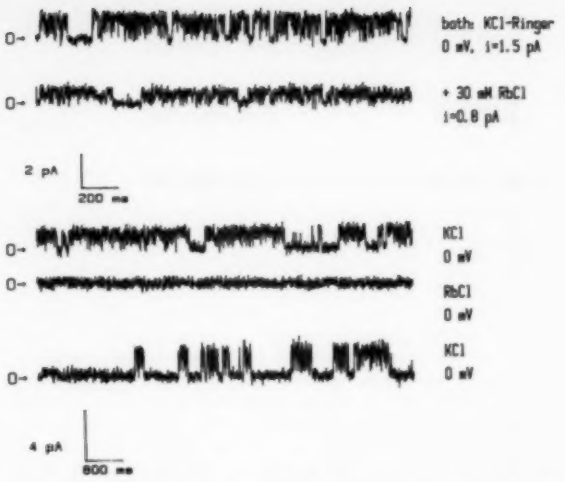

Fig. 7. Effect of rubidium on single K^+ channels in a cell excised (inside out) patch of the basolateral membrane of a rectal gland cell. Pipette NaCl, bath KCl-10^{-6} Ca^{2+} (Table 1). Clamp potential 0 mV. 0 → indicates the zero current level. Channel openings in the upward direction indicate K^+ flow from the bath (cytosolic side) into the pipette, driven by the chemical potential of K^+. Addition of 30 mmol/l RbCl to the bath, reduced the single channel current reversibly. The *lower panel* shows a typical experiment in which bath KCl-10^{-6} Ca^{2+} (*upper trace*) was replaced by RbCl-10^{-6} Ca^{2+} (cf. Table 1) solution. No significant single channel current is detectable in presence of bath RbCl. The effect is reversible

The effect of Rb^+ is shown in Fig. 7. The pipette was filled with NaCl solution and the bath consisted of KCl-10^{-6} Ca^{2+} (Table 1). The addition of 30 mmol/l Rb^+ to the KCl-10^{-6} Ca^{2+} solution, reduced the single channel amplitude to 0.8 pA. The inhibition by Rb^+ was fully reversible. The lower panel of this figure shows an experiment in which the cytosolic solution was changed from KCl-10^{-6} Ca^{2+} to RbCl-10^{-6} Ca^{2+} (Table 1). The positive current carried by K^+ was absent in the presence of Rb^+. Even at pipette negative voltages, no Rb^+ current could be generated through this channel. Therefore, Rb^+ is even an inhibitor of the K^+ current at lower concentrations. Both kinds of experiments were performed three times, and the results were identical to that shown in Fig. 7. Comparable observations, namely that Rb^+ does not conduct current through single K^+ channels, has been reported previously for the salivary gland [5], and we (unpublished observation) have also shown that the K^+ channel of MDCK cells did not conduct Rb^+ and was blocked by this ion. The present studies demonstrate that the RGT K^+ channel distinguishes between K^+ and other monovalent alkali-cations (Na^+, Rb^+, and Cs^+). Rb^+ blocks the channel, Cs^+ has less of an inhibitory effect, and Na^+, though not permeating, does not inhibit.

Finally, we tested several agents known to inhibit conductance to other ions to determine whether they

affected the basolateral K^+ channel in the rectal gland. No inhibitory action of chloride channel blockers of the phenylalkylaminobenzoic acid type, previously reported by this laboratory [39], was observed. In addition, we studied the effect of ouabain since it has been reported to inhibit K^+ conductance of the basolateral membrane in this and in other tissues [9, 22, 37]. There was no effect on single K^+ channels in the rectal gland in concentrations up to 1 mmol/l. Finally, and entirely expectedly, amiloride ($\leqslant 10^{-3}$ mol/l) and the stilbene derivative SITS ($\leqslant 10^{-3}$ mol/l) were without effect.

Discussion

To "fingerprint" a given channel, many different experiments are required and one might argue that we have examined several K^+ channels of different properties in the present study. This is not likely since all the channels we have described have very similar properties in terms of their current amplitude, their K^+ selectivity, as well as their kinetical appearance [also cf. ref. 13]. Furthermore, we have attempted (and succeeded) to test most of the above maneuvres consecutively in the same channel. Therefore, our conclusion that this K^+ channel is sensitive to known blockers but not to other agents such as Ca^{2+}, rests not only on unpaired but also on paired observations. Specifically, we are certain that different types of blockers all act on the same channel.

The K^+ channel in the basolateral membrane of the rectal gland serves to recycle this ion after its uptake by the $Na^+2Cl^-K^+$ carrier and by the $(Na^+ + K^+)$-ATPase [9]. In this respect, this channel is similar to the K^+ channel in a variety of epithelia, and, more specifically, to that of exocrine glands such as that present in pancreas, in trachea and in the colon [17, 27, 40]. For some of these channels it has been shown directly, or has been postulated, that the cytosolic Ca^{2+} activity regulates the open probability of the K^+ channel [27, 40]. In fact, in exocrine glands such as the salivary glands and pancreas it has been shown that the rate of Na^+Cl^--secretion is primarily regulated by the K^+ channel [21]. Inasmuch as the K^+ channel opens in response to the increased cytosolic (messenger) Ca^{2+} concentration, the cell hyperpolarizes and increases its driving force for a passive chloride exit via the apical chloride channel. We have postulated that the situation is quite different in the rectal gland of the dogfish [12, 13]. We have shown that the primary event in this gland is the "opening" of chloride channels [12]. In accordance with this discrepancy to other excretory glands, the K^+ channel, identified here by the patch clamp technique, is not activated directly by increases in cytosolic calcium activity. Reductions to less than 10^{-9} mol/l had no detectable effect on the open probability of this channel. In fact, we have made a rather surprising observation; namely that high Ca^{2+} activities on the cytosolic side reduced the open probability of this channel. Significant reductions in the open probability were observed at 10^{-4} mol/l and higher activities. It is not very likely that cytosolic activities of calcium as high as 10^{-4} mol/l will occur physiologically. On the other hand, we have thus far not examined in detail the effects of intermediate calcium activities ($10^{-6}-10^{-5}$ mol/l). After inhibition of the $(Na^+ + K^+)$-ATPase, high cytosolic calcium activities are expected [38]. These high activities of calcium could be responsible for the observed inhibition of the K^+ conductance [10]. Therefore, the K^+ channel in the rectal gland appears to function differently from that observed in other cells, and specifically from that present in several other exocrine glands.

For many K^+ channels it has been postulated that they are modulated by cytosolic and/or by extracellular pH. It was concluded from such experiments that alkalinization increases and that acidification reduces the K^+ conductance [15, 24–26]. The present results examine this issue more rigorously then in previous studies since the pH was controlled on the cytosolic side. The effects observed here are qualitatively similar to that reported in intact cells. However, the effects are small when considered in quantitative terms. We have observed a reduction/increase in the current amplitude by some 15% when the pH was acidified/alkalinized by one unit. As cytosolic pH is well regulated and will deviate much less than one unit from the systemic pH [3, 43] it is likely that cytosolic pH plays only a minor role in the direct regulation of the K^+ channel in the rectal gland. In the intact cell, alterations in pH may exert effects on the K^+ conductance by indirect mechanisms.

Up to this point it should be evident that this K^+ channel, unlike other epithelial K^+ channels, is not strongly regulated either by cytosolic Ca^{2+} or by cytosolic pH. Thus, it is pertinent to ask whether this K^+ channel is unique and different in behaviour from other K^+ channels in yet other aspects. Therefore, we employed putative blockers, and were rather surprised to find that they all inhibited the single K^+ channels in the rectal gland. In fact, fingerprinting of the K^+ channel by its sensitivity to some, but not to other blockers, proved unsuccessful. TEA^+, quinidine, quinine, Ba^{2+} and lidocaine all were inhibitors. The sensitivity towards TEA^+ and lidocaine was rather poor, which in the case of TEA is not surprising as it is supposed to act from the extracellular side. Ba^{2+}, quinine and quinidine were more effective.

With respect to the possible effect of Rb^+ we were aware of previous data in excretory glands where it has been claimed that Rb^+ binds so tightly to K^+ channels that a Rb^+ current is not conducted [5]. We were quite surprised to find that, in the rectal gland K^+ channel, Rb^+ was not conducted, confirming the above model of Rb^+ action. In addition, we demonstrated that Rb^+ even blocks single K^+ channel currents in the basolateral membrane of rectal gland at 10–30 mmol/l. This leads to the conclusion that the K^+ channel in the rectal gland is highly selective for K^+. In extension this finding indicates that Rb^+ fluxes do not necessarily reflect corresponding K^+ fluxes in this tissue. In other words, Rb^+ is not useful as a tracer for K^+ fluxes through this type of K^+ channel, especially if Rb^+ is used at a concentration where it may block K^+ channels.

Finally, we attampted to compare the K^+ channel described in this study to that in other cells. We have found both distinct differences from other K^+ channels, and similarities with respect to sensitivities to inhibitors. From these data one could argue that we have described yet another K^+ channel, implying that there are fundamentally different K^+ channels in the different tissues. On the other hand, one could emphasize the striking similarities. Close inspection of the kinetic appearance of this channel, for example, reveals that major kinetic properties are not distinguishable from that observed for other K^+ channels. The channel is highly selective for K^+ over Na^+, and the single K^+ current appears in phases of activity (bursts). It shows

flickering within the burst phase. Similar kinetic properties were observed in K^+ channels of other tissues [1, 6, 18, 29].

If the present K^+ channel has so many similarities with K^+ channels of other epithelia, why should one observe such striking differences with respect to Ca^{2+} sensitivity, with one K^+ channel being activated by cytosolic Ca^{2+} and the other being insensitive? Obviously, this question is not resolved. Ca^{2+} activated channels, and Ca^{2+} inhibited channels could resemble two entities. Viewed from a functional point, both channels serve the same purpose: they are required for K^+ recirculation across the basolateral membrane and they complement the K^+ uptake systems such as the $Na^+2Cl^-K^+$ carrier as well as the $(Na^+ + K^+)$-ATPase. In the rectal gland, in the trachea, in the colon and probably some other organs, the regulation of secretion is primarily modulating the chloride not the potassium conductance. Conversely, in other exocrine glands, such as the pancreas acinar cell, the primarily regulated ionic channel may very well be that of K^+ [21].

Acknowledgements. The authors are grateful to Prof. Dr. K. J. Ullrich and Prof. Dr. J. Hayslett for their critical comments on the manuscript. We also gratefully acknowledge the technical assistance by Jörg Dreinhöfer, Vinzenz Greger and Walter Greger.

References

1. Benhan CD, Bolton TB, Lang RJ, Takewaki T (1985) The mechanism of action of Ba^{2+}-activated K^+-channels in arterial and intestinal smooth muscle cell membranes. Pflügers Arch 403:120–127
2. Blatz AL, Magleby KL (1984) Ion conductance and selectivity of single calcium-activated potassium channels in cultured rat muscle. J Gen Physiol 84:1–23
3. Boron WF, Boulpaep EL (1983) Intracellular pH regulation in the renal proximal tubule of the salamander. J Gen Physiol 81:29–52
4. Findlay I, Dunne MJ, Ullrich S, Wollheim CB, Petersen OH (1985) Quinine inhibits Ca^{2+}-independent K^+ channels whereas tetraethylammonium inhibits Ca^{2+}-activated K^+ channels in insulin-secreting cells. FEBS Lett 185:1–8
5. Gallacher DV, Maruyama Y, Petersen OH (1984) Patch-clamp study of rubidium and potassium conductances in single cation channels from mammalian exocrine acini. Pflügers Arch 401:361–367
6. Gögelein H, Greger R (1984) Single channel recordings from basolateral and apical membranes of renal proximal tubules. Pflügers Arch 401:424–426
7. Greger R (1985) Application of electrical measurements in the isolated in vitro perfused tubule. Mol Physiol 8:11–22
8. Greger R, Hampel W (1981) A modified system for in vitro perfusion of isolated renal tubules. Pflügers Arch 189:175–176
9. Greger R, Schlatter E (1984) Mechanism of NaCl secretion in the rectal gland of spiny dogfish (*Squalus acanthias*). I. Experiments in isolated in vitro perfused rectal gland tubules. Pflügers Arch 402:63–75
10. Greger R, Schlatter E (1984) Mechanism of NaCl secretion in rectal gland tubules of spiny dogfish (*Squalus acanthias*). II. Effects of inhibitors. Pflügers Arch 402:364–375
11. Greger R, Schlatter E, Wang F, Forrest Jr JN (1984) Mechanism of NaCl secretion in rectal gland tubules of spiny dogfish (*Squalus acanthias*). III. Effects of stimulation of secretion by cyclic AMP. Pflügers Arch 402:376–384
12. Greger R, Schlatter E, Gögelein H (1985) Cl^--channels in the apical cell membrane of the rectal gland "induced" by cAMP. Pflügers Arch 403:446–448
13. Greger R, Gögelein H, Schlatter E (1987) Potassium channels in the basolateral membrane of the rectal gland of the dogfish (*Squalus acanthias*). Pflügers Arch 409:100–106
14. Grygorczyk R, Schwarz W (1985) Ca^{2+}-activated K^+ permeability in human erythrocytes: Modulation and single-channel events. Eur Biophys J 12:57–65
15. Guggino WB, Stanton BA, Giebisch G (1982) Regulation of apical potassium conductance in the isolated early distal tubule of the amphiuma kidney. Biophys J 37:338a
16. Hamill OP, Marty A, Neher E, Sakmann B, Sigworth FJ (1981) Improved patch-clamp technique for high resolution current recording from cells and cell-free membrane patches. Pflügers Arch 391:85–100
17. Heintze K, Steward CP, Frizzell RA (1983) Sodium-dependent chloride secretion across rabbit descending colon. Am J Physiol 244:G357–G365
18. Hunter M, Lopes AG, Boulpaep EL, Giebisch GH (1984) Single channel recordings of calcium-activated potassium channels in the apical membrane of rabbit cortical collecting tubules. Proc Natl Acad Sci USA 81:4237–4239
19. Iwatsuki N, Petersen OH (1985) Action of tetraethylammonium on calcium-activated potassium channels in pig pancreatic acinar cells studied by patch-clamp single-channel and whole-cell current recording. J Membr Biol 86:139–144
20. Iwatsuki N, Petersen OH (1985) Inhibition of Ca^{2+}-activated K^+ channels in pig pancreatic acinar cells by Ba^{2+}, Ca^{2+}, quinine and quinidine. Biochim Biophys Acta 819:249–257
21. Maruyama Y, Petersen OH (1984) Control of K^+ conductance by cholecystokinin and Ca^{2+} in single pancreatic acinar cells studied by the patch-clamp technique. J Membr Biol 79:293–300
22. Messner G, Wang W, Paulmichl M, Oberleithner H, Lang F (1985) Ouabain decreases apparent potassium-conductance in proximal tubules of the amphibian kidney. Pflügers Arch 404:131–137
23. Nagel W (1979) Inhibition of potassium conductance by barium in frog skin epithelium. Biochim Biophys Acta 552:346–357
24. Oberleithner H, Dietl P, Münich G, Weigt M, Schwab A (1985) Relationship between luminal Na^+/H^+ exchange and luminal K^+ conductance in diluting segment of frog kidney. Pflügers Arch 405:S110–S114
25. O'Neil R, Sansom SC (1984) Characterization of apical cell membrane Na^+ and K^+ conductances of cortical collecting duct using microelectrode techniques. Am J Physiol F14–F24
26. Paulmichl M, Gstraunthaler G, Lang F (1985) Electric properties of madin darby canine kidney cells. Effects of extracellular potassium and bicarbonate. Pflügers Arch 405:102–107
27. Petersen OH, Maruyama Y (1984) Calcium-activated potassium channels and their role in secretion. Nature 307:693–696
28. Portzehl H, Caldwell PC, Rüegg JC (1964) The dependence of contraction and relaxation of muscle fibres from the crab *Maia squinado* on the internal concentration of free calcium ions. Biochim Biophys Acta 79:581–591
29. Sakmann B, Trube G (1984) Conductance properties of single inwardly rectifying potassium channels in ventricular cells from guinea-pig heart. J Physiol 347:641–657
30. Standen NB, Stanfield PR, Ward TA (1985) Properties of single potassium channels in vesicles formed from the sarcolemma of frog skeletal muscle. J Physiol 364:339–358
31. Van Driessche W (1984) Physiological role of apical potassium ion channels in frog skin. J Physiol 356:79–95
32. Van Driessche W, Gögelein H (1978) Potassium channels in the apical membrane of the toad gallbladder. Nature 275:665–667
33. Van Driessche W, Zeiske W (1980) Spontaneous fluctuations of potassium channels in the apical membrane of frog skin. J Physiol 299:101–116
34. Van Driessche W, Hillyard SD, Cantiello H (1985) Investigations of basolateral K^+ channels of the tadpole skin epithelium with noise analysis. Fed Proc 44:1567
35. Vergara C, Latorre R (1983) Kinetics of Ca^{2+}-activated K^+ channels from rabbit muscle incorporated into planar bilayers. J Gen Physiol 82:543–568
36. Vergara C, Moczydlowski E, Latorre (1984) Conduction, blockade and gating in a Ca^{2+}-activated K^+ channel incorporated into planar lipid bilayers. Biophys J 45:73–76

37. Voelkl H, Geibel J, Greger R, Lang F (1986) Effects of ouabain and temperature on cell membrane potentials in isolated perfused straight proximal tubules of the mouse kidney. Pflügers Arch 407:252–257
38. Wang W, Messner G, Oberleithner H, Lang F, Deetjen P (1984) The effect of ouabain on intracellular activities of K^+, Na^+, Cl^-, H^+ and Ca^{2+} in proximal tubules of frog kidneys. Pflügers Arch 401:6–13
39. Wangemann P, Wittner M, Di Stefano A, Englert HC, Lang HJ, Schlatter E, Greger R (1986) Cl^--channel blockers in the thick ascending limb of the loop of Henle. Structure activity relationship. Pflügers Arch 407 (Suppl 2):S128–S141
40. Welsh MJ (1983) Intracellular chloride activities in canine tracheal epithelium. J Clin Invest 71:1392–1401
41. Windhager EE (1983) Regulation role of intracellular calcium ions in epithelial Na transport. Annu Rev Physiol 45:519–532
42. Yellen G (1984) Ionic permeation and blockade in Ca^{2+}-activated K^+ channels of bovine chromaffin cells. J Gen Physiol 84:157–186
43. Yoshitomi K, Frömter E (1984) Cell pH of rat renal proximal tubule in vivo and the conductive nature of peritubular HCO_3^- (OH^-) exit. Pflügers Arch 402:300–305
44. Zeiske W, Van Driessche W (1979) Saturable K^+ pathway across the outer border of frog skin (*Rana temporaria*): Kinetics and inhibition by Cs^+ and other cations. J Membr Biol 47:77–96

Received July 4, 1986/Accepted January 5, 1987

Pflügers Arch (1987) 409:114–121

Pflügers Archiv
European Journal of Physiology
© Springer-Verlag 1987

Chloride channels in the luminal membrane of the rectal gland of the dogfish (*Squalus acanthias*)*

Properties of the "larger" conductance channel

Rainer Greger[1,3], **Eberhard Schlatter**[1,3], **and Heinz Gögelein**[2,3]

[1] Lehrstuhl II Physiologie, Hermann-Herder-Strasse 7, D-7800 Freiburg, Federal Republic of Germany
[2] Max-Planck-Institut für Biophysik, Kennedyallee 70, D-6000 Frankfurt 70, Federal Republic of Germany
[3] Mount Desert Island Biological Laboratory, Salsbury Cove, ME 04672, USA

Abstract. The rectal gland of the dogfish (*Squalus acanthias*) secretes chloride via a chloride channel present in the apical cell membrane. Using the patch clamp technique in isolated perfused rectal gland tubules [7], two types of chloride channels are demonstrable in the apical membrane of cyclic AMP treated tubule segments. A small channel of about 11 pS and another channel of 40–50 pS are present. The small channel is described in the succeeding report. With NaCl on both sides (excised patches) the current amplitude of the larger channel is an almost linear function of the voltage (±50 mV). However, the open probability of this channel is grossly reduced at negative clamp potentials (corresponding to cell hyperpolarization). Therefore, the macroscopic Cl^- current through this channel is reduced with hyperpolarization on the cytosolic side. An analysis of time constants of this channel reveals that at depolarized voltages two open and two closed time constants of about 1 ms and of about 10 ms, respectively, are demonstrable. With hyperpolarized voltages the larger open state time constant is reduced significantly. This type of chloride channel is blocked reversibly by diphenylamine-2-carboxylate (10^{-4} mol/l) and by 5-nitro-2-(3-phenylpropylamino)-benzoate (10^{-5} mol/l). The channel is selective for Cl^- over Na^+ and K^+ as well as over Br^-. It is, however, permeable for NO_3^-. Since this channel is very rare or absent in non-stimulated rectal gland tubules, it is very likely that this type of channel is responsible for hormone and cAMP dependent chloride secretion in this organ.

Key words: Chloride channel – Diphenylamine-2-carboxylate – 5-Nitro-2-(3-phenylpropylamino)-benzoate – Rectal gland – Dogfish

Introduction

The rectal gland of the shark secretes NaCl when stimulated by hormones like VIP [4]. These hormones generate cyclic AMP as the cytosolic second messenger [23]. We have shown previously that cyclic AMP increases the chloride conductance in the apical membrane of these cells [9]. Furthermore, a study utilizing the patch clamp technique revealed that the increase in apical membrane chloride conductance is caused by the activation of chloride channels in previously channel free membrane patches [10]. On the other hand, it was shown that K^+ channels were present in nonstimulated and in stimulated (dibutyryl cAMP treated) membrane patches of the basolateral membrane [10]. The present study was performed to characterize the chloride channels of stimulated rectal glands with respect to their current-voltage relationship, their kinetic behaviour, ionic selectivity and their interaction with a new class of substances which have been described as blockers of chloride channels in the basolateral membrane of the cortical thick ascending limb of the loop of Henle [3, 24]. The present results indicate that the chloride channel has a single channel conductance of 40–50 pS, that it is selective for chloride, and that it is inhibited by the above mentioned chloride channel blockers. The channel is voltage dependent. Its open probability is high with positive (depolarizing) voltages and reduced with negative (hyperpolarizing) voltages.

Methods

Rectal gland tubules were dissected and perfused in vitro as described previously [7]. All experiments were performed at room temperature (about 20° C). The methods of patch clamp recording and data analysis have also been described in detail in preceding reports [6, 12]. To approach the apical membrane, patch pipettes were inserted into the open lumen and were advanced to make contact with the luminal membrane some 50 to 200 µm upstream of the open end. Alternatively, the rectal gland tubule segment was split at branching points by mechanical dissection such that the luminal surface was accessible. When a giga seal was obtained, currents were recorded with the electrode at the cell (cell attached mode). Usually, it was difficult to keep the patch pipette at the cell, and the membrane patch was excised (incidently or intentionally). This led to excised inside-out patches [14]. Sometimes the excision led to the formation of vesicles. These vesicles were ruptured by brief air exposure [14]. All tubules were bathed with a NaCl solution (Table 1) containing dibutyryl-cyclic AMP (dbcAMP) ($5 \cdot 10^{-4}$ mol/l), adenosine ($5 \cdot 10^{-4}$ mol/l) and forskolin ($5 \cdot 10^{-6}$ mol/l) (stimulation agents), as to ascertain stimulation of NaCl secretion. When excised, several different solutions (summarized in Table 1) were tested in the bath, corresponding to the cytosolic side. The pH of all solutions was adjusted to 7.5 with NaOH. Currents of negatively charged ions flowing out of the pipette into the cell (in cell attached mode) or to the cytosolic side (in cell excised mode) are referred to as positive (upward) currents. The sign of the clamp voltage *Vc* refers to the bath with respect to the patch pipette.

* Supported by Deutsche Forschungsgemeinschaft Gr 480 and by NSF and NIH grants to the MDIBL
Offprint requests to: R. Greger

Table 1. Composition of solutions. Concentrations in mmol/l

Abbreviation	Na^+	K^+	Ca^{2+}	Mg^{2+}	Cl^-	Hepes	D-Glucose	Urea	EGTA	Mannitol	Br^-	NO_3^-	TMA^+
NaCl	275	4	2.5	3	285	10	5	350	0	0	0	0	0
1/2 NaCl	140	4	2.5	3	150	10	5	350	0	270	0	0	0
KCl	5	274	0.97	3	282	10	5	350	1	0	0	0	0
NaBr	275	4	2.5	3	15	10	5	350	0	0	270	0	0
$NaNO_3$	275	4	2.5	3	15	10	5	350	0	0	0	270	0
TMACl	5	4	2.5	3	285	10	5	350	0	0	0	0	270

When the Cl^- activity was equal on both sides of the membrane patch, the current-voltage (I/V) relations were fitted by linear regression analysis. When the Cl^- activities were different, the I/V curves were fitted by the Goldman-Hodgkin-Katz current equation

$$I = \frac{F^2}{RT} z P_{Cl} V \frac{Cl_i - Cl_o e^{(zFV/RT)}}{1 - e^{(zFV/RT)}},$$

where I and V are the single channel current and membrane voltage, R, T, F and z have their usual meaning, Cl_o and Cl_i are the Cl^- activities in the pipette and on the cytosolic side, respectively. P_{Cl} is the single channel permeability coefficient for Cl^-. The value of P_{Cl} was obtained by linear regression analyses. The single channel conductance g, calculated from the differential $\delta I/\delta V$, is a nonlinear function of the voltage. Therefore, g was calculated at infinite potentials, $g(V_\infty)$, where the single channel current becomes a linear function of the clamp potential. In addition, we calculated g at the luminal membrane voltage, $g(V_{lu})$, corresponding to the single channel conductance of stimulated cells. All data are presented as original recordings; series are given as mean values ± SEM.

Results

Cell attached experiments

Figure 1 (upper half) is a typical recording of a cell attached luminal membrane patch. The pipette was filled with NaCl-shark Ringer (NaCl solution, Table 1), and the bath contained NaCl solution, to which the stimulating agents (cf. Methods) were added. It is evident that negative current events are observed at zero clamp voltage. By definition these current events represent either outflow of anions (from cell to pipette), or cation inflow. At negative clamp voltages the current amplitudes are increased, and it becomes clearly apparent now that the current amplitude fluctuates between discrete current levels. A close inspection reveals that the current fluctuates between six discrete levels of approximately equal magnitude. Clamping the patch to depolarized voltages reduces the current amplitude. The zero current potential was +24 mV in this experiment. The current-voltage relationship for one single current level of this recording is shown in the lower half of this figure. The data points were fitted by the Goldman-Hodgkin-Katz current equation, assuming a cytosolic Cl^- activity of 50 mmol/l and a luminal membrane potential of −60 mV. The single channel permeability coefficient of the demonstrated experiment was $0.11 \cdot 10^{-12}$ cm³/s and the single channel conductance at the luminal membrane potential $g(V_{lu})$ was 32 pS. Figure 2 is an analysis of the current amplitudes of the recording at a clamp potential of −36 mV. The number of events per bin is plotted versus the current amplitude: six peaks with equal distance (2 pA) from each other are clearly apparent. Therefore, it is likely that 6 functional channels were present in this membrane patch. Obviously, we are unable to distinguish between the two possibilities that one individual channel has several identical subunits of equal conductance and, the alternative, that several identical channels contribute to this current pattern. It is highly likely that, what we may call "single event" in the cell attached recordings, represent one functional channel since we have observed in most of these 7 experiments that only fewer, mostly one current level was persisting upon excision; and this current level corresponded closely in its amplitude to the "single event" observed in the corresponding cell attached experiment.

In 6 similar experiments, 4 experiments with KCl in the pipette and 2 experiments with NaCl in the pipette, a single "event" conductance at the cell resting potential $g(V_{lu})$ of 31 ± 5 pS, was observed. The mean zero current potential was 51 ± 12 mV, which is somewhat higher than that predicted by microelectrode recordings [8].

"Larger" versus "small" channel

On occasion, in excised membrane patches, we found a far smaller channel with a slope conductance of about 11 pS. First we assumed that this was the same channel, but recorded in a vesicle. In a patched vesicle only part of the applied clamp voltage is present across the channel. Therefore, the conductance will be underestimated [14]. This appeared the more attractive, as excision of patches in this preparation led quite frequently to vesicle formation. However, on occasions, we observed both the larger and the smaller channel in the same patch. A typical experiment is shown in Fig. 3. The pipette was filled with NaCl solution (Table 1), and the same solution was present in the bath. The patch was excised. At a positive voltage of 40 mV a large and a small current level were clearly apparent. Whereas the large channel flickered to the closed state, the small channel appeared to stay open for longer periods of time. This experiment excludes the vesicle hypothesis. Apparently, two types of channels (of different amplitudes and kinetics) coexist in the same patch. Both channels seem to be chloride selective (see below and [11]). A frequency distribution of the single channel conductances of both channels is given in Fig. 4. Note that the two collectives are clearly distinct. One distribution has a mean value of 45 ± 2 pS ($n = 31$), the other is far smaller with a slope conductance of about 11 ± 1 pS ($n = 21$). The small channel will be subject of an accompanying report [11].

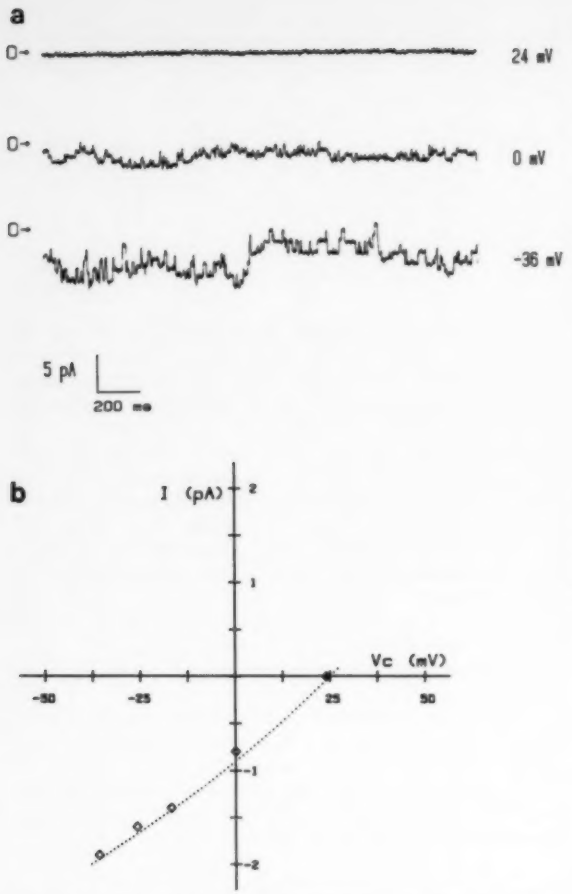

Fig. 1a, b. Cl^- channels in a cell attached patch of a luminal membrane of a rectal gland cell. Pipette and bath: NaCl solution (Table 1). **a** shows typical current recordings at different clamp potentials (indicated at the *right side*). 0 → indicates the zero current level. Six channels of similar amplitude are present in this membrane patch. The channels open in the downward direction, indicating Cl^- current flow from the cell into the patch pipette. **b** displays the current-voltage relationship for an individual current level. The single channel current (I) is plotted as a function of the clamp voltage (*Vc*). The data points are fitted by the Goldman-Hodgkin-Katz current equation (*dotted line*), assuming an intracellular Cl^- activity of 50 mmol/l and a membrane potential of −60 mV. The *filled symbol* indicates a signal to noise ration of ≤ 2

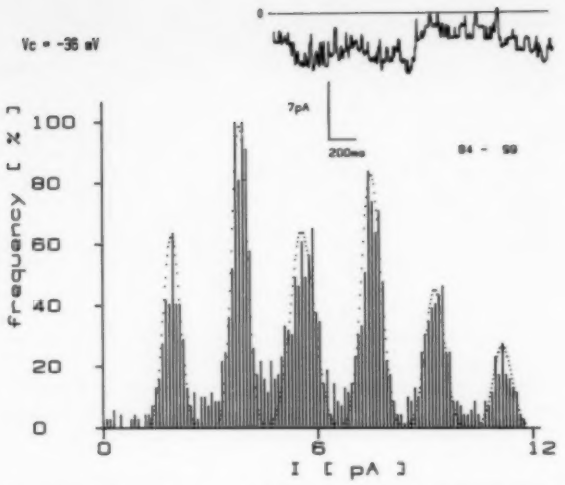

Fig. 2. Amplitude histogram of the record displayed in the *inset* of this figure. The clamp potential was −40 mV. The *ordinate* is the relative frequency with which the current level rests at a certain value. The *abscissa* is the current scale. The zero point marks the zero current level. As the channels open into the downward (negative) direction, the negative value of the current is displayed in the figure. The *dotted lines* were obtained by fitting Gaussian curves to the data. Note that the peaks are equidistant (≈ 2 pA)

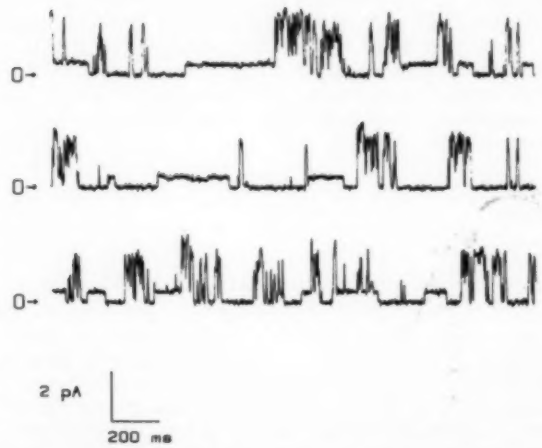

Fig. 3. Single Cl^- channel recordings of a cell excised (inside out oriented) luminal membrane of a rectal gland. Pipette and bath contained NaCl solution. The clamp potential was +40 mV in all records. 0 → indicates the zero current level. Two channels, differing in amplitude and kinetical appearance, open in the upward direction, corresponding to Cl^- flow from the pipette interior (extracellular side) into the bath

Kinetics of the "larger" chloride channel

Next we examined the "larger" channel in excised patches, with NaCl solutions (Table 1) on both sides. A typical experiment is shown in Fig. 5. The upper panel of this figure (Fig. 5a) shows the original recording. Figure 5b gives the current-voltage relationship, and Fig. 5c shows the open probability of this channel as a function of the clamp voltage. The channel permits current flow into both directions. Whereas the current amplitude is a linear function of the clamp potential (Fig. 5b), the open probability is strongly potential dependent (Fig. 5c). Long openings are only observed at positive clamp voltages (corresponding to depolarization), whereas, brief openings occur at negative clamp voltages (Fig. 5a). Consequently, the correlation of the open state probability versus the clamp potential (Fig. 5c) reveals that the open state probability of this channel is increased with positive clamp voltage, but is reduced with negative clamp potential. A series of these experiments ($n = 29$) revealed that the single channel conductance

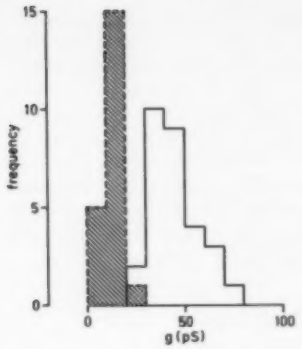

Fig. 4. Frequency distribution of single channel slope conductances g of luminal Cl^- channels in cell excised (inside out) patches of rectal gland tubules. The values of g were obtained by linear regression of the corresponding current-voltage relationship (cf. Fig. 5b). The *shadowed area* corresponds to the small conductance channel [$g = 11 \pm 1$ pS ($n = 21$)], the *white area* corresponds to the larger Cl^- channel [$g = 45 \pm 2$ pS ($n = 31$)]. Note that both distributions are clearly separated. Still 3 channels fall into the overlapping range of 20–30 pS. One of these channels had a slow kinetics, and the other two had fast kinetics. Correspondingly, the former was classified as small, and the latter two as large channels

with symmetric NaCl solution was 45 ± 2 pS. It made little difference whether the bath consisted of NaCl or KCl solution. For instance with KCl in the pipette and NaCl in the bath, the mean single channel conductance was 55 ± 4 pS ($n = 12$). In all three series the current-voltage relationships were linear within the range of the clamp voltages employed. Also, the voltage dependence of the open state probability was qualitatively similar in all experiments of these series. Figure 6 illustrates the dependence of the statistical means of the open state probability (Po) on the clamp voltage (Vc). This figure indicates that the open state probability increases with positive voltages, irrespective of the fact whether the bath solution was NaCl or KCl. For the span of clamp voltages employed (± 40 mV) the open state probability varies by a factor of about 3.

It was possible to analyse the open and closed time distributions of single channel fluctuations [6, 22] in several of these recordings. A typical example is given in Fig. 7, where a cell excised patch with NaCl solution on both sides, was analysed. The clamp potential was +25 mV. For the closed as well as for the open state, two time constants of 1 and 8 ms, and 0.6 and 5 ms, respectively, were determined. A summary of several such analyses is provided in Fig. 8. It is apparent that the time constants are voltage dependent. The longer time constants t_2 show a strong dependence,

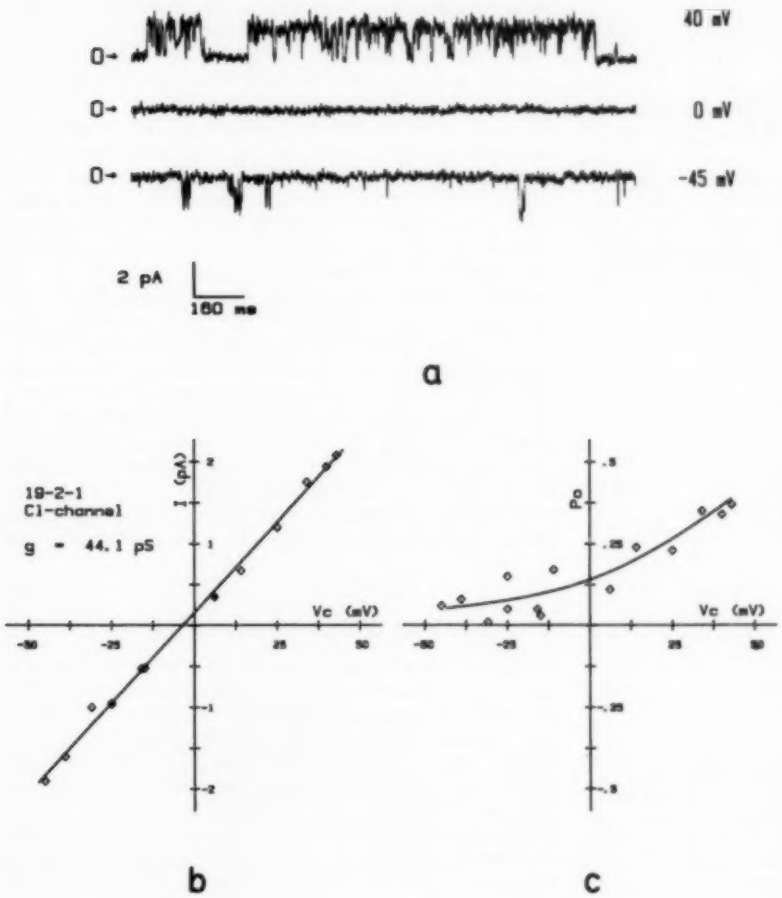

Fig. 5a–c
Single channel recordings of luminal Cl^- channels in a cell excised (inside out oriented) membrane patch of a rectal gland cell. Pipette and bath contained NaCl solution. **a** Single channels are displayed at different clamp potentials (indicated at the *right side*). 0 → indicates the zero current level. At positive clamp voltages, single channels open in the upward direction, indicating Cl^- flow from the pipette into the bath. At 0 mV clamp voltage (*middle trace*), no channel activity is apparent. At negative clamp voltages, single channel openings in the downward direction are apparent, corresponding to Cl^- flow from the bath (cytosolic side) into the pipette. Note that there is less channel activity at negative clamp potentials. **b** Current-voltage relationship of the single channels shown in **a**. The single channel current I is plotted as a function of the clamp voltage Vc. The data points were fitted by linear regression (*solid line*). The *filled symbols* indicate a signal to baseline noise ratio of ≤ 2. The single channel slope conductance was 44 pS. **c** Relationship between open state probability Po of this single Cl^- channel and clamp potential Vc. The solid line was drawn by eye

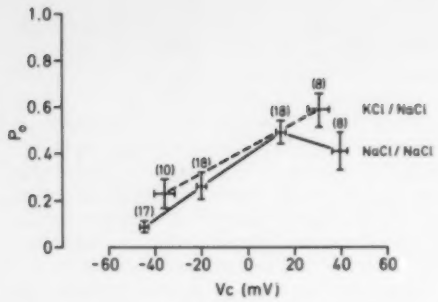

Fig. 6. Relationship between statistical mean values of open state probabilities *Po* and clamp potentials *Vc* of single Cl^- channels in cell excised (inside out oriented) luminal membrane patches of rectal gland cells. The *solid line* connects data points obtained with NaCl in the pipette and in the bath. The *interrupted line* connects points recorded with KCl in the pipette and NaCl in the bath. The numbers of experiments are given in brackets

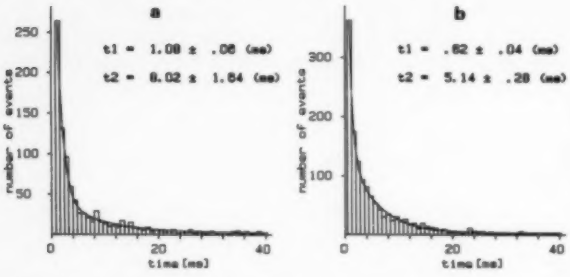

Fig. 7. Closed (**a**) and open (**b**) time histograms of a single Cl^- channel in a cell excised (inside out oriented) luminal membrane patch of a rectal gland cell. Pipette and bath contained NaCl solution. The clamp potential was 25 mV. Data were sampled at intervals of 0.4 ms. The Bessel filter was set to a 3 dB point at 0.5 kHz. Both distributions were fitted by the sum of two exponential curves. The short and long time constants (*t1* and *t2*) are displayed in the respective figure

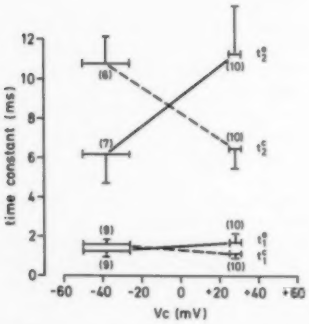

Fig. 8. Statistical mean values ± SEM of open and closed time constants as a function of the clamp potential *Vc*. The data were obtained from single Cl^- channels in cell excised (inside out oriented) luminal membranes of rectal gland cells. t_1^o and t_2^o are the short and long time constants for the open state; t_1^c and t_2^c are the short and long time constants for the closed state

whereas the shorter time constants t_1 are less voltage dependent. With positive clamp voltage (depolarization), the long open state time constant t_2^o doubles, whereas the long closed state time constant t_2^c falls to some 50%. Similar, but less marked changes are noted for the short time constants. This quantitative analysis of the time constants corresponds to the above findings (Figs. 5a, c; 6) that the open probability of these channels is increased with positive clamp voltages. Consequently, the increase in open probability occurs not because the open state occurs more frequently, but because the individual open event lasts longer.

Selectivity of the "larger" chloride channel

Next we examined the selectivity of the "larger" chloride channel. To determine the selectivity for Cl^- over Na^+, dilute NaCl solution (1/2 NaCl, Table 1) was placed at the cytosolic side. The current-voltage relations of such an experiment are shown in Fig. 9. The control experiment (NaCl on both sides), shown in Fig. 9a yielded a linear current-voltage relationship, with a zero-current potential of 0 mV and a single channel conductance of 51 pS. With 1/2 NaCl solution on the cytosolic side, however, the zero current potential is shifted to the negative range by 17 mV. This finding suggests that the channel is selective for Cl^- over Na^+. The zero current potential of −17 mV leads to an infinite permselectivity for chloride. In fact, a Goldman fit with the assumption of strict chloride permselectivity leads to a fair superposition of the calculated curve and the data points (dotted line in Fig. 9b). The single channel conductance, calculated with the Goldman-Hodgkin-Katz equation, at infinite negative potential was 27 pS and that at infinite positive potential was 54 pS. The latter value corresponds well with the single channel conductance obtained with NaCl on both sides. The selectivity of the channel for Cl^- over Na^+ was confirmed in another experiment where NaCl was replaced by tetramethylammonium chloride on the cytosolic side (TMACl solution, Table 1). In this experiment channel activity was observed in both current directions. The zero current potential stayed 0 mV (data not shown). Therefore, chloride is the permeating ion.

Next we examined the permselectivity to other anions, and replaced chloride by nitrate or bromide on the cytosolic side. The channels were poorly permeable for bromide ($n = 3$, not shown). In contrast, nitrate permeated this channel better than chloride. This is apparent from Fig. 10. The open probability of this channel increased from 0.03 (bath NaCl) to 0.96 (bath $NaNO_3$). Also the slope conductance increased from 68 pS to 90 pS in this experiment. Similar findings were made in the entire series of 4 experiments.

Effect of chloride channel blockers

Finally we have examined a new class of substances that have been characterized as chloride channel blockers in the thick ascending limb segment of the loop of Henle [3, 24]. We have tested diphenylamine-2-carboxylate ($n = 5$), torasemide ($n = 3$), 4-nitrodiphenylamine-2-carboxylic acid ($n = 1$), 5-2-(4-phenylbutylamino)-benzoic acid ($n = 1$) and 5-nitro-2-(3-phenylpropylamino)-benzoate (NPPB) ($n = 4$). A typical experiment is shown in Fig. 11. It is evident that NPPB blocks the channel activity completely and reversibly. Typically it took some 30 – 60 s for the compound to become

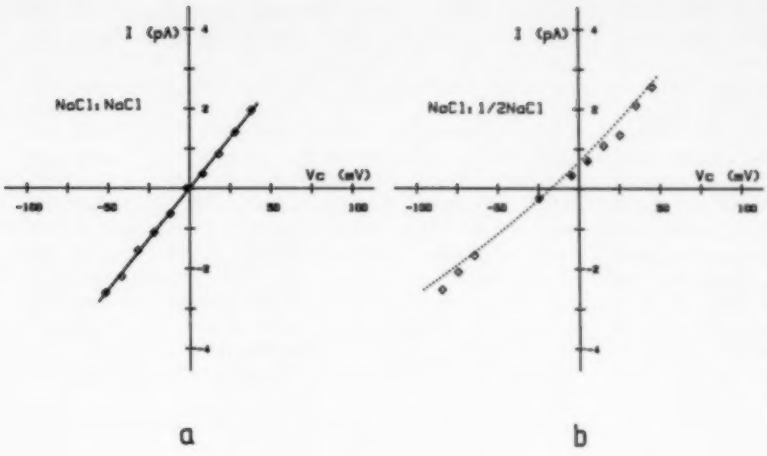

Fig. 9a, b
Current-voltage relationships of a single Cl^- channel in a cell excised (inside out oriented) luminal membrane patch of a rectal gland cell. The single channel conductances I are plotted as functions of the clamp potentials *Vc*. (**a**) Pipette NaCl, bath NaCl solution (Table 1). The data points were fitted by linear regression (*solid line*), yielding a single channel slope conductance of 51 pS. (**b**) Pipette NaCl, bath 1/2 NaCl solution (Table 1). The data were fitted by the Goldman-Hodgkin-Katz current equation (*dotted line*), yielding a single channel permeability coefficient P_{Cl} of $70 \cdot 10^{-13}$ cm³/s, a single channel conductance at infinite positive voltage of 54 pS, and a single channel conductance at infinite negative voltage of 27 pS

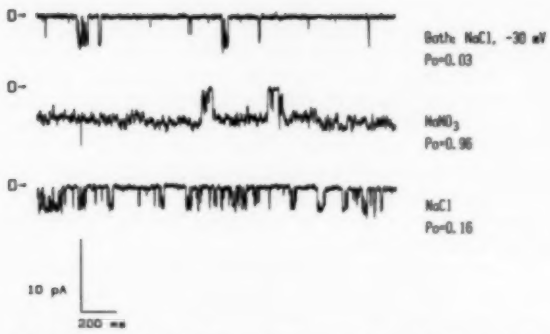

Fig. 10. Effect of $NaNO_3$ on a single Cl^- channel in a cell excised (inside out oriented) luminal patch of a rectal gland cell. The clamp potential was −30 mV in all displayed records. 0 → indicates the zero current level. The channel opens in the downward direction, indicating Cl^- flow from the bath (cytosolic side) into the pipette. The *upper* and *lower traces* were recorded with NaCl solution in the pipette and in the bath. In the *middle trace* the bath was replaced by $NaNO_3$ solution (Table 1). The corresponding open state probabilites *Po* are given on the *right side* of each record. Note the pronounced and reversible increase in *Po*, due to bath $NaNO_3$. In addition, the single channel current increased from 2.5 pA (bath NaCl) to 3.1 pA (bath $NaNO_3$). Also this effect on the single channel amplitude was reversible (*lowest trace*)

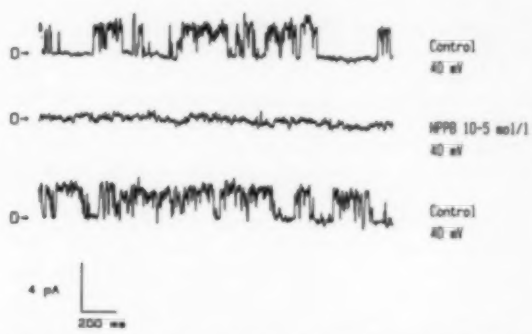

Fig. 11. Effect of the Cl^- channel blocker 5-nitro-2-(3-phenylpropylamino)-benzoate (NPPB) on single Cl^- channels in a cell excised (inside out oriented) luminal membrane of a rectal gland cell. Pipette and bath: NaCl solution. The clamp voltage was +40 mV in all displayed records. 0 → indicates the zero current level. Single channel openings in the upward direction are apparent, corresponding to Cl^- flow from the pipette (extracellular side) into the bath. The *middle trace* was recorded 60 s after the addition of 10^{-5} mmol/l of NPPB to the bath. Note the complete and reversible inhibition of the Cl^- channels by NPPB

effective, and, similarly, the recovery of channel activity took several minutes. These delays cannot be accounted for by the rate of bath exchange (about 5 Hz). Thus, it is feasible that these compounds act only from the outside of the channel, and that in our experiments the compounds had to permeate the membrane from the cytosolic side (bath) into the pipette before they were able to block the channel. These compounds are lipophilic in the protonated form [24], and may permeate the cell membrane. All five compounds tested inhibited the chloride channels reversibly. The required concentrations were $< 10^{-5}$ mol/l for 5-nitro-2-(3-phenylpropylamino)-benzoate and $< 10^{-4}$ mol/l for all the others. This sequence, of 5-nitro-2-(phenylpropylamino)-benzoate being more potent than e.g. diphenylamine-2-carboxylate, also corresponds to our previous data on the chloride channel in the thick ascending limb of Henle. It is worth noting that the small type of anion channel, which will be described in the next report [11], was not blocked by the above inhibitors.

Discussion

In the present study we aimed to characterize further the chloride channel of the rectal gland. We have confirmed that this kind of channel is only present in the luminal cell membrane of this tissue [10]. We also have reproduced our findings [10] that the incidence of this channel in luminal membranes of rectal gland is high in stimulated, i.e. dibutyryl-cyclic-AMP treated cells, but that it is infrequently demonstrable in untreated tissues.

The present study indicates that two types of anion channels are found in this preparation. Only the channel with the higher (40 − 50 pS) conductance is subject of this present report.

In cell attached patches we have observed that channel activity occurs frequently in "clusters". These clusters may represent several channels of equal conductance or identical substates of one individual channel. Cluster appearance of chloride channel activity has been previously found in the electroplax [18], in pulmonary alveolar cells [17], and in molluscan neurones [5]. In excised patches, clusters were seen only rarely in our experiments. In fact, in most instances only one to two current levels were apparent in excised membrane patches. The similarity of the slope conductance of the individual current level (cell attached) to the slope conductance determined in excised patches suggests that the clusters correspond to several superimposed channels rather than superimposed substates. The reduction of number of active channels per patch observed upon excision may be explained by the difference in composition of the bath perfusate and the cytosol. In addition, the excision may interrupt some thus far not understood activation pathway. One such factor may be calcium activity in the cytosol. Therefore, we have varied the bath (corresponding to cytosolic side) calcium activity from less than 10^{-9} to $5 \cdot 10^{-3}$ mol/l. No clear effect was seen in three such experiments (not shown). Therefore, we suggest that the inactivation of channel activity in excised membrane patches is not caused by variations in the calcium activity but by as yet unknown factors. In this context, it is important to note that a chloride channel in the apical membrane of the trachea, in sharp contrast to our findings, was activated by excision [25].

The large chloride channel described here falls into the conductance range reported for the trachea [21], and the colonic cell channels [13, and unpublished results from the author's laboratory]. On the other hand, all the above channels have a smaller conductance than that of the MDCK cell [16], of the urinary bladder [15], of A6 cells [19], of myotubes [1], and of cultured pulmonary alveolar cells [20]. The present channel shows no rectification of the single channel amplitude. However, its kinetics are strongly voltage dependent. Depolarization increased and hyperpolarization reduces the open state probability. The analysis of the open and closed state time constants revealed that this voltage dependence of the open state probability is caused by a corresponding effect on the open and closed time constants. Positive clamp potentials increase the duration of the long open state time constants. Negative clamp voltages have the opposite effect. The macroscopic current through this conductive pathway will be rectified as a consequence of the voltage dependence of the open probability. This voltage dependence of this chloride channel may suggest that this channel will be strongly inactivated by the physiological membrane voltage of -64 mV across this cell membrane [7], and may, therefore, be irrelevant as a chloride exit mechanism. In contrast, we have found that the same channel is very active in cell attached patches, alluding again to the fact that this channel is gated by some unknown cytosolic factor.

Recently, rectifying chloride have been reported for the trachea [25]. These channels, in excised patches, showed rectification of the single channel amplitude as well as of the open state probability. Both parameters increased with depolarization. Therefore, these channels behave analogously to the one described here with regard to the open state probability; they differ with respect to the voltage dependence of the current amplitude.

The experiments to determine the selectivity of this channel reveal that it is selective for anions as compared to cations. Three findings support this view: 1. The current direction in cell attached patches is only compatible with Cl^- exit from, or Na^+ entry into the cell. The zero current potential for Cl^- exit should be around $+30$ to $+50$ mV, and $+120$ to $+130$ mV for Na^+ entry [9]. We found values around $+50$ mV, suggesting that Cl^- was in the main conducting ion. 2. The experiments with diluted NaCl, as well as with TMACl on the cytosolic side strongly suggest that this channel is chloride selective. 3. This channel also discriminates between anions. Bromide is poorly permeable, but nitrate permeates easily. In fact, nitrate does not only augment the channel conductance, in addition, it increases the open state probability. A higher permeability for NO_3^- than for Cl^- was reported for channels in Aplysia neurones [2].

Finally, chloride conductance blockers have been tested for this chloride channel. It was found that these agents block the channel activity reversibly, probably from the outside of the channel. These data correspond to macroscopic conductance measurements in the rectal gland [8]. Single channels of similar kinetic behaviour and of comparable conductance have meanwhile been identified in the basolateral membrane of the proximal tubule [6], in the basolateral membrane of the thick ascending limb (unpublished from the author's laboratory) and in colonic carcinoma cell lines (T84 and HT29, unpublished from the author's laboratory). In all these channels, chloride channel blockers were effective. This may suggest that these channels belong to a single category.

In conclusion, the present study describes the characteristics of a chloride channel in the luminal membrane of the rectal gland. This channel, most probably, is responsible for the hormone dependent chloride exit from this cell. This channel requires stimulation to become active, it is present with a rather high frequency per area luminal membrane, and it is blocked by agents that have been shown to block specifically the conductive chloride exit.

Acknowledgements. The authors acknowledge gratefully the assistance by Vinzenz and Walter Greger and by Jörg Dreinhöfer.

References

1. Blatz L, Magleby KL (1983) Single voltage-dependent chloride-selective channels of large conductance in cultured rat muscle. Biophys J 43:237–241
2. Chesnoy-Marchais D, Evans MG (1984) Two types of chloride channels in outside-out patches from Aplysia neurones. J Physiol 357:64P
3. DiStefano A, Wittner M, Schlatter E, Lang HJ, Englert H, Greger R (1985) Diphenylamine-2-carboxylate, a blocker of the Cl^--conductive pathway in Cl^--transporting epithelia. Pflügers Arch (Suppl 1):S95–S100
4. Epstein FH (1979) The shark rectal gland: a model for the active transport of chloride. Yale J Biol Med 52:517–523
5. Geletyuk VI, Kazachenko VN (1985) Single Cl^- channels in molluscan neurones: multiplicity of the conductance states. J Membr Biol 86:9–15
6. Gögelein H, Greger R (1986) A voltage-dependent channel in the basolateral membrane of late proximal tubules of the rabbit kidney. Pflügers Arch (Suppl 2):S142–S148
7. Greger R, Schlatter E (1984) Mechanism of NaCl secretion in the rectal gland of spiny dogfish (*Squalus acanthias*). I. Experi-

ments in isolated in vitro perfused rectal gland tubules. Pflügers Arch 402:63–75
8. Greger R, Schlatter E (1984) Mechanism of NaCl secretion in rectal gland tubules of spiny dogfish (*Squalus acanthias*). II. Effects of inhibitors. Pflügers Arch 402:364–375
9. Greger R, Schlatter R, Wang F, Forrest JN Jr (1984) Mechanism of NaCl secretion in rectal gland tubules of spiny dogfish (*Spualus acanthias*). III. Effects of stimulation of secretion by cyclic AMP. Pflügers Arch 402:376–384
10. Greger R, Schlatter E, Gögelein H (1985) Cl^- channels in the apical cell membrane of the rectal gland "induced" by cAMP. Pflügers Arch 403:446–448
11. Gögelein H, Schlatter E, Greger R (1987) The "small" conductance chloride channel in the luminal membrane of the rectal gland of the dogfish (*Squalus acanthias*). Pflügers Arch 409:122–125
12. Greger R, Gögelein H, Schlatter E (1987) Potassium channels in the basolateral membrane of the rectal gland of the dogfish (*Squalus acanthias*). Pflügers Arch 409:100–106
13. Halm D, Rechkemmer G, Frizzell R (1986) Single-channel recording from a secretory epithelial cell line, T84. Fed Proc 45:741
14. Hamill OP, Marty A, Neher E, Sakmann B, Sigworth FJ (1981) Improved patch-clamp techniques for high-resolution current recording from cells and cell-free membrane patches. Pflügers Arch 391:85–100
15. Hanrahan JW, Alles WP, Lewis SA (1985) Single anion-selective channels in basolateral membrane of a mammalian tight epithelium. Proc Natl Acad Sci USA 82:7791–7795
16. Kolb HA, Brown CDA, Murer H (1985) Identification of a voltage-dependent anion channel in the apical membrane of a Cl^--secretory epithelium (MDCK). Pflügers Arch 403:262–265
17. Krouse ME, Schneider GT, Gage PW (1986) A large anion-selective channel has seven conductance levels. Nature 319:58–60
18. Miller C (1982) Open-state substructure of single chloride channels from Torpedo electroplax. Philos Trans R Soc Lond B299:401–411
19. Nelson DJ, Tang JM, Palmer LG (1984) Single-channel recordings of apical membrane chloride conductance in A6 epithelial cells. J Membr Biol 80:81–89
20. Schneider GT, Cook DI, Gage PW, Young JA (1985) Voltage sensitive, high-conductance chloride channels in the luminal membrane of cultured pulmonary alveolar (type II) cells. Pflügers Arch 404:354–357
21. Shoemaker RL, Frizzell RA, Dwyer TM, Farley JM (1986) Single chloride channel currents from canine tracheal epithelial cells. Biochim Biophys Acta 858:235–242
22. Sigworth F (1983) An example of analysis. In: Sakmann B, Neher E (eds) Single channel recording. Plenum Press, New York London, pp 301–322
23. Silva P, Stoff J, Field M, Fine L, Forrest JN, Epstein FH (1977) Mechanism of active chloride secretion by shark rectal gland: role of Na-K-ATPase in chloride transport. Am J Physiol 233(4):F298–F306
24. Wangemann P, Wittner M, DiStefano A, Englert HC, Lang HJ, Schlatter E, Greger R (1986) Cl^--channel blockers in the thick ascending limb of the loop of Henle. Structure activity relationship. Pflügers Arch 407(Suppl 2):S128–S141
25. Welsh MJ (1986) Single apical membrane anion channels in primary cultures of canine tracheal epithelium. Pflügers Arch 407(Suppl 2):S116–S122

Received July 11, 1986/Accepted January 5, 1987

Pflügers Arch (1987) 409:122–125

Pflügers Archiv
European Journal of Physiology
© Springer-Verlag 1987

The "small" conductance chloride channel in the luminal membrane of the rectal gland of the dogfish (*Squalus acanthias*)*

Heinz Gögelein[1,2], Eberhard Schlatter[2,3], and Rainer Greger[2,3]

[1] Max-Planck-Institut für Biophysik, Kennedyallee 70, D-6000 Frankfurt 70, Federal Republic of Germany
[2] Mount Desert Island Biological Laboratory, Salsbury Cove, ME 04672, USA
[3] Lehrstuhl II Physiologie, Universität Freiburg i. Br., Hermann-Herder-Strasse 7, D-7800 Freiburg, Federal Republic of Germany

Abstract. Besides the "larger" Cl^- channel, with a single channel conductance of about 45 pS, a "small" channel was observed in the luminal membrane of the dogfish rectal gland [9]. In cell excised (inside out) patches with NaCl solution on both sides, the latter channel had a single channel conductance of 11 ± 1 pS ($n = 21$), and its current-voltage relationship was linear in the voltage range +90 to −90 mV. The open state probability increased moderately with negative clamp potentials. Ionic replacement studies revealed a high selectivity of Cl^- over gluconate, sulfate, and iodide, whereas bromide was permeable to some extent. Also the channel is impermeable for Na^+. The Cl^- channel blocker 5-nitro-2-(3-phenylpropylamino)-benzoate did not affect this "small" conductance Cl^- channel. It can be concluded that the luminal membrane of stimulated rectal gland cells possesses two types of Cl^- channels, which differ markedly in their characteristics.

Key words: "Small" chloride channel – Luminal membrane – Patch clamp – Rectal gland – Dogfish

Introduction

In previous studies [8, 9] it was demonstrated that Cl^- channels with a single channel conductance of about 45 pS exist in the luminal membrane of stimulated cells of the dogfish rectal gland. It was concluded that these channels are responsible for the increase in luminal membrane conductance observed after stimulation of isolated perfused tubules [10]. These Cl^- channels were voltage dependent and could be blocked by 5-nitro-2-(3-phenylpropylamino)-benzoate, an agent that blocks Cl^- conductance in the thick ascending limb of rabbit kidney [14]. In addition to this Cl^- channel, we observed a channel with lower conductance ($g = 11$ pS) in the luminal membrane of excised patches. This "small" conductance channel could be observed in some instances in the same membrane patch as the "larger" Cl^- channel [9]. In this paper we shall demonstrate that this small channel is also permeable for Cl^-. In contrast to the "larger" Cl^- channel, it is not inhibited by the above mentioned Cl^- channel blocker, and it is not activated by positive clamp potentials.

* Supported by Deutsche Forschungsgemeinschaft Gr 480/8 and by NSF and NIH grants to the MDIBL
Offprint requests to: R. Greger

Methods

The patch clamp method was applied to isolated segments of rectal gland tubules of the dogfish (*Squalus acanthias*), which were mounted on one side on a perfusion system [4, 6]. A patch pipette could be inserted through the open end of the noncannulated side and brought in contact with the luminal membrane. Alternatively, tubules could be split longitudinally at branching points, enabling free access to luminal cell membranes. Details about the patch clamp technique and data analysis have been reported previously [5, 7] and are similar to those described by Hamill et al. [11]. The small conductance of this channel required a filter setting of 300–800 Hz (3dB). All experiments reported here were performed with excised (inside out oriented) membrane patches. Single channel currents of Cl^- ions flowing from the pipette into the bath are displayed as upward deflections. The sign of the clamp potential refers to the bath (cytosolic side) with respect to the patch pipette interior. The tubules were stimulated by addition of adenosine ($5 \cdot 10^{-4}$ mol/l), dibutyryl cyclic adenosinemonophosphate ($5 \cdot 10^{-4}$ mol/l), and forskolin ($5 \cdot 10^{-6}$ mol/l) to the bathing solution. Solutions tested are given in Table 1. The pH of all solutions was adjusted to 7.5 by NaOH. The experiments were performed at room temperature (about 20°C). Data are presented as individual recordings and as mean values ± SEM.

Results

Figure 1 demonstrates a typical experiment of a excised (inside out) luminal membrane patch. Both the pipette and bath were filled with NaCl solution (Table 1). The upper part of the figure demonstrates that no channel activity was present at 0 mV clamp voltage (middle record). At positive clamp voltage, channel openings in the upward direction were observed (upper record), whereas at negative clamp potentials the channels opened in the downward direction (lower record). Inspection of the single channel recordings of Fig. 1 reveals that up to three current levels of same amplitude were present, indicating that three channels existed in this membrane patch. These channels had simple kinetical appearance; they opened and closed without indications of flickering. Only rarely were brief closing events (*Nachschlag* phenomenon) observed. The current-voltage (IV) relation, shown in the lower part of Fig. 1, demonstrates that the single channel current (I) was a linear function of the clamp voltage (Vc) in the investigated potential range of

Table 1. Composition of solutions. Concentrations in mmol/l

Abbreviation	Na^+	K^+	Ca^{2+}	Mg^{2+}	Cl^-	Hepes	D-Glucose	Urea	EGTA	Gluconate	TMA^+
NaCl	275	4	2.5	3	285	10	5	350	0	0	0
KCl	5	274	0.97	3	282	10	5	350	1	0	0
Na-gluconate	279	0	10	3	26	10	5	350	0	274	0
TMACl	5	0	2.5	3	285	10	5	350	0	0	274

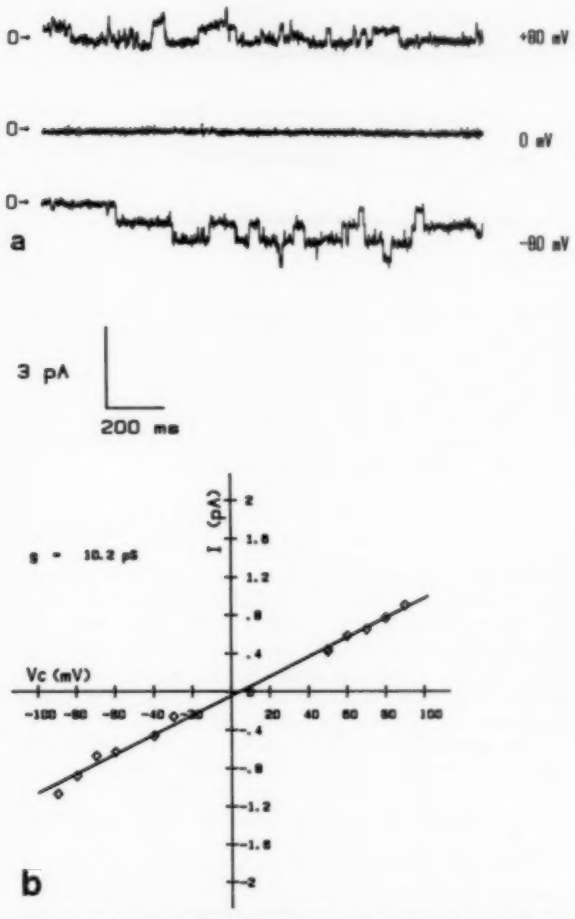

Fig. 1a, b. Single channel recordings of luminal Cl^- channels in a cell excised (inside out) membrane patch of a rectal gland cell. Pipette and bath contained NaCl solutions. **a** Single channels are displayed at different clamp potentials (indicated at the right side). *0* → indicates the zero current level. At positive clamp voltage, single channels open in the upward direction (*upper trace*), indicating Cl^- flow from the pipette into the bath. At 0 mV clamp voltage (*middle trace*), no channel activity is apparent. At negative clamp voltage, single channel openings in the downward direction were present, corresponding to Cl^- flow from the bath (cytosolic side) into the pipette (*lower trace*). Note that up to three current levels of equal amplitude are apparent, indicating the presence of three channels. **b** Current-voltage relationship of one current level of the single channel recording, shown in the upper panel. The single channel current I is plotted as a function of the clamp voltage *Vc*. The *open symbols* refer to a current over noise ratio of ≤ 2. The data points were fitted by linear regression (*solid line*). The single channel slope conductance was 10 pS

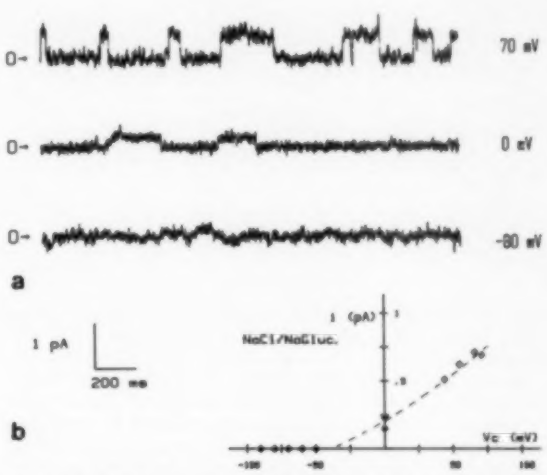

Fig. 2a, b. Single channel recordings of luminal Cl^- channels in a cell excised (inside out) membrane patch of a rectal gland cell. The pipette contained NaCl, the bath Na-gluconate solution (cf. Table 1). **a** Single channels are displayed at different clamp potentials (indicated at the right side). *0* → indicates the zero current level. At positive clamp voltages (*upper trace*), single channels open in the upward direction, indicating Cl^- flow from the pipette into the bath (cytosolic side). At negative potentials (*lower trace*) no significant channel activity is apparent, indicating that gluconate cannot permeate the channel. **b** Current-voltage relationship of the single Cl^- channels shown in **a**. The single channel current I is plotted as a function of the clamp voltage *Vc*. The *closed symbols* refer to a current over noise ratio of ≤ 2. The data points were fitted by hand

+90 to −90 mV. In addition, the zero current potential was 0 mV. It can be concluded that this channel has no rectifying properties with respect to its current amplitude. Similar observations were made in all 21 experiments, performed under the above described conditions. The mean single channel conductance was 11 ± 1 pS ($n = 21$). Because of its rather low single channel conductance, it was difficult to measure the dependence of the open state probability (P_0) as a function of the clamp voltage. However, in 5 experiments we had clear evidence that the channel was more active at negative potentials than at positive ones (see also Fig. 1). Consequently, this Cl^- channel differs from the larger one described in the accompanying report [9].

Some experiments with cell excised patches were also performed with KCl and NaCl solutions (Table 1) on the two sides of the membrane patch. With KCl in the pipette (2 experiments), or with KCl in the bath (3 experiments), the appearance of single channels was similar to that observed when NaCl bathed both sides (Fig. 1). Moreover,

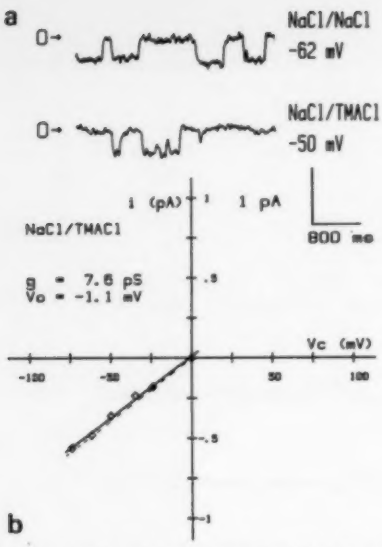

Fig. 3. Single channel recordings of luminal Cl^- channels in a cell excised (inside out) membrane patch of a rectal gland cell. The pipette contained NaCl, the bath contained the same solution or tetramethylammoniumchloride (TMACl) (cf. Table 1). **a** Single channels are displayed at negative clamp voltages. *0* → indicates the zero current level. **b** Current-voltage relationship of the single Cl^- channels shown in *a*. The single channel current I is plotted as a function of the clamp voltage *Vc*. The data points and the solid regression line correspond to the experimental condition TMACl. The *dotted line* was obtained under control conditions (NaCl). The closed symbols refer to a current over noise ratio of ≤ 2. Note that the linear regressions are virtually identical under both conditions (bath NaCl versus TMACl) indicating that the channel is impermeable for Na^+

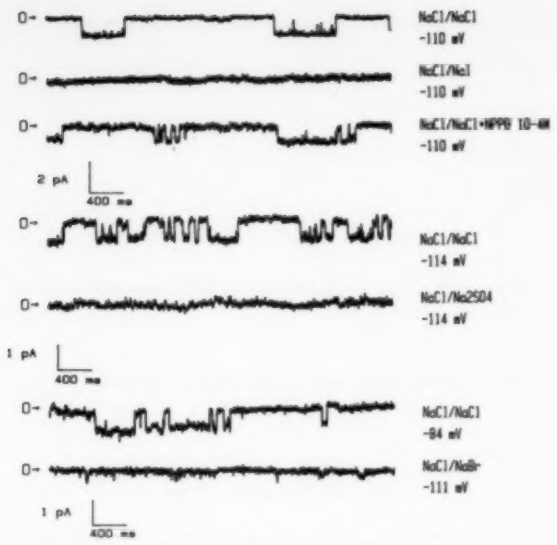

Fig. 4. Single channel recordings of luminal Cl^- channels in cell excised (inside out) membrane patches of rectal gland cells. *Upper panel*, the replacement of Cl^- by I^- in the bath abolishes entirely the channel activity. Addition of 5-nitro-2-(3-phenylpropylamino)-benzoate (NPPB) to the NaCl solution has no effect. *Middle panel*, replacement of Cl^- by SO_4^{2-} abolishes the channel activity. *Lower panel*, replacement of Cl^- by Br^- reduces the current amplitude markedly to approximately 20% of control

current-voltage relationships were linear and zero current potentials were 0 mV. These findings indicate that this channel either does not discriminate between Na^+ and K^+ ions, and/or that it is only permeable for chloride ions and not for the cations.

In order to investigate the selectivity of this channel between cations and anions, experiments were performed, in which Na-gluconate (Table 1) was placed in the bath. Figure 2 demonstrates one typical experiment. The control experiment (NaCl solution on both sides) yielded a linear current-voltage curve, with a single slope conductance of 10 pS. The zero current potential was 0 mV (data not shown). When the bath NaCl solution was replaced by Na-gluconate, single channel openings in the upward direction were recorded at positive clamp potentials (upper records in Fig. 2). However, clamping the patch to negative potentials as high as −90 mV (lower records in Fig. 2) did not produce detectable channel activity. These results indicate that this channel is impermeable to sodium and is markedly more permeable to Cl^- ions than for gluconate. The current-voltage relation shown in the lower part of Fig. 2 confirms this conclusion. Similar observations were made in three experiments.

Selectivity for Cl^- over Na^+ was confirmed in one additional experiment (Fig. 3), where the pipette was filled with NaCl solution and the bath was changed from NaCl to KCl and finally to tetramethylammonium (TMACl) solution (Table 1). With NaCl of KCl in the bath, the channels had a conductance of 8 pS. With TMACl in the bath, only negative voltages were examined. Single downward channels were observed, yielding a single channel slope conductance of 8 pS. The I/V curve crossed the zero point. These results confirmed that Cl^- was the conducting ion.

The permeability of this channel to some other anions was tested. Typical data are summarized in Fig. 4. These experiments were usually performed at high negative clamp voltages, since we expected that negative voltages would lead to corresponding current events of the replacing anion. We observed that sulfate ($n = 3$) and iodide ($n = 3$) did not permeate the channel, whereas bromide ($n = 3$) permeated, but its permeability was smaller than that for Cl^-.

We also investigated the effect of the Cl^- channel blocker 5-nitro-2-(3-phenylpropylamino)-benzoate (Fig. 4). Addition of 10^{-5} mol/l of this substance to the cytosolic side of cell excised patches had no significant effect on single channel fluctuations (8 observations).

Discussion

We have shown in this study that the "small" conductance channel is highly selective for Cl^- with respect to Na^+. As channel appearance was unaltered, when bath NaCl was exchanged for KCl, it can be concluded that this channel is also impermeable for K^+ ions. With respect to anions, this channel was apparently impermeable for sulfate, gluconate, and iodide, but had a low permeability for bromide.

Consequently, this channel has similar selectivity properties as the "larger" Cl^- channel described in the preceding study [9]. Both channels, however, differed significantly with respect to their single channel conductance, kinetic appearance, voltage dependence and sensitivity to blockers. The kinetic appearance of the "larger" Cl^- channel was characterized by burst-like fluctuations, with brief closing events within a burst [9]. The kinetics of the "larger" Cl^- channel was voltage dependent, which correlated with a voltage dependence of the open and closed state time constants [9]. In contrast to this finding, the "small" channel showed simple open and closed kinetics. It should be recalled, however, that the small conductance of this channel required low pass filtering at 300–800 Hz (3dB). Therefore, fast openings or closings could have been overlooked in our study. It is not surprizing then that we observed events denoted as the *Nachschlag* phenomenon [2] (cf. Fig. 1). The open state probability of the "larger" Cl^- channel increased significantly with positive clamp voltage, while the open probability of the "small" channel was apparently less affected by the clamp potential and, in contrast to the "larger" channel, was increased at negative voltages. Lastly, the effect of the potent Cl^- channel blocker 5-nitro-2-(3-phenylpropylamino)-benzoate [14] was tested on the "small" Cl^- channel activity. In sharp contrast to the "larger" channel, this substance had no significant effect on the "small" conductance Cl^- channel. In conclusion, two types of Cl^- channels of different characteristics exist in the luminal membrane of the dogfish rectal gland cell. Cl^- permeable channels with a similar single channel conductance of unitary events as the "small" Cl^- channel, described in the present study, were observed in the electric organ of *Torpedo californica* [12], in *Aplysia* neurones [1], in molluscan neurones [3], in tracheal epithelial cells [13], and in cultured colonic cells (HT29 and T84) (unpublished observations from the author's laboratory).

All experiments described in this study were performed with stimulated cells (cf. Methods). Therefore, it is unresolved whether this "small" channel was induced by hormonal stimulation, as it was the case with the "larger" channel. The pronounced differences between channel properties of both Cl^- channels suggests that their concurrent presence in this same membrane may serve different physiological needs of the cells. While the "larger" Cl^- channel provides a means for the pronounced increase in luminal Cl^- conductance after stimulation [10], the "small" Cl^- channel may be active both in nonstimulated and stimulated cells and account for a low Cl^- conductance in the former state [10].

Acknowledgements. The authors acknowledge gratefully the assistance of Jörg Dreinhöfer and of Vinzenz and Walter Greger.

References

1. Chesnoy-Marchais D, Evans MG (1984) Two types of chloride channels in outside-out patches from Aplysia neurones. J Physiol 357:64P
2. Colquhoun D, Sakmann B (1983) Bursts of openings in transmitter-activated ion channels. In: Sakmann B, Neher E (eds) Single channel recording. Plenum Press, New York London, pp 345–364
3. Geletyuk VI, Kazachenko VN (1985) Single Cl^- channels in molluscan neurones: multiplicity of the conductance states. J Membr Biol 86:9–15
4. Gögelein H, Greger R (1984) Single channel recordings from basolateral and apical membranes of renal proximal tubules. Pflügers Arch 401:424–426
5. Gögelein H, Greger R (1986) A voltage-dependent ionic channel in the basolateral membrane of late proximal tubules of the rabbit kidney. Pflügers Arch 407 (Suppl 2):S142–S148
6. Greger R, Hampel W (1981) A modified system for in vitro perfusion of isolated renal tubules. Pflügers Arch 389:175–176
7. Greger R, Schlatter E, Wang F, Forrest JN Jr (1984) Mechanism of NaCl secretion in rectal gland tubular of spiny dogfish (*Squalus acanthias*). III. Effects of stimulation of secretion by cyclic AMP. Pflügers Arch 402:376–384
8. Greger R, Schlatter E, Gögelein H (1985) Cl^- channels in the apical cell membrane of the rectal gland "induced" by cAMP. Pflügers Arch 403:446–448
9. Greger R, Schlatter E, Gögelein H (1987) Chloride channels in the luminal membrane of the rectal gland of the dogfish (*Squalus acanthias*). Properties of the "larger" conductance channel. Pflügers Arch 409:114–121
10. Greger R, Gögelein H, Schlatter E (1987) Potassium channels in the basolateral membrane of the rectal gland of the dogfish (*Squalus acanthias*). Pflügers Arch 409:100–106
11. Hamill OP, Marty A, Neher E, Sakmann B, Sigworth FJ (1981) Improved patch-clamp techniques for high-resolution current recording from cells and cell-free membrane patches. Pflügers Arch 391:85–100
12. Miller C, White MM (1984) Dimeric structure of single chloride channels from Torpedo electroplax. Proc Natl Acad Sci USA 81:2772–2775
13. Shoemaker RL, Frizzell RA, Dwyer TM, Farley JM (1986) Single chloride channel currents from canine tracheal epithelial cells. Biochim Biophys Acta 858:235–242
14. Wangemann P, Wittner M, Di Stefano A, Englert HC, Lang HJ, Schlatter E, Greger R (1986) Cl^--channel blockers in the thick ascending limb of the loop of Henle. Structure activity relationship. Pflügers Arch 407 (Suppl 2):S128–S141

Received July 11, 1986/Accepted January 5, 1987

Pflügers Arch (1987) 409:126–131

Pflügers Archiv
European Journal of Physiology
© Springer-Verlag 1987

Effects of potassium bicarbonate on distal nephron Na-K-ATPase in adrenalectomized rabbits

Lal C. Garg and Neelam Narang

Department of Pharmacology and Therapeutics, University of Florida, College of Medicine, Box J-267, J. Hillis Miller Health Center, Gainesville, FL 32610, USA

Abstract. Na-K-ATPase activity in the connecting tubule (CNT) and cortical collecting duct (CCD) has been shown to be influenced by KCl both in the presence and in the absence of aldosterone. To investigate if the aldosterone-independent effect of K^+ on Na-K-ATPase can be produced by other K^+ salts, we studied the effects of dietary $KHCO_3$ on Na-K-ATPase and ouabain-insensitive Mg-ATPase activities in four nephron segments of adrenalectomized (ADX) rabbits. The segments examined were: the distal convoluted tubule (DCT), CNT, CCD and medullary collecting duct (MCD). All diets were similar in composition except their $KHCO_3$ contents which were 100, 300, 500 and 700 meq/kg in groups 1 to 4 respectively. Increasing $KHCO_3$ in the diet increased K^+ excretion (7×) and urine pH (6.6 to 8.3). Na-K-ATPase activity in the CCD increased > 200% as dietary $KHCO_3$ was increased to 700 meq/kg. There was a linear relation between Na-K-ATPase activity in this segment and steady state plasma K^+ as well as K^+ excretion in the urine. However, Na-K-ATPase activity in the CCD was lower in $KHCO_3$-fed ADX rabbits than the KCl-fed animals studied previously under similar conditions. There were no significant differences in Na-K-ATPase activities in DCT, CNT and MCD among the four groups given different $KHCO_3$-diets. It is concluded that dietary intake of $KHCO_3$ can also influence Na-K-ATPase activity in the CCD independent of aldosterone.

Key words: Na-K-ATPase – Mg-ATPase – Distal convoluted tubule – Connecting tubule – Cortical and medullary collecting ducts

Introduction

Sodium-potassium-adenosine triphosphatase (Na-K-ATPase) is known to be involved in the secretion of potassium in the mammalian nephron [11]. Potassium secretion occurs in the distal segments [24] and ouabain, an inhibitor of Na-K-ATPase, has been shown to abolish potassium secretion in the isolated cortical collecting duct (CCD) of the rabbit [7]. It has been demonstrated that both Na-K-ATPase activity and potassium secretion in the CCD is increased by an increase in plasma aldosterone concentration [5, 15]. In addition, dietary potassium has been shown to increase Na-K-ATPase activity and potassium excretion [16]. The effect of dietary potassium on Na-K-ATPase activity occurs mainly in the CCD [2, 6, 13]. A part of the effect of dietary potassium on Na-K-ATPase activity may be mediated by the plasma aldosterone level which is also increased during potassium loading [1]. Recently, we have demonstrated that dietary potassium when given in the form of potassium chloride can increase both Na-K-ATPase activity in the CCD and potassium excretion in the urine independent of aldosterone [4]. The purpose of the present study was to determine if the aldosterone-independent effect of dietary potassium on Na-K-ATPase activity in the CCD is dependent on chloride or can also be produced by other anions e.g. bicarbonate. In this communication, we report the effects of dietary potassium bicarbonate on the activities of Na-K-ATPase as well as ouabain-insensitive Mg-ATPase in four segments of distal nephron in adrenalectomized (ADX) rabbits.

Methods

Animals. Male New Zealand white rabbits (1–1.5 kg) were bilaterally adrenalectomized and divided into four groups. Absence of aldosterone in plasma samples indicated the accuracy of adrenalectomy. All the animals were given 0.12 M NaCl water to drink and four different diets (Teklad, Madison, WI, USA) to eat for 7–12 days before microdissection of nephron segments. Group 1 received basic diet[1] with 100 meq/kg of potassium bicarbonate. Groups 2, 3, and 4 were given diets containing 300, 500, and 700 meq/kg of potassium bicarbonate respectively (Table 1), with a slight decrease in sucrose and corn starch. Normal laboratory diets for rabbits contain 300 meq K^+/kg. To determine the intake of sodium and potassium, the intake of diets and NaCl water was monitored throughout the study.

Collection and analysis of urine and plasma. Animals were kept in the metabolic cages 48 h prior to microdissection for urine collection. Blood was collected from the neck stump into a container with heparin at the time of decapitation. The plasma was separated from blood by centrifugation at

Abbreviations used: ADX, adrenalectomized; ATPase, adenosine triphosphatase; CCD, cortical collecting duct; CNT, connecting tubule; DCT, distal convoluted tubule; MCD, medullary collecting duct

Offprint requests to: L. C. Garg

[1] *Composition of the basic diet.* Sucrose, 18.1%; corn starch, 18.0%; high protein casein and other amino acids, 17.7%; dextrose, 15.0%; cellulose fiber, 15.0% dehydrated alfalfa meal, 6.0%; corn oil, 5%; vitamin mix, 1.2%; NaCl, 1.11% and other minerals, 2.5%

Table 1. Dietary potassium content, food intake, body and kidney weights of adrenalectomized rabbits

Treatment group	Dietary K^+ content (meq/kg)	*n*	Food intake (g/day)	K^+ intake (meq/day)	Na^+ intake (meq/day)	Body wt. (g)	Kidney wt. (g)
1	Low (100)	6	43 ± 2	4 ± 0.2	22 ± 2	1,398 ± 33	4.40 ± 0.22
2	Normal (300)	6	50 ± 3	15 ± 1*	32 ± 2	1,321 ± 68	5.10 ± 0.45
3	High (500)	8	35 ± 4	17 ± 2*	27 ± 2	1,363 ± 44	4.72 ± 0.25
4	Very high (700)	6	38 ± 6	27 ± 4**	24 ± 3	1,368 ± 31	4.64 ± 0.18

Each value represents the mean ± SEM of *n* animals
Na^+ intake includes Na^+ taken in food as well as in drinking water
The body and kidney weights were determined on the day of sacrifice
* $p < 0.05$ vs. group 1
** $p < 0.05$ vs. groups 1, 2, and 3

3,000 × *g* for 10 min and stored frozen at −20° C, until ready for analysis. Urine was collected from the bladder for measuring pH and total CO_2 content. The pH was measured on a digital pH meter (Fisher Scientific Co., Orlando, FL, USA) at 25° C. Na^+ and K^+ in the plasma and urine were determined by a flame photometer (Model 143, Instrumentation Laboratory, Lexington, MA, USA). Plasma aldosterone concentrations were determined by radioimmunoassay (Hazelton Laboratory, Vienna, VA, USA). Total CO_2 content in plasma and urine was determined with a CO_2 analyzer (Instrumentation Laboratory). Urine and plasma creatinines were determined by the Jeffe reaction [8].

Microdissection and preparation of nephron segments. Nephron segments were microdissected from the slices of kidney as has been described earlier [5]. The left kidney was removed and perfused immediately with chilled dissection buffer containing 0.1% collagenase (Type I, 140 U/mg, Sigma Chemical Co., St. Louis, MO, USA). The dissection buffer contained (in mM): NaCl, 136; KCl, 3; K_2HPO_4, 1; $MgSO_4$, 1.2; $CaCl_2$, 2; Na lactate, 4; Na citrate, 1; l-alanine, 6; and glucose, 5.5. Several slices of cortex and medulla were incubated in dissection buffer (containing collagenase) with 100% O_2 at 37° C for 30 – 60 min. Distal convoluted tubules (DCT) and connecting tubules (CNT) were dissected from the superficial tangential slice. Cortical collecting ducts of superficial nephron segments (CCD) were dissected from the medullary rays of cortex. CNT were the granular portion between the bright (DCT) and the light (initial CCD) portions of the distal tubule [10a]. Medullary collecting ducts (MCD) were taken out from the inner stripe of outer medulla. All the dissection was done under a stereomicroscope in the dissection buffer at 4° C. The segments were straightened and their lengths were measured using an eyepiece micrometer. Each tubule was transferred to a small test tube with 100 µl of hypotonic solution which contained: imidazole, 1 mM; $MgCl_2$, 1 mM; EDTA, 0.25 mM; and bovine serum albumin, 0.1%. The samples were then frozen in a mixture of dry ice and acetone. After 40 min, the samples were thawed and 100 µl of imidazole buffer was added to each sample. The composition of this imidazole buffer (in mM) was: NaCl, 300; NH_4Cl, 200; $MgCl_2$, 10; imidazole, 100; and pH adjusted to 7.4 with HCl.

Determination of Na-K-ATPase activity. Na-K-ATPase activity was determined by the method described earlier [5]. The assay is based on the hydrolysis of ATP to ADP which is coupled to oxidation of NADH. The final composition of the reaction mixture was: NaCl, 100 mM; NH_4Cl, 66.7 mM; imidazole, 50.3 mM; $MgCl_2$, 3.7 mM; EDTA, 0.08 mM; Na_2ATP, 1.1 mM; phosphoenolpyruvate, 0.6 mM; NADH, 0.017 mM; pyruvate kinase, 3.1 U/ml; and lactate dehydrogenase, 4.1 U/ml. The reaction was performed in 300 µl of solution at 37° C for 30 min. In half of the samples, 1 mM ouabain was included in the buffer. All the reactants were used in excess so that the only limiting factor was the generation of ADP from ATP by nephron segment ATPase. The rate of ATP hydrolysis is stoichiometrically related to rate of NADH depletion which was measured in a fluorometer (Turner Model 111) in a custom made cuvette. The total ATPase activity (in the absence of ouabain) and the Mg-ATPase activity (in the presence of ouabain) were determined in triplicate. The difference between the total ATPase and Mg-ATPase is calculated as Na-K-ATPase activity. The ATPase activity was expressed as pmol ADP per min per mm tubule.

Statistical analysis. Statistical comparisons among the four groups were performed by analysis of variance and Duncan's multiple range test (with modification for unequal sample sizes). The null hypothesis was rejected at the 0.05 level of significance. The relationship between K^+ excretion and Na-K-ATPase as well as plasma K^+ and the enzyme activity in the CCD were determined by the regression analysis with and without transformation of the data.

Results

Food intake, animal and kidney weights

There was not significant difference in the food intake in the four groups of animals. Dietary intake of potassium in group 4 was, therefore, approximately 7 times of that in group 1. Total intake of sodium in both food and drinking water was not significantly different among the four groups. Furthermore, there was no significant difference in the body weights and kidney weights at the time of sacrifice in the four groups (Table 1).

Plasma and urine electrolytes

There were no significant differences in sodium concentration and total carbon dioxide content in the plasma among the four groups. Although mean plasma potassium level and

Table 2. Plasma and urine electrolytes

Treatment group	n	P_{Na} (meq/l)	P_{rCO_2} (meq/l)	P_K (meq/l)	C_{Cr} (ml/min)	$U_{Na} \cdot V$ (meq/day)	$U_K \cdot V$ (meq/day)	FE_K (%)	$U_{rCO_2} \cdot V$ (meq/day)	U_{pH}
1	6	139 ± 2	26 ± 2	4.3 ± 0.30	2.0 ± 0.2	22 ± 3	2.5 ± 0.5	19.8 ± 2.9	4.6 ± 2.3	6.6 ± 0.47
2	6	134 ± 6	27 ± 1	4.6 ± 0.32	2.8 ± 0.4	29 ± 3	10.6 ± 0.4*	74.3 ± 9.3*	13.2 ± 2.0*	8.2 ± 0.16*
3	8	133 ± 3	28 ± 2	4.7 ± 0.22	3.1 ± 0.4	21 ± 4	11.4 ± 2.0*	61.6 ± 12.0*	14.5 ± 2.7*	8.3 ± 0.12*
4	6	136 ± 2	27 ± 2	5.0 ± 0.24	3.4 ± 0.1	23 ± 5	17.0 ± 2.0**	106.2 ± 13.2**	13.9 ± 2.6*	8.3 ± 0.11*

Each value represents the mean ± SEM of n animals
* $p < 0.05$ vs. group 1
** $p < 0.05$ vs. groups 1, 2, and 3

Table 3. Na-K-ATPase activity in rabbit nephron segments

Treatment group	n	DCT	CNT	CCD	MCD
1	6	72 ± 13	80 ± 6	3.6 ± 0.8	8.5 ± 2.0
2	5–6	53 ± 10	72 ± 10	8.8 ± 2.0*	8.1 ± 2.0
3	5–8	64 ± 5	80 ± 7	8.1 ± 2.0*	4.0 ± 0.8
4	5–6	71 ± 5	71 ± 5	13.6 ± 2.0**	8.0 ± 1.0

The enzyme activity is expressed as pmol · min^{-1} · mm^{-1}
Each value represents the mean ± SEM of n animals
* $p < 0.05$ vs. group 1
** $p < 0.05$ vs. groups 1, 2, and 3

the creatinine clearance increased in group 1 to group 4, the differences were not statistically significant (Table 2).

There was no significant difference in the urinary excretion of Na^+ among the four groups. However, the rates of excretion of potassium and total CO_2 and the urinary pH were significantly higher in groups 2 to 4 compared to those in group 1. The excretion of potassium in group 4 was also significantly higher than in groups 2 and 3. The fractional excretion of K^+ was only 20% in group 1 but increased to 106% in group 4.

Na-K-ATPase

There were no significant differences in Na-K-ATPase activities in the DCT, CNT and MCD among the four groups (Table 3). On the other hand, Na-K-ATPase activity in the CCD increased as the dietary intake of potassium was increased in group 1 to group 4. The enzyme activity in the CCD in groups 2 to 4 was significantly higher than in group 1. In addition, the enzyme activity in the CCD in group 4 was also significantly higher than in groups 1, 2, and 3.

There was a linear relationship between Na-K-ATPase activity in the CCD and steady-state plasma K^+ (Fig. 1) as well as excretion of potassium (Fig. 2). There was no significant relationship between Na-K-ATPase activities in the other three segments (DCT, CNT, and MCD) and the excretion of potassium or plasma K^+.

Mg-ATPase

Mg-ATPase activity in all the four segments decreased as the dietary intake of potassium bicarbonate was increased from group 1 to group 4 (Table 4). However, except in the CCD, the differences were statistically significant only in group 3 and 4 vs group 1 and 2.

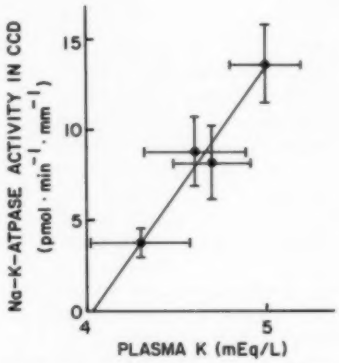

Fig. 1. Relationship between Na-K-ATPase activity in the CCD and steady state plasma K^+ in the $KHCO_3$-diet animals. The regression equation for the relationship is $y = -56 + 13.8x$ with $r = 0.98$

Discussion

The present results confirm our recent observation [4] that Na-K-ATPase can be stimulated by dietary intake of potassium in the absence of aldosterone. Furthermore, our previous [4] and present results have established that a sevenfold increase in dietary potassium (for 7–12 days) can produce a > 200% increase in Na-K-ATPase activity in the CCD in ADX rabbits whether potassium is given in the form of KCl or $KHCO_3$. In addition, Na-K-ATPase activity in the CCD was linearly related to steady state plasma K^+ (Fig. 1). However, Na-K-ATPase activity in the CCD as well as steady state plasma K^+ were lower in all $KHCO_3$-diet groups in the present study than the corresponding KCl-diet groups studied previously under similar conditions [4] (Fig. 3). A positive relationship between plasma K^+ and Na-K-ATPase activity in the CCD in both $KHCO_3$-diet and KCl-diet in ADX rabbits suggest that the steady-state concentration of K^+ in the plasma is an intrinsic regulator of Na-K-ATPase activity in the CCD in the absence of aldosterone.

An increase in Na^+ load has been shown to increase Na-K-ATPase activity in the CCD [11]. Therefore, it is possible that the decreased Na-K-ATPase activity is not due to lower plasma K^+ but is due to decreased Na^+ load to the CCD of $KHCO_3$-diet animals as compared to KCl-diet animals. However, neither the filtered Na^+ load nor the Na^+ excretion in $KHCO_3$-diet were significantly different from KCl-diet animals (Table 5). Therefore, it is unlikely that the differences in Na-K-ATPase activity in CCD are due to

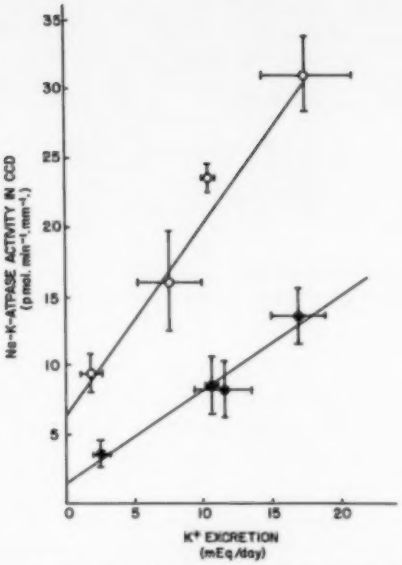

Fig. 2. Relationship between Na-K-ATPase activity in the CCD and K^+ excretion in ADX rabbits given either $KHCO_3$ or KCl diets. (●) represent data from $KHCO_3$-diet animals. (○) represent data from KCl-diet animals reported in [4]. Values represent mean ± SE in each direction. The regression equation for the relationship in $KHCO_3$-diet animals is $y = 1.54 + 0.67x$ with a correlation coefficient (r) of 0.93. The regression equation for the relationship in KCl-animals is $y = 6.6 + 1.4x$ with $r = 0.98$. The slopes and the intercepts of the two regression lines are significantly different from each other ($p < 0.05$)

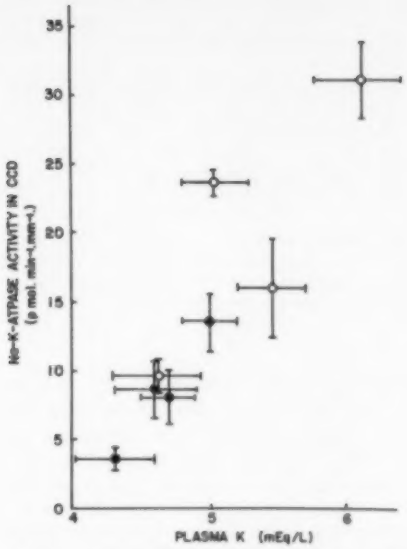

Fig. 3. Relationship between Na-K-ATPase activity in the CCD and steady state plasma K^+. Symbols used are same as in Fig. 2 and values are mean ± SE. The regression equation for the overall relationship is $y = -57 + 14.2x$ with $r = 0.90$

Table 4. Mg-ATPase activity in rabbit nephron segments

Treatment group	*n*	DCT	CNT	CCD	MCD
1	6	78 ± 13	87 ± 8	28 ± 2	29 ± 2
2	5–6	64 ± 6	102 ± 13	23 ± 1*	31 ± 3
3	5–8	43 ± 7**	46 ± 8**	12 ± 2**	9 ± 1**
4	5–6	31 ± 2**	29 ± 3**	11 ± 1**	10 ± 2**

The enzyme activity is expressed as pmol · min^{-1} · mm^{-1}
Each value represents the mean ± SEM of *n* animals
* $p < 0.05$ vs. group 1
** $p < 0.05$ vs. groups 1 and 2

decreased Na^+ load in $KHCO_3$-diet animals when compared to KCl-diet animals.

The urinary excretion of K^+ is usually dependent on distal tubular secretion of K^+ which has been shown to be dependent on Na-K-ATPase activity in this part of the nephron [7, 12, 18, 19]. As stated above, Na-K-ATPase activity in the CCD was lower in $KHCO_3$-diet animals than in KCl-diet animals reported in our previous study [4]. On the other hand, there was no difference in the urinary excretion of potassium between $KHCO_3$-diet and KCl-diet animals. When the relationship between Na-K-ATPase activity in CCD and urinary excretion of potassium was examined in $KHCO_3$-diet and KCl-diet ADX rabbits, there was a significant difference in the intercepts (but not in the slopes) of the two regression lines (Fig. 2). The reasons for similar K^+ excretions but different Na-K-ATPase activities in the CCD from $KHCO_3$-diet and KCl-diet animals are not known. However, it is possible that K^+ secretion in the CCD was higher in KCl-diet animals than in $KHCO_3$-diet animals. The lack of difference in K^+ excretion in animals on two different types of diets may be due to greater K^+ reabsorption in the MCD in KCl-diet animals than in $KHCO_3$-diet animals.

Actual potassium secretion in the CCD in $KHCO_3$-diet or KCl-diet ADX rabbits is not known. It has been shown that K^+ secretion in rat distal tubule is higher in metabolic alkalosis than in metabolic acidosis [18]. However, no metabolic alkalosis was produced in our $KHCO_3$-diet ADX rabbits (Table 2). This may be due to intake of NaCl in drinking water as it has been shown that chronic metabolic alkalosis cannot be induced in dogs if chloride is available in their diet [14]. Therefore, metabolic alkalosis would not be a reason for the difference in Na-K-ATPase activity and K^+ secretion (if any) in the CCD between $KHCO_3$-diet and KCl-diet animals.

Another explanation for the presence of higher Na-K-ATPase activity in the CCD in KCl-diet ADX rabbits [4] than in $KHCO_3$-diet animals at same rate of potassium excretions (Fig. 2) may lie in a recently proposed model of potassium secretion [3, 24]. In this model, an additional potassium transport mechanism involving a co-transport of potassium and chloride from cell to lumen takes place when tubular fluid concentration of Cl^- in the CNT and initial CCD is decreased in the rat. If it is assumed that the proposed KCl co-transport system in the apical membrane is a primary active process (i.e. independent of peritubular Na-K-ATPase) and the chloride in the tubular fluid in the CCD of our $KHCO_3$-loaded ADX rabbits is low, then the differences in Na-K-ATPase activity in the CCD of $KHCO_3$-

Table 5. Comparison of filtered Na^+ load and Na^+ excretion between KCl and $KHCO_3$ diets

Treatment group	Filtered Na^+ load (meq/h)		Na^+ excretion (meq/h)		Urine flow (ml/h)	
	KCl-diet[a]	$KHCO_3$-diet	KCl-diet[a]	$KHCO_3$-diet	KCl-diet[a]	$KHCO_3$-diet
1	14 ± 4	17 ± 2	0.79 ± 0.20	0.90 ± 0.10	2.8 ± 0.6	4.1 ± 0.5
2	16 ± 2	23 ± 4	0.80 ± 0.10	1.20 ± 0.15	3.3 ± 1.2	4.8 ± 0.7
3	19 ± 3	23 ± 3	0.60 ± 0.15	0.89 ± 0.16	3.4 ± 0.7	4.7 ± 0.8
4	15 ± 3	28 ± 8	1.00 ± 0.30	0.97 ± 0.20	5.4 ± 1.8	5.3 ± 1.2

[a] Data for KCl diet is taken from [4]

Filtered Na^+ load and Na^+ excretion are not significantly different from each other among the eight groups when tested by ANOVA. In addition, there were no significant differences in Na^+ loads and Na^+ excretions in two groups given same K^+ content but different diets (KCl vs. $KHCO_3$) when analyzed by Student's *t*-test

loaded and KCl-loaded ADX rabbits (Fig. 2) can be explained as follows. Potassium will be secreted by two mechanisms in $KHCO_3$-loaded ADX rabbits (a) the peritubular Na-K-ATPase and the apical conductive pathway and (b) by neural KCl co-transport system. On the other hand, in KCl-loaded animals [4], the chloride concentration in the tubular fluid will be high and potassium secretion should occur only by peritubular Na-K-ATPase and an apical conductive pathway. If that is the case, a higher Na-K-ATPase activity in the CCD would be required in KCl-loaded animals than in $KHCO_3$-loaded animals to produce similar degree of potassium secretion.

Our results are consistent with the results obtained from studies on electrolyte transport in the CCD of ADX rabbits [21–23]. For example, Wingo et al. [23] have demonstrated that an increase in dietary potassium can increase potassium secretion in the CCD from ADX rabbits. Furthermore, it has been shown that potassium secretion in the CCD is inhibited by ouabain [21]. However, under conditions when sodium transport was inhibited (by amiloride), the inhibition of potassium secretion in the CCD from ADX rabbits was less than complete [22]. Our results along with these results [21–23] indicate that an increase in Na-K-ATPase activity in the CCD is at least partially responsible for increased potassium secretion in this segment in ADX rabbits even in the absence of mineralocorticoids. Furthermore, Hirsch et al. [9] have demonstrated that potassium loading produces an amplification of basolateral membranes in the initial CCD of ADX rats maintained on fixed doses of adrenal steroids. Our results when taken together with those of others [9, 21–23] indicate that potassium loading produces an increase in Na-K-ATPase activity, potassium secretion and basolateral membrane area in the CCD of ADX animals as it does in adrenal intact animals [2, 13, 18].

In the present study, we did not find a significant change in Na-K-ATPase activity in the DCT and MCD after modulation of $KHCO_3$ in the animal diet. These results are consistent with the absence of potassium secretion in the DCT and MCD [19, 24]. However, potassium has been shown to be secreted in the late distal tubule (which includes the CNT and initial CCD). We found a significant (50%) increase in Na-K-ATPase activity in the CNT after loading ADX rabbits with KCl [4] but not after loading with $KHCO_3$ (Table 3). The reason for the lack of a significant change in Na-K-ATPase activity in the CNT with $KHCO_3$ diet in ADX rabbits is not apparent.

A large (sevenfold) increase in potassium excretion compared to a small (fourfold) increase in Na-K-ATPase activity (and probably K^+ secretion) in the CCD in both KCl-diet and $KHCO_3$-diet animals may be due to potassium recycling. The concept of potassium recycling [10, 20] involves a net secretion of potassium in the CNT and CCD and reabsorption of potassium in the MCD. The reabsorbed potassium enters the proximal straight tubule (PST) and thin descending limb (TDL) and is again reabsorbed in the medullary thick ascending limb (MTAL). Thus, the effect of kyperkalemia in both KCl-diet and $KHCO_3$-diet animals on K^+ excretion is probably amplified by the potassium recycling process.

In summary, a seven-fold increase in $KHCO_3$ in the diet produced a seven-fold increase in the excretion of potassium in the urine in ADX rabbits. This was accompanied by four-fold increase in Na-K-ATPase activity in the CCD without any significant change in the enzyme activity in the DCT, CNT and MCD. There was a linear relationship between Na-K-ATPase activity in the CCD and steady state plasma K^+ as well as urinary excretion of potassium in ADX rabbits. However, Na-K-ATPase activity in the CCD and steady state plasma K^+ were lower in $KHCO_3$-fed ADX rabbits than the KCl-fed animals studied previously under similar conditions [4]. Our results suggests that plasma K^+ is an intrinsic regulator of Na-K-ATPase activity in the CCD even in the absence of aldosterone.

Acknowledgements. We thank Maciej Kapturczak for technical assistance, and Drs. Charles Wingo, Christopher Wilcox, Craig Tisher and Allen Neims for their advice and discussions. This work was supported by National Science Foundation grant, DCB-8213821 and DCB-8518000.

References

1. Boyd JE, Palmore WP, Mulrow PJ (1971) Role of potassium in the control of aldosterone secretion in the rat. Endocrinology 88:556–565
2. Doucet A, Katz AI (1980) Renal potassium adaptation: Na-K-ATPase activity along the nephron after chronic potassium loading. Am J Physiol 238:F380–F386
3. Ellison DH, Velazquez H, Wright FS (1985) Stimulation of distal potassium secretion by low lumen chloride in the presence of barium. Am J Physiol 248:F638–F649
4. Garg LC, Narang N (1985) Renal adaptation to potassium in adrenalectionized rabbit: Role of distal tubular Na-K-ATPase. J Clin Invest 76:1065–1070
5. Garg LC, Knepper MA, Burg MB (1981) Mineralocorticoid effects on Na-K-ATPase in individual nephron segments. Am J Physiol 240:F536–F544

6. Garg LC, Mackie S, Tisher CC (1982) Effect of low potassium diet on Na-K-ATPase in rat nephron segments. Pflügers Arch 394:113–117
7. Grantham JJ, Burg MB, Orloff J (1970) The nature of transtubular Na and K transport in isolated rabbit renal collecting tubules. J Clin Invest 49:1815–1826
8. Henry RJ, Cannon DC, Winkelman JW (1974) Clinical chemistry. Harper and Row, New York, p 543
9. Hirsch D, Kashgarian M, Boulpaep EL, Hayslett JP (1984) Role of aldosterone in the mechanism of potassium adaptation in the initial collecting tubule. Kidney Int 26:798–807
10. Jamison RL, Work J, Schaffer JA (1982) New pathways for potassium transport in the kidney. Am J Physiol 242:F297–F312
10a. Kaissling B, Kriz W (1979) Structural analysis of the rabbit kidney. Adv Anat Embryol Cell Biol 56:1–123
11. Katz AI (1982) Renal Na-K-ATPase: its role in tubular sodium and potassium transport. Am J Physiol 242:F217–F219
12. Koeppen BM, Biagi BA, Giebisch G (1983) Intracellular microelectrode characterization of the rabbit cortical collecting duct. Am J Physiol 244:F35–F47
13. Le Hir M, Kaissling B, Dubach UC (1982) Distal tubular segments in the rabbit kidney after adaptation to altered Na- and K-intake. II. Changes in Na-K-ATPase. Cell Tissue Res 224:493–503
14. Lemieux G, Kiss A, Lemieux C, Ibanez RJ, Aranda MR (1985) Renal tubular biochemistry during acute and chronic metabolic alkalosis in the dog. Kidney Int 27:908–918
15. Schwartz GJ, Burg MB (1978) Mineralocorticoid effects on cation transport by cortical collecting tubules in vitro. Am J Physiol 235:F576–F585
16. Silva P, Hayslett JP, Epstein FH (1973) The role of Na-K-activated adenosine triphosphatase in potassium adaptation-stimulation of enzymatic activity by potassium loading. J Clin Invest 52:2665–2671
17. Stanton BA, Giebisch G (1982) Effects on pH on potassium transport by renal distal tubule. Am J Physiol 242:F544–F551
18. Stanton BA, Biemesderfer D, Wade JB, Giebisch G (1981) Structural and functional study of the rat distal nephron: effects of potassium adaptation and depletion. Kidney Int 19:36–48
19. Stokes JB (1982) Na and K transport across the cortical and outer medullary collecting tubule of the rabbit: evidence for diffusion across the outer medullary portion. Am J Physiol 242:F514–F520
20. Stokes JB (1982) Consequences of potassium recycling in the renal medulla. J Clin Invest 70:219–229
21. Wingo CS (1984) Effect of ouabain on K^+ secretion in cortical collecting tubules from adrenalectomized rabbits. Am J Physiol 247:F588–F595
22. Wingo CS (1985) Cortical collecting tubule potassium secretion: effect of amiloride, ouabain and luminal sodium concentration. Kidney Int 27:886–891
23. Wingo CS, Seldin SW, Kokko JP, Jacobson HR (1982) Dietary modulation of active potassium secretion in the cortical collecting tubules from adrenalectomized rabbits. J Clin Invest 70:579–586
24. Wright FS, Giebisch G (1985) Regulation of potassium excretion. In: Seldin DW, Giebisch G eds) The kidney. Physiology and pathophysiology, vol 2. Raven Press, New York, pp 1223–1249

Received August 18, 1986/Accepted January 5, 1987

Pflügers Arch (1987) 409:132–137

Pflügers Archiv
European Journal of Physiology
© Springer-Verlag 1987

Evidence for OH^-/H^+ permeation across the peritubular cell membrane of rat renal proximal tubule in HCO_3^--free solutions

B.C. Burckhardt and E. Frömter

Zentrum der Physiologie, Johann Wolfgang Goethe-Universität, Theodor Stern-Kai 7, D-6000 Frankfurt 70, Federal Republic of Germany

Abstract. Membrane potentials and intracellular pH were measured on rat renal proximal tubular cells in vivo to test whether sodium-bicarbonate cotransport across the peritubular cell membrane accepts OH^- (or H^+ in opposite direction) or whether it requires the CO_2, HCO_3^-, $CO_3^=$ buffer to operate. It was found that step changes of peritubular pH in nominally HCO_3^--free and CO_2-free solutions produced qualitively similar initial potential responses and cell pH responses as changes in peritubular HCO_3^- concentrations. These responses, however, were considerably smaller and they were neither reduced in Na^+-free solutions nor inhibited by the stilbene derivative SITS which is known to block $Na^+(HCO_3^-)_n$ cotransport completely. We conclude that the cotransporter requires the CO_2, HCO_3^-, $CO_3^=$ buffer for its physiological operation but that high rates of OH^- or H^+ can also be transferred across the peritubular cell membrane in HCO_3^--free solutions, probably through a separate transport system.

Key words: Rat renal proximal tubule – Sodium-bicarbonate cotransport – Pertibular OH^-/H^+ permeation

Introduction

It has recently been found that buffer exit from renal proximal tubule proceeds via cotransport with Na^+ [1, 2, 5, 7, 16–18] at a stoichiometry of 2:1 [7] or 3:1 [23, 30]. However, the exact nature of the buffer species which moves and the possible involvement of other ions such as coupling to Cl^- are not yet established. Our previous observation that the electrical response to peritubular HCO_3^- removal is reduced under the influence of classical inhibitors of carbonic anhydrase (CAH) such as acetazolamide or ethoxzolamide [9, 14] and the observation of a membrane-bound carbonic anhydrase on the peritubular cell membrane [22, 28] suggested that HCO_3^- might possibly be split during transport into OH^- and CO_2 and might recombine to HCO_3^- after passing the membrane under the influence of the membrane-bound enzyme. To test this hypothesis we have investigated whether peritubular pH steps in normally HCO_3^--free solutions produce similar changes of membrane potential and cell pH as steps in peritubular HCO_3^- concentrations. Part of the results was reported in abstract form previously [Pflügers Arch (1981) 389:R40].

Offprint requests to: E. Frömter

Methods

The experiments were carried out on renal proximal tubules of anesthetized rats using standard in vivo microperfusion techniques described previously [24]. After anesthesia with intraperitonal sodium 5-ethyl-5-(1′-methyl-propyl)-2-thiobarbiturate (Inactin, Byk Gulden, Konstanz, FRG) male Wistar rats (230 g) were placed on a thermostated table, and the left kidney was exposed by flank incision, immobilized in agar and superfused with prewarmed paraffine oil. The luminal and peritubular surface of proximal tubules was perfused from multibarrelled perfusion capillaries [24] using the retrograde perfusion technique and the capillary perfusion technique described previously [13]. Cell punctures were obtained with conventional microelectrodes (filled with 2.7 molar KCl solution) or with double-barrelled microelectrodes which were constructed from self-filling double-barrelled glass tubing (Hilgenberg, Malsfeld, FRG) of unequal diameter (i.d. 0.87 mm, o.d. 1.5 mm, and i.d. 0.35 mm, o.d. 0.75 mm) as described previously [29]. The reference barrel was filled with 0.5 molar KCl solution and the selective barrel with the H^+ ligand cocktail of Fluka (Buchs, Switzerland), which is based on tridodecylamine [3]. The potential differences against the extracellular fluid compartment, which was grounded via the deskinned rat's tail, were measured with a high impedance electrometer (model FD 223 WP Instruments, New Haven, CT, USA). To improve sensitivity and response time the electrode tips were gradually bevelled in a suspension of Al_2O_3 powder agitated by magnetic stirring [12] and the electrode shaft was coated with a silver shield (Auromal 37M, Völkner Elektronik, Braunschweig, FRG) which was connected to the 1× output of the electrometer. Slope and resistance of the pH-sensitive electrodes were 56.1 SD ± 2.0 mV and about 1×10^{12} Ohm, respectively ($n = 5$). The following solutions were used (numbers indicating concentrations in mmol/l): Na^+ 144, K^+ 4.0, Ca^{2+} 1.25, Mg^{2+} 0.5, Cl^- 118.5, HCO_3^- 30, SO_4^{2-} 0.5, HPO_4^{2-} 1.0. In the HCO_3^--free solutions HCO_3^- was replaced by BES (N,N-bis(2-hydroxyethyl)-2-aminoethane sulfonic acid), HEPES (N-(2-hydroxyethyl)piperazine-N′-2-ethane sulfonic acid) or TRIS (2-amino-2-hydroxymethyl-1,3-propanediol) as specified below and in solutions with reduced buffer concentrations the missing buffer was replaced by Cl^-. If required, Na^+ was replaced by choline. pH was adjusted to the desired value by titration with 1 molar NaOH or respectively HCl and in Na^+-free solutions with choline base, HCO_3^--containing solutions were equilibrated with 5% CO_2 in O_2 unless otherwise indicated, all others were gassed with pure oxygen.

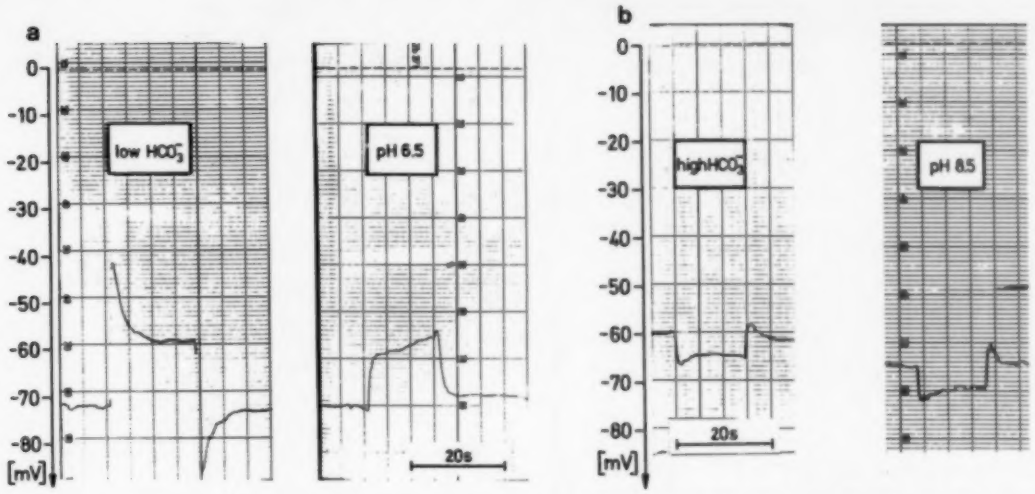

Fig. 1 a, b. Comparison of the cell potential responses to peritubular step changes in HCO_3^- concentration and pH. Sections of trace records representing membrane potential (in mV) as function of time (see *calibration bar*). **a** Response to decreasing HCO_3^- concentration from 30 to 3 mmol/l ("low HCO_3^-") at constant pH (*left*) and response to changing pH from 7.5 to 6.5 ("pH 6.5") in nominally HCO_3^--free solution buffered with BES (*right*). **b** Response to increasing HCO_3^- concentration from 30 to 60 mmol/l ("high HCO_3^-") at constant pH (*left*) and response to increasing pH from 7.5 to 8.5 ("pH 8.5") in TRIS-buffered HCO_3^--free solutions (*right*). BES- and TRIS-buffer concentrations were 10 mmol/l throughout

In some experiments SITS (4-acetamido-4′-isothiocyano-2,2′-disulfonic stilbene, 10^{-3} mol/l, obtained from Serva, Heidelberg, FRG) or $BaCl_2$ (10^{-3} mol/l) were added to the perfusion fluid. The Ba^{2+}-containing solutions were prepared without SO_4^{2-} to avoid precipitation of $BaSO_4$. All chemicals were of analytical grade and purchased from Merck (Darmstadt, FRG), except BES and HEPES which were obtained from Sigma (Taufkirchen, FRG).

Results

Membrane potential response to step changes in pH

Figure 1a compares the membrane potential response of a proximal tubular cell to 10:1 reduction of peritubular HCO_3^- concentration at constant pH with the response to a unit change of peritubular pH from 7.5 to 6.5 in nominally HCO_3^--free solutions, and Fig. 1b compares the effect of a 2-fold increase of peritubular HCO_3^- concentration (at the expense of Cl^- and at constant pH) with a unit pH change into alkaline direction. In both cases we observe an initial depolarizing (Fig. 1a) or respectively hyperpolarizing response (Fig. 1b) as expected if OH^- (or in opposite direction H^+) could permeate similarly as HCO_3^-. However, the initial response is much smaller and the secondary response is completely different: for example, instead of a recline, the acidifying pH step produces a secondary depolarization, similar to what we have observed previously upon increasing CO_2 tension [9].

Since OH^- concentration is approximately five orders of magniture smaller than HCO_3^- concentration but OH^- ions can be regenerated instantaneously from buffer base, we tested whether the magnitude of the response increased with buffering power. A small dependence was observed

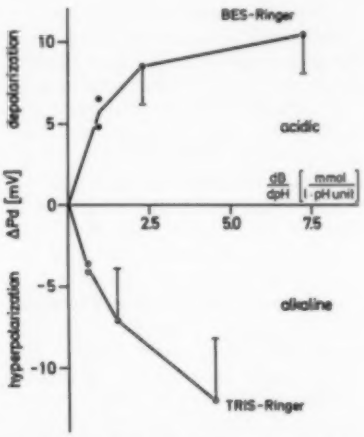

Fig. 2. Effect of buffering power on the initial cell potential response to unit pH jumps in nominally HCO_3^--free solutions. *Abscissa*: buffering power β in mmol/l × pH unit as determined by titration with 1 molar NaOH or HCl after the experiment. *Ordinate*: initial potential response to peritubular pH jumps in mV. The solutions contained respectively 1, 3, and 10 mmol/l BES (acid range) or TRIS (alkaline range) and the pH was changed from pH 7.5 to 6.5 or from pH 7.5 to 8.5

(Fig. 2) which seemed to level, however, with the highest buffering power tested (7.24 mmol/l × pH unit). Mean values of the potential change in response to pH steps and to bicarbonate concentration steps are reported in Table 1.

As previously observed with HCO_3^- concentration steps in the tubular lumen, changing pH in the luminal perfusate at constant peritubular perfusion had virtually no effect on

Table 1. Initial cell potential response to peritubular step changes of pH and of HCO_3^- concentration at constant pH

		$\Delta Pd \pm SD$ (mV)	n/m
pH	7.5 → 6.5	+ 10.4 ± 2.3	4/5
	7.5 → 8.5	− 12.0 ± 3.8	4/5
HCO_3^- (mmol/l)	30 → 3	+ 28.0 ± 7.0	6/4
	30 → 60	− 6.3 ± 1.3	6/4

Polarity: Positive ΔPd indicates depolarization, negative ΔPd indicates hyperpolarization of resting membrane potential. *n* is number of measurements on each cell, *m* number of cells investigated. In the pH experiments, HCO_3^--free solutions were used containing 10 mmol/l of BES or respecively TRIS and pH was adjusted by titration with NaOH or HCl to 7.5 and 6.5 or to 7.5 and 8.5 respectively. In the HCO_3^- experiments, the solutions containing 30, 3, and 60 mmol/l of HCO_3^- were equilibrated with respectively 5%, 0.5%, and 10% CO_2 in O_2 to achieve constant pH

the cell membrane potential (acidification by 1 pH unit from 7.5 to 6.5 in BES-Ringer depolarized the cell membrane by 0.5 SD ± 0.4 mV, each six subsequent measurements on four tubules).

Test for indirect pH effects on membrane potential

To test whether the observed fast changes in membrane potential are associated with buffer ion fluxes or represent changes in membrane permeabilities we have performed the following experiments: (1) we have used different buffers, (2) we have repeated the experiments in the presence of Ba^{2+} to block K^+ channels which are known to be pH-regulated and (3) we have measured the cell pH during changes in peritubular pH with nominally HCO_3^--free solutions.

(1) Besides BES and TRIS which had been used above we also performed experiments with HEPES-buffer (30 mmol/l in nominally HCO_3^--free solutions). However, since HEPES has a pK of 7.31 at 37°C [15] the pH steps were confined to 0.5 pH units. Acidification from 7.5 to 7.0 depolarized initially by + 3.2 SD ± 1.3 mV (one observation each in three different tubules). This was followed by a similar secondary depolarization as shown in Fig. 1a. Alkalinization on the other hand hyperpolarized (by − 4.5 mV, single observation) in agreement with the data reported above.

(2) Figure 3 shows the averaged potential time course of experiments with peritubular pH changes under control conditions and in the presence of Ba^{2+} (1 mmol/l). Each data point represents four subsequent measurements on five different tubules. It can be seen that Ba^{2+} does not affect the initial potential response but only the slow secondary response: during acidification, instead of the slow secondary depolarization, the potential remains constant under Ba^{2+}, and during alkalinization, instead of a constant hyperpolarization, the potential returns towards the control level under Ba^{2+}. We conclude from these experiments that the fast initial potential response to changes in peritubular pH in nominally HCO_3^--free solutions does not arise from changing K^+ permeability. K^+ permeability seems to change in response to pH changes, this effect, however, cannot explain the fast initial potential response.

(3) Figure 4 describes the effect on cell pH of a peritubular pH jump from 7.5 to 7.0 in nominally HCO_3^--free solutions buffered with HEPES. It can be seen that cell pH decreases gradually as expected, if OH^- moved out or

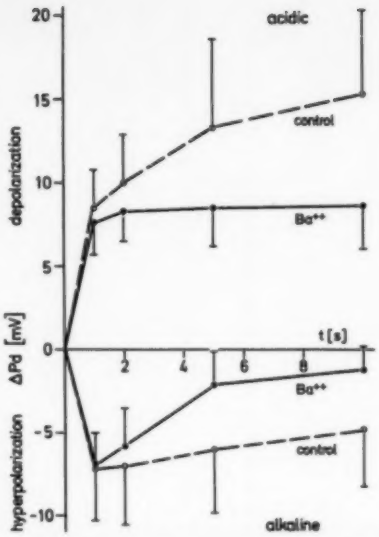

Fig. 3. Cell potential response to step changes of peritubular pH in the presence and absence of barium. *Abscissa:* time as indicated; *ordinate*: cell potential response in mV. (○——○) Averaged time course of 20 measurements with peritubular pH steps from 7.5 to 6.5 or 8.5 in BES- or TRIS-buffered (3 mmol/l) nominally HCO_3^--free solutions under control conditions. (●——●) Averaged time course of otherwise identical experiments in the presence of Ba^{2+} (1 mmol/l, also at pH 7.5). Note that initial potential response is not affected by Ba^{2+}

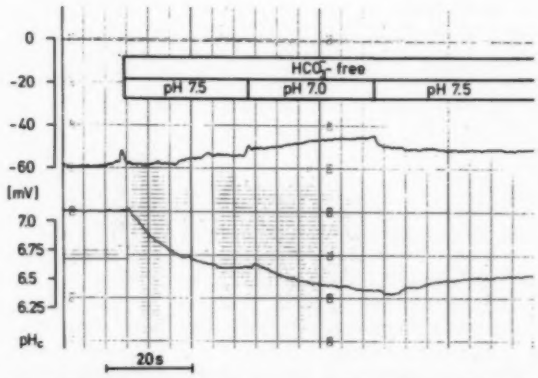

Fig. 4. Response of cell membrane potential and intracellular pH to a peritubular pH jump from pH 7.5 to 7.0. During the experiment the tubular lumen was continuously perfused with bicarbonate-free Ringer solution. *Upper trace*: potential difference in mV versus time as indicated by *bars; lower trace*: intracellular pH versus time. All solutions were buffered with HEPES (30 mmol/l). Note cell acidification in response of removing HCO_3^- and later in response to shifting pH from 7.5 to 7.0

H^+ in. As will be discussed below, however, there are also alternative interpretations for this observation.

Experiments with Na^+-free solutions and SITS

Since, thus far, the results showed a striking qualitative similarity in the initial response to pH steps and to HCO_3^-

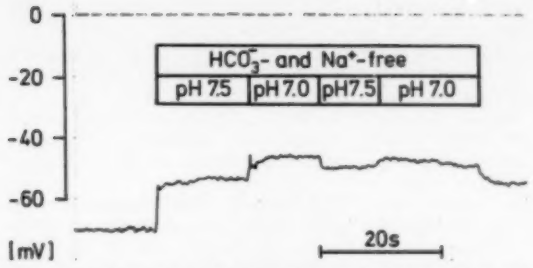

Fig. 5. Membrane potential response to peritubular pH jumps from 7.5 to 7.0 in Na^+-free, HCO_3^--free HEPES-Ringer solution. Other details as in Fig. 1

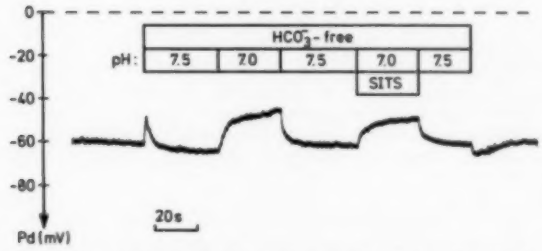

Fig. 6. Membrane potential response to peritubular pH steps from 7.5 to 7.0 in HCO_3^--free HEPES-Ringer solution under control conditions and in the presence of SITS (1 mmol/l). During the entire experiment the lumen was continuously perfused with HCO_3^--free solution. Other details as in Fig. 1

concentration steps, we have tested more directly whether both observations might be caused by the same transport mechanism. This was done by using Na^+-free solutions and SITS, since we know from previous experiments [30] that $Na^+(HCO_3^-)_n$ cotransport requires Na^+ and can be inhibited by SITS.

As shown in Fig. 5, after replacing all Na^+ in the lumen and in the peritubular compartment by choline, the potential response to acidification in nominally HCO_3^--free solutions was still preserved (note: a smaller response than in Fig. 1 was expected because the pH step in these experiments was only 0.5 units rather than one full pH unit).

Figure 6 finally shows that SITS (10^{-3} mol/l) did not eliminate the potential response after a sudden peritubular acidification in nominally HCO_3^--free solutions although SITS completely blocks $Na^+(HCO_3^-)_n$ cotransport. The data from a total of seven similar experiments including some cell pH-measurements are summarized in Table 2. We conclude from these observations that the pH-dependent membrane potential and cell pH changes in nominally HCO_3^--free solutions are independent of $Na^+(HCO_3^-)_n$ cotransport.

Discussion

In the present experiments we have tested whether OH^- (or in opposite direction H^+) might be able to migrate on the $Na^+(HCO_3^-)_n$ cotransporter through the peritubular cell membrane of rat renal proximal tubule and hence whether bicarbonate flux through this cotransporter might proceed

Table 2. Initial cell potential and cell pH response to peritubular pH steps from 7.5 to 7.0 in HEPES-Ringer under control conditions and in the presence of SITS

	$\Delta Pd \pm SD$ (mV)	$\Delta pH \pm SD^a$	n/m
Control	$+4.6 \pm 1.9$	$+0.070 \pm 0.037$	1/7
SITS (1 mmol/l)	$+3.8 \pm 0.6$	$+0.067 \pm 0.035$	1/4

Details as in Table 1, except that 30 mmol/l HEPES-Ringer was used throughout

[a] Cell pH values are taken 5 s after the peritubular pH change

in form of OH^- or respectively H^+. Although we have observed a number of experimental conditions in which OH^-/H^+ concentration steps in nominally HCO_3^--free solutions mimicked the results of similar experiments with HCO_3^- concentration steps, we eventually arrived at the conclusion that the cotransporter does not function normally in HCO_3^--free solutions and hence that it most probably transfers bicarbonate (or carbonate) rather than OH^- or H^+. This conclusion which agrees with recent reports about the renal [16] and corneal [19] sodium bicarbonate cotransporter was based mainly on the inability of sodium-free solutions and SITS-containing solutions to interfere with pH-induced changes of cell membrane potential and intracellular H^+ concentration.

The hypothesis that HCO_3^- might move through the $Na^+(HCO_3^-)_n$ cotransporter in form of OH^- (or respectively H^+ in opposite direction) had initially emerged from our observation that inhibitors of carbonic anhydrase interfere with peritubular HCO_3^- transport in vivo [9, 14] and this hypothesis seemed even more attractive after we had recently observed that the potential response from $Na^+(HCO_3^-)_n$ cotransport was already affected if only the membrane bound carbonic anhydrase on the outer surface of the peritubular cell membrane was inhibited (by dextran-bound CAH-inhibitors [10]). The fact that this hypothesis was disproven in the present experiments urges for alternative explanations of the role of membrane-bound CAH. One possible explanation might be that Na^+ and HCO_3^- move largely as ion pair as suggested by recent experiments of Boron on squid axon [6] and Jentsch and coworkers on BSC-1 cells [20] and that the reaction of 2 HCO_3^- ions and 1 Na^+ to form $NaCO_3^-$, CO_2 and H_2O is accelerated by CAH. Another possible explanation might be that the activity of $Na^+(HCO_3^-)_n$ cotransport is regulated and CAH inhibitors somehow interfere with regulation and finally it might be that CAH serves to reduce the hydration of CO_2 in context with HCO_3^- transport via a hypothetical OH^- or H^+ conductance as will be considered next.

If the potential and cell pH response to peritubular pH steps cannot be explained via $Na^+(HCO_3^-)_n$ cotransport, we have to ask which other transport mechanisms might be responsible. Could the observation result from other cotransporters or must we assume that a significant OH^- or H^+ conductance pathway is present in the peritubular cell membrane?

H^+ or OH^- flow via Na/H or Cl/HCO_3 exchangers may largely be excluded because such electroneutral countertransporters should not yield fast membrane potential changes and because the former should be inoperative in the experiments with luminal and peritubular perfusion with

Na^+-free solutions and the latter should be inhibited in the experiments with SITS.

H^+ or OH^- transport via phosphate, lactate or carboxylic acid transport systems [4, 11, 21, 25–27] may also largely be excluded because no such substrates were present in the artificial solutions or respectively the phosphate concentration was rather low.[1]

Furthermore, we can exclude that the cell pH changes were caused by buffer flux. If, contrary to all expectations, the undissociated buffer species was able to penetrate the cell membrane, the cell pH response to changes in peritubular pH, should have increased approximately linearily with increasing buffer concentration. However this was not the case. Instead, the response seemed to saturate with increasing buffer concentration, and this observation has recently been confirmed in similar experiments on isolated rabbit proximal tubule (Kondo and Frömter, unpublished observations). Moreover, we can mention that different buffer species gave essentially identical results.

On the other hand we cannot fully exclude that some of our punctures were somewhat leaky and hence that some buffer components passed through membrane leaks around the tip of the microelectrode, although we consider this possibility rather remote in view of the good reproducibility of the observations. In the latter case one might also speculate that the potential response was only a secondary consequence of a primary change in cell pH which affected one or more ionic conductances of the peritubular cell membrane. However, the observation that Ba^{2+} did not eliminate the initial membrane potential response speaks against this interpretation, at least as far as K^+ conductance is concerned.

In summary then, the present experiments would agree with the notion that the peritubular cell membrane contains a quantitatively significant OH^- or H^+ conductance or respectively a coupled rheogenic transport system which is able to transfer OH^- or H^+ in CO_2-free solutions. However, at present we cannot say whether this system functions normally in parallel with the $Na^+(HCO_3^-)_n$ cotransporter, or whether it is silent and shows up only after elimination of CO_2/HCO_3^-. The latter possibility is suggested by the fact that in HCO_3^- containing solutions SITS blocked the response to peritubular pH changes almost completely [8, 30] while in the present experiments in HCO_3^--free solutions it did not. Following this line of reasoning it also would seem possible that there is only one transport system present, which under physiological conditions transports Na^+ and HCO_3^- and in CO_2-free solutions loses its sensitivity to Na^+ and to SITS and transports OH^- or H^+ ions.

Acknowledgements. The experiments were supported by the Deutsche Forschungsgemeinschaft. The technical assistance of Mrs. N. Stallmach and secretarial assistance of Mrs. U. Merseburg and G. Selbach are gratefully acknowledged.

References

1. Alpern RJ (1985) Mechanism of basolateral membrane $H^+/OH^-/HCO_3^-$ transport in the rat proximal convoluted tubule: a sodium-coupled electrogenic process. J Gen Physiol 86:613–636
2. Alpern JA, Chambers M (1986) Cell pH in the rat proximal convoluted tubule. Regulation by luminal and peritubular pH and sodium concentration. J Clin Invest 78:502–510
3. Amman D, Lanter F, Steiner RA, Schulthess P, Shijo Y, Simon W (1981) Neutral carrier based hydrogen ion selective microelectrode for extra- and intracellular studies. Anal Chem 53:2267–2269
4. Barac-Nieto M, Murer H, Kinne R (1982) Asymmetry in the transport system of lactate by basolateral and brush border membranes of rat kidney cortex. Pflügers Arch 392:366–371
5. Biagi BA, Sohtell M (1986) Electrophysiology of basolateral bicarbonate transport in the rabbit proximal tubule. Am J Physiol 250:F267–272
6. Boron WF (1985) Intracellular pH-regulating mechanism of the squid axon. Relation between the external Na^+ and HCO_3^- dependences. J Gen Physiol 85:325–345
7. Boron WF, Boulpaep EL (1983) Intracellular pH regulation in the renal proximal tubule of the salamander. Basolateral HCO_3^- transport. J Gen Physiol 81:53–94
8. Burckhardt B-Ch, Cassola AC, Frömter E (1984) Electrophysiological analysis of bicarbonate permeation across the peritubular cell membrane of rat kidney proximal tubule. II. Exclusion of HCO_3^--effects on other ion permeabilities and of coupled electroneutral HCO_3^--transport. Pflügers Arch 401:43–51
9. Burckhardt B-Ch, Sato K, Frömter E (1984) Electrophysiological analysis of bicarbonate permeation across the peritubular cell membrane of rat kidney proximal tubule. I. Basic observations. Pflügers Arch 401:34–42
10. Burckhardt B-Ch, Geers C, Frömter E (1985) Role of membrane-bound carbonic anhydrase in HCO_3^- transport across rat renal proximal tubular cell membranes. Pflügers Arch 405 (Suppl 2): R 31
11. Burckhardt G (1984) Sodium-dependent dicarboxylate transport in rat renal basolateral membrane vesicles. Pflügers Arch 401:254–261
12. Cassola AC, Mollenhauer M, Frömter E (1983) The intracellular chloride activity of rat kidney proximal tubular cells. Pflügers Arch 399:259–265
13. Frömter E, Geßner K (1974) Active transport potentials, membrane diffusion potentials, and streaming potentials across rat kidney proximal tubule. Pflügers Arch 351:85–98
14. Frömter E, Sato K (1976) Electrical events in active H^+/HCO_3^- transport across rat kidney proximal tubular epithelium. In: Kasbekar DK, Sachs G, Rehm WS (eds) Gastric hydrogen ion secretion. Dekker, New York, pp 382–403
15. Good NE, Winget D, Winter W, Connolly N, Izawa S, Singh RM (1966) Hydrogen ion buffers for biological research. Biochemistry 5:467–477
16. Grassl SM, Aronson PS (1986) Na^+/HCO_3^- co-transport in basolateral membrane vesicles isolated from rabbit renal cortex. J Biol Chem 261:8778–8783
17. Guggino WB, London R, Boulpaep EL, Giebisch G (1983) Chloride transport across the basolateral cell membrane of the Necturus proximal tubule: Dependence on bicarbonate and sodium. J Membr Biol 71:227–240
18. Jentsch TJ, Schill BS, Schwartz P, Matthes H, Keller SK, Wiederholt M (1985) Kidney epithelial cells of monkey origin (BSC-1) express a sodium bicarbonate cotransport. Characterization by $^{22}Na^+$ flux measurements. J Biol Chem 260:15554–15560
19. Jentsch TJ, Stahlknecht TR, Hollwede H, Fischer DG, Keller SK, Wiederholt M (1985) A bicarbonate-dependent process inhibitable by disulfonic stilbenes and a Na^+/H^+ exchange mediate $^{22}Na^+$ uptake into cultured bovine corneal endothelium. J Biol Chem 260:795–801
20. Jentsch TJ, Schwartz P, Schill BS, Langner B, Lepple AP, Keller SK, Wiederholt M (1986) Kinetic properties of the sodium bicarbonate (carbonate) symport in monkey kidney epithelial cells (BSC-1). J Biol Chem 261:10673–10679

[1] When replacing bicarbonate by equivalent concentrations of other anions, we have previously noticed that phosphate was as poorly permeable as chloride [9]. This excludes significant OH^-/H^+ transport through phosphate flux

21. Murer H, Burckhardt G (1983) Membrane transport of anions across epithelia of mammalian small intestine and kidney proximal tubule. Rev Physiol Biochem Pharmacol 96:1–51
22. Sanyal G, Pessah VI, Maren TH (1981) Kinetics and inhibition of membrane-bound carbonic anhydrase from canine renal cortex. Biochim Biophys Acta 657:128–137
23. Soleimani M, Grassl SM, Aronson PS (1986) Stoichiometry of the Na-HCO_3 cotransport system in renal basolateral membrane vesicles. Clin Res (abstract) 34:609A
24. Ullrich KJ, Frömter E, Baumann K (1969) Micropuncture and microanalysis in kidney physiology. In: Passow H, Stämpfli R (eds) Laboratory techniques in membrane biophysics. Springer, Berlin Heidelberg New York, pp 106–109
25. Ullrich KJ, Rumrich G, Klöss S (1978) Phosphate transport in the proximal convolution of rat kidney. III. Effect of extracellular and intracellular pH. Pflügers Arch 377:33–42
26. Ullrich KJ, Rumrich G, Klöss S (1982) Reabsorption of monocarboxylic acids in the proximal tubule of the rat kidney. I. Transport kinetics of D-lactate, Na^+-dependence, pH-dependence and effect of inhibitors. Pflügers Arch 395:212–219
27. Ullrich KH, Fasold H, Rumrich G, Klöss S (1984) Secretion and contraluminal uptake of dicarboxylic acids in the proximal convolution of the rat kidney. Pflügers Arch 400:241–249
28. Wistrand PJ, Kinne R (1977) Carbonic anhydrase activity of isolated brush border and basal-lateral membrane of renal tubular cells. Pflügers Arch 357:149–163
29. Yoshitomi K, Frömter E (1984) Cell pH of rat renal proximal tubule in vivo and the conductive nature of peritubular HCO_3^- (OH^-) exit. Pflügers Arch 402:300–305
30. Yoshitomi K, Burckhardt B-Ch, Frömter E (1985) Rheogenic sodium-bicarbonate cotransport in the peritubular cell membrane of rat proximal tubule. Pflügers Arch 405:360–366

Received September 11, 1986/Accepted February 2, 1987

Pflügers Arch (1987) 409:138–141

Pflügers Archiv
European Journal of Physiology
© Springer-Verlag 1987

Electrophysiological identification of principal and intercalated cells in the rabbit outer medullary collecting duct

Bruce M. Koeppen

Division of Nephrology, Departments of Medicine and Physiology, University of Connecticut Health Center, Farmington, CT 06032, USA

Abstract. Intracellular microelectrode techniques were used together with inhibitors of Na^+ transport (amiloride) and H^+ transport (acetazolamide and SITS[1]) to identify principal cells and intercalated cells in the outer stripe of the rabbit outer medullary collecting duct. The principal cell ($n = 9$) had a basolateral membrane voltage (V_{bl}) of -64.7 ± 3.2 mV, a fractional resistance of the apical membrane ($fR_a = R_a/R_a + R_{bl}$) of 0.82 ± 0.02, and a K^+-selective basolateral membrane. Luminal amiloride hyperpolarized V_{bl} by 10.3 ± 2.1 mV and increased fR_a to near unity ($n = 7$). Bath acetazolamide and SITS were without effect on these parameters. The intercalated cell ($n = 5$) had a V_{bl} of -25.0 ± 3.2 mV, a fR_a of 0.99 ± 0.01, and a Cl^--selective basolateral membrane. Bath acetazolamide or SITS hyperpolarized V_{bl} by 26.4 ± 8.2 mV. Luminal amiloride did not alter V_{bl} of this cell. The differential effects of the inhibitors also indicate that the principal and intercalated cells are probably not directly coupled electrically.

Key words: Collecting duct – Intercalated cell – Principal cell – Electrophysiology – Cell heterogeneity

Introduction

The outer stripe portion of the rabbit outer medullary collecting duct ($OMCD_o$) reabsorbs Na^+, and secretes both K^+ and H^+ (Stokes 1982a, b; Laski and Kurtzman 1983; Schwartz and Al-Awqati 1985). According to structure-function studies of the rabbit collecting duct the transport of these ions occurs by different cells. Specifically, Na^+ reabsorption and K^+ secretion are thought to occur via the principal cell, while the intercalated cell secretes H^+ (O'Neil and Hayhurst 1985; Schwartz and Al-Awqati 1985; Schwartz et al. 1985; Madsen and Tisher 1986).

Based on this structure-function data, techniques were developed, using intracellular microelectrodes, which allowed functional identification of principal cells and intercalated cells in this nephron segment. To this end, inhibitors of Na^+ transport (amiloride) and H^+ transport (acetazolamide and SITS) were used as probes of the principal cell and intercalated cell, respectively. As will be shown, two cell types were distinguished by their electrophysiological properties. The differential effects of these inhibitors on the electrical properties of the two cell types provided a means for their functional identification as principal cells and intercalated cells.

Offprint requests to: B. M. Koeppen

[1] 4-acetamido-4′-isothiocyanostilbene-2,2′-disulphonic acid

Materials and methods

Adult female New Zealand White rabbits (1–2 kg) were maintained on a standard laboratory chow (Purina), with free access to tap water. At the time of study the animals were anesthetized (ketamine 35 mg/kg plus xylazine 5 mg/kg) and sacrificed by guillotine decapitation. Segments of collecting duct were dissected from the outer stripe of the outer medulla, as previously described (Koeppen 1986a). The average length of the tubule segments was 780 ± 50 μm.

The techniques for tubule perfusion and the use of intracellular microelectrodes in this laboratory have been published in detail (Koeppen et al. 1983; Koeppen 1985, 1986a). Consequently, they will be described here only in brief.

Tubules were suspended between two sets of pipettes. The perfusion pipette was fit with an internal exchange pipette, which allowed the luminal fluid composition to be changed without flow or pressure transients. The perfusion rate exceeded 10 nl/min in all tubules. The distal end of the tubule was held in the collecting pipette with unpolymerized Sylgard 184 (Dow Corning, Midland, MI, USA).

The composition of the perfusion fluid and control bath solution was (in mmol/l): NaCl, 115; $NaHCO_3$, 25; Na-acetate, 10; KCl, 5; $MgCl_2$, 1.2; $CaCl_2$, 1; and glucose 5.5. A high K^+ bath solution (50 mmol/l) was made by substituting an equivalent amount of NaCl with KCl. A low Cl^- bath solution (64 mmol/l) was made by substituting an equivalent amount of NaCl with Na-gluconate. All bath solutions were warmed to 37°C, and had a pH of 7.4–7.5 when equilibrated with 95% O_2/5% CO_2. A rapid-flow bath exchange system was used, which allowed step changes in bath fluid composition to be made in less than 1 s (Koeppen 1985, 1986a).

The transepithelial voltage (V_T) was measured through the perfusion pipette. The basolateral membrane voltage (V_{bl}) was measured with glass capillary microelectrodes filled with 1 M KCl. Both voltages were referenced to the bath. When the bath ion composition was changed (high-K^+ or low-Cl^-), the values of V_T and V_{bl} were corrected for the associated change in bath bridge junction potential (Koeppen 1985, 1986a). Cable analysis was used to calculate the transepithelial resistance of the tubule (R_T), and the fractional resistance of the apical membrane ($fR_a = R_a/R_a + R_{bl}$) (Koeppen et al. 1983).

Single tubule cells were impaled under direct observation at 400 ×. However, it was not possible to visually distinguish between principal cells and intercalated cells. Acceptable impalements were characterized by a stable membrane voltage at or exceeding the value obtained immediately after cell impalement (Koeppen et al. 1983). Impalements could be maintained routinely for 20–30 min.

Amiloride has been shown to block electrogenic Na^+ reabsorption by principal cells of the collecting duct (Koeppen et al. 1983; O'Neil and Sansom 1984; O'Neil and Hayhurst 1985). Consequently, cells found to respond to luminal amiloride were functionally identified as principal cells.

The intercalated cell is thought to be involved in urine acidification (Schwartz and Al-Awqati 1985; Schwartz et al. 1985; Madsen and Tisher 1986), and acetazolamide and SITS have been shown to inhibit this process (Dobyan et al. 1982; Koeppen and Helman 1982; Lombard et al. 1983; Stone et al. 1983). Therefore, cells found to respond to bath acetazolamide or SITS were functionally identified as intercalated cells. Although acetazolamide and SITS appear to have different sites of action within the cell (Zeidel et al. 1986; Koeppen 1987), preliminary microelectrode studies have shown that their effect on the steady-state V_{bl} is similar (Koeppen 1987). Because of this, and since both inhibitors were used only as functional probes of the intercalated cell, results related to their effect on the electrical properties of the cell were pooled for ease of presentation.

The following general protocol was used. After obtaining a stable cell impalement, the electrophysiological properties of the cell were characterized with regard to V_{bl}, fR_a, and the relative conductance of the basolateral membrane to K^+ and Cl^-. Following this, the tubule was perfused with amiloride (Merck, Sharp and Dohme, West Point, PA, USA) at a concentration of 10^{-5} M, and its effect on V_{bl} and fR_a determined. After washout of the amiloride from the tubule lumen, either the carbonic anhydrase inhibitor acetazolamide (Sigma, St. Louis, MO, USA), or the disulphonic stilbene SITS (Polysciences, Warrington, PA, USA) was added to the bath, and its effect on V_{bl} and fR_a determined. Both drugs were used at a final concentration of 10^{-4} M.

All values are reported as means ± SE. Comparisons between group means were made using paired analysis, with each cell serving as its own control. *P*-values less than 0.05 were considered significant.

Results

A total of 15 tubules were studied. The mean value of V_T was -8.5 ± 5.1 mV, and the R_T averaged 34.5 ± 3.1 kΩ · cm (233 Ω · cm²). These values are similar to those reported previously for this segment (Koeppen 1986a). Two distinct cell populations could be distinguished by their electrophysiological properties. The electrical properties of the two cell types were also similar to those reported previously, and are summarized in Table 1.

Effect of inhibitors on transepithelial electrical properties

Inhibition of electrogenic Na^+ transport, by addition of amiloride to the tubule lumen, caused the V_T to reverse polarity from a mean of -11.5 ± 6.2 mV to $+15.6 \pm 3.1$ mV ($n = 12$, $P < 0.001$). Concurrently, R_T increased from 35.0 ± 3.5 kΩ · cm to 45.0 ± 4.2 kΩ · cm ($P < 0.005$). Inhibition of electrogenic H^+ secretion, by the addition of either acetazolamide or SITS to the bath, caused V_T to hyperpolarize from -10.7 ± 5.7 mV to -20.8 ± 4.9 mV ($n = 13$, $P < 0.005$). The R_T was unchanged averaging 34.6 ± 2.9 kΩ · cm and 34.1 ± 3.0 kΩ · cm in the absence and presence of these inhibitors, respectively.

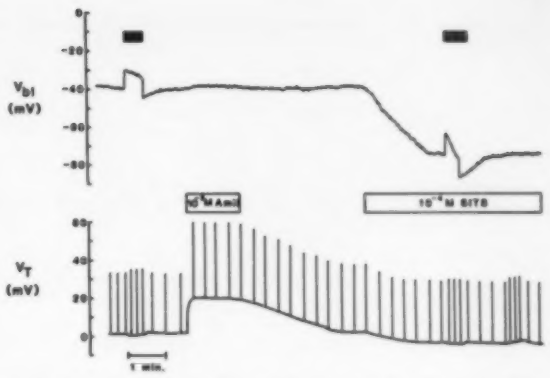

Fig. 1. Strip-chart record showing the effects of amiloride and SITS on cell type no. 1 (intercalated cell). The *black bars* represent times during which the bath [Cl^-] was reduced from 124 to 64 mmol/l. The vertical "spikes" in the V_T trace are the result of the injection of constant current pulses into the tubule lumen. The absence of current spikes in the V_{bl} trace indicates an absence of transcellular current flow ($fR_a \approx 1.0$). See text for details

Table 1. Summary of electrophysiological properties of cell types

	V_{bl}, mV	fR_a	Bath ion substitution (ΔV_{bl}, mV)	
			K^+	Cl^-
Cell type no. 1 ($n = 6$)	-25.0 ± 3.2	0.99 ± 0.01	-0.3 ± 0.4	-14.3 ± 0.4
Cell type no. 2 ($n = 9$)	-64.7 ± 3.2	0.82 ± 0.02	-31.8 ± 2.9	0.1 ± 0.4

Values are mean ± SE. Bath [K^+] was stepped from 5 to 50 mmol/l, [Cl^-] from 124 to 64 mmol/l. Depolarization of V_{bl} is indicated by negative values of ΔV_{bl}

Effect of inhibitors on cell electrical properties

The effects of amiloride and SITS on the electrical properties of the two cell types are illustrated in Figs. 1 and 2.

Cell type no. 1 ($n = 6$) was characterized by a relatively low V_{bl}, fR_a near unity, and a Cl^--selective basolateral membrane (see Table 1). As shown in Fig. 1, addition of amiloride to the tubule lumen did not alter V_{bl}. The V_T, however, did become more lumen positive, as would be expected from the inhibition of electrogenic Na^+ reabsorption in adjacent cells. By contrast, addition of SITS to the bath caused a marked hyperpolarization of V_{bl}. Concurrently, the V_T became lumen negative reflecting the inhibition of electrogenic H^+ secretion. Although not

Table 2. Effects of amiloride and acetazolamide/SITS on the electrical properties of the cell types

	V_a, mV		V_{bl}, mV		fR_a	
	Control	Expl.	Control	Expl.	Control	Expl.
Cell type no. 1						
Amiloride ($n = 5$)	31.2 ± 5.0	46.2 ± 6.1*	-27.2 ± 3.8	-27.4 ± 3.6	0.99 ± 0.01	0.99 ± 0.01
Acet./SITS ($n = 5$)	30.4 ± 4.0	43.5 ± 10.8	-24.6 ± 3.2	-51.0 ± 9.7*	0.99 ± 0.01	0.99 ± 0.01
Cell type no. 2						
Amiloride ($n = 7$)	44.9 ± 7.8	91.0 ± 5.4***	-67.4 ± 3.7	-77.7 ± 5.0**	0.82 ± 0.02	0.98 ± 0.01***
Acet./SITS ($n = 8$)	43.6 ± 10.7	36.2 ± 6.5*	-64.6 ± 2.5	-65.4 ± 3.0	0.79 ± 0.02	0.78 ± 0.01

Values are mean $\pm$ SE. * $P < 0.05$; ** $P < 0.005$; *** $P < 0.001$

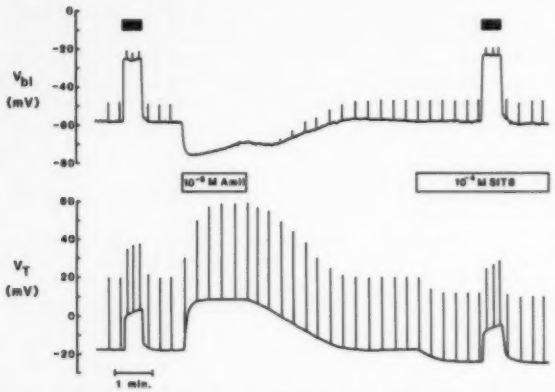

Fig. 2. Strip-chart record showing the effect of amiloride and SITS on cell type no. 2 (principal cell). The *black bars* represent times during which the bath $[K^+]$ was increased from 5 to 50 mmol/l. The vertical "spikes" in both the V_{bl} and V_T traces are the result of injection of constant current pulses into the tubule lumen. The absence of current spikes in the V_{bl} trace seen in the presence of luminal amiloride indicates blockade of transcellular current flow. See text for details

shown, the effect of acetazolamide was similar[2]. The response of this cell type to inhibitors of H^+ transport suggests that this is the intercalated cell. Table 2 summarizes the effects of inhibitors on this cell type.

Cell type no. 2 ($n = 9$), was distinguished from cell type no. 1 by having a higher value of V_{bl}, a measurable fR_a, and a K^+-selective basolateral membrane (see Table 1). As illustrated in Fig. 2, amiloride hyperpolarized V_{bl}, and blocked transcellular current flow. As a result of the inhibition of electrogenic Na^+ reabsorption, the V_T became lumen positive. SITS did not alter V_{bl} or fR_a, but did cause the lumen negative V_T to hyperpolarize, indicating an inhibition of electrogenic H^+ secretion in adjacent cells. Again not shown, the response to bath acetazolamide was similar. The effect of amiloride would indicate that this cell is the principal cell. The effects of inhibitors on cell type no. 2 are summarized in Table 2.

[2] In a separate study designed to examine the mechanism(s) of action of these inhibitors on the process of electrogenic H^+ secretion (Koeppen 1987), SITS (10^{-4} M) and acetazolamide (10^{-4} M) were found to hyperpolarize V_{bl} by 27.3 ± 5.5 mV ($n = 6$) and 20.7 ± 3.2 mV, respectively. These changes in V_{bl} were statistically indistinguishable

Discussion

In the present study microelectrode techniques were used to examine cellular heterogeneity in the rabbit $OMCD_c$. Based on electrophysiological criteria, two distinct cell types were identified. The differential effects of inhibitors of Na^+ and H^+ transport on the electrical properties of these cells provided a convenient means for their functional identification as either principal cells or intercalated cells.

The V_{bl} of cell type no. 1 hyperpolarized when either acetazolamide or SITS were added to the bath. In accordance, therefore, with available structure-function data (Schwartz and Al-Awqati 1985; Schwartz et al. 1985; Madsen and Tisher 1986), this cell is probably the intercalated cell. Since the present study was not designed to examine in detail the action of these inhibitors on the intercalated cell, it is not possible from the available data to explain the mechanism(s) responsible for the observed hyperpolarization of V_{bl}. Nevertheless, it is clear that because of their effect on V_{bl}, either acetazolamide or SITS can be used as a functional probe of this cell.

Amiloride hyperpolarized V_{bl} and increased fR_a to values near unity in cell type no. 2. These changes in the electrical properties of the cell are consistent with amiloride blockade of Na^+ channels in the apical cell membrane (Koeppen et al. 1983; O'Neil and Sansom 1984). Based on structure-function data (O'Neil and Hayhurst 1985), this response to luminal amiloride functionally identifies this cell as the principal cell.

Inhibition of electrogenic transport by one cell type would be expected to alter the membrane voltages in the second cell type owing to circular intraepithelial current flow. With the high values of fR_a seen in the two cell types ($fR_a = 0.8-1.0$), most of the voltage change would occur across the apical membrane (V_a). For example, inhibition of electrogenic Na^+ reabsorption by the principal cell (amiloride) would be expected to hyperpolarize V_a of the intercalated cell, whereas inhibition of electrogenic H^+ secretion by the intercalated cell (acetazolamide/SITS) would be expected to depolarize V_a of the principal cell. These predicted changes in V_a were in fact observed (see Table 2). It should be emphasized, however, that these current induced changes in membrane voltage do not reflect direct action of the inhibitor on the cell. Thus, the results of

the present study clearly show that at least in the rabbit $OMCD_o$, amiloride does not have a direct effect on the intercalated cell, nor do acetazolamide or SITS have direct effects on the principal cell. This taken together with the marked differences in the baseline electrical characteristics of the two cell types (see Table 1), provides strong evidence that the principal and intercalated cells are not electrically coupled.

Studies of the collecting duct have shown that changes in Na^+ transport can lead to alterations in urine acidification (Koeppen and Helman 1982; Laski and Kurtzman 1983). In view of the apparent absence of direct electrical coupling between principal and intercalated cells this interaction must be via intraepithelial current flow (see above). Accordingly, amiloride, simply by hyperpolarizing the apical membrane (see Table 2), could alter net H^+ secretion by increasing the electrical gradient against which the H^+-ATPase would have to pump.

In summary, electrophysiological techniques were used together with inhibitors to identify by functional criteria principal cells and intercalated cells in the rabbit $OMCD_o$. The intercalated cell has a relatively low V_{bl}, a Cl^--selective basolateral membrane, and no significant ion conductances in the apical membrane[3]. The principal cell has a relatively high basolateral membrane voltage, a K^+-selective basolateral membrane, and an amiloride-sensitive Na^+ conductance in the apical cell membrane. Also, these two cell types do not exhibit direct cell-to-cell electrical coupling.

Acknowledgements. Amiloride was a gift of Merck, Sharp and Dohme Research Laboratories, West Point, PA, USA. This work was supported by National Institutes of Health, Grant DK-32489, and an Established Investigatorship from the American Heart Association.

The author would like to thank Drs. P. Steinmetz and G. Giebisch for their critical review of the manuscript.

References

Dobyan DC, Magill LS, Friedman PA, Hebert SC, Bulger RE (1982) Carbonic anhydrase histochemistry in rabbit and mouse kidneys. Anat Rec 204:185–197

Koeppen BM (1985) Conductive properties of the rabbit outer medullary collecting duct: inner stripe. Am J Physiol 248: F500–F506

Koeppen BM (1986a) Conductive properties of the rabbit outer medullary collecting duct: outer stripe. Am J Physiol 250: F70–F76

Koeppen BM (1987) Proton secretion by the rabbit outer medullary collecting duct: effect of inhibitors (abstract). Kidney Int 31:410

Koeppen BM, Helman SI (1982) Acidification of luminal fluid by the rabbit cortical collecting tubule perfused in vitro. Am J Physiol 242: F521–F531

Koeppen BW, Biagi BA, Giebisch GH (1983) Intracellular microelectrode characterization of the rabbit cortical collecting duct. Am J Physiol 244: F35–F47

Laski ME, Kurtzman NE (1983) Characterization of acidification in the cortical and medullary collecting tubule of the rabbit. J Clin Invest 72:2050–2059

Lombard WE, Kokko JP, Jacobson HR (1983) Bicarbonate transport in cortical and outer medullary collecting tubules. Am J Physiol 244: F289–F296

Madsen KM, Tisher CC (1986) Structural-functional relationships along the distal nephron. Am J Physiol 250: F1–F15

O'Neil RG, Hayhurst RA (1985) Functional differentiation of the two cell types of the cortical collecting duct. Am J Physiol 248: F449–F453

O'Neil RG, Sansom SC (1984) Characterization of apical cell membrane Na^+ and K^+ conductances of cortical collecting duct using microelectrode techniques. Am J Physiol 247: F14–F24

Sansom SC, Muto S, Giebisch G (1986) Microelectrode assessment of conductive properties of "minority cells" of the rabbit cortical collecting duct (abstract). Fed Proc 45:541

Schwartz GJ, Al-Awqati Q (1985) Carbon dioxide causes exocytosis of vesicles containing H^+ pumps in isolated proximal and collecting tubules. J Clin Invest 75:1638–1644

Schwartz GJ, Barasch J, Al-Awqati, Q (1985) Plasticity of functional epithelial polarity. Nature 318:368–371

Stokes JB (1982a) Na and K transport across the cortical and outer medullary collecting tubule of the rabbit: evidence for diffusion across the outer medullary portion. Am J Physiol 242: F514–F520

Stokes JB (1982b) Ion transport by the cortical and outer medullary collecting tubule. Kidney Int 22:473–484

Stone DK, Seldin DW, Kokko JP, Jacobson HR (1983) Anion dependence of rabbit medullary collecting duct acidification. Clin Invest 71:1505–1508

Zeidel ML, Silva P, Seifter JL (1986) Intracellular pH regulation in rabbit renal medullary collecting duct cells. Role of chloride-bicarbonate exchange. J Clin Invest 77:1682–1688

[3] Recently, a cell type having similar electrical properties has been described in the cortical collecting duct of the rabbit (Sansom et al. 1986). It is likely that this is the intercalated cell of this segment

Received October 17, 1986/Accepted January 12, 1987

Pflügers Arch (1987) 409:142–144

Pflügers Archiv
European Journal of Physiology
© Springer-Verlag 1987

Intracellular pH in quiescent and stimulated ventricular myocardium

Effect of extracellular chloride concentration

D. Heinemeyer and W. Bay

II. Physiologisches Institut der Universität des Saarlandes, D-6650 Homburg/Saar, Federal Republic of Germany

Abstract. In ventricular trabeculae from guinea pig and cat heart superfused with a modified Tyrode's solution ($pH_o = 7.4$) containing either 137 mM or 103 mM Cl_o^-, intracellular pH (pH_i) was measured with H^+-sensitive double-barreled microelectrodes. In quiescent preparations pH_i was 7.26 ± 0.017 when Cl_o^- was 137 mM, and 7.38 ± 0.02 in 103 mM chloride. In 103 mM Cl_o^- containing saline stimulation of the preparation produced no acidification but in 137 mM Cl_o^- acidification occurred. The acidification was completely revesible when chloride was reduced again. When HCO_3^-/Cl^- exchange was blocked by 0.5 mM SITS, pH_i was lowered similar to the effect of increasing extracellular chloride concentration. It was concluded that when Cl_o^- is raised, the HCO_3^-/Cl^-exchanger operates as a Cl^-/Cl^- exchanger.

Key words: Intracellular pH – Ion sensitive microelectrodes – Reduced chloride saline

Introduction

The pH_i has been measured in various tissues and with different techniques [for review see 9, 10, 12, 13]. In quiescent ventricular cardiac myocytes, pH_i values of about 7.14 and 7.20 in the absence and in the presence of HCO_3^-/CO_2 buffer, respectively, have been reported [2–4]. In these measurements the extracellular chloride concentration in the Tyrode's solution was 129.5–132 mM. Extra-cellular chloride concentration is postulated to affect HCO_3^-/Cl^- exchange by competition with extracellular HCO_3^- [16] and an increase in Cl_o^- concentration has been shown to produce a fall in pH_i [15, 16]. In commonly used Tyrode's solution Cl_o^- concentration is higher than in aqueous humor or plasma of mammalians [5, 7, 17]. This could favour in vitro a steady intracellular acidosis. Little is known about pH_i in stimulated preparations. We measured pH_i in both, quiescent and stimulated preparations, bathed in a modified Tyrode's saline of a more physiological chloride concentration (103 mM). Special care was taken to maintain pH_o, pCO_2, HCO_3^- and temperature. In these conditions pH_i was found to be 7.38 ± 0.02 (SD, $n = 8$).

Methods

Experiments were done on isolated papillary muscles and trabeculae from the right ventricle (diameter 0.3–0.5 mm) of guinea pig or cat (anesthetized by pentobarbitone – Nembutal). Preparations were mounted in a chamber and equilibrated in a modified Tyrode's saline for 10–20 min before experiments were started (Fig. 1 B). Two salines were used. Saline 1 contained (in mM): NaCl 126, KCl 5.4, $CaCl_2$ 1.8, $MgCl_2$ 1.0, $NaHCO_3$ 24 and glucose 10. Saline 2 contained (in mM) NaCl 92 and methanesulfonic acid sodium salt (CH_3SO_3Na) 34, which has been reported to have no calcium binding capacity [6]. When HCO_3^-/Cl^- exchange was blocked, saline 2 contained 0.5 mM SITS (4-acetamido-4′-isothiocyanatostilben-2,2′-disulfonic-acid). Other concentrations of ions were not changed. The salines were preheated to 36° C and gassed with 5% CO_2 and 95% O_2 before $NaHCO_3$ and $CaCl_2$ were finally added. During preparation of saline 2, the warmed (but not bubbled) and CH_3SO_3Na containing saline was carefully titrated to pH 7.40 with NaOH (methanesulfonic acid sodium salt behaved in the experiments as a weak acid). Thereafter salines were bubbled and, after equilibration $NaHCO_3$ and finally $CaCl_2$ were added. This procedure minimized free HCO_3^- consumption by acid neutralization (CH_3SO_3Na) and calcium binding. A heating and gassing system (see Fig. 1 A, B) allowed the simultanious use of HCO_3^-/CO_2 buffer together with other buffers or acids (saline 2). Because there was no more a temperature dependent shift in pKa and pCO_2, the adjusted saline remained stable.

Double-barreled H^+-sensitive microelectrodes were made as recently described by Schlue and Thomas [11]. The electrodes were back filled with the proton cocktail (obtained from Fluka Chemicals, Neu-Ulm, FRG) developed by Amman et al. [1]. Only electrodes with a response slope of 54 mV/pH unit or higher were used. Each barrel was connected with one input of a differential electrometer (WPI, FD 223) via chlorided silver wires. The resolution of the electrode recording system allowed to measure changes in pH_i as small as 0.01 pH units.

Results

In quiescent preparations perfused with saline 1 pH_i values between 7.23 and 7.29 were measured (7.26 ± 0.017; mean and SD, $n = 8$). When the Cl_o^- concentration was reduced from 137 mM to 103 mM an alkalinisation of 0.09–0.15 pH units occurred (Fig. 2 A, $n = 8$). In quiescent preparations pH_i in 103 mM Cl_o^- containing saline was 7.38 ± 0.02 ($n = 8$, SD) and, when the preparation was stimulated (0.33 Hz) pH_i remained constant. In contrast, when the preparation bathed in 137 mM Cl_o^- was stimulated at the

Offprint requests to: D. Heinemeyer, Kreiskrankenhaus Ebern, Innere Medizin, D-8603 Ebern, Federal Republic of Germany

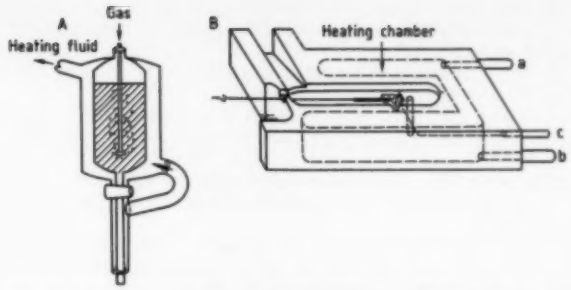

Fig. 1. A Double walled bottle (storage system) for Tyrode's solution. The saline in the inner bottle is gas saturated at 36°C, resulting in a correct pCO_2 in the recording chamber (α CO_2, $pH = f_{(T)}$). An inner gastight and heated tube connects the bottle with the experimental chamber. The system allows the simultanious use of HCO_3^-/CO_2 buffer together with other buffers or acids (saline 2). **B** Recording chamber which is warmed to 36°C by an inner perfusion. The flow in the bath (volume 0.3 ml) was 25–26 ml per min. This arrangement guarantied constant values in the saline for pH (7.40±0.03), pCO_2 (39.4±1.1 mm Hg), HCO_3^- (24.3±0.5 mM) and temperature (36±0.2°C; all mean and SD, $n = 8$). Analysis was done with a Radiometer Copenhagen ABL 4. *a* influx heating chamber; *b* efflux heating chamber; *c* influx recording chamber

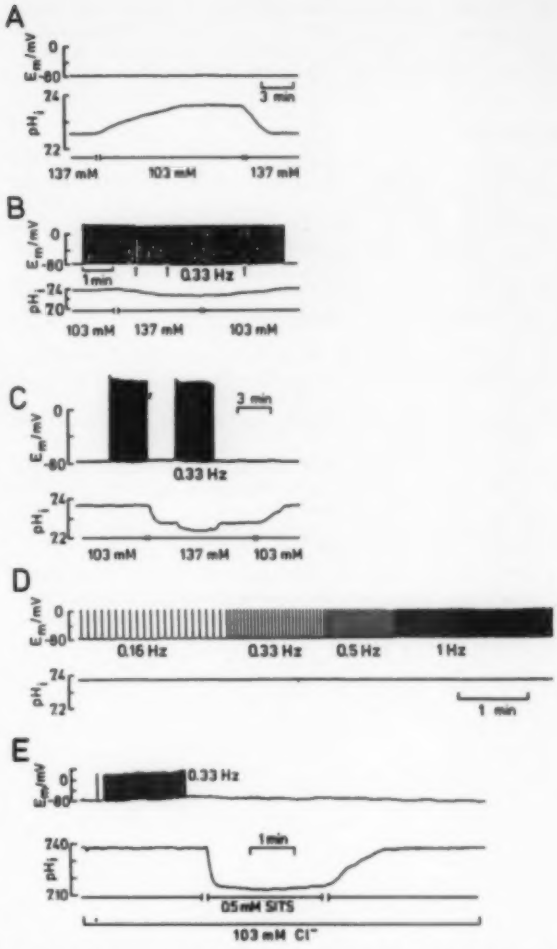

Fig. 2. A Increase in pH_i (*lower trace*) from 7.25 to 7.36 on reduction Cl_o^- from 137 mM to 103 mM. Resting potential (E_m, *upper trace*) stable at −76 mV. **B** Stimulated preparation. No acidification in 103 mM Cl_o^- in contrast to 0.14 pH units in 137 mM Cl_o^-. Complete reversibility in 103 mM Cl_o^- (*arrows* mark reinsertion of electrode). **C** No acidification on stimulation in 103 mM Cl_o^-. Cessation of stimulation and change to 137 mM Cl_o^- produced acidification of 0.09 pH units. Partial recovery on stop of stimulation, complete recovery in 103 mM Cl_o^-. **D** In 103 mM Cl_o^- pH_i remained constant up to a frequency of 1 Hz. **E** No acidification on stimulation of the preparation but on superfusion with 0.5 mM SITS reversible acidification of 0.12–0.19 pH units ($n = 3$)

same rate, pH_i decreased by 0.12–0.15 pH units (Fig. 2B). This acidification was completely reversible when Cl_o^- was reduced to 103 mM again.

These effects on pH_i by changes in Cl_o^- were studied in a preparation during periods of rest and stimulation (Fig. 2C). Acidification due to stimulation was not observed, when the saline contained 103 mM chloride. Cessation of stimulation and elevation of the Cl_o^- to 137 mM led to an acidification of 0.09 pH units. After reaching a new steady state, a second stimulation sequence produced a further acidification of 0.05 pH units. All changes were reversible when Cl_o^- was reduced to 103 mM. Stimulation of these multicellular preparations in 103 mM Cl_o^- was possible up to 1 Hz without observing an intracellular acidification (Fig. 2D). A similar acidification was observed when HCO_3^-/Cl^- exchange was blocked by 0.5 mM SITS ([15] Fig. 2E).

Discussion

The results show, that in ventricular myocardium bathed in Tyrode's saline with a stabilized HCO_3^-/CO_2 and a more physiological chloride concentration [5, 7, see saline 2 and Methods], the difference between pH_i and pH_o is negligible ($pH_i = 7.38 \pm 0.02$; SD, $n = 8$; $pH_o = 7.40 \pm 0.03$; SD; $n = 8$). pH_i is substantially higher than all previously reported values [3, 4, 10]. For the explanation of this alkaline pH_i we suggest a bicarbonate-chloride exchange [10, 13, 15, 16] were ionized free bicarbonate enters the cell [10, 13, 16]. Thus, when HCO_3^-/Cl^- exchange is blocked by SITS an intracellular acidification was observed similar to that, which occurred by raising extracellular chloride concentration from 103 mM to 137 mM. The latter effect can be explained by a chloride/chloride exchange generated in high Cl_o^- condition by competition of Cl_o^- with HCO_3^- in the exchange mechanism resulting in a more acid pH_i [16]. In the lowered Cl_o^- saline HCO_3^-/Cl_o^- exchange seems to be sufficient to maintain pH_i even in a stimulated preparation. The acidification in high Cl_o^- saline due to stimulation can be explained by an increased and frequency-dependent lactate production in these preparations [8, 14]. The lactate acidification can be neutralized in a saline with a chloride concentration reported for the extracellular fluid of man [Cl_o^- serum 103 mM, Cl_o^- interstitium (assumed) 106 mM, 5, 7].

Acknowledgements. We thank W. R. Schlue, University of Duesseldorf for introducing D. H. into the intracellular pH-measurement technique. We thank W. R. Schlue, M. Kameyama and

W. Trautwein for helpful discussion, H. Ehrler for electronical arrangements, H. Ochotzki and Mrs. E Retfalvi for technical assistance. This work was supported by the Deutsche Forschungsgemeinschaft with a grant to D. H. (He 1354/I-1/2).

References

1. Amman D, Lanter F, Steiner RA, Shijo Y, Simon W (1981) Neutral carrier based hydrogen ion selective microelectrode for extra- and intracellular studies. Anal Chem 53:2267–2269
2. De Hemptinne A (1980) Intracellular pH and surface pH in skeletal and cardiac muscle measured with a double-barreled pH microelectrode. Pflügers Arch 386:121–126
3. Ellis D, Thomas RC (1976) Microelectrode measurement of the intracellular pH of mammalian heart cells. Nature 262:224–225
4. Ellis D, Thomas RC (1976) Direct measurement of intracellular pH of mammalian cardiac muscle. J Physiol (Lond) 262:755–771
5. Gamble JL (1947) Extracellular fluid. Havard University Press, Cambridge, MA, USA
6. Kenyon JL, Gibbons WR (1977) Effects of low chloride solutions on action potentials of sheep cardiac Purkinje fibres. J Gen Physiol 70:635–660
7. Krebs HA (1950) Body size and tissue respiration. Biochim Biophys Acta 4:249–269
8. McLeod DP, Prasad K (1969) Influence of glucose on transmembrane action potential of papillary muscle. Effects of concentration, phlorizin and insulin, nonmetabolizable sugars and stimulators of glycolysis. J Gen Physiol 53:792–815
9. Nuccitelli R, Deamer D (1982) Intracellular pH: its measurement, regulation and utilisation in cellular functions. Alan R. Liss, New York
10. Roos A, Boron WF (1981) Intracellular pH. Physiol Rev 61:296–434
11. Schlue WR, Thomas RC (1985) A dual mechanism for intracellular pH regulation in leech neurons. J Physiol (Lond) 364:327–338
12. Thomas RC (1974) Intracellular pH of snail neurons with a new pH-sensitive glass microelectrode. J Physiol (Lond) 238:159–180
13. Thomas RC (1977) The role of bicarbonate, chloride and sodium ions in the regulation of intracellular pH in snail neurons. J Physiol (Lond) 273:317–338
14. Vanheel B, De Hemptinne A, Leusen I (1985) Intracellular pH and contraction of isolated rabbit and cat papillary muscle: Effect of superfusate buffering. J Mol Cell Cardiol 17:23–29
15. Vaughan-Jones RD (1979) Regulation of chloride in quiescent sheep-heart Purkinje fibres studied using intracellular chloride and pH-sensitive micro-electrodes. J Physiol (Lond) 295:111–137
16. Vaughan-Jones RD (1982) Chloride activity and its control in skeletal and cardiac muscle. Philos Trans R Soc Lond [Biol] 299:537–548
17. Wallace WM, Hastings AB (1942) The distribution of the bicarbonate ion in mammalian muscle. J Biol Chem 144:637

Received December 10, 1986/Accepted February 13, 1987

Pflügers Arch (1987) 409:145–151

Pflügers Archiv
European Journal of Physiology
© Springer-Verlag 1987

Reflex inhibition of efferent renal sympathetic nerve activity by 5-hydroxytryptamine and nicotine is elicited by different epicardial receptors*

B. Mohr, A. H. Bom, A. J. Kaumann, and V. Thämer**

Physiologisches Institut, Lehrstuhl 1, Universität Düsseldorf, Moorenstrasse 5, D-4000 Düsseldorf, Federal Republic of Germany

Abstract. Intrapericardial administration of 5-hydroxytryptamine (5-HT) induced reflex effects consisting in an inhibition of renal sympathetic nerve activity (RSNA), bradycardia and a fall in blood pressure. Nicotine caused the same reflex effects as 5-HT. The reflex effects of both 5-HT and nicotine were abolished by vagotomy. MDL 72222, an antagonist at 5-HT M-receptors, abolished or attenuated the decreases in RSNA, heart rate and blood pressure induced by 5-HT, leaving the reflex effects of nicotine unchanged. In the absence of MDL 72222 the reflex bradycardia partially concealed a positive chronotropic response to 5-HT. After blockade of the bradycardia response by MDL 72222, 5-HT elicited a significant tachycardia, which was not altered by propranolol and phentolamine, but was prevented by phenoxybenzamine. 5-HT probably reaches the sinoatrial node and activates 5-HT receptors that mediate directly the increase in heart rate. The nicotine receptor antagonist hexamethonium selectively abolished or attenuated the reflex effects of nicotine without interfering with those of 5-HT. We conclude that 5-HT and nicotine elicit similar reflex effects in epicardial vagal nerve endings by stimulation of M-receptors or nicotine receptors, respectively.

Key words: Renal nerve activity – Heart rate – 5-Hydroxytryptamine – Nicotine – MDL 72222 – Hexamethonium

Introduction

The cardiovascular changes that follow an intravenous injection of 5-hydroxytryptamine (5-HT) can be regarded as net result of direct and reflex effects on heart and blood vessels. In most species the response to 5-HT is triphasic: an initial depressor effect, a short lasting pressor effect and finally a prolonged depressor effect (Douglas 1965). The initial component is due to a reflex bradycardia (Comroe et al. 1953; Mott and Paintal 1953; Schneider and Yonkman 1954); the second component is probably related to the sum of positive inotropic effects, tachycardia and arterial constriction; the late component is due to arterial vasodilation (Kalkman et al. 1983).

The changes in blood pressure and heart rate which are reflexly mediated may result from excitation of sensory vagal afferents in different organs, e.g. type J pulmonary receptors (Paintal 1955), cardiac receptors (Zakusov 1962) and carotid body chemoreceptors (Black et al. 1972; Kirby and McQueen 1984). Injection of 5-HT into the blood stream may additionally induce a depressor response mediated by stimulation of 5-HT receptors in the central nervous system (Takahashi 1985). The purpose of the present work was to analyse the reflex changes elicited by exclusive stimulation of epicardial sensory afferents by 5-HT. To avoid the complex mosaic of effects due to activation of multiple mechanism by i.v. administration, we administered 5-HT intrapericardially (i.pc.). To investigate whether an inhibition of efferent sympathetic nerve activity is part of the reflex effects, as described for nicotine (Öberg and Thoren 1973), we measured renal sympathetic nerve activity (RSNA) during i.pc. administration of 5-HT. MDL 72222 blocks the reflex bradycardia of 5-HT in the rat (Fozard 1984) by competing with 5-HT for M-receptors (Gaddum and Picarelli 1957; recently reclassified as 5-HT_3-receptors by Bradley et al. 1986) on the afferent vagal fibres. Hexamethonium prevents the action of nicotine on nonmedullated vagal fibres (Volle and Koelle 1975).

In order to find out whether the reflex effects of 5-HT and nicotine are induced through nonspecific or specific epicardial receptors we used the M-receptor antagonist MDL 72222 (1αH, 3α,5αH-tropan-3-yl-3,5-dichlorobenzoate) and the nicotine receptor antagonist hexamethonium. The results show that 5-HT causes the Bezold-Jarisch reflex and a decrease of RSNA through epicardial M-receptors located on afferent vagal fibers.

Methods

The experiments were performed on 29 cats weighing 1.9–4.9 kg anaesthetized with chloralose (60 mg/kg i.v.). A tracheal cannula was inserted and the cats were ventilated artificially with air supplemented with oxygen. The arterial pCO_2 and pH were measured periodically and the values were maintained within the physiological range by adjusting either the tidal volume or the respiratory frequency. The arterial pO_2 exceeded 100 mm Hg. The arterial pCO_2 was maintained between 25 and 30 mm Hg and pH between 7.35 and 7.45. Body temperature was kept between 37° C and 39° C by external heating.

* This study was supported in part by grant SFB 30 Kardiologie of the Deutsche Forschungsgemeinschaft

** Present address: ICI Pharmaceuticals Division, Mereside Alderley Park, Macclesfield, Cheshire SK10 4TG, UK

Offprint requests to: V. Thämer

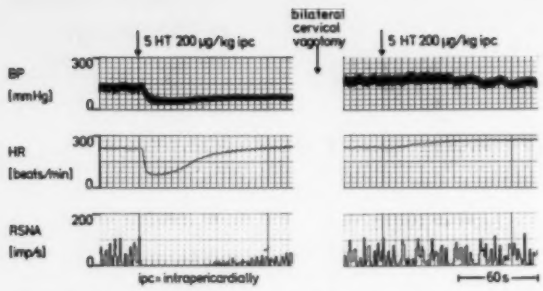

Fig. 1. Effect of intrapericardial administration of 5-HT on blood pressure (BP), heart rate (HR) and renal sympathetic nerve activity (RSNA) before and after vagotomy

Surgical procedure. After a leftsided thoracotomy the pericardium was opened. For administration of drugs a silastic catheter was introduced into the pericardial sac and sutured to the pericardium in such a way that its tip lay over the apical portion of the left ventricular surface.

Haemodynamic measurements. Blood pressure was measured in a femoral artery through a catheter connected to a Statham P23 Gb transducer. Heart rate was measured with a cardiotachometer (Gould, Oxnard, CA, USA) which was triggered by the arterial pressure wave.

Recording of nerve activity. A branch of the renal sympathetic nerve was dissected free from the surrounding tissue and cut distally. The nerve was covered with mineral oil and placed on bipolar platinum electrodes. Nerve activity was recorded as previously described by Vogt and Thämer (1980).

Experimental protocol. The protocol was started 30 min after completing the surgical preparation.

For stimulation of epicardial receptors 5-HT or nicotine were injected i.pc. The drugs were diluted in 0.9% NaCl at room temperature and the injected volume was always 1 ml. Injection of 1 ml of 0.9% NaCl at room temperature did not elicit reflex changes. In six preliminary experiments we found that no tachyphylaxis occurred following repeated administration of 5-HT and nicotine and the reproducibility of each type of stimulation was good.

We used doses of 5-HT and nicotine which produced a decrease of at least 30% in either heart rate or RSNA. Two minutes after administration of 5-HT or nicotine i.pc. the drugs were washed out with 20 ml 0.9% NaCl warmed to 37° C. The interval between two injections was 30 min. The antagonists MDL 72222 and hexamethonium were applied i.pc. 2 min before application of 5-HT or nicotine. The dose of MDL 72222 was increased (0.1 – 10 µg/kg) until it reduced or abolished the reflex effects of 5-HT. 30 min later this blocking dose of MDL 72222 was injected i.pc. again and its effect on the reflex changes of nicotine investigated. In another series of experiments the dose of hexamethonium was increased (10 – 40 µg/kg) until the reflex effects of nicotine were abolished or greatly diminished. After 30 min this blocking dose of hexamethonium was applied i.pc. again and its effect on the reflex effects of 5-HT was studied.

Statistical analysis. Data are given as mean values ± standard error of the mean. Student's *t*-test for paired observation was used to assess the significance of differences of mean values.

Table 1. Intrapericardial doses of 5-HT needed to elicit a decrease of at least 30% in either heart rate or RSNA and the corresponding intrapericardial doses of MDL 72222, which blocked the reflex

No. of animal	Dose of 5-HT (µg/kg)	Dose of MDL 72222 (µg/kg)
1	20	1
2	30	0.1
3	60	1
4	60	1
5	70	1
6	80	0.1
7	80	0.5
8	80	1
9	80	10
10	100	1
11	130	1
12	200	0.5
13	300	1

In cats 14 – 19 the blocking agent was hexamethonium and results are shown in Fig. 6

Results

Effects of 5-HT

5-HT was administered i.pc. in 29 cats, which showed a variable sensitivity for 5-HT: in 10 of the 29 cats 5-HT failed to produce reflex effects to doses up to 300 µg/kg. It cannot be excluded that higher doses would have initiated a reflex. Nevertheless in all 10 cats pronounced reflex responses could be elicited when 5-HT was injected i.v. in doses from 15 to 300 µg/kg.

In the remaining 19 cats 3 different types of reflex effects were observed: a decrease in RSNA, bradycardia and a fall in blood pressure (Figs. 1 – 3 and 6). The dose of 5-HT required to cause at least a 30% decrease in heart rate or RSNA varied from 20 to 300 µg/kg. To assure that the observed reflex effects were mediated via vagal afferent fibres, vagotomy was performed in 6 animals. After this procedure the 5-HT-induced decreases in RSNA, heart rate and blood pressure were abolished and 5-HT caused tachycardia (Fig. 1, Table 2).

In 3 of the vagotomized cats propranolol (0.5 mg/kg) and phentolamine (1 mg/kg) were administered jointly i.v. This lowered mean arterial blood pressure from 108 ± 22 mm Hg to 70 ± 25 mm Hg and decreased heart rate, but the 5-HT-induced increase in heart rate persisted (Table 2).

In the other 3 vagotomized cats i.v. administration of phenoxybenzamine (5 mg/kg) led to a fall in mean arterial blood pressure from 150 ± 15 mm Hg to 77 ± 6 mm Hg, while heart rate increased (Table 2). The pretreatment with phenoxybenzamine abolished the 5-HT mediated tachycardia (Table 2).

Effects of nicotine

Nicotine in a dose of 10 or 20 µg/kg consistently elicited decreases of RSNA, heart rate and blood pressure in each animal (Figs. 4, 5).

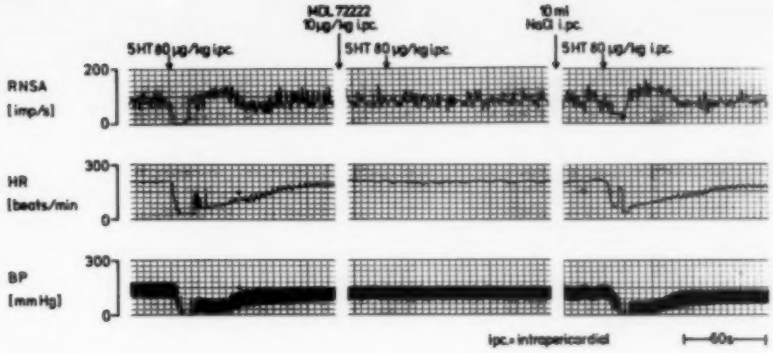

Fig. 2
Reversible blockade of the reflex effect of 5-HT by MDL 72222. (BP) arterial pressure; (HR) heart rate; (RSNA) renal sympathetic nerve activity

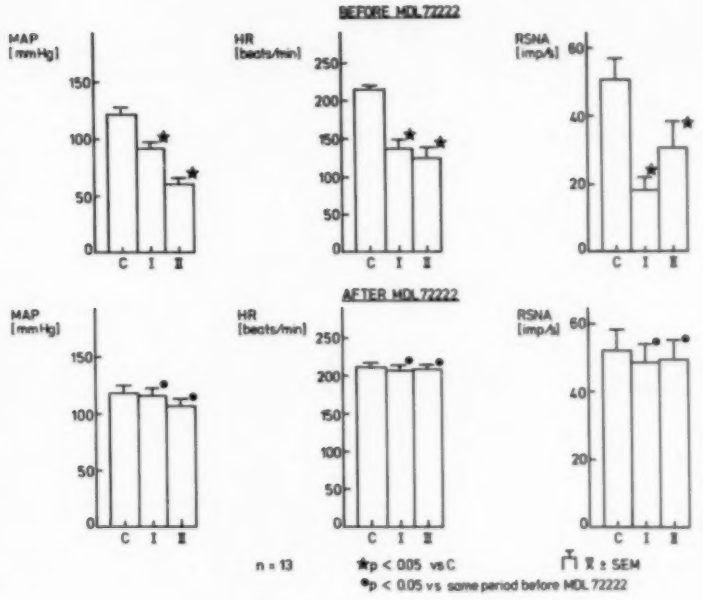

Fig. 3
Selective blockade of the reflex effects of 5-HT by MDL 72222. (MAP) mean arterial pressure, (HR) heart rate, (RSNA) renal sympathetic nerve activity. *C* control; *I* average value for the period of 1 to 15 s after the administration of 5-HT; *II* average value for the period of 16 to 30 s after the administration of 5-HT; *n* = number of cats

Blockade by MDL 72222 of the reflex effects of 5-HT

I.pc. administration of MDL 72222 did not change RSNA, heart rate and blood pressure, but greatly diminished or abolished the response in RSNA, heart rate and blood pressure to 5-HT (Figs. 2, 3). With the exception of one experiment (cat no. 9 in Table 1) we found that 1 µg/kg MDL 72222 was sufficient to block the reflex effects of 5-HT; sometimes a blockade could be obtained with even lower dosages (Table 1). The inhibitory effect of MDL 72222 was reversible; after washing the pericardial sac with 0.9% NaCl the reflex could be induced again with 5-HT. Reversibility of blockade was even observed when the concentration of MDL 72222 was unusually high (Fig. 2).

The response in heart rate to 5-HT was biphasic in the absence of MDL 72222; following the bradycardia there was a trend to a positive chronotropic response. Heart rate fell from 215 ± 6 to a minimum of 125 ± 14 beats/min and reached a value of 227 ± 6 beats/min after 2 min. This late tachycardia became significant when the bradycardia was abolished by MDL 72222; heart rate significantly increased from 210 ± 7 to 235 ± 4 beats/min after 2 min ($p < 0.05$, $n = 13$).

Lack of effect of MDL 72222 on the nicotine-induced reflex

The dose of MDL 72222, (0.1 – 10 µg/kg) which blocked the reflex effects of 5-HT did not alter the reflex response to nicotine (Fig. 4).

Effect of hexamethonium on the reflex effects of nicotine

I.pc. administration of hexamethonium did not cause significant changes in RSNA, heart rate and blood pressure. A dose of 10 to 40 µg/kg hexamethonium greatly diminished the nicotine-induced bradycardia, decrease in RSNA and fall in blood pressure (Fig. 5).

Hexamethonium does not block the 5-HT induced reflex

The dose of hexamethonium, which diminished the reflex response to nicotine did not change the fall in heart rate and

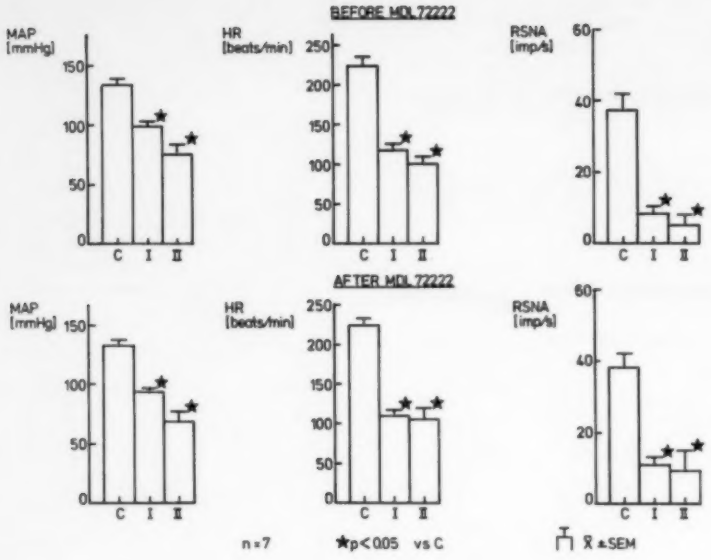

Fig. 4
Lack of blockade of the reflex effects of nicotine by MDL 72222. Details were equivalent to those of Fig. 3

Table 2
Effect of vagotomy and combinations with propranolol, phentolamine and phenoxybenzamine on the positive chronotropic response to 5-HT

	n	Heart rate (beats/min)		
		Control	Vagotomy	Vagotomy + 0.5 mg/kg i.v. propranolol + 1 mg/kg i.v. phentolamine
Before 5-HT	3	218 ± 14	217 ± 9	185 ± 9
2 min after 5-HT		248 ± 8	248 ± 11	230 ± 25
	n	Heart rate (beats/min)		
		Control	Vagotomy	Vagotomy + 5 mg/kg i.v. phenoxybenzamine
Before 5-HT	3	217 ± 16	227 ± 9	250 ± 18
2 min after 5-HT		235 ± 46	262 ± 11	245 ± 15

blood pressure and the inhibition of RSNA induced by 5-HT (Fig. 6).

Discussion

Our experiments demonstrate that 5-HT can induce pronounced reflex effects by stimulation of epicardial receptors. The reflex response includes a bradycardia as well as an inhibition of RSNA and a fall in blood pressure. All 3 responses were abolished by vagotomy, indicating that the decrease in RSNA is also mediated by excitation of sensory vagal afferents, as already known for the bradycardia and early hypotension elicited by i.v. administration of 5-HT (Comroe et al. 1953; Schneider and Yonkman 1954; Kottegoda and Mott 1955).

We assume that sympathetic inhibition is not restricted to the renal bed because: (1) the reflex pattern of other chemical agents like nicotine includes a strong vasodilatation in the skeletal muscle (Öberg and Thorén 1973) and (2) Kottegoda and Mott (1955) described an increase in blood flow in the cat's hind limb after i.v. injection of 5-HT, which persisted after administration of atropine but was abolished by vagotomy. We also found that ip.c. 5-HT reduced efferent nerve activity in cardiac nerves (Bom et al. 1985). These findings suggest that sympathetic inhibition as well as bradycardia contribute to the early fall in blood pressure induced by 5-HT.

Page (1952) and Comroe et al. (1953) observed a considerable variability in the sensitivity of cats to 5-HT injected i.v. Our data also show that the sensitivity of cats to 5-HT administered i.pc. was very variable: in 10 of 29 cats no reflex effects could be induced, while the remaining 19 cats required doses from 20 to 300 µg/kg to show clear reflex responses. In all the cats without reflex response to 5-HT i.pc., marked reflex responses were obtained when 5-HT was administered i.v. A general lack of receptors sensitive to 5-HT is therefore unlikely.

One explanation for the variable sensitivity for 5-HT might be a quite different number and distribution of 5-HT receptors on the epicardial surface of individual cats.

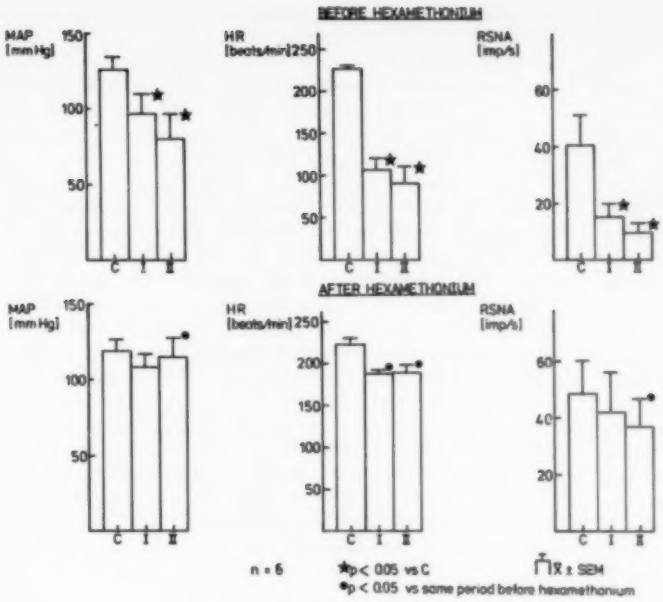

Fig. 5
Blockade of the reflex effects of nicotine by hexamethonium. Details were equivalent to those of Fig. 3

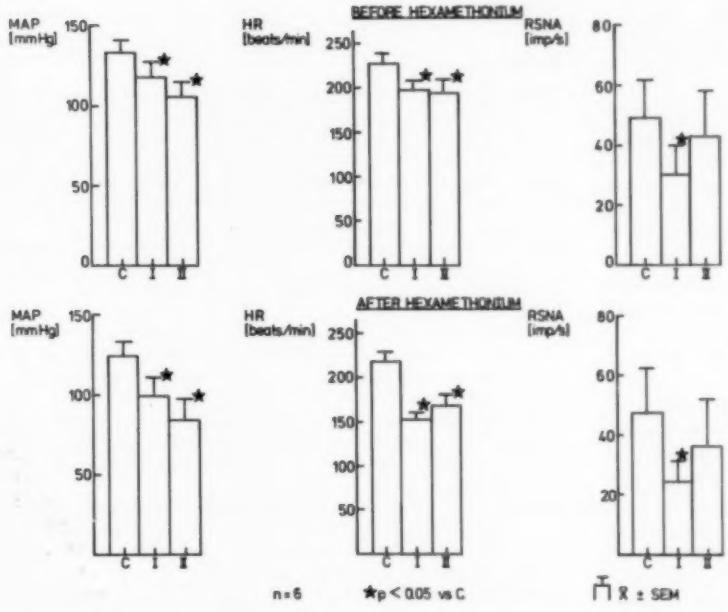

Fig. 6
Lack of blockade of the reflex effects of 5-HT by hexamethonium. Details were equivalent to those of Fig. 3

Although we know the total dose of 5-HT injected i.pc., variability in actual 5-HT concentrations due to differences in the quantity of pericardial fluid in the respective heart regions is possible. These factors could also account for the variability of the reflex responses. These explanations, however, appear unlikely because cats should have shown the same variability in sensitivity to the blocking agent MDL 72222 and this was not observed. Another explanation could be an interaction of a vagal depressor response and a counteracting sympathetic reflex. Reimann and Weaver (1980) reported that epicardial application of bradykinin, which is able to stimulate vagal as well as sympathetic afferent fibers, leads to variable reflex responses in cats. They observed excitatory responses, inhibitory responses or no changes in blood pressure and RSNA, whereas the response was always inhibitory after thoracic sympathectomy and always excitatory after vagotomy. Therefore they assumed that the varying responses of individual cats depended on the relative density of sympathetic and vagal receptors accessible to the chemical or the relative excitability of the two afferent

groups. The same could be true for 5-HT because this substance does not only stimulate vagal afferent fibres but also cardiac afferent sympathetic fibres (Uchida et al. 1969). However, the participation of afferent sympathetic fibres appears unlikely for 2 reasons: (1) we never saw an excitatory response in the intact animal and (2) even after vagotomy none of the six cats showed an increase in blood pressure and RSNA. Zimpfer et al. (1981) described a depression of chemoreceptor reflex responses with the anaesthetic α-chloralose in dogs. Although there was no difference regarding doses of α-chloralose among cats in our experiments, a different sensitivity to α-chloralose leading to varying reflex responses might be an explanation for the variability in the sensitivity to 5-HT.

To block the reflex effects of 5-HT we used the 5-HT antagonist MDL 72222, which has been shown to block selectively: (1) the excitatory action of 5-HT on sympathetic nerve terminals of the rabbit heart (Fozard and Gittos 1983), (2) the rapid response of cat carotid body chemoreceptors to 5-HT (Kirby and McQueen 1984) and (3) the 5-HT induced depolarization in the nodose ganglion and the superior cervical ganglion of the rabbit (Azami et al. 1985). Fozard (1984) also reported a marked attenuation by MDL 72222 of the heart rate and blood pressure response of the rat to i.v. 5-HT.

We were able to prevent the reflex effects of 5-HT by MDL 72222, whereas the reflex effects of nicotine were unchanged. This evidence is compatible with a selective blockade of vagal 5-HT receptors of the M-type (Gaddum and Picarelli 1957; Fozzard 1984; Richardson et al. 1985) by MDL 72222.

MDL 72222 selectively inhibited the positive chronotropic response to 5-HT in the isolated rabbit heart (Fozard 1984). In contrast, we found in the cat that marginal tachycardia developed with 5-HT, which became more pronounced when the bradycardic response to 5-HT was blocked by MDL 72222 or vagotomy. Therefore, MDL 72222 is not an antagonist at the receptor site responsible for the tachycardia in the cat. This is in agreement with the earlier findings of Trendelenburg (1960), who showed striking differences in the mechanism by which 5-HT induces a positive chronotropic response in the isolated atrium of rabbit and cat.

In the rabbit 5-HT seems to act by a release of noradrenaline from sympathetic nerve endings because the effects were prevented by reserpine pretreatment, whereas in the cat reserpine had no specific effects against 5-HT. This indicates that the positive chronotropic action of 5-HT in the cat is not mediated by endogenous catecholamines. In analogy to these experiments on isolated tissues we were not able to block the 5-HT mediated tachycardia in the cat by the α-receptor antagonist phentolamine and the β-receptor antagonist propranolol. Kaumann (1983, 1985a, b) has shown that the positive chronotropic effects of 5-HT on isolated kitten atria are irreversibly blocked by phenoxybenzamine. We confirmed this in vivo in three experiments in vagotomized cats where 5-HT did not induce an increase in heart rate after administration of phenoxybenzamine.

The nature of myocardial 5-HT receptors is not completely understood. 5-HT has a relatively low affinity for cat sinoatrial receptors (Kaumann 1983, 1985a, b) suggesting involvement of 5-HT_2-receptors. However concentrations of ketanserin saturating 5-HT_2-receptors do not antagonize the positive chronotropic effects of 5-HT in kitten atria, ruling out their 5-HT_2-nature.

Surprisingly, some drugs with high affinity for 5-HT_1-receptors also do not antagonize the positive chronotropic effects of 5-HT in kitten atria. Thus it has been concluded that sinoatrial 5-HT receptors of kitten heart are neither 5-HT_1 nor 5-HT_2 (Kaumann 1985a, 1986).

The nicotinic antagonist hexamethonium selectively blocked the reflex effects of nicotine, but did not change the responses in heart rate, RSNA and blood pressure to 5-HT. Hexamethonium applied i.pc. did not change control conditions in heart rate, blood pressure and RSNA. The dosage was too low to block transmission in sympathetic ganglia if absorption would have occurred, but it might have blocked transmission in parasympathetic ganglia, which are situated in the subepicardial region. This is unlikely for 2 reasons: (1) heart rate did not rise after application of hexamethonium and (2) the bradycardia induced by 5-HT was unchanged after application of hexamethonium.

We conclude that reflex bradycardia and reflex decrease of RSNA can be elicited on epicardial sensory vagal afferents by specific activation of M-receptors with 5-HT or of nicotinic receptors with nicotine.

Acknowledgement. We thank Dr. John Fozard (Merrell, Strasbourg, France) for a generous gift of MDL 72222.

We are grateful to Cornelia Thomalla for excellent technical assistance and for careful preparation of the figures and of the manuscript.

References

Azami J, Fozard JR, Round AA, Wallis DI (1985) The depolarizing action of 5-hydroxytryptamine on rabbit vagal primary afferent and sympathetic neurones and its selective blockade by MDL 72222. Naunyn-Schmiedebergs Arch Pharmacol 328:423–429

Black AMS, Comroe JH, Jacobs L (1972) Species difference in carotid body response of cat and dog to dopamine and serotonin. Am J Physiol 223:1097–1102

Bom AH, Mohr B, Kaumann AJ, Thämer V (1985) Are the cardiac reflex effects of nicotine, 5-HT and aortic occlusion mediated by specific receptors? Pflügers Archiv 403 R 29 (Suppl)

Bradley PB, Engel G, Feniuk W, Fozard JR, Humphrey PPA, Middlemiss DN, Mylecharane EJ, Richardson BP, Saxena PR (1986) Proposals for the classification and nomenclature of functional receptors for 5-hydroxytryptamine. Neuropharmacology 25:563–576

Comroe JR, van Lingen B, Stroud RC, Roncoroni A (1953) Reflex and direct cardiopulmonary effects of 5-OH-tryptamine (serotonin). Their possible role in pulmonary and coronary thrombosis. Am J Physiol 173:379–386

Douglas WW (1965) 5-hydroxytryptamine and antagonists; polypeptides – angiotensin and kinins. In: Goodman LS, Gilman A (eds) The pharmacological basis of therapeutics, 3rd edn. Macmillan, New York, pp 644–653

Fozard JR (1984) MDL 72222: a potent and highly selective antagonist at neuronal 5-hydroxytryptamine receptors. Naunyn-Schmiedebergs Arch Pharmacol 326:36–44

Fozard JR, Gittos MW (1983) Selective blockade of 5-hydroxytryptamine neuronal receptors by benzoic acid esters of tropine. Br J Pharmacol 80:511P

Gaddum JH, Picarelli ZP (1957) Two kinds of tryptamine receptor. Br J Pharmacol 12:323–328

Kalkman HD, Boddeke HWGM, Doods HN, Timmermans PBMWM, van Zwieten PA (1983) Hypotensive activity of serotonin receptor antagonists in rat is related to their affinity for 5-HT_1 receptors. Eur J Pharmacol 91:155–156

Kaumann AJ (1983) A classification of heart serotonin receptors. Naunyn-Schmiedebergs Arch Pharmacol 322:R42

Kaumann AJ (1985a) Two classes of myocardial 5-hydroxytryptamine receptors, which are neither 5-HT_1 nor 5-HT_2. J Cardiovasc Pharmacol 7: 576–578

Kaumann AJ (1985b) Multiple-receptor subtypes and response in autonomic effectors. Trends Auton Pharmacol 3:51–59

Kaumann AJ (1986) Further differences between 5-HT receptors of atrium and ventricle in cat heart. Br J Pharmacol 89:546T

Kirby CC, McQueen DS (1984) Effects of the antagonists MDL 72222 and ketanserin on responses of cat carotid body chemoreceptors to 5-hydroxytryptamine. Br J Pharmacol 83:259–269

Kottegoda SR, Mott JC (1955) Cardiovascular and respiratory actions of 5-hydroxytryptamine in the cat. Br J Pharmacol 10:66–72

Mott JC, Paintal AS (1953) The action of 5-hydroxytryptamine on pulmonary and cardiovascular vagal afferent fibres and its reflex respiratory effects. Br J Pharmacol 8:238–241

Öberg B, Thoren P (1973) Circulatory responses to stimulation of left ventricular receptors in the cat. Acta Physiol Scand 88:8–22

Page I (1952) The vascular action of natural serotonin, 5- and 7-hydroxytryptamine and tryptamine. J Pharmacol Exp Ther 105:58–73

Paintal AS (1955) Impulses in vagal afferent fibres from specific pulmonary deflation receptors. The response of these receptors to phenyl diguanide, potato starch, 5-hydroxytryptamine and nicotine, and their role in respiratory and cardiovascular reflexes. Q J Exp Physiol 40:89–111

Reimann KA, Weaver LC (1980) Contrasting reflexes evoked by chemical activation of cardiac afferent nerves. Am J Physiol 239:H316–H325

Richardson BP, Engel G, Donatsch P, Stadler PA (1985) Identification of serotonin M-receptor subtypes and their specific blockade by a new class of drugs. Nature 316:126–131

Schneider JA, Yonkman FF (1954) Species differences in the respiratory and cardiovascular response to serotonin (5-hydroxytryptamine). J Pharmacol Exp Ther 111:84–98

Takahashi H (1985) Cardiovascular and sympathetic responses to intracarotid and intravenous injections of serotonin in rats. Naunyn-Schmiedebergs Arch Pharmacol 329:222–226

Trendelenburg U (1960) The action of histamine and 5-hydroxytryptamine on isolated mammalian atria. J Pharmacol Exp Ther 130:450–460

Uchida Y, Kamisaka K, Ueda H (1969) Responses of the cardiac sympathetic receptors to various substances. Jpn Heart J 10:225–242

Vogt A, Thämer V (1980) Vagal and sympathetic reflexes of left ventricular origin on the efferent activity of cardiac and renal nerves on anaesthetized cats. Basic Res Cardiol 75:635–645

Volle RL, Koelle GB (1975) Ganglionic stimulating and blocking agents. In: Goodman LS, Gilman A (eds) The pharmacological basis of therapeutics, 5th edn. Macmillan, New York, pp 565–574

Zakusov VV (1962) Principles of pharmacological influence on coronary chemoreflex. Arch Int Pharmacodyn Ther 140:646–654

Zimpfer M, Sit PS, Vatner SV (1981) Effects of anaesthesia on the canine carotid chemoreceptor reflex. Circ Res 48:400–406

Received April 4, 1986/Accepted January 7, 1987

Pflügers Arch (1987) 409:152–157

Pflügers Archiv
European Journal of Physiology
© Springer-Verlag 1987

Quantitative evaluation of optical reflection spectra of blood-free perfused guinea pig brain using a nonlinear multicomponent analysis

U. Heinrich, J. Hoffmann, and D. W. Lübbers

Max-Planck-Institut für Systemphysiologie, Rheinlanddamm 201, D-4600 Dortmund 1, Federal Republic of Germany

Abstract. After developing a blood-free perfused preparation of the guinea pig brain a nonlinear multicomponent analysis (NLMCA) of the reflection spectra of the brain surface was worked out by which the redox state of cytochrome aa_3, *c*, and *b* could be evaluated quantitatively and almost continuously. The NLMCA allowed to simulate the tissue reflection spectra in such a way that only a small statistical error remained between the recorded and the computed spectra. Using redox states of cytochrome aa_3 and *c* as an intracellular oxygen probe it was found that in order to supply the guinea brain with sufficient oxygen by a saline medium equilibrated with 95% oxygen and 5% CO_2 the temperature had to be reduced to 18–20° C. At this temperature cytochrome aa_3 was 95% oxidized.

Key words: Redox state of cytochromes – Blood-free brain perfusion – Reflection photometry – Nonlinear multicomponent analysis

Introduction

By reflection photometry it is possible to monitor continuously and non-invasively tissue oxygen supply, since hemoglobin, myoglobin, and cytochromes have characteristic absorption spectra. The development of the photometric technique permits a rather accurate measurement of tissue reflection spectra, however, the question how to evaluate quantitatively reflection spectra has only been partly solved. Mostly, the two wavelengths method is used by which the extinction difference between the isosbestic and the measuring wavelength is monitored [2, 3, 25]. However, it is known that the two wavelengths method can give erroneous results [6, 11, 14, 15, 29]. Further difficulties arise in a blood-perfused organ, because the amplitudes of the hemoglobin bands are much larger than those of the cytochromes. Since in vivo hemoglobin changes very often its concentration, the existence of stable isosbestic points in such a multicomponent system is highly questionable [14].

The relative concentrations of components in a multicomponent system can be found without using isosbestic points by applying the multicomponent analysis. For this analysis the spectra of all components have to be known. Then, according to the least square method of Gauss the mixture of components is calculated which fits the measured spectra at the best [19, 21, 28]. In order to evaluate reflection spectra the influence of scattered light has to be taken into account [see 8, 17]. Lübbers and Wodick have shown that the spectral changes caused by the scattered light within the tissue can be described – and visualized – by a transformation function [22, 32]. This function describes for each wavelength the relationship between the extinction of the component in solution using transmitted light ("true" spectra, standard spectra) and the extinction of the same component within the tissue (reflection spectra).

In the following we will show that in the wavelength range between 510 and 630 nm the transformation function of the hemoglobin-free perfused guinea pig brain can be well approximated by a 3-parametric hyperbola. With such a nonlinear multicomponent analysis (NLMCA) the redox state of cytochromes can be quantitatively evaluated. We found that in the hemoglobin-free perfused guinea pig brain at 18–20° C there are no signs of an insufficient tissue O_2 supply, at 24° C single cells are anoxic, whereas at 37° C about 40% of the tissue is anoxic when equilibrating the perfusion medium with carbogen.

Method

Hemoglobin-free perfusion of the guinea pig brain. Guinea pigs weighing 200–400 g were pretreated with 0.5 ml Liquemin 30 min before starting the experiments and anaesthetized by nembutal (6 mg/100 g b.w.) adding 0.1 mg atropin.

The perfusion medium consisted of a macrodex 6% solution with the addition of 20 mmol·l^{-1} $NaHCO_3$ and papaverine (4.0 mg/100 ml). The perfusate was heated up to 18° C, 24° C, and 37° C, respectively, and equilibrated with carbogen (95% O_2 + 5% CO_2; pH 7.3) using a disk oxygenator. The perfusion was carried out by a perfusion pump with constant volume; the resulting perfusion pressure was about 70 cm H_2O. The perfusion rate was 30 ml/min. 15% to 20% of the medium runs through the brain corresponding to a blood flow of about 200 ml/(100 g · min) [16].

Animals were tracheotomized and during surgery artificially ventilated. After ligation of the vessels lying in the axilla the thorax was opened [10, 16, 27]. The lung was then carefully moved to the right and the influx catheter (made of PVC) fixed in the abdominal aorta. Incision was done with the aid of eye scissors. To facilitate the introduction of the catheter some drops of the papaverine-containing perfusate were dropped on the incision spot. After fixation of the catheter, perfusion was started. The efflux catheter

Offprint requests to: D. W. Lübbers

was now inserted in the inferior cavian vein and moved up to the right ventricle and fixed. The efflux catheter tip was manufactured out of V_2A steel with additional holes on the sides, thereby guaranteeing an uninterrupted flow of the perfusate. To isolate the brain circulation ligations were tightened around the pulmonary artery and the aorta at the heart base.

Now, the animal was turned in the abdominal position and trephinized, mostly in the posterior part of the scull, about 5 mm lateral of the sinus sagittalis. The prepared hole was about 1 cm^2 in size. After a period of 10–15 min, the cerebral cortex was blood-free so that photometric measurements could be started. Great care had to be taken not to produce any pressure or mechanical irritation of the brain. For photometric measurements the dura and the subarachnoid space were left intact. After outwashing the blood, with intact dura the perfusion time with saline medium was at 18°C about 1,5 h, at 24°C 1 h, at 37°C only 45 min.

Photometric measurements. Recordings of reflection spectra of the perfused brain were performed by the rapid spectrometer T 13/3, a double-beam photometer with a measuring frequency of 25 kHz [20]. The recording time for one spectrum amounts to 10 ms; therefore, spontaneous movements of the brain can be neglected. Under suitable conditions the constancy of the zero line is better than 0.003 OD and allows the reading of differences in optical density of 0.001 OD [26]. Wavelength resolution is 0.6 nm; wavelength reproducibility is 0.1 nm. The spectral halfband width was in our measurements 1 nm. Usually, for evaluation a series of eight spectra is averaged.

As basic spectra transmission spectra of solutions of cytochrome aa_3, cytochrome *c*, and cytochrome *b* were used [9]. Special care was taken to obtain spectra of fully reduced and oxidized cytochrome without destroying the molecules. Since it could not always be avoided that a small amount of blood (mostly from the bone) entered the measuring field during the experiment, the spectra of oxygenated and deoxygenated hemoglobin were also included in the set of basic spectra, thus obtaining a set of nine basic spectra.

For reflection measurements the light guide of the photometer is brought in 1–2 mm distance to the brain surface. In some cases a droplet of saline is used to improve the contact between light guide and dura and to avoid contact with the surrounding air.

Measuring data were digitalized (14 bit) and evaluated by a computer (Honeywell 516).

In most of the experiments the relative concentrations of cytochromes were determined from a strongly reduced reflection spectra and used for the following evaluations. By this restriction the error in the evaluation of the more oxidized spectra was reduced.

Results

Evaluation method: Nonlinear multicomponent analysis (NLMCA) of the reflection spectra of the hemoglobin-free perfused guinea pig brain

The spectra of diluted homogenate of the hemoglobin-free perfused guinea pig brain is determined by the spectra of oxidized and reduced cytochrome aa_3, *c*, and *b*, i.e. by six components. Similarly, as for diluted mitochondria, the Lambert-Beer law also holds for diluted brain homogenates in transmission [27, 33]:

$$I = I_0 \cdot 10^{-a(\lambda)\cdot z} \tag{1}$$

$$-\log\frac{I}{I_0} = a(\lambda)\cdot z = y(\lambda)\,. \tag{2}$$

Equation (2) shows that the absorbance, $a(\lambda)$, is linearly proportional to the logarithm of the intensity of the incident light, I_0, divided by the intensity of the transmitted light, I. z is the length of the lightpath. $y(\lambda)$ denotes the measured absorption spectra.

In our case $a(\lambda)$ is the sum of the six cytochrome components

$$a(\lambda) = \sum_i c_i \cdot a_i; \quad i = 1\ldots6 \tag{3}$$

with c_i = concentration of component i; a_i = molar absorptivity of the component i.

If the Lambert-Beer law is valid, a linear multicomponent analysis can be performed presupposing that the "true" absorption spectra of all components (the set of basic spectra of standard (spectra) are known i.e. the absorption spectra of each component in solution measured by transmitted light. The relative concentrations, c_i, of the set of six basic components are determined by the least square method of Gauss [19, 21, 28]. The best fit between the measured spectra, $y(\lambda)$, and the spectra of the calculated mixture of the components is accomplished, if Eq. (4) becomes a minimum.

$$\sum_\lambda [y(\lambda) - \sum_i c_i \cdot a_i(\lambda)\cdot z]^2 = \min\,. \tag{4}$$

However, for the evaluation of the brain reflection spectra this simple measure was insufficient. Wodick and Lübbers [25, 37, 40] found that for constant scattering under such conditions the relationship between the intensity of incident light and the intensity of the light leaving the sample can be described by

$$I = I_0 \int w(s,z)\cdot 10^{-a(\lambda)\cdot z}dz \tag{5}$$

where $w(s,z)$ = the distribution of the light paths, z, within the sample. This light path distribution is mainly influenced by the scattering of the sample, which is described by the scattering coefficient, s. It has been shown that for a small wavelength dependency of scattering s could be described by a constant and a wavelength-dependent term [27].

$$s = s_0 + s_1\cdot\lambda\,. \tag{6}$$

Using Eq. (6) we obtain for the measured absorption spectra

$$y(\lambda) = -\lg\frac{I}{I_0} = -\lg\int w(s_0,z)\cdot 10^{(a(\lambda)+c_s\lambda)\cdot z}dz \tag{7}$$

$$y(\lambda) = H(a(\lambda) + c_s\cdot\lambda) \tag{8}$$

H denotes the transformation function by which the basic spectra of the components are transformed in the reflection spectra. By spectra of the mixture of the components [13].

$$H^{-1}(y(\lambda)) = \sum_i (c_i\cdot a_i + c_s\cdot\lambda)\,. \tag{9}$$

Experiments with brain homogenates showed that H^{-1} is a monotonously increasing one to one function [27], which

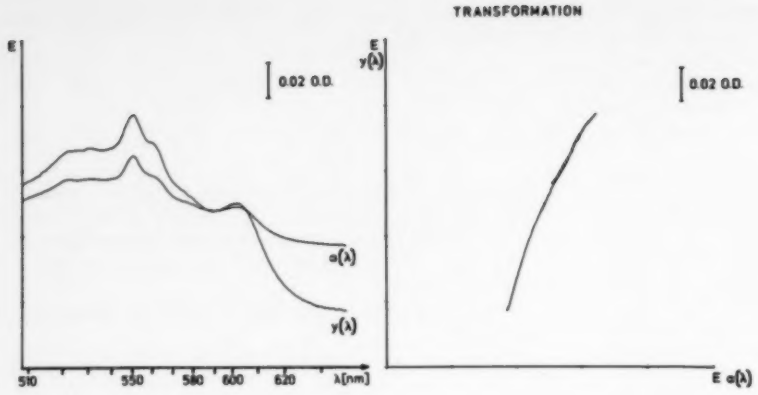

Fig. 1
A measured tissue reflection spectrum, $y(\lambda)$, the transformation, and the computed "true" spectrum, $a(\lambda)$ (blood-free perfused guinea pig brain). The peak at 550 nm corresponds to cytochrome *c*, the shoulder at 562 nm to cytochrome *b*, and the peak at 605 nm to cytochrome aa_3

can be rather well approximated by a three parametric hyperbola

$$H^{-1}(y(\lambda)) = (b_1 \cdot y(\lambda) + b_2)/(b_3 \cdot y(\lambda) + 1) = \sum_i (c_i \cdot a_i + c_s \cdot \lambda). \quad (10)$$

Using Eq. (9) a nonlinear multicomponent analysis has been performed to evaluate the tissue reflection spectra of the hemoglobin-free perfused guinea pig brain. For this analysis the spectra are normalized so that the mean of the extinctions becomes zero and the extinctions vary in the interval between -1 and $+1$. In the first step of the analysis the constants b_2 and b_3 are set to zero and b_1 to 1. With these assumed values of the constants and the set of basic components [see Eq. (9)] a linear multicomponent analysis is performed and the constants c_i and c_s are calculated. In the second step the just calculated constants are used to determine the three parameters b_1, b_2, and b_3 of the hyperbola. Using the calculated parameters, b_1, b_2, b_3, these steps are repeated until the minimum of the least square error [see Eq. (4)] is reached.

Application of the nonlinear multicomponent analysis to the Hb-free perfused brain

The nonlinear multicomponent analysis as described above was applied to measure the redox state of the cytochromes in the hemoglobin-free perfused guinea pig brain in situ. Figure 1 shows a typical reflection spectrum of the anoxic brain $y(\lambda)$. The peak of cytochrome aa_3 at 605 nm, the peak of cytochrome *c* at 550 nm, and the peak of cytochrome *b* at 562 nm are clearly visible. The other spectrum shows the calculated "true" spectrum $a(\lambda)$, which would be obtained by measuring the cytochrome mixture in a cuvette with transmitted light. On the left side the transformation function is depicted:

$$y(\lambda) = H(\sum_i c_i \cdot a_i + c_s \cdot \lambda) = -\lg \frac{I}{I_0}$$

H is clearly a monotonously increasing one to one function.

In Fig. 2 (left side) the reflection spectra is simulated by its components $[H(\sum_i c_i \cdot a_i + c_s \cdot \lambda)]$ and compared with the measured spectra. Since it can hardly be seen that there are two spectra plotted, the difference between the spectra, 5 times enlarged, is depicted on the right side. The difference amounts to about ± 0.002 OD. In this error range there is no visible wavelength-dependent systematic error.

This example of a successful simulation of reflection spectra demonstrates that the nonlinear multicomponent analysis using a proper set of basic spectra and a 3-parametric hyperbola can be used to evaluate quantitatively the redox state of the cytochrome in the hemoglobin-free perfused guinea pig brain.

In Fig. 3 a series of spectra are shown during a perfusion stop at 18°C. The series starts with a "well oxidized spectrum" (lowest trace) and ends with a "partly reduced spectrum" (uppermost trace). Besides the characteristic peaks of the cytochromes, there is a trace of the peak of oxygenated hemoglobin at 577 nm (visible between the peaks of cytochrome aa_3 and cytochrome *b*). As already mentioned, this peak is caused by traces of blood, which are outside the brain circulation. By evaluating a continuous series of spectra the cytochrome kinetics during perfusion stop can be obtained (Fig. 4). At the beginning, cytochrome aa_3 and cytochrome *c* are about 95%, and cytochrome *b* 52% oxidized. The width of the traces demonstrates the absolute error of the computation. It amounts to about 5%. In the lowest trace the mean least square error is depicted. It is 3% and shows that in these experiments the error is independent of the state of oxidation.

Table 1 shows the redox state of cytochromes using the above described perfusion conditions. It demonstrates that at 18°C the brain is well oxygenated. At 24°C first indications of insufficient brain tissue oxygen supply could be observed, whereas at 37°C almost 40% of the tissue is anoxic. The absolute values of the redox state of cytochrome *b* differ distinctly from those of the other cytochromes, but show the same trend.

Discussion

To measure photometrically concentration changes of a single component in a multicomponent system the two wavelength method can only be applied, if stable and well defined isosbestic points exist [6, 24]. Since this is often not the case, changes of isosbestic points have to be taken into account. Williams [29] describes a method which allows to determine simultaneously the concentration of four cytochromes in mitochondria. Jõbsis [14] and his group tried to solve the

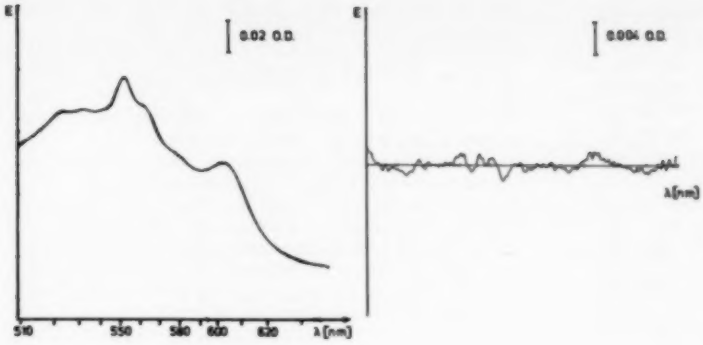

Fig. 2
Measured and simulated spectrum $[H(\sum_i c_i \cdot a_i + c_4\lambda)]$ from the blood-free perfused guinea pig brain (*left*). The remaining differences are 5 times enlarged (*right*)

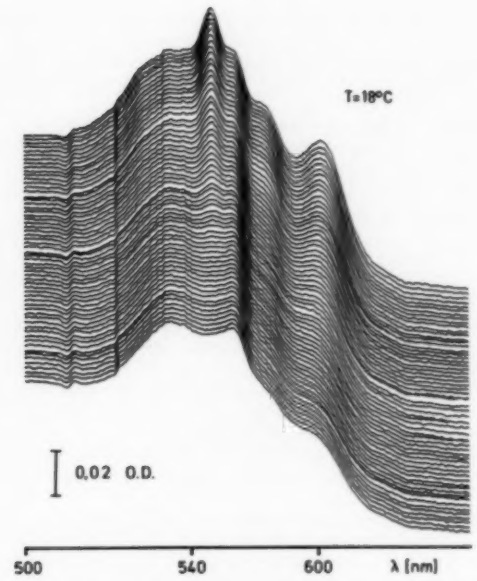

Fig. 3. Measured reflection spectra during brain perfusion and perfusion stop ($t = 18°C$). The experiment begins with the lowest trace

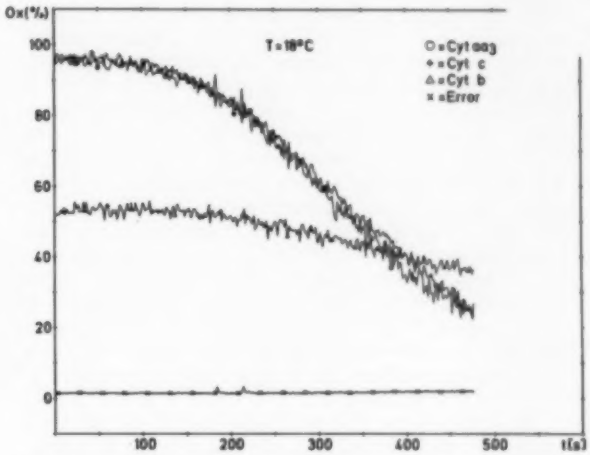

Fig. 4. Evaluation of the percentual oxidation of cytochromes during the experiment shown in Fig. 3 (perfusion stop, $t = 18°C$). The width of the traces shows the error range, by which the concentration of the different components can be determined. The trace designated error (×) depicts the mean last square error

Table 1

Temperature °C	Redox state of cytochromes % oxidation		
	aa_3	*c*	*b*
18	95	95	50
24	82	82	30
37	60	60	20

difficulties which arise, if hemoglobin is present by introducing "equibestic" points, at which the changes of light absorption related to the oxygen saturation of hemoglobin are equal [', 14, 15]. However, for tissue measurements it is not always allowed to use the same isosbestic points as found in solutions of mitochondria or homogenates, because the isosbestic points are influenced by the scattering conditions within the intact tissue [27]. To overcome this problem a multicomponent analysis has been developed which does not rely on the existence of isosbestic points and is independent of concentration changes of the components. To be successful such an analysis needs absorption spectra of all components measured over a larger wavelength range.

To simplify the optical system a hemoglobin-free perfusion of the guinea pig brain in vivo was developed. By reducing the temperature to 18°C it was possible to supply sufficient oxygen using a simple saline solution, but to overcome the vascular constriction, which accompanies the cooling of the brain, papaverine had to be added to the perfusion medium [16]. The dilated vessels permitted a relatively low perfusion pressure; this was necessary since with higher perfusion pressures edema develops. Isolated brain perfusions are known (e.g. cat [4, 7, 12], rat [1, 18]), but all these perfusions use blood and do not need hypothermia.

As it was tried to simulate the reflection spectra of the hemoglobin-free perfused guinea pig brain – first graphically – it was found that an approximation was only

possible if the experimentally measured displacement of the isosbestic points was taken into account [21, 27], but the remaining error was still rather large [23].

To find a better approximation the light path distribution [see Eq. (5)] in concentrated homogenates of the hemoglobin-free perfused guinea pig brain was investigated [21] and the transformation function of our optical system was worked out [31].

The experiments show that our optical system is well described by a 3-parametric hyperbola (see Fig. 1), if the wavelength-dependent changes are taken into account by including a polynom of 1 degree in the set of basic spectral components as a wavelength-dependent scattering [see Eq. (6)]. The transformation is bended to the abscissa. This bending causes a flattening of the absorption peaks, as it was observed for example by Duysens [5]. With this nonlinear multicomponent analysis it was possible to simulate the reflection spectra of the hemoglobin-free perfused guinea pig brain in such a way that only a small statistical error remained between the measured and the computed spectra (Fig. 2). From this successful simulation we conclude that the NLMCA allows a quantitative evaluation of the relative concentration of the cytochromes in the brain tissue in vivo. It was found that special care had to be taken to obtain spectra of fully reduced and oxidized cytochromes without destroying the substances, since the calculated absolute values depend very much on correct basic spectra. A small mean least square error did not mean that the concentrations of the components could be determined with the same error, because the determination of the relative concentration of the components depends also on the form of the spectra. However, the continuous control of the mean least square error permits to detect, to analyse, and to minimize experimental disturbances.

The experiments show that applying the NLMCA the redox state of ytochrome aa_3 and c can be used as an intracellular, in vivo oxygen sensor. In order to supply the guinea pig brain sufficiently with oxygen by a saline medium equilibrated with 95% O_2 and 5% CO_2 the temperature had to be reduced to about 20°C. Under these conditions cytochrome aa_3 was about 95% oxidized. This degree of oxidation is larger than that reported by Jöbsis [14] for a normothermic and blood perfused brain of an animal respiring air, but corresponds to values obtained with increased arterial P_{O_2}.

References

1. Andjus RK, Suhara K, Sloviter HA (1967) An isolated, perfused rat brain preparation, its spontaneous and stimulated activity. J Appl Physiol 22:1033–1039
2. Chance B (1951) Rapid and sensitive spectrophotometry. III. A double-beam apparatus. Rev Sci Instr 22:634–638
3. Chance B, Williams GR (1955) Respiratory enzymes in oxidative phosphorylation. II. Difference spectra. J Biol Chem 217:395–407
4. Chute AL, Smyth DH (1939) Metabolism of the isolated perfused cat's brain. Q J Exp Physiol 29:379–394
5. Duysens LNM (1956) The flattening of the absorption spectrum of suspensions as compared to that of solutions. Biochim Biophys Acta 19:1–11
6. Figulla HR, Hoffmann J, Lübbers DW (1984) Evaluation of reflection spectra of the isolated heart by multicomponent spectra analysis in comparison to other evaluating methods. In: Lübbers DW, Acker H, Leniger-Follert E, Goldstick TK (eds) Oxygen transport to tissue, V. Adv Exp Med Biol, vol 169. Plenum Press, New York London, pp 821–830
7. Geiger A (1953) Correlation of brain metabolism and function by the use of a brain perfusion method in situ. Physiol Rev 38:1–20
8. Hecht HG (1968) Modern aspects of reflectance spectroscopy. In: Wendtlandt WW (ed). Plenum Press, New York
9. Heinrich U (1981) Untersuchungen zur quantitativen photometrischen Analyse der Redox-Zustände der Atmungskette in vitro und in vivo am Beispiel des Gehirns. Dissertation, Bochum
10. Heinrich U, Hoffmann J, Lübbers DW (1983) Quantitative analysis of reflection spectra on the perfused brain in different states of oxygen supply. In: Bicher HI, Bruley DF (eds) Oxygen transport to tissue, IV. Adv Exp Med Biol, vol 159. Plenum Press, New York London, pp 119–127
11. Hempel FG, Jöbsis FF, La Manna JC, Rosenthal MR, Saltzman HA (1977) Oxidation of cerebral cytochrome aa_3 by oxygen plus carbon dioxide at hyperbaric pressures. J Appl Physiol 43:872–877
12. Hirsch H, Gleichmann U, Kristen H, Magazinović V (1961) Über die Beziehung zwischen O_2-Aufnahme des Gehirns und O_2-Druck im Sinusblut des Gehirns bei uneingeschränkter und eingeschränkter Durchblutung. Pflügers Arch Ges Physiol 273:213–222
13. Hoffmann J, Wodick R, Hannebauer F, Lübbers DW (1984) Quantitative analysis of reflection spectra of the surface of the guinea pig brain. In: Lübbers DW, Acker H, Leniger-Follert E, Goldstick TK (eds) Oxygen transport to tissue, V, Adv Exp Med Biol, vol 169. Plenum Press, New York London, pp 831–839
14. Jöbsis FF, Keizer JH, La Manna JC, Rosenthal M (1977) In vivo reflectance spectrophotometry of cytochrome aa_3 in the intact cerebral cortex of the cat. J Appl Physiol 43:858–872
15. Kariman K, Burkhart DS (1985) Non-invasive in vivo spectrophotometric monitoring of brain cytochrome aa_3 revisited. Brain Res 360:203–213
16. Knaust K (1967) Sauerstoffversorgung des hämoglobinfrei perfundierten Meerschweinchengehirns in vivo und in Hypothermie von 18°C. Dissertation, Marburg
17. Kortüm G (1969) Reflexionspektroskopie. Grundlagen, Methodik, Anwendungen. Springer, Berlin Heidelberg New York
18. Krieglstein G, Krieglstein J, Stock RW (1972) Suitability of isolated perfused rat brain for studying effects on cerebral metabolism. Naunyn-Schmiedeberg's Arch Pharmacol 275:124–134
19. Lübbers DW, Niesel W (1957) Über die Auswertung von spektralen Veränderungen in biologischen Objekten. Naturwissenschaften 3:59–60
20. Lübbers DW, Niesel W (1959) Der Kurzzeit-Spektralanalysator. Ein schnellarbeitendes Spektral-Photometer zur laufenden Messung von Absorptions- bzw. Extinktionsspektren. Pflügers Arch Ges Physiol 268:286–295
21. Lübbers DW, Wodick R (1969) The examination of multicomponent systems in biological materials by means of a rapid scanning photometer. Appl Optics 8:1055–1062
22. Lübbers DW, Wodick R (1972) Quantitative Analyse von Reflexionsspektren multiplikativer und additiver Gemische von Mehrkomponentensystemen mit überlagerter Störkomponente am Beispiel der menschlichen Haut. Naturwissenschaften 59:418–419
23. Lübbers DW, Wodick R (1972) Schnelle Photometrie komplizierter biochemischer Mehrkomponentensysteme. Fresenius Z Anal Chem 261:271–280
24. Makino N, Kanaide H, Yoshimura R, Nakamura M (1983) Myoglobin oxygenation remains constant during the cardiac cycle. Am J Physiol 245:H237–H243
25. Matthes K, Gross F (1939) Untersuchungen über die Absorption von rotem und ultrarotem Licht durch kohlenoxydgesättigtes, sauerstoffgesättigtes und reduziertes Blut. Arch Exp Pathol Pharmacol 191:369–380

26. Niesel W, Lübbers DW, Schneewolf D, Richter J, Botticher W (1964) Double beam spectrometer with 10 ms recording time. Rev Sci Instr 35:578–581
27. Schwickardi D (1968) Konzentration und Kinetik der Atmungsfermente am isoliert perfundierten Meerschweinchengehirn in vivo und in Hypothermie von 18°C. Dissertation, Marburg
28. Sternberg JC, Stillo HC, Schwendeman RS (1960) Spectrophotometric analysis of multicomponent systems using the least squares method in matrix form. Anal Chem 32:84–90
29. Williams JN jr (1964) A method for the simultaneous quantitative estimation of cytochromes *a*, *b*, c_1 and *c* in mitochondria. Arch Biochem Biophys 107:537–543
30. Wodick R, Lübbers DW (1973) Methoden zur Bestimmung des Lichtweges bei der Photometrie trüber Lösungen oder Gewebe mit durchfallendem oder reflektiertem Licht. Pflügers Arch 342:29–40
31. Wodick R, Lübbers DW (1973) Quantitative Analyse von Reflexionsspektren und anderen Spektren mit inhomogenen Lichtwegen an Mehrkomponentensystemen mit Hilfe der Queranalyse. I. Das Verfahren der Queranalyse bei Mehrkomponentensystemen mit unbekannten, inhomogenen Lichtwegen. Hoppe-Seylers Z Physiol Chem 354:903–915
32. Wodick R, Lübbers DW (1974) Quantitative evaluation of reflection spectra of living tissue. Hoppe-Seylers Z Physiol Chem 335:583–549
33. Wodick R, Schwickardi D, Lübbers DW (1966) Konzentration und Kinetik der Atmungsfermente im Meerschweinchengehirn in vivo. Pflügers Arch Ges Physiol 291:25

Received August 18, 1986/Accepted January 7, 1987

Pflügers Arch (1987) 409:158–162

Pflügers Archiv
European Journal of Physiology
© Springer-Verlag 1987

Forskolin inhibition of hexose transport in cardiomyocytes

Timothy P. Geisbuhler*,[1], Susan Sergeant[2], Frances L. Miramonti[1], Hyun Dju Kim[2], and Michael J. Rovetto[1]

Departments of [1]Physiology and [2]Pharmacology, University of Missouri, Medical Sciences Building, Columbia, MO 65212, USA

Abstract. The effects of insulin, forskolin, isoproterenol, and epinephrine on 3-O-methylglucose (hexose) transport and cell cyclic AMP levels were determined in adult rat cardiomyocytes. Insulin stimulated hexose transport in these cells an average of 2.5-fold. Initial hexose transport rates at 1 mM hexose were 3.75×10^{-2} nmol/mg cell protein/second in the absence of insulin, and 8.25×10^{-2} nmol/mg cell protein/second in the presence of 12.3 μM insulin. Forskolin at 5 μM nearly abolished hexose transport within 3 s of exposure, but did not increase cell cyclic AMP concentrations within 9 s. The apparent K_i for hexose transport inhibition was about 0.3 μM forskolin. Epinephrine and isoproterenol at 50 μM increased cell cyclic AMP 4-fold during 9 s exposure, but did not affect hexose transport. Treatment of cells with these catecholamines of forskolin for up to 99 s increased cell cyclic AMP, but only forskolin inhibited hexose transport. We conclude from these results that forskolin acts on hexose transport independent of its action on adenyl cyclase, and that cyclic AMP does not inhibit or stimulate hexose transport.

Key words: Heart – Myocyte – Glucose – Insulin – Catecholamines – Cyclic AMP

Introduction

Glucose uptake has been extensively studied in whole heart (Cheung et al. 1978; Morgan et al. 1961; Morgan and Neely 1972), and recently in isolated cardiomyocytes (Eckel et al. 1983; Haworth et al. 1984; Lindgren et al. 1982). The latter preparation is free of non-muscle cells, and provides a homogeneous cell suspension suitable for initial transport rate estimates. In this study we have used calcium-tolerant cardiomyocytes from adult rats to determine initial transport rates of 3-O-methylglucose (a nonmetabolized glucose analog), the effect of insulin on these rates, and the relationship of cyclic-3′,5′-AMP (cAMP) to hexose transport. This latter study was prompted by reports that isoproterenol and other agents inhibited glucose transport in adipocytes via a cAMP-dependent mechanism (Kashiwagi et al. 1983; Taylor et al. 1976). Our studies of hexose transport in myocytes demonstrate that zero-trans rates at non-saturating glucose concentrations are higher than those found in whole heart. Pre-incubation with insulin increased these rates an average of 250%. Forskolin was a potent inhibitor of hexose transport by a mechanism unrelated to elevations in cAMP concentrations.

* Supported by NIH-HL 07094
Offprint requests to: M. J. Rovetto

Methods

Myocytes were obtained by collagenase digestion of adult rat hearts, using a modification of the methods of Hohl et al. (1983) and Farmer et al. (1983). Male Sprague-Dawley rats were injected with heparin (1000 U/kg, i.p.) 30 min before anaesthesia with 75 mg sodium pentobarbital/kg, i.p. The hearts were excised and placed in ice-cold MEM-Joklik-modified buffer supplemented with 20 mM creatine, 60 mM taurine, 5 mM HEPES (this mixture is hereafter called "buffer"), 1 U heparin/ml and 0.1% bovine serum albumin (BSA), pH = 7.3. The aortas were cannulated with 2 mm i.d. stainless steel tubing, and perfused at 37°C from a static 40 mm Hg hydrostatic pressure head. The buffer was equilibrated with 100% O_2 and was not recirculated. After a 5–10 min washout period, 0.7 mg collagenase/ml (Cooper, CLS I) was added to the buffer and allowed to recirculate until the aortic perfusion pressure decreased below 40 mm Hg (30–40 min). The ventricles were minced, placed in fresh collagenase-containing buffer, and shaken at 250 rpm in a New Brunswick model G-76 gyrotory water bath (New Brunswick Scientific Co., Edison, NJ, USA) for 10 min. Calcium concentration was brought to 50 μM, and digestion continued 10 more min.

The cells were dispersed by repeated aspiration/dispersion with a plastic dispo-pipette, and filtered through a triple layer of cheesecloth. The cell suspension was diluted 1:4 with buffer containing 0.1% BSA. The cells were allowed to settle, the supernatant fluid was removed, and the cells were resuspended in buffer containing 1% BSA. This procedure was repeated twice, and the cells were suspended in glucose-free buffer containing 0.1% BSA and 1 mM pyruvate. The volume of the suspension was adjusted to 8–10 mg cell protein/ml. Calcium concentration was increased by stepwise addition of 100–200 μM $CaCl_2$ over 30 min, to a final concentration of 1 mM. The cells were settled once more, the supernatant fluid removed, and the pellet suspended in glucose-free buffer containing 0.1% BSA, 1 mM pyruvate, and 1 mM calcium. This procedure gave a cell preparation containing 75–90% rod-shaped cells, and viability by trypan blue exclusion of about 90%. Nearly all of the cells which took up the dye were hypercontracted, as less than 0.1% of the rodshaped cells were stained.

Transport studies. Buffer of the same composition as that used in the final cell suspension and containing

4 mM 3-O-methyl-D-glucose, U-^{14}C-3-O-methyl-D-glucose (0.6 μCi/ml buffer), 1 mM D-sorbitol and 1-^{3}H-D-sorbitol (3.0 μCi/ml buffer) was used for transport studies (^{3}H-sorbitol was used to correct for extracellular contamination ranging from 10–30% of the uncorrected uptake). When forskolin, isoproterenol, or epinephrine were present, these compounds were added directly to the isotope-containing buffer, so that exposure of the cells to these compounds and initiation of transport was simultaneous. To initiate transport, 0.6 ml cell suspension (representing 2–4 mg cell protein) were rapidly injected into 0.2 ml of buffer containing isotope and 3-O-methylglucose at 4× the desired final concentration. Aliquots of 0.2 ml were removed at 3, 6, and 9 s and injected into ice-cold inhibitor-stop solution containing 4 mM phloridzin and 4 mM $HgCl_2$. The cells were immediately centrifuged through 0.4 ml bromododecane into 0.1 ml 2 N perchloric acid, as described by McCune and Harris (1979) for hepatocytes. The supernatant fluid above the organic phase was removed and the tube which had been in contact with it was repeatedly washed with 50% ethanol:H_2O to remove residual radioactivity. The perchloric acid under the organic phase was diluted with 0.4 ml ice-cold water to make it less dense than the bromododecane. Following centrifugation, 0.2 ml aliquots of the diluted extract (above the organic phase) were removed for scintillation counting and cAMP analysis.

Analyses and reagents. Radioactivity was determined using a Packard Tri-Carb model 460 liquid scintillation spectrometer with appropriate corrections for quench. Cyclic-3′,5′-AMP was determined by radioimmunoassay [Steiner et al. (1969) as modified by Harper and Brooker (1975)]. Radioisotopes were purchased from New England Nuclear, Boston, MA, USA. Collagenase was obtained from Cooper Biomedical, Freehold, NJ, USA. Individual lots of this material were tested to determine suitability for myocyte preparation. Bovine serum albumin was obtained from Miles Laboratories (Naperville, IL, USA), and dialyzed 24 h against 20 volumes of physiological salt solution containing (in mM): NaCl, 111; KCl, 5; NaH_2PO_4, 10; $MgSO_4$, 1; $CaCl_2$, 0.05; creatine, 20; taurine, 60; and HEPES, 5; pH = 7.3. Forskolin was obtained from Calbiochem-Behring (San Diego, CA, USA). Isoproterenol and epinephrine were purchased from Sigma Chemical Company (St. Louis, MO, USA) and dispensed from freshly prepared stocks just prior to use. All other reagents were of the highest quality commercially available.

Results

Insulin stimulated 3-O-methylglucose transport 2.5-fold. Uptake of 3-O-methylglucose was linear in the presence and absence of insulin up to 6 s but uptake rates calculated from 9 s values decreased 20–30%. Therefore, all subsequent rates for kinetic values were calculated from values at 0, 3 and 6 s. The cells clearly were not equilibrated with the external medium, in spite of the reduction of uptake rates at 9 s; intracellular 3-O-methylglucose concentrations were 8% (no insulin) and 21% (with insulin) of those in the external medium.

Transport of 3-O-methylglucose increased as the external concentration of the sugar was increased (Fig. 1). In the absence of insulin, saturation was achieved at 5 mM hexose,

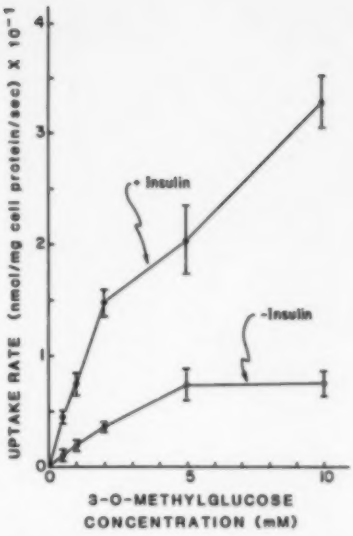

Fig. 1. Concentration dependent 3-O-methylglucose transport. Myocytes were incubated with the indicated concentrations of 3-O-methylglucose at 37°C for 3 and 6 s. Cells were incubated at least 15 min with 12.3 μM insulin (●) or an equivalent time without insulin (○) prior to estimating transport rates. Transport rates were estimated by linear regression analysis of values at 0, 3 and 6 s. Each point represents the mean ± SEM of 4 cell preparations

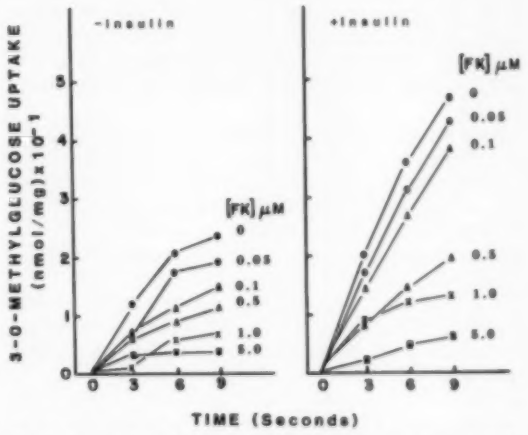

Fig. 2. Forskolin inhibition of 3-O-methylglucose transport. Transport was measured with 1 mM 3-O-methylglucose at 37°C as described in Methods. ^{3}H-3-O-methylglucose and forskolin were added simultaneously in these experiments. Each point represents the mean of 3 cell preparations

and there was no evidence for a nonspecific diffusional component. The apparent K_m for 3-O-methylglucose transport without insulin was about 2 mM (estimated from Fig. 1 at 1/2 V_{max}) or 3.5 ± 1.8 mM (estimated by nonlinear regression of data in Fig. 1). Insulin stimulated the rate of hexose transport 2- to 4-fold at each 3-O-methylucose concentration used.

Hexose transport after 9 s was inhibited 94% by 5 μM (Fig. 2) and 50 μM (data not shown) forskolin. (Forskolin

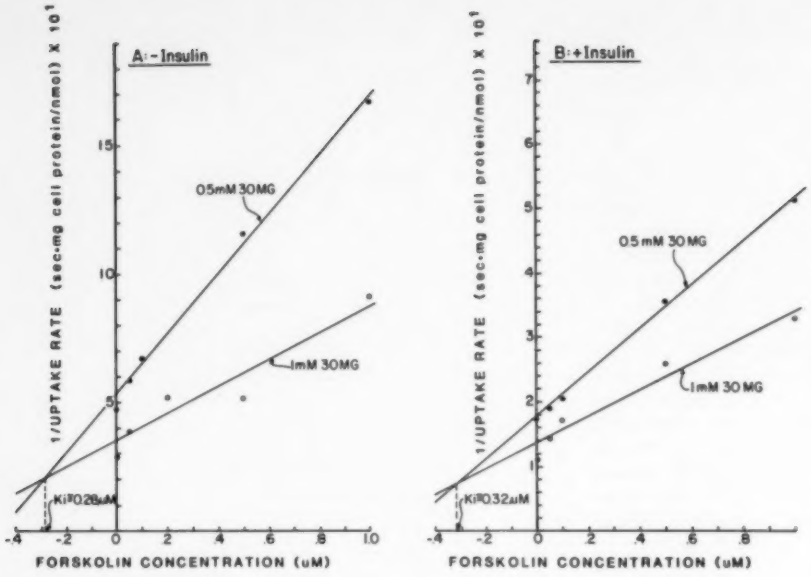

Fig. 3A, B
Dixon plot of forskolin inhibition of 3-O-methylglucose transport. Transport was measured with either 0.5 mM (●) or 1.0 mM (○) 3-O-methylglucose (3 OMG) at 37° C as described in Methods, in the absence **A** or presence **B** of 12.3 μM insulin. Transport rates were estimated as in Fig. 2. The linear regression equations for the data are: − insulin, 1/rate = 11.67 μM + 5.25 (r = 0.997) and 5.21 μM + 3.52 (r = 0.937), for 0.5 and 1 mM 3 OMG, respectively; + Insulin, 1/rate = 3.47 μM + 1.75 (r = 0.999) and 2.02 μM + 1.37 (r = 0.975) for 0.5 and 1 mM 3 OMG, respectively. Each point represents the mean of 3 cell preparations

and isotope for transport were added to the cells simultaneously.) Inhibition occurred within 3 s, and insulin did not prevent it. Progressively less inhibition was obtained at lower forskolin concentrations (Fig. 2). In the absence of insulin, uptake at 3 s was not different from controls at forskolin concentrations less than 0.5 μM. In the presence of insulin, 0.1 μM forskolin or less did not significantly inhibit transport at 3 s.

Transport of 3-O-methylglucose was examined at 0.5 and 1 mM hexose in the presence of up to 1 μM forskolin. Data from these experiments are presented as Dixon plots in Fig. 3A and B. The results indicate that forskolin is either a competitive or linear-mixed-type inhibitor of 3-O-methylglucose transport (K_i = 0.3 μM forskolin). Insulin did not significantly alter the apparent K_i (Fig. 3B).

Cell cAMP concentrations were determined in the same cells used to study effects of forskolin on hexose transport. Isoproterenol and epinephrine, which elevate cAMP through different mechanisms than forskolin, also were examined by the same protocol. No direct relationship between cell cAMP levels and short-term hexose transport could be established (Fig. 4). At a forskolin concentration which inhibited hexose transport greater than 60%, there was no detectable increase in cAMP concentrations above control levels. Isoproterenol, on the other hand, produced a 5-fold increase in cAMP by 3 s, but did not significantly affect hexose transport at any time studied.

To establish that forskolin could increase cAMP in myocytes, an experiment was conducted in which both hexose transport and cAMP levels were measured with exposure of the cells to forskolin or catecholamines for up to 99 s. After 15, 30, 60, and 90 s exposure, cells were removed from the incubation vessel and allowed to transport hexose for 9 s (forskolin or catecholamines remained in the cell suspension during this latter 9 s). The results of these experiments are shown in Fig. 5A and B. All three agents caused major changes in cyclic AMP over the time of this exper-

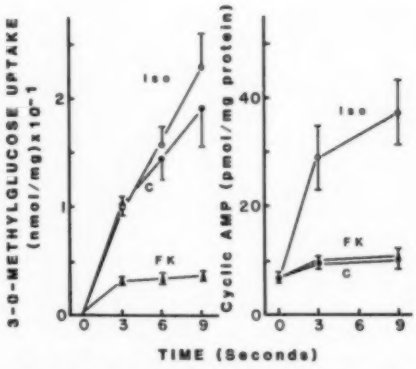

Fig. 4. Effect of forskolin and isoproterenol on hexose transport and cell cyclic amp. Transport of 1 mM 3-O-methylglucose at 37° C was estimated as described in Methods. 5 μM forskolin (*FK*, ▲) or 50 μM isoproterenol (*Iso*, ○) were added at 0 s with the isotope. Each point represents the mean ± SEM of 6 control (*C*, ●) or 3 each drug-treated cell preparations

iment (Fig. 5B). Isoproterenol and epinephrine, however, produced more rapid elevations in cyclic AMP than those observed with forskolin. In spite of the similar increases in final cyclic AMP concentrations caused by the drugs, their effects on hexose transport were strikingly different. Forskolin inhibited hexose transport 95% within 15 s of exposure to the drug (Fig. 5A, panel I), but did not significantly elevate cell cyclic AMP during this period (Fig. 5B, panel I). Isoproterenol and epinephrine inhibited transport only slightly (panels II and III), and in a manner apparently unrelated to the effects of these drugs on cell cyclic AMP (Fig. 5B, panels II and III). Insulin had no effect on cell cAMP concentrations, or on forskolin inhibition of hexose transport.

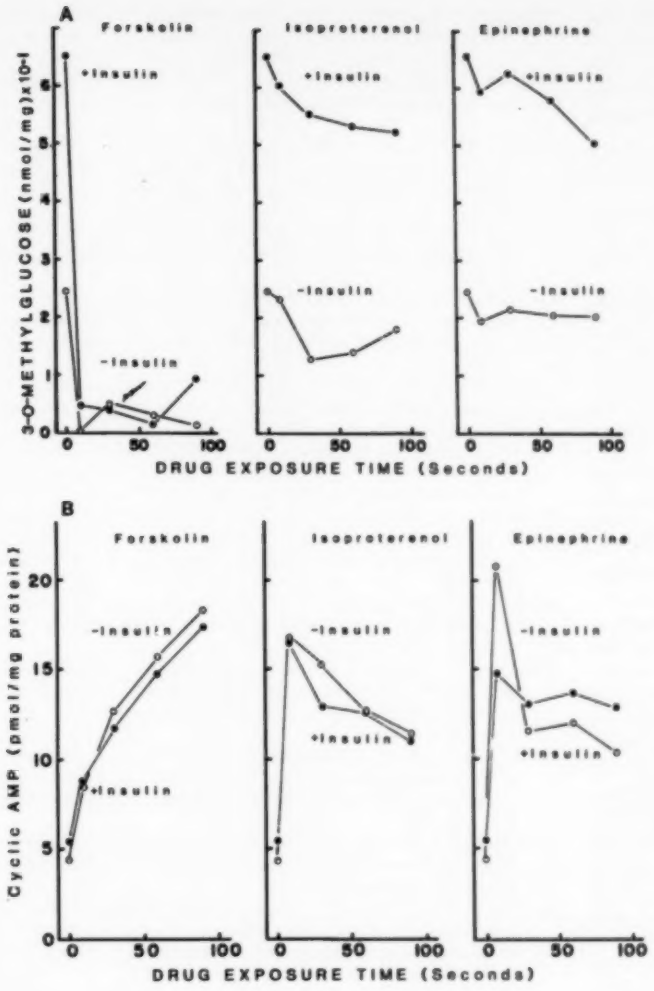

Fig. 5A, B
Effects of forskolin, isoproterenol, and epinephrine on cell cyclic amp and hexose transport. Cells were incubated at 37° C with 5 μM forskolin, 50 μM isoproterenol, or 50 μM epinephrine, removed from the incubation chamber at the indicated intervals, and allowed to transport hexose for 9 s. The indicated times refer to the time cells were incubated with drug before addition of 3-O-methylglucose for estimating uptake. The total time exposure to the drugs was an additional 9 s before transport was stopped and cells extracted for cAMP analysis **B**. Each point represents the average of duplicate samples, (○), without insulin; (●), with insulin

Because of a reported dose-dependent biphasic effect of isoproterenol on glucose transport in adipocytes (Kashiwagi et al. 1983), we also measured 3-O-methylglucose transport rates at several isoproterenol concentrations. There were no significant effects of isoproterenol on transport at 0.01, 0.05, 0.1, 1.0, 5, 10 and 50 μM (data not shown).

Discussion

Hexose uptake into cardiomyocytes has been studied by several groups, using a wide variety of approaches (Eckel et al. 1983; Gerards et al. 1982; Haworth et al. 1984; Lindgren et al. 1982). We report here a contribution to this literature, using both short time periods and rapid quenching with centrifugation to obtain initial unidirectional ("zero-trans") uptake rates for 3-O-methylglucose. Using this approach, we obtained an initial uptake velocity at 1 mM sugar of 37.5 pmol/mg cell protein. This transport was stimulated to 82.5 pmol/mg/s by incubation of myocytes with 12.3 μM insulin. These rates are in general agreement with those found by Eckel et al. (1983; 46.3 pmol/mg protein/s) and Lindgren et al. (1982; 20.4 pmol/mg/s), and very much higher than those found by Gerards et al. (1982). Obviously, these comparisons are based on recalculated values obtained from the cited studies, and therefore should be viewed with some caution. Where observed rates from the present study differ by over 100-fold, as was the case when our data are compared to those of Gerards et al. (1982), we believe that methodology (equilibrium exchange) and the method of correction for extracellular contamination (average value vs. every sample in our case) is the cause of the discrepancy. It is unlikely that the difference is due to choice of extracellular markers, as we detect no differences between 3-O-methylglucose transport rates when ^{14}C-sucrose (^{3}H-3-O-methylglucose transported), or ^{3}H-sorbitol (^{14}C-3-O-methylglucose transported), is used as the extracellular marker.

Myocytes and perfused hearts differ from each other in the estimated K_m for 3-O-methylglucose transport between 2 and 4 fold [2 mM (present study), 3.8 mM (Gerards et al. 1982), and 6.8 mM (Eckel et al. 1983) versus 7–10 mM in perfused hearts (Cheung et al. 1978)]. This difference in

apparent K_m's between myocytes and intact heart can account for the differences in transport rates at non-saturating hexose concentrations. The higher K_m for intact heart may be due to the presence of non-myocyte cells and/or diffusion resistances in extracellular and vascular spaces in the intact heart.

Insulin stimulates 3-O-methylglucose uptake in myocytes 2.5-fold. The relative stimulation of glucose uptake by insulin should be method-independent. Indeed, our average stimulation of 2.5-fold compares well with the 2.5- to 5-fold stimulation found in other myocyte systems (Eckel et al. 1983; Gerards et al. 1982; Lindgren et al. 1982).

Forskolin (5 μM) inhibits 3-O-methylglucose transport greater than 90%, apparently by a competitive or linear-mixed-type mechanism. The inhibition is almost instantaneous, as its magnitude is not different after 3 and 6 s exposure to forskolin. Inhibition also is not associated with detectable increases in cAMP, as these values do not increase above control values during 9 s exposure. This result is consistent with the findings of Mills et al. (1984) and Kashiwagi et al. (1983), who studied hexose transport in adipocytes, with those of Sergeant and Kim (1985) using erythrocytes, and with Kim et al. (1986) using platelets.

The adrenergic antagonists isoproterenol and epinephrine failed to alter hexose transport rates at any concentration level or at any exposure time studied. This result is consistent with that of Challoner (1970) who reported that norepinephrine did not stimulate glucose utilization in K^+-arrested perfused hearts. This result, taken together with the fact that these drugs produce rapid and large increases in isolated myocyte cAMP, further argues against the involvement of cAMP in hexose transport. Moreover, we do not observe in myocytes the biphasic response in hexose transport to isoproterenol found by Kashiwagi et al. (1983) in adipocytes. Stimulation of hexose transport in adipocytes by either epinephrine or isoproterenol reportedly can be suppressed by the use of phosphate-containing buffers, which may chelate calcium (Ludvigsen et al. 1980). The free calcium in the buffer we use is about 0.80 mM, and is sufficient for insulin stimulation of transport. The effects of different buffers on cardiomyocytes was not systematically examined. Therefore, the possibility exists that lower, non-physiologic phosphate concentrations allow catecholamine stimulation of hexose transport. Regardless, the data reported herein demonstrate the independence of cardiac myocyte hexose transport and cell cAMP.

Acknowledgements. This work was supported in part by grants NIH-AM 33456, NIH-HL 27336 and the Edward Mallinckrodt Foundation. The authors thank A. Francis for careful, rapid preparation of drafts and final copies of the manuscript, and Dr. R. Altschuld for an estimate of free calcium in the medium.

References

Challoner DR (1970) Glucose transport in perfused rat hearts: lack of epinephrine stimulation during arrest. Life Sci 9:477–480

Cheung JY, Conover C, Regen DM, Whitfield CF, Morgan HE (1978) Effect of insulin on kinetics of sugar transport in heart muscle. Am J Physiol 234:E70–E78

Eckel J, Pandalis G, Reinauer H (1983) Insulin action on the glucose transport system in isolated cardiocytes from adult rat. Biochem J 212:385–395

Farmer BB, Mancina M, Williams ES, Watanabe AM (1983) Isolation of calcium tolerant myocytes from adult rat hearts: review of the literature and description of a method. Life Sci 33:1–18

Gerards P, Graf W, Kammermeier H (1982) Glucose transfer studies in isolated cardiocytes of adult rats. J Mol Cell Cardiol 14:141–149

Harper JF, Brooker G (1975) Femtomole sensitive radioimmunoassay for cyclic AMP and cyclic GMP after 2-O-acetylation by acetic anhydride in aqueous solution. J Cyclic Nucleotide Res 1:207–218

Haworth RA, Hunter DR, Berkoff HA (1984) Heterogeneous response of isolated adult rat heart cells to insulin. Arch Biochem Biophys 233:106–114

Hohl CM, Altschuld RA, Brierley GP (1983) Effects of calcium on the permeability of isolated adult rat hearts cells to sodium. Arch Biochem Biophys 221:197–205

Kashiwagi A, Huecksteadt TP, Foley JE (1983) The regulation of glucose transport by cAMP stimulators via three different mechanisms in rat and human adipocytes. J Biol Chem 258:13685–13692

Kim HD, Sergeant S, Shukla SD (1986) Glucose transport in human platelets and its inhibition by forskolin. J Pharmacol Exp Ther 236:585–589

Lindgren CA, Paulson DJ, Shanahan MF (1982) Isolated cardiac myocytes. A new cellular model for studying insulin modulation of monosaccharide transport. Biochim Biophys Acta 721:385–393

Ludvigsen C, Jarett L, McDonald JM (1980) The characterization of catecholamine stimulation of glucose transport by rat adipocytes and isolated plasma membranes. Endocrinology 106:786–790

McCune SA, Harris RA (1979) Mechanism responsible for 5-(tetradecyloxy)-2-furoic acid inhibition of hepatic lipogenesis. J Biol Chem 254:10095–10101

Mills I, Moreno FJ, Fain JN (1984) Forskolin inhibition of glucose metabolism in rat adipocytes independent of adenosine 3′:5′-monophosphate accumulation and lipolysis. Endocrinology 115:1066–1069

Morgan HE, Neely JR (1972) Insulin and membrane transport. In: Steiner DF, Frienkel (eds) Handbook of physiology: Endocrinology, vol 1, chapter 20. American Physiological Society Bethesda, Maryland, pp 323–331

Morgan HE, Henderson MJ, Regen DM, park CR (1961) Regulation of glucose uptake in heart. I. The effects of insulin and anoxia on glucose transport and phosphorylation in the isolated, perfused heart of normal rats. J Biol Chem 236:253–261

Sergeant S, Kim HD (1985) Inhibition of 3-O-methylglucose transport in human erythrocytes by forskolin. J Biol Chem 260:14677–14682

Steiner AL, Kipnis DM, Utiger R, Parker C (1969) Radioimmunoassay for the measurement of adenosine 3′,5′-cyclic phosphate. Proc Natl Acad Sci USA 64:367–373

Taylor WM, Mak ML, Halperin ML (1976) Effect of 3′:5′-cyclic AMP on glucose transport in rat adipocytes. Proc Natl Acad Sci USA 73:4359–4363

Received September 1, 1986/Accepted January 22, 1987

Pflügers Arch (1987) 409:163–168

Pflügers Archiv
European Journal of Physiology
© Springer-Verlag 1987

The role of extracellular sodium on heart muscle energetics*

Jorge E. Ponce-Hornos, Patricia Bonazzola, and Alberto C. Taquini

Instituto de Investigaciones Cardiológicas, Universidad de Buenos Aires, Facultad de Medicinia, Marcelo T. de Alvear 2270, RA-1122 Buenos Aires, Argentina

Abstract. A study has been made of changing external sodium concentration $[Na]_e$, over the range 75 to 200 mmol · l^{-1}, on contractile parameters and heat production in isolated, arterially perfused, interventricular rabbit septa.- The observed changes in maximum rate of contraction with $[Na]_e$, either in the presence of a constant external Ca concentration $[Ca]_e$ or in the presence of a constant $[Na]_e^2/[Ca]_e$ ratio, paralleled those observed for tension development (T). On the other hand the maximal rate of relaxation ($-\dot{T}_{max}$) and the ratio $-\dot{T}_{max}/T$ increased. While the ratio between active heat production and developed tension remained unaltered (0.111 ± 0.003 mJ · mN^{-1} · g^{-1} dry weight), resting heat production increased with $[Na]_e^2$ with a slope of 95 ± 18 mW · g^{-1} · mol^{-2} · l^2. Under resting conditions, a decrease in $[Na]_e$ of 50 mmol · l^{-1} induced a fall in ^{42}K uptake of about 16 nmol · s^{-1} · g^{-1} without changes in ^{42}K efflux, suggesting that such an intervention depresses K influx. If the depressed K influx, induced by a decrease in $[Na]_e$ of 50 mmol · l^{-1}, is associated with a decrease in Na-K pump activity, a fall in resting heat production of about 0.64 mW · g^{-1} would be expected. This represent 56% of the calculated change in the resting heat production, 1.14 ± 0.22 mW · g^{-1} (mean ± one confidence interval), suggesting that some process in addition to a depressed Na-K pump activity may be altered by changes in $[Na]_e$.

Key words: Sodium – Potassium fluxes – Contractility – Na-K pump – Heat production – Calorimetry – Heart – Na-Ca exchange

Introduction

It is well established that the calcium responsible for heart muscle contraction is in rapid equilibrium with the calcium in the extracellular media (Philipson and Langer 1979; Philipson et al. 1980; Langer 1982). In addition it has been shown that alterations in extracellular sodium concentration $[Na]_e$, affect force development by affecting Ca movements (Niedergerke 1957; Wendt and Langer 1977a; Ponce-Hornos and Langer 1980). While the physiological basis for cardiac resting heat production have not been established, it is known that the major energy processes associated with a cardiac contraction are: the actin-activated myosin ATPase of the contractile mechanism, that transforms chemical energy into mechanical work, and the active transport of sodium (Na), potassium (K) and calcium (Ca) ions (Gibbs and Chapman 1979). Therefore, alteration in these mechanisms would be directly linked to the energy cost of excitation and contraction. In 1970, Chapman et al. found that the inotropic effects of altering the ratio $[Na]_e^2/[Ca]_e$ in the bathing medium were not correlated with the observed changes in tension-independent heat, and they suggested that de major determinants of tension-independent heat are active transport of Na and Ca ions (Chapman et al. 1970). The purpose of the present study was to define further the role of the $[Na]_e$ in myocardial energy consumption and to elucidate its relationships with mechanical function and ionic transport in mammalian myocardium.

* Supported by the Consejo Nacional de Investigaciones Cientificas y Técnicas (CONICET), Argentina

Offprint requests to: J. E. Ponce-Hornos

Methods

Biological preparation. Experiments were performed on the isolated arterially perfused rabbit heart interventricular septum at 24° C. Male rabbits (2–3 kg) were heparinized and then killed with a pentobarbital overdose. The beating heart was removed, its septal artery cannulated with PE-50 polyethylene tubing and then the septum was carefully dissected from the heart. The muscle was mounted in a Kel-F frame between two stainless steel hooks attached to an isometric tension transducer. After cannulation and mounting, the preparation was placed in the inner chamber of a calorimetric system. At the end of each experiment the tissue was removed from the calorimeter, weighed in a preweighed vial and dried at 110° C to constant weight so that the water content could be calculated. The average water content obtained in the present experiments ($82.8 \pm 0.8\%$, $n = 13$) compares well with that reported by Tillisch and Langer under 200 mM Na (Tillisch and Langer 1974).

Solutions. The muscle was perfused at a constant rate (2.5 ml · min^{-1}) with a solution containing (in mmol · l^{-1}): $CaCl_2$ 1.2; $MgCl_2$ 1.0; NaH_2PO_4 0.5; $NaHCO_3$ 24.0; KCl 6.5; dextrose 6.0 and NaCl 50, 65, 85, 120, 150 or 175 mmol · l^{-1} and made isoosmotic to 200 mM Na by adding 250, 220, 180, 110, 50 or 0 mmol · l^{-1} sucrose, respectively. A series of experiments was performed with various external Na and calcium concentrations ($[Ca]_e$) while maintaining the ratio of $[Na]_e^2/[Ca]_e$ constant at 17.5 (i.e. the ratio in control perfusate with 0.0012 mol · l^{-1} Ca and 0.145 mol · l^{-1} Na) and made isoosmotic to 200 mmol · l^{-1} Na

with sucrose. The solutions were bubbled with 95% O_2 – 5% CO_2 to achieve a pH of 7.3 – 7.4.

Mechanical and heat measurements. Complete details of the calorimetric system, calibration and stimulating procedure, together with the methods for recording both mechanical and heat outputs have been set out elsewhere (Ponce-Hornos et al. 1982; Dominguez-Mon et al. 1984). Briefly, these procedures allow a number of parameters to be recorded continuously and simultaneously: 1) resting tension (*RT*), 2) developed tension (*T*), 3) maximal rate of tension development ($+\dot{T}_{max}$), 4) maximal rate of relaxation ($-\dot{T}_{max}$), 5) perfusion pressure, 6) total heat production (H_t), 7) resting heat production (H_r) and 8) active heat production (H_a) calculated as the difference ($H_t - H_r$). In addition, contraction frequency, temperature, resting tension and composition of the perfusate, can be fully controlled throughout. Contraction frequency was controlled by external stimulation (Grass SD9 stimulator) with 2.0 V, 3.0 ms duration, square wave pulses at 0.5 Hz. Resting tension was maintained constant in each experiment and ranged between 30 and 50 mN. A 60 min equilibration period with a solution containing 145 mmol · l^{-1} Na and 110 mmol · l^{-1} sucrose, was allowed to elapsed before any experimental intervention. In all experimental conditions a period of at least 15 min was allowed so as to achieve a steady state before any heat or mechanical measurements were made. Only those heat or mechanical measurements that remained stable for at least 20 min after the 15 min equilibration period were accepted for analysis. A septum was accepted for study only if during the 60 min equilibration period a minimum and stable 100 mN tension could be developed from a resting tension of 50 mN. On this basis three septal preparations were rejected. Only those conditions of $[Na]_e$ in which the muscle remained "quiescent" in the absence of stimulation, and therefore the contractile parameters (*RT*, *T*, $+\dot{T}_{max}$ and $-\dot{T}_{max}$) and heat production (H_t and H_r) could be recorded under the same conditions of extracellular sodium, were accepted for analysis.

Calorimeter calibration was accomplished by passing a 2.1 kHz sine wave through the muscle by means of the stimulating electrodes as described elsewhere (Ponce-Hornos et al. 1982). In the present experiments the average output of the thermosensitive units recorded for the heat production under "quiescent" conditions was about 130 μV while the bandwidth noise was 1.0 μV at maximum gain (1.0 μV/div). All heat production values were expressed per gram of dry tissue.

Isotopic experiments. The isotopic activity of the whole tissue was monitored by a 5 × 3.75 cm Na-iodide crystal placed 2 – 3 cm in front of the septum. To avoid any variation in background activity during the experiment the effluent of the septum when not collected was returned by suction to a lead shielded area. For the ^{42}K (kindly supplied by Medicina Nuclear, Comisión Nacional de Energía Atómica/Buenos Aires, Argentina) uptake experiments, the muscles were perfused with solutions prepared by adding isotope (1 μCi · ml^{-1}) to a stock solution (10% concentrated), containing low Na concentration (95 mmol · l^{-1}). This solution was then divided and the appropiate amounts of NaCl, sucrose and H_2O were added to obtained the final 145 Na-sucrose solution. Thus, identical specific activities of the solutions was assured. The ^{42}K washout experiments (145 Na-sucrose) were followed for 30 min in order to achieve the monoexponential phase of intracellular ^{42}K, before switching to low Na perfusate (95 Na-sucrose) (Ponce-Hornos and Fernandez Villamil 1979). During the washout the isotopic activity of the muscle was followed continuously and the effluent collected over 1 min periods in individual vials; ^{42}K activity was later counted with a liquid scintillation system using Cerenkov counting (Ponce-Hornos and Langer 1982). Both tissue probe and effluent counts were corrected for isotopic decay and background activity and plotted semilogarithmically. The uptake curves were fitted to an equation of the form

$$y = y_\infty - \sum_{i=1}^{n} A_i \cdot e^{-m_i \cdot t} \quad (1)$$

where the sum of A_i is the asymptotic value y_∞, m_i = the rate constant of the *i*th component and t = time. To facilitate analysis the uptake data were plotted as $\log(1 - y/y_\infty)$ versus time. Similarly the efflux curves were treated with the following relation

$$y = \sum_{i=1}^{n} A_i \cdot e^{-m_i \cdot t} \quad (2)$$

where the sum of the A_i is the ^{42}K tissue content at the start of the washout and m_i as in Eq. (1). Both A_1 and m_i values were derived by a log-linear regression analysis (Ponce-Hornos and Fernandez Villamil 1980) and the y_∞ value was estimated from the specific activity of the perfusate and the total K content in the tissue. For the determination of K content the dried tissue was stored for 1 week and then it was soaked for 2 – 3 days in approximately 2 ml/g wet muscle of a 0.015 M LiOH solution, K was determined in the supernatant by internal standard flame photometry. Cellular K flux was calculated from the regression parameters of the slow exponential term assuming a parallel system (Langer and Brady 1966).

Statistics. The curves were fitted using the criterion of least squares, the correlation coefficients for both pooled data and individual experiments were considered significant if the *p* value was less than 0.05. One way analysis of variance was used for those parameters that, plotted against extracellular Na, showed a correlation coefficient which was not different from zero and did not show any systematic trend (Documenta Geigy 1962). Unless otherwise indicated, values stated in this paper represent the mean ± standard error of the mean.

Results

Energetic and mechanical effect of varying $[Na]_e$

After an equilibration period at 145 mmol · l^{-1} Na and 110 mmol · l^{-1} sucrose, two experimental sequences of altered $[Na]_e$ were used. In 5 experiments the different Na levels were changed as follows 75, 90, 110, 145, 175 and 200 mmol · l^{-1} Na while, in 5 experiments a randomized mode of the different Na levels was employed. No significant differences were found between these designs in the effects of $[Na]_e$ on either the mechanical or the energetic parameters. Therefore, analysis of both mechanical and energetic parameters were performed using the pooled data. As previously noted for amphibian and mammalian cardiac tissues, tension development was indirectly related to $[Na]_e^2$ (Tillisch

et al. 1979; Chapman 1983). As shown in Fig. 1, steady developed tension plotted as a function of $[Na]_e^2$ showed a correlation coefficient $r = -0.57$ for 43 data points with a slope $k = -0.0012 \pm 0.00027$ mN · mmol^{-2} · l^2 and intercept K = 179 ± 5 mN (slope and intercept ± one confidence interval; $t_{0.5}\ \alpha = 0.05$). Similar results were obtained when, instead of using the pooled data, the regression lines of developed tension versus $[Na]_e^2$ were calculated for each experiment.

The decrease in maximal rate of contraction with $[Na]_e$ (data not shown) was similar to that observed for developed tension so that, the ratio $+\dot{T}_{max}/T$ was constant ($F = 2.3$; $n_1 = 5$; $n_2 = 37$) over the range of $[Na]_e$ examined (see Fig. 2). The average ratio $+\dot{T}_{max}/T$ for 43 data points was 4.2 ± 0.05 s^{-1}. On the other hand the maximal rate of relaxation increased with increasing $[Na]_e$, varying from 250 ± 8 mN · s^{-1} for 75-Na perfusion to 272 ± 5 mN · s^{-1} for 200-Na perfusion ($p < 0.025$), and the ratio $-\dot{T}_{max}/T$ increased with $[Na]_e$ with a correlation coefficient $r = 0.76$ (see Fig. 2). The values of the slope and intercept calculated for 43 data points were 0.0040 ± 0.00053 s^{-1} · mmol^{-1} · l and 1.13 ± 0.02 s^{-1}, respectively. Similar results were obtained when, instead of using the pooled data the regression lines of the ratio $-\dot{T}_{max}/T$ versus $[Na]_e$ were calculated for each experiment ($r \geq 0.965$ for $n \geq 4$ data points).

As shown in Fig. 3 changing the $[Na]_e$ from 75 to 200 mmol · l^{-1} did not alter total heat production ($F < 1.0$; $n_1 = 5$; $n_2 = 37$); the average total heat production (H_t) per beat for all 43 data points was 38.9 ± 0.5 mJ · g^{-1}. Although active heat production per beat (H_a), i.e. the difference between H_t and H_r, decreased with extracellular sodium concentration, it can be seen from Fig. 3, that the ratio between active heat production per beat and developed tension (H_a/T) remained unaltered over the range of $[Na]_e$ analyzed ($F = 2.10$; $n_1 = 5$; $n_2 = 37$) suggesting that the fall of H_a associated with the increase in extracellular sodium was related to the simultaneous decrease in tension development. The average H_a/T ratio for all 43 data points was 0.111 ± 0.003 mJ · g^{-1} · mN^{-1}.

On the other hand, resting heat production increased with increasing $[Na]_e$, from 9.7 ± 0.47 mW · g^{-1} for 75-Na perfusion to 13.4 ± 0.41 mW · g^{-1} for 200-Na perfusion ($p < 0.001$) suggesting a close relationship between the electrochemical gradient for Na and the energy requirement for the maintainance of resting conditions. Since,

$$T = k \cdot [Na]_e^2 + K \tag{3}$$

and

$$H_r/T = H_t/T - H_a/T \tag{4}$$

on substituting for T from Eq. (3) in the H_r/T term of Eq. (4) we obtain

$$\frac{H_r}{k \cdot [Na]_e^2 + K} = \frac{H_t}{k \cdot [Na]_e^2 + K} - \frac{H_a}{T}$$

which can be rearranged to

$$H_r = H_t - \frac{H_a}{T} \cdot K - \frac{H_a}{T} \cdot k \cdot [Na]_e^2. \tag{5}$$

Since H_a/T, K, k and H_t are constants in the range of $[Na]_e$ analyzed, H_r versus $[Na]_e$ should be adjusted to a parabolic function. In fact, as shown in Fig. 4, resting heat production and $[Na]_e^2$ did correlate, with a $r = 0.789$ (for 43 data points). The values for the calculated slope and intercept were 95 ± 18 mW · g^{-1} · mol^{-2} · l^2 and 9.37 ± 0.20 mW · g^{-1} respectively (slope and intercept ± one confidence interval). Similar results were obtained when the regression

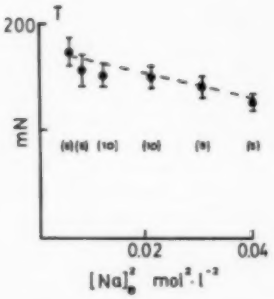

Fig. 1. Steady tension development (T) plotted against $[Na]_e^2$. *Bars* represent ± one standard error of the mean. Figures in parenthesis indicated number of experiments for each mean value. The *dashed line* was obtained by a least-squares regression analysis ($n = 43$ data points)

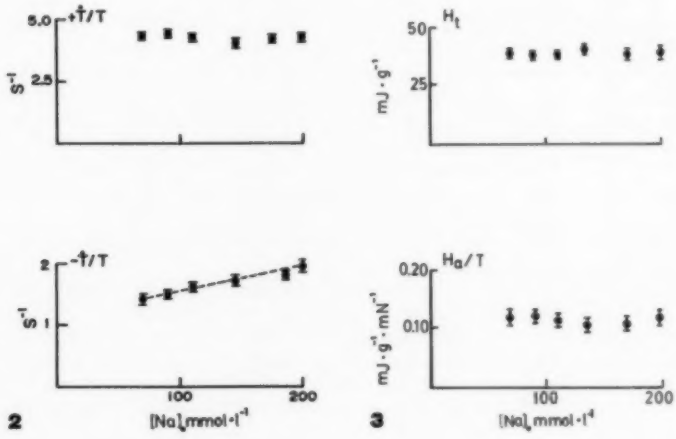

Fig. 2
Upper panel ratio between maximal rate of tension development and developed tension $+\dot{T}_{max}/T$ and *lower panel* ratio between maximal rate of relaxation and tension development, $-\dot{T}_{max}/T$, plotted against $[Na]_e$. *Dots* are means, *vertical bars* represent ± one standard error of the mean. All three contractile parameters (i.e. T, $+\dot{T}_{max}$ and $-\dot{T}_{max}$) were recorded at several values of $[Na]_e$ with each septum (see text). Number of experiments for each mean value as in Fig. 1

Fig. 3
Upper panel total heat production per beat (H_t) per gram dry tissue and *lower panel* ratio between active heat production per beat per gram dry tissue and tension development (H_a/T) plotted against $[Na]_e$. *Dots* are means, *vertical bars* represent ± one standard error of the mean. The number of experiments for each mean value as in Fig. 1

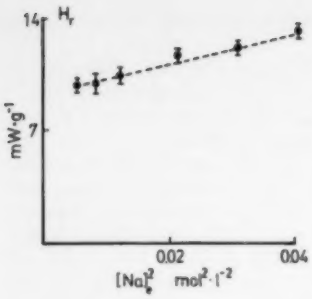

Fig. 4. Resting heat production (H_r) per gram of dry tissue plotted against $[Na]_e^2$. *Dots* are means, *vertical bars* represents ± one standard error of the mean and the number of experiments for each mean value as in Fig. 1. The *dashed line* drawn through the points was obtained by a least-squares regression analysis ($n = 43$ data points)

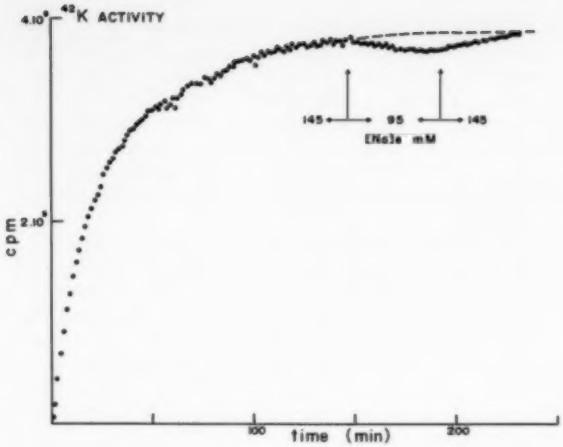

Fig. 5. Effect of changing external Na concentration on tissue ^{42}K activity. *Dashed line*, extrapolated ^{42}K uptake under various conditions. *Arrows* indicate time at which external sodium concentration was changed

parameters of resting heat production versus $[Na]_e^2$ were calculated for each experiment ($r > 0.96$ for $n = 4$ and $r > 0.90$ for $n > 4$ data points).

Energetic and mechanical effects of simultaneous alteration in $[Na]_e$ and $[Ca]_e$

In order to further clarify the apparent dependence of active heat production on tension development, $[Na]_e$ was altered simultaneously with $[Ca]_e$ while maintaining the $[Na]_e^2/[Ca]_e$ ratio constant. The experimental sequence of simultaneous alteration in $[Ca]_e$ and $[Na]_e$, after the equilibration period at 1.2 mmol · l^{-1} Ca and 145 mmol · l^{-1} Na, was as follows (in mmol · l^{-1}): 0.32/Ca−75 Na, 0.69 Ca−110 Na, 1.2 Ca−145 Na, 1.75 Ca−175 Na and 2.28 Ca−200 Na. At the end of each experiment a 1.2 Ca−145 Na perfusion period was performed. No significant differences were found between the 1.2 Ca−145 Na perfusion during the equilibration period and the 1.2 Ca−145 Na performed at the end of each experiment, neither in the mechanical nor in the energetic parameters. Under these conditions the positive inotropic effect produced by increasing $[Ca]_e$ was higher than the negative inotropic effect of increasing $[Na]_e$ so that, tension development increased in all three experiments from 112 ± 7 mN, 75 Na−0.32 Ca, to 193 ± 9 nM, at 200 Na−2.28 Ca ($p < 0.005$). The maximal rate of contraction paralleled the observed changes in tension development and the ratio $+\dot{T}_{max}/T$ remained unaltered ($F < 1.0$; $n_1 = 4$; $n_2 = 10$) over the range of simultaneous alteration of $[Na]_e$ and $[Ca]_e$ examined. The average ratio $+\dot{T}_{max}/T$ for 15 data points was 4.5 ± 0.15 s^{-1}. On the other hand, while the maximal rate of relaxation increased with the simultaneous increase in $[Na]_e$ and $[Ca]_e$, varying from 165 ± 15 mN · s^{-1} for 0.32 Ca−75 Na, to 387 ± 20 mN · s^{-1} for 2.28 Ca−200 Na ($p < 0.001$), the ratio $-\dot{T}_{max}/T$ also increased. The increase of $-\dot{T}_{max}/T$ ratio correlated with $[Na]_e$ with a correlation coefficient of $r = 0.89$. The calculated slope and intercept (± one confidence interval) for 15 data points were 0.0047 ± 0.001 s^{-1} · mmol^{-1} · l and 1.0 ± 0.06 s^{-1}, respectively. Similar results were obtained when, instead of using the pooled data, the regression lines of the ratio $-\dot{T}_{max}/T$ ratio versus $[Na]_e$ (while maintaining $[Na]_e^2/[Ca]_e$ constant) were calculated for each experiment ($r \geq 0.97$; $n = 5$).

As with alteration in $[Na]_e$ at constant $[Ca]_e$, increasing $[Na]_e$ from 75 mmol · l^{-1} to 200 mmol · l^{-1} with maintaining the ratio $[Na]_e^2/[Ca]_e$ constant, resulted in all three experiments, in a steady increase in resting heat production that correlated with $[Na]_e^2$ with $r = 0.60$ for 15 data points. The values for the calculated slope and intercept (± one confidence interval) were 70 ± 29 mW · g^{-1} · mol^{-2} · l^2 and 10.3 ± 0.46 mW · g^{-1} respectively, which are close to those obtained when $[Na]_e$ was varied and $[Ca]_e$ held constant. Similar results were obtained when the regression parameters of resting heat production versus $[Na]_e^2$ were calculated for each experiment ($r > 0.89$ for $n = 5$). On the other hand, whereas total heat production per beat increased by 10 ± 1.3 mJ · g^{-1} when $[Na]_e$ was increased from 75 Na−0.36 Ca to 200 Na−2.28 Ca ($p < 0.01$), the ratio between active heat production per beat and developed tension remained unaltered and the average ratio H_a/T for all 15 data points was 0.098 ± 0.007 mJ · g^{-1} · mN^{-1}.

Influence of $[Na]_e$ on ^{42}K exchange

The effects of changing $[Na]_e$ on the resting heat production suggested that the transport of Na through the Na-K pump in cardiac muscle could be an important determinant of resting heat production. If the increase in resting heat production, with increasing $[Na]_e$, is due to an increase in the activity of Na-K pump, one would expect an increased intracellular K content. To investigate this possibility, six ^{42}K uptake experiments were performed as follows. After a control uptake period of 150 min with a solution containing 145 Na-sucrose, the perfusate was switched to a 95 Na-sucrose perfusate. As shown in Fig. 5, under these conditions ^{42}K content fell. This effect was reversed by returning to 145 Na-sucrose perfusate.

Since a decreased content can be due to, either a decreased influx or an increased efflux, to clarify the results obtained, the following ^{42}K efflux experiments were done. The muscles were perfused with 145 Na-sucrose solution containing ^{42}K for 160 min. The washout was started by perfusion of the septum with 145 Na-sucrose free of the

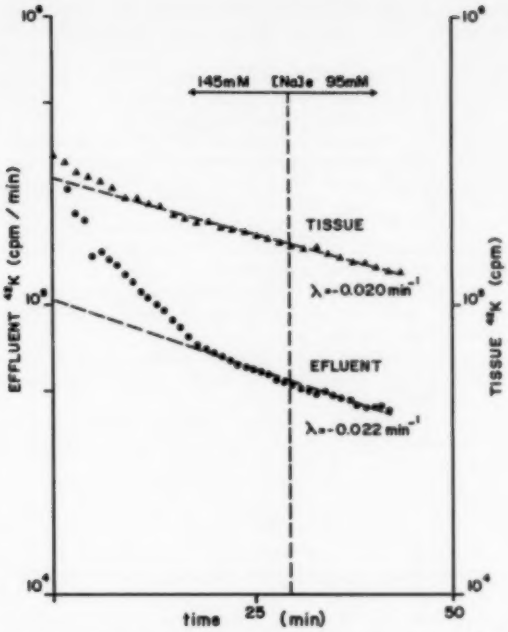

Fig. 6. Effect of changing external Na concentration on ^{42}K efflux. Simultaneous records of total tissue ^{42}K activity (▲ *right ordinate*) and effluent activity (● *left ordinate*)

isotope. After 28 min of washout with 145 Na-sucrose the solution was switched to a 95 Na-sucrose perfusate. As shown in Fig. 6, no changes in ^{42}K efflux were found, which is in agreement with the finding of Tillisch and Langer, that in a beating heart preparation no changes on ^{42}K efflux were associated to changes in $[Na]_e$ (Tillisch and Langer 1974). This clearly indicates that the depressed ^{42}K uptake during low Na perfusion is due to a depressed ^{42}K influx. The average rate constant calculated for the 6 uptake experiments under 145 Na−1.2 Ca perfusion was $0.026 \pm 0.003\ min^{-1}$ which compares well with that obtained by Wendt and Langer in the same preparation (Wendt and Langer 1977). Under these conditions calculated average K efflux was $150 \pm 23\ nmol \cdot g^{-1} \cdot s^{-1}$ which fell as $[Na]_e$ was decreased (from 145 to 95 $mmol \cdot l^{-1}$) by $16.4 \pm 2.2\ nmol \cdot g^{-1}$ ($p < 0.001$).

Discussion

The changes in parameters of mechanical performance seen in response to alterations of $[Na]_e$ in the present experiments are in agreement with those seen in previous studies (Niedergerke 1957; Wendt and Langer 1977; Tillisch et al. 1979; Chapman 1983). The observed changes in developed tension induced by increasing $[Na]_e$, either in the presence of a constant $[Ca]_e$ or with a constant $[Na]_e^2/[Ca]_e$ ratio, were proportionally the same as the changes observed in the maximal rate of tension development. This is shown by the fact that under both experimental conditions the ratio between maximal rate of tension development and developed tension $+\dot{T}_{max}/T$ remained unaltered. Conversely, the maximal rate of relaxation and the ratio $-\dot{T}_{max}/T$ significantly increased with increasing $[Na]_e$. This improvement of relaxation took place either whether $[Na]_e$ was increased in the presence of constant $[Ca]_e$ (negative inotropic effect) or in the presence of a constant $[Na]_e^2/[Ca]_e$ ratio (positive inotropic effect). This observation could be explained if an increase in $[Na]_e$ changes the driving force on the Na-Ca exchanger, improving Ca efflux and relaxation. Against this hypothesis is the fact that no effect on Ca efflux has been observed when $[Na]_e$ was reduced to as low as 36 $mmol \cdot l^{-1}$ (Wendt and Langer 1977; Ponce-Hornos and Langer 1980). On the other hand it should be noted that the sarcolemmal Ca pump seems to have lower transport rate than the Na-Ca exchange system (Caroni and Carafoli 1980). Thus, changes in the relative activity of these two other mechanisms could account for the observed changes in the rate of relaxation in the presence of a unchanged Ca efflux. Furthermore, since it has been reported that sarcolemmal Ca pump has a stoichiometry of one Ca extruded per ATP hydrolized (Caroni and Carafoli 1981) and the cell would take up three Na to remove one Ca through the Na-Ca exchanger (and the energy cost of removing Na by the Na-K pump is 1 ATP/3 Na) no changes in the energy cost of Ca extrusion would be expected. This agrees with the fact that the H_a/T ratio remained unaltered over the range of $[Na]_e$ examined.

The decrease in active heat production with the increasing in $[Na]_e$ observed in the present experiments seems then to be mainly associated to the simultaneous change in tension development. This is shown by the fact that the H_a/T ratio remained unaltered under both experimental conditions examined (i.e. changing $[Na]_e$ with or without changes in $[Ca]_e$). This agrees with findings obtained in papillary muscles, which showed that changes in extracellular Na levels do not modify the heat-tension relationship (Chapman et al. 1970). Nevertheless, since resting heat production increases with $[Na]_e$ when $[Ca]_e$ is mantained constant, total heat production per unit of tension developed increases, indicating that high Na decreases overall muscle economy. On the other hand, the decrease in total heat production per unit of tension developed observed when $[Na]_e$ was increased simultaneously with $[Ca]_e$, is in agreement with previous studies which showed that increasing $[Ca]_e$ improves overall muscle economy without altering the H_a/T ratio (Ponce-Hornos and Taquini 1986).

The fact that under "quiescent" conditions a decrease in $[Na]_e$ by 50 $mmol \cdot l^{-1}$ induces a fall in K content without altering the rate of ^{42}K efflux, leads to the conclusion that such an intervention depresses K influx. If the amount of depressed K influx, about 16 $nmol \cdot s^{-1} \cdot g^{-1}$, is associated with a decrease in the activity of the Na-K pump which has a stoichiometry of 2 K/ATP, there should be a decrease in the rate of ATP breakdown of about 8 $nmol \cdot s^{-1} \cdot g^{-1}$. In a steady-state situation, the ATP used by the pump will be resynthesized by oxidative phosphorylation, that is, 80 kJ $\cdot mol^{-1}$ of resynthesized ATP (Curtin and Woledge 1978). Therefore, a fall of 8 $nmol \cdot s^{-1} \cdot g^{-1}$ on ATP breakdown would represent a change in resting heat production of about $0.64\ mW \cdot g^{-1}$. It can be calculated from the regression parameters of the H_r versus $[Na]_e^2$ plot that, when $[Na]_e$ is reduced from 145 to 95 $mmol \cdot l^{-1}$ by sucrose substitution, a decrease in resting heat production of $1.14 \pm 0.22\ mW \cdot g^{-1}$ (mean ± one confidence interval) is induced. Furthermore, this change is similar to the $0.84 \pm 0.35\ mW \cdot g^{-1}$ calculated from the regression parameters of the H_r versus $[Na]_e^2$ plot obtained when $[Na]_e$ was altered simultaneously with $[Ca]_e$ while maintaining the $[Na]_e^2/[Ca]_e$ ratio, constant.

This indicates that the estimated change in Na-K ATPase activity would account for about 56% of the observed change in resting heat production (or 76% if calculated from the experiments in which the ratio $[Na]_e^2/[Ca]_e$ was held constant) and it appears that some additional process might be affected by alterations in $[Na]_e$.

References

Caroni P, Carafoli E (1980) An ATP-dependent Ca-pumping system in dog heart sarcolemma. Nature 283:765–767

Caroni P, Carafoli E (1981) The calcium pumping ATPase of heart sarcolema: characterization, calmodulin dependence and partial purification. J Biol Chem 256:3263–3270

Chapman RA (1983) Control of cardiac contractility at the cellular level. Am J Physiol 245:H535–H552

Chapman JB, Gibbs CL, Gibson WR (1970) Effects of calcium and sodium on caridac contractility and heat production in rabbit papillary muscle. Circ Res 27:601–610

Curtin N, Woledge R (1978) Energy changes and muscular contraction. Physiol Rev 58:690–760

Documenta Geigy (1962) Scientific Table, 6th edn, Diem K (ed), pp 175–176

Dominguez-Mon M, Ponce-Hornos JE, Gómez R, Cannata M, Taquini AC (1984) Energetic, metabolic and contractile effects of vasopressin in mammalian heart. Methods Find Exp Clin Pharmacol 6:373–378

Gibbs CL, Chapman JB (1979) Cardiac energetic. In: Berne RM, Sperelakis N, Geiger SR (eds) Handbook of physiology, sect 2, vol 1. American Physiol Society, Bethesda, Maryland, pp 775–804

Langer GA (1982) Sodium-calcium exchange in the heart. Annu Rev Physiol 44:435–449

Langer GA, Brady AJ (1966) Potassium in dog ventricular muscle: kinetic studies of distribution and effects of varying frequency of contraction and potassium concentration of perfusate. Circ Res 18:164–177

Niedergerke R (1957) The rate of action of calcium ions on the contraction of the heart. J Physiol (Lond) 138:506–515

Philipson KD, Langer GA (1979) Sarcolemmal bound calcium and contractility in the mammalian myocardium. J Mol Cell Cardiol 11:857–875

Philipson KD, Bers DM, Nishimoto AY, Langer GA (1980) Binding of CA and Na to sarcolemmal membranes: Relation to control of myocardial contractility. Am J Physiol 238:H373–H378

Ponce-Hornos JE, Fernandez Villamil M (1979) Pitfalls in kinetic studies of multiexponential decay processes with special emphasis on desaturation curves of arterial Na. Acta Physiol Latinoam 29:275–283

Ponce-Hornos JE, Fernandez Villamil M (1980) A simple method for fitting multiexponential curves of the decay type in a hand calculator. Acta Physiol Latinoam 30:141–146

Ponce-Hornos JE, Langer GA (1980) Sodium-calcium exchange in mammalian myocardium: The effects of lithium. J Mol Cell Cardiol 12:1367–1382

Ponce-Hornos JE, Langer GA (1982) Effects of inorganic phosphate on ion exchange, energy state and contraction in mammalian heart. Am J Physiol 242:H79–H88

Ponce-Hornos JE, Taquini AC (1986) Calcium effects on contractility and heat production in mammalian myocardium. Am J Physiol 251:H127–H132

Ponce-Hornos JE, Ricchiuti NV, Langer GA (1982) On line calorimetry in the arterially perfused rabbit interventricular septum. Am J Physiol 243:H289–H295

Tillisch JH, Langer GA (1974) Myocardial mechanical responses and ionic exchange in high sodium perfusate. Circ Res 34:40–50

Tillisch JH, Fung LK, Hom PM, Langer GA (1979) Transient and steady state effects of sodium and calcium on myocardial contractile response. J Mol Cell Cardiol 11:137–148

Wendt IR, Langer GA (1977a) The sodium-calcium relationship in mammalian myocardium: effect of sodium deficient perfusion on Ca fluxes. J Mol Cell Cardiol 9:551–564

Wendt IR, Langer GA (1977b) Effects of the antibiotic ionophore X537A on contractility and ionic exchange in rabbit ventricular myocardium. Circ Res 40:489–497

Received November 21, 1985/Accepted January 15, 1987

Pflügers Arch (1987) 409:169–174

Pflügers Archiv
European Journal of Physiology
© Springer-Verlag 1987

The relationship between the cardiac contractile function, adenine nucleotides and amino acids of cardiac tissue and mitochondria at acute respiratory hypoxia

O. I. Pisarenko, E. S. Solomatina, I. M. Studneva, and V. I. Kapelko

USSR Cardiology Research Center, 3rd Cherepkovskaya Street 15A, Moscow 121552, USSR

Abstract. The effect of asphyxia and subsequent resumption of respiration on the content of adenine nucleotides and some amino acids in heart tissue and mitochondria, as well as respiration of heart mitochondria was studied in rats. The depression of cardiac contractile function during asphyxia showed a better correlation with losses in mitochondrial adenine nucleotides (ATP + ADP + AMP) than those in cardiac tissue. The decrease in the heart work index was accompanied by a decrease in state 3 respiration with glutamate and malate as well as uncoupled respiration with these substrates. This did not occur with succinate. Nonphosphorylating (state 4) respiratory rates and ADP/O ratios were slightly affected by asphyxia, when respiratory substrates of both types were used. The decreased level of glutamic acid in the tissue and mitochondria of asphyxic hearts was simultaneously observed with a significant increase of alanine in cardiac tissue and of aspartic acid in the mitochondria. The losses of intramitochondrial ATP and respiratory activity with NAD-dependent substrates during asphyxia were associated with a reduction of glutamic acid level in mitochondria. The recovery of cardiac function during resumption of respiration was related to the restoration of mitochondrial respiration supported by glutamate and malate, as well as to the restoration of mitochondrial adenine nucleotides and glutamic acid. The results suggest that the depression of cardiac function caused by acute respiratory hypoxia may be attributed to impairment of electron transport, particularly in complex I of the respiratory chain and changes in metabolism of glutamic acid.

Key words: Asphyxia – Cardiac performance – Mitochondrial respiration – Adenine nucleotides – Glutamic acid

Introduction

Myocardial hypoxia is associated with a profound fall in the adenine nucleotide pool and a compensatory rise of substrate phosphorylation in mitochondria which is coupled with a loss of glutamate and aspartate and concomitant alanine formation (Freminet 1981; Taegtmeyer 1978; Sanborn et al. 1979). Exogenous L-glutamic acid and its transaminated products – α-ketoglutaric and L-aspartic acids – can retard myocardial ATP fall and hypoxic contracture (Shertzer and Cascarano 1979; Pisarenko et al. 1985). These findings stimulated our interest in the study of the relationship between the levels of adenine nucleotides in cardiac tissue and mitochondrial respiration, as well as amino acid metabolism during acute respiratory hypoxia. The experiments have been carried out on rats in which total hypoxia of various durations was developed under conditions of asphyxia (Feinstein 1962; Hendrickx et al. 1984).

Offprint requests to: O. I. Pisarenko

Methods

Acute respiratory hypoxia in rats. Male Wistar rats weighing 250–300 g were used in this study. Artificial respiration of urethane-nacrotized (1.6 g/kg, intraperitoneally) thoracotomized animals was performed at a frequency of 60 per min using a Vita-1 animal respirator. Oxygen tension in arterial blood was 90 ± 5 mm Hg, arterial-venous difference for O_2 was equal to 40 ± 4 mm Hg, and spontaneous heart rate was 315 ± 6 beats per min. To measure the intraventricular pressure, a catheter filled with a fluid and connected with a P23Gb sensor and a "Gould Brush" amplifier was inserted into the left ventricular cavity. The initial values of heart rate and the left ventricular pressure were recorded 30 min after the artificial respiration had been initiated. At the next step, acute respiratory hypoxia of 1, 3, 5 or 10 min duration was induced in different groups of rats ($n = 8–12$) by cessation of artificial respiration. Asphyxia decreased oxygen tension in arterial blood to 22.2, 4.4 and 1.1% of the initial value after 1, 3 and 5 min, respectively. Acute hypoxia was followed by a 30 min resumption of artificial respiration at a frequency of 60 per min. The functional state of the heart was expressed as the product of the left ventricular developed pressure, ($P_{syst.} - P_{diast.}$), and the heart rate (termed thereafter as the heart work index).

At the end of in vivo experiments, the hearts were quickly excised and instantaneously frozen using Wollenberger clamps precooled in liquid nitrogen. In a separate series of experiments the excised hearts were immediately used for isolation of mitochondria. Perchloric acid extraction of hearts and mitochondrial fractions was performed as described previously (Pisarenko et al. 1985; Asimakis and Conti 1984).

Isolation of mitochondria. Mitochondria were prepared according to the method of Asimakis and Conti (1984). Each heart (wet tissue weight approximately 1 g) was minced

finely in medium I containing 250 mM sucrose, 10 mM EGTA (ethyleneglycol-bis-[-aminoethyl ether] N,N′-tetra-acetic acid) and 10 mM Tris (tris [hydroxymethyl] aminomethane), pH 7.4. The tissue was rinsed twice to remove excess of blood and was homogenized in 10 ml of medium I in a Polytron PT-20 tissue processor (Brinkman Instruments, USA). Then 10 ml of medium I were added to the homogenate, which was subsequently centrifuged at 27,000 × *g* for 10 min. The supernatant was discarded, and the pellet was resuspended in 1.5 ml of medium I containing 2.5 mg of Nagarse proteolytic enzyme. The suspension was incubated for 3 min at 4 °C and mixed with 10 ml of medium II containing 180 mM potassium chloride, 1 mM EGTA, 0.5% bovine serum albumin and 5 mM Tris, pH 7.4. This suspension was homogenized with 4 passes in a size C Potter-Elvehjem homogenizer, diluted two-fold with medium II and centrifuged at 500 × *g* for 5 min. The supernatant was centrifuged at 10,000 × *g* for 10 min. The resulting mitochondrial pellet was resuspended in 10 ml of medium III containing 180 mM potassium chloride, 0.5% bovine serum albumin and 5 mM Tris, pH 7.4. The suspension was centrifuged at 10,000 × *g* for 10 min. The mitochondrial pellet was suspended in medium III to a concentration of 12–15 mg mitochondrial protein/ml. All isolation procedures were performed at 0 to 4 °C.

Assays. The content of ATP, ADP and AMP in protein-free tissue and mitochondrial extracts were determined enzymatically, using an Aminco SPF-500 spectrofluorometer (Williamson and Corkey 1969). Tissue and mitochondrial concentrations of glutamate, aspartate and alanine were measured using a Liquimat-III amino acid analyzer with a FFM-31 fluorometric cell as described in Pisarenko et al. (1985). Protein concentrations were assayed by the method of Lowry (Lowry et al. 1951). Tissue dry weights were determined by weighing a portion of washed pellets after extraction with perchloric acid and dried at 100 °C for 12 h. The mean wet/dry weight ratio was equal to 4.5.

Mitochondrial oxygen consumption was measured in a 1.5 ml chamber of a Gilson 6/5 M oxygraph, using a Clark O_2-electrode. The assay medium contained 250 mM sucrose, 10 mM potassium chloride, 10 mM monopotassium phosphate, 1 mM EDTA (ethylenediamine tetraacetic acid) and 10 mM Tris, pH 7.4. Mitochondrial protein (approx. 1 mg) was added to the assay medium followed 1 min later by the addition of either 5 mM glutamate and 5 mM malate or 10 mM succinate plus 1.3 μM rotenone. The amount of ADP (adenosine 5′-diphosphate) added to the assay medium to stimulate state 3 respiration was equal to 200 nmol. The uncoupled respiration was initiated by the addition of 2,4-dinitrophenol (f.c. 30 μM).

Reagents. All enzymes and chemicals for assays were purchased from Sigma Chemical Company, St. Louis, MO, USA. Ion-exchange resin, lithium citrate buffers and reagents for amino acid analysis were obtained from Pierce Chemical Company, Rockford, IL, USA. The solutions were prepared using deionized water (demineralit Zerolit).

Calculations and statistics. Values are expressed as mean ± SEM. Statistical analysis was performed using the two-way analysis of variance and significance evaluated by Scheffé multiple comparison method. A P value of < 0.05 was considered significant.

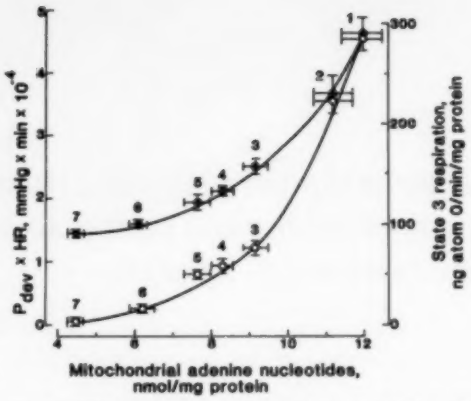

Fig. 1. Relationship between adenine nucleotides of rat heart mitochondria, cardiac function and respiratory activity of heart mitochondria. (○) Correspond to the heart work index, (●) indicate state 3 respiration, with glutamate and malate. (*1*) artificial respiration, (*2*) resumption of respiration after 5 min asphyxia (group 1), (*3*) 1 min asphyxia, (*4*) 3 min asphyxia, (*5*) 5 min asphyxia (group 1), (*6*) 5 min asphyxia (group 2), (*7*) 10 min asphyxia. Group 1: Animals, subjected to 5 min asphyxia, with a recovery of the cardiac function after resumption of respiration. Group 2: Animals with no recovery of the cardiac function under these conditions. Adenine nucleotides = ATP + ADP + AMP. $P_{dev.}$ left ventricular developed pressure, $P_{syst.} - P_{diast.}$. *HR* heart rate. Values are the mean ± SEM

Results

Cardiac function and adenine nucleotides

The cardiac function of nacrotized, thoracotomized rats during artificial respiration was characterized by the following parameters: the left ventricular systolic pressure – 139 ± 4 mm Hg, the diastolic pressure – 0 mm Hg, the heart rate – 344 ± 11 per min, the heart work index – 43055 ± 1344 mm Hg/min. Acute respiratory hypoxia caused a depression of cardiac function as well as a decrease in adenine nucleotides (ATP + ADP + AMP) in cardiac tissue and mitochondria. During the first minute of asphyxia, the 70% fall in the heart work index (Fig. 1) was associated with a 25% reduction of tissue and mitochondrial adenine nucleotides (Table 1). Later on, the decrease in the heart work index and adenine nucleotides of cardiac tissue and mitochondria slowed down. The cardiac function completely ceased after 6–10 min asphyxia. The adenine nucleotide pools in cardiac tissue and mitochondria decreased after 10 min asphyxia to 50% and 38% of the initial values, respectively (Table 1). The depletion of the adenine nucleotide pool in hypoxic myocardium was mainly due to the loss of ATP, whereas that in mitochondria was associated with the fall in both AMP and ADP. Although ATP in intact heart mitochondria is equal to only 10% of the total adenine nucleotide pool, a decrease in mitochondrial ATP was the most dramatic: after 10-min asphyxia its content was reduced to about 22% of the initial one (Table 1).

An almost complete recovery of cardiac function during the resumption of respiration was observed after 1–3 min asphyxia, when adenine nucleotides in tissue and mitochondria decreased not more than to 67–68% of the initial values (Fig. 2, Table 1). The recovery of cardiac function at the initial stage of the resumption of respiration was

accompanied by a large rise in the left ventricular pressure and heart rate when compared to asphyxic hearts. The longer the duration of the preceding hypoxia was, the slower the heart work index reached its maximum during resumption of respiration (Fig. 2).

A period of 5 min asphyxia appeared to be critical for a recovery of the cardiac function during resumption of respiration. Only in 15 animals of the total 30 subjected to 5 min asphyxia we observed a complete, although somewhat retarded, recovery of the cardiac function (group 1) (Fig. 2). In these animals, the heart work index dropped by the end of 5 min asphyxia to 15% of the initial level, the left ventricular systolic pressure decreased 2-fold (to 71 ± 7 mm Hg), while the intramitochondrial adenine nucleotide pool was 64% of the control (Fig. 1, Table 1). The cardiac function in other animals did not recover after 5 min asphyxia (group 2). In this case, the heart work index fell to 4%, the left ventricular systolic pressure decreased to 15 ± 2 mm Hg (9-fold) and intramitochondrial adenine nucleotide pool dropped to 52% of the initial value. The differences in these parameters between the two groups of animals were statistically significant, while a decrease in tissue adenine nucleotides after 5 min asphyxia was the same in both groups (approx. 63%) (Table 1). Thus, only the intramitochondrial pool of adenine nucleotides showed a close correlation with the cardiac function depression during asphyxia as well as with its subsequent recovery after resumption of respiration (Fig. 1).

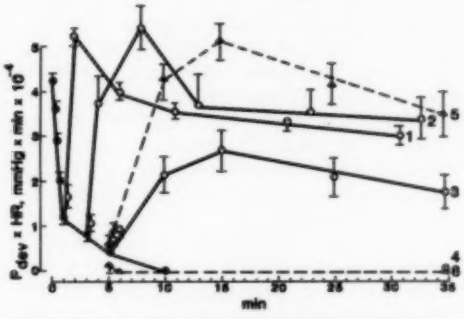

Fig. 2. Effect of asphyxia and subsequent resumption of respiration on the heart work index in narcotized rats. *Closed symbols* correspond to 10 min asphyxia, *open symbols* correspond to 30 min resumption of respiration after: (*1*) 1 min asphyxia, (*2*) 3 min asphyxia, (*3*) 5 min asphyxia (the mean values for both groups 1 and 2); (*4*) 10 min of respiration, (*5*) 5 min asphyxia (group 1), (*6*) 5 min asphyxia (group 2). (▲) Indicate the values of cardiac function in animals of groups 1 and 2 after 5 min asphyxia. Designations are the same as in Fig. 1. Values are the mean ± SEM

Mitochondrial respiratory function

The respiratory function of mitochondria isolated from control hearts (after 30 min artificial respiration) was evaluated by the following parameters: respiratory control index 7.10 ± 0.05; ADP/O 2.9 ± 0.1; state 3 respiration 290 ± 10 ng-atom O/min/mg protein when glutamate plus malate were used as respiratory substrates. The addition of water soluble cytochrome *c* to mitochondria from control hearts (45 nmol cytochrome *c*/mg mitochondrial protein) had no effect on state 3 respiration and only slightly improved oxidative phosphorylation in mitochondria from hypoxic hearts, thus indicating that there were no significant cytochrome *c* losses during mitochondrial isolation.

Polarographic assays of mitochondria isolated from hypoxic hearts revealed that state 3 respiration with glutamate and malate was less the longer the duration of asphyxia (Table 2). After 10 min asphyxia ADP-stimulated respiration with these substrates decreased 3-fold. The uncoupled respiratory rates showed a comparable decrease during asphyxia (Table 2). However, asphyxia had no effect on state 4 respiration with NAD-dependent substrates: it increased insignificantly from 41 ± 1 ng-atom O/min/mg protein in artificial respiration to 45 ± 3 ng-atom O/min/mg protein after 10 min asphyxia. After 5 min respiratory arrest the ADP/O ratio decreased slightly (from 2.9 ± 0.1 in the control to 2.4 ± 0.2), i.e. the coupling efficiency of hypoxic mitochondria remained sufficiently high. During further 5 min asphyxia the ADP/O ratio fell to 2.0 ± 0.2. The recovery of the cardiac function after 5 min asphyxia was associated with a restoration of 80% of state 3 respiration, while no recovery of phosphorylating respiration was observed in mitochondria of those animals in which cardiac

Table 1. Adenine nucleotide content in heart mitochondria and cardiac tissue of rats. Experimental conditions and the analytical procedures are described in Methods. Group 1: Animals in which cardiac performance recovered during resumption of respiration. Group 2: Animals with no recovery of cardiac performance after resumption of respiration. Total = ATP + ADP + AMP

	Tissue, μmol/g dry weight				Mitochondria, nmol/mg mitochondrial protein			
	ATP	ADP	AMP	Total	ATP	ADP	AMP	Total
Artificial respiration	25.20 ± 0.94	4.14 ± 0.18	0.57 ± 0.05	30.02 ± 1.12	1.31 ± 0.12	4.40 ± 0.31	6.34 ± 0.42	12.09 ± 0.61
Asphyxia								
1 min	18.00 ± 0.76[a]	3.87 ± 0.14	0.54 ± 0.04	22.41 ± 0.90[a]	1.08 ± 0.11	3.82 ± 0.20	4.40 ± 0.51	9.25 ± 0.47
3 min	15.35 ± 0.68[a]	4.05 ± 0.11	0.72 ± 0.06	20.12 ± 0.74[a]	0.98 ± 0.08	3.15 ± 0.16	4.14 ± 0.52[a]	8.27 ± 0.40[a]
5 min (group 1)	14.04 ± 0.56[a]	3.96 ± 0.14	0.81 ± 0.07[a]	18.91 ± 0.70[a]	0.84 ± 0.09[a]	3.25 ± 0.21[a]	3.71 ± 0.30[a]	7.76 ± 0.31[a]
(Group 2)	13.51 ± 0.60[a]	3.90 ± 0.13	0.87 ± 0.08[a]	18.25 ± 0.70[a]	0.43 ± 0.06[a,b]	2.58 ± 0.24[a]	3.27 ± 0.32[a]	6.22 ± 0.32[a,b]
10 min	10.52 ± 0.46	3.68 ± 0.12	0.79 ± 0.09	15.02 ± 0.61[a]	0.29 ± 0.04[a]	2.07 ± 0.18[a]	2.23 ± 0.21[a]	4.51 ± 0.24[a]
Resumption of respiration after 5 min asphyxia (group 1)	23.40 ± 1.10	3.68 ± 0.20	0.69 ± 0.08	27.80 ± 1.26	0.96 ± 0.08	4.32 ± 0.24	5.50 ± 0.47	10.87 ± 0.64

Significant difference: [a] from artificial respiration; [b] from the corresponding value of group 1. Values are the mean ± SEM of 10–12 experiments

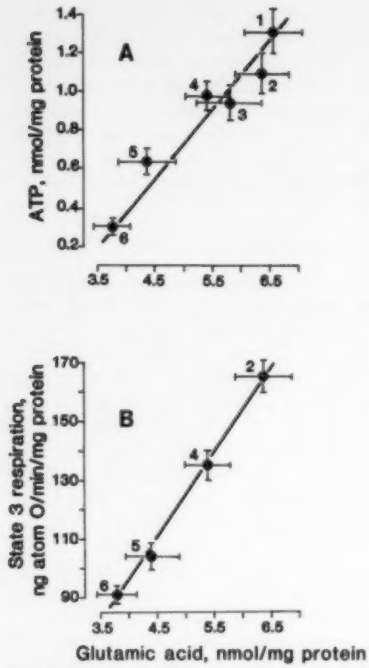

Fig. 3. Relationship between the content of glutamic acid and ATP in rat heart mitochondria (**A**) and between mitochondrial glutamic acid and state 3 respiration supported by glutamate and malate (**B**). (*1*) Artificial respiration, (*2*) 1 min asphyxia, (*3*) resumption of respiration after 5 min asphyxia (group 1), (*4*) 3 min asphyxia, (*5*) 5 min asphyxia (for both groups 1 and 2), (*6*) 10 min asphyxia. Values are the mean ± SEM of 6–10 experiments

performance remained depressed during resumption of breathing.

State 3 respiration supported by succinate changed less than that with glutamate and malate, showing only a 25% decrease after 10 min asphyxia (Table 2). Nonphosphorylating (State 4) respiratory rates of hypoxic mitochondria with succinate did not differ significantly from the initial value and averaged 74 ± 6 ng-atom/O/min/mg protein. The ADP/O ratio, as in the case of glutamate and malate, was only slightly decreased (from 1.8 ± 0.1 in the control to 1.5 ± 0.2 after 10 min respiratory arrest). Recovery of cardiac function during restoration following 5 min asphyxia was associated with a complete recovery of succinate-supported state 3 respiration.

Amino acids of cardiac tissue and mitochondria

After 10 min asphyxia the glutamic acid content in mitochondria was reduced by 40%, while that in heart tissue – by 23% (Table 3). The loss of glutamic acid from mitochondria after 5 min asphyxia was not directly related to the level of the cardiac contractile function. However, after resumption of respiration, the recovery of the cardiac function, mitochondrial respiration and adenine nucleotides was accompanied by a rise in mitochondrial glutamate level to nearly the initial level (5.83 ± 0.60 nmol/mg protein), whereas the heart failure and mitochondrial dysfunction during this period were associated with a lowered glutamate content in mitochondria. Figure 3A demonstrates the relationship between glutamate and ATP levels in heart mitochondria during asphyxia, resumption of respiration and artificial respiration in rats. Similar relationship was found between mitochondrial glutamate and exchangeable (ATP + ADP) adenine nucleotides (not shown). The de-

Table 2. Mitochondrial respiration. Values are the mean ± SEM of 6–8 experiments

	State 3 respiration, ng-atom O/min/mg protein		
	Glutamate + malate	Glutamate + malate + uncoupler	Succinate + rotenone
Artificial respiration	284 ± 9	280 ± 9	270 ± 9
Asphyxia			
5 min (group 1)	117 ± 7[a]	131 ± 12[a]	226 ± 10[a]
(group 2)	97 ± 6[a]	122 ± 10[a]	222 ± 10[a]
10 min	91 ± 6[a]	106 ± 9[a]	197 ± 8[a]
Resumption of respiration after 5 min asphyxia (group 1)	228 ± 12[a]	219 ± 11[a]	261 ± 11

[a] Significant difference from artificial respiration

Table 3. Amino acid content in heart mitochondria and cardiac tissue of rats. Tissue concentrations are expressed in μmol/g dry weight, mitochondrial concentrations are expressed in nmol/mg mitochondrial protein. Values are the mean ± SEM of 8–10 experiments

	Glutamic acid		Alanine		Aspartic acid	
	Tissue	Mitochondria	Tissue	Mitochondria	Tissue	Mitochondria
Artificial respiration	23.50 ± 1.08	6.51 ± 0.48	5.14 ± 0.37	1.48 ± 0.08	6.75 ± 0.78	0.88 ± 0.06
Asphyxia						
5 min	20.12 ± 0.70	4.42 ± 0.51	6.83 ± 0.74	1.24 ± 0.09	5.32 ± 0.64	1.23 ± 0.09
10 min	18.27 ± 0.71[a]	3.80 ± 0.36[a]	7.64 ± 0.71[a]	1.64 ± 0.12	4.62 ± 0.58	2.93 ± 0.11[a]

[a] Significant difference from artificial respiration

crease in the mitochondrial pool of glutamic acid was related to the loss of state 3 respiration with glutamate and malate during asphyxia (Fig. 3B).

The glutamic acid fall in cardiac tissue during asphyxia corresponded to alanine formation. The content of alanine in heart tissue increased 1.5-fold after 10 min asphyxia, while no significant changes in mitochondrial alanine pool were observed (Table 3). Asphyxia resulted in a significant rise in the level of mitochondrial aspartic acid but did not alter its tissue content.

Discussion

The disturbance in myocardial energy production during asphyxia features both hypoxic and ischemic influences. During the first 1–3 min asphyxia, when the circulation is maintained at a sufficiently high level, the heart is mainly subjected to hypoxia. During the first minute of asphyxia, the heart work index fell to 30% of the initial level, whereas the ATP level in the myocardium decreased by 29% (Fig. 2, Table 1). These findings are consistent with the report (Hearse 1979) on hypoxic perfusion of isolated rat heart. A sharp decrease in the left ventricular systolic pressure and the heart rate, as well as an increase in the end-diastolic pressure from 0 to 7 mm Hg are in a good agreement with the data of other authors who used the same or similar models (Feinstein 1962; Hendrickx et al. 1984). After 5 min asphyxia the bradycardia and a drastic fall of the left ventricular systolic pressure resulted in a sharp decline of the mean arterial pressure, as well as in the acute coronary flow insufficiency (Hendrickx et al. 1984).

Our results show that the cardiac function recovery after resumption of respiration following 5 min asphyxia was observed only in experiments where the mean left ventricular systolic pressure was at least 70 mm Hg. Presumably, in this case the aortic pressure is high enough to maintain the coronary flow at a fairly high level necessary for hypoxic heart contraction. A sharp fall of the left ventricular systolic pressure and, accordingly, of the aortic pressure, by the end of 5 min asphyxia further aggravated the heart function disturbances due to myocardial ischemia and prevented its recovery after resumption of respiration.

It is noteworthy that with an increase in the duration of asphyxia, a more pronounced fall in adenine nucleotides was observed in isolated mitochondria than in the cardiac tissue. Although the mechanism of the loss of adenine nucleotides from the matrix is not known (Asimakis and Conti 1984, 1985), it may be attributed to a damage of mitochondrial inner membrane (Sordahl and Stewart 1980; Stoner and Sirak 1973). The present study showed that a decrease in mitochondrial adenine nucleotides of rat hearts, which occurred as a result of asphyxia, was mainly accompanied by the loss in mitochondrial phosphorylating and uncoupled respiration supported by glutamate and malate, but not by succinate. It may thus be suggested that mitochondrial dysfunction, correlating with a more prominent fall in the cardiac function (Fig. 1), is due to disturbance in electron transport, particularly in complex I of the respiratory chain. This suggestion is consistent with the data of Rouslin and Millard (1980), who found that the inhibition of activity of NADH-CoQ reductase in myocardial ischemia accounts nearly quantitatively for the decrease in mitochondrial phosphorylating respiration with NAD-dependent substrates. In contrast, complexes III, IV and succinic dehydrogenase appear to be relatively resistant to ischemic damage (Jennings et al. 1957; Wachstein and Meisel 1955; Rouslin and Millard 1980). It is possible that disturbance of the integrity of the respiratory chain components within the mitochondrial membrane may be related to the observed loss of adenine nucleotides.

The reduction of adenine nucleotides as well as glutamate in mitochondria of hypoxic hearts is probably not an artifact of isolation procedure since mitochondria from ischemic heart tissue contain normal amounts of NADH and Mg^{2+} in spite of a more conspicious decrease in adenine nucleotides, and additional washing of these mitochondria does not result in further loss of adenine nucleotides (La Noue et al. 1981). Moreover, the authors suggest that the loss is specific for adenine nucleotides, since the pyridine nucleotide pool is not greatly affected. However, we did not assess mitochondrial pyridine nucleotides and Mg^{2+} in this study. Hence, one may also assume that the effects observed with isolated mitochondria of hypoxic hearts are due in part to inhibition of NAD-linked α-ketoacid dehydrogenases because of the loss of nicotinamide coenzymes (Klein et al. 1981) or Mg^{2+}.

The present study also demonstrates the relationship between the losses in mitochondrial respiratory activity, adenine nucleotides and changes in amino acid metabolism in rat hearts during asphyxia. The decrease in myocardial glutamic and aspartic acids and concomitant alanine production, observed under acute hypoxia, are consistent with the previous report of Freminet (1981). The rearrangement in metabolism of these amino acids results in the formation of α-ketoglutarate and oxaloacetate and, as a consequence, in the activation of energy yielding reactions in the tricarboxylic acid cycle coupled with succinate accumulation (Taegtmeyer 1978; Sanborn et al. 1979). The data presented in Table 3 indicate the participation of amino acids of heart mitochondria in metabolic response to respiratory arrest. This is especially related to glutamic acid, since the relative fall in glutamate pool in mitochondria of hypoxic hearts was more conspicious than that in the cardiac tissue. This may be due to aspartate aminotransferase and inhibition of glutamate influx into the matrix caused by the depression of mitochondrial glutamate/aspartate translocase under hypoxia (La Noue et al. 1973; Kauppinen et al. 1983). This assumption agrees with the elevation of aspartic acid intramitochondrial content in asphyxic hearts (Table 3). The operation of mitochondrial glutamate dehydrogenase towards deamination of glutamic acid seems to be unlikely because of high $NADH/NAD^+$ ratio under oxygen deprivation. The direct relationship between glutamic acid and ATP levels in heart mitochondria (Fig. 3A), as well as mitochondrial glutamate and state 3 respiration (Fig. 3B) is in a good agreement with the ability of exogenous glutamate to diminish ATP losses in ischemic and hypoxic hearts with simultaneous recovery of intracellular glutamate content to normal values (Pisarenko et al. 1983, 1985). This effect is accompanied by the maintenance of a higher level of cardiac performance in animal experiments and men (Shertzer and Cascarano 1979; Bittl and Shine 1983; Pisarenko et al. 1986). Thus, the data obtained strongly suggest that profound changes in intermediary metabolism of substrates, which can be of physiological importance (such as glutamic acid), are tightly linked with mitochondrial dysfunctions and depression of cardiac performance in acute hypoxia.

References

Asimakis GK, Conti VR (1984) Myocardial ischemia: correlation of mitochondrial adenine nucleotide and respiratory function. J Mol Cell Cardiol 16:439–448

Asimakis GK, Conti VR (1985) Phosphate-induced efflux of adenine nucleotides from heart mitochondria. Am J Physiol 249:H1009–1016

Bittl J, Shine KI (1983) Protection of ischemic rabbit myocardium by glutamic acid. Am J Physiol 245:H406–412

Feinstein MB (1962) Effects of experimental congestive heart failure, ouabain and asphyxia on the high-energy phosphate and creatine content of the guinea pig heart. Circ Res 10:333–346

Freminet A (1981) Carbohydrate and amino acid metabolism during acute hypoxia in rats: blood and heart metabolites. Comp Biochem Physiol 70B:427–433

Hearse DJ (1979) Oxygen deprivation and early myocardial contractile failure: a reassessment of the possible role of adenosine triphosphate. Am J Cardiol 44:1115–1121

Hendrickx HHL, Rao GR, Safar P, Gilsvold SE (1984) Asphyxia, cardiac arrest and resuscitation in rats. 1. Short term recovery. Resuscitation 12:97–116

Jennings RB, Kaltenbach JP, Smethers GW (1957) Enzymatic changes in acute myocardial ischemic injury. Arch Pathol 64:10–16

Kauppinen RA, Hiltunen JK, Hassinen IE (1983) Mitochondrial membrane potential, transmembrane difference in NAD^+ redox potential and the equilibrium of the glutamate-aspartate translocase in the isolated perfused rat heart. Biochim Biophys Acta 725:425–433

Klein HH, Schaper J, Puschmann St, Nienaber Ch, Kreuzer H, Shaper W (1981) Loss of canine myocardial nicotinamide adenine dinucleotides determines the transition from reversible to irreversible ischemic damage of myocardial cells. Basic Res Cardiol 76:612–621

La Noue KF, Walajtys EI, Williamson JR (1973) Regulation of glutamate metabolism and interactions with the citric acid cycle in rat heart mitochondria. J Biol Chem 248:7171–7183

La Noue KF, Watts JA, Koch CP (1981) Adenine nucleotide transport during cardiac ischemia. Am J Physiol 241:H663–671

Lowry OH, Rosebrough NJ, Farr AL, Randall RJ (1951) Protein measurements with the Folin phenol reagent. J Biol Chem 193:265–275

Pisarenko OI, Solomatina ES, Studneva IM, Ivanov VE, Kapelko VI, Smirnov VN (1983) Effect of glutamic and aspartic acids on adenine nucleotides, nitrogen compounds and contractile function during underperfusion of isolated rat heart. J Mol Cell Cardiol 15:53–60

Pisarenko OI, Solomatina ES, Ivanov VE, Studneva IM, Kapelko VI, Smirnov VN (1985) On the mechanism of enhanced ATP formation in hypoxic myocardium caused by glutamic acid. Basic Res Cardiol 80:126–134

Pisarenko OI, Lepilin MG, Ivanov VE (1986) Cardiac metabolism and performance during L-glutamic acid infusion in postoperative cardiac failure. Clin Sci 70:7–12

Rouslin W, Millard RW (1980) Canine myocardial ischemia: Defect in mitochondrial electron transfer complex. I. J Mol Cell Cardiol 12:639–645

Sanborn T, Gavis W, Berkowitz S, Perrille T, Lesch M (1979) Augmented convertion of aspartate and glutamate to succinate during anoxia in rabbit heart. Am J Physiol 273:H535–541

Shertzer HG, Cascarano J (1979) Anaerobic rat heart: mitochondrial role in calcium uptake and contractility. J Exp Zool 207:337–350

Sordahl LA, Stewart ML (1980) Mechanism(s) of altered mitochondrial calcium transport in acutely ischemic canine hearts. Circ Res 47:814–820

Stoner CD, Sirak HD (1973) Adenine nucleotide-induced contraction of the inner mitochondrial membrane. J Cell Biol 56:51–64

Taegtmeyer H (1978) Metabolic response to cardiac hypoxia. Increased production of succinate by rabbit papillary muscle. Circ Res 43:808–815

Wachstein M, Meisel E (1955) Succinic dehydrogenase activity in myocardial infarction and in induced myocardial necrosis. Am J Pathol 31:353–365

Williamson JR, Corkey BE (1969) Assays of intermediates of the citric compounds by fluorometric enzyme methods. In: Lowenstein JM (ed) Methods in enzymology, vol XII. Academic Press, New York, pp 488–496

Received March 20, 1986/Accepted January 7, 1987

Pflügers Arch (1987) 409:175–181

Pflügers Archiv
European Journal of Physiology
© Springer-Verlag 1987

Changes in cold- and heat-defence following electrolytic lesions of raphe nuclei in the guinea-pig

Zoltán Szelényi* and Peter Hinckel

Physiologisches Institut, Universität Giessen, Aulweg 129, D-6300 Giessen, Federal Republic of Germany

Abstract. In conscious guinea-pigs the effects of electrolytic lesions of the nucleus raphe magnus (NRM) and of adjacent areas in the lower brainstem on cold- and heat-defence were studied. Changes in core temperature, heat production and heat loss effectors as well as their threshold temperatures were compared in the same animals before and after lesioning. As an additional index of heat loss, ear skin temperature and a derived parameter – vasomotor index – were also measured. Three days after NRM lesion the fall in core temperature evoked by an exposure to 14–15°C was smaller than before lesion, furthermore the body temperature threshold for shivering increased. Cold-induced heat production was also higher following NRM lesions. Lesions outside the NRM or sham-operation did not influence cold-defence. After NRM lesion heat-defence was also improved; the rise in core temperature elicited by an exposure to 36–37°C was smaller and the body temperature threshold for ear skin vasoconstriction during recovery from hyperthermia decreased. No change in respiratory evaporative heat loss could be observed after NRM lesion. Lesions outside the NRM or sham-operation did not influence heat-defence. An attempt has been made to explain the observed improvements in cold- and heat-defence by discussing relevant data on mechanisms in central temperature control.

Key words: Temperature regulation – Cold-defence – Heat-defence – Nucleus raphe magnus lesion – Body temperature thresholds

Introduction

Recently interest has been increased on the role of the lower brainstem in various aspects of central body temperature control [see 4, 5]. One of the sites of importance at that level of the brain has proved to be the raphe system, traditionally looked upon as an anatomical and functional entity with similar neurochemical architecture in different mammalian species [14, 16]. Although new lines of evidence from a large number of studies utilizing a sophisticated neurochemical repertoire have demonstrated considerable heterogeneity in the "chemical wiring" within the different raphe nuclei, some convergence in our understanding of the function of this part of the brain has occurred during the last decade.

One major area of research has been involved in studies on the role of some raphe areas in modulation of nociceptive spinal mechanisms [1, 8]. However, non-noxious information from peripheral receptors, including thermal information within the physiological range also reaches the central controlling sites through the lower brainstem. It has been suggested that the nucleus raphe magnus (NRM) may act as a relay station of warm-receptive information ascending from the skin [3, 7, 19]. The same raphe nucleus has been shown to be the origin of pathways projecting to the hypothalamus [2], the activation of which could specifically influence warm- and cold-responsive hypothalamic units in the guinea-pig [3]. Also in the guinea-pig, electrical stimulation of NRM inhibited cold-induced thermogenesis, a response not influenced by the interruption of descending pathways known to inhibit cutaneous sensory inputs probably at the level of the dorsal horn in the spinal cord [10].

In the present study guinea-pigs were exposed to a standard cold environment before and after lesioning of the NRM to see if cold-defence would change in the manner expected from the results of the electrical stimulation experiments mentioned above. Furthermore, standard heat exposure was applied in the same animals to test the idea of the role of ponto-medullary raphe also in influencing heat-loss reactions, since electrical stimulation of the NRM could increase the activity of hypothalamic warm-responsive units [3].

Preliminary results of the present study have been reported elsewhere [17].

Methods

Twenty-one guinea-pigs of either sex aged 5–7 weeks, with an initial body weight of 310–380 g, were used. The animals were held at an ambient temperature of 21–24°C before the first experiment and also during the ensuing week which elapsed between the first and the second thermophysiological experiment.

On the morning of the experiment thermocouples were introduced into the colon (8 cm from the anus), under the back skin and on the inner surface of one of the ear-lobes using halothane anaesthesia. Electrodes for measuring integrated electrical activity were inserted into the thigh and masseter muscles on the right side and sutured in place. After the effect of the anaesthetic had worn off, the guinea-pig was fixed to a plexiglass plate with strings bound gently around the lower end of the four extremities as well as with a plaster tape around the back.

The course of the experiments was as follows:

* *Present address:* Department of Pathophysiology, University Medical School Pécs, H-7643 Pécs, Szigeti út 12, Hungary
Offprint requests to: P. Hinckel

A. Thermophysiological experiment 1

1. The animal was placed into a metabolic chamber with wall and air temperature held at 28.5°C (range 28.0–29.0°C) for 1.5–2 h, during which time body temperatures and metabolic rate became stabilized at their normal resting levels.

2. A cold exposure of 14–15°C range was then applied for 1 h, followed by a 2-h period of exposure to 28–29°C.

3. A heat-exposure of 36–37°C was then initiated, which lasted until all signs of heat-defence (i.e. polypnea, vasodilatation) had developed (1–1.5 h).

4. An additional exposure to 28–29°C concluded the experiment leading to recovery from the previous heat-induced hyperthermia.

5. Under halothane anaesthesia all electrodes and thermocouples were removed and the animal placed back into its cage.

B. Operation

Three days later an i.p. injection of nembutal (40 mg per kg body weight) was given and the animal's head placed in a stereotaxic apparatus according to the co-ordinate system of Rössner [15]. After drilling holes in the midline of the skull and incising the dura a stainless steel lesioning electrode (0.1 mm in diameter with a 0.1 mm free end) was lowered aiming at the NRM and adjacent brainstem sites.

In 14 guinea-pigs electrolytic lesions were made by using 1.0–1.5 mA current for 10 s at 2.4–6.0 V, one leg of the animal serving as reference site. In all cases two lesions, 0.3–0.6 mm apart were placed sagittally from each other. In 7 guinea-pigs no current was passed through the electrode (sham-operation). The electrode was then withdrawn, the wound sutured and the animal placed back into its cage.

C. Thermophysiological experiment 2

Three days after surgery the guinea-pig was again supplied with the electrodes and thermocouples (this time the left ear-lobe and the left masseter and thigh muscles having been used) and procedure A was repeated. Since the duration of the heat-exposure varied in different guinea-pigs during experiment A, care was taken to expose each guinea-pig to heat for the same time as was the case in the first experiment.

After an overdose of Nembutal the animal's brain was quickly removed and placed into a buffered formaldehyde solution. The localization of lesions were evaluated using standard histological methods.

The following physiological variables were measured during the whole course of experiments A and C:

1. Colonic temperature (T_{colon}).
2. Subcutaneous temperature on the back (T_{back}).
3. Surface temperature of the ear-lobe (T_{ear}).
4. Integrated electrical activity in the two muscle groups (EMA).
5. Respiratory evaporative heat loss (REHL), using temperature and humidity data at the inlet and near the outlet air flowing through the metabolic chamber.
6. Metabolic rate (MR) by measuring oxygen consumption (open system) using a paramagnetic oxygen analyser.

The variables listed were measured consecutively by a digital voltmeter and sampled every 30 s by a Hewlett-Packard 9603A measurement and control system and stored on a magnetic tape. All these data as well as mean body temperature ($\overline{T}_b = 0.5 \times T_{colon} + 0.5 \times T_{back}$) and ear-lobe vasomotor index (VMI) were recorded on-line by a Hewlett-Packard printer.

Mean body temperature thresholds for shivering thermogenesis ($\overline{T}$–SH), for rise in metabolic rate ($\overline{T}$–MR↑) were used to characterize the heat production response during cold-exposure. Similarly, the mean body temperature threshold for REHL ($\overline{T}$–REHL) was utilized to judge the onset of rise in evaporative heat loss during heat-exposure. To get a deeper insight into the functioning of heat-loss effectors an index of the vasomotor tone, VMI was utilized (Szelényi and Székely, unpublished). There is some information in the literature that – similar to the rabbit's ear temperature – ear temperature of the guinea-pig also shows signs of thermoregulatory vasomotor reactions [9]. To get information on changes in T_{ear} independent of changes in core temperature (T_{colon}) and ambient temperature (T_a), the following equation was used:

$$\text{VMI} = \frac{T_{ear} - T_a}{T_{colon} - T_a}.$$

Except for extremely rapid changes in the respective temperatures, VMI can be a useful indicator of vasomotor tone on ear-skin and theoretically its value can range from almost 0 to 1 (full vasoconstriction and vasodilatation, respectively). Preliminary experiments showed that VMI did not change reliably during heat-exposure to indicate vasodilatation-threshold. After transfer of the animal to a near-thermoneutral T_a, however, a slow recovery from the heat-induced hyperthermia (while T_{colon} and T_{ear} are declining practically in parallel) gives way to a steep fall in T_{ear} indicating vasoconstriction. When calculated in the way given above, VMI does not change during the first phase of recovery from hyperthermia, then there is a very steep fall followed by a second steady-state of the VMI value (see inset in Fig. 1). The $\overline{T}_b$ at which the start of this sudden decrease in VMI indicates onset of vasoconstriction thus may be taken as a threshold of vasomotor heat-defence in the guinea-pig (Fig. 1). This body temperature threshold ($\overline{T}$–VMI) represents another estimate of heat-defence; the lower the $\overline{T}$–VMI, the later the animal stops vasodilatation which contributes to recovery from hyperthermia.

For statistical analysis the one-sample and the multiple *t*-test were used. For the calculations of thresholds linear regression analysis was applied.

Results

Histological evaluation of the lesion sites revealed that the 14 guinea-pigs with brainstem lesions could be divided into two sub-groups according to the localization and extension of lesions (Fig. 2). In 7 guinea-pigs much of the NRM as well as – in 4 cases – the ventral part of the nucleus raphe pontis (NRP) had been destroyed ("NRM-lesion"). In the other 7 guinea-pigs the lesions either were localized more laterally – thus leaving the raphe system intact – or destroyed only the NRP or more distal and dorsal parts of the median lower brainstem. These animals were therefore grouped as "lesions outside the NRM". These latter lesions, though heterogenous in terms of their localization, can be regarded as an homogeneous group from the point of view of their leaving the NRM and its immediate surroundings intact.

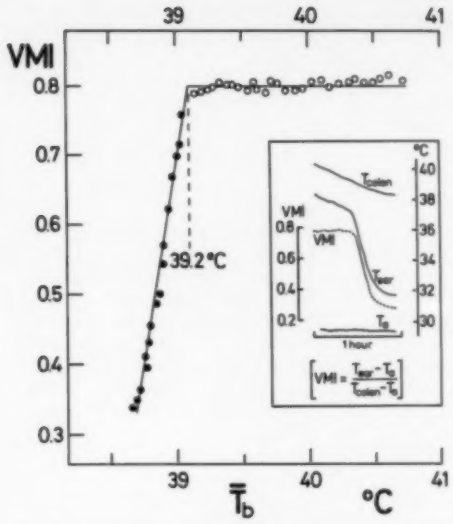

Fig. 1. Determination of ear-skin vasomotor index (VMI) and of the mean body temperature threshold ($\overline{T}_b$) for vasoconstriction during recovery from heat-induced hyperthermia. Original temperature data and equation of VMI are shown in the *inset*. Regression lines for VMI vs. $\overline{T}_b$ before (○) and after (●) the start of vasoconstriction (data sampled every minute). $\overline{T}_b = 0.5\ T_{colon} + 0.5\ T_{back\ skin}$ (the latter temperature not shown in the figure)

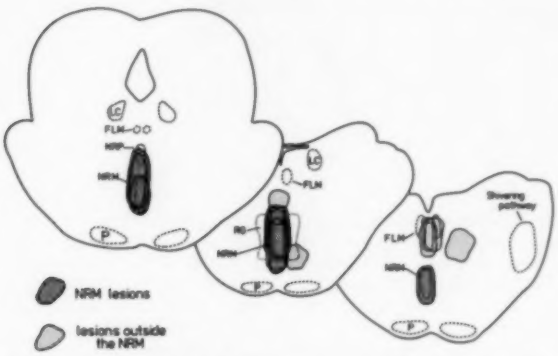

Fig. 2. Localization of the lesion sites shown on three representative frontal sections through the lower brainstem. *LC* locus coeruleus; *FLM* fasciculus longitudinalis medialis; *NRP* nucleus raphe pontis; *NRM* nucleus raphe magnus; *P* tractus corticospinalis

As a first estimate of the effects of the various lesions, cold- and heat-defence of guinea-pigs with lesions outside the NRM, within the NRM and those of the sham-operated control animals was calculated as shown in Fig. 3. In guinea-pigs with lesions outside the NRM, the T_{colon}-course during the first cold-exposure (before lesion) did not differ from that observed during the second cold-exposure (after lesion). As expected, the sham-operation did not influence the T_{colon}-course, either. Following lesions of the NRM, however, the fall in T_{colon} was significantly attenuated from minute 25 onwards indicating a more pronounced cold-defence as a result of these lesions. At the end of the cold-exposure the difference in the extent of decline in T_{colon} amounted to more than 1.5°C (left panel of Fig. 3).

An enhanced thermal stability after NRM-lesion can also be derived from the heat-defence responses of the guinea-pigs (Fig. 3, right panel), since only in the NRM-lesioned group was the rise in T_{colon} smaller during the second heat-exposure than that during the first heat-exposure. Here again the better regulation was evident from minute 25 onwards in the NRM-lesioned guinea-pigs, whereas within the two other groups no difference in the T_{colon}-course could be observed.

Figure 4 shows effects of cold- and heat-exposure (upper and lower part, respectively) before and after lesion of the NRM in a guinea-pig. Initial T_{colon} was practically identical in the two experiments carried out 7 days apart (as usual in this series). After NRM lesion the extent of fall in T_{colon} during cold-exposure was about 0.5°C less than in the control experiment. The delay for the rise in MR and EMA after the start of cold-exposure was reduced after NRM-lesion. In this experiment the levels of MR and EMA were also slightly higher at all phases of cold-exposure following NRM-lesion (upper part of Fig. 4).

The rise in T_{colon} during heat-exposure was less steep after NRM-lesion than before it and reached a lower hyperthermic value. The behaviour of VMI showed the typical qualitative changes observed in all experiments; i.e. a rapid rise at the beginning of heat-exposure – mostly due to a rapid rise in T_a (not shown in Fig. 4) – followed by some oscillation of VMI just below 1.0. Exposure to 28.5°C resulted in an initial rapid fall in VMI (as an effect of reduction in T_a) followed by a new steady-state while T_{colon} gradually declined towards the normothermic range of core temperature. Then a rapid fall in VMI ensued – earlier and from a lower value in the control experiment than after NRM-lesion – with a stabilization of T_{colon} slightly above the value observed at the beginning of the whole experiment. It is noteworthy that in the last part of the experiment VMI began to fall when T_{colon} was still high in the control experiment, whereas after NRM-lesion VMI decreased at a lower T_{colon}. In this animal REHL also increased more steeply and reached a higher value after NRM-lesion than in the control experiment.

Average threshold mean body temperatures for changes in the investigated thermoregulatory effectors and slopes of temperature-response relationships are summarized in Fig. 5. After lesions outside the NRM threshold temperature for shivering decreased, while NRM-lesion resulted in a slight but significant rise in this threshold (I). Similarly, the threshold temperature for a rise in MR decreased or increased following lesions outside or within the NRM, respectively. Thus, both indices of thermoregulatory heat production were activated at a higher mean body temperature as a result of NRM-lesions (III).

On the heat-loss side, the body temperature threshold for ear-skin vasoconstriction decreased significantly after NRM-lesion, whereas neither the lesions outside the NRM, nor sham-operation influenced vasoconstriction threshold (II). No difference in the threshold for a rise in REHL could be found in any of the three groups, that is neither NRM-lesion, nor other lesions in this study influenced the characteristics of the REHL-response during heat-exposure (IV).

NRM-lesion did not influence resting MR but led to significantly greater rises in MR during cold-exposure (expressed in absolute terms or in per cent), while average shivering activity remained unchanged. As an index for the sensitivity with which the heat production effectors were

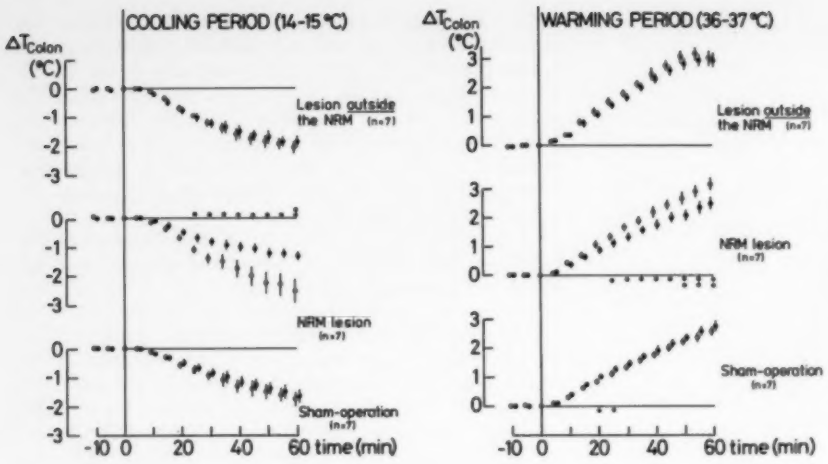
COOLING PERIOD (14-15 °C)
WARMING PERIOD (36-37 °C)
ΔT Colon (°C)
Lesion outside the NRM (n=7)
NRM lesion (n=7)
Sham-operation (n=7)
-10 0 20 40 60 time (min)

Fig. 3
Time-course of changes in colonic temperature (T_{colon}) 3 days before and after electrolytic lesions in the lower brainstem as well as before and after a sham-operation. Differences between pre- and post-lesion values of T_{colon}: * $p < 0.05$; ** $p < 0.01$; n = number of guinea-pigs. (○) before lesion; (●) after lesion

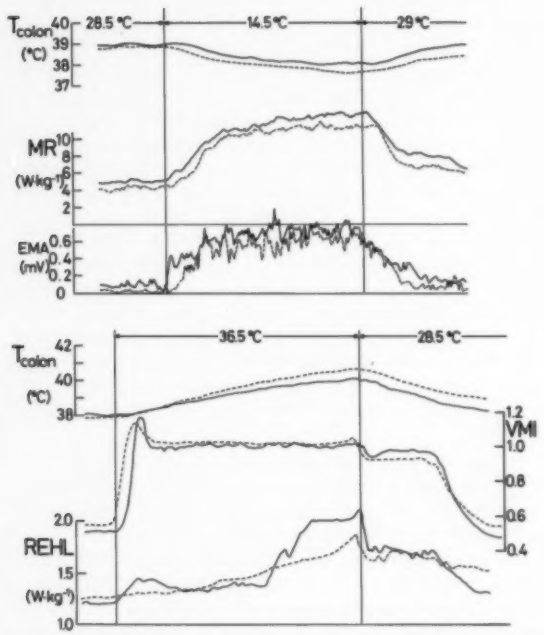

Fig. 4. Changes in colonic temperature (T_{colon}), metabolic rate (MR), integrated electrical activity in two muscle groups (EMA), respiratory evaporative heat loss (REHL) and ear-skin vasomotor index (VMI) in a guinea-pig before (——) and after (———) NRM lesion. *Upper panel:* cold exposure ($T_a = 14.5°C$), *lower panel:* heat exposure ($T_a = 36.5°C$)

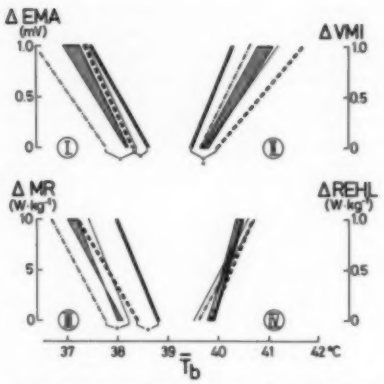

Fig. 5. Mean body temperature thresholds (indicated by the lower ends of the lines) and their slopes for heat production and heat loss effector responses. *I* Shivering activity (*EMA*); *II* Vasomotor index (*VMI*); *III* Heat production (*MR*); *IV* Respiratory evaporative heat loss (*REHL*), each plotted against mean body temperature ($\bar{T}_b$). Before (——) and after (———) NRM lesion. Before (·····) and after (–·–·–) lesions outside the NRM (e.g. in the subcoeruleus area). Range of changes before and after a sham-operation (▒). * $p < 0.05$, ** $p < 0.01$

stimulated by cold exposure, the activation of MR and EMA after a 1°C fall in T_{colon} during cold exposure was significantly larger in animals with NRM-lesions, whereas sham-operation had no such effect (Table 1).

NRM-lesion led to a small but significant fall in initial VMI (at T_a of 28.5°C) with significantly higher VMI values during the last 30 min of heat-exposure (Table 2). Neither resting REHL (measured at a T_a of 28.5°C), nor average REHL during the last 30 min of heat-exposure were modified by NRM-lesions.

Discussion

The effect of NRM-lesions on cold- and heat-defence reactions of conscious guinea-pigs have been studied in the present investigations. To make these comparisons possible several control situations had to be utilized:

(a) the same standardized procedure for cold- and heat-exposure carried out before and after operating the animal for NRM-lesion (to see the effect if any of NRM-lesion)

(b) to carry out similar studies on guinea-pigs lesioned at sites in the lower brainstem other than the NRM (to check the specificity of effect of NRM-lesions)

Table 1. Resting heat production (MR), changes in MR (ΔMR) and in shivering activity (ΔEMA) on cold exposure ($T_a = 14-15°C$) before and after a sham-operation (sham) and before and after lesioning the nucleus raphe magnus (NRML) as well as the sensitivity of changes in MR and EMA (mean ± SEM)

	Resting MR ($W\ kg^{-1}$)		ΔMR average ($W\ kg^{-1}$)		ΔEMA average (mV)	
	Before	After	Before	After	Before	After
Sham	4.3 ± 0.17	4.2 ± 0.35	$+4.8 \pm 0.35$	$+4.7 \pm 0.30$	$+0.47 \pm 0.05$	$+0.62 \pm 0.06$
	NS		NS		NS	
NRML	4.4 ± 0.28	4.4 ± 0.29	$+4.6 \pm 0.50$	$+6.1 \pm 0.39$	$+0.45 \pm 0.05$	$+0.58 \pm 0.05$
	NS		$p < 0.05$		NS	

	ΔMR (average) per degree fall in T_{colon} ($W\ kg^{-1}\ °C^{-1}$)		ΔEMA (average) per degree fall in T_{colon} ($mV\ °C^{-1}$)	
	Before	After	Before	After
Sham	$+3.2 \pm 0.84$	$+3.3 \pm 0.81$	$+0.28 \pm 0.04$	$+0.36 \pm 0.06$
	NS		NS	
NRML	$+2.5 \pm 0.79$	$+4.6 \pm 0.45$	$+0.24 \pm 0.07$	$+0.44 \pm 0.06$
	$p < 0.005$		$p < 0.05$	

NS = non-significant difference

Table 2
Ear skin vasomotor index (VMI) and respiratory evaporative heat loss (REHL) before and after a sham-operation (sham) and before and after lesioning the nucleus raphe magnus (NRML) (mean ± SEM)

	Resting VMI (at T_a of 28–29°C)		VMI during the last 30 min of exposure to 36–37°C	
	Before	After	Before	After
Sham	0.35 ± 0.01	0.29 ± 0.03	0.75 ± 0.01	0.77 ± 0.02
	NS		NS	
NRML	0.39 ± 0.02	0.32 ± 0.02	0.73 ± 0.04	0.84 ± 0.02
	$p < 0.05$		$p < 0.05$	

	Resting REHL (at T_a of 28–29°C) ($W\ kg^{-1}$)		REHL during the last 30 min of exposure to 36–37°C ($W\ kg^{-1}$)	
	Before	After	Before	After
Sham	1.58 ± 0.15	1.62 ± 0.15	2.30 ± 0.23	2.93 ± 0.19
	NS		NS	
NRML	1.17 ± 0.22	1.15 ± 0.16	2.40 ± 0.30	2.40 ± 0.20
	NS		NS	

NS = non-significant difference

(c) to conduct again similar experiments in guinea-pigs with no brainstem lesions at all (to study the influence of repetition of the same thermoregulatory procedure after 7 days).

The main finding of these experiments was that electrolytic lesions of the NRM improved both cold- and heat-defence. Consequently, the guinea-pigs with NRM-lesions regulated their body temperature with significantly smaller declines and rises in core temperature on exposure to cold and heat, respectively. In other words, under the circumstances of the cold- and the heat-challenge applied, the reduced range of changes in core temperature after NRM-lesions indicates that cold- and heat-defence of these animals was more efficient.

The body temperature threshold for increases in heat production and heat loss effectors changed in a way which resulted in some narrowing of the so-called interthreshold zones (i.e. the range of body temperature between thresholds of heat production and heat loss). In particular, the interthreshold zone between ear-skin vasoconstriction and shivering (see Figs. 5, 6) had indeed become significantly narrower, while that for rises in REHL and MR had remained unchanged, probably owing to the finding that NRM-lesions did not influence $\overline{T}$–REHL (Fig. 5). In experiments carried out in guinea-pigs with lesions outside the NRM no change in any of the interthreshold zones could be observed. However, the mean body temperature threshold for cold-induced heat production (and shivering) were shifted to lower values (see (I) and (III) in Fig. 5). This displacement in heat-production thresholds might be explained by the more dorso-lateral localization of some of these lesions, thus destroying parts of the subcoeruleus system. In fact, electrolytic lesions of the subcoeruleus area have been demonstrated to cause a similar displacement of the shivering threshold [4].

The finding that cold-induced thermogenesis and its thresholds increased following NRM-lesions is in line with recent data that electrical stimulation of the NRM inhibits cold-induced thermogenesis [10]. NRM-lesion influenced

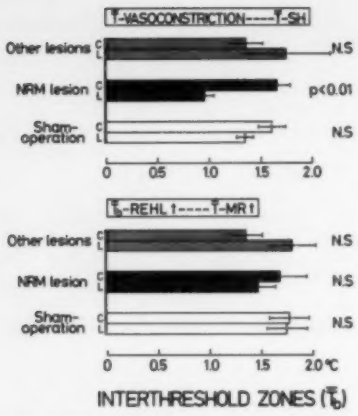

Fig. 6. Interthreshold zones expressed as ranges of mean body temperature ($\bar{T}_b$). *Upper part:* between vasoconstriction and shivering; *lower part:* between respiratory evaporative heat loss and metabolic rate; *C* control experiments; *L* experiments after lesion or sham-operation. *N.S* non-significant difference

several aspects of cold-defence ($\bar{T}$−SH, MR and the sensitivity of MR and EMA responses) with the result of more precise temperature control, while resting MR and core temperature remained the same. This indicates the role of NRM in modulating cold-induced thermogenesis without affecting general metabolic activity of the animals, thus the development of a non-specific increase in vigilance-state after lesions appears to be unlikely. This seems to support and extend the growing evidence that NRM or part of it, as well as some closely neighbouring areas (such as the nucleus reticularis gigantocellularis and the nucleus reticularis paragigantocellularis lateralis) might play a role in conveying thermal information from the periphery. Since stimulation of the NRM excited warm-responsive hypothalamic units and inhibited cold-responsive hypothalamic units [3, 12], the improvement of cold-defence observed in the present study may be interpreted as a consequence of switching off some of these ascending pathways, thus partly disinhibiting cold-responsive hypothalamic units and switching off warm-responsive units, respectively. The existence of a direct inhibitory projection from NRM to the hypothalamus has been supported recently in the cat and rat [11]. NRM-lesions must have left those ascending pathways intact, the stimulation of which activated thermoregulatory heat production [4, 18].

NRM-lesions also resulted in a partial improvement of heat-defence in the guinea-pig; the body temperature threshold for the development of ear-skin vasoconstriction during recovery from hyperthermia decreased and the level of vasodilatation during heat-exposure was higher. Although no change in REHL could be demonstrated after NRM-lesions, heat-defence of these guinea-pigs increased as judged from the smaller rise of core temperature.

It is known that in guinea-pigs no genuine thermal polypnea exists; during heat exposure respiratory frequency increases gradually with the degree of hyperthermia without any clear-cut transition to thermal polypnea [6] as is the case in the rabbit. This has been reinforced by our experience in this study by measuring REHL during heat-exposure showing steep rises only after a considerable hyperthermia had already developed and even in this case it was generally accompanied by gross movements and excitement of the animals. The lack of influence of NRM-lesion on REHL as observed in the present study would, therefore, only mean that an emergency-like mechanism of heat-loss in the guinea-pig has remained unaffected by these lesions.

Ear-skin temperature as well as the derived variable (VMI) utilized to indicate changes in thermoregulatory vasomotor tone proved to be the only measured heat-loss parameter, which was clearly affected by NRM-lesions in connection with heat-exposure. In guinea-pigs subcutaneously measured trunk-skin temperature behaves very similarly to core temperature (especially during heat-exposure) and in this site no thermoregulatory vasomotor reaction can be observed. In contrast, ear-skin temperature (as well as skin temperature on the four paws) shows changes during heat-exposure typical for skin areas possessing thermoregulatory vasomotorics. Since these parts of the skin (two ear-lobes and four paws) represent 16% of the body surface area in the guinea-pig (Szelényi, unpublished), the large changes of temperature here at constant core and ambient temperatures should indicate a sizable modification of non-REHL. In addition, the fact that ear-skin temperature (and VMI for that matter) decreased sharply at a certain point in the course of recovery from hyperthermia in the present study (see Figs. 1 and 4) justifies the use of VMI and its threshold-value to characterize the heat-loss response as applied in this study.

The slightly improved heat-defence as evidenced also by the reduction of VMI-threshold after NRM-lesions in the present study can be interpreted as a sign of activation of at least one of the measured heat-loss responses in the heat. Since NRM-stimulation has been shown to inhibit REHL slightly in the guinea-pig (Hinckel, unpublished), one would expect an increase in heat loss and facilitation of heat-loss mechanisms during heat-exposure. Although REHL was not influenced by NRM-lesion in the present study, the decrease in VMI-threshold indicated at least a partial improvement of heat-defence, which seems compatible with a role of NRM in limiting heat-loss responses to hyperthermia.

Obviously, more data are needed on the role of the raphe system in the central control of body temperature. Besides the present experiments, only one study seems to have been published in which the thermoregulatory consequences of NRM lesions in conscious animals have been followed [13]. In pigeons NRM-lesion did not cause any gross disturbance of thermoregulation in cold and heat, but the day-night oscillation of core temperature – about 2°C in this species – has disappeared. This disappearance of the day-night rhythm in body temperature might be a similar phenomenon as the improvement of cold- and heat-defence seen in the present study in guinea-pigs.

Acknowledgements. The authors gratefully acknowledge the advice of Professor Dr. K. Brück and the assistence of Mrs. Inge Stei, Mr. G. Schade and Ch. Lenz. This work was supported by a DFG scholarship to Z. S.

References

1. Basbaum AI, Fields HL (1984) Endogenous pain control system: Brainstem spinal pathways and endorphin circuitry. Annu Rev Neurosci 7:309–338

2. Bobillier P, Seguin S, Petitjean F, Salvert D, Touret M, Jouvet M (1976) The raphe nuclei of the cat brain stem: a topographical atlas of their efferent projections as revealed by autoradiography. Brain Res 113:449–486
3. Brück K, Hinckel P (1980) Thermoregulatory noradrenergic and serotonergic pathways to hypothalamic units. J Physiol 304:193–202
4. Brück K, Hinckel P (1982) Thermoafferent systems and their adaptive modifications. Pharmacol Ther 17:357–381
5. Brück K, Hinckel P (1984) Thermal afferents to the hypothalamus and thermal adaptation. J Therm Biol 9:7–10
6. Brück K, Wünnenberg W, Gallmeier H, Ziehm B (1970) Shift of threshold temperature for shivering and heat polypnea as a mode of thermal adaptation. Pflügers Arch 321:159–172
7. Dickenson AH (1977) Specific responses of rat raphe neurones to skin temperature. J Physiol 273:277–293
8. Dubner R, Bennett GJ (1983) Spinal and trigeminal mechanisms of nociception. Annu Rev Neurosci 6:381–418
9. Grant RT (1963) Vasodilatation and body warming in the rat. J Physiol 167:311–317
10. Hinckel P, Cristante L, Brück K (1983) Inhibitory effects of the lower brain stem on shivering. J Therm Biol 8:129–131
11. Lumb BM, Wolstencroft JH (1985) Electrophysiological studies of a rostral projection from the nucleus raphe magnus to the hypothalamus in the rat and cat. Brain Res 327:336–339
12. Matsumura K, Nakayama T, Ishikawa Y (1984) Effects of median raphe electrical stimulation on the preoptic thermosensitive neurons in rats. In: Hales JRS (ed) Thermal physiology. Raven Press, New York, pp 87–90
13. Necker R, Wegner L (1981) Effects of nucleus raphe lesions and p-CPA on temperature regulation and day-night rhythm of body temperature in pigeons. In: Szelényi Z, Székely M (eds) Contributions to thermal physiology. Pergamon, Oxford, Akadémiai Kiadó, Budapest, pp 29–31
14. Parent A, Poitras D, Dubé L (1984) Comparative anatomy of central monoaminergic systems. In: Björklund A, Hökfelt T (eds) Handbook of chemical neuroanatomy, vol 3, Classical transmitters and transmitter receptors in the CNS, part II. Elsevier, Amsterdam, New York, Oxford, pp 409–439
15. Rössner W (1965) Stereotaktischer Hirnatlas vom Meerschweinchen. Pallas, München
16. Steinbusch HWM (1984) Serotonin-immunoreactive neurons and their projections in the CNS. In: Björklund A, Hökfelt T, Kuhar MJ (eds) Handbook of chemical neuroanatomy, vol 3, Classical transmitters and transmitter receptors in the CNS, part II. Elsevier, Amsterdam, New York, Oxford, pp 68–125
17. Szelényi Z, Hinckel P (1984) Improvement of cold- and heat-defence following electrolytic lesions of raphe nuclei in the guinea-pig. Pflügers Arch 402:R39
18. Szelényi Z, Zeisberger E, Brück K (1977) A hypothalamic alpha-adrenergic mechanism mediating the thermogenic response to electrical stimulation of the lower brain-stem in the guinea-pig. Pflügers Arch 370:19–23
19. Taylor DCM (1982) The effects of nucleus raphe magnus lesions on an ascending thermal pathway in the rat. J Physiol 326:309–318

Received July 15, 1986/Accepted January 30, 1987

Pflügers Arch (1987) 409:182–187

Pflügers Archiv
European Journal of Physiology
© Springer-Verlag 1987

Effects of prolactin on Na-K-ATPase activity along the rat nephron

L. Bussieres, K. Laborde, M. Dechaux, and C. Sachs

Département de Physiologie, C. H. U. Necker-Enfants Malades, 156 rue de Vaugirard, F-75730 Paris Cedex 15, France

Abstract. To test prolactin (PRL) action on osmoregulation in mammals, we evaluated in the rat the effect of this hormone on a major enzyme in renal regulation of water and electrolyte: renal Na-K-ATPase. Enzyme activity was determined by cytochemistry in medullary ascending limb (MAL) and distal convoluted tubule (DCT) from rats treated either by bromocriptine, or by PRL. Three hours after a bromocriptine injection (0.1 mg/100 g IP) a significant decrease of Na-K-ATPase activity is observed in both MAL (80% of control values, $p < 0.001$) and DCT (78%, $p < 0.01$). Reciprocally, a significant ($p < 0.001$) increase in enzyme activity is induced 3 h after a single PRL injection (140 µg/100 g IM), in both segments (MAL: 165%, DCT: 172% of control activities) and persists 6 h after the injection (MAL: 130%, DCT: 118%). Na-K-ATPase activity was correlated to plasma PRL levels ($r = 0.78$ in DCT, $r = 0.89$ in MAL). A direct effect of PRL on the tubule is suggested by results from experiments in which PRL, at various concentrations, is added in vitro on renal slices before Na-K-ATPase activity measurements. The increase in Na-K-ATPase activity exhibits a log-dose dependency with PRL concentration ($p < 0.01$) and is still observed when AVP antagonist is added before PRL incubation, ruling out the possible role of AVP contamination of PRL. These results suggest a direct effect of PRL on renal Na-K-ATPase in MAL and DCT.

Key words: Na-K-ATPase – Prolactin – Single nephron segment – Vasopressin

Introduction

One of the most and frequently reported functions of prolactin (PRL) is the regulation of membrane permeability to salt and water in different species. In lower vertebrates, PRL is an important osmoregulator, inhibiting sodium excretion in the fish when adapting from salt to fresh water environments [6, 36]. In higher vertebrates, PRL has been reported to be involved in renal salt and water conservation both in man [4, 8, 21] and in experimental animals [9, 24, 31], although the subject is still controversial [10, 26, 39]. In other respects, at the cellular level, investigations on the possible mechanism of PRL action have demonstrated activation of Na-K transport across such different epithelia as mammary gland [7, 18], amniotic membrane [23], and isolated toad bladder [14]. As Na-K-ATPase is an ubiquituous [22] key enzyme for Na transport it was tempting to speculate a role for PRL on the enzyme. To test whether such a mechanism could also apply to mammals, we examined in this study the effect of PRL on renal Na-K-ATPase activity in the rat. Results provide evidence for a specific effect of PRL on Na-K-ATPase activity in the medullary thick ascending limb of Henle's loop (MAL) and in the distal convoluted tubule (DCT) of the rat nephron, in a range of concentrations observed in some physiological situations.

Offprint requests to: K. Laborde

Methods

Animals

Experiments were performed on male Sprague-Dawley rats (Charles River Breeding Laboratories) weighing 150–200 g. All animals were fed a standard laboratory diet and had free access to tap water.

Experiment design

(a) In vivo studies. In this first set of experiments, the short time effects on renal Na-K-ATPase induced by modifications of the in vivo levels of circulating PRL were investigated: rats were subjected to a single injection either of bromocriptine, (IP 0.1 mg/100 g BW), or of ovine prolactin (oPRL) (IM 140 µg/100 g BW) and were sacrificed 3 or 6 h later. In bromocriptine experiments animals were also sacrificed 12 and 24 h after injection. Controls received the respective vehicles only. Bromocriptine solution was prepared by dissolving an equal weight of tartaric acid and bromocriptine (bromocriptine mesylate CB 154 Sandoz, Basel, Switzerland) in absolute alcohol, and adjusted with 0.9% saline to the desired concentration. Ovine PRL, (NIADDK, 30.5 UI/mg) was chosen for its lower arginine vasopressin (AVP) contamination (< 0.5% on a molar basis) and was first dissolved in 0.03 M NaH CO_3 in 0.15 M NaCl pH: 10.8; after solubilization, pH was adjusted to 7.5.

(b) In vitro studies. Animals were pretreated with bromocriptine (0.25 mg/100 g/12 h IP, 3 times), and sacrificed 3 h after the last injection. oPRL (at various concentrations) or AVP (10^{-12} M) were added afterwards during the in vitro procedure, both with or without previous incubation with an AVP antagonist (see later: preincubation).

All animals were killed by nitrogen asphyxiation at the same time in order to avoid diurnal variations. Blood was collected immediately prior to sacrifice from the abdominal aorta for PRL and aldosterone measurements and kidneys removed for Na-K-ATPase determination.

Enzyme determination

(a) Principle. In all studies (in vitro or in vivo), enzyme determination was made by quantitative cytochemistry, a method that allows in situ measurements of enzyme activities, directly at the cellular level. The procedure for measuring Na-K-ATPase activity was derived from the original one described by Chayen et al. [13], in which phosphate liberated from ATP forms a precipitate with a lead agent (lead ammonium citrate/acatete complex: LACA). This precipitate is quantified by scanning and integrating microdensitometry. This method which has previously been validated in our laboratory [38], gives results similar to those obtained by microdissection, and has shown to be highly reproductible. The differents steps of the procedure are described below.

(b) Tissue preparation. Immediately after sacrifice kidneys are removed, cut into segments and frozen to $-70°$ C in n-hexane which had been cooled by a surrounding bath of crushed solid carbon dioxide in methanol. These operating procedures have been shown to prevent water crystallisation in tissues [12]. The segments were stored at $-70°$ C until 8 µm sections were produced in a Bright low temperature cryostat fitted with an automatic cutting device. The cabinet temperature was maintained at $-25°$ C, and the knife cooled with solid carbon dioxide. Serial sections were transfered to glass slides and stored in the cryostat until they were assessed for ATPase activity (within 2 h). They were then surrounded by a plastic ring into which incubation media were successively poured.

(c) Preincubation. (1) Normally, a 40% (w/v) solution of Polypep (Sigma 5115) in 0.2 M Tris buffer (pH 7.5) was first added to each section for 10 min to remove free phosphate that otherwise could produce a background coloration.

(2) In in vitro studies, different hormones were added to the Polypep solution at this time: AVP (10^{-12} M) or oPRL (12.5; 125; 1250 ng/ml), and allowed to incubate (20 min) alone or after a 20 min incubation with a competitive AVP inhibitor (pressor antagonist d$(CH_2)_5$-D-Tyr-(Me) VAVP, antidiuretic antagonist d$(CH_2)_5$-D-Tyr (Et) VAVP) (80 ng/ml).

(d) Incubation. The preincubation medium is discarded by aspiration and immediately replaced by prewarmed (37° C) incubation medium. Total ATPase activity was measured in sections exposed to the following medium: 40% solution (w/v) of Polypep in 0.2 M Tris buffer containing sodium chloride (150 mM), magnesium sulphide (20 mM), potassium chloride (5 mM), vanadate-free ATP (16.5 mM), levamizole (1 mM) and lead ammonium citrate/acetate complex (32 mg/ml), final pH being adjusted to 7.5. Alternate sections were treated with the same reaction medium containing ouabain octahydrate (1 mM). Sections were exposed to the reaction medium for 15 min at 37° C and then washed in Coplin jars with cold 0.2 M Tris buffer (pH 7.5). They were finally immersed in hydrogen sulphide satured water (1 – 2 min) in order to reveal the brown lead phosphate precipitate. Subsequently they were rinsed several times with distilled water, allowed to dry, and mounted in Z5 medium.

All chemical reagents were purchased from Sigma, St. Louis, MO, USA.

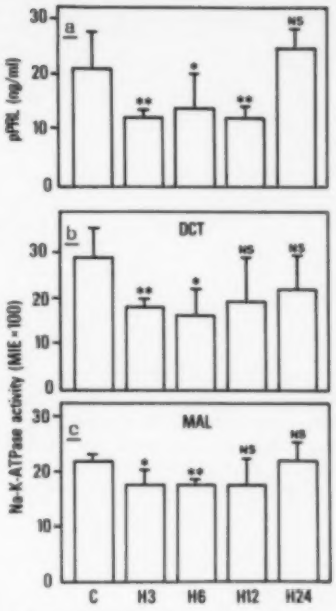

Fig. 1. Effect of in vivo bromocriptine injection (0.1 mg/100 g BW) on pPRL concentration (**a**), and Na-K-ATPase activity in MAL (**b**) and DCT (**c**). H_3, H_6, H_{12}, H_{24} represent hours between injection and sacrifice. Controls (*C*) received vehicle only. Number of rats studied was: H_3, H_6, H_{12}, H_{24}: 6; *C*: 18. Values are means ± SD. Comparison of bromocriptine injected rats and controls by unpaired *t*-test

(e) Scanning and integrating microdensitometry. Absorbance of the reaction product, at 485 nm wavelength was measured in situ by means of a Vickers M-85 microdensitometer with a ×40 objective. The area of the measuring field was 47.8 µm² and the diameter of the flying spot 0.5 µm in the plane of the section. The mask was precisely set over the tubule basal membrane. Absorbance values (MIE) recorded were normalized by reference to an internal absolute calibrated filter and expressed as percent of mean integrated extinction (% M.I.E.). Absorbance was measured in ten different DCT or MAL on each slice. By their coloration and cellular structure differences, it was very easy to discriminate PCT, DCT and MAL. Generally, for each rat, three slices without ouabain and three with ouabain were quantified, the mean computed and Na-K-ATPase activity (% MIE) was taken as the difference of the two means. Statistical comparisons were assessed by the Student's *t*-tests for paired and unpaired data (* $p < 0.05$, ** $p < 0.01$, *** $p < 0.001$).

(f) Aldosterone and prolactin determination. Aldosterone and prolactin were determined in the plasma of all rats. Blood was collected from the abdominal aorta in heparin-

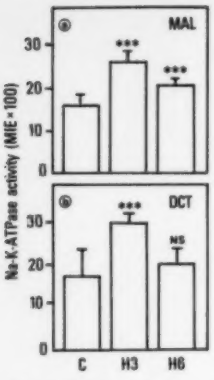

Fig. 2. Effect of in vivo oPRL injection (140 µg/100 g BW) on Na-K-ATPase activity in MAL (**a**) and DCT (**b**). H_3, H_6 represent hours between injection and sacrifice. Controls (*C*) received vehicle only. Number of rats studied was: H_3, H_6: 6; *C*: 12. Values are means ± SD. Comparison of oPRL-treated rats and controls by unpaired *t*-test

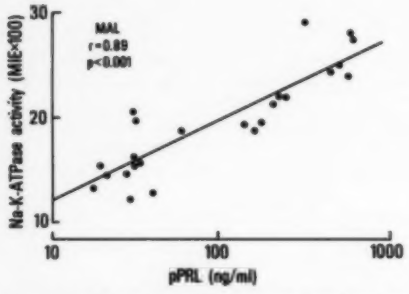

Fig. 3. In vivo oPRL injection: relationship between Na-K-ATPase activity in MAL and pPRL concentration

ized (for aldosterone) or EGTA (for prolactin) tubes, immediately prior to sacrifice. Aldosterone was measured by a modified Pham Huu Trung and Corvol radioimmunoassay [28]. Plasma ovine prolactin was measured by Kahn's radioimmunoassay (Lactation Laboratory I.N.R.A., Jouy-en-Josas, France). There was no cross-reaction between ovine prolactin and endogenous rat prolactin. Inter and intra assay variations are: 11% and 7% for aldosterone, 7% and 5% for PRL radioimmunoassays.

Results

In vivo experiments

Injections of bromocriptine (Fig. 1a) resulted in a significant fall in plasma PRL concentration (pPRL) (56%, 65% and 57% of control values 3, 6 and 12 h after injection respectively); pPRL levels did not differ from control values 24 h after the injection. Therefore in subsequent experiments when PRL secretion was to be inhibited, injections were repeated every 12 h. Plasma aldosterone concentration (PAC) was not affected by bromocriptine injection except 3 h after injection: 13.9 ± 7 (control), 27.5 ± 7 (3 h), 9.9 ± 1.8 (6 h), 11.9 ± 9.8 (12 h), 15.2 ± 7.6 ng/100 ml (24 h). The effect of bromocriptine injection on DCT and MAL Na-K-ATPase activity appeared to be similar in both segments: a significant ($p < 0.001$) decrease in Na-K-ATPase activity (80% in MAL, 78% DCT of control values) was observed 3 h after injection. Activity mimicked closely the PRL concentration pattern: the activity was still decreased 6 h after injection (MAL: 80%, DCT: 71%) and progressively normalized afterwards (Fig. 1b, c).

oPRL injection produced opposite effects: high pPRL levels were obtained: 22.4 ± 8 ng/ml (control); 517 ± 100 ng/ml (3 h); 200 ± 36 ng/ml (6 h), and in both segments activity increased respectively: 165% at 3 h and 130% at 6 h in MAL, 172% at 3 h and 118% at 6 h in DCT as compared to control values (Fig. 2). Moreover Na-K-ATPase activity was then well correlated to PRL levels ($r = 0.78$ in DCT, $r = 0.89$ in MAL) (Fig. 3) but not to aldosterone levels which were not affected by PRL injection (7.96 ± 3.75 ng/100 ml (controls); 10.5 ± 4.8 ng/100 ml (3 h); 11.05 ± 5.15 ng/100 ml (6 h).

In vitro experiments

In these experiments, all animals were first treated by bromocriptine in order to reduce circulating PRL (7.98 ± 4 ng/ml). Levels of 7.98 ± 4 ng/ml were thus produced. Renal Na-K-ATPase activity obtained under these conditions was low (MAL: 12.7 ± 4.5 (MIEX100), DCT: 16.1 ± 3.5 (MIEX100)]. Addition of oPRL in vitro, during preincubation (20 min), stimulated Na-K-ATPase activity in MAL and DCT (Table 1). In both segments, the increase was dose dependent (MAL $p < 0.01, r = 0.98$); (DCT $p < 0.01$, $r = 0.98$) (Fig. 4). In MAL, addition of 12.5 ng/ml oPRL was sufficient to induce a significative increase in enzyme activity ($p < 0.001$); in DCT, 125 ng/ml was necessary to produce the same effect. Addition of AVP (10^{-12} M) (Table 1) produced a similar effect on Na-K-ATPase activity, which was more striking in MAL (213% increase) than in DCT (155% increase). This effect was completely inhibited by addition of an AVP antagonist 20 min prior incubation with AVP. In contrast the increase in Na-K-ATPase activity induced by oPRL was not affected by prior addition of AVP antagonist (Fig. 5a, b).

Discussion

It is tempting to speculate for the existence of a renal function of PRL in mammals, similar to the osmoregulatory one well established in lower species. Indeed the conservation of the osmoregulatory sequence during evolution [19], the ability of the mammal molecule to exert significant osmoregulatory activities when injected into teleost [6], and the demonstration of specific renal receptors in mammal kidney [25] advocate in favor of this hypothesis. Unfortunately most studies have failed to demonstrate such an effect. Difficulties arise from two sets of facts: (1) the impossibility in the in vivo studies to discriminate between direct and indirect effects of PRL [16] and (2) the vasopressin like nature of the effects observed, which renders their specificity doubtful, especially as contamination of PRL preparation by antidiuretic hormones (AVP) has been extensively reported [10, 39]. By studying at the renal level the effect of PRL, the purpose of this work was to answer to the following questions: (1) has PRL any effect on renal Na-K-ATPase that could explain

Table 1. Influence of oPRL (12.5, 125, 1250 ng/ml) or AVP (10^{-12} M) in vitro addition on Na-K-ATPase activity. Activities are compared to activities obtained in absence of hormones addition. n = number of animals studied. Comparison between hormone-added slices and no hormone-added slices by paired t-test

PRL (ng/ml)		0	12.5	125	1250	0
AVP (M)		0	0	0	0	10^{-12}
	MAL	12.7 ± 4.5	$17.6 \pm 2.6^{**}$	$20.0 \pm 1^{***}$	$29.9 \pm 3.9^{***}$	$27.1 \pm 1^{***}$
Na-K-ATPase activity (MIEx100) mean ± SD	DCT	16.1 ± 3.5 $n = 12$	16.8 ± 4.9 NS $n = 12$	$23.4 \pm 3.7^{**}$ $n = 12$	$27.3 \pm 3.7^{***}$ $n = 12$	$25.0 \pm 1^{***}$ $n = 3$

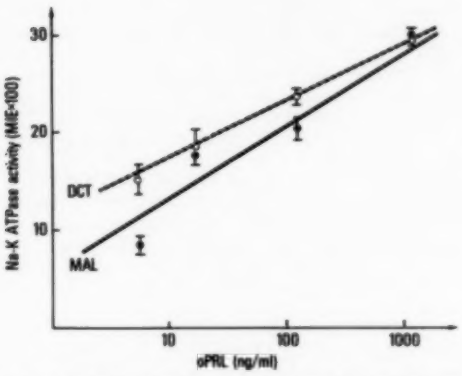

Fig. 4. Relationship between Na-K-ATPase activity in MAL (●) and in DCT (○) and the different concentrations of oPRL added in vitro (0, 12.5, 125, 1250 ng/ml). Values are means ± SD

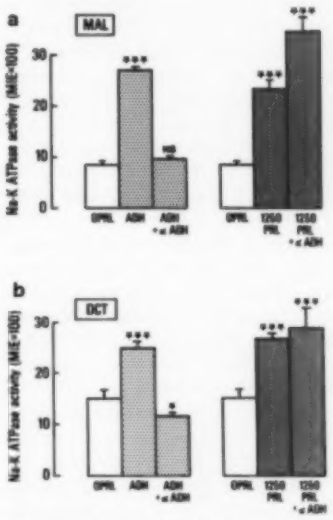

Fig. 5. Effects of oPRL and AVP addition in vitro on Na-K-ATPase activity in MAL (**a**) and DCT (**b**), with or without AVP antagonist (α ADH). Comparison between hormone-added slices and no hormone-added slices by paired t-test. Animals were treated prior sacrifice by three injections of bromocriptine

effects on renal ion transport? (2) Is this effect specific? (3) In which segment of the nephron and by which mechanism does PRL exert its action? (4) Is it consistent with a physiological role of this hormone on ionic transport?

Our first set of in vivo experiments shows that renal Na-K-ATPase activity can be affected by PRL: inhibition of PRL secretion results in a decrease in the enzyme activity and oPRL injection produces opposite effects. Moreover these changes in Na-K-ATPase activity are contemporary of PRL variation and correlated to the hormone levels.

However the specificity of this effect cannot be assessed firmly as many other parameters may interfere in this in vivo situation. This effect might have been produced by an indirect bromocriptine-dopamine agonist-aldosterone pathway or by the possible existence of AVP impurities in the PRL preparation. Effectively bromocriptine has dopamine agonist properties; aldosterone is under dopaminergic control [1, 11] and kidney Na-K-ATPase is regulated by aldosterone [22].

A better analysis of our in vivo results and mainly our in vitro experiments allows to rule out the different possibilities steming out from the above mentioned hypothesis.

Thus the observed changes in Na-K-ATPase activity could have been linked more to PAC than to PRL modifications. This latter hypothesis is ruled out by the absence of correlation between the decrease of Na-K-ATPase activity and the changes in aldosterone while the former is well correlated to PRL modifications. Dopamine itself could be responsible of the effect observed, as renal blood flow modifications [36] or direct tubular effect induced by this mediator have been demonstrated [5]. The restoration of Na-K-ATPase activity by in vitro addition of PRL demonstrates that this decrease in Na-K-ATPase activity induced by bromocriptine was due to PRL deficiency and not to dopamine action. Ultimately the stimulation of the enzyme by PRL could be secondary, due to an AVP contamination of the PRL preparation used. AVP addition produces similar stimulation of the enzyme in the same segments of the nephron. This effect of AVP on Na-K-ATPase has been recently reported although in MAL only, and with much lower AVP concentration [29]. However assuming a contamination of 2 mU AVP/mg powder, 12.5 ng/ml of PRL would correspond to 25×10^{-6} mU AVP/ml, a concentration far below the 10×10^{-3} mU AVP/ml necessary to cause partial antidiuresis [41]. Even more, preincubation with AVP inhibitor completely abolished AVP effect, but failed to have any influence on PRL action.

Therefore our study indicates MAL and DCT as preferential target segments for PRL. Despite systematic measurement of enzyme activity was not realized in PCT, previous works strongly suggested that this portion of the tube was not affected by PRL. This result was at variance with most

labelling studies [15, 25] that demonstrated that renal receptors to PRL were situated in proximal tubule. It should be noted that lower but specific binding was found in distal structures [15, 25] and autoradiographic techniques revealed a selective and prolonged localisation of purified PRL in MAL and DCT [17].

The mechanism of PRL action on the pump in these segments still must be further investigated. This study does not allow to discriminate between an increase in the number of pump units or an increase in catalytic site activity. PRL could exert its action directly through a mediator or indirectly by restoring a factor inhibited by bromocriptine. AVP is a wellknown AMPc activator and the increase in active Na reabsorption in MAL induced by the hormone in some species is linked to AMPc formation [32, 34], although the precise mechanism of Na-K-ATPase stimulation in this situation is still debated [35]. In contrast, the cellular mediator of PRL action is still unknown: AMPc is a poor candidate for the hormone action, at least in the mammary gland [33], as PRL would lead to a decrease in cellular AMPc content [27]. However it must be noted that some authors reported that prolactin induced stimulation of rat medullary adenylate cyclase in vitro [17].

The last question to be raised is the physiological importance of such action of PRL. The dose dependency experiment shows that in vitro addition of 12.5 ng/ml in MAL, and 125 ng/ml in DCT are sufficient to promote a significant enzyme activity. A recent study of Pippard et al. [30] demonstrated a similar effect of PRL on Na-K-ATPase but in a range of PRL concentration far below from $0.4 \cdot 10^{-4}$ to 0.4 ng/ml. Na-K-ATPase activity was also measured in this work by microdensitometry, but important differences in the incubation procedure may explain the discrepancy observed with our results. In vivo stimulated enzyme was studied with higher PRL levels (200 – 500 ng/ml) but still in the range observed during lactation and pregnancy in these species [40]. It is noteworthy that an increase in fractional Na reabsorption in MAL has been documented in pseudopregnant and pregnant rats with characteristic high PRL secretion [2, 3, 20]. We hypothesize that, in these situations, PRL could have an osmoregulatory role: by stimulating Na-K-ATPase activity, PRL could facilitate water and sodium reabsorption along the nephron.

Acknowledgements. The authors are grateful to Dr. Grouselle (College de France), Dr. Epelbaum (Inserm U 159), and Dr. Khan (INRA, Jouy-en-Josas) for performing prolactin determination. They are indebted to Dr. Doucet (College de France) for helpfull discussion. They also thank Mrs. R. Hernandez and Miss F. Briant for secretarial assistance. L. Bussieres is a student from Paris VI University (3e cycle d' Endocrinologie, Prof. P. Hemon).

References

1. Aguilera G, Catt KJ (1984) Dopaminergic modulation of aldosterone secretion in the rat. Endocrinology 114:176 – 181
2. Atherton JC (1983) Glomerular filtration rate and salt and water reabsorption during pregnancy in the conscious rat. J Physiol 334:493 – 504
3. Atherton JC, Bu'Lock D, Pirie SC (1982) The effect of pseudopregnancy on glomerular filtration rate and salt and water reabsorption in the rat. J Physiol 324:11 – 20
4. Baumann G, Marynick SP, Winters SJ, Loriaux DL (1977) The effect of osmotic stimuli on prolactin secretion and renal water excretion in normal man and in chronic hyperprolactinemia. J Clin Endocrinol Metab 44:199 – 202
5. Bello-Reuss E, Higashi Y, Kaneda Y (1982) Dopamine decreases fluid reabsorption in straight portions of rabbit proximal tubule. Am J Physiol 243:F634 – F639
6. Bern HA, Loretz CA, Bisbee CA (1980) Prolactin and transport in fishes and mammals. Prog Reprod Biol 6:166 – 171
7. Bisbee CA (1981) Prolactin effects on ion transport across cultured mouse mammary epithelium. Am J Physiol 240:C110 – C115
8. Buckman MT, Peake GT, Rubertson G (1976) Hyperprolactinemia influences renal function in man. Metabolism 25:509 – 516
9. Burstyn PGR (1978) Sodium and water metabolism under the influence of prolactin, aldosterone, and antidiuretic hormone. J Physiol 275:39 – 50
10. Carey RM, Johanson AJ, Seif SM (1977) The effects of ovine prolactin on water and electrolyte excretion in man are attributable to vasopressin contamination. J Clin Endocrinol Metab 44:850 – 858
11. Carey RM, Thorner MO, Ortt EM (1979) Effects of metoclopramide and bromocriptine on the renin-angiotensin-aldosterone system in man. J Clin Invest 63:727 – 735
12. Chayen J, Bitensky L (1981) Cytochemistry in the bioassay of hormones. J Clin Pathol 34:575 – 588
13. Chayen J, Forst GTB, Doods RA, Bitensky L, Pitchfork J, Baylis PH, Barrnet RJ (1981) The use of hidden metal captive reagent for the measurement of Na^+-K^+ATPase activity: a new concept in cytochemistry. Histochemistry 71:533 – 541
14. Dalton T, Snart RS (1969) Effect of prolactin on the active transport of sodium by the isolated toad bladder. J Endocrinol 43:VI – VII
15. Donatsch P, Richardson B (1975) Localisation of prolactin in rat kidney tissue using a double-antibody technique. J Endocrinol 66:101 – 106
16. Elkarib AO, Garland HO, Green R (1983) Acute and chronic effects of progesterone and prolactin on renal function in the rat. J Physiol 337:389 – 400
17. Evan AP, Palmer GC, Lucci MS, Solomon S (1977) Prolactin-induced stimulation of rat renal adenylate cyclase and autoradiographic localisation to the distal nephron. Nephron 18:266 – 276
18. Falconer IR, Forsyth IA, Wilson BM, Dils R (1978) Inhibition by low concentrations of ouabain of prolactin-induced lactogenesis in rabbit mammary-gland explants. Biochem J 172:509 – 516
19. Farmer SW, Papkoff H, Bewley TA, Nishioka RS, Bern HA, Li CH (1977) Isolation and properties of teleost prolactin. Gen Comp Endocrinol 31:60 – 71
20. Garland HO, Green R (1982) Micropuncture study of changes in glomerular filtration and ion and water handling by the rat kidney during pregnancy. J Physiol 329:389 – 409
21. Horrobin DF, Lloyd IJ, Lipton A, Burstyn PG, Durkin N, Muiruri KL (1971) Actions of prolactin on human renal function. Lancet 2:352 – 354
22. Katz AI (1982) Renal Na-K-ATPase: its role in tubular sodium and potassium transport. Am J Physiol 242:F207 – F219
23. Leontic EA, Tyson JE (1977) Prolactin and fetal osmoregulation: water transport across isolated human amnion. Am J Physiol 232:R124 – R127
24. Marshall S, Gelato M, Meites J (1975) Serum prolactin levels and prolactin binding activity in adrenals and kidney of male rats after dehydratation, salt loading, and unilateral nephrectomy. Proc Soc Exp Biol Med 149:185 – 188
25. Montjoy K, Cowden EA, Dobbie JW, Ratcliffe JG (1980) Prolactin receptors in the rat kidney. J Endocrinol 87:47 – 54
26. North WG, Gellai M, Sokol HW, Adler RA (1981) Demonstration that rat prolactin has no intrinsic antidiuretic activity in the rat. Horm Res 15:55 – 64
27. Perry JW, Oka T (1980) Cyclic AMP as negative regulator of hormonally induced lactogenesis in mouse mammary gland organ culture. Proc Natl Acad Sci USA 77:2093 – 2097
28. Pham Huu Trung MT, Corvol P (1974) Direct radioimmunoassay of plasma aldosterone. Steroids 24:587 – 594

29. Pippard C, Baylis PH (1984) The stimulation of Na-K-ATPase activity in the medullar of the rat kidney by (arginine) vasopressin and its analogues. Clin Sci 66:561–567
30. Pippard C, Baylis PH (1986) Prolactin stimulates Na-K-ATPase activity located in the outer renal medulla of the rat. J Endocrinol 108:95–99
31. Riley AL, Hagen TC, Stefaniak JE (1978) Effect of prolactin on glomerular filtration rate. Clin Sci 55:335–339
32. Rouffignac C De, Corman B, Roinel N (1983) Stimulation by antidiuretic hormone of electrolyte tubular reabsorption in rat kidney. Am J Physiol 244:F156–F164
33. Sapag-Hagard M, Greenbaum AL (1974) The role of cyclic nucleotides in the development and function of rat mammary tissue. FEBS Lett 46:180–183
34. Sasaki S, Imai M (1980) Effects of vasopressin on water and NaCl transport across the in vitro perfused medullary thick ascending limb of Henle's loop of mouse, rat, and rabbit kidneys. Pflügers Arch 383:215–221
35. Schlatter E, Greger R (1985) cAMP increases the basolateral Cl^- conductance in the isolated perfused medullary thick ascending limb of Henle's loop of the mouse. Pflügers Arch 405:367–376
36. Seri I, Aperia A (1986) Dopamine regulation of glomerular filtration rate and renal blood flow in young and adult rat. Helv Paediatr Acta 41:127
37. Singh SP, Singh TP (1984) Diurnal variations in prolactin secretion and serum Na^+ and K^+ concentrations in the Freshwater catfish Clarias batrachus. Ann Endocrinol (Paris) 45:137–141
38. Snarska J, Laborde K, Bachelet M, Bader C, Ulmann A (1983) Localisation par cytophotométrie de la Na-K-ATPase le long du néphron de rat. Néphrologie 4:94
39. Vorherr H, Vorherr UF, Salomon S (1978) Contamination of prolactin preparations by antidiuretic hormone and oxytocin. Am J Physiol 234:F318–F324
40. Walker J, Garland HO (1985) Single nephron function during prolactin-induced pseudopregnancy in the rat. J Endocrinol 107:127–131
41. Waters AK (1977) Augmentation of vasopressin antidiuresis by prolactin with a note on the contamination of international standard prolactin. J Endocrinol 75:435–436

Received March 17, 1986/Accepted January 13, 1987

Pflügers Arch (1987) 409:188–193

Pflügers Archiv
European Journal of Physiology
© Springer-Verlag 1987

Structural and functional response of the isolated toad skin to mucosal lithium

S. M. L. Sanioto[1] and A. Sesso[2]

[1] Institute of Biomedical Sciences, Department of Physiology and Biophysics, University of São Paulo, BR-05508, São Paulo, SP, Brazil
[2] School of Medicine, Molecular Pathology Laboratory, Department of Pathology, University of São Paulo, BR-01246, São Paulo, SP, Brazil

Abstract. Structural and functional changes induced by long-term Li-exposure of the outer surface of toad skin was studied. Electron microscopy revealed that total Na by Li replacement in the outer compartment of short-circuited toad skin promotes a conspicuous cellular damage expressed as focal swollen cells with altered intercellular spaces and nuclear morphology. Short-circuit current (SCC) decreases by about 70% over the first 60 min after 115 mmol/l Li-exposure. An amiloride sensitive transepithelial Li transport remains intact over a further 150 min despite the epithelial damage, indicating that the pathways across the apical barrier are functioning. Increase of the paracellular permeability is detected by elevation of Na-efflux. Partial 50% or 10% Na by Li replacements induce minor structural alterations and are not sufficient to trigger appreciable Na-efflux and SCC alterations. Therefore, low Li concentrations are less effective than 115 mmol/l in promoting morphofunctional responses. Although ouabain and Li reduce the SCC, ouabain does not promote structural lesions, showing that Li-inhibition of Na transport by itself is not responsible for the observed morphological alterations. In the light of this study, Li utilization as a tool to investigate transepithelial Na transport requires careful judgement.

Key words: Toad skin – Lithium – Na-transport – Ouabain

Introduction

In frog skin, Li enters the cell compartment, where it accumulates [13, 20, 21, 25], crossing by electrodiffusion the apical barrier via amiloride sensitive Na channels [3, 17, 20, 21, 23]. The mechanism of Li extrusion across the basolateral membranes is less clear [20, 31]. Li acts as an inhibitor of the Na, K-ATPase in microsomal preparations from frog skin [30] and rat kidney epithelia [12]. Therefore, it should not be effectively pumped in toad skin. It is unlikely that passive diffusion contributes significantly to Li transport across the basolateral membranes, considering the low Na permeability of this structure.

Previous results [1] have shown that total Na by Li replacement in the solution bathing the outer surface of toad skin under short-circuit conditions, promotes an unspecific permeability increase of the epithelium to Na, K and sucrose, suggesting an increase of the paracellular permeability. This effect is due to an intracellular action of this ion, since blockade of Li entrance into cells by amiloride, or long-term pretreatment with ouabain, prevents the Li induced increase of Na, K and sucrose permeabilities.

The present work was carried out to investigate a correlation between epithelial cell fine structure and the reported permeability increases induced by Li. The effects of total or partial Na by Li replacement in the outer bathing solution upon the short-circuit current (SCC), Na-efflux and the structure of the epithelium were analysed. A comparative study of the effect of ouabain and Li, both inhibitors of the Na, K-ATPase, upon the SCC and the fine structure of the epithelium was also performed.

Offprint requests to: S. M. L. Sanioto

Materials and methods

The studies were carried out in modified Ussing-Zerahn chambers, according to methods previously described [1, 4, 28, 32, 33]. Special precautions were taken to prevent interference of skin edge damage on isotope efflux by using hemichambers provided with a silicone grease gasket (High Vacuum Grease) located at the internal rim of the hemichamber in contact with the epithelial side of the skin. This precaution was necessary to measure the low levels of isotope efflux occuring in the present experiments. A nylon mesh in contact with the corial side was used to prevent skin stretching during changes of the solution in the outer compartment.

Abdominal skins of the toad *Bufo marinus ictericus* were used and the experiments were performed at room temperature (20–24° C). A voltage clamp unit was connected to the preparation through saturated KCl agar bridges and saturated KCl calomel half-cells (for voltage measurements) and Cu-$CuSO_4$ half-cells (for current passing).

For morphological observations, the experiments were performed in open- as well as in short-circuited paired half-skins of the same toad: one half-skin being the control of the Li-treated half-skin. The two half-skins were equilibrated for 120 min or more with NaCl-Ringer's solution on both sides. In the other, after equilibration, the outer solution was replaced by 115.0 mmol/l LiCl-Ringer's solution (100% LiCl-R), or by 57.5 mmol/l Li-NaCl-Ringer's solution (50% LiCl-R) or by 11.5 mmol/l Li-NaCl-Ringer's solution (10% LiCl-R), according to the protocol. 150 min elapsed before both half skins were fixed in the hemichambers with 1% glutaraldehyde and 1.5% paraformaldehyde buffered at pH 7.3 with 0.08 mmol/l sodium cacodilate at the tempera-

ture of ice. Fragments with 1–3 mm were cut and immersed for 120 min in a series of graded ethanol solutions and embedded in araldite. The skins were so oriented as to furnish sections perpendicular to the surface of the epithelium. For light microscopic studies, 0.5 μm thick sections were stained with azur A and methylene blue. Ultrathin sections were contrasted with uranyl acetate and lead citrate and analysed in a Zeiss E M 9 S 2 electron microscope.

For isotope measurements, experiments were carried out in short-circuited skins of different toads. An equilibration period of approximately 120 min or more with NaCl-Ringer's solution bathing both skin surfaces, elapsed before the addition of 100 μCi of 24-Na (Institute of Energetic and Nuclear Research, São Paulo, Brazil) to the solution bathing the inner skin surface (corial side). Every 5 min, the outer compartment solution was completely drained into counting vials for 24-Na assay by the Cerenkov effect [24], in a liquid scintillation counter (Beckman, Mod. L-S 8000). Short-circuit condition was maintained throughout the experiments, except for 5–10 s during drainage of the outer compartment. Collections from the outer compartment started immediately following addition of the isotope to the inner solution. After an equilibration period, long enough for the Na efflux to attain a stationary state, 10 control determinations of the Na efflux were carried out. Then, the outer bathing medium was replaced by LiCl or Li-NaCl-Ringer's solutions and the collections were performed.

Na-efflux is the efflux of sodium from the inner to the outer compartment calculated by the rate of 24-Na appearance in the outer compartment and the specific activity of sodium in the inner bathing solution.

Solutions used were (in mmol/l): NaCl-Ringer's solution (NaCl-R): NaCl 115.0, $KHCO_3$ 2.5, $CaCl_2$ 1.0: 100% LiCl-Ringer's solution (100% LiCl-R): LiCl 115.0, $KHCO_3$ 2.5, $CaCl_2$ 1.0; 50% Li-NaCl-Ringer's solution (50% LiCl-R): LiCl 57.5, NaCl 57.5, $KHCO_3$ 2.5, $CaCl_2$ 1.0; 10% Li-NaCl-Ringer's solution (10% LiCl-R): LiCl 11.5, NaCl 103.5, $KHCO_3$ 2.5, $CaCl_2$ 1.0. All solutions had pH 8.2 after aeration.

Drugs used were: Ouabain from Sigma Chemical Company, St. Louis, MO, USA; glutaraldehyde, paraformaldehyde, sodium cacodilate, osmium tetroxide, uranyl acetate, lead citrate, azur A, methylene blue and araldite from Ladd Industry, Inc., Burlington, Vermont, USA.

SCC and Na-efflux are presented as mean ± standard error and n is the number of experiments.

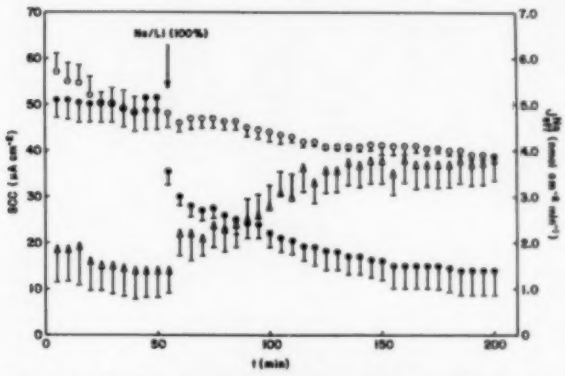

Fig. 1. Effect of substitution of NaCl-Ringer's solution by 100% LiCl-Ringer's solution in the outer compartment of toad skin mounted in an Ussing-Zerahn chamber upon the steady-state 24-Na-efflux (J^{Na}_{ml}) (△) (n = 5) and the short-circuit current (SCC) (●) in the Li-treated half-skins (n = 5) compared with the values of the SCC in the control half-skins (○) (n = 5). Inner bathing solutions were NaCl-Ringer's solutions

Results

Effect of 100% LiCl-Ringer's solution in the outer compartment upon SCC, Na-efflux and structure of the epithelium

Figure 1 shows the time course of the SCC in control and in Li-treated half-skins, and the values of Na-efflux before and after total Na by Li substitution in the outer bathing medium. This ionic replacement induces a decrease of the SCC with time, reaching a plateau (30% of the control values) 150 min after Li-exposure. Na-efflux starts to increase soon after the ionic replacement, reaching stabilization after 150 min with values 2.5-fold higher than the control ones.

Under light and electron microscopy, the epithelia exposed to 115 mmol/l LiCl-R during 150 min, show pro-

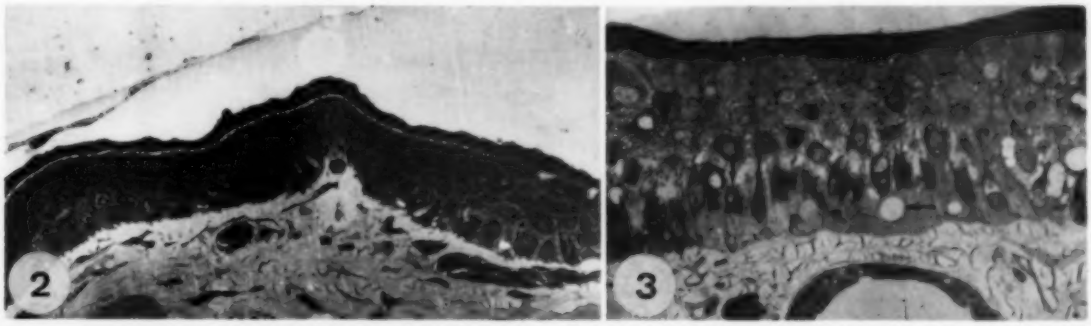

Fig. 2, 3. Semi-thin sections from control half-skin (2) and from long-term 115 mmol/l Li-treated half-skin (3). In all epithelial layers of the Li-exposed epithelium the cells appear swollen, thereby causing lowering of the density of the cytoplasm and an increase in the epithelium width. *Arrow* indicates a vacuole in the stratum germinativum cell layer. *Arrow head* points to a compressed cell nucleus (see also Fig. 5). *Vertical arrows* indicate hyperchromatic nuclei located on the apical pole of the cells of the innermost cell layer of the epithelium. (×480)

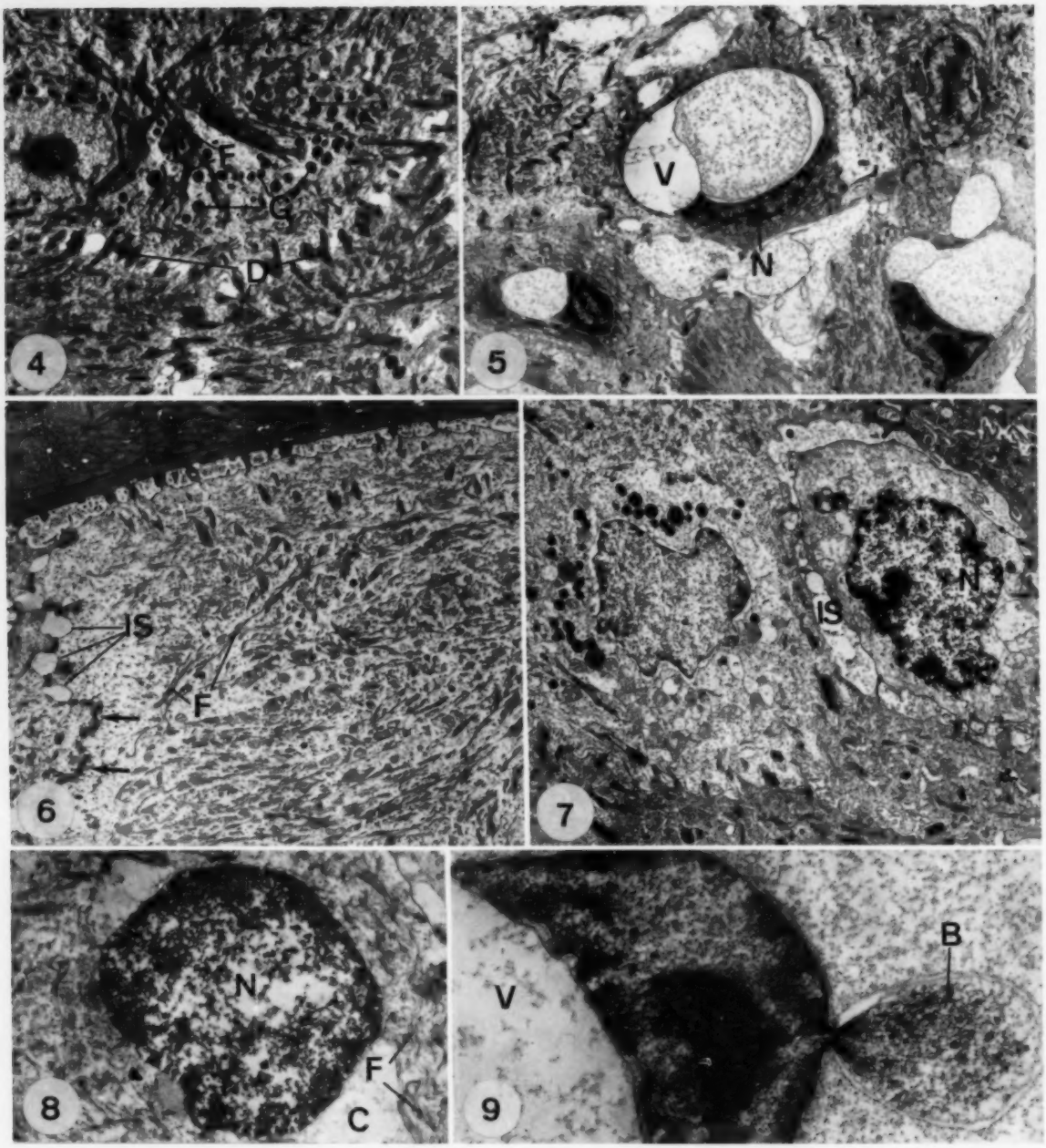

Fig. 4. Cells of the first cell layer of the stratum granulosum from control epithelium showing tonofilament bundles (*F*), electron-dense granules (*G*) and parallel disposed desmosamal plaques (*D*). (×5,700)

Fig. 5. Swollen cells in the stratum spinosum from 100% LiCl-Ringer's solution treated epithelium. Large-sized clear vacuole (*V*) displaces and compresses the cell nucleus (*N*) which shows demi-lune profile and electron-dense content. (×3,100)

Fig. 6. Swollen cells of the first cell layer of the stratum granulosum from 100% LiCl-Ringer's solution treated epithelium. Dispersed tonofilament bundles (*F*) Dilated intercellular spaces (*IS*). The lateral desmosomes (*arrows*) which normally are parallel to the stratum corneum, appear aligned orthogonally to this cell layer. Compare with Fig. 4. (×5,700)

Fig. 7. Dilated intercellular spaces (*IS*) and nucleus (*N*) with abnormal chromatin aggregation of stratum granulosum cells from 50% Li-NaCl-Ringer's solution treated epithelium. (×5,700)

Fig. 8. Altered chromatin material aggregation in nucleus (*N*) from a swollen stratum granulosum cell from 100% LiCl-Ringer's solution treated epithelium. (*C*) Perinuclear clear spaces. (*F*) Dispersed tonofilament bundles. (×9,600)

Fig. 9. Bleb (*B*) containing chromatin material from a nucleus compressed by a vacuole (*V*) in a cell of the stratum spinosum from 100% LiCl-Ringer's solution treated epithelium. (×12,600)

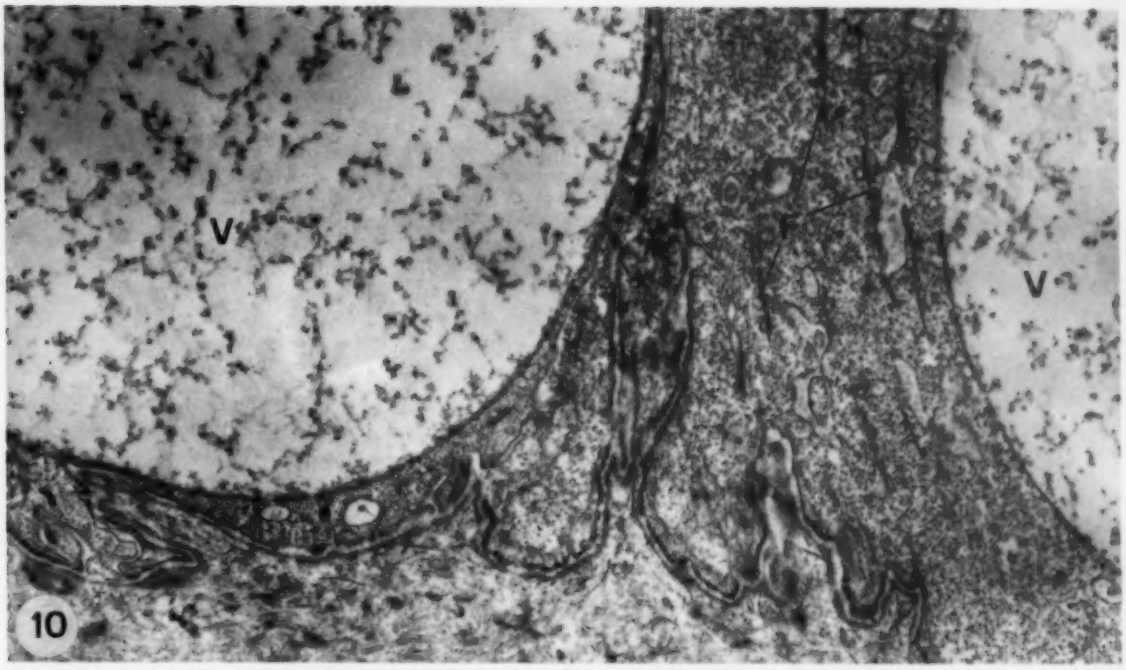

Fig. 10. Two epithelial basal layer swollen cells with dispersed tonofilament bundles (*F*) and large sized clear vacuoles (*V*) (as compared to arrows in Fig. 3). (×15,500)

nounced morphological alterations. Figures 2 and 3 show the light microscopic structure of control and 100% Li-treated epithelia, respectively. As compared to the control, the long-term Li-exposed epithelium is clearly edematous with markedly swollen and vacuolized cells in all cell layers. The swollen cells present cytoplasmic rarefaction with dispersed tonofilaments (Figs. 6 and 8) as compared to the cells of the control epithelium (Fig. 4). Consequent to cell swelling, an altered disposition of desmosomes is also seen (Figs. 6 and 8). Although small and large-sized clear vacuoles are observed in all cell layers, they are predominantly found in the spinosum (Figs. 5 and 9) and germinativum strata (Fig. 10). In these layers, the nuclei are occasionally located on the apical pole of the cells (Fig. 3) and frequently large-sized clear vacuoles compressed the cell nucleus which shows demi-lune profiles and marked electron-dense content (Fig. 5). Irregular nuclear profiles are common findings. Altered chromatin aggregations (Fig. 8) as well as nuclear blebs (Fig. 9) can be observed in all cell layers, suggesting cellular injury. Damaged epithelia present irregular and broadened intercellular spaces (Figs. 6 and 7). This pattern of lesion of the epithelia is similar in open- as well as in short-circuited skins undergoing long-term 115 mmol/l mucosal LiCl-R treatment.

Effect of 50% and 10% LiCl-Ringer's solutions in the outer compartment upon SCC, Na-Efflux and structure of the epithelium

These studies were performed in paired half-skins of the same toad. One half-skin was treated with 50% Li-NaCl-R, and the other with 10% Li-NaCl-R.

Although no appreciable alterations are observed in Na-efflux and SCC (Figs. 11a, b), under light and electron microscopy, these epithelia show proportionally minor and less frequent morphological alterations as compared to the epithelia treated with 100% LiCl-R. Figure 7 shows swollen stratum granulosum cells from 50% Li-treated skin.

Comparison of the effects of 10^{-3} mmol/l ouabain and 100% LiCl-Ringer's solutions upon SCC and structure of the epithelium

These experiments were carried out in paired half-skins of the same toad. After equilibration, the inner bathing solution of one half-skin was replaced by NaCl-R containing 10^{-3} mmol/l ouabain. At the same time, the outer bathing solution of the other half-skin was replaced by 100% LiCl-R.

As can be seen in Fig. 12, ouabain and Li induce a marked decrease of the SCC with time. The decrease induced by ouabain is greater than that observed with Li. In the Li-treated half-skins, the SCC attains within 150 min a stationary state at 30% of the control value. In the ouabain-treated half-skins, the SCC decreases steadly with time reaching values near zero within 150 min.

The fine structure of the ouabain-treated epithelia does not differ from those of the skins bathed with NaCl-R on both sides. In contrast, the Li-exposed epithelia show the pattern of lesions described above.

Discussion

The main finding of the present work is that long-term 115 mmol/l Li-exposure of the outer surface of short-circuited toad skin promotes both, conspicuous structural lesions of all cell layers of the epithelium and functional

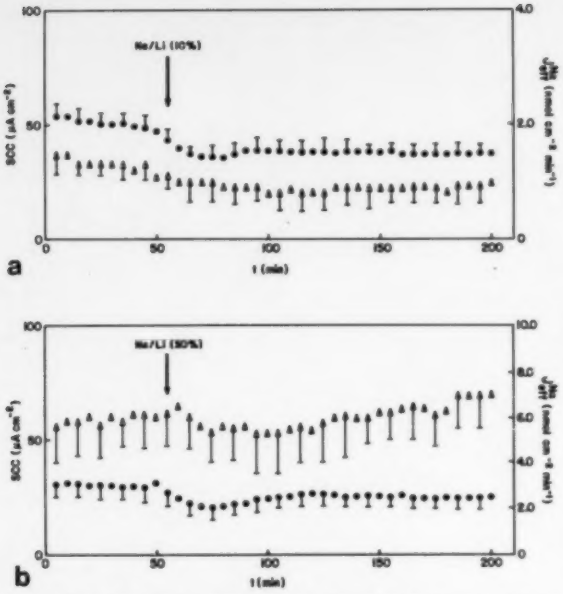

Fig. 11. Effect of substitution of NaCl-Ringer's solutions containing 10% (**a**) and 50% (**b**) Li replacing equimolar amount of Na in the outer compartment upon the steady-state of 24-Na-efflux (J^{Na}_{eff}) (△) and short-circuit current (SCC) (●). **a** ($n = 5$); **b** ($n = 5$). The inner bathing solution were NaCl-Ringer's solutions

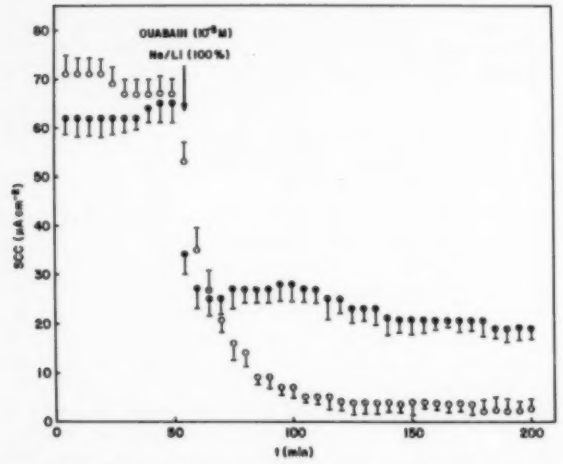

Fig. 12. Effect of substitution of NaCl-Ringer's solution in the outer compartment in the Li-treated half-skins (●) compared to the effect of 10 mmol/l ouabain in the inner NaCl-Ringer's solution in the other half-skins (○) upon short-circuit current (SCC). The Li-treated half-skins ($n = 5$) are bathed with NaCl-Ringer's solution at the inner surface. The ouabain treated half-skins ($n = 5$) are bathed with NaCl-Ringer's solution on both sides throughout the experiments

alterations. In contrast, 11.5 or 57.5 mmol/l Li-exposure induces focal structural changes with no detectable functional counterpart.

Li induced polyuria and vasopressin resistant diabetes insipidus have been associated with renal structural changes in man [2, 10, 14, 18] and rat [7, 8, 11, 15, 19, 22, 26] as well as in the isolated toad urinary bladder [9]. Such alterations are comparable to those described in the present work. The morphological changes predominantly described in distal tubule and collecting duct cells include general dilations of the tubules with variable epithelial cell swelling as consequence of cytoplasmic vacuolization as well as broadened and infiltrated intercellular spaces, nuclear polymorphism and hyperchromatism, eventually with nuclear pyknosis.

Our results show that total Na by Li replacement in the outer bathing solution induces pronounced epithelial alterations and suggest some relationship between functional and structural response. 115 mmol/l LiCl-R in contact with the mucosal side of the epithelium promotes a decrease of approximately 70% in the SCC. A stable SCC of 15 to 20 μA cm^{-2} continues for 90–150 min, or for hours, as described by other authors in amphibian epithelium [6, 16]. This positive SCC indicates a net transepithelial Li-flux from mucosa to serosa down its chemical gradient, as demonstrated in frog skin [16, 20, 27]. A previous report [1] had shown that this SCC is inhibitable by amiloride. This observation suggested that the pathway across the apical barrier is not severely affected by long-term Li-exposure, despite the pronounced structural alterations described in this paper.

Simultaneous to the decrease of SCC, Na-efflux increases in response to external Li. This Na-efflux increase does not occur via amiloride sensitive Na channels of the apical barrier, suggesting an opening of the paracellular pathway due to an action of Li ions upon intracellular structures [1]. Opening of the tight-junctions in response to Li seems to involve structural components of the cytoskeleton, particularly the microfilaments. Abnormal cytoplasmic aggregation of microfilaments was observed in rat renal collecting duct cells in the Li-induced polyuria [11]. Although the structure of the tight-junctions cannot be seen in thin section electron microscopy, our results show that long-term 115 mmol/l Li-exposure promotes morphological alterations in both, cell and intercellular spaces. These observations correlate with functional changes, suggesting that the Li-effects may result from altered cellular function. A very large number of metabolic, biochemical and clinical side effects of Li have been extensively reported in man and animals. However, the mechanisms by which Li alters cell function to induce these effects are still unknown.

The degree of Li induced structural alterations appears to depend on the Li concentration in the solution bathing the mucosal surface of the skins. Partial Na by Li substitution is not sufficient to trigger an increase of the Na-efflux and a decrease of SCC. In contrast, when KCl-Ringer's solution was used as outer bathing medium, 10% K by Li substitution induces an increase of the paracellular permeability, as reported previously [1]. It was already mentioned that Li-induced polyuria in rats, and severe Li-intoxication in man and animals, correlate with morphological renal lesions. It is of interest to remember that during administration of Li to animals or man, although systemic Li levels remain low, elevated concentrations can be found along the nephron, specially in the terminal segments. These Li-effects can be prevented by a high NaCl intake [29]. Our results show that, in the presence of NaCl, long-term 11.5 or 57.5 Li-exposure is less effective in promoting structural and functional alterations. Therefore, these observations, apart from suggesting that Na could prevent the Li-induced permeability increase and the active transepithelial Na transport inhibi-

tion, support the idea of a competition between Na and Li ions for a common pathway or entrance mechanisms, as described in amphibian skin [5, 20, 23].

The movement of Li across the isolated amphibian skin resembles in many aspects the transepithelial Na transport. Although Li can be used as a Na substitute in the amiloride sensitive Na channels of the apical membranes from frog skin [20, 21, 25], it does not act as a Na substitute on the Na, K-ATPase from basolateral membranes of frog skin [30] and rat kidney [12].

Our results show that ouabain and Li, both inhibitors of the Na, K-ATPase, promote decrease of the SCC, ouabain being more effective than Li. However, whereas ouabain does not alter the epithelial structure, Li has a striking morphological effect. This indicates that Na transport inhibition by itself is not responsible for the structural alterations.

Due to Li effects on structure and function of the toad skin described in the present and previous studies [1], the use of Li as a tool to investigate the mechanisms of transepithelial Na transport should be undertaken with care in many experimental approaches.

Acknowledgements. We are specially grateful to Prof. F. Lacaz-Vieira for helpful discussions and criticism of our manuscript. We would also like to thank Prof. G. Malnic for carefull revision of the text. We thank Mr. Helio Correa, Mr. Roberto Vieira and Mrs. Tarcira Magali P. Martins for the skilfull technical assistance. Mr. Roberto S. do Nascimento performed the illustrations and Mr. Wilson Roberto C. Azevedo the photographic work. This study was supported by the grants of FAPESP 84/1374-7 and FINEP B-76-81258.

References

1. Aboulafia J, Sanioto SML, Lacaz-Vieira F (1983) Cellular Li opens paracellular path in toad skin: amiloride blockable effect. J Membr Biol 74:59–65
2. Aurell M, Svalander C, Allin L, Alling C (1981) Renal function and biopsy findings in patients on long-term lithium treatment. Kidney Int 20:663–670
3. Benos DJ, Mandel LJ, Simon SA (1980) Cationic selectivity and competition at the sodium entry site in frog skin. J Gen Physiol 76:233–247
4. Bevevino LH, Lacaz-Vieira F (1982) Control of sodium permeability of the outer barrier in toad skin. J Membr Biol 66:97–107
5. Biber TUL, Curran PF (1970) Direct measurement of uptake of sodium at the outer surface of the frog skin. J Gen Physiol 56:83–99
6. Candia OA, Chiarandini DJ (1973) Transport of lithium and rectification by frog skin. Biochim Biophys Acta 307:578–589
7. Christensen S, Hansen BB, Faarup P (1982) Functional and structural changes in the rat kidney by long-term lithium treatment. Renal Physiol 5:95–104
8. Evan AP, Ollerick DA (1972) The effect of lithium carbonate on the structure of the rat kidney. Am J Anat 134:97–106
9. Fernandez-Repollet E, LeFurgey A, Hardy MA, Tisher CC (1983) Structural and functional response of toad urinary bladder to LiCl. Kidney Int 24:719–730
10. Forrest JM Jr, Cohen AD, Torretti J, Himmelhoch JM, Epstein FH (1974) On the mechanism of lithium-induced diabetis insipidus in man and rat. J Clin Invest 53:1115–1123
11. Forrest JM Jr, Marcy TW, Biemesderfer D, Kashgarian M (1981) Cytoskeletal defect in cortical collecting duct cells in lithium-induced polyuria. Kidney Int 19:200
12. Gutman Y, Hochman S, Wald H (1973) The differential effect of Li on microsomal ATPase in cortex, medulla and papilla of the rat kidney. Biochim Biophys Acta 298:284–290
13. Hansen HH, Zerahn K (1964) Concentration of lithium, sodium and potassium in epithelial cells of the isolated frog skin during active transport of lithium. Acta Physiol Scand 60:189–196
14. Hestbech J, Hansen HE, Amdisen A, Olsen S (1977) Chronic renal lesions following long-term treatment with lithium. Kidney Int 12:205–213
15. Hestbech J, Olesen OV, Thomsen K (1978) Lithium-induced focal interstitial fibrosis in rat kidney. Acta Pathol Microbiol Immunol Scand 36:195–197
16. Hughes MP, Macknight ADC (1982) Cellular lithium and transepithelial transport across toad urinary bladder. J Membr Biol 70:69–88
17. Hullin RP (1975) The effects of lithium on electrolyte balance and body fluids. In: Johnson FM (ed) Lithium research and therapy. Academic Press, London, pp 359–379
18. Jørgensen F, Larsen S, Spanager B, Clausen E, Tango M, Brinch E, Brun C (1984) Kidney function and quantitative histological changes in patients on long-term lithium therapy. Acta Psychiatr Scand 70:455–462
19. Kling MA, Fox JG, Johnston SM, Tolkoff-Rubbin NE, Rubin RH, Colvin R (1984) Effects of long-term lithium administration on renal structure and function in rats. A distinctive tubular lesion. Lab Invest 50:526–535
20. Leblanc G (1972) The mechanism of lithium accumulation in the isolated frog skin epithelium. Pflügers Arch 337:1–18
21. Li JHY, Lindemann B (1982) Movement of Na and Li across the apical membrane of frog skin. In: Emrich JBA, Lux HH (eds) Basic mechanisms in the action of lithium. Excerpta Medica, Amsterdam, pp 23–35
22. MacAuliffe WG, Olesen OV (1983) Effects of lithium on the structure of the rat kidney. Nephron 34:114–124
23. Morel F, Leblanc G (1975) Transient current changes and Na compartmentalization in frog skin epithelium. Pflügers Arch 358:135–157
24. Moyer BJ (1962) A survey of Cerenkov counter technique. In: Snell AH (ed) Nuclear instruments and their uses, vol 1. Wiley and Sons, New York, pp 166–193
25. Nagel W (1977) Influence of lithium upon the intracellular potential of frog skin epithelium. J Membr Biol 37:347–359
26. Nørgaard T, Faarup P, Hansen BB, Kristensen AR, Christensen S (1985) Correlation between distal nephron enzyme activity structure and function in rats during lithium plus neuroleptic treatment. Renal Physiol 8:50–61
27. Reinach PS, Candia OA, Siegel GJ (1975) Lithium transport across isolated frog skin epithelium. J Membr Biol 25:75–92
28. Sanioto SML, Aboulafia J (1985) Lack of PCMB action upon the outer barrier sodium permeability in the absence of Na in toad skin. Pflügers Arch 403:115–119
29. Schou M (1958) Lithium studies. I. Toxicity. Acta Pharmacol Toxicol 15:70–84
30. Siegel GJ, Tormay A, Candia OA (1975) Microsomal (Na-K)-activated ATPase from frog skin epithelium: cation activations and some effects of inhibitors. Biochim Biophys Acta 389:557–566
31. Ussing HH (1960) The frog skin potential. J Gen Physiol 43:135–147
32. Varanda WA, Lacaz-Vieira F (1978) Transients in toad skin: short-circuit current and ionic fluxes related to inner sodium substitution by monovalent cations. J Membr Biol 39:369–385
33. Varanda WA, Lacaz-Vieira F (1979) Transient potassium fluxes in toad skin. J Membr Biol 49:199–233

Received July 24/Accepted December 8, 1986

Pflügers Arch (1987) 409:194–199

Pflügers Archiv
European Journal of Physiology
© Springer-Verlag 1987

Amiloride-sensitive sodium transport of the rat distal colon during early postnatal development *

J. Pácha, M. Popp, and K. Čapek

Czechoslovak Academy of Sciences, Institute of Physiology, CS-142 20 Prague 4 – Krč, Vídeňská 1083, Czechoslovakia

Abstract. To evaluate developmental changes in colonic sodium transport, the sensitivity of the transepithelial potential and short-circuit current to amiloride was investigated. The amiloride-sensitive short-circuit current (I_{sc}^{Na}), which represents the electrogenic sodium transport through Na^+ channels, rose significantly from day 5, reached a peak on day 10, and entirely disappeared after weaning. The maximum rate of electrogenic, amiloride-sensitive sodium transport was 12.0 μEq/cm² · h. The I_{sc}^{Na} was suppressed by adrenalectomy and/or premature weaning but not by a mineralocorticoid antagonist, spironolactone. On the contrary, treatments which increase aldosterone levels in vivo (low-sodium diet, furosemide-induced natriuresis, high dietary intake of potassium) stimulated the I_{sc}^{Na}. The effect of adrenalectomy increased during postnatal development. The sensitivity of I_{sc}^{Na} to aldosterone was highest at the end of the weaning period. High-sodium diet, which causes a decrease in circulating aldosterone, was associated with a partial inhibition of I_{sc}^{Na} ($P < 0.016$). These data suggest that the distal colon of neonatal rats can transport sodium via an electrogenic, amiloride-sensitive mechanism and that adrenocortical hormones exert the main regulatory control of this pathway.

Key words: Sodium transport – Amiloride – Colon – Rat – Ontogeny

Introduction

It is generally accepted that during the early postnatal period, major developmental changes of transport, enzymology and cellularity occur in most parts of the mammalian gastrointestinal tract. These maturation events and their underlying mechanisms have been investigated predominantly in the small intestine [17], whereas relatively little attention has been paid to developmental changes in the colon. Studies on the new-born pig have demonstrated that the proximal colon ceases to transport neutral amino acids [28] and that the distal colon begins to transport sodium via an electrogenic, amiloride-sensitive mechanism [7]. The development of this mechanism is dependent on aldosterone and can be blocked through the action of aldosterone antagonist canrenoate [10]. Several studies indicate that the immature rat colon also undergoes both enzymatic and absorptive changes during the suckling and weaning periods [3, 16, 26], but there are few data concerning sodium transport [11]. We, therefore, decided to investigate the development of sodium transport and the influence of adrenal hormones that are traditionally associated with maturation of the digestive tract [17]. The rat distal colon was chosen because in adult animals gluco- and mineralocorticoids not only increase the total capacity of sodium transport but also induce changes of the transport mechanism in this segment of large intestine. They suppress that part of sodium absorption which is predominantly electroneutral and insensitive to amiloride [4, 13] and induce a new sodium transport system that is electrogenic and amiloride-sensitive and is responsible for the amiloride-sensitive short-circuit current [25, 31, 33]. The cellular mechanism of this electrogenic system is well understood and has been recently reviewed by Schultz [27].

The present work was undertaken to examine the developmental changes of the sodium transport and to see what role, if any, adrenal hormones might play in controlling the early postnatal sodium transport by the rat distal colon.

Methods

Experiments were performed on young or adult male Wistar rats that were provided with a standard diet (1% NaCl), low-sodium diet (0.15% NaCl) and high-sodium diet (8% NaCl), respectively, and tap water ad libitum. The day of birth was regarded as day 0. Approximately 24 h post partum all litters were reduced to 8 or 9 pups. Each litter was housed with the mother until day 30 when weaning was completed by removal her.

The rats were killed by decapitation and their abdominal cavities were opened by mid-line incision for exposure of the large intestine. The distal colon was dissected just above the pelvic brim (length 15 mm) and cleaned using Ringer's solution. After stripping off the serosa and muscularis propria, the mucosa with portions of submucosa was mounted in an Ussing chamber (surface area 3.14 mm²) bathed on both sides with Ringer's solution at 37° C and continuously oxygenated (95% O_2 + 5% CO_2). The solution contained (in mmol/l): Na^-, 140.0; K^+, 5.2; Ca^{2+}, 1.2; Mg^{2+}, 1.2; Cl^-, 119.8; HCO_3^-, 25.0; HPO_4^{2-}, 2.4; $H_2PO_4^-$, 0.4; glucose, 10.0 (pH 7.4). To obtain a good electrical seal, the inside

* Parts of this study have been presented at the 6th Symposium on Developmental Pharmacology, Schloss Reinhardsbrunn 1986

Offprint requests to: J. Pácha at the above address

faces of both half chambers were covered with a layer of silicone grease and gently pressed together.

The tissues were short-circuited with a voltage clamp device, using saturated, calomel half-cells connected to the bathing solution compartments through agar bridges and Ag/AgCl electrodes immersed directly into the bathing solutions. Both the series resistance of the bathing solution between the potential electrodes and the tissue, and the potential electrode asymmetry were automatically compensated. The short-circuit current (I_{sc}) and transepithelial potential (PD) were monitored on a pen recorder. The tissue was continuously short-circuited, except when the external circuit was opened in order to provide measurements of the instantaneous PD. The transepithelial resistance was calculated from the PD and I_{sc}. Amiloride, a specific blocker of sodium channels, was added to the mucosal side of the tissue to reach a final concentration of 10^{-4} mol/l.

The study comprised 7 series of experiments. In the first series, 73 pieces of distal colon were used to test wether the I_{sc} was as sensitive to amiloride during the early postnatal period, compared as in adult rats. The amiloride-sensitive I_{sc} (I_{sc}^{Na}) was calculated as ($I_{sc} - I_{sc}^{R}$), where I_{sc}^{R} represents the amiloride-insensitive part of I_{sc}. In some experiments ($n = 29$), the effect of sodium removal on I_{sc} was observed. Na-free solution was prepared by equimolar substitution of all the Na^+ with choline.

In series 2 ($n = 42$), we tested the effect of adrenalectomy on the I_{sc}^{Na} in 12, 18, and 28-day-old rats. Bilateral adrenalectomy or a sham operation were performed through a dorsal incision under ether anaesthesia on postnatal day 9, 15, and 25. The pups were returned to their mothers after operation.

In series 3 ($n = 13$), adrenalectomy was combined with premature weaning. Adrenalectomy was performed on day 15 and premature weaning on day 16. I_{sc}^{Na} was measured on day 18.

In series 4 ($n = 85$), spironolactone, a competitive mineralocorticoid antagonist, was used to determine the mode of corticosteroid regulation of colonic sodium transport. Spironolactone was administered by intraperitoneal injections (20 mg/kg per day) or by stomach tube (75 mg/kg per day) for 4 days from day 1 or 14 after birth. The I_{sc}^{Na} was measured 24 h after the last administration.

In series 5 ($n = 8$), 15-day-old animals were fed a high-sodium diet for 14 days in order to decrease the plasma level of aldosterone. The sensitivity of colon to amiloride (I_{sc}^{Na}) was investigated on day 30.

In series 6 ($n = 8$), distal colons of 20-day-old rats were used to test the effect of anion substitution on the I_{sc}. After the electrical parameters had reached a steady-state in the normal Ringer's solution, this solution was replaced by the chloride-free solution (SO_4-Ringer), which was composed of (in mmol/l) Na^+, 140.0; K^+, 5.2; Ca^{2+}, 1.2; Mg^{2+}, 1.2; SO_4^{2-}, 59.9; HCO_3^-, 25.0; HPO_4^{2-}, 2.4; $H_2PO_4^-$, 0.4; glucose, 10.0; and mannitol, 55.0.

In series 7 ($n = 56$), we evaluated the effect of mineralocorticoids on rat colonic sodium transport. In order to raise aldosterone levels in vivo a low-sodium diet, furosemide-induced natriuresis, or high dietary intake of potassium were employed. The low-sodium diet was given immediately after birth. Furosemide (30 mg/kg per day, i.p.) was administered for 4 days prior to the experiment. The potassium intake was increased by replacing drinking water by a 1% KCl solution from day 23 to 30 when I_{sc}^{Na} was measured.

Chemicals of highest grade purity were purchased from Sigma (St. Louis, MO, USA) and Labora (Brno, Czechoslovakia). Amiloride was obtained from Merck, Sharp & Dohme (Hoddesdon, GB), spironolactone (Aldactone) from Boehringer (Mannheim, FRG), and furosemide from Spofa (Prague, Czechoslovakia).

All data are expressed as means ± SEM. Statistical analysis was performed using the unpaired Student's t-test. A value of $P < 0.05$ was accepted to indicate statistical significance.

Results

In series 1, distal colons taken from young rats of different ages were used to investigate the transepithelial electrical properties (Table 1) and to test their sensitivity to amiloride (Fig. 1). Comparing the tissue resistance of adult rats in Table 1 with that found in the adult distal colon measured in larger chambers [25, 31–33], it is obvious that the small diameter of our chamber did not lead to tissue damage. The total I_{sc} measured in the absence of amiloride increased throughout the first 20 days of postnatal life, decreased from day 20 until 35 and then remained stable. In contrast with adult rats, the distal colon of young animals was sensitive to amiloride during the suckling and weaning periods. I_{sc}^{Na} rose significantly after birth, reached its peak on day 10 and entirely disappeared after weaning. I_{sc}^{R} increased sharply from the 10th day to reach the adult value on day 20. Replacement of sodium with choline resulted in a marked reduction in I_{sc} of amiloride-treated colons, so that a negligible or negative I_{sc} were recorded. This electrogenic, amiloride-insensitive I_{sc} which represents electrogenic, amiloride-insensitive sodium absorption [4] followed the developmental pattern for I_{sc}^{R} (Table 2).

In adulthood, sensitivity of the rat distal colon to amiloride can be induced by corticosteroids and therefore, the effect of adrenalectomy on I_{sc}^{Na} was tested in series 2. The sham operation per se did not decrease I_{sc}^{Na}. However, adrenalectomy suppressed it substantially (Fig. 2). This finding indicates that adrenocortical hormones represent the principal factor determining colonic electrogenic sodium transport during early postnatal life.

Comparing the I_{sc}^{Na} of sham operated and adrenalectomized animals (Fig. 2), a substantial increase of the inhibiting effect of adrenalectomy is evident during postnatal development. In series 3, we, therefore, tested whether milk intake interferes with the effect of adrenalectomy. As is shown in Fig. 2, weaning may influence the I_{sc}^{Na} in sham operated and adrenalectomized animals ($P < 0.05$). The finding that I_{sc}^{Na} fell after premature weaning and that milk contains glucocorticoids [20] might explain the quantitative differences of the effect of adrenalectomy on I_{sc}^{Na} at various ages and indicates the significance of milk for the control of sodium transport in the gastrointestinal tract.

To distinguish whether mineralo- or glucocorticoids are responsible for the electrogenic, amiloride-sensitive sodium transport, the capacity of spironolactone for inhibiting I_{sc}^{Na} in 5 and 18-day-old rats was examined in series 4 (Table 3). Our data showed that the I_{sc}^{Na} was not decreased by spironolactone even if we used usual doses and modes of administration, rather that spironolactone might increase I_{sc}^{Na} in a dose-dependent manner.

Table 1. Developmental patterns for electrical properties of distal colon from young and adult rats

Parameter	Age (days)					
	5	10	20	30	50	Adult
Transepithelial potential (mV)	3.8 ± 0.6	5.7 ± 2.4	7.4 ± 1.1	4.6 ± 0.6	9.6 ± 1.0	9.4 ± 0.7
Short-circuit current ($\mu A/cm^2$)	82 ± 17	163 ± 15	224 ± 34	147 ± 23	84 ± 8	74 ± 6
Tissue resistance ($\Omega \cdot cm^2$)	48 ± 5	52 ± 6	38 ± 2	45 ± 5	114 ± 14	129 ± 9
n	15	6	15	13	9	10

Values are means ± SEM; *n* = number of animals

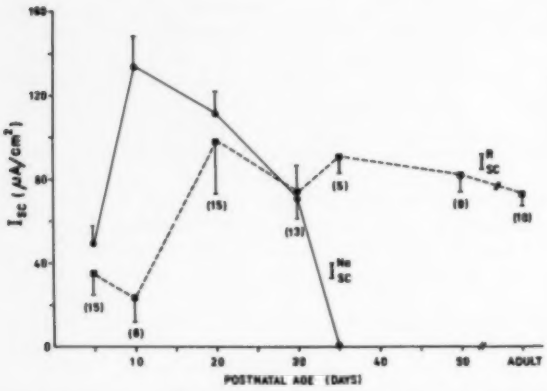

Fig. 1. Developmental patterns for the amiloride-sensitive (I^{Na}_{sc}, ——) and the amiloride-insensitive short-circuit current (I^{R}_{sc}, – – –). Values are given as means ± SEM. Numbers of animals are given in parentheses

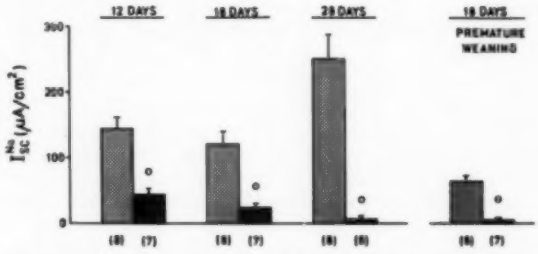

Fig. 2. Amiloride-sensitive short-circuit current (I^{Na}_{sc}) of the rat distal colon 3 days after adrenalectomy (*dark columns*), or sham operation (*dotted columns*). The operations were performed on day 9, 15, and 25, respectively, and the animals were either kept with their lactating dams or prematurely weaned on day 16. Values are given as means ± SEM. Numbers of animals investigated are indicated in parentheses. (○) Values significantly different ($P < 0.05$) from sham operated animals. The I^{Na}_{sc} of the prematurely weaned, adrenalectomized rats was significantly different ($P < 0.05$) from that of the adrenalectomized 12- and 18-day-old animals

Table 2. Development of electrogenic, amiloride-insensitive sodium transport in the distal colon of rat

Age	5	10	20	30	Adult
${}_{R}I^{Na}_{sc}$	19 ± 7	84 ± 13	116 ± 9	136 ± 14	70 ± 7
n	6	5	7	5	6

Values are means ± SEM, *n* = number of animals. ${}_{R}I^{Na}_{sc}$ was calculated as ($I^{R}_{sc} - I^{F}_{sc}$), where I^{R}_{sc} represents the amiloride-insensitive part of I_{sc} and I^{F}_{sc} the value of I_{sc} after replacement of NaCl-Ringer with a sodium-free solution. ${}_{R}I^{Na}_{sc}$ in $\mu A/cm^2$

In series 5, we tested, whether a lower plasma level of aldosterone might change the electrogenic, amiloride-sensitive sodium transport (Table 4). In this set of experiments the animals were provided with a high-sodium diet under which circulating aldosterone was decreased [9]. The results indicated that high-sodium intake was associated with a partial inhibition of I^{Na}_{sc} ($P < 0.016$), however, the effect of adrenalectomy was more pronounced.

To test whether sodium absorptive capacity is maximal under basal conditions the effect of chloride-free Ringer's solution on I^{Na}_{sc} was examined in series 6. The replacement of chloride by sulphate stimulated the electrogenic sodium absorption (Fig. 3) to the similar extent as in the adult colon [25, 30]. The substitution of sulphate for chloride caused an elevation of I_{sc} (+109 ± 18%) as well as I^{Na}_{sc} (+165 ± 27%). The electrogenic, amiloride-sensitive sodium transport was increased from 4.7 $\mu Eq/cm^2 \cdot h$ to 12.0 $\mu Eq/cm^2 \cdot h$ in 20-day-old rats.

The last series of experiments comprised experiment in which we attempted to define the significance of aldosterone for the regulation of sodium absorption in the early postnatal life. As the electrogenic sodium transport in young rats was not maximal under basal conditions, we tried to stimulate the electrogenic sodium absorption in further experiments by procedures known to elevate plasma levels of aldosterone [22, 29, 31]. A high dietary intake of potassium or furosemide increased the amiloride-sensitivity of the descending colon of 20 and 30-day-old rats (Table 5). The low sodium diet elevated the I^{Na}_{sc} in 30-day-old rats, but was without significant effect on younger or older animals (Fig. 4) although furosemide was able to increase the I^{Na}_{sc} in younger (Table 5), as well as adult rats [33].

Discussion

We used amiloride for estimating the contribution of sodium transport to the electrogenic behaviour of colonic epithelium

Table 3. Effect of spironolactone on amiloride-sensitive short-circuit current (I_{sc}^{Na}) in the distal colon of young rats

Age	I_{sc}^{Na} (μA/cm²)				
	Group A		Group B		Intact
	Spironolactone	Saline	Spironolactone	Saline	
5-day-old rats	109 ± 16 (6)*	62 ± 13 (7)	68 ± 10 (9)	69 ± 15 (9)	50 ± 8 (15)
18-day-old rats	177 ± 18 (9)*,**	100 ± 14 (9)	106 ± 27 (7)	112 ± 25 (5)	109 ± 15 (9)

Values are means ± SEM; numbers of animals are shown in parentheses. Group A: Spironolactone (75 mg/kg BW per day) or saline were given by stomach tube for 4 days. Group B: Spironolactone (20 mg/kg BW per day) or saline were given by i.p. injections for 4 days. * Statistical significance ($P < 0.05$) from intact rats. ** Statistical significance ($P < 0.05$) from saline-treated rats

Table 4. Effect of high-sodium diet on amiloride-sensitive short-circuit current in the distal colon of 30-day-old rats

	High-sodium diet	Controls
Amiloride-sensitive short-circuit current (μA/cm²)	33 ± 7 (15)	71 ± 13 (13)

Values are means ± SEM; numbers of animals are shown in parentheses. The rats were fed a standard diet (1% NaCl) or a high-sodium diet (8% NaCl) for 14 days

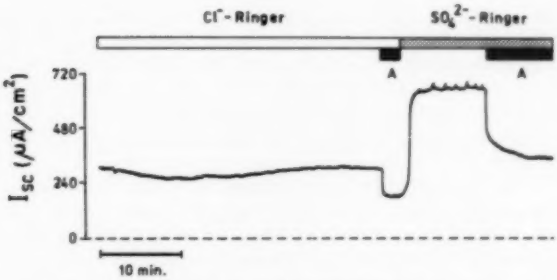

Fig. 3. Effect of amiloride (A, 10^{-4} mol/l) and chloride-free solution (SO_4^{2-}-Ringer) on the short-circuit current (I_{sc}) in the distal colon of 20-day-old rats. Replacement of Ringer's solution by SO_4^{2-}-Ringer rapidly increased the total short-circuit current and its amiloride-sensitive part

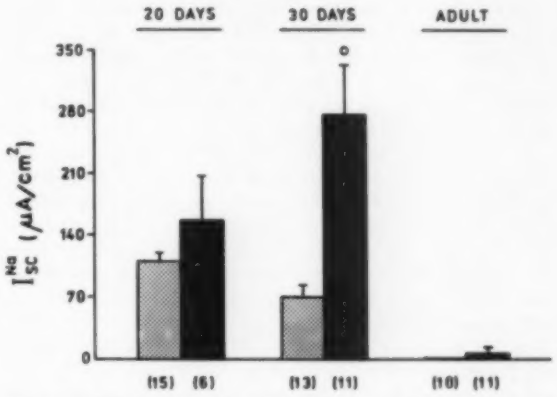

Fig. 4. Effect of low-sodium diet (0.15% NaCl, *dark columns*) and standard diet (1% NaCl, *dotted columns*) on the amiloride-sensitive short-circuit current (I_{sc}^{Na}). Values are given as means ± SEM. Numbers of animals investigated are indicated in parentheses. (○) Denote values significantly different ($P < 0.05$) from corresponding controls

in young rats. These experiments demonstrated that there is electrogenic, amiloride-sensitive sodium transport in young rats. This finding therefore contrasts with the suggestion that this mechanism is absent in the distal colon in the absence of the stimulatory action of corticosteroids [25, 31, 33], and demonstrates striking differences between the neonatal and adult colon. As animals require a great supply of sodium to sustain their growth during the early postnatal period, it seems hardly surprising that the young rats absorb sodium in a similar manner to that induced by sodium-deficiency in adult animals [31, 33]. It seems likely that sodium uses an electrogenic, amiloride-sensitive pathway to cross the mucosa of the distal colon in the newborn rat, and that this pathway is replaced by an electrogenic, amiloride-insensitive Na^+ transport during the weaning period. Furthermore, the time courses of the ontogeny of I_{sc}^{R} and ${}_{R}I_{sc}^{Na}$ indicate a delayed postnatal development of the electrogenic, amiloride-insensitive processes, which are typical of the adult colon [4, 13]. The discrepancy between ${}_{R}I_{sc}^{Na}$ and I_{sc}^{R} in the neonatal colon appears to be due to potassium secretion (unpublished observations).

The same pattern of development of I_{sc}^{Na} was observed previously in the pig colon [7]. In that study, however, only the first 10 postnatal days were investigated. Nevertheless, these comparable findings in young pigs are very interesting because the mechanism of sodium absorption in the adult pig [1] and adult rat colon [4, 13] seems to be very similar. The greater I_{sc}^{Na} in the absence of chloride means that the maximal rate of sodium absorption in young rats might be double that of the adult rat [25] and rabbit distal colon [27].

Although the present results demonstrate that adrenal hormones are necessary for the maintenance of I_{sc}^{Na}, it was not possible to detect any depression of I_{sc}^{Na} after spironolactone in young rats even though mineralocorticoid receptors were found in the adult colonic mucosa [5]. However, our experiments involving administration of exogenous deoxycorticosterone acetate by i.p. injection, indicated that its effect can be blocked by simultaneously giving spironolactone [24]. Identical results were obtained in studies with exogenous aldosterone [18, 32]. By contrast, the present results and the data of Will and co-workers [32] indicate that the effect of endogenous aldosterone of adrenal-intact rats cannot be abolished by spironolactone. It is difficult to explain this difference, but it is of interest

Table 5. Effect of furosemide and high dietary intake of potassium on amiloride-sensitive short-circuit current in the distal colon of young rats

	20-day-old rats		30-day-old rats	
	Furosemide	Controls	High K^+ intake	Controls
Amiloride-sensitive short-circuit current ($\mu A/cm^2$)	419 ± 71 (11)*	177 ± 19 (9)	611 ± 77 (8)*	71 ± 13 (13)

Values are means ± SEM; numbers of animals are shown in parentheses. The rats drank water or 1% KCl solution from day 23 to 30 or they were given i.p. injections of either furosemide (30 mg/kg BW per day) or saline for 4 days. * Statistical significance ($P < 0.05$) from controls

that prolonged administration of spironolactone resulted in a loss of Na and compensatory activation of the renin-angiotensin-aldosterone system [6]. Furthermore, there is a discrepancy between the plasma level of aldosterone and the I_{sc}^{Na} during postnatal development. After birth, there is a decrease in plasma aldosterone in many mammals including rodents [8, 10, 14, 15]. In rats aged 10–14 days there are very low levels of aldosterone which subsequently increase sharply and reach adult levels on day 18 [11]. The sodium repletion which causes a decrease in circulating aldosterone [9] suppressed I_{sc}^{Na} partially. Thus our data suggest that the enhanced electrogenic, amiloride-sensitive sodium transport in young rats may be due not only to mineralocorticoids but also to glucocorticoids, the cytosolic receptors of which are also present in the epithelium of the rat colon [23]. Age-related changes in rat plasma corticosterone follow a similar developmental pattern to that mentioned above for aldosterone [17, 19, 21]. On the other hand, there are data indicating that glucocorticoid hormones are present in milk and that they may be involved in controlling the transport of ions and of water in the gastrointestinal tract [20]. In accordance with this hypothesis [20] our experiments involving adrenalectomy and/or premature weaning confirmed the importance of milk for the I_{sc}^{Na} and demonstrated that the I_{sc}^{Na} of the adrenalectomized animals decreased during the period of weaning in parallel with the milk intake [2, 17].

To determine whether aldosterone is involved in the physiological regulation of sodium transport in the developing colon, the effect of sodium depletion was investigated. In agreement with the findings of Finkel and Aperia [11], our experiments with a low-sodium diet demonstrated that immature colonic mucosa is sensitive to aldosterone. Their finding that 20-day-old rats, are also sensitive to low-sodium diet, was probably due to greater sodium depletion. Hence in a second set of experiments this controversial result was investigated. I_{sc}^{Na} was measured in 20-day-old rats treated with furosemide in the dose which stimulates maximal diuresis and natriuresis in young rats [34] and consequently increases plasma level of aldosterone. This attempt to stimulate the I_{sc}^{Na} was successful. As furosemide is known to enhance plasma renin activity and induce a delayed aldosterone response in newborn mammals [15], we suppose that in young rats the activation of the renin-angiotensin-aldosterone system by furosemide also increases sodium transport in the developing colon.

Hence, it seems to be evident that the distal colon of young rats is sensitive to aldosterone. Independent evidence for the same conclusion comes from the experiments with the high dietary intake of potassium. The control of aldosterone secretion depends not only on the renin-angiotensin system but also on potassium ions [15] and thus high potassium intake elevates the endogenous plasma level of aldosterone without any effect on corticosterone [22]. Although the mechanism of potassium adaptation in K^+-loaded animals with intact adrenal glands is complicated, a recent study on the distal colon of rats has demonstrated that the mechanism of potassium adaptation requires the presence of aldosterone and dietary potassium acting in an additive fashion and that the adaptation depends on mineralocorticoids [12]. In agreement with this findings we were able to demonstrate stimulation of I_{sc}^{Na} by high potassium intake in young rats. The I_{sc}^{Na} was in fact considerably enhanced. However, it was only 1.8 times higher than I_{sc}^{Na} in the chloride-free solution even though it has been demonstrated that a potassium-rich diet may stimulate the plasma level of aldosterone by up to 660% [22] and that a prolonged high level of aldosterone may further increase the amiloride-sensitive conductance and the activity of Na-K-ATPase [33].

The marked difference between the effect of a low-sodium diet in groups of adult, and in 20 and 30-day-old rats indicates that the low-sodium diet used in our experiments was "a weak stimulus" for inducing sodium deficiency and that the rat colon has an enhanced sensitivity to aldosterone at the end of the weaning period. This finding is entirely consistent with the results of Finkel and Aperia [15].

In conclusion, the present study provides data on the development of sodium transport in the distal colon. While the distal colon of adult rats possesses an electroneutral and electrogenic, amiloride-insensitive sodium transport, in young rats there is an electrogenic, amiloride-sensitive one, which disappears after weaning. This electrogenic type of sodium transport depends essentially on the presence of adrenal steroids, namely mineralocorticoids and glucocorticoids.

Acknowledgements. The authors wish to thank Drs. P. Hník, J. Jelínek and J. Zicha for fruitful discussions on this study and for helpful suggestions throughout the experimental work and during completion of the manuscript.

References

1. Argenzio RA, Whipp SC (1983) Effect of theophylline and heat-stable enterotoxin of *Escherichia coli* on transcellular and paracellular ion movement across isolated porcine colon. Can J Physiol Pharmacol 61:1138–1148

2. Babický A, Ošťádalová I, Pařízek J, Kolář J, Bíbr B (1970) Use of radioisotope techniques for determining the weaning period in experimental animals. Physiol Bohemoslov 19:457–467
3. Batt ER, Schachter D (1969) Developmental pattern of some intestinal transport mechanisms in newborn rats and mice. Am J Physiol 216:1064–1068
4. Binder HJ, Rawlins CL (1973) Electrolyte transport across isolated large intestinal mucosa. Am J Physiol 225:1232–1239
5. Binder HJ, White A, Whiting D, Hayslett J (1986) Demonstration of specific high affinity receptors for aldosterone in cytosol of rat colon. Endocrinology 118:628–631
6. Chabert PR, Guelpa-Decorzant C, Riondel AM, Vallotton MD (1984) Effect of spironolactone on electrolytes, renin, ACTH and corticosteroids in the rat. J Steroid Biochem 20:1253–1259
7. Cremaschi D, Ferguson DR, Henin S, James PS, Meyer G, Smith MW (1979) Post-natal development of amiloride sensitive sodium transport in pig distal colon. J Physiol 292:481–494
8. Dalle M, Giry J, Gay M, Delost P (1978) Perinatal changes in plasma and adrenal corticosterone and aldosterone concentrations in the mouse. J Endocrinol 76:303–309
9. Douglas J, Hansen J, Catt KJ (1978) Relationship between plasma renin activity and plasma aldosterone in the rat after dietary electrolyte changes. Endocrinology 103:60–65
10. Ferguson DR, James PS, Paterson JYF, Saunders JC, Smith MW (1979) Aldosterone induced changes in colonic sodium transport occurring naturally during development in the neonatal pig. J Physiol 292:495-504
11. Finkel Y, Aperia A (1986) Role of aldosterone for control of colonic NaKATPase activity in weanling rats. Pediatr Res 20:242–245
12. Foster ES, Jones WJ, Hayslett JP, Binder HJ (1985) Role of aldosterone and dietary potassium in potassium adaptation in the distal colon of the rat. Gastroenterology 88:41–46
13. Gazitúa S, Robinson JWL (1982) Ion fluxes and electrical characteristics of the short-circuited rat colon in vitro. Pflügers Arch 349:32–37
14. Giry J, Delost P (1977) Changes in the concentrations of aldosterone in the plasma and adrenal glands of the foetus, the newborn, and the pregnant guinea-pig during the perinatal period. Acta Endocrinol 84:133–141
15. Giry J, Safwate A, Barlet J-P (1985) Control of aldosterone secretion in domestic mammals during the perinatal period. Reprod Nutr Dév 25:993–1005
16. Helander HF (1975) Enzyme patterns and protein absorption in rat colon during development. Acta Anat 91:330–349
17. Henning SJ (1981) Postnatal development: coordination of feeding, digestion, and metabolism. Am J Physiol 241:G199–G214
18. Horster M, Lückhoff A (1983) Aldosterone on sodium transport of rat distal colon in long-term adrenalectomy during acute and chronic substitution. J Physiol 340:503–511
19. Kamoun A (1970) Activité corti-surrénale au cours de la gestation de la lactation et du développement pré et post-natal chez le rat. I. Concentration et cinétique de disparition de la corticostérone. J Physiol (Paris) 62:5–32
20. Kulski JK, Hartmann PE (1981) Changes in the concentration of cortisol in milk during different stages of human lactation. Aust J Exp Biol Med Sci 59:769–778
21. Malinowska KW, Hardy RN, Nathanielsz PW (1972) Plasma adrenocorticosteroid concentrations immediately after birth in the rat, rabbit and guinea-pig. Experientia 28:1366–1367
22. Martin RS, Jones WJ, Hayslett JP (1983) Animal model to study the effect of adrenal hormones on epithelial function. Kidney Int 24:386–391
23. Marusic ET, Hayslett JP, Binder HJ (1981) Corticosteroid-binding studies in cytosol of colonic mucosa of the rat. Am J Physiol 240:G417–G423
24. Pácha J, Popp M, Čapek K (1987) Effects of deoxycorticosterone acetate on the electrical properties of rat large intestine: segmental differences. Physiol Bohemoslov (in press)
25. Perrone RD, Jenks SL (1984) Suppression of coupled Na-Cl absorption by aldosterone and dexamethasone in rat distal colon in vitro. Am J Physiol 246:F785–F793
26. Potter GD, Burlingame SM (1986) Glucose-coupled sodium absorption in the developing rat colon. Am J Physiol 250:G221–G226
27. Schultz SG (1984) A cellular model for active sodium absorption by mammalian colon. Annu Rev Physiol 46:435–451
28. Sepúlveda FV, Smith MW (1979) Different mechanisms for neutral amiño acid uptake by new-born pig colon. J Physiol 286:479–490
29. Spät A, Tarján E, Tóth G (1979) Hyperaldosteronism in the sodium-depleted rat: Mode of aldosterone-stimulating action of frusemide. J Endocrinol 82:7–15
30. Turnheim K, Frizzell RA, Schultz SG (1977) Effect of anions on amiloride-sensitive, active sodium transport across rabbit colon, in vitro. J Membr Biol 37:63–84
31. Will PC, Cortright RN, DeLisle RC, Douglas JG, Hopfer U (1985) Regulation of amiloride-sensitive electrogenic sodium transport in the rat colon by steroid hormones. Am J Physiol 248:G124–G132
32. Will PC, Cortright RN, Groseclose RG, Hopfer U (1985) Amiloride-sensitive salt and fluid absorption in small intestine of sodium-depleted rats. Am J Physiol 248:G133–G141
33. Will PC, Lebowitz JL, Hopfer U (1980) Induction of amiloride-sensitive sodium transport in the rat colon by mineralocorticoids. Am J Physiol 238:F261–F268
34. Zaumseil J, Kersten L, Bräunlich H (1975) Altersabhängige Wirkungen von Furosemid bei Ratten. Arch Int Pharmacodyn Ther 218:167–176

Received August 5, 1986/Accepted January 5, 1987

Pflügers Arch (1987) 409:200–207

Pflügers Archiv
European Journal of Physiology
© Springer-Verlag 1987

Evidence for a Na^+/H^+ exchanger at the basolateral membranes of the isolated frog skin epithelium: Effect of amiloride analogues

Jordi Ehrenfeld[1], Edward J. Cragoe[2] Jr., and Brian J. Harvey[1]

[1] Laboratoire Jean Maetz du Department de Biologie du CEA, PB 68, F-06230 Villefranche Sur Mer, France
[2] Merck Sharp and Dohme Research Laboratories, West Point, PA 19486, USA

Abstract. We have investigated the possible existence of a Na^+/H^+ ion exchanger in the frog skin epithelium by using isotopic methods and two amiloride analogues: 5-(N-ethyl-N-isopropyl)-amiloride (EIPA) and phenamil. We found phenamil to be a specific blocker of sodium entry to its cellular transport compartment since it inhibited both the transepithelial Na^+ influxes (J_{13}) with a K_i of $4 \cdot 10^{-7}$ mol/l and the Na^+ pool (control: 77 ± 4 neq $\cdot h^{-1} \cdot cm^{-2}$; phenamil: 21 ± 1 neq $\cdot h^{-1} \cdot cm^{-2}$). On the contrary EIPA (10^{-5} mol/l) had no effect on J_{13} nor on the apical Na^+ conductance. Acidification of the epithelium by passing from a normal Ringer (25 mmol/l HCO_3^-, 5% CO_2, pH 7.34) to a HCO_3^--free Ringer (5% CO_2, pH 6.20) while blocking the Na^+ conductance with phenamil, produced a large stimulation of Na^+ influxes exclusively across the basolateral membranes (J_{32}), after return to a normal Ringer ($J_{32} = 706 \pm 76$ and 1635 ± 199 neq $\cdot h^{-1} \cdot cm^{-2}$ in control and acid-loaded epithelia respectively). The stimulation of J_{32} was initiated when the epithelia were acid-loaded with Ringer of pH lower than 6.90 and was blocked by amiloride ($K_i = 7 \cdot 10^{-6}$ mol/l) and EIPA ($K_i = 5 \cdot 10^{-7}$ mol/l) whereas phenamil had no effect. In Na^+-loaded epithelia (ouabain treated) the Na^+ efflux across the basolateral membranes was stimulated by an inwardly directed proton gradient and was blocked by EIPA (10^{-5} mol/l) or amiloride (10^{-4} mol/l), a result suggesting reversibility of the mechanism. We conclude that a Na^+ permeability mediated by a Na^+/H^+ ion exchanger exists in the basolateral membranes, which is stimulated by intracellular acidification and is sensitive to amiloride or EIPA. This exchanger is proposed to be involved in intracellular pH regulation.

Key words: Na^+/H^+ exchanger – Frog skin – EIPA – Phenamil

Introduction

Many ion transporting epithelia have the ability to excrete protons and this property is often associated with the capacity of the epithelia to absorb sodium ions. In tight epithelia such as the turtle and toad urinary bladder [27, 39], the frog skin [15] and certain segments of the mammalian renal collecting tubule [41] the mechanism of acid secretion is that of an active proton transport. In the frog skin, this H^+ transport was shown to be mediated by an electrogenic pump located at the apical side of the epithelium [16]; furthermore we have recently found that at the basolateral side of the epithelium a Cl^-/HCO_3^- exchange mechanism contributes to the stability of cell pH and to overall net H^+ excretion [13].

In acidotic conditions, the frog skin and urinary bladder respond to an acidification of the internal medium by increasing the capacity of the H^+ pumping mechanism [8, 15, 18]. This physiological regulation of transepithelial H^+ efflux must also be associated with a regulation of cell pH. However the question could be posed whether the H^+ pump and Cl^-/HCO_3^- exchange are the unique regulatory mechanisms. Indeed, recent evidence suggests that a plasma membrane Na^+/H^+ exchanger plays a critical role in the regulation of intracellular pH in a variety of cells [2, 6, 11, 20, 33], and in epithelia like the *Necturus* gallbladder [17, 45], renal tubular cells [5, 24, 28], and toad bladder cells [26].

In the kinetic studies presented here, we have investigated the possible existence of a Na^+/H^+ exchange mechanism involved in cell pH regulation following an acid load of the isolated frog skin epithelium. The use of two amiloride analogues phenamil and EIPA were found to be useful in determining the localisation and characteristics of the exchanger.

Material and methods

Rana esculenta frogs were kept at 15°C without food in running tap water. The frogs were used within 10 days of arrival in the laboratory. The ventral skin was used for the experiments. Large sheets of epithelium were isolated by the technique of Aceves and Erlij [1].

The normal Ringer used contained bicarbonate (24 mmol/l) and was gased with a mixture of 5% CO_2 and 95% O_2; its pH was 7.34 and it contained (in mmol/l): NaCl 85; $NaHCO_3$ 24; KCl 2.5; $CaCl_2$ 2; $MgSO_4$ 2; Na_2HPO_4 2.5; KH_2PO_4 1.2 and glucose 11.

The so-called "acid Ringer" had an identical ionic composition except that sodium bicarbonate was replaced by sodium sulfate, it's pH after gasing with 5% CO_2 was 6.20. Epithelia incubated in this Ringer are denoted as "acid treated epithelia". In chamber experiments, the apical solution was a 1 mmol/l Na_2SO_4 solution buffered at pH 7.34 (2 mmol/l imidazole) or a normal Ringer or an "acid Ringer".

Kinetic studies. For measurements of the unidirectional Na transepithelial influxes (J_{13})[1], the ventral skin was mounted

Offprint requests to: J. Ehrenfeld

[1] Subscripts 1, 2, and 3 of J_{13}, J_{23}, J_{32} refer to mucosal, cellular and serosal compartments respectively

between two lucite chambers of 7 ml capacity and of exposed area 7 cm^2, and equilibrated for 1 h with normal Ringer on both sides. J_{13} was measured with the isotope ^{22}Na (0.4 μCi/ml) added to the mucosal solution. After a 20 min equilibration period, the appearance of the isotope was followed in the serosal solution as a function of time. The radioactivity of the ^{22}Na samples was measured with an automatic counting system (MR 252 Kontron, France) and the sodium concentration of the solutions was determined by flame photometry (Eppendorf, FRG). The fluxes (J_{13}) were calculated in neq · h^{-1} · cm^{-2} and expressed as means ± SE of the mean.

Determination of the Na pool, basolateral Na uptake (J_{32}) and Na outflux (J_{23}). For the chamber experiments, paired pieces of epithelium (1.13 cm^2) were mounted in Ussing chambers. Loading the epithelium with ^{22}Na (10 μCi/ml) was performed in normal Ringer, either from the apical or the basolateral side as indicated in the text.

For beaker experiments we cut pieces of epithelia (12–13 pieces of 1.13 cm^2) from a single large sheet of isolated epithelium. Each piece of epithelium was then sandwiched between two nylon meshes (Millipore, USA) to avoid curling and thus to maximise the exposed surface. The ^{22}Na loading was identical to chamber experiments except that the loading proceeded through both membranes of the epithelium. In most beaker experiments, we used phenamil to block the apical conductive Na entry and under this condition, the ^{22}Na loading of the epithelia occurred essentially through the basolateral membranes. Beaker experiments were more convenient to perform than chamber experiments since a large number of pieces of epithelia could be obtained which allowed a more detailed statistical analysis.

Treatment of the epithelia for the washout procedure was similar to that used by Stoddard and Helman [40]. Briefly the washout solution contained ouabain ($5 \cdot 10^{-4}$ mol/l), furosemide (10^{-3} mol/l) and amiloride (10^{-4} mol/l) to block the different Na^+ transport mechanisms of the epithelium in order to reduce to a maximum the Na efflux from the epithelium. The analysis of the ^{22}Na efflux plotted as a function of time is that of a two compartment system, corresponding to an extracellular space $t^1/_2 \simeq 1$ min) and to single cell Na compartment ($t_{1/2} \simeq 20$ min). The evaluation of the initial ^{22}Na quantity (Q_o) before washing the epithelium was calculated from linear regression analysis of the second ^{22}Na washout component. The Na pool (A) was then estimated from the equivalent relationship between intra- and extracellular specific radioactivity and expressed as neq · cm^{-2}

$$A = Q_o \times \frac{A_R}{Q_R \times S}$$

where A is the Na pool, Q_o the ^{22}Na initial radioactivity of the epithelium (after 2 h of loading with the isotope), A_R the amount of Na^+ of the Ringer solution and Q_R the quantity of ^{22}Na radioactivity of the corresponding Ringer solution and S the surface area of the epithelium.

The unidirectional ^{22}Na leak efflux (J_{23}) could be calculated as $J_{23} = 0.693\ A/t^1/_2$ (see [40]) and expressed in neq · h^{-1} · cm^{-2}.

The estimation of the unidirectional ^{22}Na uptake (J_{32}) through the basolateral membranes requires a ^{22}Na loading time of sufficiently short duration which must be in the linear range of the loading as a function of time and long enough to allow precise measurements of the radioactivity in the epithelium. A loading time of 2 min (see Fig. 1) was chosen to fulfill both of the above conditions. This loading time underestimates J_{32} but permits an accurate qualitative estimation of Na transport across the basolateral membrane thus allowing a comparison between different experimental conditions. Data analysis and plotting were carried out using a Hewlett Packard micro computer.

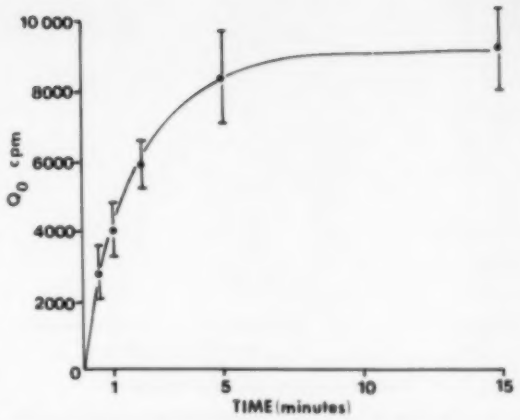

Fig. 1. The amount of cell ^{22}Na uptake (cpm) plotted as a function of time (min) of loading with the isotope. The epithelia were bathed in beakers in normal Ringer containing phenamil (10^{-5} mol/l)

I-V Relationship of the apical Na^+ conductive pathway. To determine the specificity of the amiloride analogues, we wished to test their effects on the apical membrane Na^+ conductance (G_{Na}). G_{Na} was calculated from the amiloride sensitive "instantaneous" current-voltage relationship of the apical membrane under short-circuit conditions. The recording of current(I)-voltage(V) curves was performed by a technique similar to that used by Thomas et al. [42]. Briefly, the I-V relationship of the apical Na^+ conductive pathway was obtained from the difference of the I-V curves recorded by an intracellular microelectrode, under control spontaneous Na^+ transport conditions and those recorded 2–3 min after complete inhibition of the short circuit current (I_{sc}) following the addition of 10^{-4} mol/l amiloride to the apical solution.

The conductance was estimated from the slope of the I-V relationship at zero net current. Intracellular pH (pH_i) was measured using double barreled ion sensitive microelectrodes by techniques previously described [22].

Drugs. Amiloride (Merck, Sharp & Dohme, Research Laboratories, West Point, PA, USA) and its analogues were synthesized as previously described [10]. Ouabain and furosemide were purchased from Sigma Chemical Co. (St. Louis, MO, USA).

Results

Amiloride analogues and Na^+ transport

Two amiloride analogues, 3,5-diamino-6-chloro N (benzeneamino) aminoethylene pyrazine carboxamide (phenamil)

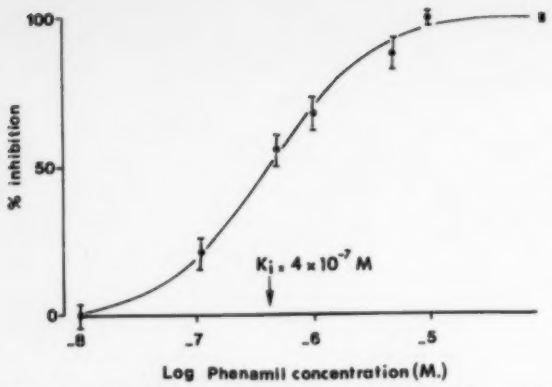

Fig. 2. Log dose-response of J_{13} versus phenamil concentration. Skins were mounted in Ussing chambers with a mucosal Na concentration of 114 mmol/l. All data points were normalized to the initial J_{13}. J_{13} in the control period was 408 ± 181 neq $\cdot$ h^{-1} $\cdot$ cm^{-2} (n = 6). In *abscissa*, the logarithm of the phenamil concentration is shown

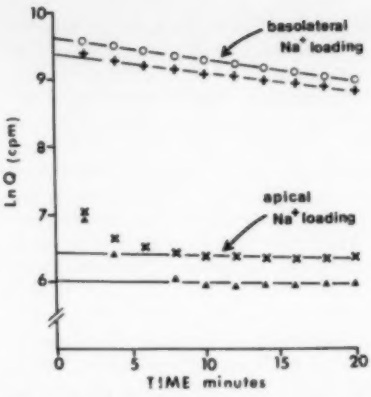

Fig. 4. Washout kinetics of paired epithelia both treated with phenamil (10^{-5} mol/l) and loaded with ^{22}Na for 2 min from the apical (*lower trace*) and basolateral side (*upper trace*). *Ordinate:* Naperian logarithm of the ^{22}Na accumulation in the epithelium. *Abscissa:* time course of the washout kinetics of two typical paired epithelia. (○), (×), (+) and (▲) represent symbols used for the first paired typical epithelia and the second one respectively

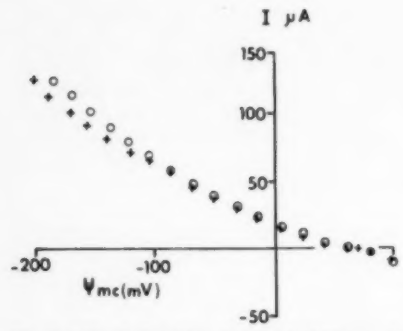

Fig. 3. I-V relationship of the apical Na conductive pathway. On *ordinate* the Na current (amiloride inhibited current) expressed in μA. was plotted versus the apical membrane potential (*abscissa*). The exposed frog skin surface was 1 cm^2. Control (+) and EIPA: (○)

and 5-(N-ethyl-N-isopropyl)-amiloride (EIPA), were tested on the transepithelial sodium influx (J_{13}) measured across the isolated frog skin mounted in Ussing chambers. Experiments were performed in open-circuit conditions (n = 6). Phenamil inhibited the J_{13} at all doses tested higher than 10^{-8} mol/l (Fig. 2). Maximal inhibition was observed at 10^{-5} mol/l. The apparent K_I was found to be $4 \cdot 10^{-7}$ mol/l with 114 mmol/l Na^+ in the Ringer. However, when the solution bathing the apical side of the skin was a low sodium containing solution (2 mmol/l Na), a K_I of $4 \cdot 10^{-8}$ mol/l was calculated.

On the other hand, EIPA added to the mucosal bath at a dose of 10^{-5} mol/l had no effect either on J_{13} or on the amiloride-sensitive Na conductance (G^a_{Na}) of the apical membrane measured by the I-V relationship of the apical Na conductive pathway (Fig. 3). Thus, J_{13} was 636 ± 144 neq $\cdot$ h^{-1} $\cdot$ cm^{-2} and 773 ± 144 neq $\cdot$ h^{-1} $\cdot$ cm^{-2} (n = 6) for control and EIPA experiments respectively, whereas G^a_{Na} was 0.153 mS/cm^2 and 0.169 mS/cm^2 for the control and EIPA treated epithelia respectively.

Cell acidification of the epithelium increases the Na pool and the Na fluxes across the basolateral membranes

We confirmed that phenamil inhibited J_{13} by blocking the apical Na^+ entry step by the following experiments. Paired isolated epithelia mounted in Ussing chambers were loaded for 2 min with ^{22}Na either from the apical side or the basolateral side. When phenamil was used to block Na entry from the mucosal side (Fig. 4) the amount of ^{22}Na loading the epithelium from the apical side was very low, and the calculated Na pool approached the detection limit for this technique. However, when loading of the phenamil treated epithelium was performed from the basolateral side, a finite pool 24 times larger than that originating from the apical side, was measured.

These experiments are in agreement with those reported by Stoddard and Helman [40] and show that a finite pool can be estimated, when the apical Na^+ entry is blocked, reflecting the existence of a Na^+ permeability at the basolateral membranes of the epithelium.

We took advantage of this finding to evaluate the Na^+ pool in pieces of epithelia soaked in Ringer ("beaker experiments") in the absence or presence of phenamil (10^{-5} mol/l); in the latter situation apical Na entry is blocked. We found that equilibration of the epithelium with ^{22}Na was achieved after 2 h of incubation. The Na^+ pool measured in the absence of phenamil, after 2 h of loading the epithelia with ^{22}Na, was 77.3 ± 4.0 neq $\cdot$ cm^{-2} (Table 1). Phenamil (10^{-5} mol/l) reduced considerably both the Na^+ pool (to a mean value of 21.5 ± 1 neq $\cdot$ cm^{-2}) and the half-time of washout kinetics (to a mean value of 13.9 ± 0.9 min). From our measurements of the cell water content per cm^2 of tissue (6.18 ± 0.31 μl/cm^2), the cell sodium concentration was decreased from a control value of 12.5 mmol/l to 3.5 mmol/l of cell water after the addition of phenamil. These results agree with measurements of the Na^+ transport pool reported by others using amiloride [23, 30, 34, 40].

Attempts to create a cell acidification was performed by incubating the epithelia in HCO_3^- free Ringer gased with

5% CO_2, pH 6.2 ("acid Ringer") for $1^1/_2$ h. A cell pH decrease is to be expected considering (1) the permeability of CO_2 through cell membranes, (2) the low pH of the incubating Ringer, and (3) bicarbonate efflux into the bicarbonate free Ringer. We found that perfusing the serosal Ringer with such an "acid Ringer" leads to a cell pH decrease from 7.27 ± 0.03 ($n = 8$) (control) to 6.89 ± 0.03 ($n = 7$) ("acid Ringer") as measured with ion selective microelectrodes. The Na pool was therefore measured after incubation of the epithelia, in the presence of phenamil (10^{-5} mol/l), in an acid Ringer (HCO_3^- free Ringer gased with 5% CO_2 pH 6.2) which resulted in an increase of the Na^+ pool which averaged 48.4 ± 6.2 neq $\cdot$ cm^{-2} corresponding to a cell concentration of 7.8 mmol/l cell water.

Cell acidification has also been reported using weak organic acids (see [21]). Incubation of the epithelia, in the presence of phenamil, with the weak acid, butyrate (20 mmol/l) added to a normal Ringer solution also produced an increase of the Na^+ pool (25.9 ± 1.3 neq/cm^2; $n = 4$; compare to 21.5 ± 1 neq $\cdot$ cm^{-2} in normal Ringer $p < 0.002$) which was however less pronounced than that observed with acid Ringer.

Thus, incubation of the epithelia in solutions known to acidify the cell produces an increase in the cell Na^+ concentration.

In order to determine the mechanism and sidedness of this increase in the Na pool in acid-treated epithelia, we measured the unidirectional $^{22}Na^+$ fluxes across the basolateral membranes (J_{32}) in control and acid loaded epithelia treated with phenamil and incubated in beakers. Acid loading was achieved by pre-incubating the epithelia in beakers for 90 min in "acid Ringer" (HCO_3^- free 5% CO_2 pH 6.2). On return to control Ringer (pH 7.34), this treatment creates a large outwardly directed proton gradient and during this period, the epithelia were loaded for 2 min with ^{22}Na. The calculated Na fluxes (J_{32}) were 706 ± 76 neq $\cdot$ $h^{-1} \cdot cm^{-2}$ and 1635 ± 199 neq $\cdot$ $h^{-1} \cdot cm^{-2}$ ($n = 12$) for control and acid loaded epithelia respectively. As can be seen J_{32} was increased twofold indicating an increase in the Na transport mechanism across the basolateral membrane following an intracellular acid load of the epithelia. It must be remarked that the acid stimulated J_{32} measured immediately post acid load probably underestimates the maxima stimulated Na flux since the activity of the Na/H exchanger should decrease with recovery of intracellular pH. In fact, we found that after 5 min post acid load (after return to control Ringer) J_{32} had decayed to 50% of the stimulated flux value (unpublished results).

We further explored the stimulation of J_{32} following cell acidification by incubating pieces of epithelia in Ringer solutions of different pH gased with 5% CO_2 and containing varying amounts of HCO_3^- in the aim to acidify the epithelial cells to varying degrees. As shown in Fig. 5 ($n = 5$), the J_{32} was stimulated at preincubation Ringer pH values lower than 6.90. This result suggests that the cell pH must reach a certain pH value in order to stimulate the Na^+ uptake mechanism.

We found no stimulation of J_{13} through isolated frog skins mounted in Ussing chambers, in the presence of phenamil (10^{-5} mol/l), either after incubation of the skins in a HCO_3^- free Ringer (gased with 5% CO_2, pH = 6.20) or after return to a normal Ringer pH = 7.34 (control: 58 ± 11 neq $\cdot$ $h^{-1} \cdot cm^{-2}$; "acid Ringer": 57 ± 8 neq $\cdot$ $h^{-1} \cdot cm^{-2}$; return to control Ringer: 44 ± 5 neq $\cdot$ $h^{-1} \cdot cm^{-2}$).

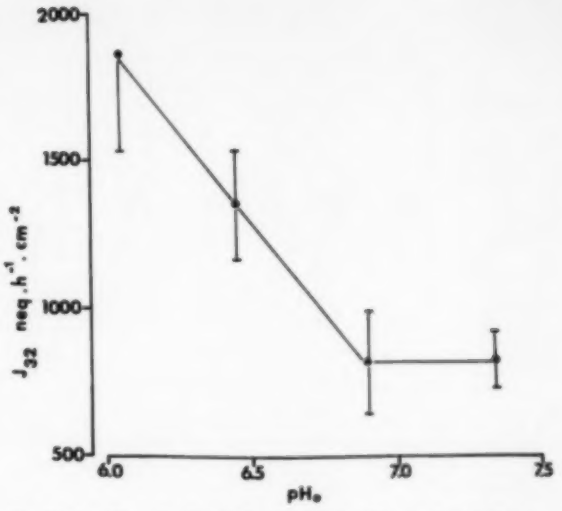

Fig. 5. The effect of cell acidification on J_{32}. Pieces of epithelia were peincubated in Ringer solution containing different amounts of bicarbonate, gased with 5% CO_2 and having the different pH values reported on the *abscissa* of the figure. The time of ^{22}Na uptake (2 min) in the presence of phenamil (10^{-5} mol/l), the washing period and the analysis were identical for all epithelia, after this preincubation period. *Ordinate:* represents J_{32} in neq $\cdot$ $h^{-1} \cdot cm^{-2}$ ($n = 5$)

Therefore, the increase in the Na^+ pool following an acid load occurred solely across the basolateral membranes of the epithelium.

Amiloride and EIPA inhibit the acid-stimulated Na uptake across the basolateral membranes

High concentrations of amiloride have been shown to inhibit Na^+/H^+ exchangers in a variety of isolated cells and epithelia [35]. The analogue of amiloride, EIPA was found to be more potent in this respect [44]. Amiloride also blocks G^s_{Na}, but as shown above EIPA was without effect on G^s_{Na}. Thus, EIPA may be considered as a selective inhibitor of a Na^+/H^+ exchanger.

We have tested amiloride and EIPA on the ^{22}Na uptake across the basolateral membranes of the epithelium after blocking the apical conductive Na^+ entry with phenamil (10^{-5} mol/l), in acid loaded epithelia (experiments in beakers).

As can be seen in Fig. 6, the acid stimulated J_{32} was clearly and similarly reduced by EIPA (10^{-5} mol/l) or amiloride (10^{-4} mol/l and 10^{-3} mol/l). The remaining component of J_{32} which was not inhibited by these drugs (550 ± 27 neq $\cdot$ $h^{-1} \cdot cm^{-2}$; $n = 16$) was lower than J_{32} in control epithelia (non-acid loaded epithelia; see above; $p < 0.001$), suggesting that (1) the acid stimulated component of J_{32} was completely blocked by amiloride or EIPA and (2) the non-acid stimulated epithelia possess a small amiloride and EIPA sensitive component of J_{32}.

We have assumed that phenamil was without effect on Na/H exchanger. We tested this assumption by measuring the acid stimulated Na influx in the presence of phenamil (10^{-5} mol/l) on the basolateral side of paired epithelia mounted in Ussing chambers. No effect of phenamil was

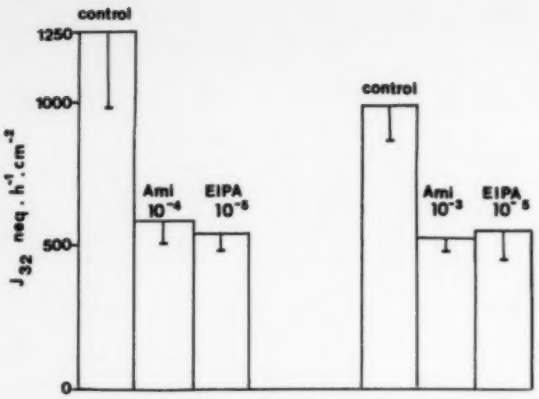

Fig. 6. Comparative effects of EIPA and amiloride on the basolateral Na influxes (J_{32}), in phenamil and acid pre-treated epithelia bathed in beakers. EIPA (10^{-5} mol/l) was compared with the effects of amiloride at 10^{-3} mol/l and 10^{-4} mol/l

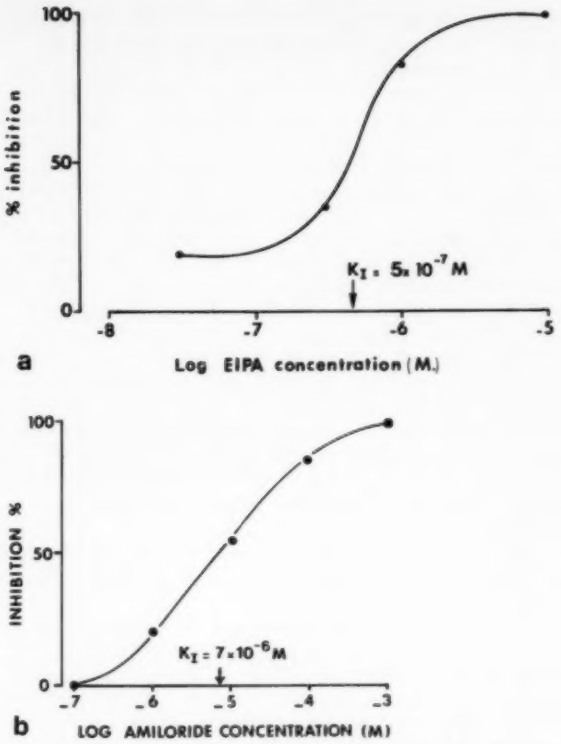

Fig. 7. Log dose-response curve of J_{32} versus EIPA (**a**) or amiloride (**b**) concentrations. The Ringer sodium concentration was 114 mmol/l all data points were normalized to the initial J_{32}. On the *abscissa*, the logarithm of the EIPA or amiloride concentration is given. Experiments were on acid pre-treated epithelia in the presence of phenamil (10^{-5} mol/l) in beakers. On return to normal Ringer the epithelium was loaded with ^{22}Na for 2 min in the presence of phenamil (10^{-5} mol/l). Significance between control and epithelial treated with EIPA at dose (in mol/l) of $3 \cdot 10^{-8}$, $3 \cdot 10^{-7}$, and $3 \cdot 10^{-6}$ and 10^{-5} were n.s., $p < 0.05$, $p < 0.001$ and $p < 0.001$ respectively. Significance between control and amiloride treated epithelia at dose (in mol/l) of 10^{-6}, 10^{-5}, 10^{-4} and 10^{-3} were n.s. $p < 0.05$, $p < 0.001$ and $p < 0.001$ respectively

found on these Na influxes: $J_{32} = 971 \pm 259$ neq $\cdot$ h^{-1} $\cdot$ cm^{-2} and 1296 ± 456 neq $\cdot$ h^{-1} $\cdot$ cm^{-2}) in control and phenamil treated epithelia ($n = 5$; difference not significant).

The dose-response relationship of the EIPA effect is illustrated in Fig. 7; the apparent K_I for EIPA was 5×10^{-7} mol/l ($n = 5$) with a Ringer Na^+ concentration of 114 mmol/l. A K_I of $7 \cdot 10^{-6}$ mol/l ($n = 5$) was estimated with amiloride, a value ten times larger than that found with EIPA.

In summary, acid loading the epithelium induces an increase in the Na pool originating from the basolateral side and an increase in J_{32} which can be blocked by amiloride and EIPA. These results provide evidence that in acid loaded epithelia, a large fraction of the Na uptake through the basolateral membranes occurs via a Na/H exchanger.

Reversibility of the exchanger

In physiological conditions, the Na^+ gradient is directed across the basolateral membranes, from the serosal medium to the cells. In order to reduce this gradient, we have loaded the cells with Na^+ and ^{22}Na, by blocking the Na-K pump with ouabain for 2 h. In these experiments phenamil was not added during the first 90 min in order that Na loading could proceed faster across both barriers. The ^{22}Na kinetics were then performed in the presence of phenamil.

The Na pool measured in the presence of ouabain (2 h), was increased and found to be 406 ± 11 neq $\cdot$ cm^2 ($n = 68$), a value corresponding to a cell sodium concentration of 66 mmol/l of cell water.

Washout kinetics of such Na^+ loaded epithelial were then performed in media containing ouabain $5 \cdot 10^{-4}$ mol/l, furosemide 10^{-3} mol/l and phenamil 10^{-5} mol/l. As can be seen in Table 2 increasing the Na^+ concentration of the epithelia cells increased the J_{23} fluxes (compare Table 2 to Table 1).

An eventual Na/H exchanger functioning in reverse mode would be expected to be accelerated by decreasing the external pH, creating an inwardly directed proton gradient. Such a situation was observed when the washout kinetics were performed in acid Ringer, the $t^1/_2$ of Na efflux was reduced from 27.1 to 20.6 min and J_{23} was increased from 394 ± 29 to 583 ± 29 neq $\cdot$ h^{-1} $\cdot$ cm^{-2}. EIPA (10^{-5} mol/l) blocked the acid stimulated Na efflux to values close to those measured when normal Ringer was used as the washout solution.

Discussion

The original Koefoed-Johnsen and Ussing model [25] postulated the existence of a Na^+ conductance located on the apical membrane of the Na^+ transporting cells in series with a K^+ conductance located on the basolateral membranes (b.l.m.). This model applied to tight epithelia in steady-state conditions and has been widely confirmed. However, in addition to the dominant K^+ conductive pathway, other ion transport mechanisms have been identified at the b.l.m. Recent studies have described an electrically silent Cl^-/HCO_3^- exchange mechanism [13] and Ussing [43] has reported the presence of a neutral Na/K/2 Cl cotrans-

Table 1. Effects of phenamil (10^{-5} mol/l) and of an acid load on the Na^+ pool (neq · cm^{-2}), on the half time of washout (min) and on the J_{23} (neq · h^{-1} · cm^{-2}) in frog skin epithelia

	Pool (neq · cm^{-2})	$t^1/_2$ (min)	$J23$ (neq · h^{-1} · cm^{-2})
Normal Ringer ($n = 8$)	77.3 ± 4.0	18.7 ± 1.2	107 ± 11
Normal Ringer + Phenamil 10^{-5} mol/l ($n = 12$)	21.5 ± 1.0	13.9 ± 0.9	42 ± 3
Acid Ringer + Phenamil 10^{-5} mol/l ($n = 12$)	48.4 ± 6.2	10.9 ± 0.8	115 ± 16

Table 2. Reversal of the Na/H exchanger. The epithelia were loaded with ^{22}Na for 2 h in the presence of ouabain ($5 \cdot 10^{-4}$ mol/l) and phenamil (10^{-5} mol/l). Washout kinetics of the epithelia were then performed in the different media listed in the table; the Na pool, the half time of washing and the J_{23} were expressed in neq · cm^{-2}, minutes and neq · h^{-1} · cm^{-2} respectively

Washout media	Pool (neq · cm^{-2})	$t^1/_2$ (min)	J_{23} (neq · h^{-1} · cm^{-2})
Normal Ringer ($n = 14$)	402 ± 26	27.1 ± 1.6	394 ± 29
Acid Ringer ($n = 14$)	456 ± 27	20.6 ± 1.3	583 ± 29
Acid Ringer ($n = 14$)	456 ± 27	20.6 ± 1.3	538 ± 29
Acid Ringer + EIPA 10^{-5} mol/l ($n = 13$)	418 ± 25	32.0 ± 1.2	337 ± 20

port activated by an osmotic shock. Furthermore, Stoddard and Helman [40] demonstrated the existence of a non-negligeable basolateral Na^+ permeability, supporting the idea that a finite Na^+ pool arises from Na^+ influx across the basolateral side. Such Na^+ influx appears to be non-conductive since Na^+ substitution of the serosal side of the epithelium does not produce any immediate change in the electrical potential of the b.l.m. ([29], Harvey and Ehrenfeld, unpublished results).

Our study confirms the existence of a Na^+ permeability at the b.l.m. of the frog skin epithelium. The following evidence supports the existence of an acid-stimulated Na^+/H^+ exchanger: (1) The Na^+ pool was increased from 21.5 ± 1 neq · h^{-1} · cm^{-2} to 48.4 ± 6.2 neq · h^{-1} · cm^{-2} and J_{32} was increased twofold after acid loading the epithelia. (2) J_{32} was found to be a function of the outwardly directed proton gradient. (3) Amiloride and EIPA, two potent inhibitors of the Na^+/H^+ transporter in other systems, blocked the acid stimulated J_{32}. (4) J_{23} (Na^+ efflux) was increased by an inwardly directed proton gradient and blocked by amiloride and EIPA.

The localization of the Na^+/H^+ exchanger in epithelia cells appears to be largely dependent on the origin of the epithelia. In leaky epithelia such as *Necturus* gallbladder [45], rabbit proximal tubule [36, 37], the diluting segment of frog kidney [32] and the small intestine, the Na^+/H^+ transporter is located at the apical side of the epithelium. Conversely, in the rabbit cortical tubule, the Na^+/H^+ exchanger is confined to the b.l.m. of the epithelium [7]. In vivo, the solutions bathing both sides of the frog skin have a completely different ionic composition: the serosal side has a high Na^+ concentration (114 mmol/l), whereas the frogs live in an external medium of very low Na^+ concentrations (often lower than 1 mmol/l). In these conditions, a Na^+/H^+ exchanger whose normal function depends on the existence of a favourable inwardly directed Na^+ gradient, would not be expected to be located at the apical side of the epithelium. Indeed, from our experimental results we can advance arguments to eliminate the possible existence of the exchanger at the apical membrane of the epithelium: (1) we have observed in chamber experiments, that all ^{22}Na influx across the apical membrane was inhibited by the specific Na^+ channel blocker phenamil. (2) Acid loading of the epithelium did not uncover an apical Na^+/H^+ exchanger since under these conditions phenamil also blocks all ^{22}Na influx. (3) The specific Na^+/H^+ exchanger inhibitor EIPA did not affect Na^+ fluxes across the apical membranes. All these results argue strongly against the existence of a Na^+/H^+ exchanger at the apical membrane as has been postulated by Drewnowska and Biber [12]. Moreover, our experimental results directly support the presence of the Na^+/H^+ exchanger to the basolateral membrane only: Na^+ influxes (J_{32}) stimulated by an acid load occurred solely across the basolateral membrane of the epithelium and were inhibited by amiloride and EIPA, the latter being a specific blocker of Na^+/H^+ exchanger.

Since the frog skin epithelium possesses a high Na^+ conductance on the apical membranes, we used amiloride analogues, phenamil and EIPA, to distinguish between a Na^+ conductance and a Na^+/H^+ exchanger. Indeed, apical applied phenamil was found to be a very specific blocker of Na^+ transport by blocking conductive Na^+ entry to its transport compartment; the K_i of $4 \cdot 10^{-7}$ mol/l in the presence of 114 mmol/l of Na^+ was very close to the value reported by Garvin et al. [19] in the toad urinary bladder. On the other hand, phenamil at a dose of 10^{-5} mol/l on the basolateral side was found to be ineffective on the Na^+/H^+ exchanger (as measured by the acid stimulated J_{32} in experiments were the epithelium was mounted in chambers). The absence of effect of phenamil on the Na^+/H^+ exchanger of the chick cardiac cells and astrocytoma C_6 cells was also found by Frelin and Vigne (personal communication).

Conversely to phenamil, EIPA was, at a dose of 10^{-5} mol/l, applied at the apical side, ineffective on the Na^+ transport as measured by J_{13} or the Na^+ conductance of the apical membrane, whereas it was very effective on the Na^+/H^+ antiport. At an external Na^+ concentration of 114 mmol/l, we determined a K_i of $5 \cdot 10^{-7}$ mol/l for the inhibition of Na^+/H^+ exchange by EIPA. This value is closer to that reported for chick cardiac cells or chick skeletal muscle cells ($K_i = 1.5 \cdot 10^{-7}$ mol/l) [44] than that of $2.9 \cdot 10^{-6}$ mol/l reported for the intact renal proximal tubular cells with a low Na^+ concentration (1 mmol/l) in the external medium [31].

Recently, in proximal tubules, EIPA was found to block the ouabain sensitive O_2 consumption (a measure of Na^+ pump activity and mitochondrial production of ATP) at doses larger than 10^{-4} mol/l [38]. No effect was found at doses lower than 10^{-4} mol/l. Since in this study, the highest

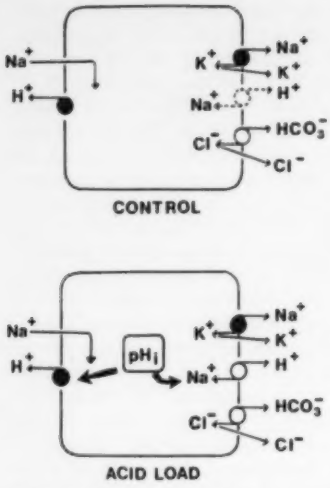

Fig. 8. Cell pH regulation an transepithelial acid transport. Schematic representation of the frog skin epithelium in normal and acidotic conditions. Following and acid load, the transepithelial acid transport is increased by the stimulation of the apical proton pump in series with the basolateral Cl^-/HCO_3^- exchanger. Cell pH regulation could be achieved by the "switching on" of the basolateral Na^+/H^+ exchanger, both mechanisms tending to restore the normal cell pH

dose used was 10^{-5} mol/l with a K_I for the inhibition of the Na^+/H^+ exchanger of $5 \cdot 10^{-7}$ mol/l, it is reasonable to conclude that EIPA was blocking the Na^+ fluxes through the b.l.m., by acting directly on the Na^+/H^+ antiport.

Under physiological conditions, an inwardly directed Na^+ gradient of sevenfold [23] is maintained across the b.l.m. of the frog skin epithelium by the extrusion of Na^+ via the Na^+/K^+ ATPase; the proton chemical gradient is outwardly directed since the internal pH was found to be close to 7.20 (present study; [22]) at a serosal Ringer pH of 7.34. Thus a large thermodynamic driving force favours the net entry of Na^+ in exchange for internal H^+. In many unstimulated epithelia [4] and non-epithelia cell types [21], the antiport appears to be quiescent when the cytoplasmic pH is in the physiological range. It has been proposed that the activation of the Na^+/H^+ exchanger results from the protonation of an internal modifier site after cell pH has decreased. The results presented in this study are supportive of this view (see Table 1 and Fig. 5). However, we found that EIPA (10^{-5} mol/l) added to epithelia incubated in normal Ringer (non acidotic epithelia), produced a small inhibition (less than 20%) of J_{32}. This finding suggest that under steady-state conditions, the Na^+/H^+ exchanger, although functioning at a low rate was still present. In Table 1 it can be observed that the Na^+ pool was increased in acid loaded epithelia despite the continuing presence of a low external pH (6.20). The latter ought to reduce the outwardly directed H^+ gradient and slow down the normal function of the exchanger (Na^+ in, H^+ out) and thus reduce the Na^+ pool. However, we observed the opposite effect: an increase in the Na^+ pool. We interprete this result as being due to the dominant effect of internal H^+ (intracellular acidification) to activate the Na^+/H^+ exchanger whose main driving force (the Na^+ gradient) is still intact. Also, a direct effect of low pH_i on Na^+/K^+ ATPase activity cannot be excluded. Indeed, Eaton et al. (1984) have demonstrated in the urinary bladder that intracellular acidification produced a blockade of the Na^+/K^+ pump.

In summary, this study demonstrates the existence of a Na^+/H^+ exchanger located at the b.l.m. of the frog skin epithelium; its stimulation by cellular acidification makes it a good candidate as a mechanism involved in the regulation of intracellular pH. An apical proton pump in series with a Cl^-/HCO_3^- exchanger located on the b.l.m. of the epithelium has been described in previous studies [13, 15, 16] as the mechanism of active proton excretion in the frog skin. Furthermore this mechanism was shown to participate in maintaining cell pH [22]. A schematic view of the frog skin epithelium and the H^+ extrusion mechanisms following an acidotic shock is illustrated in Fig. 8. The relation between transepithelial acid transport and pH_i regulation can be interpreted as follows: in steady-state conditions, the proton pump at the apical membrane in series with the Cl^-/HCO_3^- exchange mechanism is responsible for the transepithelial acid/base transport. The Na^+/H^+ exchanger in these conditions is functioning at a low rate as the internal pH_i is close to the threshold cell pH for Na^+/H^+ activation. When the internal pH_i is lowered by an acid load, the apical proton pump increases its capacity of transepithelial acid secretion [15] and the basolateral Na^+/H^+ exchanger is switched on. The relative contribution of both systems to cell pH regulation remains to be studied.

Acknowledgements. The technical assistance of C. Raschi and A. Giovagnoli is gratefully acknowledged. This work was supported by grants from the Centre National de la Recherche Scientifique (Physiologie des Membranes U.A 638 associée au CEA).

References

1. Aceves J, Erlij D (1971) Sodium transport across the isolated epithelium of the frog skin. J Physiol (Lond) 212:195–210
2. Aickin CC, Thomas RC (1977) An investigation of the ionic mechanism of intracellular pH regulation in mouse soleus muscle fibres. J Physiol (Lond) 273:295–316
3. Aronson PS (1985) Kinetic properties of the plasma membrane Na^+/H^+ exchanger. Annu Rev Physiol 47:545–560
4. Aronson PS, Nee J, Suhm MA (1982) Modifier role of internal H^+ in activating the Na^+/H^+ exchanger in renal microvillus membrane vesicles. Nature 299:161–163
5. Boron WF, Boulpaep EL (1983) Intracellular pH regulation in the renal proximal tubule of the salamander: Na-H exchange. J Gen Physiol 81:29–52
6. Cala PM (1980) Volume regulation by Amphiuma red blood cells. The membrane potential and its implications regarding the nature of the ionflux pathways. J Gen Physiol 76:683–708
7. Chaillet JR, Lopes AG, Boron WF (1985) Basolateral Na-H exchange in the rabbit cortical collecting tubule. J Gen Physiol 86:795–812
8. Cohen HL, Steinmetz PR (1980) Control of active proton transport in turtle urinary bladder by cell pH. J Gen Physiol 76:381–393
9. Cox TC, Helman SI (1983) Effects of ouabain and furosemide on basolateral membrane Na efflux of frog skin. Am J Physiol 245:F312–F321
10. Cragoe EJ Jr, Woltersdorf OW, Bicking JB, Kwong SF, Jones JH (1967) Pyrazine diuretics. II. N-Amidino-3-amino-5-substituted-6-halopyrazine carboxamides. J Med Chem 10:66–75
11. Deitmer JW, Ellis D (1980) Interactions between the regulation of the intracellular pH and sodium activity of sheep cardiac Purkinje fibers. J Physiol (Lond) 304:471–488

12. Drewnovska K, Biber TUL (1985) Active transport and exchange diffusion of Cl across the isolated skin of Rana pipiens. Am J Physiol 249:F424–F431
13. Duranti E, Ehrenfeld J, Harvey B (1986) Acid secretion through the *Rana esculenta* skin: involvement of an anion-exchange mechanism at the basolateral membrane. J Physiol (Lond) 386:195–211
14. Eaton DC, Hamilton KL, Johnson KE (1984) Intracellular acidosis blocks the basolateral Na-K in rabbit urinary bladder. Am J Physiol 247:F946–F954
15. Ehrenfeld J, Garcia-Romeu F (1977) Active hydrogen excretion and sodium absorption through isolated frog skin. Am J Physiol 233:F46–F54
16. Ehrenfeld J, Garcia-Romeu F, Harvey BJ (1985) Electrogenic active proton pump in *Rana esculenta* skin and its role in sodium ion transport. J Physiol (Lond) 359:331–355
17. Ericson AC, Spring KR (1982) Volume regulation by Necturus gallbladder: apical Na^+/H^+ and Cl^--HCO_3^- exchange. Am J Physiol 243:C146–150
18. Frazier LW (1984) Characteristics of proton excretion in normal and acidotic toad urinary bladder. Biochim Biophys Acta 817:75–84
19. Garvin JF, Simon SA, Cragoe EJ Jr, Mandel LJ (1985) Phenamil: An irreversible inhibitor of sodium channels in the toad urinary bladder. J Membrane Biol 87:45–54
20. Grinstein S, Rothstein A (1986) Mechanisms of regulation of the Na^+/H^+ exchanger. J Membr Biol 90:112
21. Grinstein S, Clarke CA, Rothstein A (1983) Activation of Na^+/H^+ exchange in lymphocytes by osmotically induced volume changes and by cytoplasmic acidification. J Gen Physiol 82:619–638.
22. Harvey BJ, Ehrenfeld J (1986) Regulation of intracellular sodium and pH by the electrogenic H^+ pump in frog skin. Pflügers Arch 406:362–366
23. Harvey BJ, Kernan RP (1984) Intracellular ionic activities in frog skin in relation to external sodium concentration and in the presence of amiloride and/or ouabain. J Physiol (Lond) 349:501–517
24. Kinsella JL, Aronson PS (1980) Properties of the Na^+/H^+ exchanger in renal microvillus membrane vesicles. Am J Physiol 238:F461–469
25. Koefoed-Johnsen V, Ussing HH (1958) The nature of the frog skin potential. Acta Physiol Scand 42:298
26. Labelle EF, Eaton DC (1983) Amiloride-inhibited Na^+ uptake into toad bladder microsomes is Na-H exchange. Biochim Biophys Acta 733:194–197
27. Ludens JH, Fanestil DD (1972) Acidification of urine by the isolated urinary bladder of the toad. Am J Physiol 223:1338–1344
28. Murer H, Hopfer U, Kinne R (1976) Sodium-proton antiport in brush-border membrane vesicles from rat small intestine and kidney. Biochem J 154:597–604
29. Nagel W (1977) The dependence of the electrical potential across the membranes of the frog skin upon concentration of sodium in the mucosal solution. J Physiol (Lond) 269:777–796
30. Nagel W, Garcia-Diaz JF, McD Armstrong W (1981) Intracellular ionic activities in frog skin. J Membr Biol 61:127–134
31. Nord EP, Goldfarb D, Mikhail N, Moradeshagi P, Hafezi A, Vaystub S, Cragoe, EJ Jr, Fine LG (1986) Characteristics of the Na^+/H^+ antiporter in the intact renal proximal tubular cell. Am J Physiol 250:F539–550
32. Oberleithner H, Lang F, Messner G, Wang W (1984) Mechanism of hydrogen ion transport in the diluting segment of frog kidney. Pflügers Arch 402:272–280
33. Pouyssegur J, Chambard JC, Franchi A, Paris S, Van Obbergen-Schilling (1982) Growth factor activation of an amiloride-sensitive Na^+/H^+ exchange system in quiescent fibroblasts: coupling to ribosomal proteins phosphorylation. Proc Natl Acad Sci USA 79:3935–3939
34. Rick RA, Dorge A, Von Arnim E, Thurau K (1978) Electron microprobe analysis of frog skin epithelium: evidence for a syncitial sodium transport compartment. J Membr Biol 39:313–331
35. Roos A, Boron WF (1981) Intracellular pH. Physiol Rev 61:296–434
36. Sasaki S, Skiigai T, Takeuchi J (1985) Intracellular pH in the isolated perfused rabbit proximal straight tubule. Am J Physiol 249:F417–F423
37. Schwartz GJ (1981) Na^+-dependent H^+ efflux from proximal tubule: evidence for reversible Na^+/H^+ exchange. Am J Physiol 241:F380–F385
38. Soltoff SP, Cragoe, EJ Jr, Mandel LJ (1986) Amiloride analogues inhibit proximal tubule metabolism. Am J Physiol 250:C744–C747
39. Steinmezt PR, Omachi RS, Frazier HS (1967) Independence of hydrogen ion secretion and transport of other electrolytes in the turtle bladder. J Clin Invest 46:1541–1548
40. Stoddard JS, Helman SI (1985) Dependence of intracellular Na^+ concentration on apical and basolateral membrane Na^+ influx in frog skin. Am J Physiol 249:F662–F671
41. Stoner LC, Burg MB, Orloff J (1974) Ion transport in cortical collecting tubule: effect of amiloride. Am J Physiol 227:453–459
42. Thomas SR, Suzuki Y, Thompson SM, Schultz SG (1983) Electrophysiology of Necturus urinary bladder: "Instantaneous" current-voltage relations in the presence of varying mucosal sodium concentration. J Membr Biol 73:157–175
43. Ussing HH (1982) Volume regulation of frog skin epithelium. Acta Physiol Scand 114:363–369
44. Vigne P, Frelin C, Cragoe EJ Jr, Lazdunski M (1983) Structure-activity relationship of amiloride and certain of its analogues in relation to the blockade of the Na^+/H^+ exchange system. Mol Pharmacol 25:131–136
45. Weinman SA, Reuss L (1982) Na^+/H^+ exchange at the apical membrane of Necturus gallbladder. J Gen Physiol 80:299–321

Received October 6, 1986/Accepted January 29, 1987

Pflügers Arch (1987) 409:208–213

Pflügers Archiv
European Journal of Physiology
© Springer-Verlag 1987

A quantitative study of the dependence of feline cold receptor activity on the calcium concentration

Klaus Schäfer

Institut für Zoophysiologie, Universtität Hohenheim, Garbenstrasse 30, D-7000 Stuttgart 70, Federal Republic of Germany

Abstract. An isolated preparation of the cat tongue was developed to study quantitatively the relation between single cold receptor activity and calcium concentration. The activity recorded from lingual cold fibres of the isolated preparation was identical to that observed by previous authors in lingual cold receptors of whole animals. A perfusing solution containing excess calcium (5 mmol/l) suppressed discharge at constant temperatures as well as the dynamic response to rapid cooling. Reduced calcium levels (0.5 mmol/l) enhanced cold fibre activity at adapting temperatures above 15°C. Cold receptor activity was linearly inversely related to the logarithm of calcium concentration at adapting temperatures above 20°C. The linear relation was valid for both the discharge at constant temperatures and the dynamic peak frequency during cooling steps. From this relation it was calculated that at 25°C an elevation of 0.1 mmol/l external calcium above the control value (1.53 mmol/l) reduces static firing rate by 0.35 impulses per second. It is concluded that neither the in vitro conditions nor the application of various external calcium concentrations impair cold receptor function. The data are consistent with the hypothesis of a calcium-stimulated outward current controlling the static and dynamic response characteristics of cold receptors.

Key words: Cold receptors – Afferent discharge – Calcium dependence – Sensory processes

Introduction

Sensory transduction in peripheral thermoreceptors involves a calcium-dependent process (Hensel and Schäfer 1974). In cold receptors this process is supposed to be a calcium-stimulated outward conductance controlling afferent activity (Braun et al. 1980). Changes of cold receptor activity induced by various levels of external calcium are in agreement with the hypothesis of calcium channels and calcium-dependent outward currents being present in cold receptors (Schäfer et al. 1982). Calcium currents through neuronal calcium channels vary with the external calcium concentration (Akaike et al. 1978), affecting the intracellular calcium level and the calcium-activated outward conductance (Lux and Hofmeier 1982). Quantitative data concerning the proportion between external calcium levels and afferent discharges might improve the understanding of the sensory transducer process of cold receptors. Since studies on whole animals do not allow the control of extracellular calcium concentrations, experiments on isolated organ preparations seem desirable to gain insight into the conditions, under which the calcium-dependent receptor process is initiated.

Therefore an isolated preparation of the cat tongue was developed with the aim to establish a quantitative relation between receptor activity and external calcium. This approach was expected to elucidate the following two questions: First, to what degree do the calcium-induced modifications of cold receptor activity accord with the known properties of calcium controlled neuronal conductances, and secondly, is the cold receptor sensitivity to calcium in a range that might influence the sensory process under physiological conditions? I here present evidence that minute changes of external calcium affect cold receptor activity to a degree which might be considered to have physiological implications. Furthermore the changes of cold fibre discharge induced by various external calcium levels accord with properties of neuronal calcium channels, namely with the nonlinear dependence of the calcium current on the extracellular calcium concentration. Additionally, the changes of cold receptor activity in intact animals are comparable with those in the isolated organ preparation, indicating a specific action of calcium in both cases. A preliminary account of these experiments has been published (Schäfer 1985).

Methods

Six adult cats were anaesthetized with intravenous sodium pentobarbital (35 mg/kg). To obtain free access to the whole tongue, after ligature of the mandibular artery the mandibula was resected from the apex to the angle. Both lingual arteries were cannulated and after start of perfusion the tongue was excised. The isolated tongue was placed upside down within the Perspex recording chamber (Fig. 1), with the apical part located on a nickel-plated brass thermode, and was secured to the baseplate with fine surgical thread. The isolated preparation was perfused with a modified Krebs solution containing (mmol/l): 118.40 NaCl, 26.60 $NaHCO_3$, 2.83 KCl, 1.32 KH_2PO_4, 1.46 $MgSO_4$, 1.53 $CaCl_2$, and 11.6 glucose. Perfusion pressure was provided by gravity and corresponded to the mean arterial blood pressure monitored in cats (on average 120 mm Hg, Altmann and Dittmer 1974). Flow of perfusate was adjusted to about 0.2 ml/g/min, which is in the range reported for lingual blood flow in cats (0.29 ml/g/min; Alm and Bill 1973). The solutions used to perfuse the isolated organ were

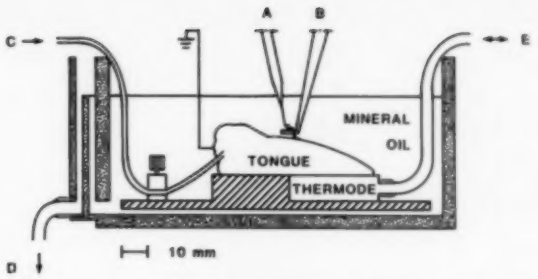

Fig. 1. Lateral view of the Perspex recording chamber. The isolated tongue is secured to a baseplate with surgical thread. *A*, recording electrode (polished flattened platinum wire); *B*, dissection plate; *C*, tubing connected with lingual arteries to perfuse the tongue; *D*, outlet of waste solution (the spillway was designed to keep the level of mineral oil within the chamber constant independently from the flow of perfusate); *E*, tubing to connect the thermode with the multiway tap

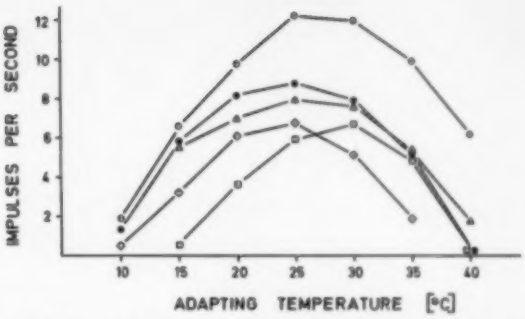

Fig. 2. Average impulse activity of lingual cold fibres as a function of thermode temperature. Data from the isolated tongue preparation compared with published data from whole animals. (●), isolated tongue preparation, $n = 17$; (□), Hensel and Zotterman 1951, $n = 6$; (◇), Dodt 1953, $n = 5$; (△), Benzing et al. 1969, $n = 44$ (cited after Hensel 1973); (○), Bade et al. 1979, $n = 27$

aerated with a mixture of 95% oxygen and 5% carbon dioxide, the final pH of the solution being 7.40. Control and experimental solutions differed in their calcium content. Calcium concentration of the control solution was 1.53 mmol/l, corresponding to an calcium activity of 1.35 mmol/l, which was evaluated with the aid of a calcium-sensitive electrode (Orion system 99-20). Serum calcium activity was determined in cats by the same system to be 1.36 mmol/l on the average. Calcium concentrations of the experimental solutions were 0.5 mmol/l ("low calcium") and 5.0 mmol/l ("high calcium"), respectively. Any variation in calcium concentration was compensated for by a corresponding change in sodium concentration, so that the total cation concentration remained constant.

After the lingual nerve had been exposed, the branch serving the apical part of the tongue was isolated and dissected into small strands on a small black Perspex plate. The strands were placed on a fine platinum wire for monopolar recording of single unit activity. The indifferent electrode was inserted in nearby tissue. Receptive fields of identified cold fibres were stimulated by a water-circulated thermode with an area of 35×35 mm, connected with seven water baths controlled at 40°, 35°, 30°, 25°, 20°, 15° and 10°C. With a multiway tap, successive cooling steps of 5°C were applied within the range of static temperatures available, the period between each step being 3 to 5 min. The slope of the temperature change against time was nonlinear, but 80% of the final temperature was reached within 3 s. A thermocouple was attached to a groove in the stimulating surface of the thermode. The whole isolated tongue was kept under mineral oil. The venous outflow of perfusate was removed from the chamber by a spillway, which allowed the level of mineral oil to be kept constant throughout the experiment, independently of the flow of perfusate (Fig. 1).

Having recorded the control values of cold fibre activity at constant temperatures and following cooling steps (e. g. static and dynamic responses), the tongue was perfused with either the "low calcium" or "high calcium" solution. After the appropriate stimulation series had been completed, a second control series was added. If the signal-to-noise ratio of the impulses allowed a further recording, cold fibre activity was monitored during a second experimental series, using the perfusion solution which was not tested so far. After this stimulation series had been completed, a third control series was added, if possible.

Data were stored on magnetic tape for off-line analysis. Responses to constant temperatures were measured as the average number of impulses/s within a period of 1 min prior to a temperature change. This ensured that the receptor activity had been stabilized at least 1 min prior to the measuring period. Dynamic responses to the 5°C cooling steps were characterized by the peak frequency obtained during the decrease of temperature; measuring period was 0.5 s.

Results

A total of 17 single afferent fibres showing the characteristics of specific cold fibres (Hensel 1981) were identified, and their response properties were recorded under control perfusion conditions. The activity of these fibres at various constant temperatures was compared to data of lingual cold receptors studied in the intact animal in different laboratories (Hensel and Zotterman 1951; Dodt 1953; Benzing et al. 1969; Bade et al. 1979). As shown in Fig. 2, responses to static thermal stimuli of fibres from the isolated preparation are in good agreement with those observed by various authors in the intact animal, thus indicating that cold receptor function is not interfered with by the isolation of the tongue. Furthermore, a discharge consisting of impulse groups separated by pauses (burst discharge), which has been repeatedly described for lingual cold fibres of the intact animal (Hensel 1981), was also apparent in fibres of the isolated preparation.

In 5 experiments, static and dynamic activity of cold receptors was recorded while perfusing the tongue with a solution containing either excess or reduced calcium. Moreover, a complete set of data was obtained during perfusion with both low and high calcium solution in additional 6 experiments. After each experimental perfusion with either low or high calcium, a control perfusion was added. The recording of an entire stimulation series took at least 3.5 h to be completed, consisting of 3 control and 2 experimental runs. After approximately 8 h of perfusion, the responses of mechanically as well as of thermally sensitive units to adequate stimulation deteriorated, and after 8 h occasional-

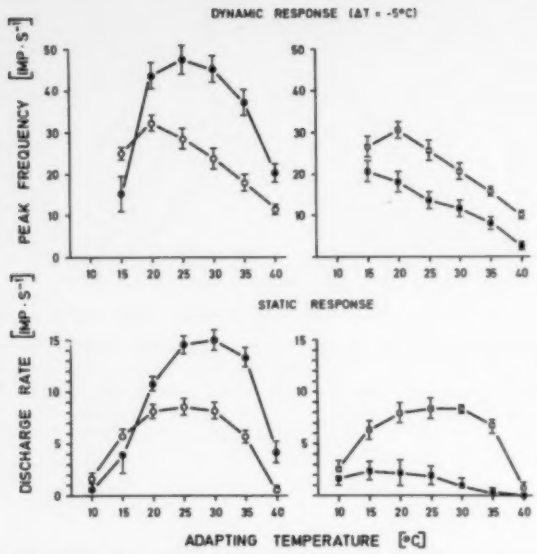

Fig. 3. Effect of three different extracellular calcium concentrations on static and dynamic responses of cold receptors of the isolated tongue preparation. *Upper diagrams*, dynamic response (peak frequency following a 5° C cooling step from adapting temperature); *lower diagrams*, mean static firing rate (sampling period 1 min). *Left diagrams*, effect of lowered external calcium (○, control; ●, 0.5 mmol/l calcium, $n = 11$); *right diagrams*, effect of elevated external calcium (□, control; ■, 5 mmol/l calcium, $n = 6$). *Bars* indicate SEM

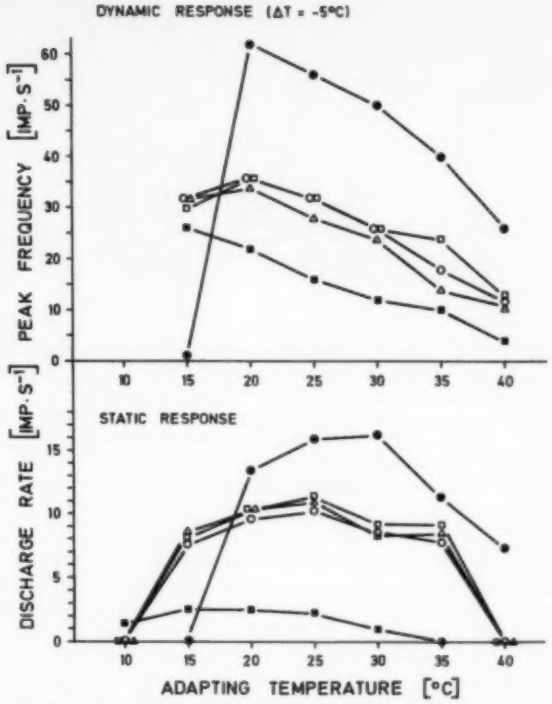

Fig. 4. Response characteristics of a single cold fibre at control conditions before and after perfusion with a solution containing reduced or excess calcium. *Upper diagram*, dynamic peak frequency following a 5° C cooling step from adapting temperature; *lower diagram*, mean static firing rate. Perfusion protocol: (○) first control; (●) 0.5 mmol/l calcium; (□) second control; (■) 5 mmol/l calcium; (△) third control. This experiment took more than 4 h to be completed

ly a separation of the mucous membrane from the underlying tissues could be observed. It was therefore concluded that the tongue generally does not survive for periods longer than 8 h after isolation.

After switching from the actual perfusing solution to solutions of different calcium concentration, the cold receptor activity adjusted to a new steady-state level within an average of 1.8 min. This period includes a delay of 0.5 min due to the dead space in the tubing. The temporal pattern of adjustment of discharge rate was identical for the various changes of calcium concentrations which were applied. Compared to control conditions, perfusion with solutions containing excess calcium suppressed cold receptor activity at constant temperatures and reduced the dynamic peak frequency following rapid cooling steps. Data were obtained from 6 cold fibres during perfusion with the solution containing 5 mmol/l calcium, and are presented in Fig. 3.

Perfusion with the low calcium solution induced a temperature-dependent modulation of cold receptor discharge. At low temperature, impulse activity was suppressed, but at temperatures exceeding 15° C discharge was enhanced both at constant temperatures and during the dynamic response to rapid cooling. Data of 11 cold fibres completely recorded during control and low calcium perfusion conditions are given in Fig. 3. The similarity of the two cold fibre samples concerning their responses to either constant temperatures or rapid cooling steps under control conditions indicates that a homogeneous population of cold receptors was studied.

The maximal sensitivity to thermal stimuli was shifted to higher temperatures by 2.7° C (static temperatures) and 3.2° C (rapid cooling steps) during perfusion with solutions containing reduced calcium. Perfusion with "high calcium" solutions resulted in a shift of the maximal sensitivity in the opposite direction, with the respective values reduced by 12.5° C (static sensitivity) and 3.3° C (dynamic sensitivity). The values are calculated from the data of fibres presented in Fig. 3. In this figure, the shifts are well visible.

These changes, which are induced by perfusion with solutions containing either reduced or excess calcium, are qualitatively identical to those, which can be obtained by lowering or elevating extracellular calcium systemically in whole animals (Schäfer et al. 1982). However, the effects of altered external calcium levels are less pronounced in the intact animal, indicating smaller changes of free extracellular calcium in these experiments.

The exposure of cold receptors to either reduced or elevated external calcium levels for periods of up to 1 h did not impair their cellular function, since the induced effects were perfectly reversible and reproducible. As illustrated in Fig. 4, no permanent modification of cold receptor response characteristics could be observed. Static and dynamic responses were essentially identical, when various control series of an individual cold fibre were compared, which were recorded subsequently to the respective experimental stimulation series.

A temperature-dependence of the effect of calcium on cold receptor activity was revealed by comparing the relative

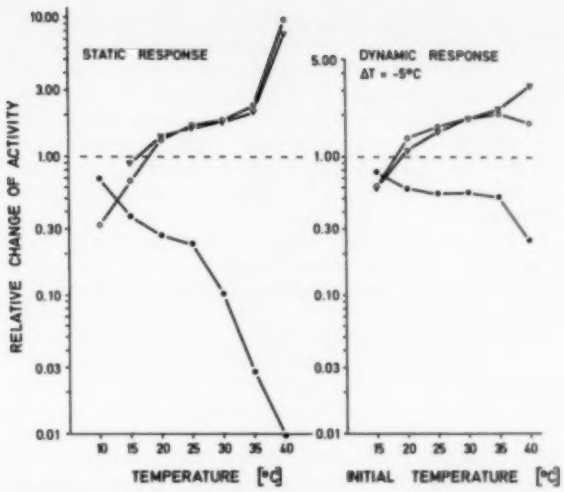

Fig. 5. Temperature dependence of the effect of reduced and elevated external calcium levels on cold receptor activity. For comparison, the effects of external menthol on the cold receptor responses have been added. The data are plotted as relative changes. Control values are represented by "1,00". *Left diagram*, static firing rate; *right diagram*, dynamic peak frequency following 5°C cooling from adapting temperature. (○) 0.5 mmol/l calcium; (●) 5 mmol/l calcium. Same data as shown in Fig. 3. (▽) 50 µmol/l menthol, $n = 3$

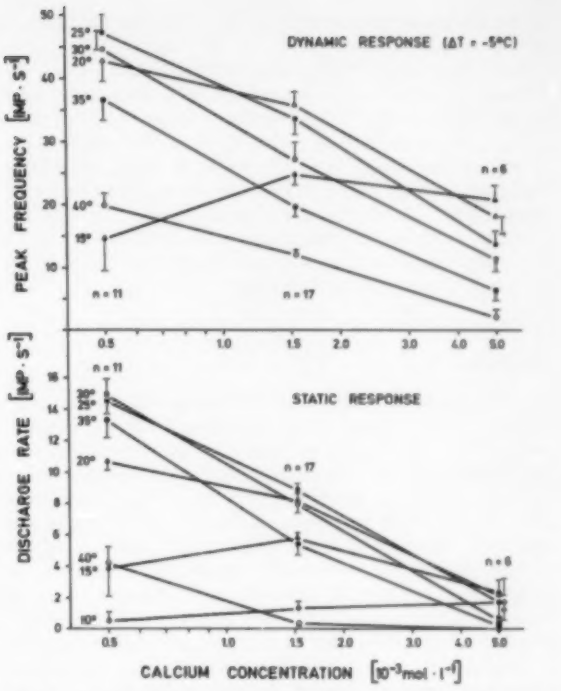

Fig. 6. Dynamic peak frequency following cooling (*upper diagrams*) and mean static firing rate (*lower diagrams*) as a function of extracellular calcium concentration. Adapting temperatures as indicated. Control values correspond to a calcium concentration of 1.53 mmol/l (see Methods). *Bars* indicate SEM. Pooled data of all fibres. For various adapting temperatures a regression analysis was performed (see text), the respective correlation coefficients are given in the following: Dynamic response, −0.83 (40°C); −0.76 (35°C); −0.77 (30°C); −0.75 (25°C); −0.68 (20°C); static response, −0.85 (35°C); −0.88 (30°C); −0.86 (25°C); 0.27 (10°C)

changes of activity induced by excess or reduced calcium. The data are plotted in Fig. 5. Static responses were considerably more affected by the altered calcium concentration than the dynamic responses to rapid cooling. This has been as well observed in the whole animal, when the calcium concentration was modified by administration of either calcium salts or the calcium chelating agent EDTA (Schäfer et al. 1982). At adapting temperatures below 20°C, perfusion with both reduced and excess calcium containing solutions suppressed cold fibre activity, the depressing action being effective at static as well as at dynamic thermal conditions. The stimulating effect of low calcium and the inhibiting effect of high calcium, however, generally increased with warming in the temperature range between 20° and 40°C, and maximal modification of receptor discharge was obtained at high stimulation temperatures (Fig. 5). The relative changes of receptor activity induced by lowered or elevated external calcium levels are rather symmetrical, indicating that the effects are based on a common mechanism. Recently it has been shown that menthol specifically and selectively impairs the conductance of neuronal calcium channels (Swandulla et al. 1986, 1987). The relative changes of cold fibre activity induced by perfusing the isolated tongue with a solution containing 50 µmol/l menthol have been added in Fig. 5 for comparison. The data are from Schäfer et al. (1986). It is apparent by these data that reduced external calcium and menthol both affect the cold receptor responses quite uniformly.

Plotting the available data on linear-logarithmic coordinates indicated the existence of a linear inverse relationship between the cold receptor activity and the logarithm of the calcium concentration at adapting temperatures above 20°C. This suspected linear dependence of receptor response on the logarithm of the calcium concentration applied to both the impulse activity at constant temperatures and the dynamic peak frequency during rapid cooling steps (Fig. 6). Therefore the relationship of each set of data obtained during the various stimulus conditions was tested for the appropriatenes of a simple linear regression model. The null hypothesis, i.e. a linear relationship, was rejected for the data obtained during 40°C, 20°C and 15°C of maintained temperatures, and for the data obtained during cooling from 15°C adapting temperature. For the remaining sets of data a simple linear regression analysis was performed; the corresponding coefficients of correlation are given in the legend of Fig. 6. The observed behaviour could be described by the following equation:

$$f = a - b \log_{10}[\mathrm{Ca}]$$

where f is the cold receptor activity, a is a constant, b is the slope of the relation, and [Ca] is the calcium concentration of the solution used to perfuse the isolated tongue. The function is considered to apply to the impulse activity at any adapting temperature above 20°C. The deviation of the 40°C relation may result from the complete inhibition of a number of receptors at normal and high calcium concentrations, causing a deflection of the relation because the impulse frequency cannot bear a negative sign.

At thermoneutral conditions, the nasal skin temperature of cats can be assumed to be in the range of 20°–25°C (Hensel and Banet 1982). Therefore the calculation of the slope of the relation per decade external calcium was based on the data for 25°C adapting temperature. For the static firing rate, the term *b* amounts to −12.5 impulses/s, the corresponding value for the dynamic peak frequency following cooling being −33.3 impulses/s. This proves a considerable sensitivity of the cold receptor to external calcium: mean static firing rate is reduced at 25°C by 0.35 impulses/s, when external calcium is elevated by 0.1 mmol/l above the control value.

Discussion

One main result of the study is the finding that cold receptor function is not impaired by recording from an isolated perfused organ preparation. This technique therefore allows the investigation of sensory processes quantitatively under in vitro conditions, which might be of general importance since the response properties of feline cold receptors are similar to those of primate cold sensors (Hensel 1976). Additionally, the data provide conclusive evidence for a participation of calcium channels and calcium-stimulated outward conductances in the process of sensory transduction in cold receptors. The relative changes of cold receptor activity induced by low and high external calcium levels are comparable in studies on the isolated tongue and on whole animals (Schäfer et al. 1982), indicating a specific action of calcium on the receptive structures.

The results will be discussed in two ways. First, the data will be related to membrane mechanisms possibly involved in sensory transduction, and secondly, possible implications of the observed calcium effects for sensory signal processing will be addressed.

Sensory processes

In general a nonlinear relationship between external ionic concentration and afferent activity is to be expected, because the amplitude of the receptor potential is predicted by the Nernst equation to depend logarithmically on the ionic activity, and also because for biological sensors a simple linear relationship has been assumed to exist between the amplitude of the receptor potential and the frequency of the afferent impulses (Uttal 1973; Duncan 1981). But do the data accord with the known properties of neuronal ionic channels? Current through calcium channels varies nonlinearly with external calcium concentration (Akaike et al. 1978; Gorman and Thomas 1980a), the relation being hyperbolic, because the calcium current saturates with elevation of external calcium concentration. However, calcium does not affect the receptor potential as a current carrier in cold receptors, since elevation of external calcium does not increase afferent activity by depolarizing the sensory membrane. Yet, various membrane conductances are controlled by the level of intracellular free calcium, which also depends nonlinearly on external calcium (Gorman and Thomas 1980a). The data indicate that a calcium-activated outward current is involved, masking the direct effect of the calcium channel by its considerably higher conductance (Akaike et al. 1978; Lux and Hofmeier 1982). The calcium-stimulated outward current is linearly related to the intracellular calcium activity (Gorman and Thomas 1980b), and a nonlinear relation of external calcium and calcium-dependent outward conductance including saturation has been observed (Lux and Hofmeier 1982). These data concerning the properties of calcium-dependent neuronal channels accord reasonably well with the results of the present study to support the view that cold receptor function is controlled by calcium channels and by calcium-stimulated outward conductances.

There is additional evidence indicating that calcium-controlled conductances are involved in cold receptor transducer processes. Menthol induces changes of cold receptor activity, which are perfectly identical to those induced by reduced external calcium levels (Fig. 5, see also Schäfer et al. 1986). At comparable effective doses, menthol was recently discovered to specifically and selectively impair invertebrate and vertebrate neuronal calcium conductances (Swandulla et al. 1986, 1987), which was associated with a concomitant decrease of the calcium-sensitive potassium outward current (D. Swandulla, K. Schäfer, and H. D. Lux, unpublished observations). Likewise, the increasing effect of calcium on cold receptor activity with higher temperatures corresponds to the temperature dependence of neuronal calcium channels (Lux and Brown 1984).

Reduced extracellular calcium levels induce depolarizing shifts of membrane potential in invertebrate and vertebrate bursting neurons, whereas elevated calcium results in hyperpolarisation (Gola and Selverston 1981; Legendre et al. 1985); the induced changes of potential being associated with concomitant modifications of discharge rate (Legendre et al. 1985).

Activity of these neurons is controlled by calcium currents and by calcium-stimulated conductances. The considerable conformity of the calcium-induced changes of membrane potential in these neurons with the mechanisms proposed to underly the calcium induced modifications of afferent activity in cold sensors further support the view that identical processes might be involved in the control of membrane potential in both cell types.

Possible functional implications

The data presented here show that in cold receptors both the discharge at maintained temperatures and the dynamic response to cooling steps are similarly affected by alterations of external calcium. A calcium-activated conductance is supposed to control the static and dynamic response properties of crustacean stretch receptors (Ottoson and Swerup 1982), indicating a more general functional significance of calcium-dependent processes in sensory transduction. The inherent property of such processes to act as negative feedback systems may serve to increase the temporal resolution of the sensory process to step increments of stimulus. The results of this study and earlier observations (Schäfer et al. 1982, 1986) suggest that calcium contributes to the decline of impulse frequency after the initial increase during dynamic responses. Therefore the enhancement of the dynamic response by low calcium could result from the impaired activation of the calcium-stimulated outward conductance. In analogy, the reduction of dynamic peak frequency could result from an excessive activation by high calcium.

Within the physiologically relevant temperature range of 20°C–40°C, the dependence of cold fibre discharge on

external calcium levels can be described by a logarithmic relation. At 25° C a reduction of mean cold receptor activity of 0.35 impulses/s can be calculated for an elevation of 0.1 mmol/l free external calcium above the control value (1.34 mmol/l). Since peripheral warm receptors are either excited by elevated calcium levels (Hensel and Schäfer 1974), or any modulating effect of calcium on warm receptor activity requires higher effective doses (Schäfer, unpublished observations), the observed sensitivity of peripheral cold receptors to calcium could be of functional significance. Increases of 0.1 mmol/l of plasma ionized calcium have been observed to occur during physical work (Greenleaf et al. 1979), and a calcium-dependent additional factor has been suggested to affect thermoregulation during exercise (Greenleaf 1979). Therefore the idea of a peripheral calcium controlled sensory process being involved in thermoregulation is tempting. Thermoregulatory responses to altered plasma calcium levels have been observed in various species (Nielsen 1974a, b). However, the data accumulated so far do not allow to decide if the afferent or the efferent pathway within the thermoregulatory control system is most sensitive to calcium. Central actions of peripheral calcium can be excluded, since the calcium activity within the CNS is maintained fairly constant despite considerable and long-lasting changes in the plasma calcium activity (Tai et al. 1986). There is no doubt that further experiments and additional evidence are needed to elucidate the mechanisms of the thermoregulatory effects of peripheral calcium.

Acknowledgements. I am greatly indebted to Dr. R. F. Hellon for helpful comments on this manuscript, and to R. Binder and A. Garriss for skillful and reliable assistance. The research was supported by the Deutsche Forschungsgemeinschaft.

References

Akaike N, Lee KS, Brown AM (1978) The calcium current of Helix neuron. J Gen Physiol 71:509–531

Alm A, Bill A (1973) The effect of stimulation of the cervical sympathetic chain on retinal oxygen tension and on uveal, retinal and cerebral blood flow in cats. Acta Physiol Scand 88:84–94

Altman PL, Dittmer DS (1974) Biology data book, vol III. Federation of American Societies for Experimental Biology, Bethesda, MD

Bade H, Braun HA, Hensel H (1979) Static burst parameters of lingual cold receptors in the cat. Pflügers Arch 382:1–5

Benzing H, Hensel H, Wurster RD (1969) Integrated static activity of lingual cold receptors in the cat. Pflügers Arch 311:50–54

Braun HA, Bade H, Hensel H (1980) Static and dynamic discharge patterns of bursting cold fibres related to hypothetical receptor mechanisms. Pflügers Arch 386:1–9

Dodt E (1953) The behaviour of thermoreceptors at low and high temperatures with special reference to Ebbecke's temperature phenomena. Acta Physiol Scand 27:295–314

Duncan CJ (1981) The transducer mechanism of sense organs. In: Laverack MS, Cosens DJ (eds) Sense organs. Blackie, Glasgow, pp 100–111

Gola M, Selverston A (1981) Ionic requirements for bursting activity in lobster stomatogastric neurons. J Comp Physiol 145:191–207

Gorman ALF, Thomas MV (1980a) Intracellular calcium accumulation during depolarization in a molluscan neurone. J Physiol (Lond) 308:259–285

Gorman ALF, Thomas MV (1980b) Potassium conductance and internal calcium accumulation in a molluscan neurone. J Physiol (Lond) 308:287–313

Greenleaf JE (1979) Hypothermia and exercise. In: Robertshaw D (ed) Environmental physiology III, International reviews of physiology, vol 20. University Park Press, Baltimore, pp 157–208

Greenleaf JE, Beaumont W Van, Brock PJ, Morse JT, Mangseth GR (1979) Plasma volume and electrolyte shifts with heavy exercise in sitting and supine positions. Am J Physiol 236:R206–R214

Hensel H (1973) Cutaneous thermoreceptors. In: Iggo A (ed) Handbook of sensory physiology, vol II. Springer, Berlin Heidelberg New York, pp 79–110

Hensel H (1976) Correlation of neural activity and thermal sensation in man. In: Zotterman Y (ed) Sensory functions of the skin. Pergamon, Oxford, pp 331–353

Hensel H (1981) Thermoreception and temperature regulation. Academic Press, London

Hensel H, Banet M (1982) Adaptive changes in cats after long-term-exposure to various temperatures. J Appl Physiol 52:1008–1012

Hensel H, Schäfer K (1974) Effects of calcium on warm and cold receptors. Pflügers Arch 352:87–90

Hensel H, Zotterman Y (1951) Quantitative Beziehungen zwischen der Entladung einzelner Kältefasern und der Temperatur. Acta Physiol Scand 23:291–319

Legendre P, McKenzie JS, Dupouy B, Vincent JD (1985) Evidence for bursting pacemaker neurones in cultured spinal cord cells. Neuroscience 16:753–767

Lux HD, Brown AM (1984) Patch and whole cell calcium currents recorded simultaneously in snail neurons. J Gen Physiol 83:727–750

Lux HD, Hofmeier G (1982) Properties of a calcium- and voltage-activated potassium current in Helix pomatia neurons. Pflügers Arch 394:61–69

Nielsen B (1974a) Actions of intravenous Ca^{2+} and Na^{+} on body temperature in rabbits. Acta Physiol Scand 90:445–450

Nielsen B (1974b) Effect of changes in plasma Na^{+} and Ca^{2+} ion concentration on body temperature during exercise. Acta Physiol Scand 91:123–129

Ottoson D, Swerup C (1982) Studies on the role of calcium in adaptation of the crustacean stretch receptor. Effects of intracellular injection of calcium, EGTA, and TEA. Brain Res 244:337–341

Schäfer K (1985) Cold receptor activity quantitatively related to calcium concentration. Pflügers Arch 403:R52

Schäfer K, Braun HA, Hensel H (1982) Static and dynamic activity of cold receptors at various calcium levels. J Neurophysiol 47:1017–1028

Schäfer K, Braun HA, Isenberg C (1986) Effect of menthol on cold receptor activity: Analysis of receptor processes. J Gen Physiol 88:757–776

Swandulla D, Schäfer K, Lux HD (1986) Calcium channel current inactivation is selectively modulated by menthol. Neurosci Lett 68:23–28

Swandulla D, Carbone E, Schäfer K, Lux HD (1987) Effect of menthol on two types of Ca currents in cultured sensory neurons of vertebrates. Pflügers Arch 409:52–59

Tai CY, Smith QR, Rapoport SI (1986) Calcium influxes into brain and cerebrospinal fluid are linearly related to plasma ionized calcium concentration. Brain Res 385:227–236

Uttal WR (1973) The psychobiology of sensory coding. Harper and Row, New York

Received September 24, 1986/Accepted February 13, 1987

Pflügers Arch (1987) 409:214–216

Pflügers Archiv
European Journal of Physiology
© Springer-Verlag 1987

Effects of thyroid hormone on the action potential and membrane currents of guinea pig ventricular myocytes

Ofer Binah, Irit Rubinstein, and Eran Gilat

Department of Physiology and Biophysics, Faculty of Medicine and Rappaport Family Institute for Research in the Medical Sciences, Technion-Israel Institute of Technology, Haifa 31096, Israel

Abstract. We studied the effects of thyroid hormone on the action potential and membrane currents recorded from enzymatically dissociated guinea pig ventricular myocytes, by means of the whole-cell recording technique. Hypothyroidism was associated with an increase in action potential duration, whereas hyperthyroidism was associated with a decrease in duration. These effects are similar to those reported in multicellular preparations. Hypo- and hyperthyroidism were also associated with a decrease and an increase, respectively, in the slope of the action potential plateau. Resting potential and action potential amplitude were unaffected by the alterations in the thyroid state. The voltage-clamp experiments revealed that as compared with euthyroid myocytes, the peak calcium current was bigger in hyperthyroid myocytes and smaller in hypothyroid myocytes. The potassium outward current (at a membrane potential = 50 mV) was of similar amplitude in hypo- and euthyroid myocytes and bigger in hyperthyroid myocytes. Our major conclusion is that thyroid hormones regulate the amplitude of the calcium current and that this effect may be responsible in part for the modulation of myocardial contractility by thyroid hormones.

Key words: Thyroid hormone – Guinea pig ventricular myocytes – Transmembrane action potential – Membrane currents

Introduction

During the course of a previous study on the relationships between the thyroid state and ventricular action potential characteristics, we found that action potential duration is inversely correlated ($r = -0.91$) with oxygen consumption across a wide range of species (from man to shrew), and that in guinea pig ventricular muscle, hypothyroidism is associated with a longer action potential duration, whereas hyperthyroidism is associated with a marked shortening of action potential duration and a faster rate of repolarization [1, 2]. Other authors have reported similar results in rabbit atrial, sinoatrial, and ventricular action potential duration [3, 6, 11]. The mechanisms responsible for the electrophysiological effects of thyroid hormones are still unknown, and progress in this direction has probably been hampered by the fact that thyroid hormones have multiple actions, induced either directly or indirectly [8, 10]. As the whole-cell recording technique now provides us with a powerful tool to study the mechanisms responsible for thyroid hormone action, our main objectives in the present study were: (1) to determine whether changes in ventricular action potential characteristics due to alterations in thyroid state could also be demonstrated in isolated myocytes, and (2) to provide preliminary data on the membrane currents that are affected by thyroid hormones.

Offprint requests to: O. Binah

Materials and methods

Guinea pig ventricular myocytes were enzymatically dissociated according to procedures described elsewhere [5], with slight modifications. Myocytes were superfused with modified Tyrode's solution (at 24.5°C) containing (mM): NaCl, 140; KCl, 4; $CaCl_2$, 1.8; $MgCl_2$, 1; glucose, 10; HEPES, 5. pH was adjusted to 7.4. Recordings were carried out with L/M-EPC 7 (List Medical, Darmstadt, FRG) by means of heat-polished electrodes (Kimble, Toledo, OH, USA) with tip resistance of 1–2 mΩ. The electrode solution contained (mM): K-aspartate, 100; KCl, 20; $MgCl_2$, 3.5; KH_2PO_4, 20; Na_2ATP, 3; EGTA, 1. pH was adjusted to 7.4.

In the current-clamp experiments, myocytes were stimulated through the electrode at a cycle length of 2 s. In the voltage-clamp experiments, command pulses as well as the membrane current sampling were under digital computer control (Data General, DG-20). Command pulses were generated by a 10-bit digital-to-analogue converter and were delivered at a cycle length of 5 s from a holding potential of −40 mV. The membrane current was filtered at 1 kHz, sampled by means of a 10-bit analogue-to-digital convertor and stored on a 15-MB hard disk for off-line analysis. The amplitude of the calcium current (I_{Ca}) was measured at the peak of the net inward current, and the potassium outward current (I_K) was measured as the current level 300 ms after the onset of the clamp pulse.

Hyperthyroidism was induced by intraperitoneal injections of L-thyroxine, 150 μg/kg, for 8–11 days. Hypothyroidism was induced by maintaining guinea pigs on regular Purina chow and drinking water containing 0.05% propylthiouracyl for 45 days. Drugs were obtained from Sigma, St. Louis, MO, USA. Free thyroxine levels were determined in the serum using a commercial kit (Clinical Assays, Cambridge, MA, USA).

Results

In the hypothyroid, euthyroid, and hyperthyroid guinea pigs, free thyroxine levels (mean ± SEM) were 0.20 ± 0.02,

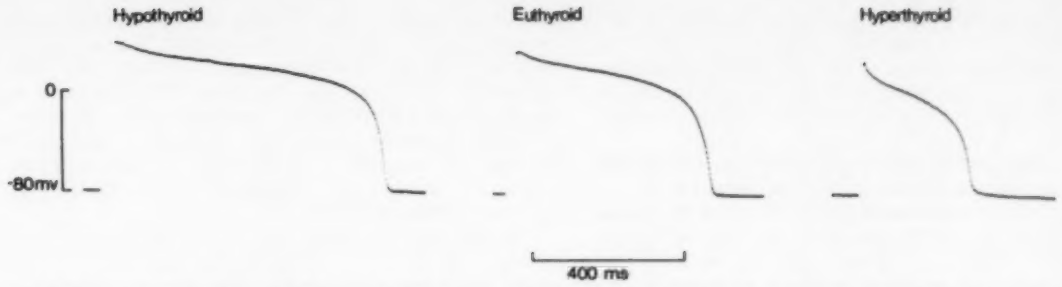

Fig. 1. Representative action potentials recorded from ventricular myocytes isolated from hypothyroid, euthyroid, and hyperthyroid guinea pigs. Cycle length = 2 s; temperature = 24.5°C

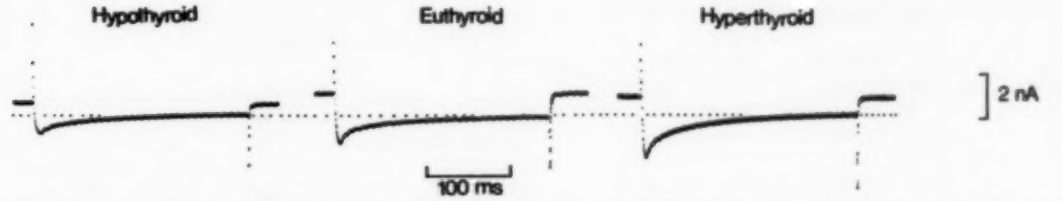

Fig. 2. Representative membrane currents from hypothyroid, euthyroid, and hyperthyroid guinea pig ventricular myocytes. Holding potential = −40 mV; command pulse = 50 mV; cycle length = 5 s; temperature = 24.5°C

Table 1. Effects of hypothyroidism and hyperthyroidism on action potentials from guinea pig ventricular myocytes

	No. of myocytes	RP (mV)	AP amp (mV)	APD_{30} (ms)	APD_{50} (ms)	APD_{90} (ms)	Slope of plateau (mV/ms)
Euthyroid	15	-83.0 ± 0.9	130.9 ± 1.6	359.0 ± 24.0	449.2 ± 25.0	499.0 ± 23.9	0.23 ± 0.02
Hypothyroid	20	-80.8 ± 0.6	134.8 ± 0.7	513.7 ± 34.7*	592.5 ± 31.5*	635.1 ± 28.9**	0.17 ± 0.02***
Hyperthyroid	17	-81.8 ± 1.0	129.3 ± 1.6	243.8 ± 23.8*	323.5 ± 19.3**	360.0 ± 19.6**	0.36 ± 0.03***

Values are means ± SEM. The slope of the plateau of the action potential was calculated from the linear part of the voltage trace
The P values are compared with the euthyroid (control) values. * $P < 0.005$, ** $P < 0.001$, *** $P < 0.05$
RP, resting potential; AP amp, action potential amplitude; APD_{30}, APD_{50}, and APD_{90}, action potential duration at 30, 50, and 90% repolarization, respectively

1.17 ± 0.09, and > 23.5 µg/dl, respectively. Figure 1 depicts action potentials recorded from ventricular myocytes isolated from hypothyroid, euthyroid, and hyperthyroid guinea pigs. These recordings demonstrate that hypo- and hyperthyroidism are associated with marked alterations in action potential configuration, the most pronounced changes being an increase in action potential duration in the hypothyroid state and a decrease in duration in the hyperthyroid state. Hypo- and hyperthyroidism were also associated with a decrease and an increase, respectively, in the slope of the action potential plateau. Table 1 summarizes action potential characteristics in the different thyroid states. Compared with euthyroid myocytes, action potential duration at 30, 50, and 90% repolarization was longer in the hypothyroid and shorter in the hyperthyroid myocytes. Action potential amplitude and resting potential were not affected by the alterations in the thyroid state.

We then studied the effects of thyroid hormones on I_{Ca} and on I_K. In the euthyroid (18 cells), hyperthyroid (23 cells), and hypothyroid (21 cells) myocytes, the peak I_{Ca} was (mean ± SEM): -1.20 ± 0.17, -1.68 ± 0.17, and -0.70 ± 0.05 nA, respectively ($P < 0.05$, hyperthyroid versus euthyroid myocytes; $P < 0.001$, hypothyroid versus euthyroid myocytes). In the euthyroid, hyperthyroid, and hypothyroid myocytes, I_K at a membrane potential of 50 mV was: 0.34 ± 0.06, 0.73 ± 0.13, and 0.33 ± 0.04 nA, respectively ($P < 0.025$, hyperthyroid versus euthyroid). Figure 2 depicts representative membrane currents recorded from hypothyroid, euthyroid, and hyperthyroid myocytes in response to a command pulse of 50 mV delivered from a holding potential of −40 mV. It is illustrated that in the hypothyroid myocyte I_{Ca} was smaller, whereas in the hyperthyroid myocyte I_{Ca} was bigger than the current in the euthyroid myocyte.

Discussion

The present study demonstrates that hypo- and hyperthyroidism are associated with alterations in the action potential and membrane currents of guinea pig ventricular myocytes. With respect to the action potential, the main findings were that hyperthyroidism was associated with a decrease in action potential duration, whereas an increase

in duration occurred in hypothyroidism. These findings are very similar to those reported by us and by others in multicellular preparations [1–3, 6, 11], thereby rendering guinea pig ventricular myocytes an appropriate model for studying the electrophysiological effects of thyroid hormones.

While additional information is required to understand the fundamental mechanisms of thyroid hormone action, the present study demonstrates for the first time, by means of direct measurement of the membrane current, that thyroid hormones modulate the amplitude of the I_{Ca}. It should be noted that the effects of thyroid hormones on action potential duration and on I_{Ca} are not in disagreement. Thus, thyroid hormones can increase peak I_{Ca} and, at the same time, attenuate the plateau and decrease action potential duration by affecting other currents such as I_K and perhaps the early outward current and the tetrodotoxin-sensitive window current.

The effect of thyroid hormones on myocardial contractility has long been recognized, and this effect has been proposed to result from the regulation of myosin ATPase isozymes (V_1, V_2, and V_3) by thyroid hormones. Hence, thyroid hormones stimulate the synthesis and predominance of the high-activity V_1 form, whereas hypothyroidism results in low-activity V_3 predominance [8].

The effect of thyroid hormones on I_{Ca} is of importance, since it suggests that these hormones affect myocardial contractility not only by regulating myosin ATPase isozymes expression, but also by modulating the amplitude of I_{Ca}. There are several reports that suggest that alterations in myosin ATPase are not the only mechanism responsible for thyroid hormone action on myocardial contractility. Goodkind and his collegues [4] studied the "effect of thyroxine on ventricular myocardial contractility and ATPase activity in guinea pigs." They reported that one day after thyroxine administration, the developed tension and maximal rate of rise of tension in the right ventricular papillary muscles was greater than normal, whereas myosin ATPase activity was unchanged. Based on these findings, they suggested that the rapid effect of thyroxine probably results from the effect of the hormone on excitation contraction coupling. Since then, several other studies have provided more direct evidence suggesting that thyroid hormones affect Ca^{2+} ATPase activity and Ca^{2+} uptake [9, 12]. More recently, Kim and Smith [7] studied the effect of thyroid hormones on cellular Ca^{2+} content and trans-sarcolemmal influx and efflux in cultured chick ventricular cells. They found that, among other effects, 10^{-8} M T_3 in the growth medium increases Ca^{2+} influx (verapamil inhibitable) via the slow Ca^{2+} channels. Thus, our study shows that I_{Ca} (measured directly) is in fact increased by thyroid hormone. The possibility that this effect on I_{Ca} is mediated, at least in part, by an increase in membrane area can be tested in principle by expressing the amplitude of I_{Ca} as current density, by estimating membrane area from measurements of passive electrical properties. However, this procedure would provide reliable results only if the increase in area resulted from the addition of a "functional membrane", i.e., one containing Ca^{2+} channels. As it has been shown that hyperthyroidism (in rabbits) is associated with a dilatation of ventricular muscle t-tubules [11], which do not necessarily contain Ca^{2+} channel, it appears that only by means of single-Ca^{2+}-channel recording would it be possible to provide more definitive answers.

The mechanisms responsible for the effect of thyroid hormones on I_{Ca} are yet to be investigated, and detailed studies are needed to determine whether these effects are induced indirectly, via synthesis of proteins that are part of the ionic channel, or through a more direct effect on the channel, such as by modifying the channel protein phosphorylation state.

References

1. Binah O, Arieli R, Beck R, Rosen MR, Palti Y (1985) Modulation of ventricular electrophysiological properties by metabolic rate [Abstract]. Circulation 72 (Suppl 3):231
2. Binah O, Arieli R, Beck R, Rosen MR, Palti Y (1987) Ventricular electrophysiological properties: is interspecies variability related to the thyroid state? Am J Physiol (in press)
3. Freedberg AS, Papp JG, Vaughan-Williams EM (1970) The effect of altered thyroid state on atrial intracellular potentials. J Physiol (Lond) 207:357–369
4. Goodkind J, Dambach GE, Thyrum PT, Luchi R (1974) Effect of thyroxine on ventricular myocardial contractility and ATPase activity in guinea pigs. Am J Physiol 226:66–72
5. Isenberg G, Klöckner U (1982) Calcium-tolerant ventricular myocytes prepared by preincubation in a "KB medium". Pflügers Arch 395:6–18
6. Johnson PN, Freedberg AS, Marshall JM (1973) Action of thyroid hormone on the transmembrane potentials from sinoatrial node cells and atrial muscle cells in isolated atria of rabbits. Cardiology 58:273–289
7. Kim D, Smith TW (1985) Effect of thyroid hormone on calcium handling in cultured chick ventricular cells. J Physiol (Lond) 364:131–149
8. Morkin E, Flink IL, Goldman S (1983) Biochemical and physiologic effects of thyroid hormones on cardiac performance. Prog Cardiovasc Dis 25:435–464
9. Nayler WG, Merrillees NCR, Chipperfield D, Kurtz JB (1984) Influence of hyperthyroidism on the uptake and binding of calcium by cardiac microsomal fractions and on mitochondrial structure. Cardiovasc Res 5:469–482
10. Oppenheimer JH (1979) Thyroid hormone action at the cellular level. Science 203:971–979
11. Sharp NA, Neel DS, Parsons RL (1985) Influence of thyroid hormone level on the electrical and mechanical properties of rabbit papillary muscle. J Mol Cell Cardiol 17:119–132
12. Suko J (1973) The calcium pump of cardiac sarcoplasmic reticulum: functional alterations of different levels of thyroid state in rabbits. J Physiol 228:563–581

Received October 30, 1986/Accepted January 21, 1987

Pflügers Arch (1987) 409:217–219

Pflügers Archiv
European Journal of Physiology
© Springer-Verlag 1987

Short communication

Suppression of charge movement by calcium antagonists is not related to calcium channel block

K. B. Walsh, S. H. Bryant, and A. Schwartz

Department of Pharmacology and Cell Biophysics, University of Cincinnati, Cincinnati, OH 45267-0575, USA

Abstract.
The calcium channel-inhibiting drugs nitrendipine and diltiazem represent two important classes of organic calcium antagonists. In the present study, the effect of these drugs on calcium currents and charge displacement currents in bullfrog semitendinosus muscle fibers was examined using a vaseline gap voltage clamp. Nitrendipine (10 μM) reduced the quantity of charge that moved both during the ON phase (Q_{ON}) and the OFF phase (Q_{OFF}) of charge movement. This action appeared to be most selective for Q_{ON}. However, at this same concentration, nitrendipine had no blocking action on inward calcium currents. In contrast to these findings, diltiazem blocked calcium currents in a concentration-dependent manner, while slightly increasing the quantity of charge moved during Q_{ON} and Q_{OFF}. The enhancement of charge movement by diltiazem resulted from two actions. First, diltiazem shifted the voltage-dependence of charge movement to more negative potentials. Second, diltiazem increased the maximum amount of charge moved. (Supported by NIH NS 03178 and HL 07382.)

Key words:
Calcium antagonist drugs, calcium currents, charge movement.

Introduction

Voltage-dependent charge movement first observed by Schneider and Chandler (1973) in frog skeletal muscle, has remained a viable mechanism for linking excitation of the transverse tubular (t-tubular) membrane with release of calcium (Ca^{++}) from the sarcoplasmic reticulum (SR). Many pharmacological agents, including local anesthetics, which suppress contraction produce a reduction in charge movement (Hui, 1983; Huang, 1982). Recently, based chiefly on experiments showing that charge movement could also be reduced in the presence of the dihydropyridine Ca^{++} channel antagonist nifedipine, investigators have suggested that part if not all of charge movement is associated with t-tubular Ca^{++} channels (Hui et al., 1984; Lamb, 1986; Rios et al., 1986). In the present study it is demonstrated that Ca^{++} channel block can be pharmacologically dissociated from charge movement suppression using other Ca^{++} channel blocking drugs. Nitrendipine at a concentration that has no blocking action on inward Ca^{++} currents, greatly reduced charge movement. In contrast, a concentration of diltiazem which was found to block Ca^{++} currents enhanced charge movement.

Methods

Experiments were performed on segments of single muscle fibers obtained from the bullfrog (Rana Catesbiana) semitendinosus muscle. Ca^{++} currents and charge displacement currents were recorded using a modified triple vaseline gap voltage clamp (Hille and Campbell, 1976), following standard procedures (Decoursey et al., 1982). Charge-displacement currents were acquired using the D/A and A/D capabilities of the laboratory's DEC-LSI 11/02 computer. Command voltages of varying amplitude and duration were delivered to the voltage clamp amplifier from the D/A converter (DT 2781) and linear components of the current records first reduced using an analogue leak and capacity transient subtractor. After reducing the linear components of the current records, charge displacement currents were obtained by digitally subtracting four current records associated with hyperpolarizing steps of P/4 amplitude from the record generated by a depolarizing step of amplitude P applied from a holding potential of -90 mV. Charge records were filtered at 2.5 KHZ using an 8-pole Bessel filter, sampled at 200 μsec per point by an A/D converter (DT 2782) and stored on a hard disk. For recording Ca^{++} currents, fibers were held at a holding potential of -90 mV from which depolarizing steps 1.8 sec in duration were applied every 2 min from a pulse generator. Ca^{++} current records were sampled at 6 msec intervals for 500 points. The external solution (pool A) contained (in mM): $TMACH_3SO_3$, 120; $CaCl_2$, 10 (Ca^{++} current), 2 (charge movement); HEPES, 10; and 10^{-6} g/ml tetrodotoxin. In addition charge movement records were recorded in the presence of 10 mM $NiCl_2$. The internal solution (pools B, C, E) contained (in mM): CsAspartate, 120; EGTA, 5; Hepes, 10; and ATP, 3. All solutions were adjusted to pH 7.2-7.3, and had an osmolarity of 240-250 mOsmol.

Results

Figure 1A shows charge movement records obtained during test pulses to -30 mV. Charge movement becomes discernible when linear components of capacity are subtracted and ionic currents are blocked. Charge movement records are composed of two phases: the ON phase of the charge movement (Q_{ON}), which occurs during the onset of depolarization, and the OFF phase of the charge movement (Q_{OFF}), which occurs following the termination of depolarization (Schneider and Chandler, 1973). Addition of the dihydropyridine blocker nitrendipine resulted in a time-dependent reduction in the quantity of charge moved during Q_{ON} and Q_{OFF} (Figure 1A). This action appeared to be most selective for Q_{ON} with the quantity of charge moved during Q_{ON} being reduced from 15.3 to 4.8 nC/μF, after 20 min exposure to nitrendipine. Q_{OFF} decreased from 16.9 to 13.8 nC/μF during this same time. A slight depressive effect was also noted in Q_{ON} with 5μM nitrendipine (not shown).

These results suggested that a component of charge movement (predominately in Q_{ON}) might be related to current flow through t-tubule Ca^{++} channels, since we (unpublished work), as well as others (Schwartz et al., 1985) have found that these currents are blocked by nitrendipine in English

Offprint requests to: S.H. Bryant

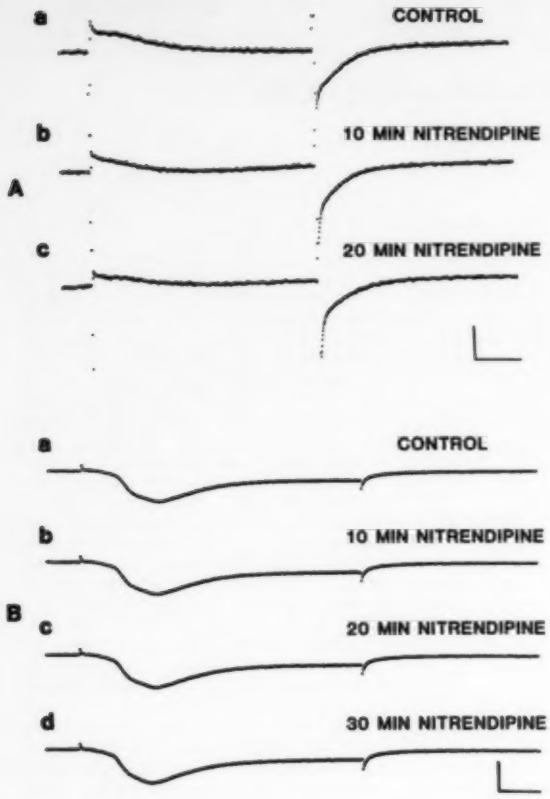

Figure 1. Charge displacement currents and Ca^{++} currents recorded in the presence of nitrendipine. A: Charge displacement currents recorded at 10.0°C during step depolarizations to -30 mV, before (a), 10 min (b) and 20 min (c) after addition of 10 M nitrendipine. All traces are averages of four sweeps. Vertical calibration equals 2 A/F and horizontal calibration equals equals 20 msec. B: Ca^{++} currents recorded at 22.1°C during step depolarizations to -27 mV, before (a), 10 min (b), 20 min (c), and 30 min (d) after addition of 10 M nitrendipine. Vertical calibration equals 75 A/cm^2 and horizontal calibration equals 250 msec.

grass frog (Rana temporaria) muscle fibers. In order to confirm this in the bullfrog fibers, Ca^{++} currents were recorded under conditions similar to those used to measure charge movement. Figure 1B shows Ca^{++} current records obtained during test steps to -27 mV. These currents revealed kinetics similar to those reported previously (Sanchez and Stefani, 1978; Stanfield, 1977; Almers and Palade, 1981), could be reduced by substitution of Mg^{++} for Ca^{++}, and were blocked by 0.5 mM Cd^{++}. Surprisingly, there was no reduction in the amplitude of the Ca^{++} current in the presence of nitrendipine, even up to 30 min after addition of the drug to the chamber (Figure 1B).

Since charge movement was suppressed with nitrendipine at a concentration that produced no blockage of the Ca^{++} current, it was of interest to determine what effect, if any, an agent that blocked the Ca^{++} current would have on charge movement. The Ca^{++} antagonist drug diltiazem was found to be

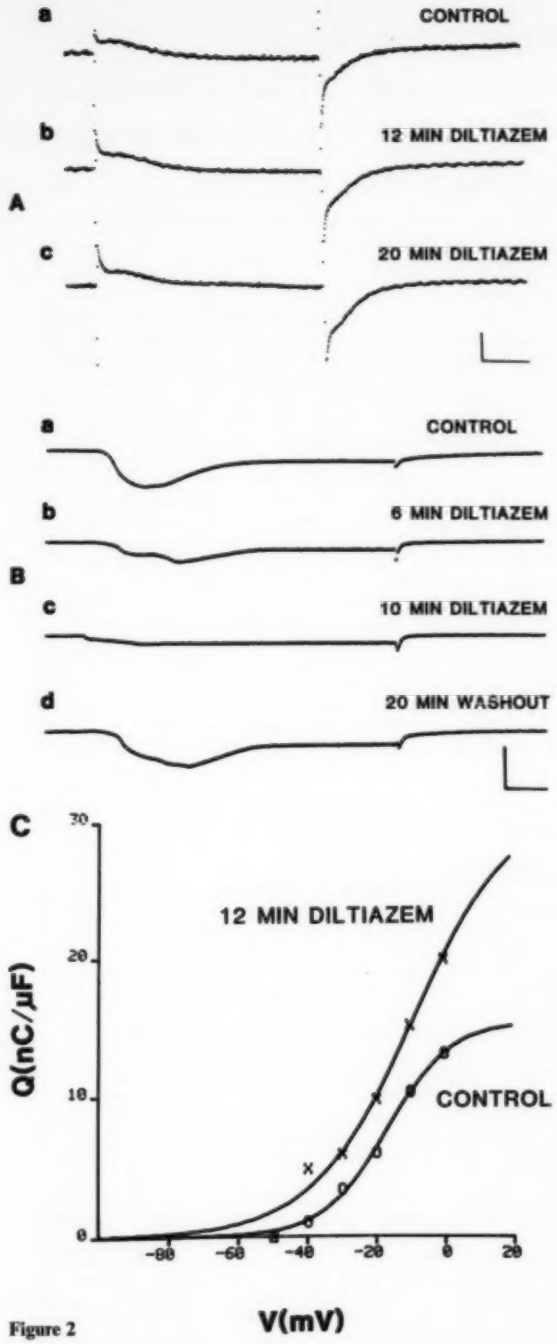

Figure 2

suitable for this purpose. High concentrations of diltiazem are required to reduce the amplitude of the Ca^{++} current in skeletal muscle (Almers and McClesky, 1984; Walsh et al., 1986). Figure 2B shows the blocking effect of 0.5 mM d-cis diltiazem on the Ca^{++} current. At this concentration, onset of block occurred 2 min after addition of diltiazem and reached its peak effect 8 min later. In the

Figure 2. Charge displacement currents and Ca^{++} currents recorded in the presence of diltiazem. A: Charge displacement currents recorded at 10.2° C during step depolarizations to -10 mV, before (a), 12 min (b) and 20 min (c) after addition of 0.25 mM d-cis diltiazem. All traces are averages of four sweeps. Vertical calibration equals 2 μA/μF and horizontal calibration equals 20 msec. B: Ca^{++} currents recorded at 21.8° C during step depolarizations to -16 mV before (a), 6 min (b) and 10 min (c) after addition of 0.5 mM d-cis diltiazem and 20 min after washout (d). Vertical calibration equals 75 $\mu A/cm^2$ and horizontal calibration equals 250 msec. Effect of diltiazem on the steady-state distribution of Q_{ON} as a function of potential (V). Values of Q_{ON} at each V, were obtained before (O) and 12 min (X) after the addition of 0.25 mM d-cis diltiazem. The smooth curves were fit with $Q = Q_{max}/(1 + \exp[-(V - \overline{V})/k])$, where in the absence of diltiazem, Q_{max} = 15.5 nC/μF, $\overline{V}$ = -16.3 mV and k = 9.4 mV, and in the presence of diltiazem Qmax = 31.6 nC/μF, $\overline{V}$ = -8.7 mV and k = 14.6 mV.

experiment shown in Figure 2B, diltiazem reduced the fractional current amplitude to 0.08. Blockage of Ca^{++} currents by diltiazem was concentration-dependent with the 50% blocking concentration being 190 μM.

In contrast to the suppressing action nitrendipine produced on charge movement, Figure 2A illustrates that diltiazem, at a concentration that reduced the Ca^{++} current, slightly enhanced charge movement. In the presence of diltiazem, Q_{ON} increased from 10.9 nC/μF to 12.1 and 14.4 nC/μF, respectively, 10 and 20 min after drug addition. During the same time, diltiazem increased Q_{OFF} from 17.4 nC/μF to 22.9 and 28.2 nC/μF. Overall in five experiments, 0.25 mM diltiazem increased the quantity of charge moved (mean ± S.E.) during Q_{ON} and Q_{OFF} by 19.6 ± 7.5% and 20.6 ± 5.0% respectively. A similar action was observed with 0.5 mM diltiazem. In Figure 2C the amount of charge moved as a function of the test potential is plotted for Q_{ON} recorded before and after the addition of 0.25 mM diltiazem. It can be seen that enhancement of charge movement resulted from two actions of diltiazem. First, diltiazem shifted the voltage-dependence of charge movement to more negative potentials. Second, diltiazem increased the maximum amount of charge moved (Qmax) from 15.5 to 31.5 nC/μF. Similar changes were observed in Q_{OFF}.

Taken together, the results of this study indicate that there is no relationship between block of skeletal muscle Ca^{++} channels and suppression of charge movement brought about by Ca^{++} antagonist drugs. Instead it is proposed that the action of each of these drugs on charge movement results from the binding of the drugs to specific receptor sites, known to be present in the t-tubular membrane (Fosset et al., 1983; Galizzi et al., 1986). Depending on the drug, these sites may or may not be associated with Ca^{++} channels. Although skeletal muscle t-tubular membrane is considered one of the richest sources of dihydropyridine binding sites (Fosset et al., 1983), the functional role of these sites has remained unknown (Schwartz et al., 1985; Schwartz and Triggle, 1984). The present work suggests that these sites may play an important role in excitation-contraction coupling. Along these lines, enhancement of charge movement by diltiazem may be involved in the twitch potentiating action of this drug in skeletal muscle (Gonzalez-Serratos et al., 1982).

References

Almers W, McClesky EW (1984) Non-selective conductance in calcium channels of frog muscle: calcium selectivity in a single-file pore. J Physiol 353: 585-608

Almers W Palade PT (1981) Slow calcium and potassium currents across frog muscle membrane: measurements with a vaseline-gap technique. J Physiol 312: 159-176

DeCoursey TE, Bryant SH, Lipicky RJ (1982) Sodium currents in human skeletal muscle fibers. Muscle a Nerve 5: 614-618

Fosset M, Jaimovich E, Delpont E, Lazdunski M (1983) [^{3}H]Nitrendipine receptors in skeletal muscle: properties and preferential localization in transverse tubules. J Biol Chem 258: 6086-6092

Galizzi J, Borsotto M, Fosset M, Lazdunski M (1986) Characterization and photoaffinity labeling of receptor sites for the Ca^{2+} channel inhibitors d-cis-Diltiazem, (+/-)-Bepridil, Desmethoxy-verapamil, and (+)-PN 200-110 in skeletal muscle transverse tubule membranes. J Biol Chem 261: 1393-1397

Gonzalez-Serratos H, Valle-Aguilera R, Lathrop DA, del Carmen-Garcia M (1982) Slow inward calcium currents have no obvious role in muscle excitation-contraction coupling. Nature 298: 292-294

Hille B, Campbell DT (1976) An improved vaseline gap voltage clamp for skeletal muscle fibers. J Gen Physiol 67: 265-293

Huang CL-H (1982) Pharmacological separation of charge movement components in frog skeletal muscle. J Physiol 324: 375-387

Hui CS (1983) Pharmacological studies of charge movement in frog skeletal muscle. J Physiol 337: 509-529

Hui CS, Milton RL, Eisenberg RS (1984) Charge movement in skeletal muscle fibers paralyzed by the calcium-entry blocker D600. Proc Natl Acad Sci 81: 2582-2585

Lamb GD (1986) Components of asymmetric charge movement in contracting skeletal muscle fibres of the rabbit. Biophys J 49: 12a

Rios E, Brum G, Stefani E (1986) E-C coupling effects of interventions that reduce slow Ca current suggest a role of T-tubule Ca channels in skeletal muscle function. Biophys J 49: 13a

Sanchez JA, Stefani E (1978) Inward calcium current in twitch muscle fibres of the frog. J Physiol 283: 197-209

Schneider MF, Chandler WK (1973) Voltage dependent charge movement in skeletal muscle: a possible step in excitation-contraction coupling. Nature 242: 244-246

Schwartz A, Triggle DJ (1984) Cellular action of calcium channel blocking drugs. Ann Rev Med 35: 325-356

Schwartz LM, McClesky EW, Almers W (1985) Dihydropyridine receptors in muscle are voltage-dependent but most are not functional calcium channels. Nature 314: 747-751

Stanfield PR (1977) A calcium dependent inward current in frog skeletal muscle fibres. Pflugers Arch 368: 267-270

Walsh KB, Bryant SH, Schwartz A (1986) Effect of calcium antagonist drugs on calcium currents in mammalian skeletal muscle fibers. J Pharm Exp Ther 236: 403-407

Received September 3, 1986 / Accepted December 3, 1986

Pflügers Arch (1987) 409:220–222

Pflügers Archiv
European Journal of Physiology
© Springer-Verlag 1987

Short communication

Isolated perfused rat kidney and liver combined

A new experimental model

H. Daugaard, M. Egfjord, and K. Olgaard

Medical Department P, Division of Nephrology, and Department of Experimental Pathology, Rigshospitalet, DK-2100 Copenhagen, Denmark

ABSTRACT Interaction between hepatic and renal metabolism is found in many endocrine systems. We therefore developed a new experimental model, combining the isolated perfused rat kidney and rat liver. Krebs-Henseleit buffer with bovine serum albumin 67 $g \cdot l^{-1}$ and amino acids was recirculated to both organs through two rolling pumps, four 8 µm Millipore filters and two specially designed membrane lungs. The kidney was cannulated by a modification of the technique described by Nishiitsutsuji-Uwo 1967 and the liver was cannulated by a modification of the technique described by Hems 1966. Kidney function: Perfusion pressure 12.4 ± 1.1 kPa (93 ± 8 mmHg), flow 28 ± 6 $ml \cdot min^{-1} \cdot g^{-1}$, FR_{Na} 94.0 ± 2.9 %, GFR 491 ± 191 $\mu l \cdot min^{-1} \cdot g^{-1}$, urine production 48 ± 34 $\mu l \cdot min^{-1} \cdot g^{-1}$, FE_K 60 ± 36 %. Liver function: Flow 25 $ml \cdot min^{-1}$ (fixed), portal vein pressure 12 ± 3 cm H_2O, bile flow 0.18 ± 0.13 $ml \cdot h^{-1}$, oxygen consumption 2.0 ± 0.2 $\mu mol \cdot min^{-1} \cdot g^{-1}$. Only minor differences were found between single perfusions (N = 25) and combined perfusions (N = 6). We conclude that it is possible to combine the isolated perfused rat kidney and rat liver without impairment of the function of either.

KEY WORDS Rat, isolated perfused kidney, isolated perfused liver, combination of

INTRODUCTION The present investigation compares the results from a model using the combined isolated perfused rat kidney and rat liver with the results from the single perfused organs. This new model makes it possible to study interactions between hepatic metabolism and renal excretion of a certain hormone or pharmacon without the disturbing influences from other organs found in many in vivo studies. Thus, total metabolism in the liver and the kidney can be investigated under well-defined conditions chosen by the investigator.

METHODS Perfusion medium: All experiments were performed with modified Krebs-Henseleit bicarbonate buffer containing glucose 5 $mmol \cdot l^{-1}$, 67 $g \cdot l^{-1}$ bovine serum albumin (fraction V, Miles Laboratories, Inc, Illinois, U.S.A.) and all 20 physiological L-amino acids.

Electrolyte composition ($mmol \cdot l^{-1}$): Na 141; K 5.0; Ca 3.0; Mg 0.7; SO_4 0.7; HCO_3 25; Cl 122; PO_4 3.0; lactate 4.0. Albumin concentrates for the perfusions were dialysed versus Krebs-Henseleit bicarbonate buffer for 48 h. Amino acid composition was the same as described before (Epstein et al. 1982). Travasol 10% (Travenol Laboratories, Inc, Illinois, U.S.A.) 10 ml per liter of perfusate was used as the source of most of the amino acids. The remainder were added individually (Sigma cell culture reagents, Sigma Chemical Company, Mo., U.S.A.). Perfusates were prefiltered through 0.22 µm Millipore filters (GVWP 04700, Millipore Corp., Mass., U.S.A.). No antibiotics were added. When gassed with 95 % O_2 – 5 % CO_2 the perfusates maintained a pH of 7.30 – 7.40.

Kidney perfusion: Experiments were performed on male Wistar rats weighing from 368 g to 466 g maintained on a standard pellet diet and allowed water ad libitum. The animals were anesthetised with sodium pentobarbital 2.5 % 1.7 – 2.0 ml intraperitoneally and given 0.9 ml of 20 % mannitol intravenously prior to surgery. The right kidney was cannulated with a 19 gauge blunted needle via the superior mesenteric artery without interruption of flow by a modification of the technique described before (Nishiitsutsuji-Uwo et al. 1967). Heparin 500 I.E. were given intravenously immediately before cannulation. Ligatures were placed around the right renal artery proximal and distal to the origin of the adrenal artery that was not ligated. The ureter was not cannulated but dissected free about three cm distal to the kidney and guided directly into the urine sampling vials in the perfusion chamber. Arterial pressure was monitored with a strain gauge transducer and perfusate flow was adjusted manually to bring the calculated pressure distal to the tip of the cannula into the range of 12.7 – 14 kPa (95 – 105 mmHg). The weight of the left kidney was used as an estimate of the weight of the right kidney.

Liver perfusion: Female Wistar rats weighing from 180 g to 227 g were fasted 24 hours before the experiments, but allowed free access to water. Nebumal anesthesia 6 mg per 100 g rat body weight was given intraperitoneally. The operative technique was a modification of that described before (Hems et al. 1966). The bile duct was cannulated with a short length of Portex PE-10 tubing inserted into a PE-50 tubing connected to a 1 ml-syringe for bile collection. The portal vein was cannulated with a 14 G catheter (Deseret Comp., Utah, U.S.A.) and single pass perfusion was started with oxygenated perfusate at a flowrate of 8 $ml \cdot min^{-1}$. The inferior caval vein was cannulated through the right atrium with another 14 G catheter. The tip of the catheter was fixed at the level of the diaphragm with a ligature around the inferior caval vein close to the right atrium. The inferior caval vein was then ligated below the liver and the liver was dissected free and placed in the perfusion chamber hanging in the portal cannula and supported by a Petri dish. Recirculation was established and the flowrate was gradually increased to either 25 $ml \cdot min^{-1}$ or 35 $ml \cdot min^{-1}$ and then kept constant throughout the experiment.

Combined perfusions: These experiments were performed by two operators, permitting the two organs (one from each rat) to be cannulated at the same time. The organs were allowed to equilibrate for 30 minutes followed by another 30 – minute period for sampling before the liver and the kidney were combined, in order to use the function of the single organs as control for the combined model. Perfusate and in-line filters were then changed and the volume of the perfusate was adjusted to 200 ml. The coupled organs were then perfused for two hours, the perfusate recirculating between the liver and kidney in a parallel mode.

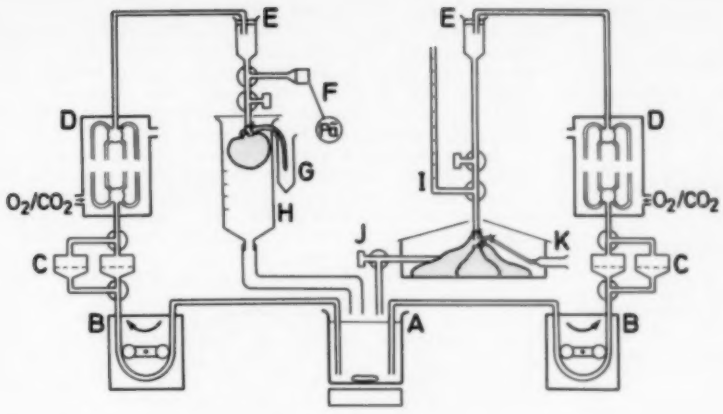

FIGURE 1.

Schematic outline of the system for combined liver and kidney perfusion:
A: Perfusate reservoir with stirrer
B: Roller pumps
C: 8um filters
D: Silastic lungs
E: Bubble traps
F: Pressure transducer
G: Vial for urine collection
H: Kidney chamber
I: Manometer connected to portal vein catheter
J: Caval catheter with sampling port
K: Bile catheter and syringe for bile collection.

Perfusion circuit (fig. 1): The circuit was contained in a thermostated plexiglass chamber ensuring a constant perfusate temperature of 36 - 37 °C. The circuit for each organ consisted of one peristaltic pump (MultiPerpex, LKB, Bromma, Sweden), two parallel in-line 8 µm filters (SCWP 04700, Millipore, Mass., U.S.A.) and one membrane lung consisting of four parallel 3.8 m - coils of Silastic tubing (Cat.no. 602-235, Dow Corning, Michigan, U.S.A.) connected with specially designed fittings (Ole Dich Instrumentmakers, Copenhagen, Denmark). This lung could withstand the high pressures needed in the kidney-circuit. When supplied with a standard gas mixture of 95 % O_2 - 5 % CO_2 the lung delivered perfusate at the necessary flow rates (20 - 40 ml·min^{-1}) with a pO_2 of 67 - 80 kPa (500 - 600 mmHg). Priming volume in each circuit was only 50 ml.

Analytical methods: Glomerular filtration rate (GFR) was determined as inulin clearance by a colorimetric method. Sodium and potassium were measured by flame photometry (Instrumentation Laboratories, Inc, Mass., U.S.A.). PO_2, PCO_2 and acid base status were measured by a blood gas system (ABL 4, Radiometer, Copenhagen, Denmark). Glucose was measured enzymatically by the hexokinase - glucose-6-phosphate dehydrogenase method and lactate was measured by the lactate dehydrogenase method after deproteinization with 1 molar percloric acid.

Data and statistical analysis: The data are given as means ± SD. Student's t test and parametric linear regression were used. All significance limits are two-sided.

RESULTS Kidney function: Eight kidneys were perfused as controls and six kidneys were perfused in combination with the isolated liver. A total of 118 observations of each functional parameter were obtained from these 14 perfusions. The results are shown in table 1. GFR and fractional sodium reabsorption (FR_{Na}) were found to decrease significantly ($p < 0.01$) with time, whereas urine production and fractional potassium excretion (FE_K) increased significantly ($p < 0.01$) with time. Therefore the results are given separately for each of the three hours of perfusion. A significant correlation was also found between perfusate flow and GFR ($r = 0.55$; $p < 0.001$). Three additional experiments were performed with single-pass perfusion of the isolated kidney and PAH 2 mg·l^{-1} added to the perfusate. PAH-clearances of 2.7 - 5.8 ml·min^{-1} were found in these perfusions.

Liver function: Results are shown in table 2. Oxygen consumption did not vary significantly with perfusion time throughout the observation period. Eighteen perfusions were performed with the isolated liver alone, without amino acids and glucose added to the medium and at a flowrate of 25 ml·min^{-1}. In this series we found a rate of gluconeogenesis from L-lactate 10 mmol·l^{-1} of 0.56 ± 0.23 µmol·min^{-1}·g^{-1} and a ratio of lactate elimination to glucose production of 2.01 ± 0.57 at comparable oxygen consumptions.

Table 1. Results from 14 kidney perfusions.

	Liver in circuit	Perfusion time (minutes) 30-60	60-120	120-180
Number of observations	(-)	14	19	26
	(+)	*	30	29
GFR µl·min^{-1}·g^{-1}	(-)	615±282	695±305	562±210
	(+)	*	491±191	420±156
P			<0.05	<0.01
FR_{Na} %	(-)	96.6±1.3	93.9±3.6	92.0±3.7
	(+)	*	94.0±2.9	91.0±3.3
P			NS	NS
FE_K %	(-)	26±17	80±43	90±26
	(+)	*	60±36	82±32
P			NS	NS
Urine production µl·min^{-1}·g^{-1}	(-)	30±20	70±53	70±39
	(+)	*	48±34	57±31
P			NS	NS
Perfusate flow ml·min^{-1}·g^{-1}	(-)	28±6	32±2	31±2
	(+)	*	28±6	27±5
P			<0.005	<0.001
Perfusion pressure mmHg	(-)	102±13	100±7	108±18
	(+)	*	93±8	96±6
P			<0.005	<0.005

Values are means ± SD. Abbreviations: GFR, glomerular filtration rate; FR_{Na}, fractional sodium reabsorption; FE_K, fractional potassium excretion.
Sampling was started 30 minutes after cannulation of the kidney.
* Kidney and liver were combined 60 minutes after cannulation of the kidney.

Table 2. Results from 24 liver perfusions.

	Kidney in circuit	Control	P
Number of livers	6	18	
Rat weight: g	206±15	194±12	NS
Liver wet weight: g	7.65±1.09	6.25±0.65	<0.005
Portal vein pressure cm H_2O	10±2	10±3	NS
Bile flow: $ml \cdot h^{-1}$	0.18±0.13	0.21±0.09	NS
Oxygen consumption:			
O_2 $\mu mol \cdot min^{-1}$	15.17±1.00	15.22±2.35	NS
O_2 $\mu mol \cdot min^{-1}$ per g_{-1}	2.00±0.20	2.46±0.46	<0.005
Flow (fixed) $ml \cdot min^{-1}$	25	25	NS

Combined perfused liver and kidney: No statistically significant differences were found between combined and single kidney perfusions concerning urine production, fractional sodium reabsorption and fractional potassium excretion (Table 1). GFR was lower in the combined perfusions and perfusate flow and perfusion pressure was also significantly lower in the combined perfusions.

Oxygen consumption per liver was not different in combined and single perfusions, whereas oxygen consumption calculated per gram liver was significantly lower in the combined perfusions than in the control group (Table 2). Liver weight was significantly higher in combined perfusions than in single perfusions, although rat weight was not significantly different in the two groups. Eight additional perfusions were carried out with a perfusate flow to the liver of 35 $ml \cdot min^{-1}$. In these perfusions oxygen consumption was 3.18 ± 0.47 $\mu mol \cdot min^{-1} \cdot g^{-1}$ in single livers and 3.02 ± 0.16 $\mu mol \cdot min^{-1} \cdot g^{-1}$ in combined perfusions. Average bile flow and portal vein pressure did not differ in the two groups.

DISCUSSION It is generally accepted, that for practical and economical reasons, single pass perfusion of the kidney is not feasible (Maack 1980). Moreover, preliminary studies in our laboratory showed deterioration of kidney function if single pass perfusion was used for more than 10 to 15 minutes. Therefore a recirculating system was chosen. In this recirculating system a parallel rather than serial perfusion setup for the combined kidney and liver was used, because parallel perfusion has the closest resemblance to the situation in vivo.

In the present study it was possible to combine the isolated perfused rat kidney and rat liver and obtain function of the combined organs that equalled that reported in other investigations using the single perfused organs (Friedmann and Rasmussen 1970; Gleim et al. 1984; Maack 1980; Rabkin et al. 1980). Only minor differences were found between single perfusions and combined perfusions. The function tests used were those generally accepted in the litterature of the isolated perfused organs.

Oxygen consumption per total liver was nearly identical in single and combined perfusions, and liver function did not differ from what has been found in other investigations using hemoglobin-free media (Friedmann and Rasmussen 1970; Rabkin et al. 1980). However, liver weight was significantly higher in combined perfusions than in single perfusions, and a lower oxygen consumption as expressed per gram liver was found in combined perfusions. The higher liver weight may be due to random variation. The weight was determined as wet weight at the end of the perfusions, and an influence from the kidney during the combined perfusions could not be excluded. The single livers, perfused at 25 $ml \cdot min^{-1}$, had an oxygen consumption per gram that was in the normal range, whereas the corresponding coupled livers were on the low side. Perfusions with liver flow 35 $ml \cdot min^{-1}$ resulted in high normal oxygen consumptions in both single and coupled livers. The same tendency towards lower oxygen consumption in coupled perfusions was found in these perfusions, even though no differences in liver weight could be demonstrated in this small series.

In the kidney a slightly lower, but acceptable GFR was found in combined perfusions. This could be explained by the unintended lower perfusion pressure and perfusate flow in this group. The perfusion pressure was controlled by the investigators by regulation of the perfusate flow. When GFR was corrected for the differences in perfusate flow using the significant correlation between perfusate flow and GFR then the difference between GFR in single and combined perfusions diminished and was no longer significant. However, when single and combined perfusions with the same perfusion pressure were matched, GFR was still significantly lower in combined perfusions.

The possible effects of introducing catheters with necessarily narrow lumina into the ureter have been discussed before (Schurek and Alt 1981). In this study the ureter was not cannulated, and peristalsis was visible distally to the cut end hanging down in the urine sampling vial. However, urine production was similar to that reported in other studies (Gleim et al. 1984; Maack 1980).

The described perfusion system developed for this combined perfusion model permits an easy access to the two organs and can be assembled in 10 minutes. The main purpose of these experiments was to optimise and characterise the present model. Thus the isolated perfused liver and kidney may be combined immediately after cannulation and perfused for at least 2 hours. This new model may prove of value in studies of hormone metabolism and pharmacokinetics.

ACKNOWLEDGMENTS The present investigation was kindly supported by grants from The Danish Medical Research Council, The P. Carl Petersen Foundation, The Helen and Ejnar Bjørnow Foundation, The Dagmar Marshall Foundation, The Jytte Hommsen born Købler's Foundation, The Elin Hartelius Foundation, The Gerda and Aage Haensch's Foundation, The Viholm-Foundation, The Novo Foundation, The Foundation of 1870, and King Christian X's Foundation.

REFERENCES

Epstein FH, Brosnan JT, Tange JD, Ross BD (1982) Improved function with amino acids in the isolated perfused kidney. Am J Physiol 243:F284-F292

Friedmann N, Rasmussen H (1970) Calcium, manganese and hepatic gluconeogenesis. Biochim Biophys Acta 222:41-52

Gleim GW, Kao-Lo G, Maude DL (1984) Pressure natriuresis and prostaglandin secretion by perfused rat kidney. Kidney Int 25 (5):683-688

Hems R, Ross BD, Berry MN, Krebs HA (1966) Gluconeogenesis in the perfused rat liver. Biochem J 101: 284-292

Maack T (1980) Physiological evaluation of the isolated perfused rat kidney. Am J Physiol 238:F71-F78

Nishiitsutsuji-Uwo JM, Ross BD, Krebs HA (1967) Metabolic activities of the isolated perfused rat kidney. Biochem J 103:852-862

Rabkin R, Ghazelech S, Share L, Crofton J, Unterhalter SA (1980) Removal of immunoreactive arginine vasopressin by the perfused rat liver. Endocrinology 106:930-934

Schurek HJ, Alt JM (1981) Effect of albumin on the function of perfused rat kidney. Am J Physiol 240:F569-F576

Received September 11, 1986 / Accepted March 5, 1987

Pflügers Archiv
European Journal of Physiology

Instructions for authors

General information
Manuscripts must be submitted in triplicate to the appropriate Subject Editor, who then selects a Field Editor to be responsible for having the papers evaluated.

Manuscripts must be written in English. Correct use of the language is the responsibility of the author.

Manuscripts which are returned to the authors for revision should be sent back within 6 weeks, otherwise they will be considered withdrawn.

Format
Manuscripts should be typed in double-spacing, leaving wide margins on one side of the paper only.

The desired position of figures and tables should be marked in the margin. Form and content should be checked carefully to exclude the need for correction in proof. Authors will be charged for changes introduced after the text has been set in type.

Each paper is limited to 8 printed pages. DM 150,00 will be charged for each page exceeding this limit.

Eight printed pages equal about 24 typewritten pages DIN A4 with 33 lines per page and 65 typewriter strokes per line. If an article contains illustrations, the space occupied by the figures must be allowed for in the length of the text.

Each article must be complete in itself, i.e., comprehensible without detailed knowledge of a previous or subsequent publication by the same author(s).

1. The **title page** should contain:

a) The title. (For bibliographic reasons, double titles are undesirable, particularly if the authors of the main and subsidiary parts are different.)

b) The name(s) of the author(s) and of the institution. (The latter can appear in the local language.) If there are several institutions, please make the affiliations clear. Give full address(es).

c) "Offprint requests to ..." (name of the author).

2. **Abstract** and **Key words:**

a) The manuscript must be preceded by an abstract stating the main points (not more than 200 words).

b) Below the abstract up to 8 key words are to be given for subject indexing. Key words should be taken from *Index Medicus* or composed on similar lines.

3. **Footnotes** other than those referring to the title heading should be numbered consecutively.

4. The list of **references** should include only works referred to in the text. References should be styled as follows:

Lee JM, Hill RM (1972) Responses of midbrain cells to blur. Pflügers Arch 336: 213–216

Hille B (1971) Voltage clamp studies on myelinated nerve fibres. In: Adelman WJ (ed) Biophysics and physiology of excitable membranes, chapter 12. Van Nostrand Reinhold, New York, p 242

Citations in the text should be by author and date or by numbers in square brackets. References should be listed at the end of the paper in alphabetical order under the first author's name. If an author who is cited also coauthored additional papers that are cited, and if he is the first author listed, the order should be as follow:

First author and one coauthor – list first alphabetically by coauthor, and then chronologically. First author and more than one coauthor – list chronologically (not alphabetically by the second author), since only the first author's name and "et al." followed by the year of publication will be used in the text.

In the event that more than one paper by the same author or team of authors was published in the same year, the letters a, b, c, etc., should follow the year – e.g. Schwartz (1971 a) – in both the text and the reference list if references are cited by author and year.

Works that have been accepted for publication but not yet released should be included in the reference list with the words "in press" in parentheses after the abbreviated name of the journal concerned. References must be verified by the author(s) against the original documents.

Personal communications should be cited only as an exception and preferably documented by a written statement, e.g.: Müller H: Personal communication, letter of October 31, 1972. This document need not be submitted to the journal but must be available in the file of the author(s). Oral communications should be mentioned in acknowledgements.

5. **Legends.** The figure legends should be sufficient to allow each figure to be understood without reference to the text. Each figure should have a short title followed by a concise description. All abbreviations and symbols appearing in the figure must be explained in the legend. Information given in the legends should not be repeated in the text.

6. **Figures** should not be regarded as mere illustrations but restricted to the minimum needed to clarify the text. Previously published figures cannot be accepted. The same data should not be presented in both graph and table form. As a rule, requests for color reproductions cannot be approved unless the author(s) bear(s) the costs.
All figures, whether photographs, graphs, or diagrams, should be numbered consecutively throughout and submitted on separate sheets. The figures should either match the size of the column width (8.6 cm) the entire page (17.7 cm) or be 12.8 cm in width with the legend at the side. The maximum length is 24 cm including the legend printed at its foot. Several figures may be grouped into a plate on one page.

Line drawings. Please submit good-quality glossy prints in the desired final size. The size of the letters should be in an appropriate and legible proportion to the size of the figures.

Halftone illustrations. Please submit well-contrasted photographic prints, trimmed at right angles and in the desired final size. Inscriptions should be about 3 mm high.

7. **Generic names** of drugs are preferred. If trade names are used, the generic name should be stated in full at first mention.

8. It is recommended that the Système International d'Unités (SI) be used for the numerical expression of the results of measurements. For details see Pflügers Arch (1977) 368:1–2.

Short communications
Short communications are limited to 3 printed pages, i.e., 6 columns. They must be submitted in triplicate to the appropriate Subject Editor and typed so as to fit the column width (11.5×33.0 cm). There is a limit of 2 figures and 8 references. To ensure rapid publication, the Subject Editor will enclose special stationery and instructions for producing camera-ready copy when the letter of acceptance is sent to the author(s). Once submitted in camera-ready form, a Short communication will be included in the next issue, which means it can appear in print within 3–6 weeks.

Offprints
Fifty (50) offprints of each paper are supplied free of charge. Additional offprints are available in lots of 100, provided the order is received with corrected proofs.

Pflügers Archiv
European Journal of Physiology

(Continuation of table of contents)

Vol. 409 No. 1–2 June 1987

B. M. Koeppen: Electrophysiological identification of principal and intercalated cells in the rabbit outer medullary collecting duct **138**

L. Bussieres, K. Laborde, M. Dechaux, C. Sachs: Effects of prolactin on Na-K-ATPase activity along the rat nephron **182**

S. M. L. Sanioto, A. Sesso: Structural and functional response of the isolated toad skin to mucosal lithium **188**

J. Pácha, M. Popp, K. Čapek: Amiloride-sensitive sodium transport of the rat distal colon during early postnatal development **194**

J. Ehrenfeld, E. J. Cragoe Jr., B. J. Harvey: Evidence for a Na^+/H^+ exchanger at the basolateral membranes of the isolated frog skin epithelium: Effect of amiloride analogues **200**

Short communication

H. Daugaard, M. Egfjord, K. Olgaard: Isolated perfused rat kidney and liver combined. A new experimental model **217**

C Excitable tissues and central nervous physiology

G. Droogmans, I. Declerck, R. Casteels: Effect of adrenergic agonists on Ca^{2+}-channel currents in single vascular smooth muscle cells **7**

A. R. Marchand, D. Manzoni, O. Pompeiano, G. Stampacchia: Effects of stimulation of vestibular and neck receptors on Deiters neurons projecting to the lumbosacral cord **13**

O. Pompeiano, S. Manzoni, A. R. Marchand, G. Stampacchia: Effects of roll tilt of the animal and neck rotation on different size vestibulospinal neurons in decerebrate cats with the cerebellum intact **24**

G. Cecchi, F. Colomo, V. Lombardi, G. Piazzesi: Stiffness of frog muscle fibres during rise of tension and relaxation in fixed-end or length-clamped tetani **39**

J. Kassotis, S. F. Steinberg, S. R. J. Bilezikian, R. B. Robinson: An inexpensive dual-excitation apparatus for fluorescence microscopy **47**

D. Swandulla, E. Carbone, K. Schäfer, H. D. Lux: Effect of menthol on two types of Ca currents in cultured sensory neurons of vertebrates **52**

D. Heinemeyer, W. Bay: Intracellular pH in quiescent and stimulated ventricular myocardium. Effect of extracellular chloride concentration **142**

K. Schäfer: A quantitative study of the dependence of feline cold receptor activity on the calcium concentration **208**

O. Binah, I. Rubinstein, E. Gilat: Effects of thyroid hormone on the action potential and membrane currents of guinea pig ventricular myocytes **214**

Short communication

K. B. Walsh, S. H. Bryant, A. Schwartz: Suppression of charge movement by calcium antagonists is not related to calcium channel block **220**

Indexed in *Current Contents*

Announcement

International Symposium on Surfactant Replacement Therapy

14–15th November 1987, Medical Faculty of Erasmus University Rotterdam

For further information please contact: Dr. B. Lachmann, Department of Anesthesiology, Erasmus University, Postbox 1738, NL-3000 DR, Rotterdam, The Netherlands, Telephone: (31) 10-4634393